

Disulfide Polymerizable Phosphatidylcholines:  
Characterization of Membrane Physical Properties  
and Investigations of *in vivo* Behavior.

Thesis by  
Tracy Marie Handel

*In Partial Fulfillment  
of the Requirements for  
the Degree of Doctor of Philosophy*

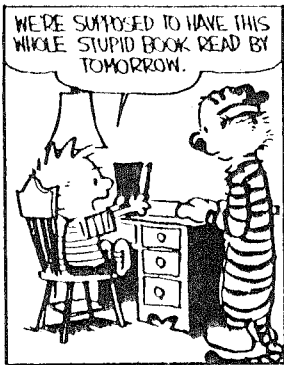
*California Institute of Technology  
Pasadena, California*

1989

*submitted January 18, 1989*

*To the Examining Committee and Anyone Else Who Considers Reading this Thesis.....*

**CALVIN AND HOBBS** By Bill Watterson



## Acknowledgements

I'm glad it's over, but, on the other hand, I have to say my years at Caltech have been extremely rewarding and filled with memorable experiences. I suspect that in the future, it will be difficult to find another institution where the scientific enthusiasm, encouragement and freedom rivals that found at Caltech. Needless to say, it is not the institution itself which has made "my Caltech years" so fantastic, but rather the people I have met and worked with. I owe a lot to many people.

My deepest gratitude goes to my research advisor, John Baldeschwieler. With his support and contagious enthusiasm, it was virtually impossible not to really enjoy and become perhaps too absorbed in my research. I must admit, the satisfaction one derives from working in the JDB lab also arises from the fact that the scientific areas he has chosen to delve into are incredibly exciting. Finally, I thank him for giving me every opportunity to develop myself as an independent and creative scientist. I could not have asked for a better mentor.

I am also very grateful to have been able to work with such a nice group of people as those in the JDB lab. The camaraderie of the group really softened some of the rough times I managed to put myself in. I am particularly indebted to the Bio-half of the group not only for their good scientific ideas but for their friendship and for taking pretty good care of me over the course of the past several years.

In addition to the student members of the JDB group, there are a number of people I really must thank for both friendship and science. James Yesinowski is perhaps one of the people to whom I am most indebted for teaching me the ropes of NMR spectroscopy -- not only did he show me how to change probes, implement 2-D pulse sequences and carry out magic angle spinning experiments, but he also introduced me

to some of the more amusing sides of NMR spectroscopy like inhaling helium while filling the magnet. Another collaborator who has substantially affected my stay at Caltech includes Jack Blazyk who introduced me to the wonders of vibrational spectroscopy and really played an integral role in helping me get my project moving. Mary Roberts and Elise Gabriel are two of a kind -- they were not only great for bouncing ideas off of, but also for keeping me smiling. Depression and discouragement just are not part of their vocabulary. Sean Sullivan has been a true friend since his postdoctoral stay at Caltech. He provided me with music, running companionship, and was a great surgical partner.

The people I am most indebted to I save for last. Tom Goliber has been my best friend for the past nine years. I thank him for getting me away from the lab and into the mountains, for keeping me laughing, for music, and for showing me by his own example that it is possible to do good science without compromising the other important aspects of ones life. Finally I thank my family for supporting my desire to go back to graduate school even if they they didn't quite understand the driving force, and my parents especially for giving me what it takes to to get a Ph.D.

## Abstract

In the past ten years, polymerizeable amphiphiles have been recognized as an important class of synthetic phospholipids due to their ability to modify the mechanical and chemical stability of membranes. The motivation behind studies of polymerizeable phospholipids is based on the potential importance of stable membranes in a wide variety of applications including reactivity control, encapsulation technologies and drug delivery. However, compared to nonpolymerizeable lipids, there is a relative paucity of information correlating membrane physical properties with the structure of the polymeric lipid. The present investigation involves the synthesis of a series of disulfide polymerizeable phosphatidylcholines, the characterization of the physical properties of membranes formed from these lipids, and an investigation of the biodistributions, vascular clearance rates and degradation rates of these liposomes *in vivo*.

The structures of the lipids under investigation are analogous to saturated phosphatidylcholines but with a thiol either alpha to the carbonyl of the acyl chain ( $\alpha$ -THIOL) or at the chain terminus ( $\omega$ -THIOL). It is found that the presence and position of the polymerizeable moiety drastically alters the physical characteristics of the membranes. A variety of physical techniques have been utilized to understand both the bulk properties of the lipids such as morphology and permeability, as well as the molecular details of the lipid conformation and dynamics. On the basis of such studies including Raman, FT-IR and DSC, it appears that the presence of the polymerizeable group at the interfacial region ( $\alpha$ -THIOLS) causes a reduction in the lipid packing and an increase in chain disorder compared to nonpolymerizeable analogs. For the monomeric form of the  $\alpha$ -THIOLS, the decreased interlipid interaction may be ascribed to the presence of an additional hydrophilic pendant group at the interface that interferes

with tight crystalline packing, most likely by a combination of steric and hydration effects. In contrast to the general expectations for polymerized versus nonpolymerized phospholipids, upon polymerization, the membrane disorder is augmented even further. We believe this to be a consequence of the conformational restrictions of polymerization which inhibit the ability of the polymeric lipids to adopt a highly ordered and uniform packing state. Instead it is suspected that the reduced conformational freedom of polymerized lipids promotes the formation of surface defects between unlinked polymer chains. As a morphological consequence, the polymeric  $\alpha$ -THIOLS tend to form smaller and largely unilamellar vesicles on dispersion in water. Furthermore because of the disorder in the hydrocarbon chain region, they are quite permeable to entrapped solutes and when administered *in vivo*, are cleared rapidly from the circulatory system. The latter effect is likely the result of facilitated absorption of opsonizing proteins into the disordered membrane surface which subsequently accelerates vascular clearance and uptake by the cells of the reticuloendothelial system (RES).

On the basis  $^{31}\text{P}$  NMR relaxation measurements, it was observed that the motion of the headgroups in polymeric  $\alpha$ -THIOLS was reduced relative to nonpolymerizable analogs. Furthermore a reduced chemical shift anisotropy of polymeric  $\alpha$ -THIOLS in the liquid-crystalline state relative to nonpolymerizable lipids was observed and suggests an alteration in the average orientation of the headgroup for the polymer. Because the headgroup of phosphatidylcholines is zwitterionic, changes in the average orientation can have marked effects on the electrostatic properties of the membrane surface, which in turn can affect membrane morphology and interactions with cell-surfaces and proteins.

For  $\omega$ -THIOLS, a distinctly different behavior was observed compared to the  $\alpha$ -THIOLS. For the monomers and especially the polymers, results from vibrational

spectroscopy and DSC suggest that the membrane conformational order and rigidity is increased relative to nonpolymerizable phosphatidylcholine analogues. However, in contrast to the  $\alpha$ -THIOLS that form normal self-sealed liposomal structures in both the monomeric and polymeric state, polymerization induces the transformation of  $\omega$ -THIOLS into bilayer fragments lacking an internal aqueous compartment. The most likely explanation for this was derived from  $^{13}\text{C}$  NMR relaxation experiments, which indicated that the mobility at the bilayer midplane of polymeric  $\omega$ -THIOLS is as restricted as the interfacial region. This contrasts to nonpolymerizable phospholipids and  $\alpha$ -THIOLS, which have the bilayer interior as the most fluid portion of the membrane. The rigidity at the midplane may prohibit the ability of the polymeric  $\omega$ -THIOLS to form curved or continuous multilamellar sheets or to respond to transient defects in the membrane without fragmentation.

An interesting and unexpected result concerning the  $\omega$ -THIOLS was retention of a phase transition after polymerization. For most polymeric lipids that have the polymerizable moiety at the chain terminus, polymerization has resulted in the disappearance of the transition due to crosslinking of the hydrocarbon chains. The presence of the transition in polymerized  $\omega$ -THIOLS may be evidence for the fact that polymerization results in a predominance of *intra*- rather than *inter-leaflet* coupled chains.

## TABLE OF CONTENTS

Acknowledgements .....	
Abstract.....	
I. Introduction .....	1
References.....	24
II. Morphological Properties of Aqueous Dispersions of Disulfide Polymerized Phosphatidylcholines.....	31
Introduction.....	31
Materials and Methods.....	34
Results.....	39
Discussion.....	105
References.....	115
III. Investigation of the Phase Transition Properties of Disulfide Polymerizable Phosphatidylcholine Bilayers by DSC, FT-IR and Fluorescence Polarization. .	119
Introduction.....	119
Materials and Methods.....	120
Results.....	123
Discussion.....	170
References.....	178
IV. Investigations of the Acyl Chain Conformations and Membrane Packing Characteristics of Disulfide Polymerizable Phospholipids by Raman and FT-IR . Spectroscopy.....	182
Introduction.....	182

Materials and Methods .....	183
Results and Discussion .....	184
Conclusions .....	236
References.....	238
Appendix .....	240
V. Investigations of the Dynamic Properties of Polymerized Phosphatidylcholines by $^{13}\text{C}$ and $^1\text{H}$ NMR.....	252
Introduction .....	252
Materials and Methods .....	255
Background .....	260
Results and Discussion .....	275
Conclusions.....	333
References.....	343
VI. Investigations of the Dynamics and Conformation of the Headgroup of Polymerized Phospholipid Membranes by $^{31}\text{P}$ NMR .....	347
Introduction .....	347
Materials and Methods.....	348
Results and Discussion .....	350
Conclusions.....	390
References.....	391

VII. <i>In Vitro</i> and <i>In Vivo</i> Investigations of the Stability, Blood Clearance Rates and Biodistributions of Disulfide Polymerized Phosphatidylcholine Liposomes . . .	393
Introduction . . . . .	393
Materials and Methods . . . . .	396
Background and Theory . . . . .	403
Results and Discussion . . . . .	409
Conclusions . . . . .	469
References . . . . .	472
VIII. Synthesis and Polymerization . . . . .	477
Materials and Methods . . . . .	477
Synthesis . . . . .	480
Representative Spectra . . . . .	497
Polymerization . . . . .	513
References . . . . .	534
IX. Concluding Remarks . . . . .	535

---

---

## Chapter I

---

---

### *INTRODUCTION*

---

---

Since the original discovery in the 1960s that certain phospholipids when dispersed in water, form concentric bilayers separated by aqueous compartments (liposomes or vesicles) there has been a tremendous effort directed toward membrane research. In the biological sciences, the similarity between liposomes and cell membranes have led to their use as simplified model membranes for studies of various processes including membrane fusion (1-4), protein structure and function (5,6), and cellular recognition (7,8). Also, the compartmentalized nature of liposomes has been particularly attractive for biophysical studies of reconstituted membrane proteins involved in vectorial processes such as proton pumping and molecular transport (9,10).

In addition to purely academic studies, many technological applications have been envisioned. These include liposomes for reactivity control (11-13), solar energy conversion (11), as semiconductors (14,15), and as erythrocyte substitutes for oxygen transport (16-18). Perhaps, however, the most interesting and promising potential of liposomes is in drug delivery (see references 19-23 for reviews). Several therapeutic and diagnostic delivery strategies have in fact been conceived and developed including: (i) targeted delivery to designated tissues via liposomes modified with specific recognition elements such as antibodies, carbohydrates and peptides (the most coveted and complicated delivery scheme) (24-30) (ii) passive delivery of liposomes to highly metabolic (i.e. tumors) or anatomically accessible cells (31) and (iii) slow release of

drugs and other materials from liposomes circulating in the blood and lymph, or resident in particular tissues (32,33). In addition to the obvious advantages inherent in the various delivery schemes, additional benefits of liposomal delivery include the fact that many types of materials (drugs, enzymes, immunomodulators, e.g. lymphokines) may be entrapped in a single type of liposome and transported into cells via liposomal endocytosis, thereby circumventing the pharmacokinetics of the encapsulant and alleviating any difficulty the untrapped material might otherwise have in crossing the cell membrane. Secondly, because the liposomes prevent entrapped material from ubiquitous uptake by all cell types, diseased or healthy, drug toxicity is often reduced as is the required dose for efficacy. Finally, encapsulation of the drug inhibits enzymatic degradation. Given the possibility of using such simple delivery systems to home in on diseased cells such as malignant and aids-infected cells, or to deliver activating factors to the immune system in an effort to stimulate the body's own defense mechanisms, it is easy to understand the interest in implementing liposome technology. This area is in fact a major theme of the research efforts of the Baldeschwieler group, and an underlying motivation for the studies presented in this thesis.

Unfortunately, the simplicity of the ideas are equalled by the complexity of their implementation. Whether for pure biophysical studies or drug delivery applications, a major caveat of liposomes which has prevented their widespread application has been their general instability with regard to leakage of entrapped material, chemical degradation, membrane fusion, and susceptibility to mechanical stress. Fundamental studies on the correlation between liposome composition and the above properties have demonstrated that the most stable liposomes are promoted by saturated gel-state phospholipids and cholesterol (34). In synthetic efforts to achieve greater chemical stability, the susceptible ester linkage of phospholipids has been replaced by ether, carbamyl, and alkyl linkages with the desired results (35-38). More recently, the

concept of polymerizable phospholipids has been introduced in an attempt to circumvent all of the above obstacles. Since their initial conception, many different types of polymeric lipids have been designed (for a review see reference 62) using a variety of polymerizable moieties (diacetylene, butadiene, methacrylate, amide and thiol groups) positioned at various locations along the lipid chain or in the headgroup (39-62). A schematic drawing of representative polymerizable lipids is shown in Figure 1. In many cases, polymerized liposomes have shown superior resistance to chemical and mechanical degradation, solubilization by organic solvents, and fusion, than have non-polymerized liposomes. This would be expected particularly for highly cross-linked lipid matrices. Liposome permeabilities have also been generally reduced for polymeric liposomes *compared to their monomeric counterparts*. On the other hand, while few studies have made direct comparisons with nonpolymerizable liposomes, it appears that relative to nonpolymerizable liposomes, permeabilities are rather structure dependent – sometimes worse, sometimes better. Nonetheless, the use of polymerizable lipids as surrogate membranes seems a promising approach to obviating the difficulties encountered with nonpolymerizable liposomes. Unfortunately, there is at present a huge number of polymeric lipids which have been synthesized and a relative paucity of data concerning the relationship between lipid structure and the membrane physical properties, thus making difficult *a priori* prediction of what types of lipids will yield the desired characteristics.

For this reason, the main objective of the work described in this thesis was to examine systematically and in detail, the physical properties of a particular class of polymerizable phospholipids. Since our long range goals include the use of liposomes as drug delivery systems, their *in vitro* behavior was also studied. The class of polymeric lipids we have chosen to evaluate were thiol-containing lipids shown in Figure 2 (A and B). These lipids (where N=11,16 for A and N=16 for B) were

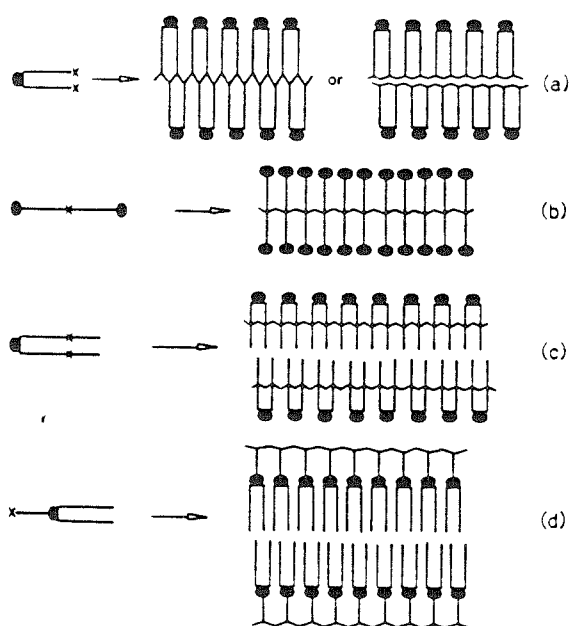
originally synthesized and studied in the Regen group (49,51) and have been extended here to include a wide range of chain lengths. In addition, we have also prepared mixed chain dimerizable phosphatidylcholines as shown in Figure 2 (C and D). Our reasons for choosing to study this particular type of lipid was based on the considerations summarized below.

(i) The nature of the polymerization is such that lipids with *widely varying chain lengths* may be readily synthesized. This offers many possibilities for systematic studies of structure-property relationships, and the ability to manipulate the lipid physical state. Not only can one alter the thermal properties of the lipids (such as the gel to liquid-crystalline phase transition temperature) but different aggregate morphologies may also be formed by appropriate choice of chain length. Saturated lecithins with chain lengths  $N=12$  to  $16$ , for example, are known to form bilayers with gel to liquid-crystalline transition temperatures ranging from  $-1.8^\circ$  ( $N=12$ ) to  $54.7^\circ$  ( $N = 18$ ) (63). For acyl chain lengths  $N = 6$  to  $8$ , micelles are formed above a critical micelle concentration (64,65). If similar trends are exhibited by polymerizable lipids, it should be possible to prepare both polymeric liposomes *and* polymeric micelles. Micelles, due to their (i) generally smaller size and (ii) ability to solubilize hydrophobic solutes, could conceivably provide interesting alternatives to liposomal drug delivery systems for the transport of hydrophobic drugs and other water-insoluble materials to target tissue. In this regard polymeric micelles should be much more stable than nonpolymerized micelles due to the fact that they do not possess a critical micelle concentration below which only monomers are obtained.

(ii) The ability to alter the *position of the polymerizable group* may provide an additional "handle" with which to manipulate and study the physical properties of the membrane. As an example, for lipid B (referred to as  $\alpha$ -THIOL or  $\alpha$ -N where N is the length of the acyl chain), polymerization may occur only within a given leaflet of the

**Figure 1**

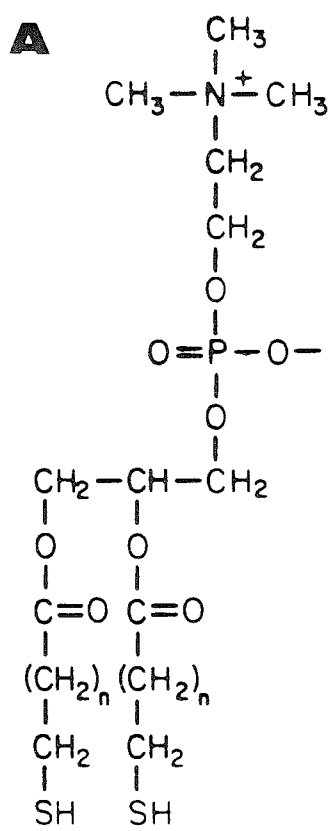
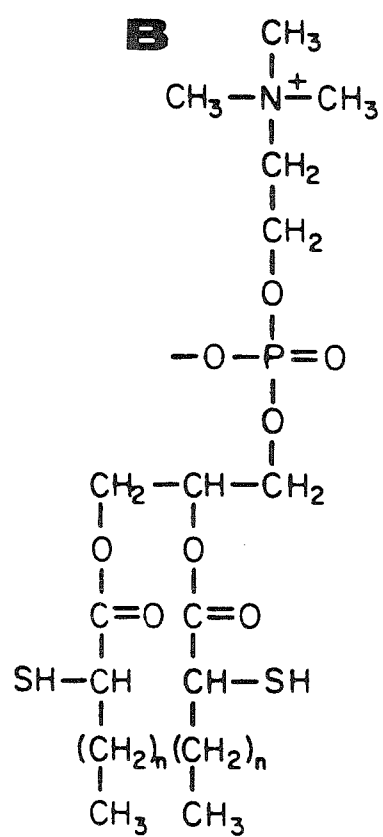
Schematic representation of some polymerizable lipid structures which have been described in the literature.

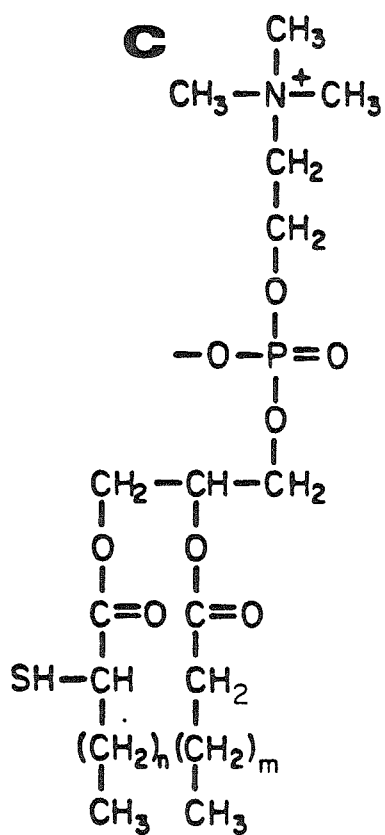
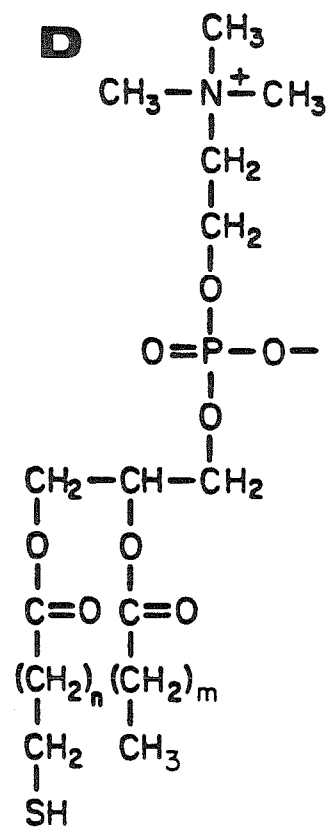


Scheme 1. Possible preparation of polymer model membranes ( $x$  = polymerizable group). (a—c): polymerization preserving head-group properties; d: polymerization preserving chain mobility

**Figure 2**

Structure of the disulfide polymerizeable phosphatidylcholines studied in this thesis: **A.** 1,2-di(N-mercaptoacyl)-L- $\alpha$ -phosphatidylcholine ( $\omega$ -THIOL) ; **B.** 1,2-di(2-mercaptoacyl)-L- $\alpha$ -phosphatidylcholine ( $\alpha$ -THIOL); **C.** 1-(N-acyl)-2-(N-mercaptoacyl)-L- $\alpha$ -phosphatidylcholine (mixed-chain  $\omega$ -THIOL); and **D.** 1-(N-acyl)-2-(2-mercaptoacyl)-L- $\alpha$ -phosphatidylcholine (mixed-chain  $\alpha$ -THIOL). N refers to the number of carbons in the acyl chains. Throughout the thesis, the notation for the  $\omega$ -THIOLS and  $\alpha$ -THIOLS is  $\omega$ -N and  $\alpha$ -N, respectively, to denote both the position of the polymerizeable moiety and the length of the acyl chains.

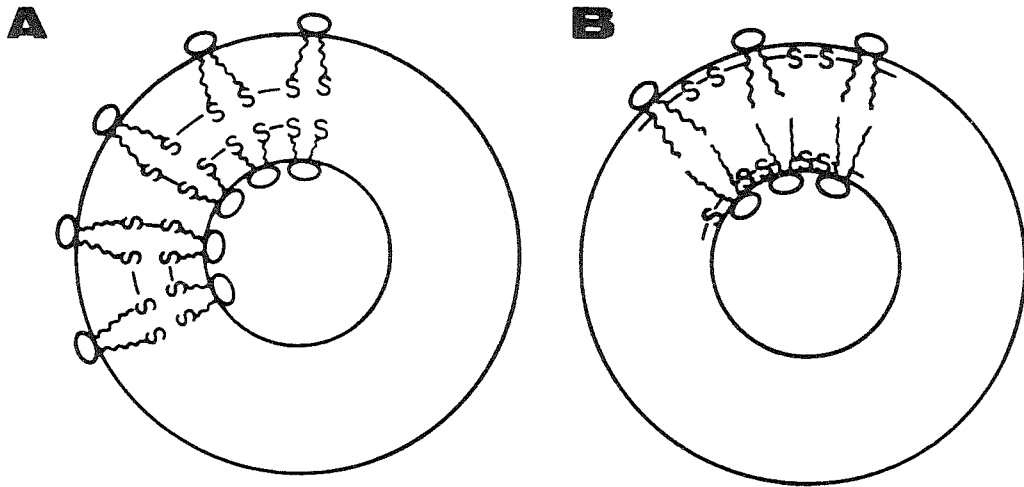
 $\omega$ -THIOL $\alpha$ -THIOL

MIXED CHAIN  $\alpha$ -THIOLMIXED CHAIN  $\omega$ -THIOL

**Figure 3**

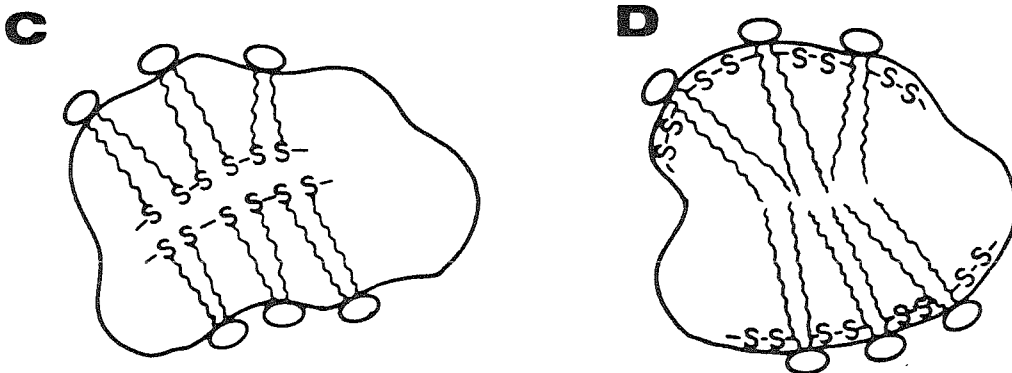
Schematic of polymerized liposomes and micelles of  $\alpha$ -THIOLS and  $\omega$ -THIOLS:  
A. polymerized  $\omega$ -THIOL liposome; B. polymerized  $\alpha$ -THIOL liposome; C.  
polymerized  $\omega$ -THIOL micelle; and D. polymerized  $\alpha$ -THIOL "micelle".

## VESICLES



---

"MICELLES"



bilayer. By contrast, for lipid A (referred to as  $\omega$ -THIOL or  $\omega$ -N) there is a possibility for polymerization across the two leaflets as well. This is depicted in Figure 3, which shows what one might envision for polymeric micelles and liposomes composed of these two lipid types. To consider the potential consequences of this, one should contrast these lipids with conventional nonpolymerizable lipids. In the case of the  $\alpha$ -THIOLS, an interesting analogy with nonpolymerizable lipids is the fact that the disulfide group is positioned near the interfacial region, which is the most rigid part of a normal bilayer (66,67). Thus one might expect the  $\alpha$ -THIOLS to retain the fluidity gradient observed for most phospholipid membranes. By contrast, the  $\omega$ -THIOLS should have restricted motion by virtue of polymerization at the bilayer midplane, which is generally the most fluid portion of biomembranes. In that respect,  $\omega$ -THIOLS are similar to some methacrylate-based lipids that also have polymerizable groups at the chain terminus. The effects of such alterations of chain length and position of the polymerizable group on morphology, membrane fluidity, chain mobility and permeability will be addressed in subsequent chapters.

(iii) Finally, the disulfide linkage is biodegradable, which is an important consideration for *in vivo* use. Diacetylene, butadiene, and methacrylate-based liposomes may not be degradable by the cellular machinery of the body, with potential toxic consequences. Furthermore, given a liposome that is stable under the conditions of an *in vivo* experiment (i.e. 37°C, in serum), once inside the target cell, some type of mechanism is necessary to release entrapped material. In the absence of passive leakage (which is undesirable because that implies release of entrapped solutes will be continuous prior to localization in the target tissue) it is not clear what mechanisms would bring about degradation of such liposomal matrices to release the contents. Ringsdorf et al. have devised a clever "corked liposome" composed of a phase separated mixture of fluorinated butadiene lipids and disulfide-linked single chain

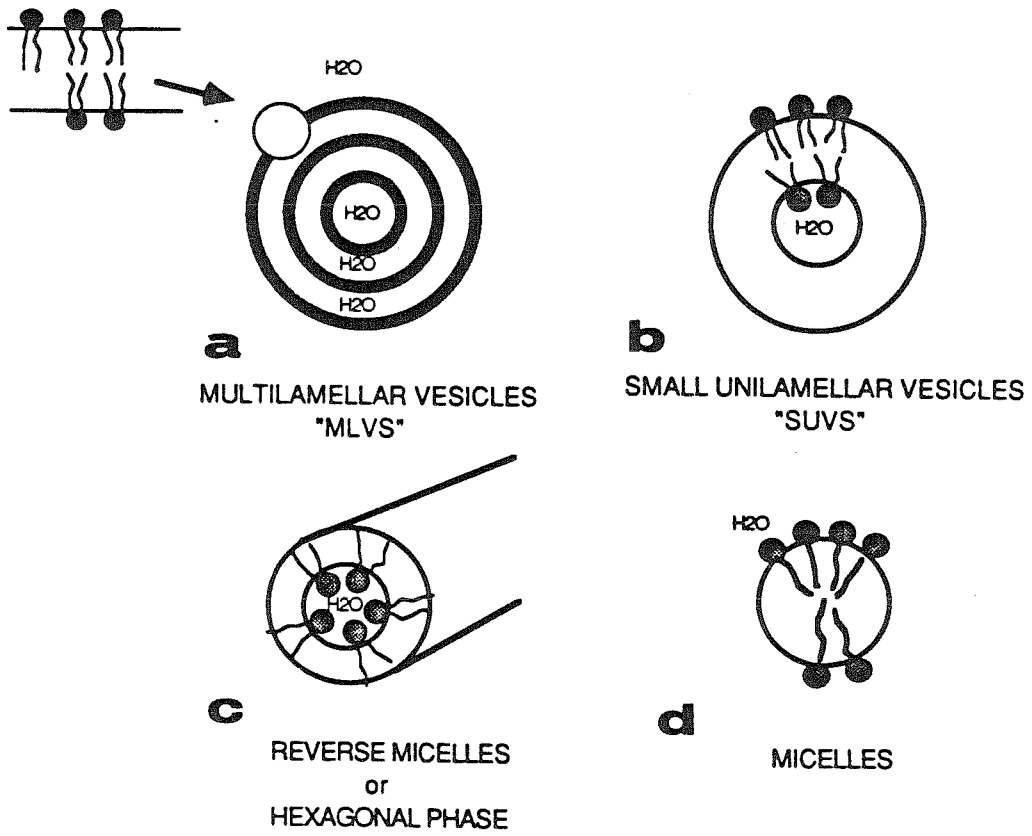
amphiphiles (68). Treatment of the liposomes with reducing agents such as dithionite cleaves the disulfides into water soluble lysolipids, which are leached out of the membrane, leaving behind "holes". Presumably, in an *in vivo* experiment, once inside the target tissue, similar mechanisms would be operative to dispense the entrapped material. As an alternative, a purely disulfide based liposome should be *completely* degradable once inside the reductive environment of a tumor or subject to the high concentrations of reductases known to be present in the lysosomal compartments of most cells. Thus we chose to study the lipids illustrated in Figure 2. The thesis is divided into several chapters, which address the following issues:

Chapter II: In chapter II, we examine the morphology of the polymeric lipids to confirm formation of their expected lamellar or micellar structures and to evaluate their sizes. Expectations are based on the known morphologies of nonpolymerizable analogs and the initial reports of Regen et al. for  $\alpha$ -16,  $\omega$ -11 and  $\omega$ -16. In actuality, however, a variety of aggregate structures may be formed by amphiphiles depending on the details of their molecular structure such as head group size, charge and hydration, as well as chain length and degree of unsaturation (69). Useful theories have been developed that allow prediction of the morphologies formed by lipids and lipid mixtures based essentially on these features but which have been generalized into less precise designations of molecular geometry (i.e. headgroup area, chain length and volume) (69-71). Morphologies that are pertinent to this thesis are illustrated in Figure 4. The basic unit of lamellar structures (Figure 4, A and B) is the bilayer that consists of two opposed sheets of lipid where the hydrocarbon tails are sequestered toward the membrane interior away from water, and the hydrophilic headgroups exposed to the aqueous medium (see insert). Typically, upon dispersion in water, long chain phosphatidylcholines (N=12-18) form large (5 to 20  $\mu\text{m}$ ) self-sealed concentric lamellae separated by aqueous compartments, structures commonly referred to as

**Figure 4**

Schematic diagram of the types of lipid morphologies that may be formed on dispersion of phospholipids in water. **A.** Multilamellar vesicles (MLVs) **B.** Small unilamellar vesicles (SUVs) **C.** Hexagonal phase tubules; and **D.** Micelles.

MEMBRANE MORPHOLOGIES



multilamellar vesicles or MLVs (Figure 4A). Sonication, pressurized filtration (72), reverse evaporation from organic solvent (73) and other methods (74,75) can be utilized to reduce the MLVs to unilamellar vesicles consisting of small or large single bilayers ( SUVs and LUVs, respectively) enclosing an aqueous compartment (Figure 4B). Certain lipids and lipid mixtures have also been found to promote spontaneous formation of unilamellar vesicles (76,77). By contrast, short chain lipids ( $N = 6-8$ ) or single chain amphiphiles with bulky or charged headgroups form spherical or ellipsoidal micelles on solubilization in water (Figure 4D). These structures are characterized by a generally smaller size (20-100Å ), a lack of an internal aqueous compartment, and are considered to be in dynamic equilibrium with the monomeric species on a much faster time scale than lipids in lamellar phases. The third most commonly encountered morphology is that of the hexagonal II phase or reversed micelles shown in Figure 4C. While important structures, particularly in regard to membrane fusion, these will not be discussed. Throughout this thesis, we will be concerned primarily with lamellar structures and to a lesser extent, micelles.

A variety of techniques were used to discriminate among the various macroscopic aggregates. Electron microscopy is particularly useful for visualizing both unilamellar and multilamellar structures and was a primary tool used in this investigation. Micelles are not readily observed by this technique due to their small size, fragility, and less well-defined morphology. Therefore, encapsulation of aqueous solutes was also used to distinguish between lamellar and micellar structures via the presence or absence of an aqueous compartment. Quasi-elastic light scattering, which measures the Brownian motion of the particles, was a useful adjunct to electron microscopy for particle sizing. Finally,  $^{31}\text{P}$  NMR spectra of lipid dispersions was used to identify the presence of morphological or size changes in lipid dispersions. This is possible due to the fact that lipid dispersions generally give rise to asymmetric powder patterns or broadened

symmetrical peaks due to incomplete motional averaging of the chemical shift tensors and dipolar interactions. The shape of the powder spectra is generally diagnostic of the presence of lamellar, hexagonal and micellar phases, but is also sensitive to aggregate size, head group motion, and head group orientation with respect to axis of motional averaging (78-80).

Chapter III: In chapter III, the phase transition behavior of the polymeric liposomes is described. The significance of the information derived from these studies will be more apparent after a brief introduction to the nature of the molecular reorganizations that occur during the so-called gel to liquid-crystalline transition:

For a typical phosphatidylcholine in the gel state (Figure 5), the lipids are packed in well-ordered crystalline arrays characterized by an extended all-trans configuration of the chains\*. As the temperature is raised, at some point an endothermic phase transition occurs during which the chains become highly disordered by a lateral expansion of the lipids, a decrease in the bilayer thickness, and the introduction of trans-gauche rotational isomers in the chain (81). The temperature at which the gel to liquid-crystalline phase transition ( $T_m$ ) occurs and the enthalpy ( $\Delta H$ ) associated with it has been extensively studied and demonstrated to depend on the details of the molecular structure of the lipid (chain length, degree of unsaturation, head group size and charge) and to reflect the *intermolecular* interactions of the lipids in the bilayer. In general, for phosphatidylcholines such as those used in this study, increasing the chain length increases the transition temperature and enthalpy as would be expected for increased van der Waals interactions between the chains. Unsaturation of the chains which increases the effective molecular volume of the chains and reduces the intermolecular

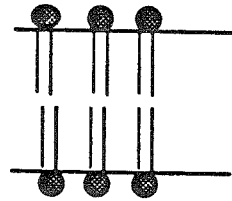
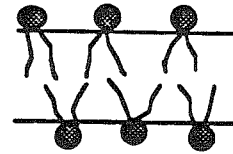
---

\* For simplicity, we ignore the poorly understood pretransition, which has been associated with the change of the chains from a tilted (all-trans) orientation with respect to the bilayer normal to a perpendicular orientation. The pretransition is a lower enthalpy transition than the "main" or gel to liquid-crystalline transition.

**Figure 5**

Schematic representation of the change in bilayer dimensions and lipid conformation on passing between the gel and liquid-crystalline phases.

## LAMELLAR PHASE TRANSITIONS

 $P_{\beta'}$  (GEL STATE) $L_{\alpha}$  (FLUID STATE)

interactions via the introduction of gauche-gauche bends, drastically decreases the  $T_m$  and  $\Delta H$ . As an example, DSPC, an 18-carbon saturated phosphatidylcholine (PC), has a  $T_m$  and a  $\Delta H$  of 54.9 °C and 10.7 kcal/mole, respectively, while DOPC, a monounsaturated 18-carbon analogue has corresponding values of -22 °C and 7.6 kcal/mole.

The morphology of the lipid (SUVs, LUVs or MLVs) has also been found to affect the thermal properties. For example, multilamellar vesicles give rise to transitions that are sharper and elevated by  $\approx 5$  degrees relative to SUVs due to the disorder in the latter, which is thought to arise from the packing constraints imposed by the small radius of curvature (81,82). Clearly evaluation of the parameters and characteristics associated with the gel to liquid-crystalline phase transition can provide abundant information concerning the molecular organization of the lipids in the bilayer and how it is affected by modifications of the lipid structure. In this study we were particularly interested in the effect on the thermal properties of the addition of the sulfhydryl groups in the monomeric lipids compared to nonpolymerizable phosphatidylcholine analogues, and the effect of subsequent polymerization. Furthermore, the position of the polymerizable group should have a marked effect not only on the temperature of the phase transition, but on its presence or absence as well. One might expect to observe a phase transition for the  $\alpha$ -THIOLS whereas polymerization of the  $\omega$ -THIOLS could conceivably result in restricted chain motion such that no transition is observed.

The wealth of structural information one can derive from analysis of the thermal properties is not the only motivation for these studies. Knowledge of the position of the temperature of the phase transition is critical for encapsulation technologies since it is well known that release of entrapped material as well as vulnerability to lipoproteins, and lipases is maximal at the phase transition (34). This is thought to arise from the fact

that at the transition temperature, 50% of the lipids are in the gel state and 50% are liquid-crystalline. It is believed that the boundaries between the two domains give rise to poorly organized regions of the bilayer that are highly susceptible to disruption and through which rapid leakage can occur. Consequently, it is important to know if the position of the transition coincides with temperatures the liposomes will be subject to for particular applications (i.e. room temperature and 37°C for *in vivo* use).

Several methods were used to study the thermal properties of the polymerizable lipids. While many provide similar data (i.e.  $T_m$ ), all contain complimentary information. The most straightforward way to examine the thermal transitions is by differential scanning calorimetry (DSC), a technique that monitors the excess heat absorbed by a system as it goes through a transition. The information one can derive from such studies includes the position and breadth of the phase transition, the enthalpy, and the cooperativity, all of which are useful in understanding the structure and organization of membranes, polymeric or not. Fluorescence polarization as a function of temperature is also a common method for determining the phase transition temperature (82). In addition, steady-state polarization of fluorescent probes (i.e. diphenylhexatriene (DPH)) embedded in the bilayer can be used to examine the "fluidity" and fluorescence order parameters of membranes as a function of composition, and to detect membrane perturbations induced by the addition of other components such as cholesterol (83).

Chapter IV. Having established some of the *general* properties of the polymerizable lipids shown in Figure 2, one can begin to ask more direct questions concerning the *molecular* rather than *bulk* properties of these lipids. In Chapter IV, Raman and FT-IR were utilized to examine the chain packing and conformation of the acyl chains in monomeric and polymeric  $\alpha$ - and  $\omega$ -THIOLS compared to model membranes. The information derived from these studies (are the lipids ordered or disordered and what

happens on polymerization?) are then evaluated in light of the investigations of Chapter II concerning the thermal and release properties of these lipids.

Chapter V and VI. In Chapters V and VI, the dynamic properties of the polymeric membranes are studied. Chapter V describes spin-lattice relaxation and linewidth studies by  $^{13}\text{C}$  and  $^1\text{H}$  NMR, which are intended primarily to (i) examine the effect of polymerization on the motions of the acyl chains and the regions of the membrane surrounding the polymerizable moiety and (ii) to examine if the polymeric lipids possess a mobility gradient from the glycerol backbone to the acyl chains. The latter is a characteristic feature of most natural and synthetic biomembranes and may be largely correlated to the gross morphological features of the polymerized lipid aggregates investigated in Chapter II.

In Chapter VI, the dynamics (and conformation) of the headgroup are examined. Our particular interest in the properties of the headgroup stem from the fact that it is at the membrane interface where interactions with proteins, cell surfaces and other biological materials initially take place. Furthermore, from a more fundamental viewpoint, we were curious as to the effect of polymerization, on the motions and conformation of the headgroup. Are we just modifying the hydrocarbon interior or are remote portions of the membrane affected? A number of studies have suggested that the spin-lattice relaxation of the headgroup phosphate moiety can be accounted for by a single correlation time on the order of nanoseconds for reorientation about the P-O bond adjacent to the glycerol backbone (84). Based on these results, one might not expect a major effect on the mobility of the choline headgroup due to polymerization at either the interface (as in the  $\alpha$ -THIOLS) or in a distant position such as at the chain terminus in the  $\omega$ -THIOLS. In Chapter VI, these questions are addressed by a variety of experiments including:

(i) The temperature dependence of the  $^{31}\text{P}$  spin-lattice relaxation time to find the minimum in the  $T_1$  profile. This enables a direct determination of the effective rotational correlation time ( $\tau_c$ ) of the headgroup because at the minimum,  $\tau_c$  is on the order of the inverse of the larmor frequency.

(ii) Evaluation of  $^{31}\text{P}$  NMR powder spectra of unsonicated dispersions of the polymerized lipids versus nonpolymerizable analogues to examine conformation and mobility at various temperatures.

(iii) The cross polarization time ( $\tau_{\text{PH}}$ ) for transfer of magnetization from vicinal protons to the phosphorous of the headgroup. As in (i),  $\tau_{\text{PH}}$  reflects the dynamics of the headgroup. Thus we can examine differences in the cross polarization rates for polymeric versus monomeric phospholipids.

Chapter VII. In Chapter VII is a description of the *in vivo* experiments which were carried out to examine the potential of these lipid systems as drug delivery vehicles in laboratory animals. In particular, Perturbed Angular Correlation Spectroscopy (PAC) was used to examine the blood clearance rate, the biodistribution and the intracellular degradation rates of intravenously injected polymerized versus nonpolymerized SUVs. The motivation behind these experiments was to see if polymerization might extend the lifetime of liposomes in the blood and thereby enhance passive targeting of liposomes to extravascular tissues other than the liver and spleen. In addition, polymerized multilamellar vesicles were also prepared to investigate their utility as slow release systems since polymerization would be expected to slow the rate degradation and release of entrapped solutes relative to nonpolymerizable analogues. The latter experiments therefore included investigations of the tissue distributions, clearance rates and most importantly, intracellular degradation rates of polymeric and nonpolymeric

MLVs. The results of these experiments are discussed in light of what has been learned from the investigations described in chapters II through VI.

Chapter VIII. The work in Chapters II through VII was exciting and extremely educational. Chapter VIII describes the painful synthesis and polymerization of the compounds under study.

### REFERENCES

1. Ellens, H., Bentz, J. and Szoka, F.C. (1986) *Biochemistry* **25**, 4141.
2. Ellens, H., Bentz, J. and Szoka, F.C. *Biochemistry* **25**, 285.
3. Siegel, D.P. (1986) *Biophys. J.* **49**, 1171-1183.
4. Novick, S.L. and Hoekstra, D. (1988) *Proc. Natl. Acad. Sci. U.S.A.* **85**, 7433-7437.
5. Yeagle, P.L., Selinsky, B.S. and Albert, A. (1984) *Biophys. J.* **45**, 1085-1089.
6. Batenburg, A.M., Demel, R.A., Verkleij, A.J. and de Kruiff, B. (1988) *Biochemistry* **27**, 5678-5685.
7. Finkelstein, M.C. and Weissmann in : *Liposomes from Physical Structure to Therapeutic Applications* ; Knight, C.G. (Ed.); Elsevier: North Holland Biomedical Press, 1981; 443.
8. Connor, J., and Huang, L. (1986) *Cancer Research* **46**, 3431-3435
9. Fendler, J.H. in: *Membrane Mimetic Chemistry* ; Wiley-Interscience: New York, 1982.
10. Pabst, R., Ringsdorf, H., Koch, H. and Dose, K. (1983) *FEBS Lett.* **154**, 5-9.
11. Fendler, J.H. and Tundo, P. (1984) *Acc. Chem. Res.* **17**, 3-8.

12. Ishiswatari, T. and Fendler, J.H. (1984) *J. Am. Chem. Soc.* **106**, 1908-1912.
13. Fendler, J.H. and Hinze, W.L. (1981) *J. Am. Chem. Soc.* **103**, 5439-5447.
14. Zhao, X.K., Boral, S., Rolandi, R. and Fendler, J. (1988) *J. Am. Chem. Soc.* **110**, 1012-1024.
15. Tricot, Y. and Fendler, J.H. (1984) *J. Am. Chem. Soc.* **106**, 2475-2476.
16. Hayward, J.A., Levine, D.M., Newfeld, L., Simon, S.r., Johnston, D.S. and Chapman, D. (1985) *FEBS Lett.* **187**, 261-266.
17. Djordjevich, L. and Miller, I.F. (1980) *Exp. Hematol.* **8**, 584-592.
18. Gaber, B.P., Yager, P., Sheridan, J.P. and Cgang, E.L. (1983) *FEBS Lett.* **153**, 285-288.
19. Gregoriadis, G. in: *Drug Carriers in Biology and Medicine* ; Academic Press: London, 1979.
20. Kimelberg, H.K. and Mayhew, E.G. in: *CRC Crit. Rev. Toxicol.* 1978, 25-79.
21. Juliano, R.L., and Layton, D. in : *Drug Delivery Systems: Characteristics and Biomedical Applications* ; Juliano, R. (Ed.); New York: Oxford University Press, 1980; 189-236.
22. Gregoriadis, G., Senior, J. and Trouet, A. *Targeting of Drugs* ; Plenum Press: New York, 1982.
23. Juliano, R.L. in : *Liposomes from Physical Structure to Therapeutic Applications* ; Knight, C.G. (Ed.); Elsevier: North Holland Biomedical Press, 1981; 391.
24. Baldeschwieler, J.D., (19 ) *Ann. N.Y. Acad. Sci.* **446**, 349-367.
25. Connor, J. and Huang, L. (1986) *Cancer Res.* **46**, 3431-3435.
26. Huang, A., Kennel, S.J., and Huang, L. (1983) *J. Biol. Chem.* **258**, 14034-14040.

27. Szoka, F.C. and Mayhew, E. (1983) *Biochem. Biophys. Res. Comm.* **110**, 140-146.
28. Leserman, L.D., Machy, P. and Barbet, J. in: *Liposome Technology* ; Gregoriadis, G. (Ed.); Boca Raton: CRC Press, 1984; Vol. III, 29-40.
29. Huang, L., Huang, A. and Kennel S. in: *Liposome Technology* ; Gregoriadis, G. (Ed.); Boca Raton: CRC Press, 1984; Vol. III, 51-62.
30. Ponpipom, M.M., Shen, T.Y., Baldeschwieler, J.D. and Wu, P. in: *Liposome Technology* ; Gregoriadis, G. (Ed.); Boca Raton: CRC Press, 1984; Vol. III, 95-116.
31. Proffitt, R.T., Williams, L.E., Presant, L.A., Tin, G.W., Uliana, J.A., Gamble, R.C. and Baldeschwieler, J.D. (1983) *Science* **29**, 502-505.
32. Derksen, J.T.P., Baldeschwieler, J.D. and Scherphof, G.L. (1989) *Proc. Natl. Acad. Sci. U.S.A.*, accepted for publication.
33. Deshmukh, D.S., Bear, W.D., Wisniewski, H.M. and Brockerhoff, H. (1978) *Biochim. Biophys. Acta.* **82**, 328-334.
34. Scherphof, G., Damen, J. and Wilschut, J. in: *Liposome Technology* ; Gregoriadis, G. (Ed.); Boca Raton: CRC Press, 1984; Vol. III, 205-224.
35. Gupta, C.M. and Bali, A. (1981) *Biochim. Biophys. Acta.* **663**, 506-515.
36. Agarwal, K., Bali, A. and Gupta, C.M. (1986) *Biochim. Biophys. Acta.* **883**, 468-475.
37. Bali, A., Dhawan, S. and Gupta, C.M. (1983) *FEBS Lett.* **153**, 373-377.
38. Deshmukh, D.S., Bear, W.D. Wisniewski, H.M. and Brockerhoff, H. (1978) *Biochem. Biophys. Res. Comm.* **82**, 328,334.
39. Akimoto, A., Klaus, D. Gros, L., Ringsdorf, H. and Schupp, H. (1981) *Angew. Chem. Int. Ed. Engl.* **20**, 90-91.
40. Gros, L., Ringsdorf, H. and Schupp, H. (1981) *Angew. Chem. Int. Ed. Engl.* **20**, 305-325.

41. Büschl, R., Folda, T. and Ringsdorf, H. (1984) *Makromol. Chem. Suppl.* **6**, 245-258.
42. Wagner, N., Dose, K., Koch, H. and Ringsdorf, H. (1981) *FEBS Lett.* **132**, 313-318.
43. Dorn, K., Klingbiel, R.T. Specht, D.P. Tyminski, P.N., Ringsdorf, H. and O'Brien, D.F. (1984) *J. Am. Chem. Soc.* **106**, 1627-1633.
44. Ringsdorf, H., Schlarb, B., Tyminski, P.N. and O'Brien, D.F. (1988) *Macromolecules* **21**, 671-677.
45. Kippenberg, D., Rosenquist, K., Odberg, L., Tundo, P. and Fendler, J. (1983) *J. Am. Chem. Soc.* **105**, 1129-1135.
46. Weber, B., Dodrer, N. and Regen, S. (1987) *J. Am. Chem. Soc.* **109**, 4419,4421.
47. Sodownik, A., Stefely, J. and Regen, S.L. (1986) *J. Am. Chem. Soc.* **108**, 7789-7791.
48. Regen, S.L. (1985) *Ann. N.Y. Acad. Sci.* **446**, 296-307.
49. Samuel, N.K.P., Singh, M., Yamaguchi, K. and Regen, S.L. (1985) *J. Am. Chem. Soc.* **107**, 42-47.
50. Regen, S., Singh, A., Oehme, G. and Singh, M. (1981) *Biochem. Biophys. Res. Comm.* **101**, 131-136.
51. Regen, S.L., Yamaguchi, K., Samuel, N.K.P., and Singh, M. (1983) *J. Am. Chem. Soc.* **105**, 6354.
52. Regen, S.L., Singh, A., Oehme, G. and Singh, M. (1982) *J. Am. Chem. Soc.* **104**, 791-795.
53. Regen, S. L., Czech, B. and Singh, A. (1980) *J. Am. Chem. Soc.* **102**, 6638-6640.
54. Akimoto, A., Dorn, K., Gros, L. Ringsdorf, H. and Schupp, H. (1981) *Angew. Chem. Int. Ed. Engl.* **20**, 90-91.

55. Hub, H., Hupfer, B., Koch, H. and Ringsdorf, H. (1980) *Angew. Chem. Int. Ed. Engl.* **19**, 938-940.
56. Hupfer, B., Ringsdorf, H. and Schupp, H. (1983) *Chem. Phys. Lipids* **33**, 355-374.
57. O'Brien, D.F., Whitesides, T., Klingbiel, R. (1981) *J. Polymer Sci.: Polymer Letters Ed.* **19**, 95-101.
58. O'Brien, D.F., Klingbiel, R.T., Specht, D.P. and Tyminski, P.N. (1985) *Ann. N.Y. Acad. Sci.* **446**, 282-295.
59. Lopez, E., O'Brien, D.F., Whitesides, T.H. (1982) *Biochim. Biophys. Acta.* **693**, 437-443.
60. Elbert, R., Laschewsky, A. and Ringsdorf, H. (1985) *J. Am. Chem. Soc.* **107**, 4134-4141.
61. Neumann, R. and Ringsdorf, H. (1986) *J. Am. Chem. Soc.* **108**, 487-490.
62. Laschewsky, A., Ringsdorf, H and Sneider, J. (1986) *Die Angewandte Makromolekulare Chemie* **145/146**, 1-17.
63. Szoka, F. and Papahadjopoulos, D. (1980) *Ann. Rev. Biophys. and Bioeng.* **9**, 467-508.
64. Tausk, R.J.M., Kormiggett, J., Oudshoorn, C. and Overbeek, J. (1974) *Biophys. Chem.* **1**, 175-183.
65. Tausk, R.J.M., Oudshoorn, C. and Overbeek, J. (1974) *Biophys Chem.* **2**, 53-63.
66. Browning, J. in : in : *Liposomes from Physical Structure to Therapeutic Applications* ; Knight, C.G. (Ed.); Elsevier: North Holland Biomedical Press, 1981; 189.
67. Burns, R.A. and Roberts, M.F. (1980) *Biochemistry* **19**, 3106-3113.
68. Büschl, R., Folda, T. and Ringsdorf, H. (1984) *Makromol. Chem., Suppl.* **6**, 245-258.

69. Israelachvilli, J.N., Marcelja, S. and Horn, R.G. (1980) *Q. Rev. Biophys.* **13**, 121-200
70. Israelachvilli, J.N., Mitchell, J. and Ninham, B.W. (197) *Biochim. Biophys. Acta.* **470**, 185-201.
71. Mitchell, J. and Ninham, B.W. (1981) *J. Chem. Soc., Faraday Trans. 2* **77**, 601-629.
72. Mayer, L.D., Hope, M.J., and Cullis, P.R. (1986) *Biochim. Biophys. Acta.* **858**, 161-168.
73. Szoka, F. and Papahadjopoulos, D. (1978) *Proc. Natl. Acad. Sci. U.S.A.* **75**, 4194-4198.
74. Batzri, S. and Korn, E.D. (1973) *Biochim. Biophys. Acta.* **298**, 1015-1019.
75. Brunner, J., Skrabol, P. and Hauser, H. (1976) *Biochim. Biophys. Acta.* **455**, 322-331.
76. Gabriel, N.E. and Roberts, M.F. (1984) *Biochemistry* **23**, 4011-4015.
77. Gabriel, N.E. and Roberts, M.F. (1986) *Biochemistry* **25**, 2812-2821.
78. Seelig, J. (1978) *Biochim. Biophys. Acta.* **515**, 105-140.
79. Cullis, P.R. and De Kruijff, B. (1978) *Biochim. Biophys. Acta.* **513**, 31-42.
80. Seelig, J. and Seelig, A. (1980) *Quat. Rev. Biophysics* **13**, 19-61.
81. Mabrey-Gaud, S. in : in : *Liposomes from Physical Structure to Therapeutic Applications* ; Knight, C.G. (Ed.); Elsevier: North Holland Biomedical Press, 1981; 105.
82. Suurkuusk, J., Lentz, B.R., Barenholz, Y., Biltonen, R.L., and Thompson, T. (1976) *Biochemistry* **15**, 1393-1401.
83. Van Blitterswijk, W.J., Van Hoeven, R.P., and Van der Meer, B.W. (1981) *Biochim. Biophys. Acta.* **644**, 323-332.

84. Milbourn, M.P. and Jeffrey, K.R. (1987) *Biophys. J.* **52** , 791-799.

---

---

## Chapter II

---

---

### *Morphological Properties of Aqueous Dispersions of Disulfide Polymerized Phosphatidylcholines*

---

#### **INTRODUCTION**

---

Attempts to stabilize synthetic phospholipid membranes via polymerization has resulted in a tremendous library of synthetic polymerizable lipids (1-12). Some of these include methacryl, diacetylene, butadiene and vinyl-based lipids, polymerizable in the acyl chain. Typical structures were shown in Figure 1 (Chapter I). In most reported cases, polymerization of the monomeric liposomes proceeded with retention of the original lipid morphology. With chain-terminating polymerizable groups such as in Figure 1A (Chapter 1), this is quite surprising since the resulting structure would seem to defy an elementary feature of basic bilayers or micelles that have the bilayer midplane as the most mobile portion of the membrane. Despite retention of the bilayer structure, however, imposition of the polymerizable moieties in the hydrocarbon region modifies the membrane interior to some extent as has been shown by reduction or loss of the phase transition and restricted motion of the chains (13-15). For some

applications this may be advantageous. For example, it is known that leakage of entrapped materials and susceptibility to lipases and lipoproteins is maximal at the phase transition and generally greater for fluid versus well-packed crystalline bilayers (16-20). Thus for *in vivo* use, an immobilized hydrocarbon region might be desirable. On the other hand, for reconstitution of proteins, a fluid bilayer interior may be critical to the proper functioning of the protein.

To achieve the benefits of polymerization without compromising rudimentary aspects of conventional bilayers, lipids have been introduced with the polymerizable moiety in the headgroup to allow decoupling of the polymerizable group from the hydrocarbon chain (Figure 1D, Chapter I). For some lipids containing methacryl headgroups separated from the glycerol backbone via ethylene oxide spacers or with amino acid headgroups, this was sufficiently successful such that liposomes could be prepared from *prepolymerized lipids* rather than by the usual route of polymerizing preformed vesicles (21-22).

Our interest in biodegradable phospholipids for *in vivo* applications has prompted us to concentrate on the thiol-containing lipids originally synthesized by Regen et al. (Figure 2, Chapter I) (23-24). These lipids, which have the polymerizable moiety either at the chain terminus ( $\omega$ -THIOLS) or adjacent to the carbonyl ( $\alpha$ -THIOL) are useful for further examinations of the effect of the position of the polymerizable group on the morphology and other membrane physical properties. In the case of the  $\omega$ -THIOLS, polymerization via oxidative disulfide formation should rigidify the bilayer interior (normally the most fluid part of the membrane) as do chain-terminating methacrylates. Thus, loss of the phase transition and immobilization of the chains might be anticipated. Furthermore, polymerization may occur both within a given leaflet as well as across the two leaflets of a bilayer. In the case of the  $\alpha$ -THIOLS, the polymerizable moiety is near the interfacial region, which in conventional bilayers is the most rigid portion (25).

Therefore the motions of the chains and headgroup may be relatively unaffected on disulfide formation. In contrast to the  $\omega$ -THIOLS, polymerization of these lipids is restricted to intra-leaflet coupling. An illustration of what might be envisioned for polymerized bilayers and micelles was shown in Figure 3 of Chapter I.

The structure of these lipids is conducive to modification of the chain length and we have therefore synthesized a reasonably sized homologous series for both types. This should allow a systematic study of the effect of both chain length and position of the polymerizable group on the properties of the disulfide-polymerized membranes. In this chapter, we extend (and reevaluate) the initial investigations by Regen et al. on the morphological behavior of these thiol based phospholipids. Questions we wished to address in this study include:

(i) Can we form liposomes from intermediate and long chain lipids and are the morphologies of the unpolymerized aggregates retained upon polymerization? In the case of the  $\omega$ -THIOLS, we can test the importance of chain mobility at the bilayer midplane on the ability of polymeric lipids to maintain closed bilayer structures.

(ii) Are micelles formed from short chain lipids in analogy to nonpolymerizable phosphatidylcholines with  $N = 6-8$ ? These types of structures may be of some utility for solubilization of hydrophobic materials within very small matrices or for reactivity control where interfacial activation is required but not compartmentalization (i.e. as for phospholipase activity (26)).

(iii) Since the  $\alpha$ -THIOLS have the polymerizable group in the region of the membrane that is motionally restricted even in nonpolymerized bilayers, is their sufficient chain mobility such that liposomes may be formed from pre-polymerized lipids?

(iv) What is the effect of "dilution" of the polymerizable group on the membrane morphology? For these studies, dimer-forming mixed-chain lipids with the polymerizable moiety only in the sn-2 chain and a saturated fatty acid in the sn-1 chain were synthesized. In addition, mixtures of the polymerizable phospholipids and cholesterol were prepared and polymerized with the expectation that smaller oligomers would be formed in such mixtures than in bilayers of the polymerizable lipids alone.

A variety of standard techniques have been used to evaluate the morphology of the aggregates formed on dispersion of these lipids in water. These include electron microscopy, encapsulation experiments, gel permeation chromatography and dynamic light scattering. In addition,  $^1\text{H}$  and  $^{31}\text{P}$  NMR are utilized because the line shapes and widths are sensitive to the aggregate size and motions of the lipid components and therefore may be diagnostic of the presence of micellar, lamellar, and hexagonal phase structures or useful in assessing changes in the morphology of these structures with temperature, polymerization, or the addition of other components (27-31).

## MATERIALS and METHODS

### Materials.

The synthesis of the thiol-containing liposomes is as described in Chapter VIII. L- $\alpha$ -dipalmitoylphosphatidylcholine (DPPC), dioleoylphosphatidylcholine (DOPC), and Dioctanoylphosphatidylcholine (D8PC) were purchased from Avanti Polar Lipids. Cholesterol (>99% purity) was obtained from Sigma.  $^3\text{H}$ -uridine was obtained from Amersham. Carboxyfluorescein was purchased from Eastman Kodak and purified by the method outlined in reference 32. Embedding reagents for thin section electron microscopy were purchased from Bioscience. All other reagents were of analytical grade and used without purification.

### Preparation of Liposomes.

Sonicated vesicles were routinely prepared by hydration of the lipids in buffer (10 mM Tris or HEPES, 135 mM NaCl, pH 7.4 or 10m M Borate, 135 mM NaCl, pH 8.5) above the phase transition. For monomeric lipids, the buffer was flushed with argon. This was followed by bath sonication with a Laboratory Supplies bath sonicator or Heat Systems 350W probe sonicator (depending on lipid type). During sonication, samples were placed under nitrogen and in a large room-temperature water bath to avoid excessive heating. Titanium particles and large liposomes were removed from the SUVs by centrifugation at 12000 x g for 5 min in an eppendorf centrifuge. Multilamellar vesicles or liposome dispersions were prepared by hydration of the lipids above the phase transition with intermittent vortexing for approximately 30 minutes.

### Polymerization of Liposomes.

*Method A.* Polymerization of the thiol-containing phospholipid was carried out by the protocol outlined by Regen et al. with small modifications of temperature and concentration (23,24). Briefly, 5 mg/ml of samples were prepared by dispersion or sonication in borate buffer containing 20 equivalents of H<sub>2</sub>O<sub>2</sub>, pH 8.5. The samples were allowed to polymerize for 4-8 hours above the phase transition.  $\alpha$ -THIOLS were polymerized 4 hours at 40°C, 50°C and 60°C ( $\alpha$ -16,  $\alpha$ -18 and  $\alpha$ -20, respectively).  $\omega$ -THIOLS were polymerized at 40°C (N=8-10), 45°C (N=11), 55°C (N=15) and 60°C (N=16). Some variations in temperature and length of polymerization have been utilized but are noted in the text. This method of polymerization was used unless mentioned otherwise.

*Method B.* Samples were prepared as dispersions in borate buffer (pH 7.4) containing 20 equivalents of H<sub>2</sub>O<sub>2</sub>. To this was added  $\mu$ liter amounts of a 0.025M Cu<sup>+2</sup>/ $\alpha$ -Phenanthroline solution until a slight pinkish tint was detected indicating the

presence of  $\text{Cu}^{+1}$ (33). The solution was subsequently stirred at room temperature until it was a slight green tint and the pH began to drop, or the sample was thiol-negative as detected with Ellman's reagent. At this point 0.1M EDTA (in 10 mM Tris, pH 7.4) was added to quench the reaction. The samples were dialyzed exhaustively with an Amicon dialysis chamber (YM10 filters), first with 0.1M EDTA to remove copper ions and subsequently with  $\text{H}_2\text{O}$ /MEOH to remove o-phenanthroline. The proton spectra of polymeric  $\omega$ -11 in  $\text{CDCl}_3$ /MEOH appeared similar to that of an  $\text{H}_2\text{O}_2$ -polymerized sample. Samples rehydrated after polymerization by this method seemed to produce smaller aggregate structures than samples prepared by method A, however. This was shown by preliminary gel permeation chromatography using calibrated columns and by  $^1\text{H}$  NMR. Whether this is due to the polymerization or dialysis with organic solvent is not known.

#### Encapsulation of Aqueous Solutes.

For studies involving entrapment of uridine, samples were prepared and polymerized as described above (Method A) except that the borate buffer contained 1 mM uridine spiked with 10  $\mu\text{Ci}$  of  $^3\text{H}$ -uridine per 0.5mls of sample. Control monomeric liposomes were prepared in an analogous fashion with the exception that the hydrating buffer was HEPES (pH 7.4) containing 1 mM uridine and 10  $\mu\text{Ci}$   $^3\text{H}$ -uridine (no  $\text{H}_2\text{O}_2$ ). Following polymerization, samples were dialyzed against an isotonic HEPES buffer for 24 h. The contents of each dialysis bag was then diluted to constant volume and aliquots taken for measurement of associated radioactivity.

Carboxyfluorescein (CF) entrapment was attempted exclusively with prepolymerized liposomes. In general, 2.5 mg of lipid was hydrated with 0.5 ml 50 mM carboxyfluorescein in HEPES buffer. Samples were warmed and intermittently vortexed above the phase transition temperature. For SUVs, hydration was followed by

bath or probe sonication. Unentrapped carboxyfluorescein was removed either by (i) dialysis against an isotonic buffer, (ii) pelleting the lipid 3-5 times from isotonic buffer by centrifugation or (iii) passage over sephadex G-25-50 spin columns (see Chapter VII for details of spin columns). Entrapped carboxyfluorescein was detected by the dequenching of fluorescence upon addition of 10% Triton-X 100. The fluorescence intensity was monitored on an SLM 4000 spectrofluorimeter with excitation and emission wavelengths of 470 and 520 nm, respectively.

### Electron Microscopy.

*Negative Stain.* Samples were prepared by applying a drop of lipid solution to freshly coated glow-discharged carbon grids. After  $\approx 30$  sec, the excess was wiped away with filter paper and the samples allowed to dry 3-5 min. The grids were subsequently stained with 1% uranyl acetate, ammonium molybdate, or phosphotungstic acid for 30-60 s, blotted with filter paper and allowed to dry thoroughly.

*Freeze Fracture.* Freeze fracture electron microscopy was done exclusively with prepolymerized samples. Lipids were hydrated at a concentration of approximately 10 mg/ml in H<sub>2</sub>O above the phase transition for 15-30 minutes. The liposomes were then pelleted by centrifugation. For DPPC, centrifugation at 2000 rpm (swinging bucket rotors, IEC Centra-8 centrifuge) was sufficient to pellet the lipid. For  $\alpha$ -THIOLS, which form smaller liposomes, ultracentrifugation (40000 rpm, SW50 rotors) was necessary. For  $\omega$ -THIOLS, the samples were simply hydrated above the phase transition with a slight excess of H<sub>2</sub>O (i.e. as a paste). In order to prevent ice crystallization, 15-20% ethylene glycol was added to the samples immediately prior to freezing. Approximately 10  $\mu$ ls was then sandwiched between copper "hats" prepared from oxygen-free high conductivity copper. The samples were rapidly frozen in freon and transferred to the sample stage of a Balzers apparatus. The samples were

subsequently cracked, etched and shadowed with platinum and carbon. Additional carbon was applied for extra support as the samples warmed to room temperature. Replicas were separated from copper hats by dipping in DMSO. After thoroughly dissolving away organics and rinsing the replicas by flotation on distilled water, the replicas were transferred to formvar-coated grids.

*Thin Section.* Samples for thin section were polymerized as described above. The lipid ( $\omega$ -16) was spun down into a pellet in 1 ml eppendorf vials (12000 x g) and hydrated with 1% OsO<sub>4</sub> (in isotonic HEPES) for 20 h at 8°C. The OsO<sub>4</sub> supernatant was then removed and the pellet washed in buffer and recentrifuged. 2% freshly prepared aqueous uranyl acetate was added and the pellets allowed to shake for 1 day at room temperature. The uranyl acetate was subsequently removed and the pellets washed with water and recentrifuged. The samples were then dehydrated with a series of ethanol stocks (50,70,80,95 % (x1) and 100% (x4)) for 5 min each. Propylene oxide was added, shaken for 15 min and removed (x2). This was followed by the addition of 50:50 epon /propylene oxide overnight. After replacing the epon/propylene oxide with fresh epon, the samples were left open to the air for several hours and subsequently hardened at 35 °C (overnight), 45 °C (8-12 h) and 60 °C (overnight). The bullets were sectioned with glass knives and stained with 2% uranyl acetate (15 min) followed by lead citrate (15 min).

All samples were visualized and photographed using a Phillips EM 201C transmission electron microscope.

### Light Scattering.

Determination of particle sizes was accomplished via dynamic light scattering using a Malvern 4700 light scattering system equipped with a goniometer, a 128 channel correlator and a 3 W Spectra Physics argon ion laser. 488 nm incident laser light was

used with the detector placed at 90 degrees relative to the incoming beam. Calculations of the particle size were based on the Stokes-Einstein equation using monomodal analysis with the software supplied by Malvern. Measurements are the average of three determinations. For certain very large particles (> 2000 nm), due to the polydispersity of the samples and the sizes outside the range of the instruments, sizes are simply denoted as > 2000 nm.

### NMR

For proton NMR, samples ( $\approx 5$  mg/ml) were hydrated with D<sub>2</sub>O (pH 6.8) or D<sub>2</sub>O/.1M NaCl. In some cases, NaAc was included as an internal standard for integration purposes. Samples for <sup>31</sup>P NMR were prepared in 10 mM Tris buffer containing 0.2mM EDTA. <sup>1</sup>H and <sup>31</sup>P NMR spectra were recorded on a Bruker AM-500 at 500 and 202 MHz, respectively.

For the proton spectra, a 45° excitation pulse ( $\approx 3$   $\mu$ s) and a 2.5 s repetition rate were used. When necessary, the HOD resonance was presaturated. For experiments involving relaxation (Mn<sup>+2</sup>) or shift (Pr<sup>+3</sup>) reagents,  $\mu$ liter amounts of 10mM stocks of MnCl<sub>2</sub> and Pr(NO<sub>3</sub>)<sub>3</sub> were titrated into 0.3-0.5 ml samples. Samples at room temperature were referenced to HOD at 4.63 ppm. At higher temperatures, the position of the choline resonance was assumed to remain constant and set to 3.1 ppm.

Phosphorous spectra were acquired with inverse gated decoupling using a 90° pulse ( $\approx 23$   $\mu$ s) and a 4 s recycle delay. During acquisition, 30-40W of continuous or broad band proton decoupling was employed.

## RESULTS

### Morphology of $\alpha$ -THIOLS.

The preparation conditions, sizes and entrapment characteristics of polymeric and monomeric  $\alpha$ -THIOLS (N = 16-20) are summarized in Table I. Monomeric  $\alpha$ -THIOLS (N= 16-20) formed turbid solutions on dispersion in buffer and opalescent small unilamellar vesicles after bath (N=16) or probe (N=18,20) sonication as indicated by their sizes and ability to encapsulate aqueous solutes. Consistent with reports by Regen et al. for  $\alpha$ -16, the sizes of all three vesicle types was retained after oxidation of the thiol groups. This is shown by the similarity in the chromatographic profiles (Figure 1) and electron micrographs (Figure 2) of monomeric and polymeric  $\alpha$ -16 SUVs as well as the negligible differences in the light scattering data for  $\alpha$ -20 SUVs before and after polymerization (Table I). The electron micrographs in Figure 3 of monomeric  $\alpha$ -10 SUVs show that even very short chain lipids can form liposomes.

*Liposomes prepared from prepolymerized  $\alpha$ -THIOLS.* Ringsdorf et al. have shown that if one can minimize the interference of polymerization with the ordering of the lipid chains, in some cases it may be possible to produce liposomes from *prepolymerized* lipids (21,22). The results of the experiments described above and the fact that the phase transitions of the  $\alpha$ -THIOLS are only slightly shifted and broadened upon polymerization (shown in Chapter III), suggested minimal perturbation of the chain packing. Therefore, attempts were made to prepare liposomes from  $\alpha$ -THIOLS which had first been oxidized as multilamellar dispersions and lyophilized. From aqueous dispersions of the lyophilized powders liposomes were indeed produced. Interestingly, the unsonicated dispersions were routinely more optically clear and obviously smaller (according to light scattering data) than the dimensions of monomeric  $\alpha$ -THIOLS and particularly compared to nonpolymerizable phosphatidylcholine dispersions (Table

**Table 1**

Summary of the sizes and entrapment characteristics of monomeric and polymeric  $\alpha$ -THIOLS . The polymerized  $\alpha$ -20 SUVs were sonicated prior to polymerization. Polymerized MLVs were samples that had been polymerized, lyophilized and redispersed.

Lipid	Preparation	Size (nm)	Entrapment of CF
$\alpha$ -20 (M) SUV's	Before Polymerization	$71.5 \pm 2.0$	+
$\alpha$ -20 (P) SUV's	After Polymerization	$81.4 \pm 1.0$	+
$\alpha$ -20 (M) MLV's <sup>a</sup>		$838 \pm 15$	+
$\alpha$ -20 (P) MLV's <sup>a</sup>	Prepolymerized	$363 \pm 3$	+
$\alpha$ -18 (P) MLV's <sup>a</sup>	Prepolymerized	$249 \pm 5$	+
$\alpha$ -16 (P) MLV's <sup>a</sup>	Prepolymerized	$468 \pm 17$	+
DPPC MLV's <sup>a</sup>		$>2000$	+

<sup>a</sup>Samples were 1.25 mg/ml in .15 NaCl

**Figure 1**

Elution profile of  $\alpha$ -16 SUVs on a sepharose 4BCL column: **A.** before polymerization; **B.** after polymerization. Peaks below 30 ml correspond to that of the lipid while peaks above 30 ml are from the buffer. The separation was carried out on a 30 x 1.2 cm Sepharose 4BCL column to which was added 0.5-1.0 mls of a liposome solution. The presence of lipid in the column was monitored using a UV detector ( $\lambda$ -280 nm).

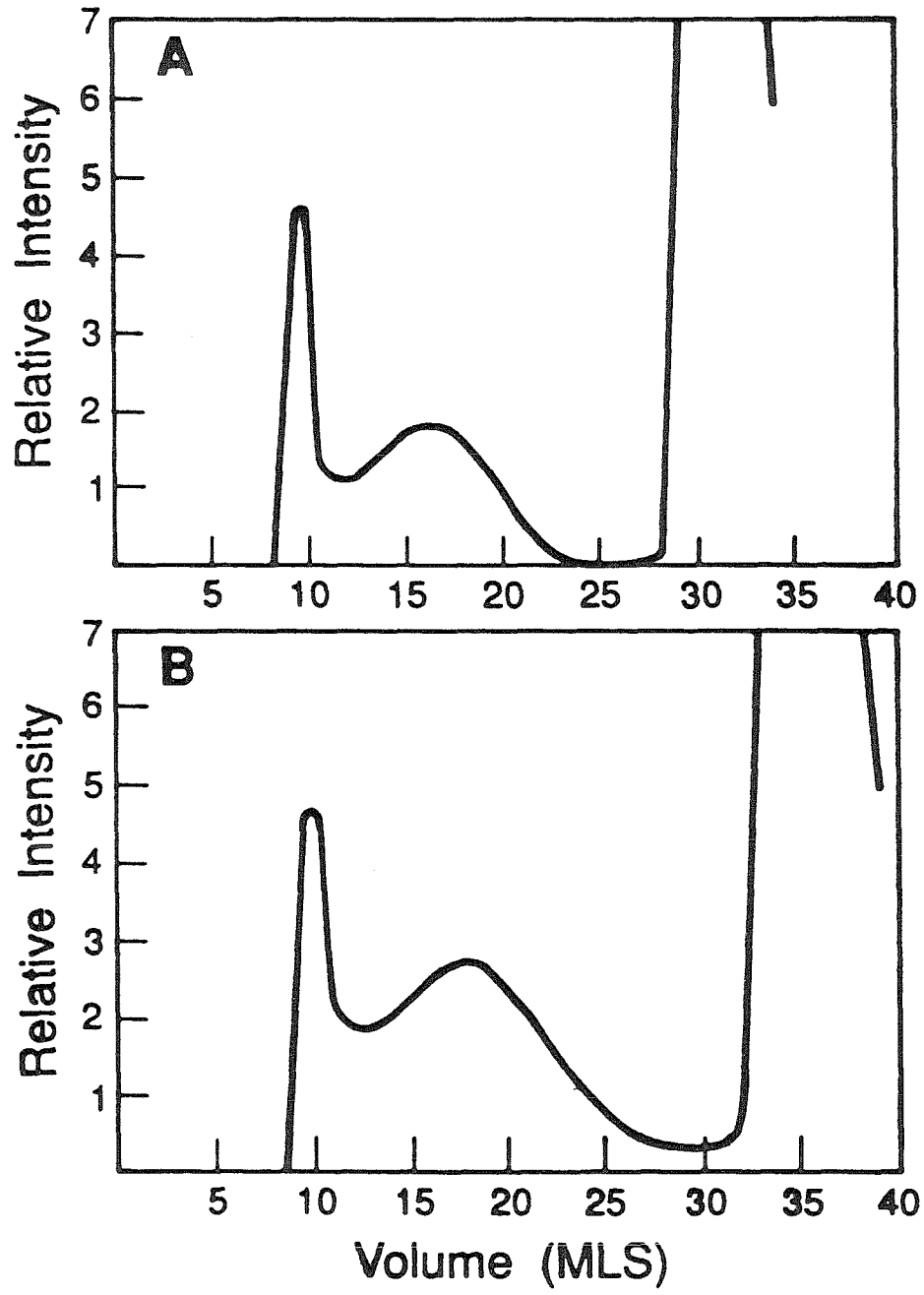
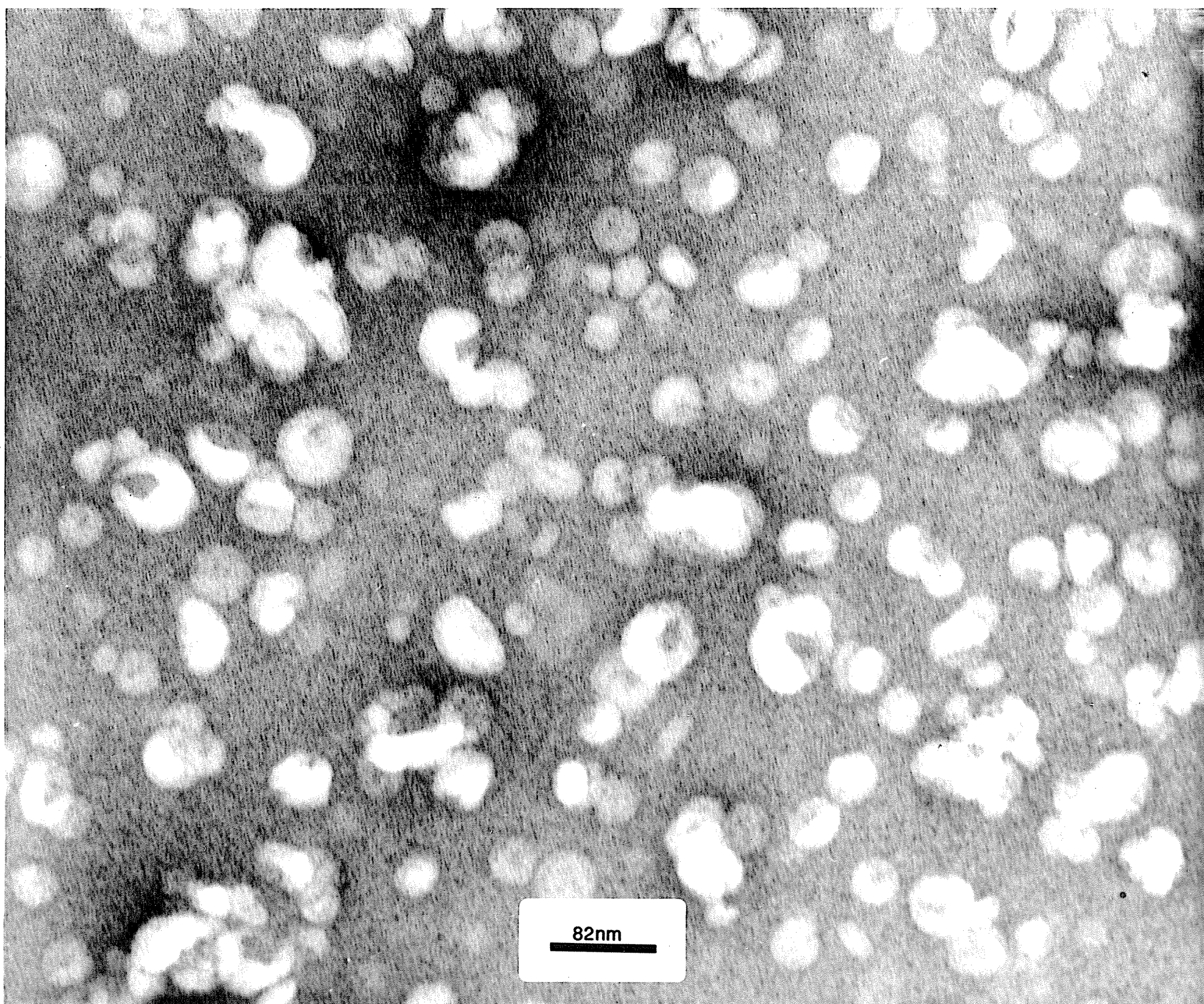
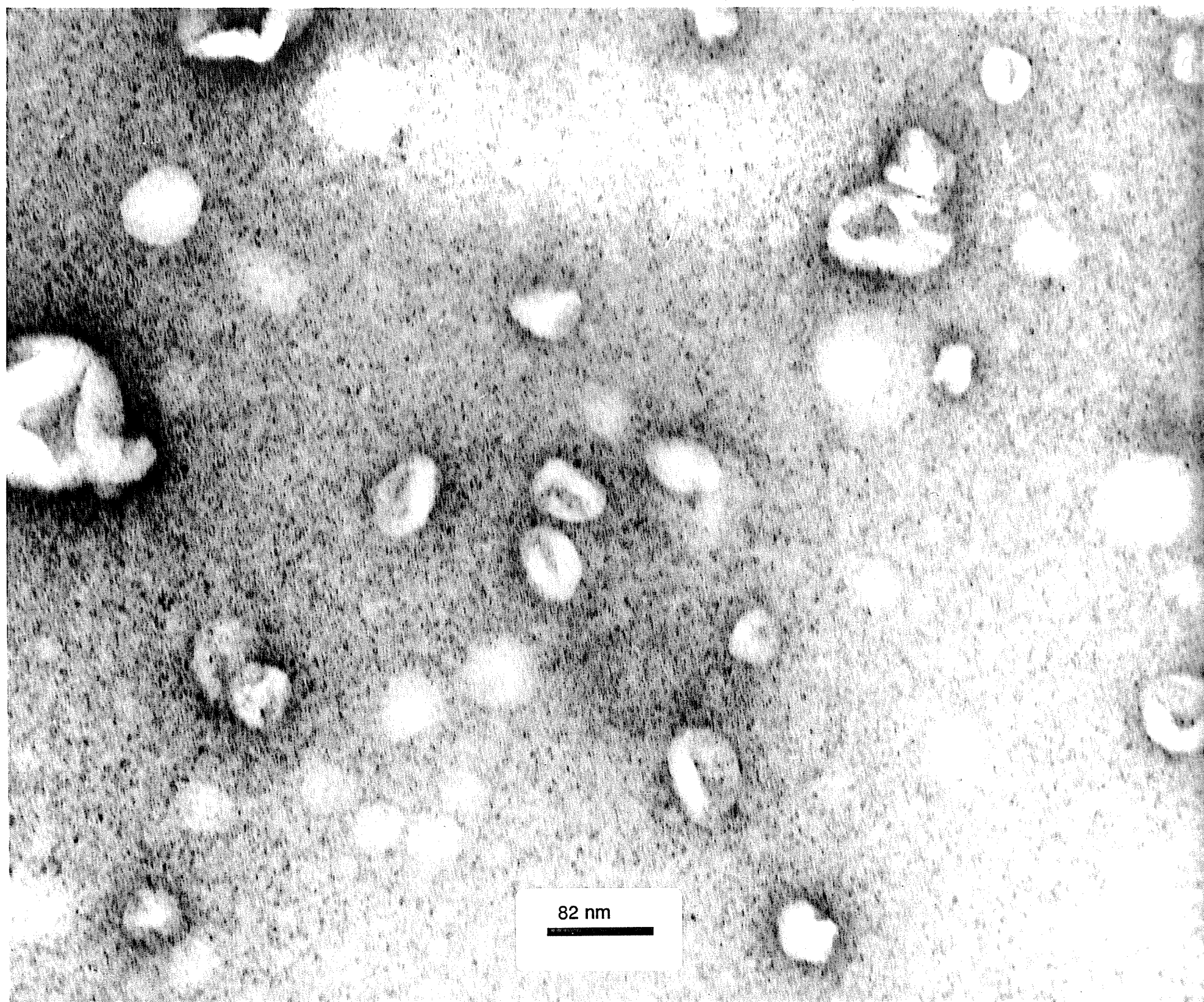


**Figure 2**

Negative stain electron micrographs of: **A.** Unpolymerized  $\alpha$ -16 and **B.** Polymerized  $\alpha$ -16.

**A**



**B**

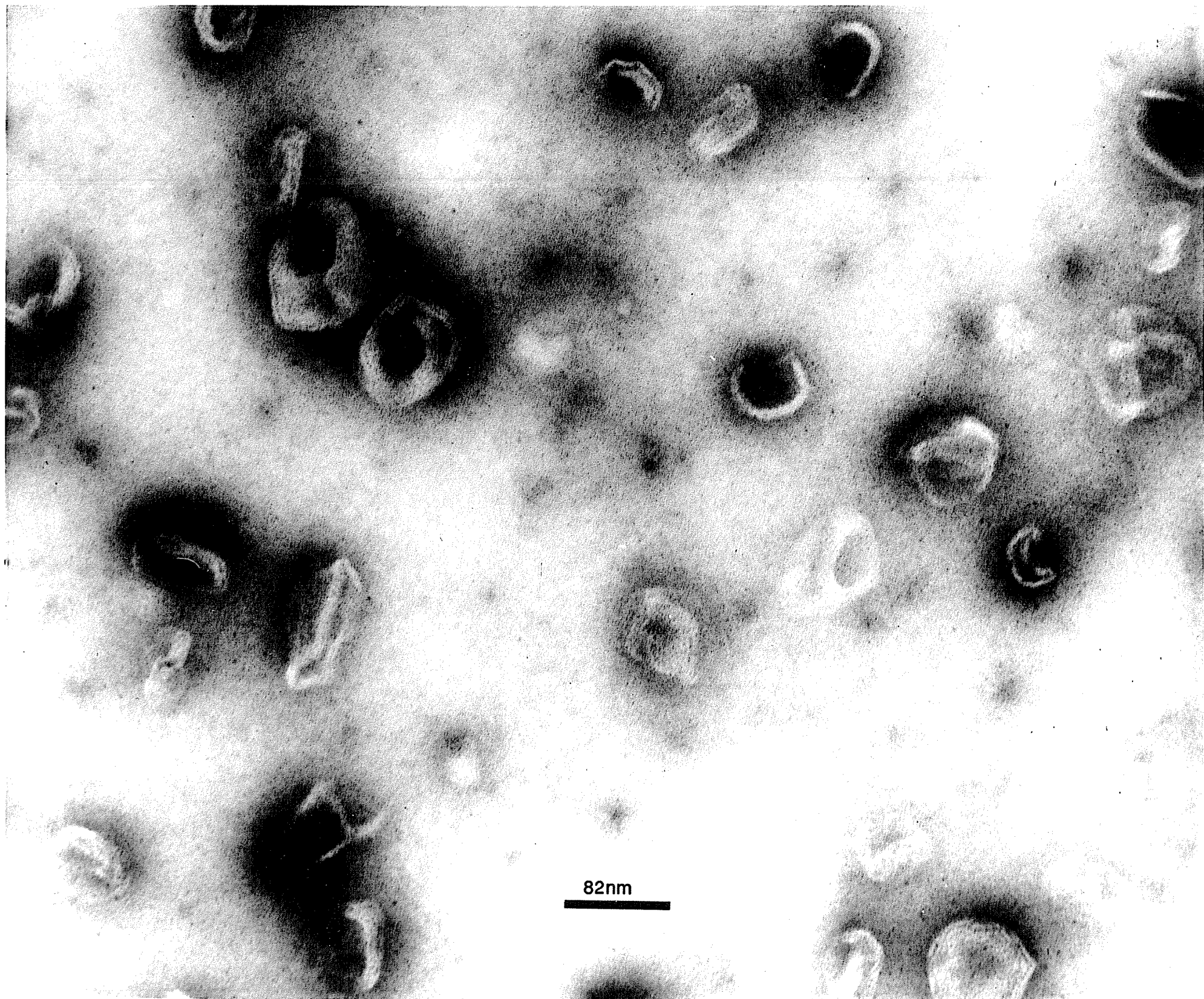
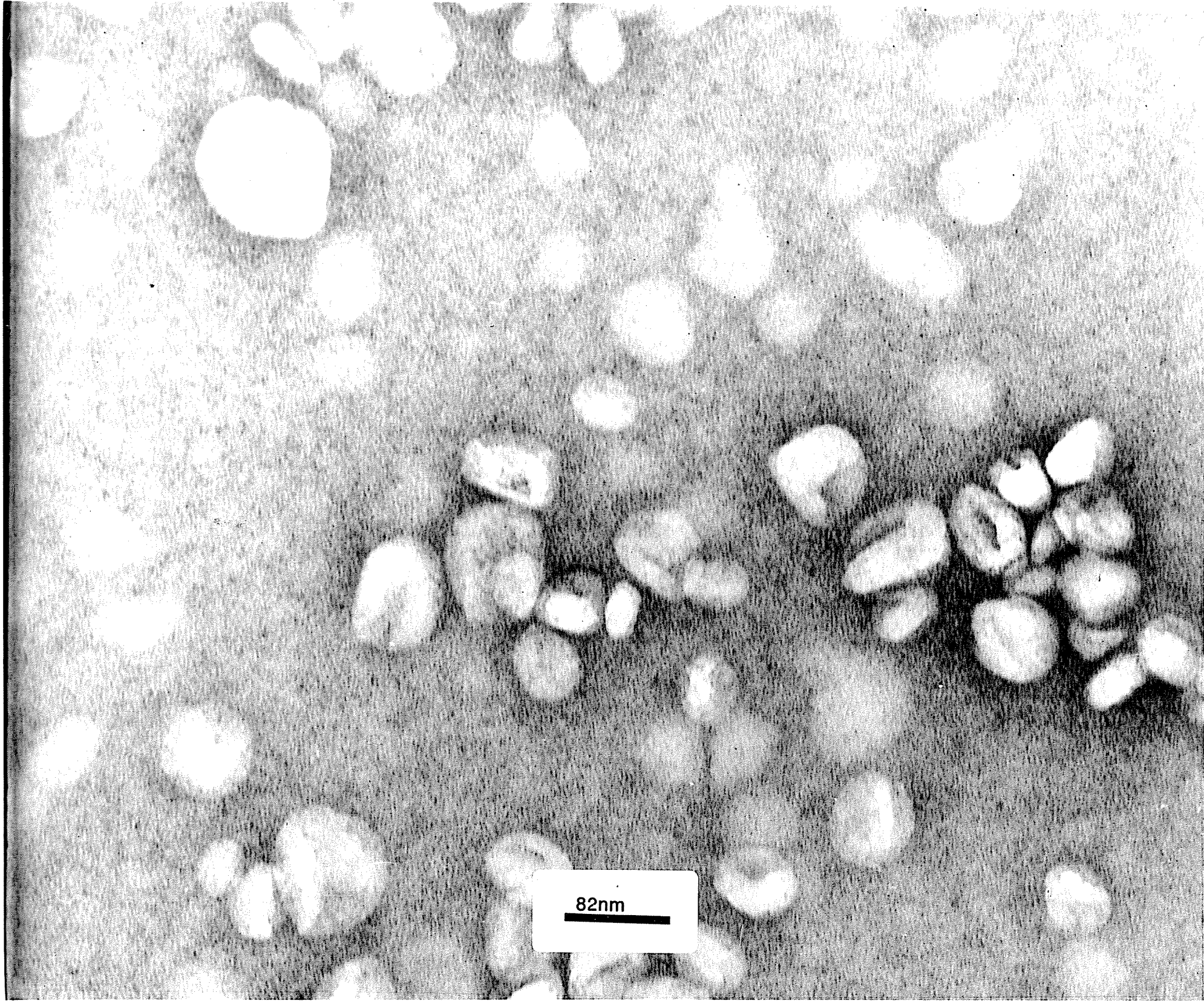
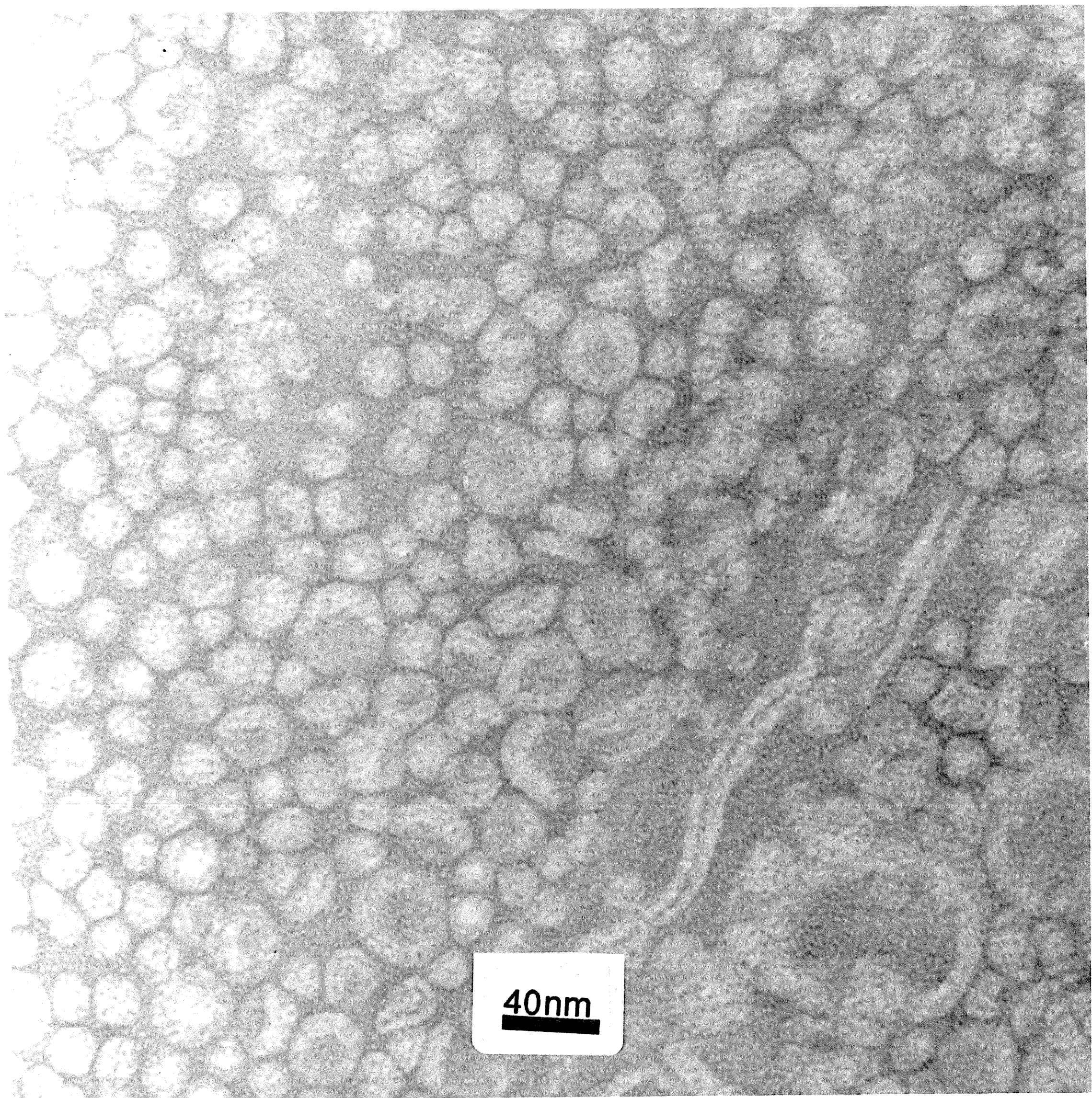


**Figure 3**

Negative stain electron micrographs of monomeric  $\alpha$ -10 SUVs.



I)\* . Furthermore on sonication of *prepolymerized* dispersions, small vesicles were formed even more readily than vesicles sonicated from the respective monomers. The electron micrographs in Figure 4 show  $\alpha$ -20 SUVs prepared by (A) sonication followed by polymerization of the monomeric lipid and (B) sonication of the prepolymerized lipid. Smaller vesicles were clearly obtained more quickly from the prepolymerized lipids. For this reason, in the work described in subsequent chapters, samples were prepared almost exclusively from lyophilized polymers.

To evaluate more carefully the apparently smaller sizes of prepolymerized  $\alpha$ -THIOL MLVs compared to nonpolymerizable phosphatidylcholines, the  $^1\text{H}$  spectra of the dispersions were examined because the linewidths are sensitive to the tumbling rate and therefore the size of the liposomes (34,35). As an example, Figure 5 shows a typical  $^1\text{H}$  spectra of DPPC SUVs above and below the phase transition, and MLVs above the phase transition, illustrating the dependence of linewidth on the overall vesicle tumbling. By comparison, Figure 6 shows MLVs of polymeric  $\alpha$ -THIOLS in the liquid-crystalline state. As can be seen, the resonances are narrower and there is a much greater contribution of the proton resonances from the  $\alpha$ -THIOL MLVs than the DPPC MLVs, despite the fact that lateral diffusion and rotation of the polymeric lipids must be slower. Using NaAc as an internal standard and integrating the resonances of the choline group, it was found that  $\approx 30\%$  of the protons contribute to the spectra. This suggests that a substantial fraction of liposomes formed by the  $\alpha$ -THIOL dispersions are small enough to be sufficiently motionally averaged by the tumbling of the vesicle to be visualized by NMR (27,34). Titration of  $\text{MnCl}_2$  into dispersions of  $\alpha$ -16 to  $\alpha$ -20 to broaden away the external choline resonances caused a limiting reduction in the intensity of the choline resonance relative to bulk methylene

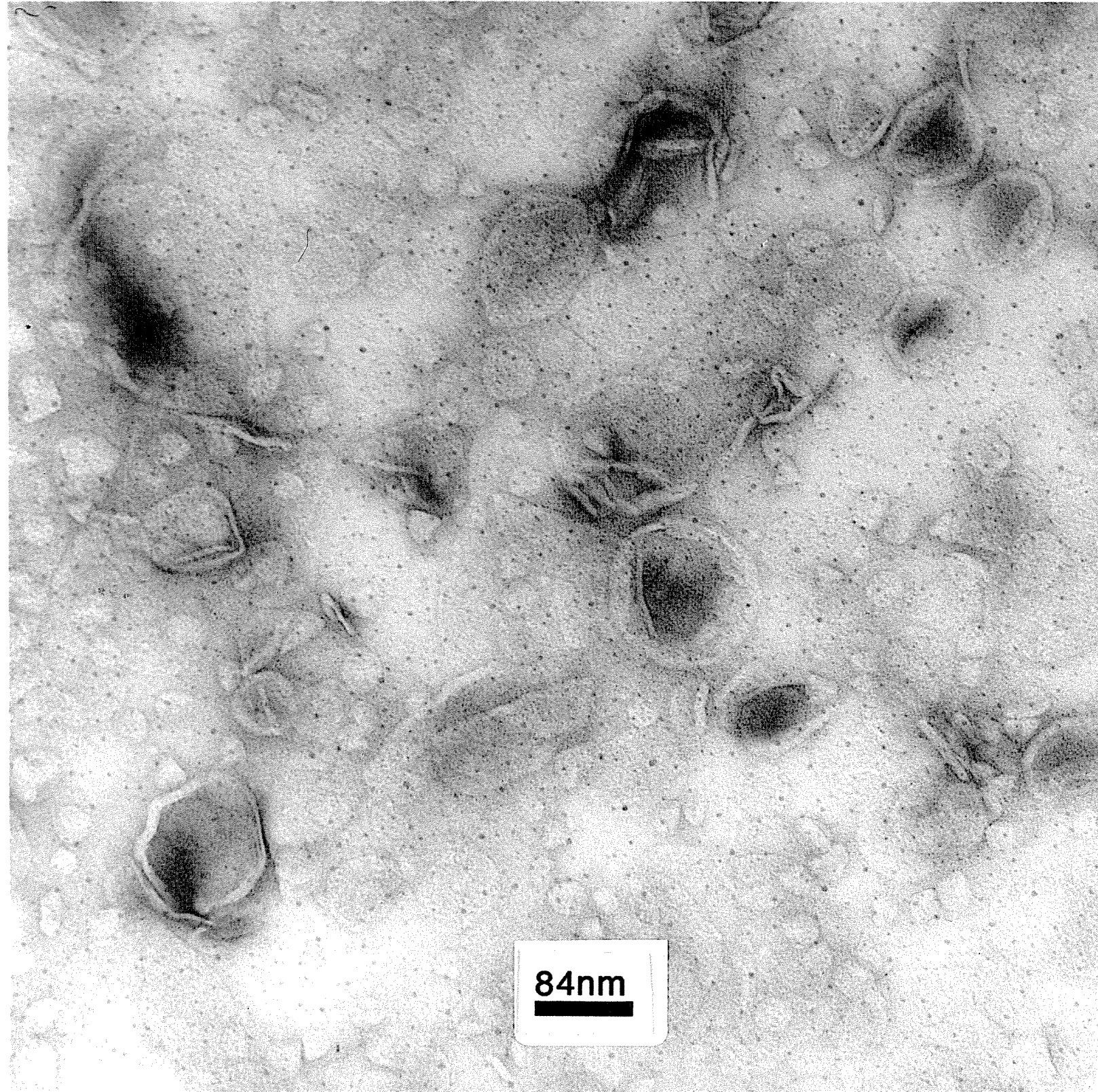
---

\* It should be noted that the value for DPPC is only an illustration of the disparity in the sizes. The value is probably quite inaccurate due to the polydispersity of the multilamellar samples as well as the fact the sizes above  $\approx 2000$  nm are outside the range of the instrument.

**Figure 4**

Negative stain electron micrographs of: **A.**  $\alpha$ -20 SUVs sonicated prior to polymerization and **B.**  $\alpha$ -20 SUVs sonicated from the lyophilized powder of the prepolymerized lipid.

**A**



**B**

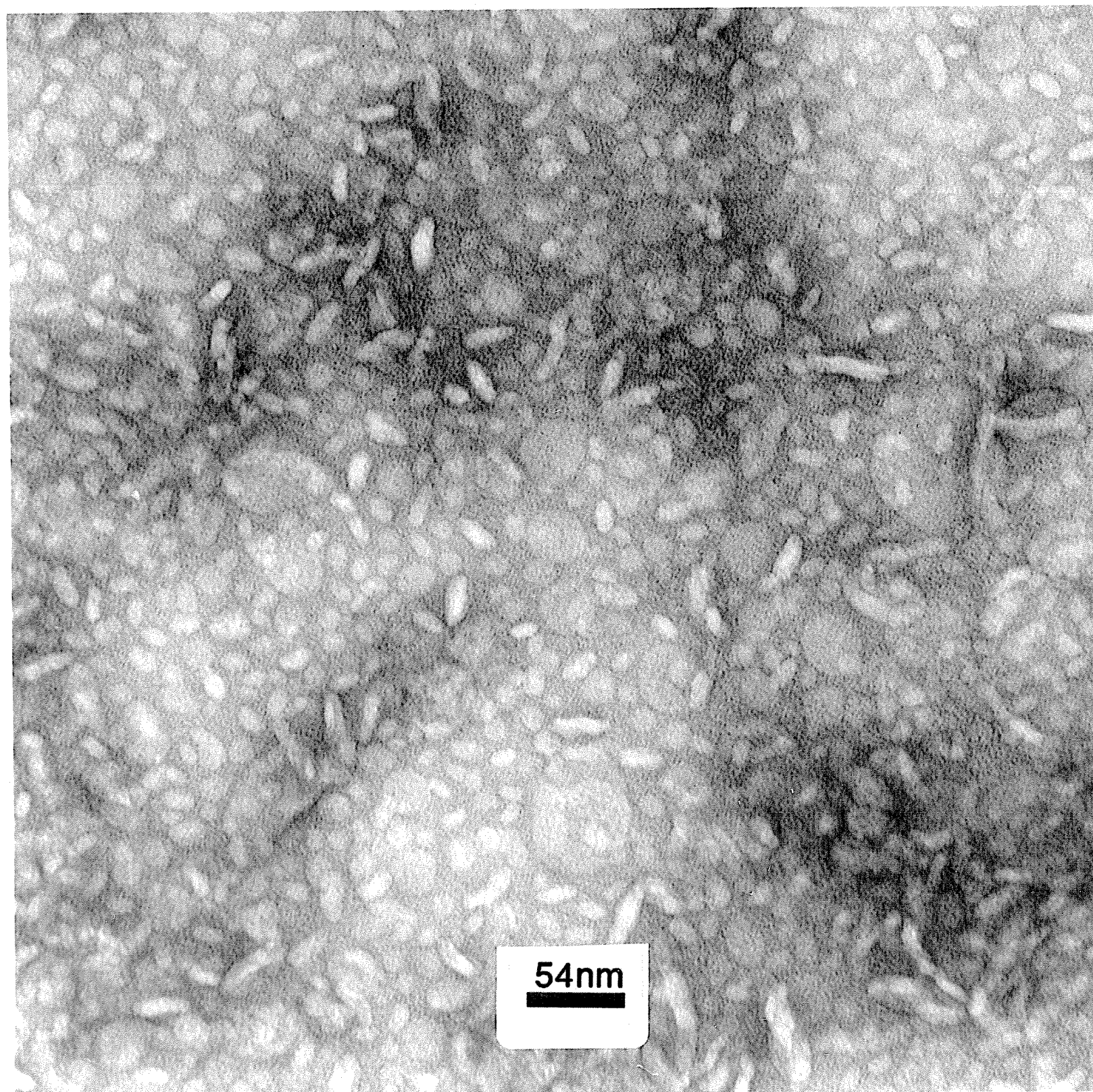


**Figure 5**

<sup>1</sup>H NMR spectra of A. DPPC SUVs at 25 °C; B. DPPC SUVs at 50 °C; C. DPPC MLVs at 47 °C.

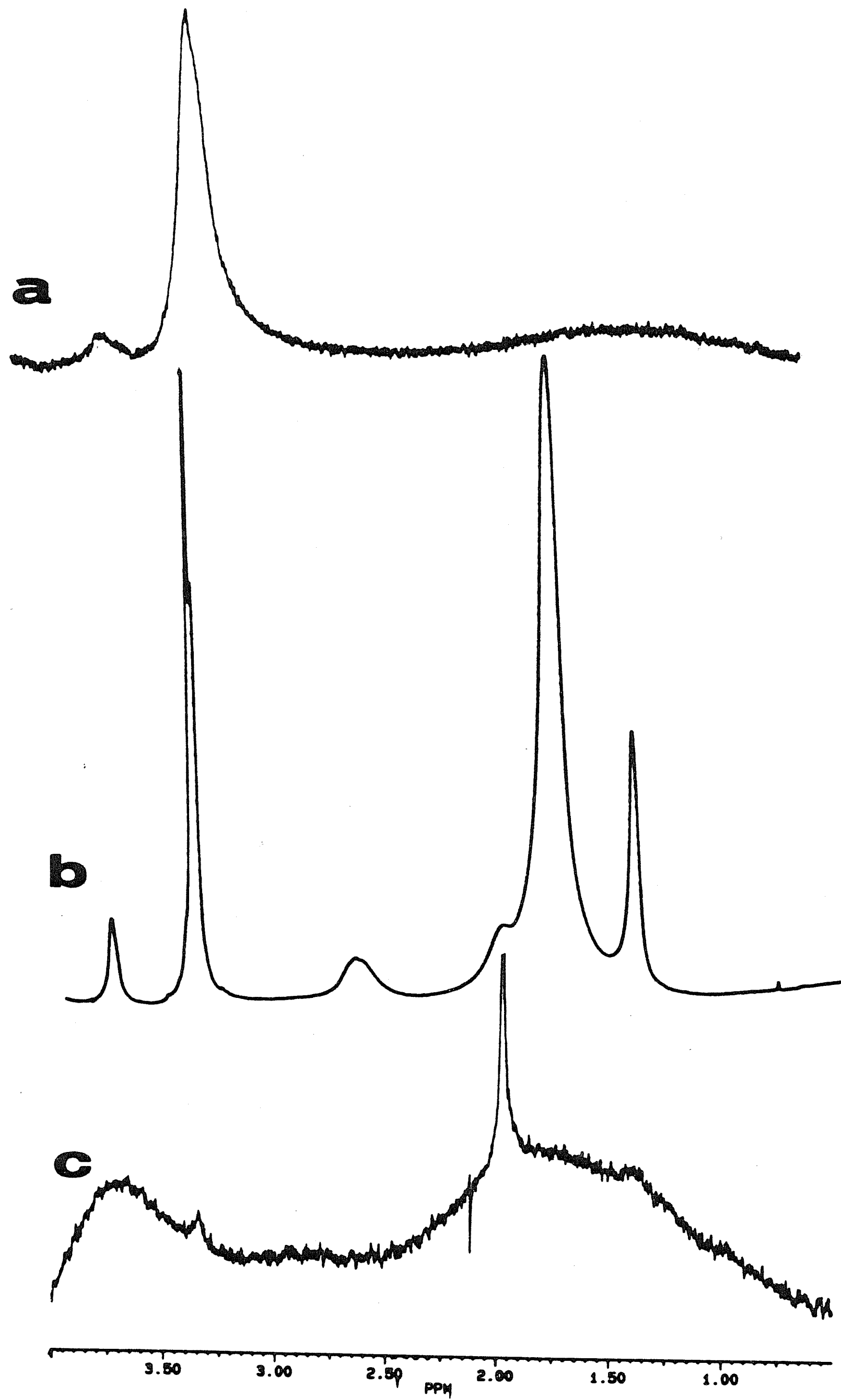
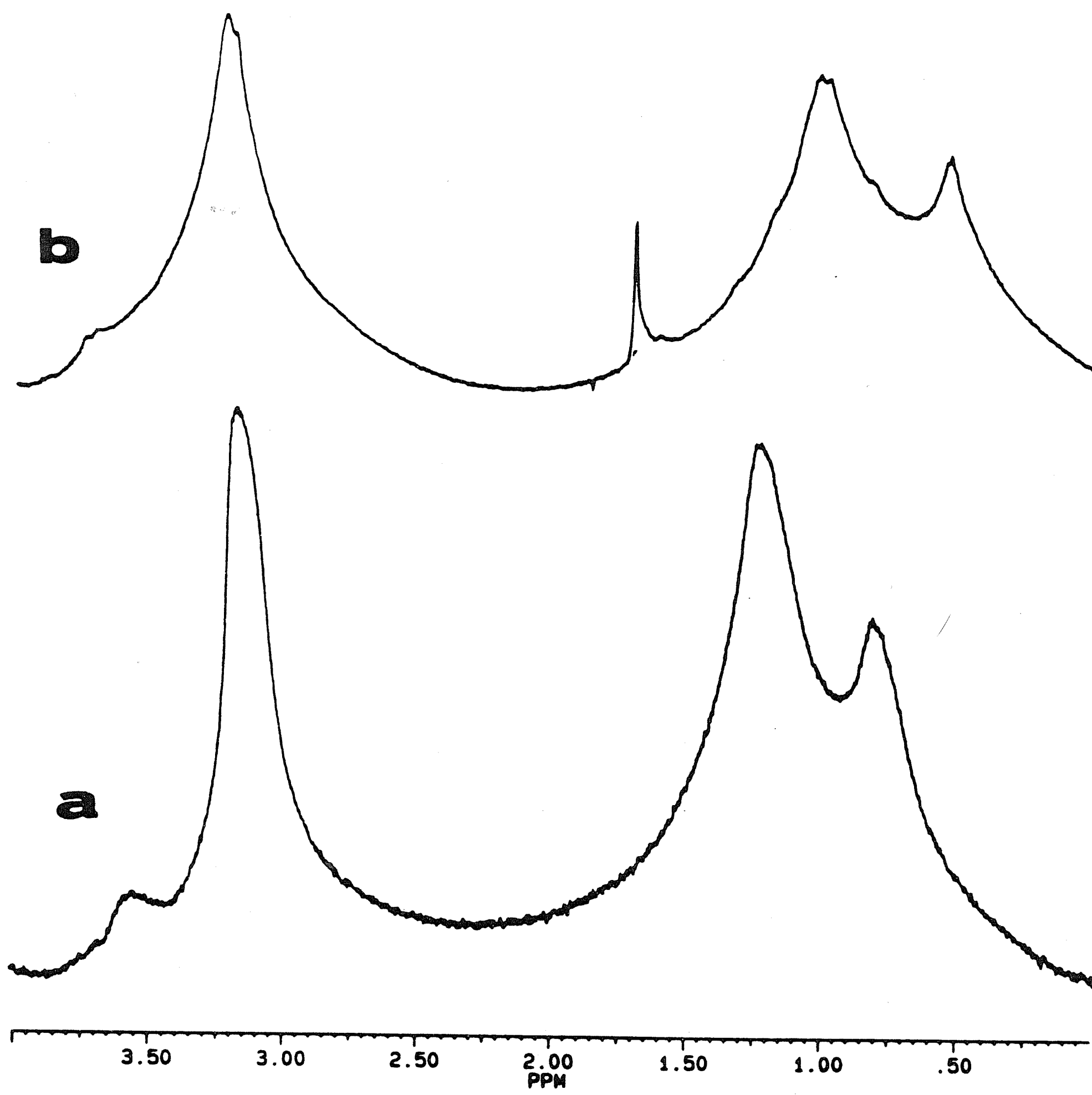


**Figure 6**

$^1\text{H}$  NMR spectra of A.  $\alpha$ -16 MLVs at 32 °C; B.  $\alpha$ -18 MLVs at 47 °C. The sharp spike in the spectrum of polymeric  $\alpha$ -18 is NaAC.



and methyl groups by  $\approx 55 \pm 15\%$ . Under the very reasonable assumption that the alkyl chain protons are unaffected by the relaxation reagent, these data also suggest that the NMR-visible liposomes are unilamellar.

To better visualize the relative sizes and lamellarity of the  $\alpha$ -THIOL dispersions, freeze fracture replicas were prepared. Figure 7 and 8 show typical multilamellar structures observed for DPPC and for monomeric  $\alpha$ -16 MLVs. By contrast, from a preparation of prepolymerized  $\alpha$ -20 liposomes, much smaller and largely unilamellar vesicles were observed both by freeze fracture (Figure 9) as well as negative stain electron microscopy (Figure 10). Qualitatively, similar results were obtained for  $\alpha$ -16 and  $\alpha$ -18 dispersions.

It should be noted that the data presented here are typical data. The sizes produced by simple dispersion of the  $\alpha$ -THIOL polymers is somewhat dependent on concentration as well as the length and temperature of hydration. As an example, Figure 11 shows  $^{31}\text{P}$  NMR powder spectra of  $\alpha$ -16 at 50 mg/ml after a hydration period of one hour at 37°C. After maintaining the sample at 45°C for 12 hours, a large isotropic component grew, indicative of the formation of smaller vesicles tumbling rapidly with respect to the NMR time scale. The size of the isotropic component increased further with prolonged incubation at 60°C (higher temperature). Similar treatment of DPPC MLVs does not result in the production of an isotropic component.

*Aggregation Tendency.* As a final point, it was found that SUVs of polymeric  $\alpha$ -THIOLS were much more resistant to aggregation than nonpolymerizable analogues. Even polymeric  $\alpha$ -20, which at room temperature is well below the phase transition temperature ( $\approx 50^\circ\text{C}$ ), remained unaltered in size for several weeks as determined by light scattering. By comparison, DPPC SUVs aggregated much more rapidly despite the fact that this lipid has a much shorter chain length. This is shown in Figure 12.

**Figure 7**

Freeze fracture electron micrographs of DPPC multilamellar dispersions.

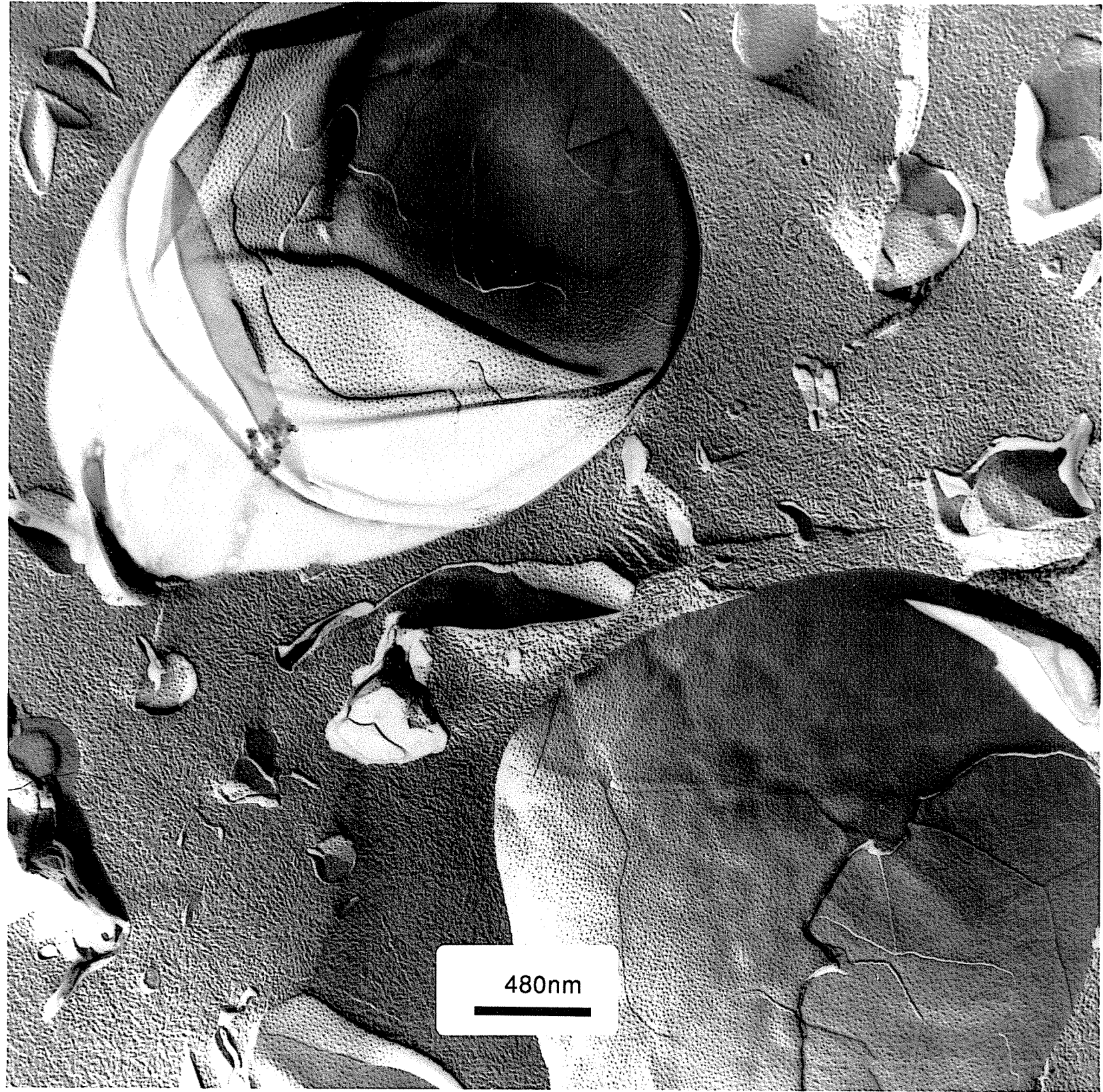


**Figure 8**

Freeze fracture electron micrographs of monomeric  $\alpha$ -16 multilamellar dispersions. The corrugation on the surface is the well-known ripple structure often observed for samples incubated between the pretransition and main gel to liquid-crystalline phase transition (26). This sample was prepared at room-temperature, which is just below the  $T_m$  of the lipid ( $\approx 25.6$  °C).

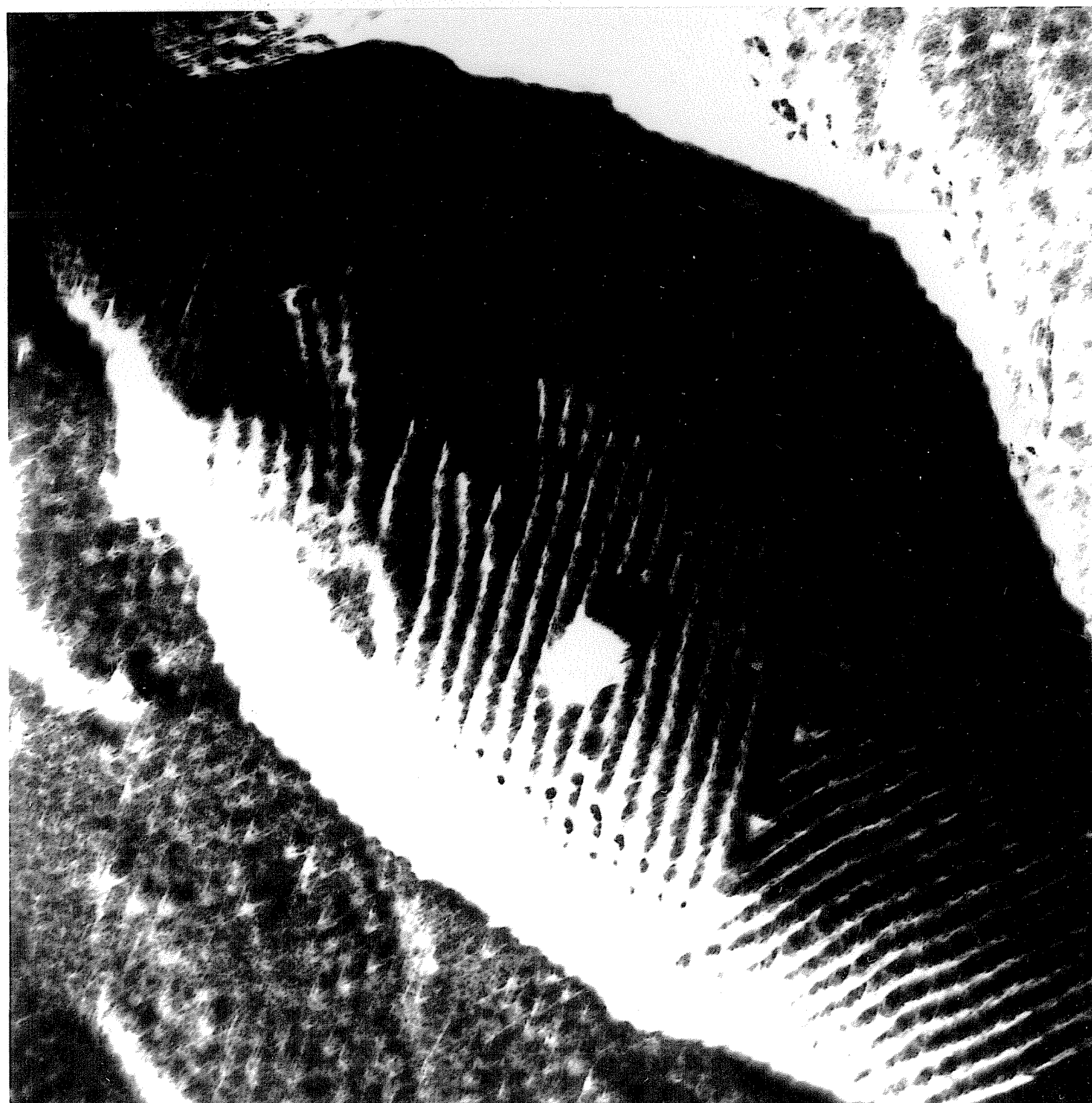


**Figure 9**

Freeze fracture electron micrographs of polymeric  $\alpha$ -20 dispersions. The samples were prepared from a lyophilized powder of the prepolymerized polymer.

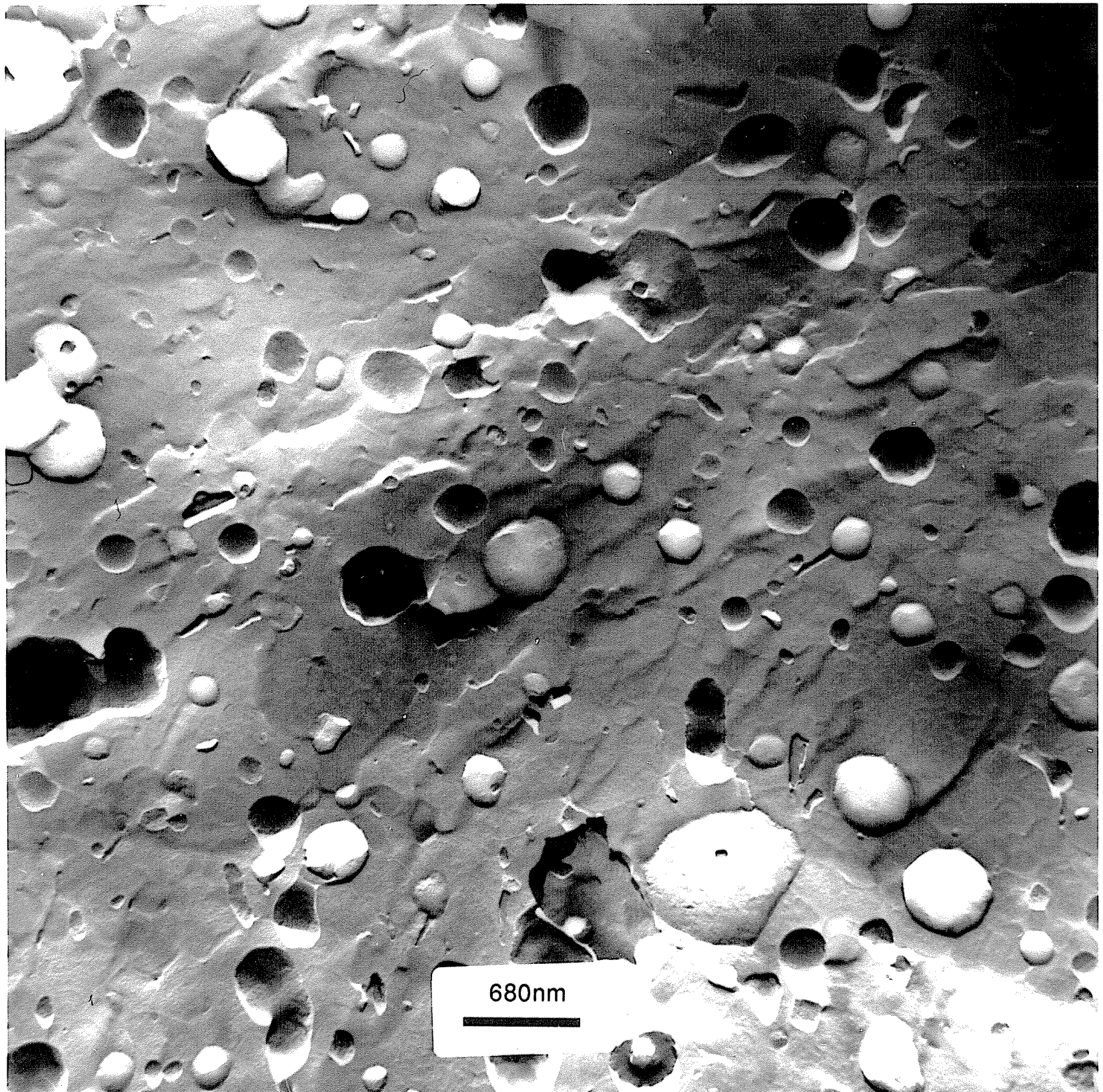
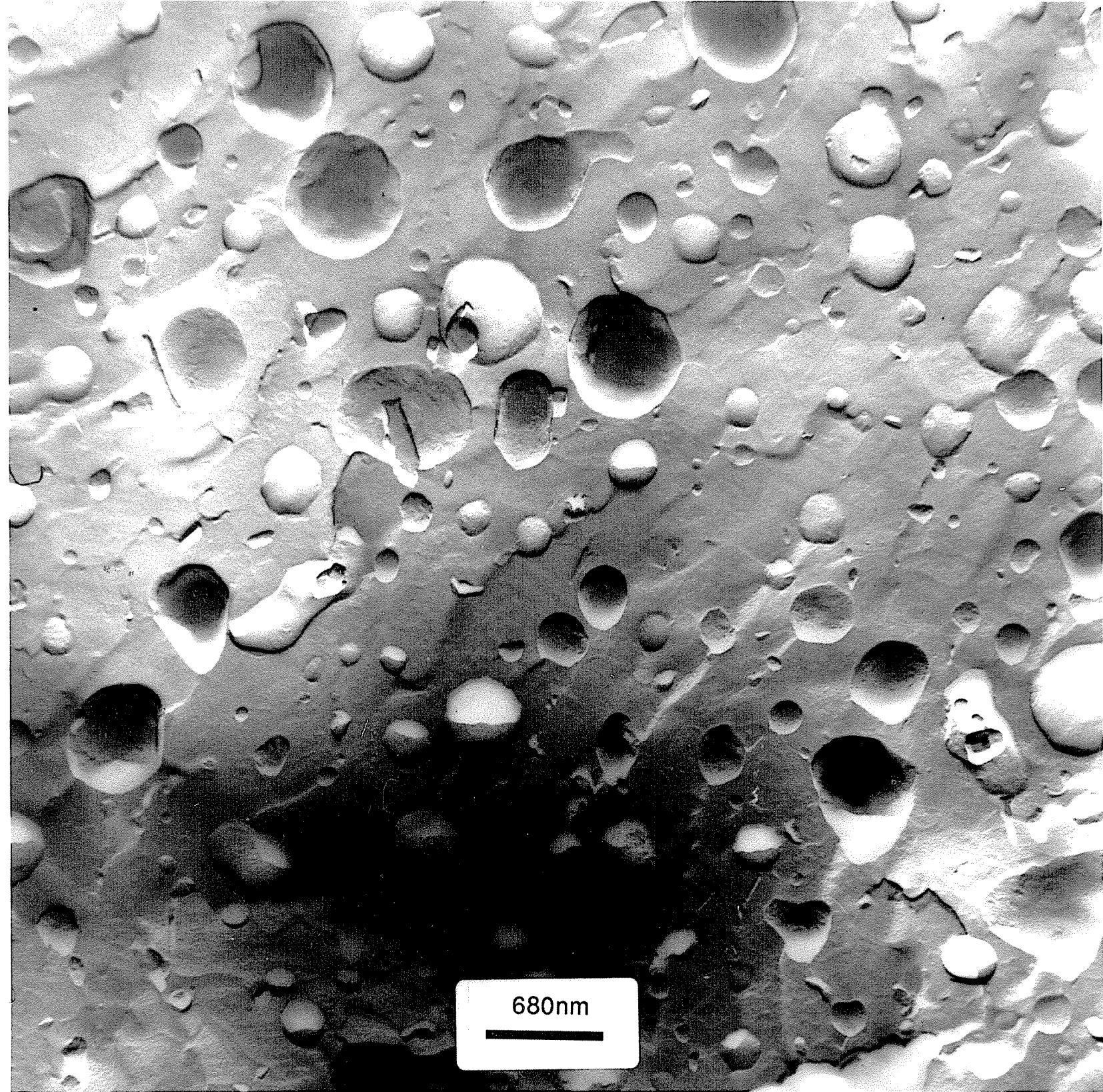


**Figure 10**

Negative stain electron micrographs of polymeric  $\alpha$ -20 dispersions. The samples were prepared from a lyophilized powder of the prepolymerized polymer.

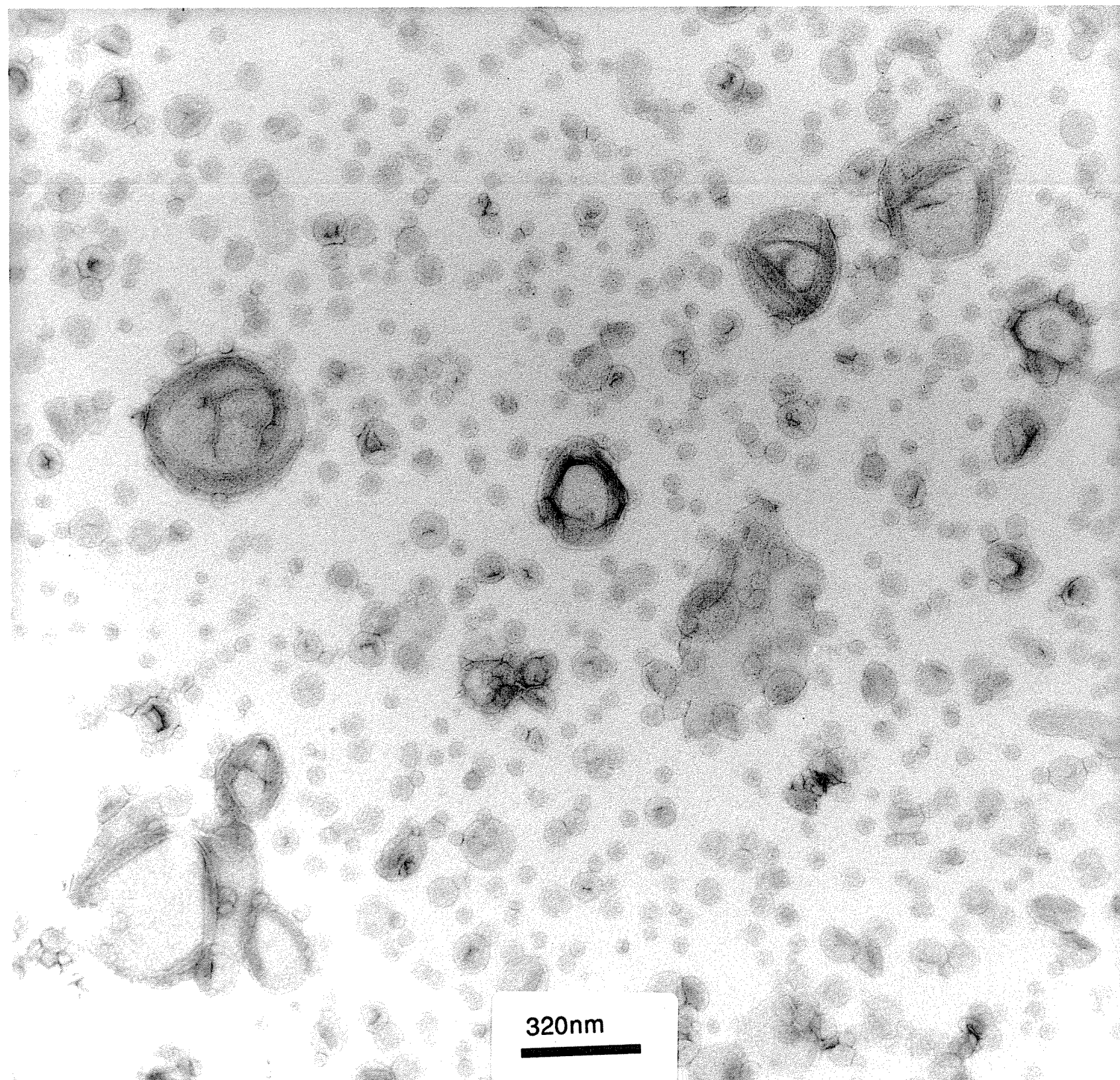
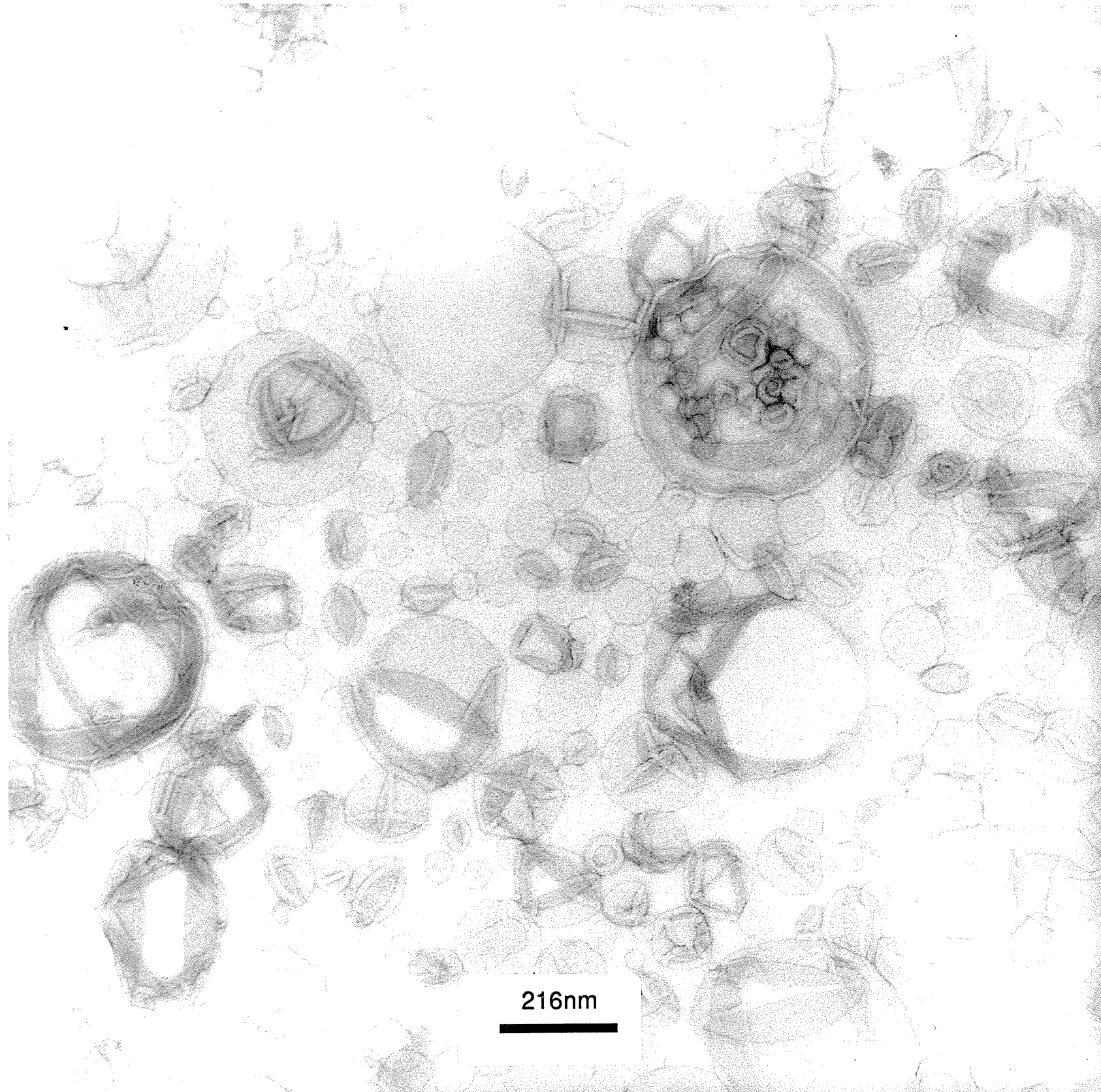


**Figure 11**

$^{31}\text{P}$  NMR spectra of polymerized  $\alpha$ -16, which had been incubated at **A.** 37°C for (1 h); **B.** 45 °C (12 h).

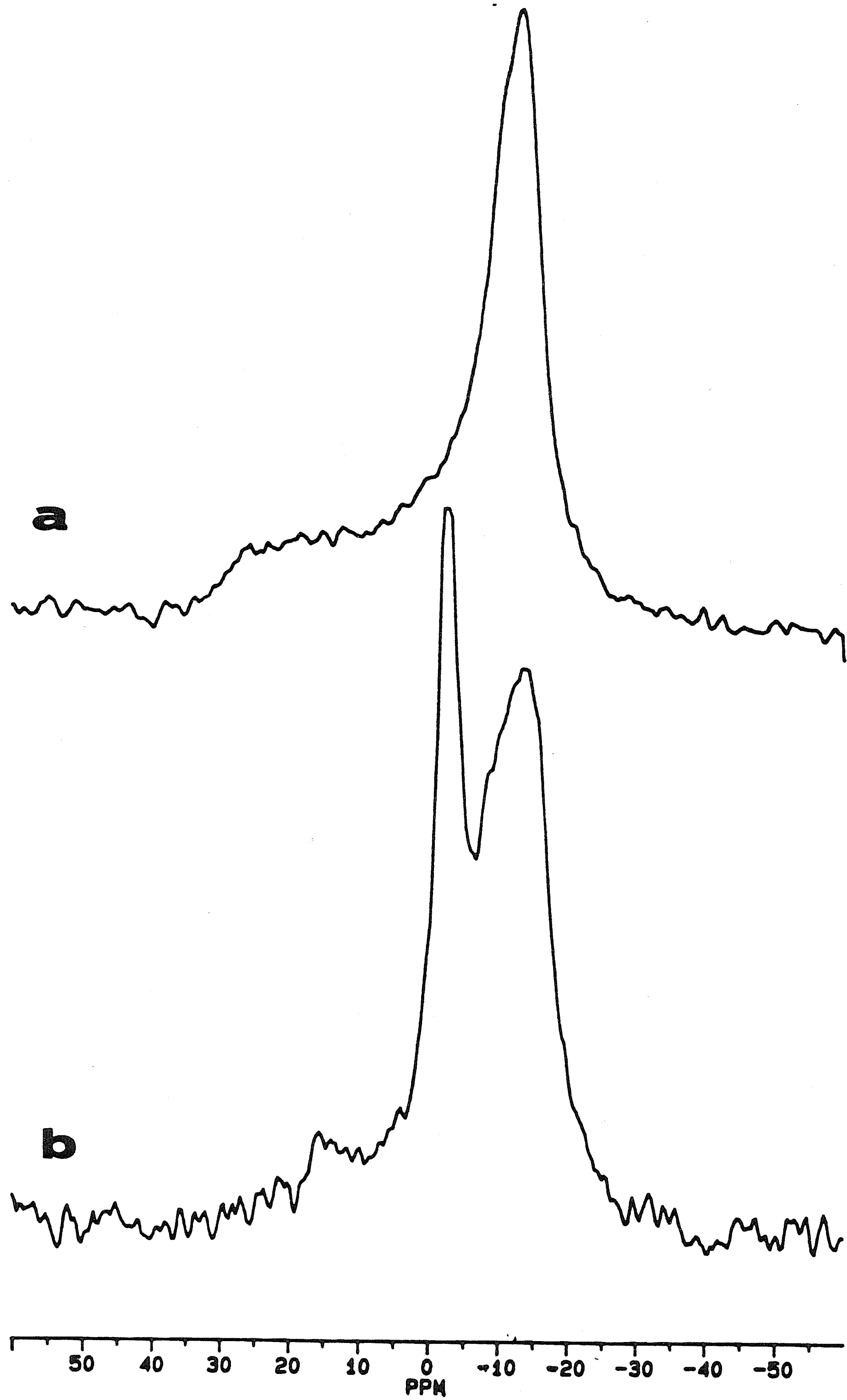
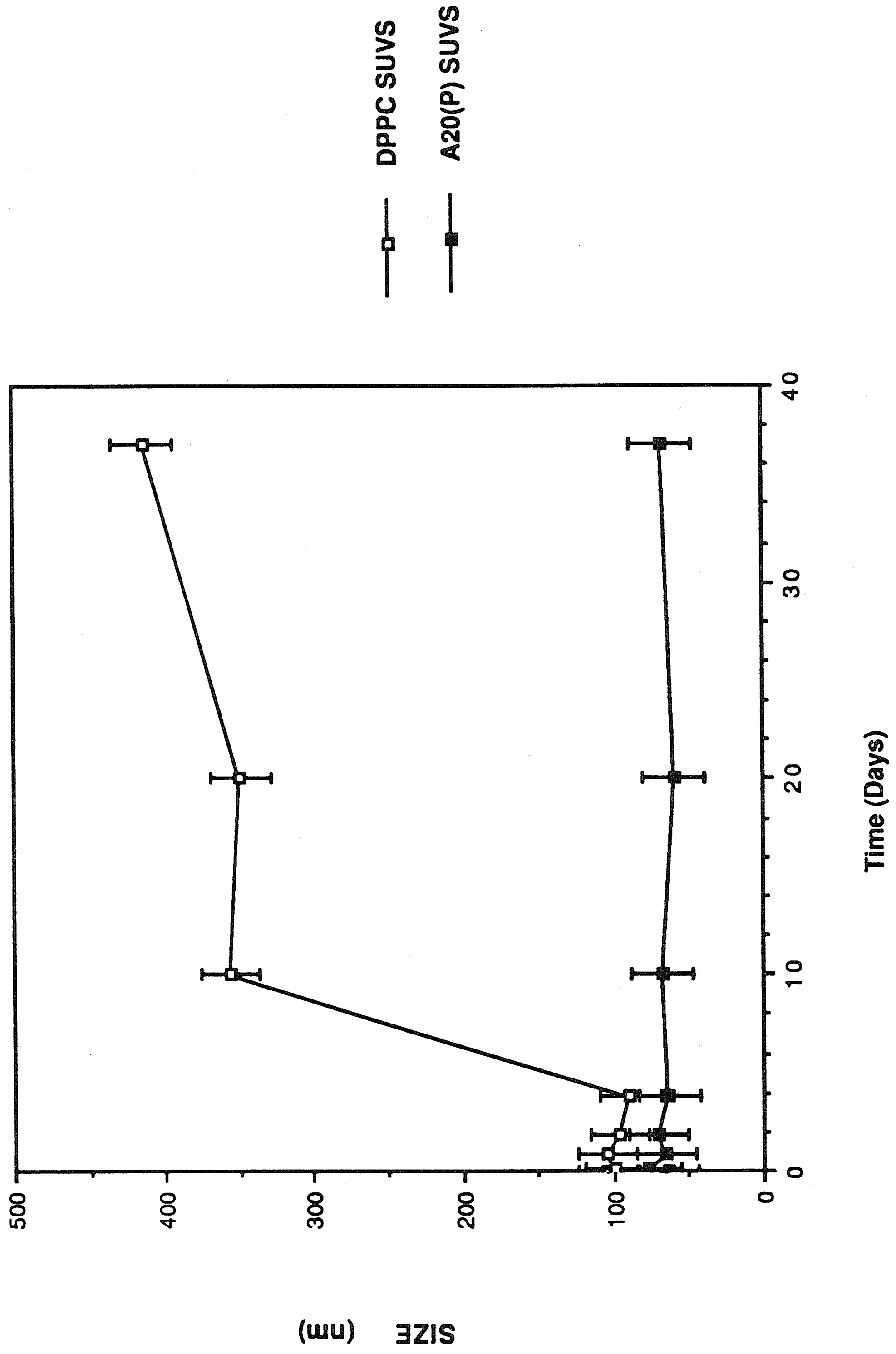


**Figure 12**

Comparison of the aggregation of polymeric  $\alpha$ -20 SUVs versus DPPC SUVs. Samples were maintained at ambient temperature throughout the duration of the experiment and therefore both lipids were in the gel state. The sizes were measured by dynamic light scattering at angle of  $90^\circ$ .



## Morphology of $\omega$ -THIOLS.

### Monomeric $\omega$ -THIOLS.

Table II shows a summary of light scattering and entrapment data for monomeric and polymeric  $\omega$ -THIOLS. For the monomeric  $\omega$ -THIOLS (N=11,15,16), entrapment of carboxyfluorescein and uridine was positive, indicating the formation of sealed liposomes. Similar encapsulation experiments were not carried out for N = 9 and 10 but turbid solutions were obtained consistent with the formation of bilayers. Preliminary freeze fracture and negative stain micrographs of monomeric  $\omega$ -9 and  $\omega$ -10 also suggested the presence of liposomes. For N = 8, optically clear solutions were obtained similar to that observed for micelle-forming phosphatidylcholines. To confirm this, the fluorescence intensity of 2-p-toluidinylnaphthalene 6-sulfonate (TNS), which is enhanced upon adsorption to membrane interfaces, was used to detect the presence of a critical micelle concentration (37). Figure 13 shows a comparison of the changes in fluorescence intensity with lipid concentration for DOPC, which forms liposomes; D8PC, which forms micelles; and monomeric  $\omega$ -8. The abrupt break in the curve at  $\approx$  0.1 mg/ml indicates the onset of micelle formation for  $\omega$ -8, similar to that exhibited by D8PC.

SUVs were easily formed from intermediate chain (N=11,12)  $\omega$ -THIOLS on bath sonication. Typical sizes of  $\omega$ -11 ranged from 200-800 Å depending on the length of sonication. For  $\omega$ -15 and  $\omega$ -16, optical clearing of solutions was obtained by probe sonication but aggregation and precipitation occurred after sonication was discontinued, consistent with the observations of Regen et al. This behavior is similar to that occasionally observed for conventional phosphatidylcholines with high transition temperatures (i.e. DSPC) and may be due to the high transition temperature and

**Table II**

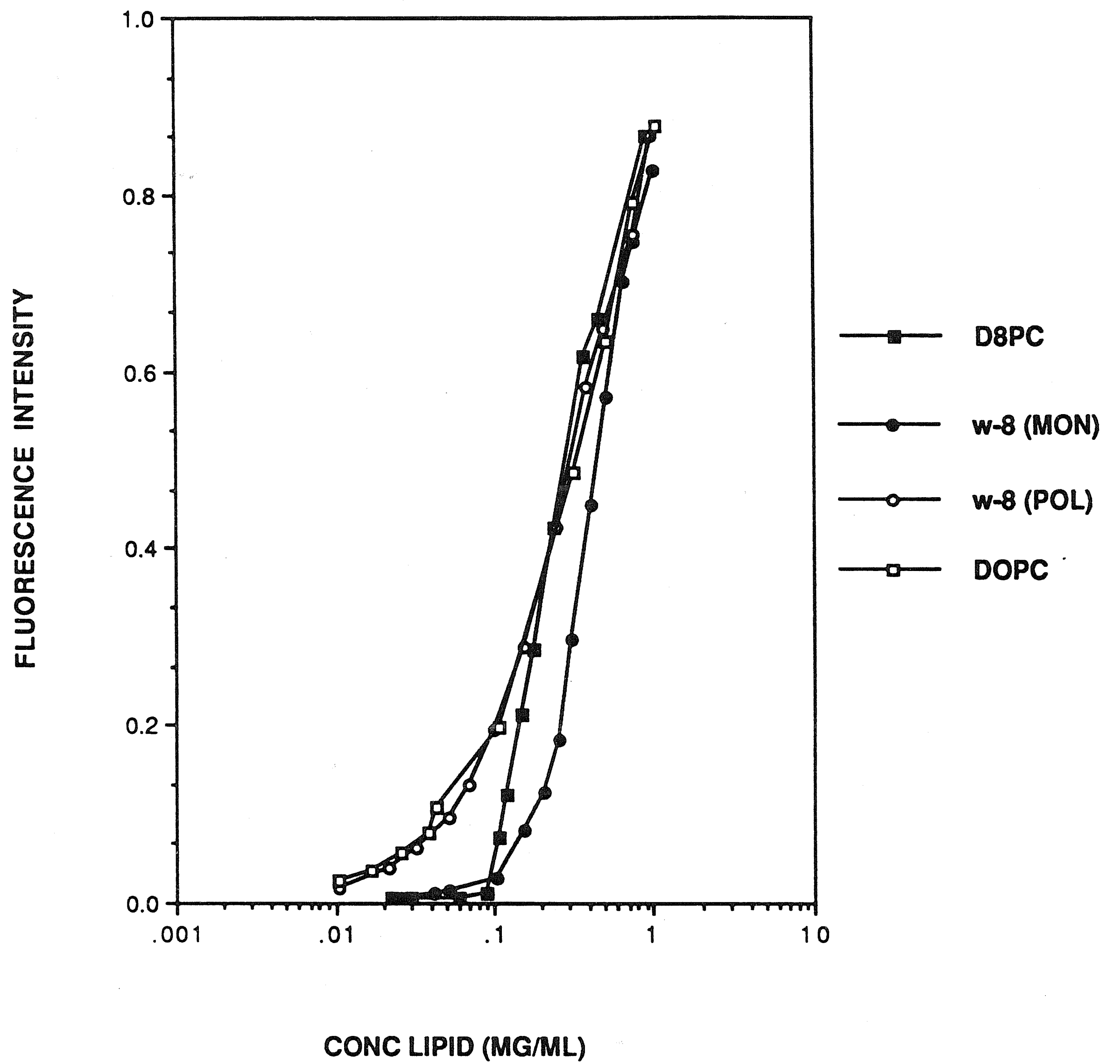
Summary of the sizes and entrapment characteristics of monomeric and polymeric  $\omega$ -THIOLS . The polymerized  $\omega$ -11 SUVs were sonicated prior to polymerization. Polymerized MLVs were samples dispersed in buffer prior to polymerization. The important points to note are: *(i)* the increase in size of  $\omega$ -11 SUVs on polymerization; *(ii)* retention of the size of  $\omega$ -11 SUVs on polymerization when cholesterol is present in the membrane (mole ratio = 2:1  $\omega$ -11:Chol); *(iii)* the ability of monomeric but not polymeric  $\omega$ -THIOLS to entrap aqueous solutes.

Lipid	Preparation	Size (nm)	<u>Entrapment</u>	
			Uridine	CF
ω-11 SUV's	Before Polymerization	79.2 ± 1.2 <sup>a</sup>	0.13%	
ω-11 SUV's	2 h After Polymerization	462 ± 61 <sup>a</sup>		
ω-11 SUV's	After Polymerization/Dialysis	>2000 <sup>b</sup>	0.017%	
ω-11/Chol SUV's	Before Polymerization	56.7 ± 1.0		
ω-11/Chol SUV's	After Polymerization	68.5 ± 2.0		
ω-15 MLV's	Before Polymerization		1.3%	+
ω-15 MLV's	After Polymerization		0.004%	
ω-16 MLV's	Before Polymerization		1.0%	+
ω-16 MLV's	After Polymerization		0.006%	+

<sup>a</sup>Samples were 5 mg/ml. <sup>b</sup>Samples were 2.2 mg/ml.

**Figure 13**

Change in the fluorescence intensity of 2-p-toluidinylnaphthalene-6-sulfonate (TNS) with increasing concentration of lipid (DOPC, D8PC, monomeric  $\omega$ -8, and polymeric  $\omega$ -8). The breaks in the curves of D8PC and monomeric  $\omega$ -8 denote the cmc. Measurements were carried out as in (37). The symbols are assigned in the legend of the figure.



strong cohesive forces of these lipids ( $T_m \approx 49^\circ\text{C}$  and  $52^\circ\text{C}$ , for  $N=15$  and  $16$ , respectively; see Chapter III). In subsequent experiments, these lipids were therefore not sonicated but rather prepared as MLVs by simple vortex mixing above the phase transition temperature. Electron micrographs of monomeric  $\omega$ -11 SUVs and  $\omega$ -16 MLVs are shown in Figure 14 and 15. An interesting point to note about the  $\omega$ -16 MLVs is the formation of long tubules frequently seen in both freeze fracture replicas and by Nomarski optics. The reason for their formation is unclear. Whether they are also present in other  $\omega$ -THIOL dispersions or are simply an artifact of a small but unavoidable amount of polymer is also unknown. However, they do form closed structures. This was confirmed by observation via fluorescence microscopy of their ability to entrap carboxyfluorescein.

### POLYMERIZED $\omega$ -THIOLS

*Oxidative Polymerization of  $\omega$ -THIOLS.* In contrast to  $\alpha$ -THIOLS, oxidative ( $\text{H}_2\text{O}_2$ ) polymerization of the  $\omega$ -THIOLS appears to greatly perturb the membrane organization for all lipids examined. Polymerization of  $\omega$ -11 SUVs resulted in a large increase in the apparent particle size. For  $\omega$ -11 SUVs, polymerization was generally carried out for 4 hours at  $45^\circ\text{C}$ . Typically, during the incubation period, no change in the optical clarity was noted. However, on standing at room temperature, the turbidity of the sample gradually increased over the course of approximately an hour, in contrast to the monomeric SUVs which remained optically clear and unchanged. While this could be due to reversible aggregation, in most cases on vortexing the sample or after prolonged incubation at  $45^\circ\text{C}$ , the solution was transformed into a completely translucent and viscous gel. In Table II, the sizes of  $\omega$ -11 SUVs measured before and after polymerization are shown. It is interesting to note that despite the complete clarity of the sample used in these experiments, the apparent size is obviously very large at this concentration. Gel permeation chromatography of a separate preparation of

**Figure 14**

Negative stain electron micrographs of monomeric bath sonicated  $\omega$ -11 SUVs.

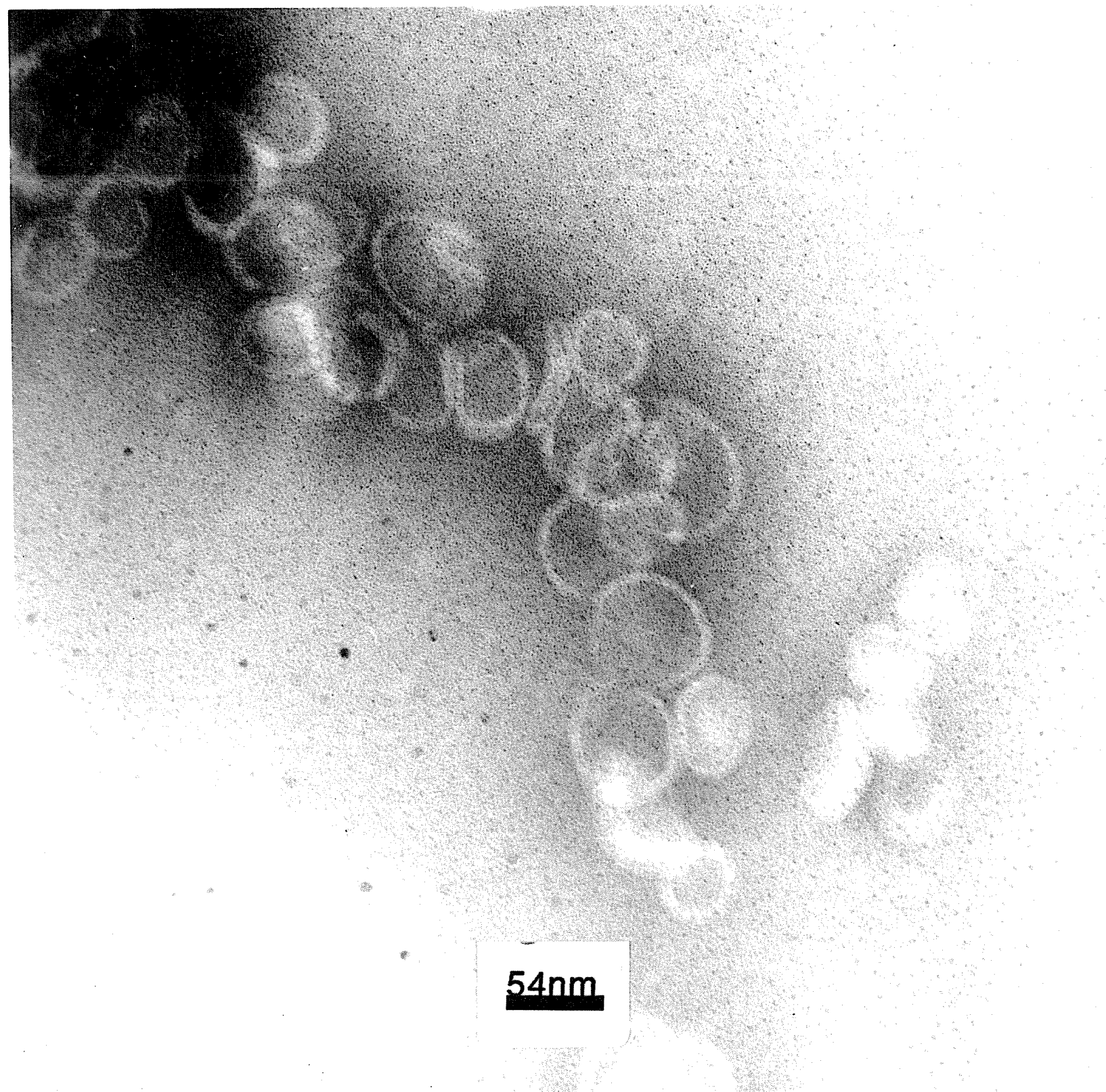
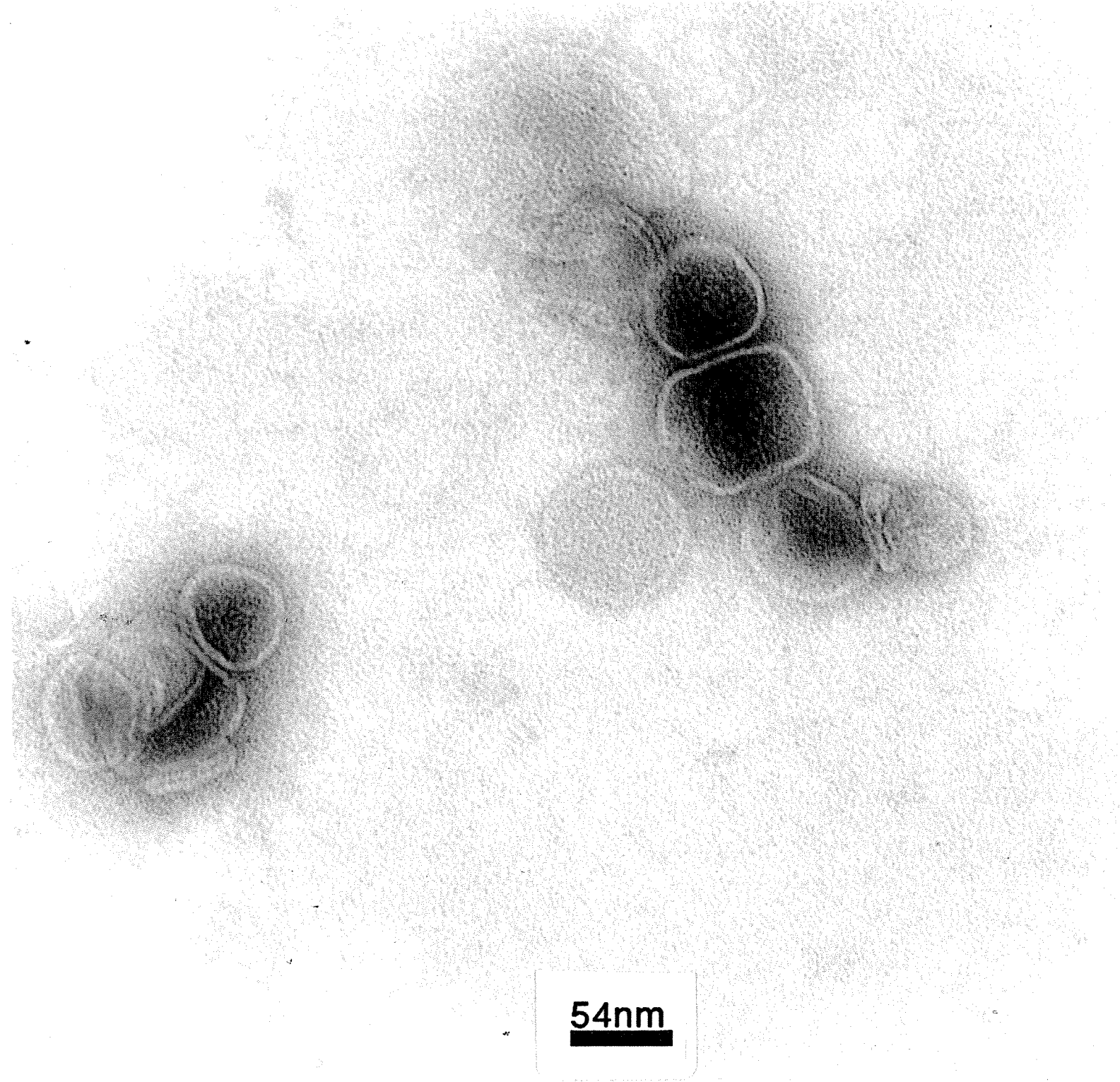
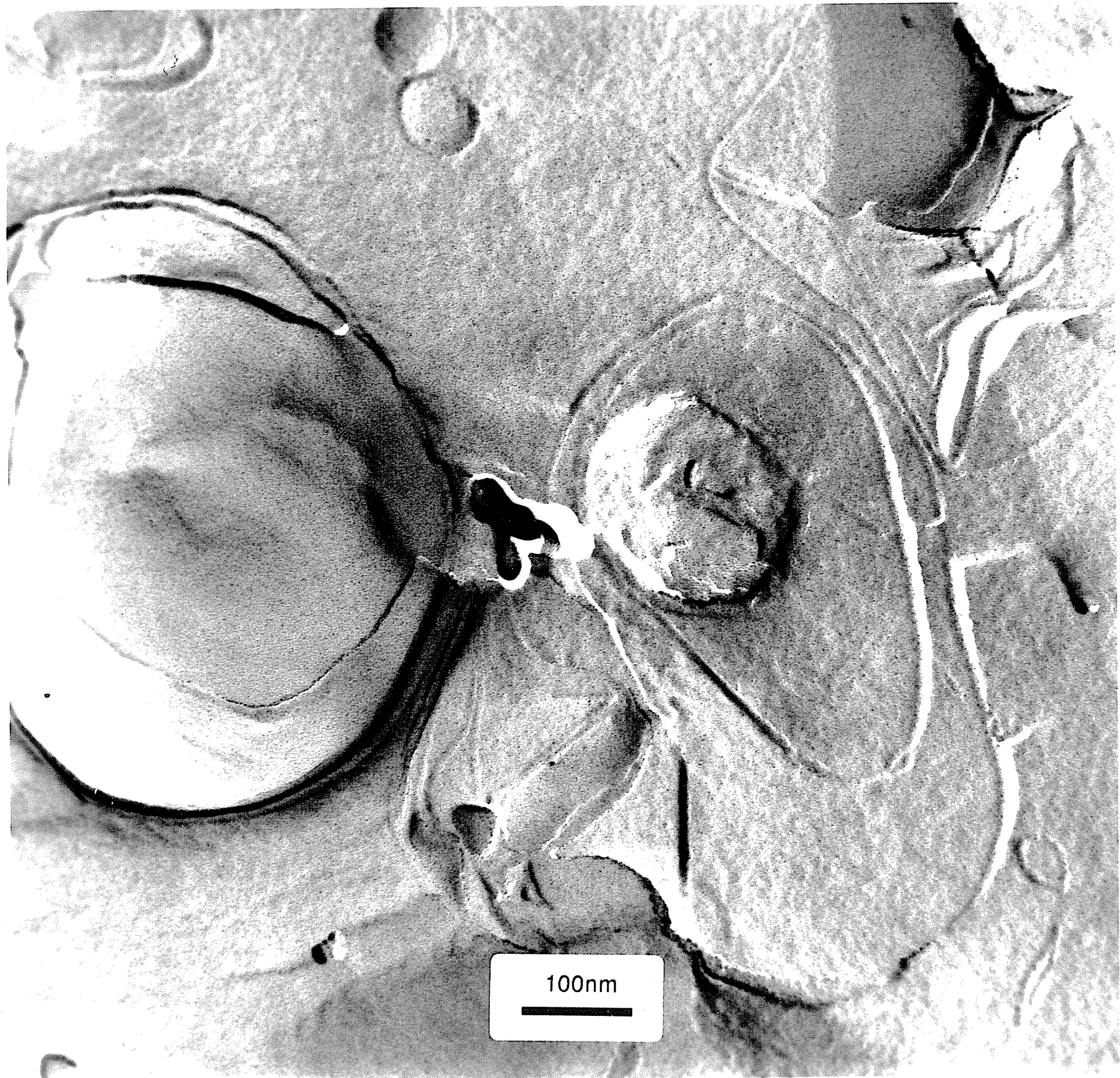


**Figure 15**

Freeze fracture electron micrographs of monomeric  $\omega$ -16 multilamellar dispersions.



$\omega$ -11 SUVs before and after polymerization corroborate the increase in particle size. (Figure 16). Similar observations were made for polymerized  $\omega$ -10 and  $\omega$ -9 SUVs.

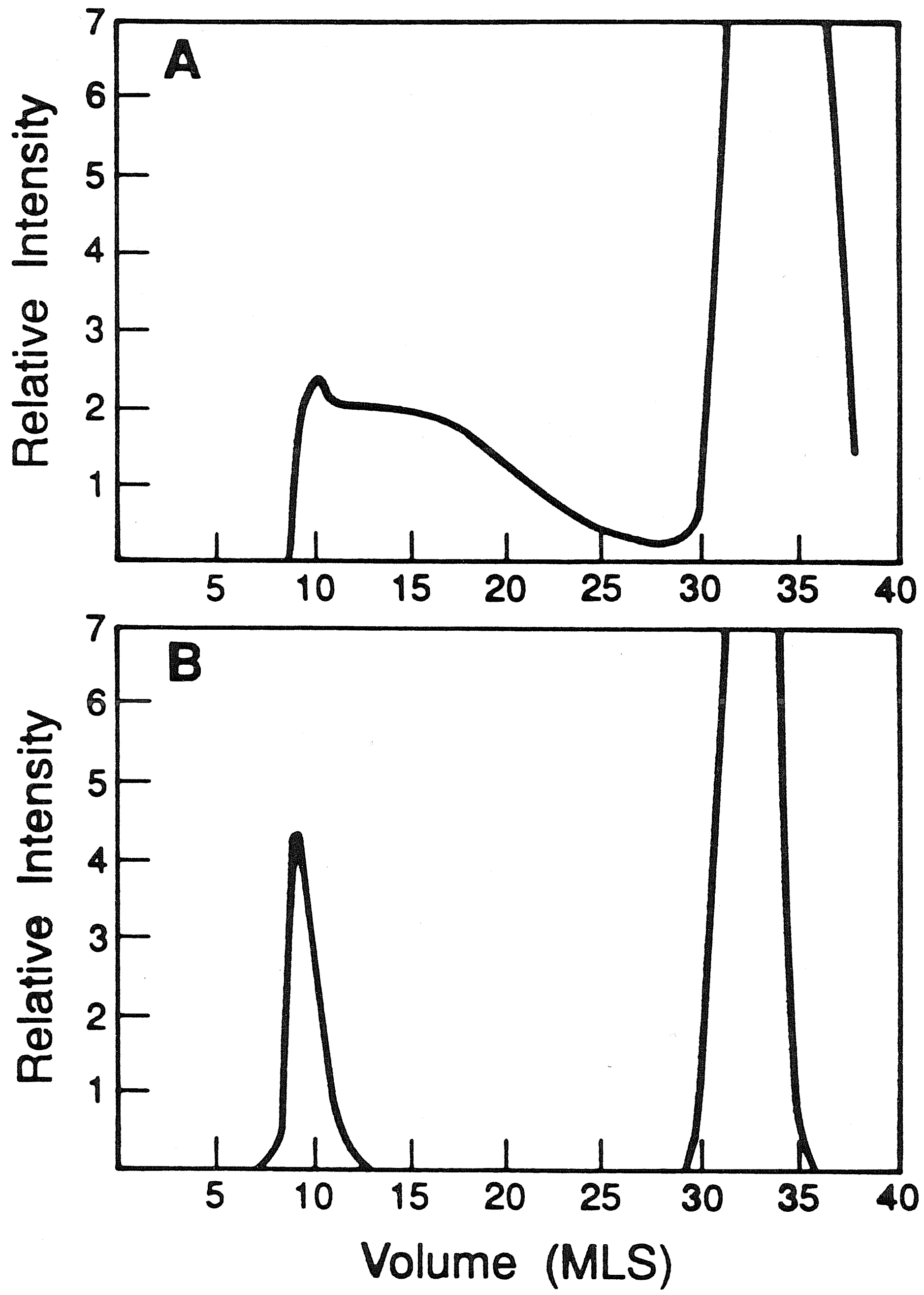
For  $\omega$ -8, the sample stayed optically clear but the characteristic cmc was lost as expected for the formation of "polymeric micelles." This is demonstrated in Figure 13, which shows the lack of an abrupt break in the plot of fluorescence intensity versus concentration for polymeric  $\omega$ -8, similar to that for the DOPC SUVs. At high concentrations, polymeric  $\omega$ -8 dispersions became very viscous and large as determined by light scattering suggesting some similarity in the morphology of these non-vesicular structures and structures formed by polymeric  $\omega$ -THIOLS with N= 9 to 11.

Concerning the tendency of these samples to aggregate and form viscous gels, it should be stressed that the apparent size, viscosity and clarity of the samples are concentration and temperature dependent. To illustrate the effects of concentration and temperature on the short chain  $\omega$ -THIOLS, Figure 17 shows the "apparent" size of polymeric  $\omega$ -10 (lyophilized and rehydrated) as a function of concentration and temperature. Similar data is shown for  $\omega$ -8 polymeric micelles and DOPC SUVs. The extreme aggregation tendency of the  $\omega$ -THIOLS is reminiscent of micellar growth or micelle-lamellar transitions but is likely due to extensive aggregation of the fragments (41-43). By comparison, for DOPC SUVs, a relatively small dependence is observed as expected for liposomes. The large size of polymeric  $\omega$ -15 and  $\omega$ -16 aggregates precluded detection of changes in size by light scattering.

Because  $\omega$ -15 and  $\omega$ -16 were routinely prepared as MLVs, changes in particle size were difficult to quantify. Optically, the samples remained turbid although the turbidity seemed to decrease and the dispersions became more gelatinous and "sticky."

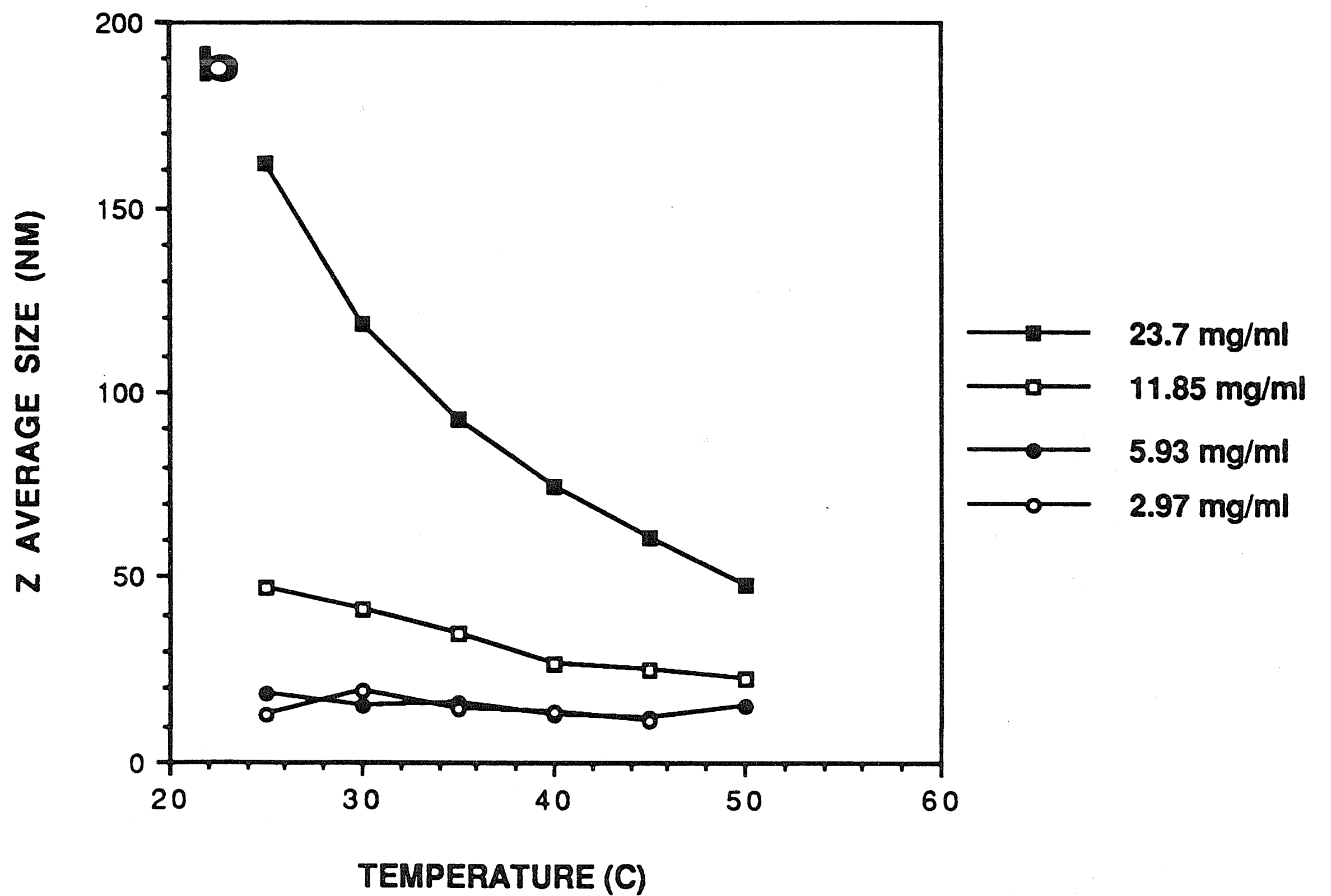
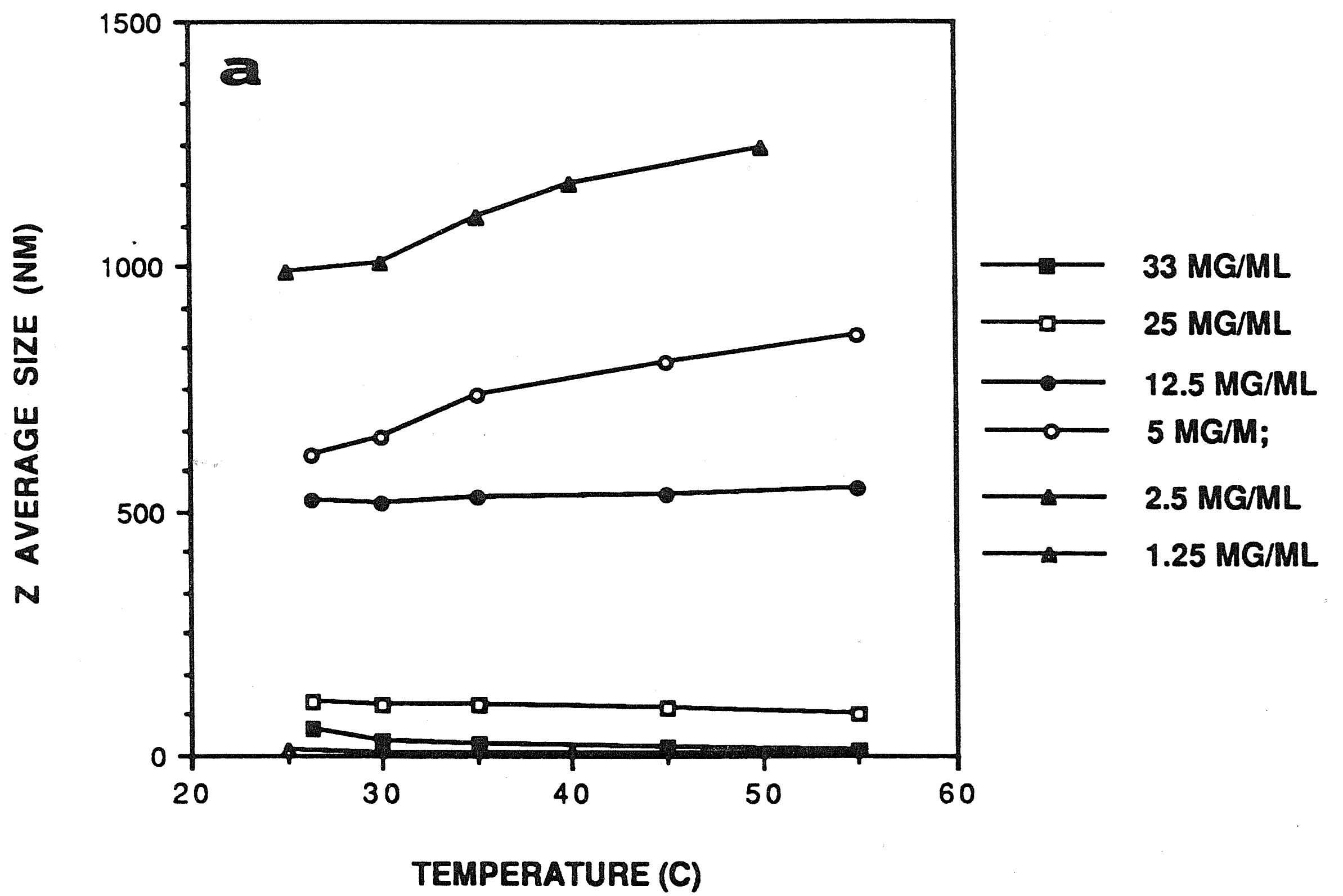
**Figure 16**

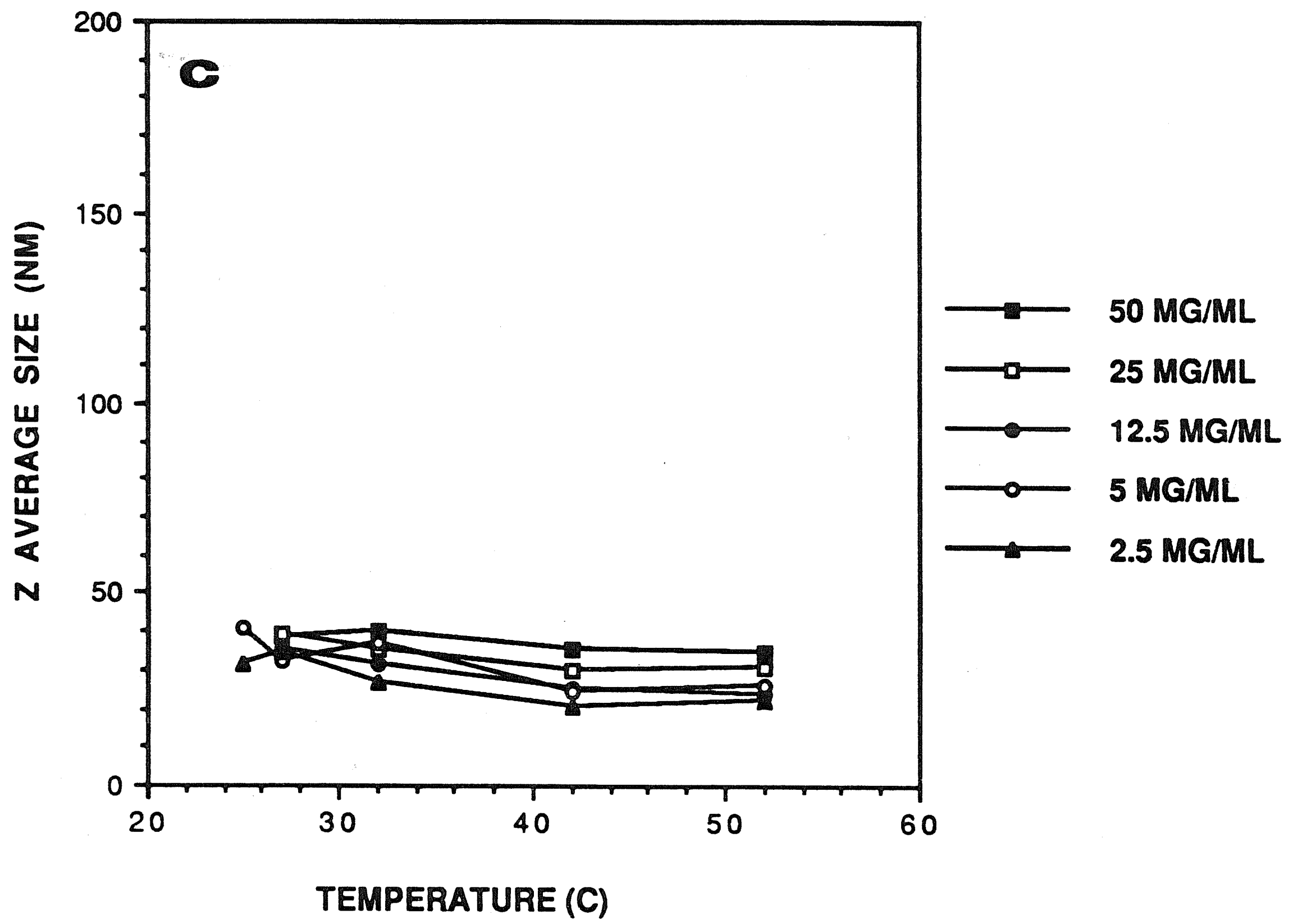
Elution profile of  $\omega$ -11 SUVs on a sepharose 4BCL column: **A.** before polymerization ; **B.** after polymerization. Peaks below 30 ml correspond to that of the lipid while peaks above 30 ml are from the buffer. The separation was carried out on a 30 x 1.2 cm Sepharose 4BCL column to which was added 0.5-1.0 mls of a liposome solution. The presence of lipid in the column was monitored using a UV detector ( $\lambda$ -280 nm). One can clearly see that in the case of the monomeric lipid (**A**), most of the sample elutes in the fractionation range of the column, whereas in the case of the polymer (**B**), the sample elutes in the void volume illustrating the polymerization-induced increase in particle size.



**Figure 17**

Concentration and temperature dependence of "the apparent size" of **A.** polymeric  $\omega$ -10; **B.** polymeric  $\omega$ -8; and **C.** DOPC SUVs. The polymeric samples had been polymerized, lyophilized and rehydrated for these experiments. However, as has been demonstrated, samples not been lyophilized display similar aggregation phenomena. This contrasts to SUVs, whose particle size is relatively concentration and temperature insensitive.





*Cu<sup>2+</sup>/Phenanthroline Polymerization.* An alternate polymerization protocol was evaluated to examine if the clearing and gelation of the short-chain  $\omega$ -THIOLS was due to degradation of the sample by lysolipid formation or hydrolysis of the choline group. The Cu<sup>2+</sup>/Phenanthroline method is gentler in that the polymerization is carried out at room temperature, pH 7.4 and for 30 minutes or less. The caveat of this method is the addition of extraneous and possibly perturbing components, and for this reason it was rarely used. Nonetheless, the results were even more dramatic. Figure 18 illustrates the gradual clarification of a vortex-mixed dispersion of  $\omega$ -11 during the course of polymerization. By contrast, similar treatment of  $\alpha$ -16 MLVs resulted in no apparent change of turbidity (Figure 18). Analysis of the presence of thiol groups using Ellman's reagent demonstrated conversion of the thiol group to the disulfide. The proton spectra of a chloroform/methanol solution of polymeric  $\omega$ -11 indicated the products of the Cu<sup>2+</sup>/Phenanthroline and H<sub>2</sub>O<sub>2</sub> polymerization were similar\* .

*Encapsulation of Aqueous Solutes in Polymerized  $\omega$ -THIOLS.* For polymeric  $\omega$ -THIOLS, attempts to entrap aqueous solutes were rather unsuccessful. This is shown by the comparison of the percentage of uridine entrapped for monomeric versus polymeric  $\omega$ -11,  $\omega$ -15 and  $\omega$ -16 (Table II). Attempts to entrap carboxyfluorescein was successful in the case of the monomers but not in the case of the polymers. The encapsulation data as well as the physical differences between monomeric and polymeric  $\omega$ -THIOLS suggest that polymerization may transform monomeric liposomes into non-vesicular structures. In the case of uridine encapsulation, the fact that a small but measurable amount of uridine is detected with the lipids could in fact be due to a small percentage of residual sealed liposomes.

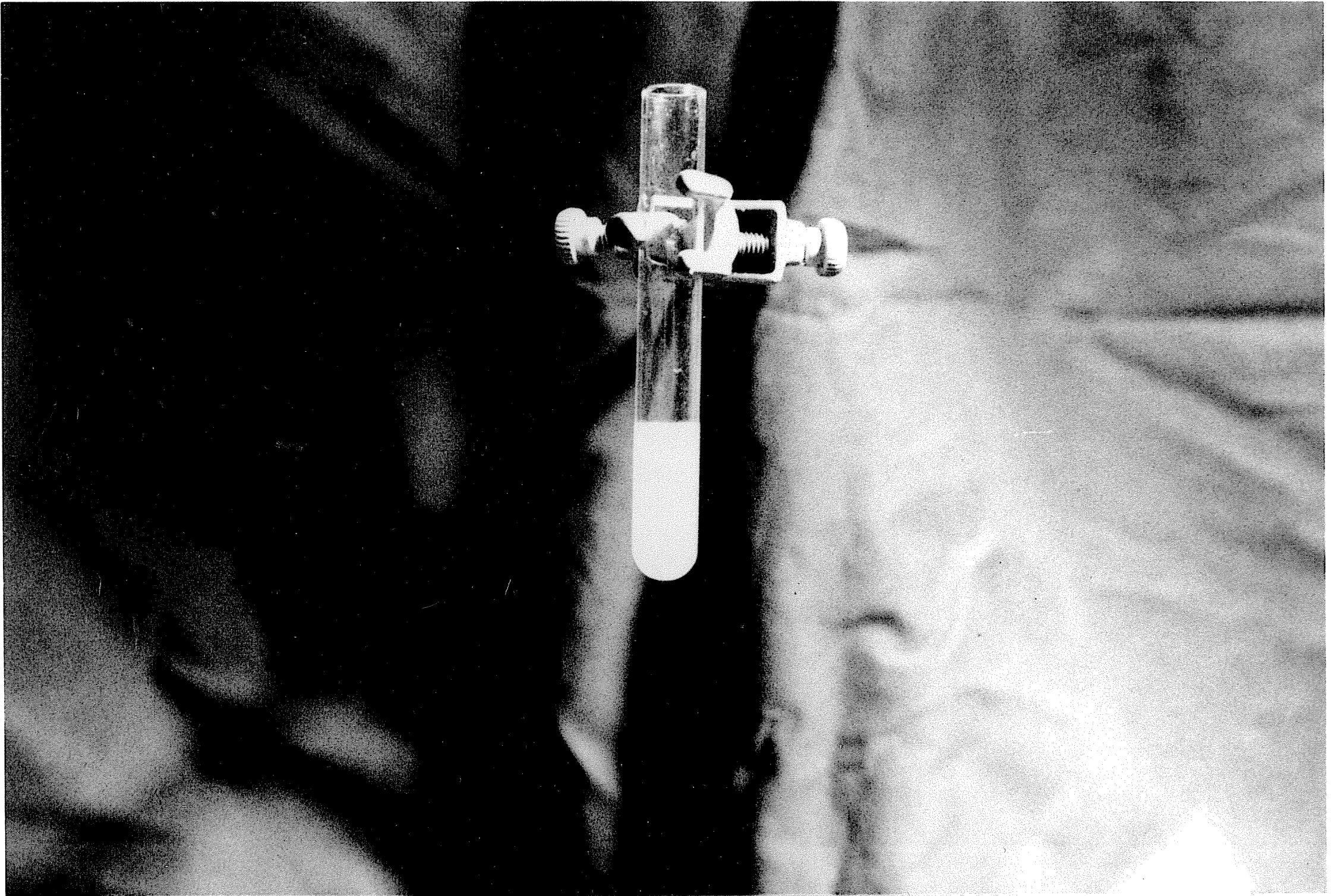
---

\* With the exception of the experiments just described all polymers described in this study were prepared by simple H<sub>2</sub>O<sub>2</sub> oxidation.

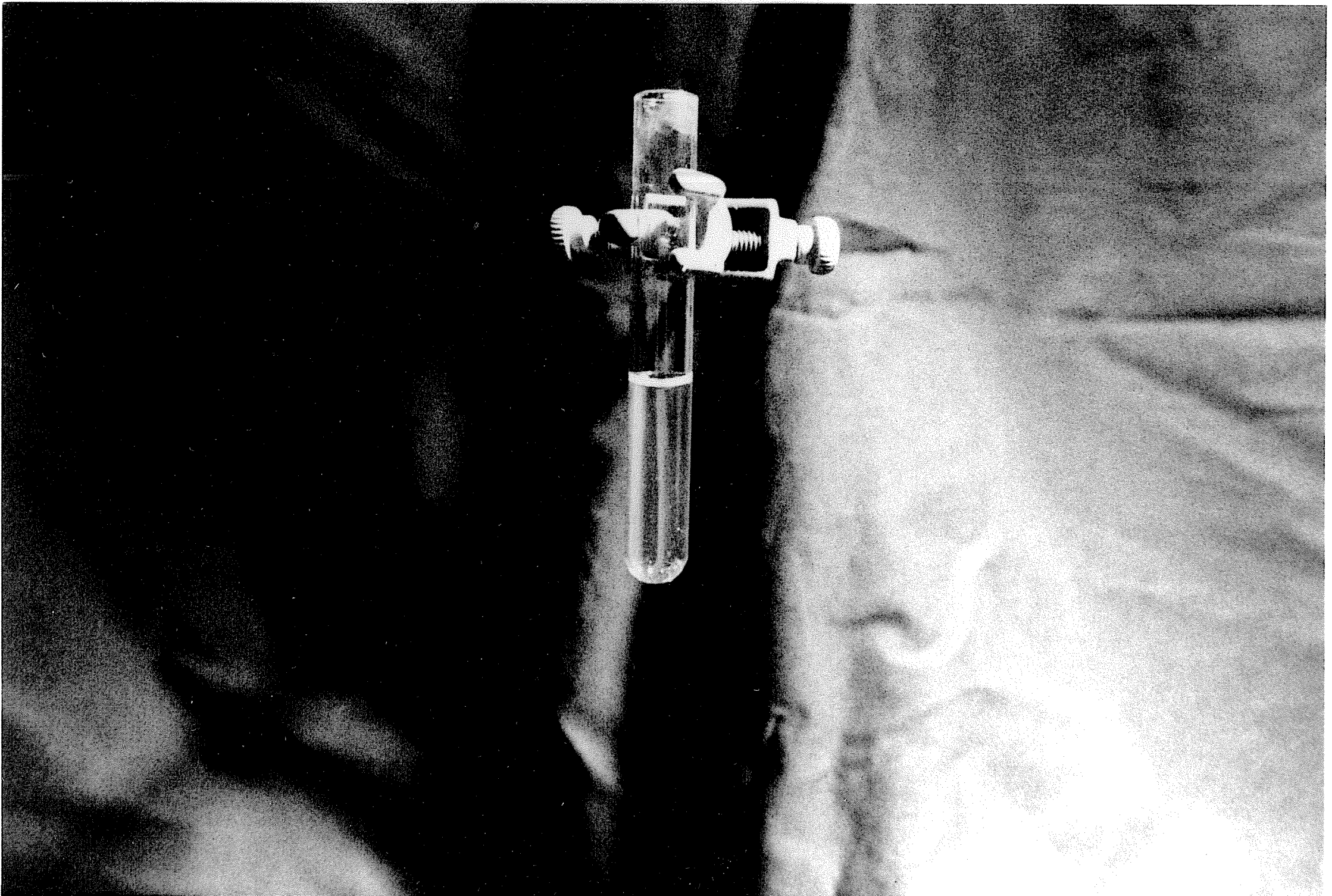
**Figure 18**

Demonstration of the morphological changes that occur in  $\omega$ -11 lipid dispersions but not in  $\alpha$ -16 dispersions on polymerization by the  $\text{Cu}^{+2}$ /Phenanthroline polymerization method. **A.** Monomeric  $\omega$ -11 before polymerization; **B.**  $\omega$ -11 after polymerization ( $\approx$  20-30 min); **C.** monomeric  $\alpha$ -16 before polymerization and **D.**  $\alpha$ -16 after polymerization.

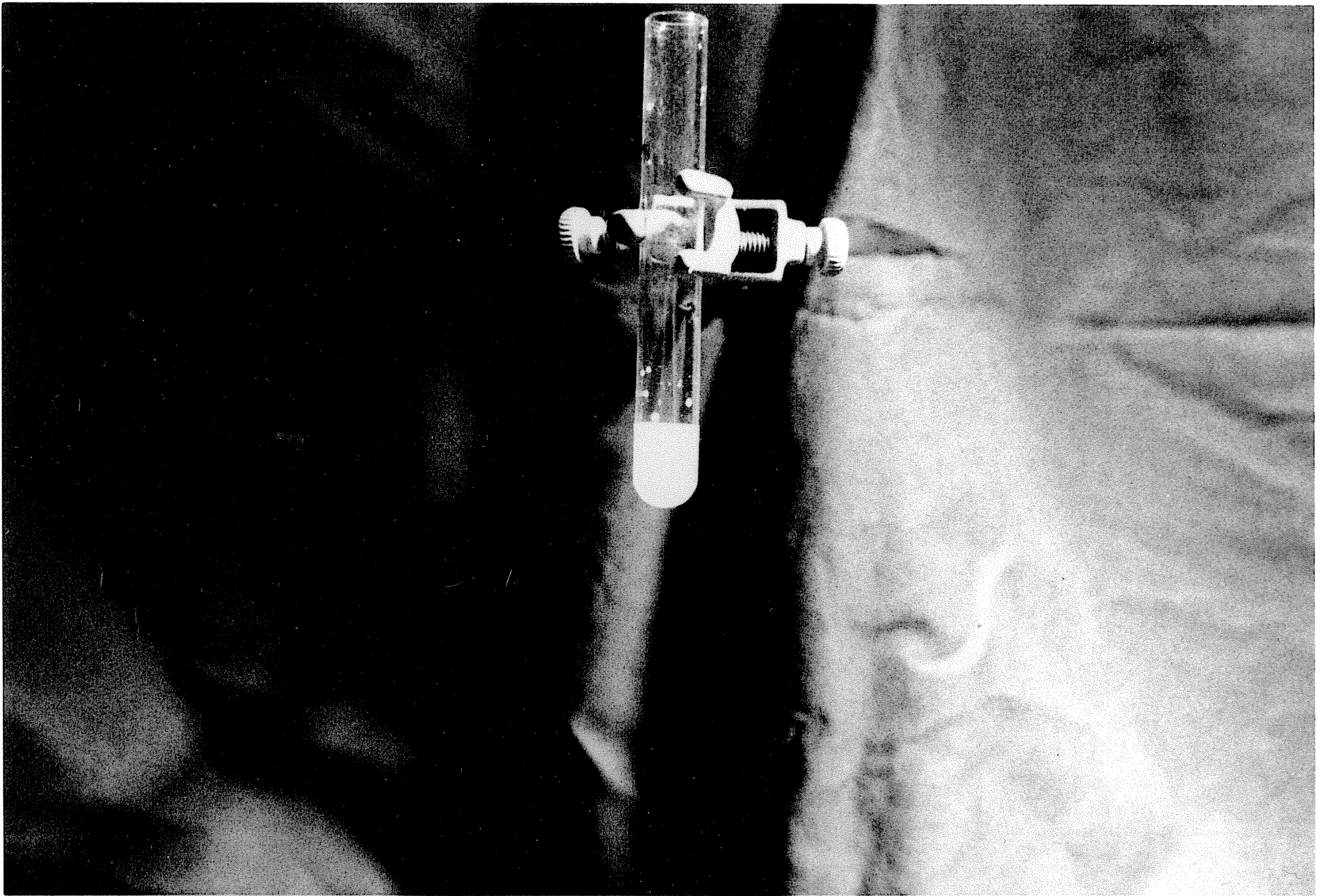
**A**



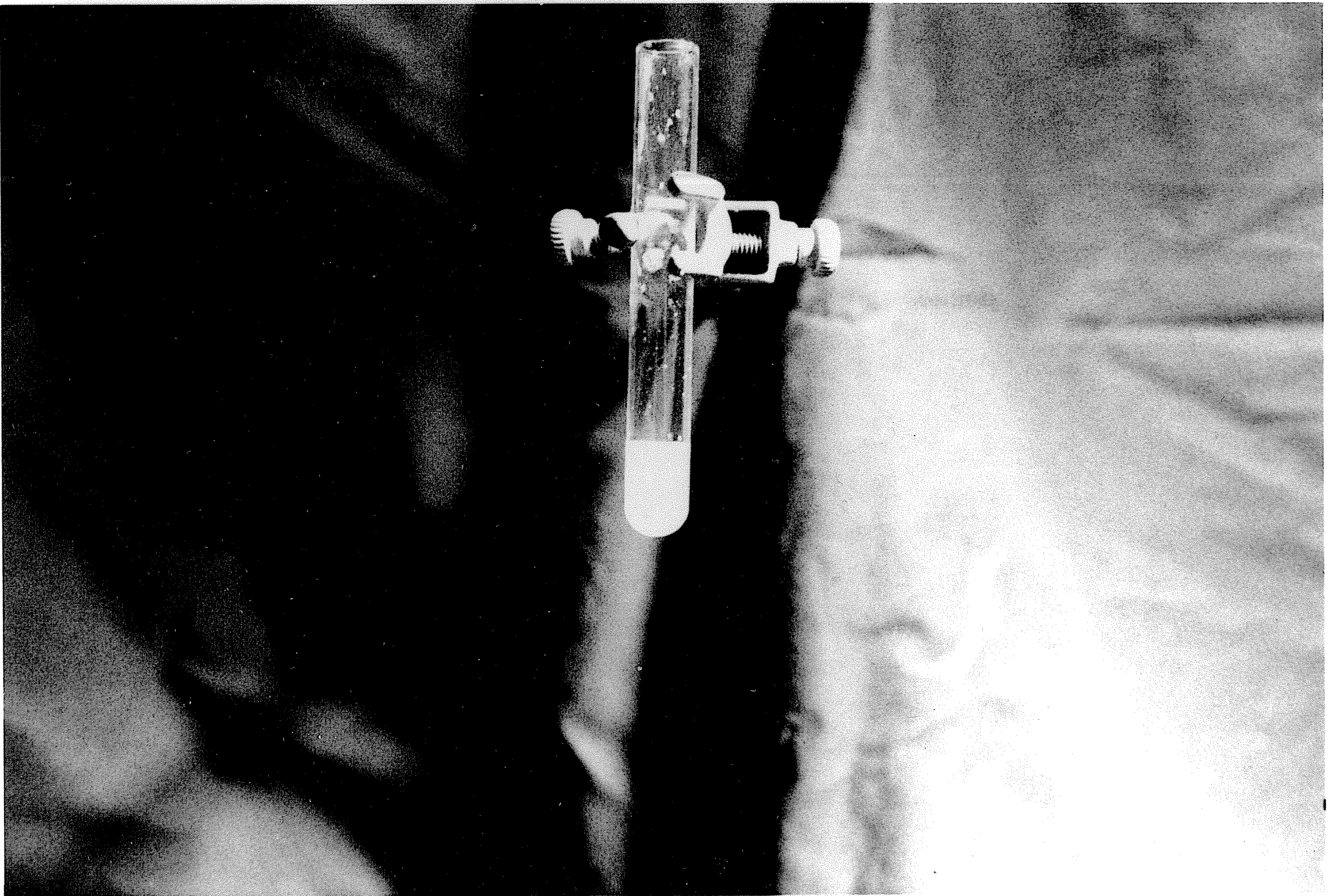
**B**



**C**



**D**



*Electron Microscopy of Polymerized  $\omega$ -THIOLS.* Using negative stain electron microscopy, visualization of the structures formed from polymeric  $\omega$ -THIOLS was not as straightforward as for the monomeric and polymeric  $\alpha$ -THIOLS or conventional liposomes. Generally, for polymeric  $\omega$ -11,  $\omega$ -15 and  $\omega$ -16, aggregated masses of material were observed without convincing resemblance to liposomes. Occasionally less aggregated structures were visible as shown in Figure 19 for polymeric  $\omega$ -15 MLVs and  $\omega$ -11 SUVs. The structures appear at low resolution as networks and at higher resolution as unsealed or crushed bilayers. Figure 19 D, which shows micrographs prepared from polymeric  $\omega$ -11 "SUVs" is similar to those shown for  $\omega$ -15 "MLVs" in the lack of distinctive liposomes.

In order to better visualize the morphology of the polymeric  $\omega$ -THIOLS, samples were prepared by thin section rather than negative stain. Figure 20 shows micrographs of polymeric  $\omega$ -16 prepared in this way. Bilayers are clearly visible but self-sealed liposomes were not observed. It appears that upon polymerization, fragmentation of the lamellae occurs. This may be a general phenomena of all the  $\omega$ -THIOLS examined\*. In the case of the shorter chain lipids (N=9-11), however, the greater hydrophilicity may promote formation of smaller fragments, perhaps with characteristics somewhat similar to those of micelles. Such structures would be consistent with the susceptibility of these lipids to aggregation and gelation. In all cases, fragmentation would account for the low entrapment of aqueous solutes.

*Preparation of  $\omega$ -THIOL Dispersions from Lyophilized Prepolymerized Lipids.*

As for the  $\alpha$ -THIOLS, samples of the  $\omega$ -THIOLS were also dialyzed and lyophilized after polymerization. The general behavior of the rehydrated samples

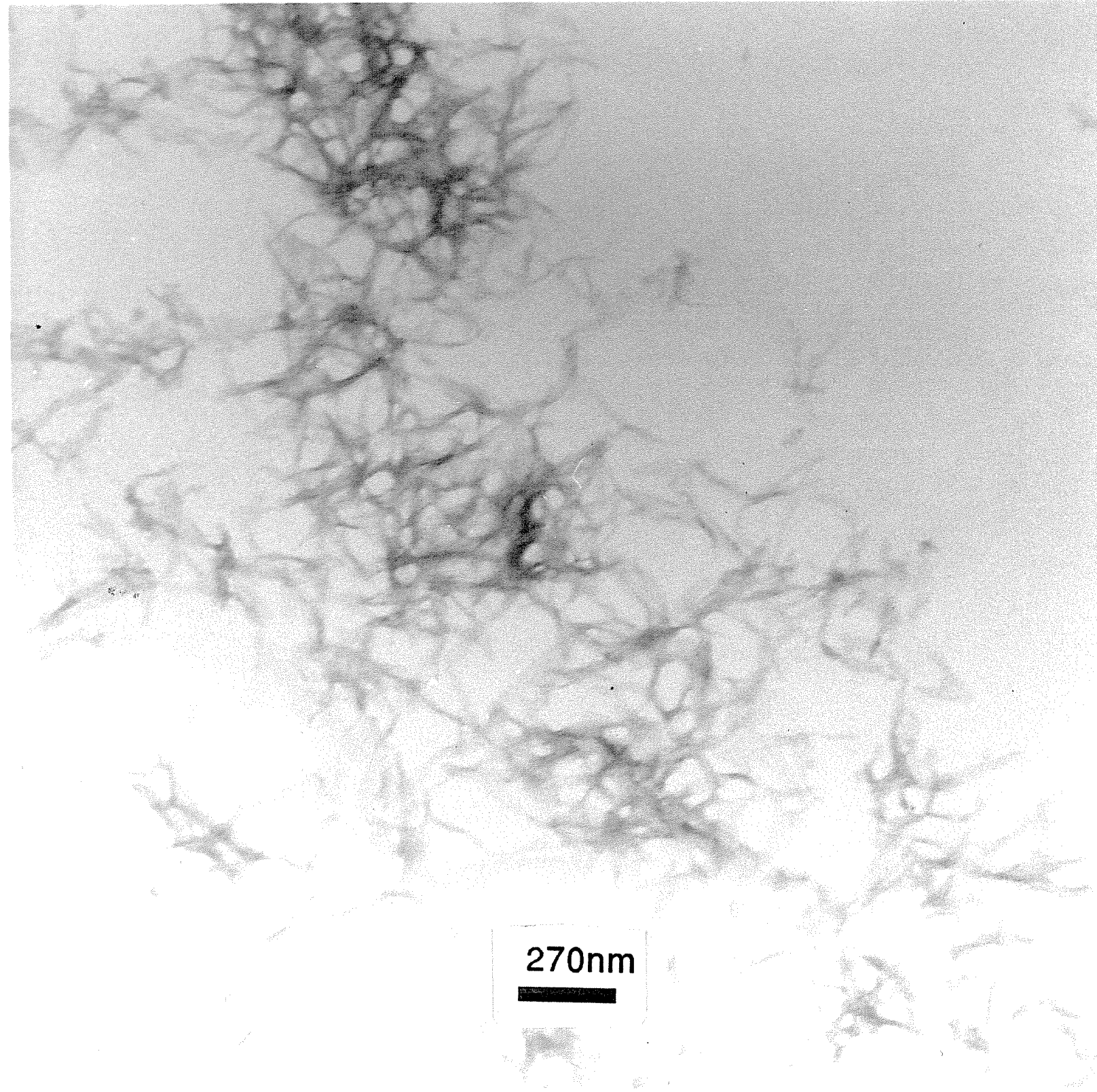
---

\* Similar EM experiments have not yet been carried out for other chain lengths.

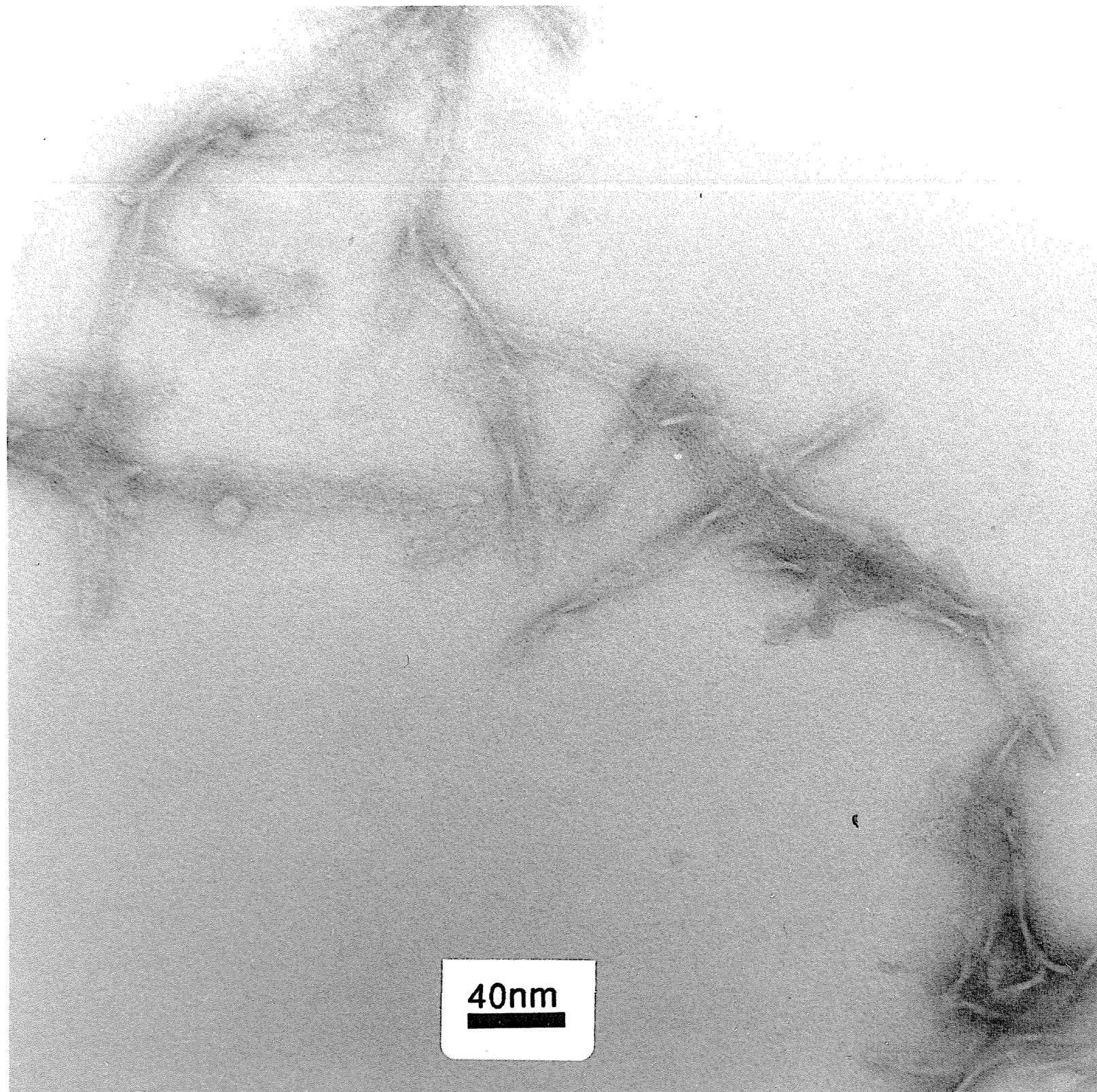
**Figure 19**

Negative stain electron micrographs of: **A - C.**  $\omega$ -15 dispersions following polymerization and dialysis; **D.**  $\omega$ -11 SUVs after polymerization and dialysis.

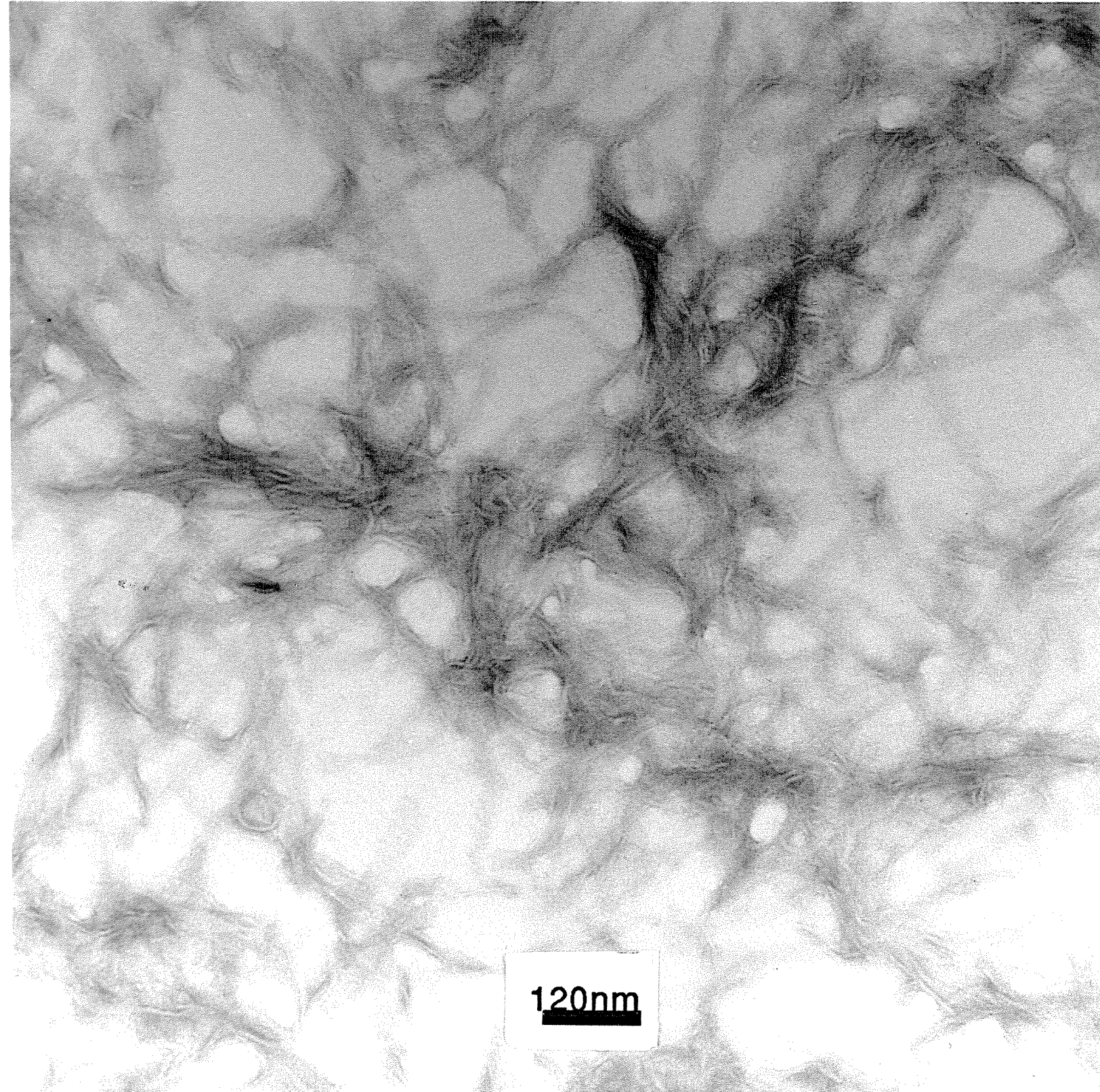
**A**



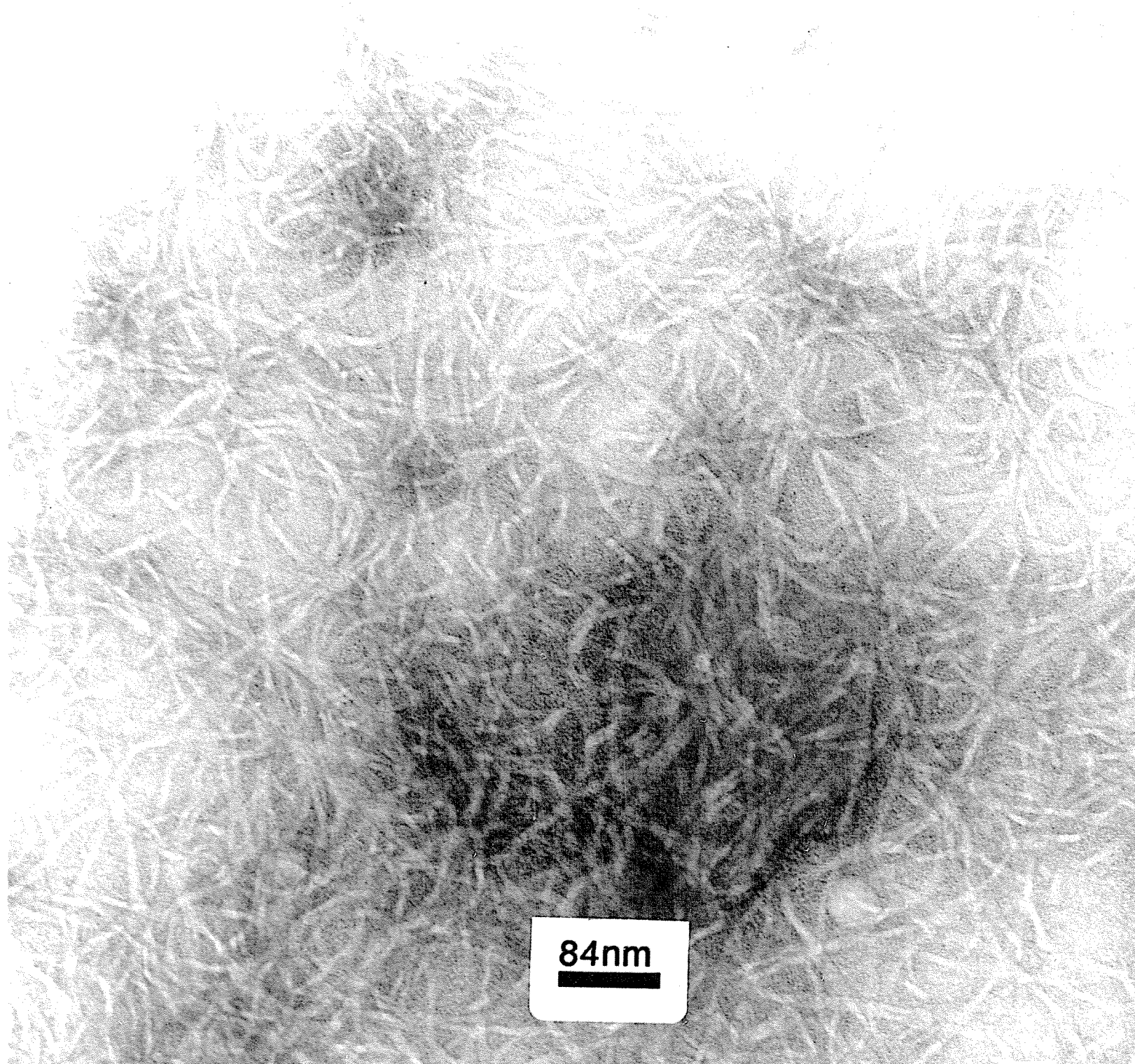
**B**



**C**

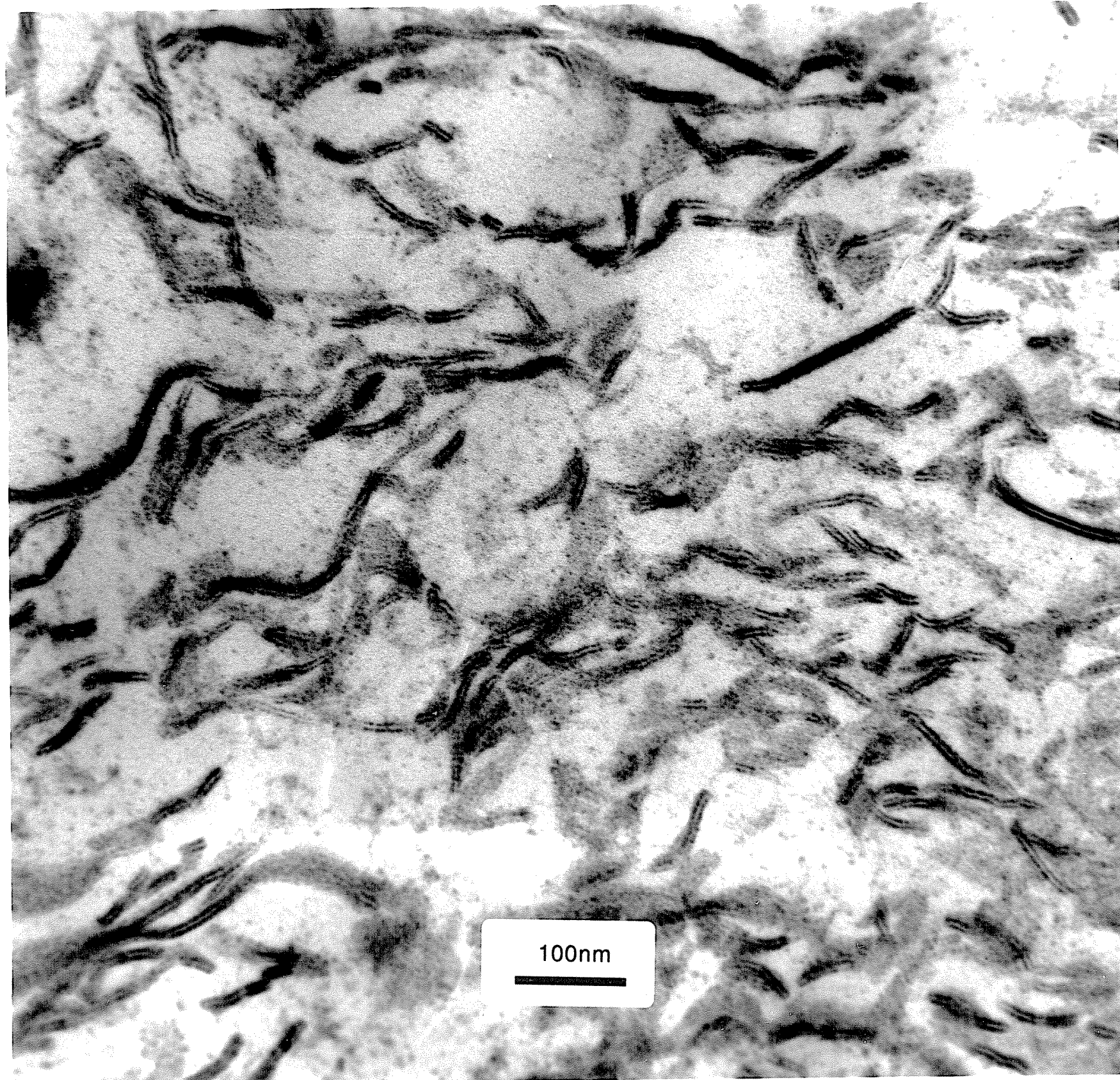
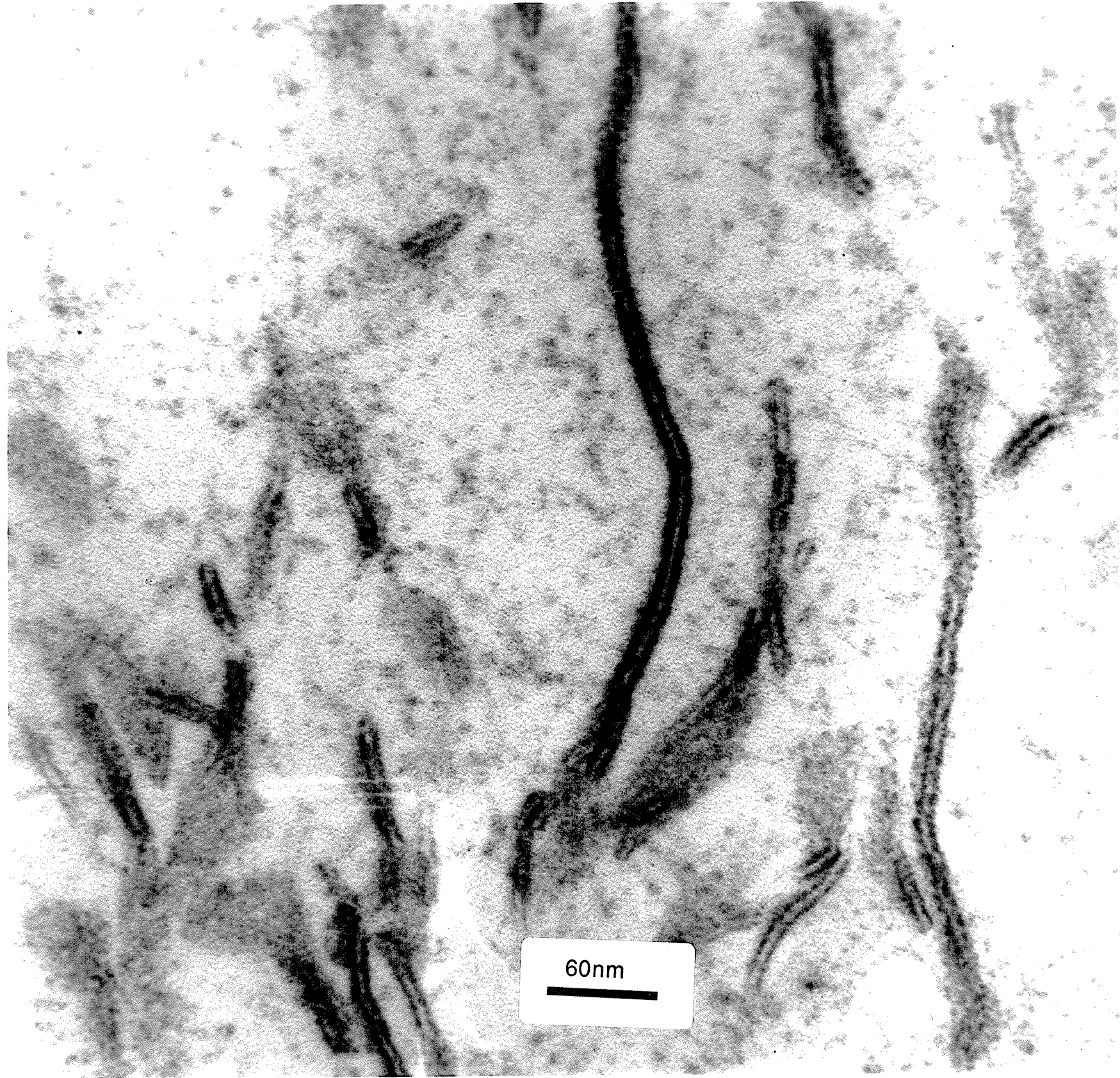


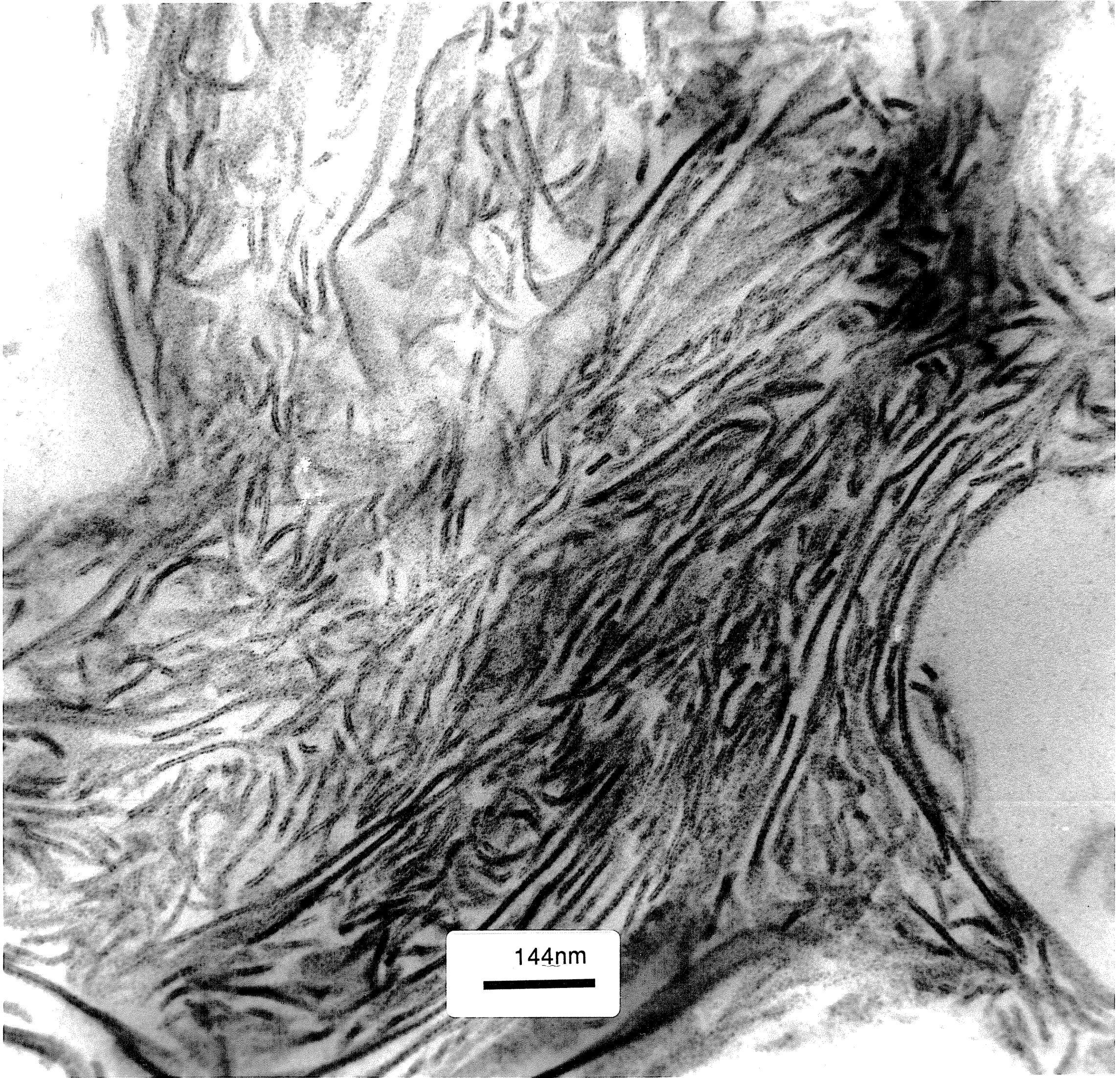
**D**



**Figure 20**

Electron micrographs of polymerized  $\omega$ -16 prepared by thin section.





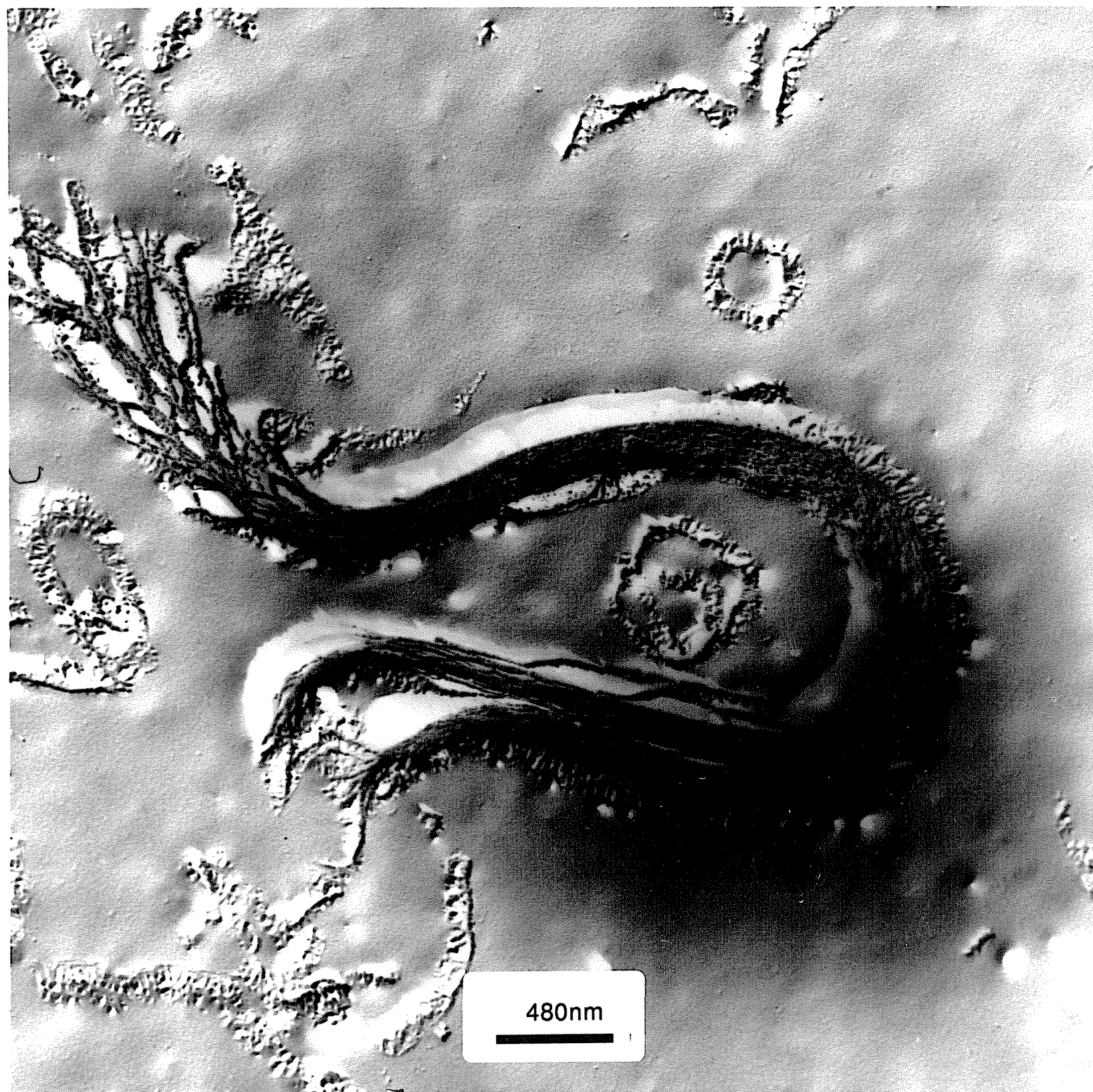
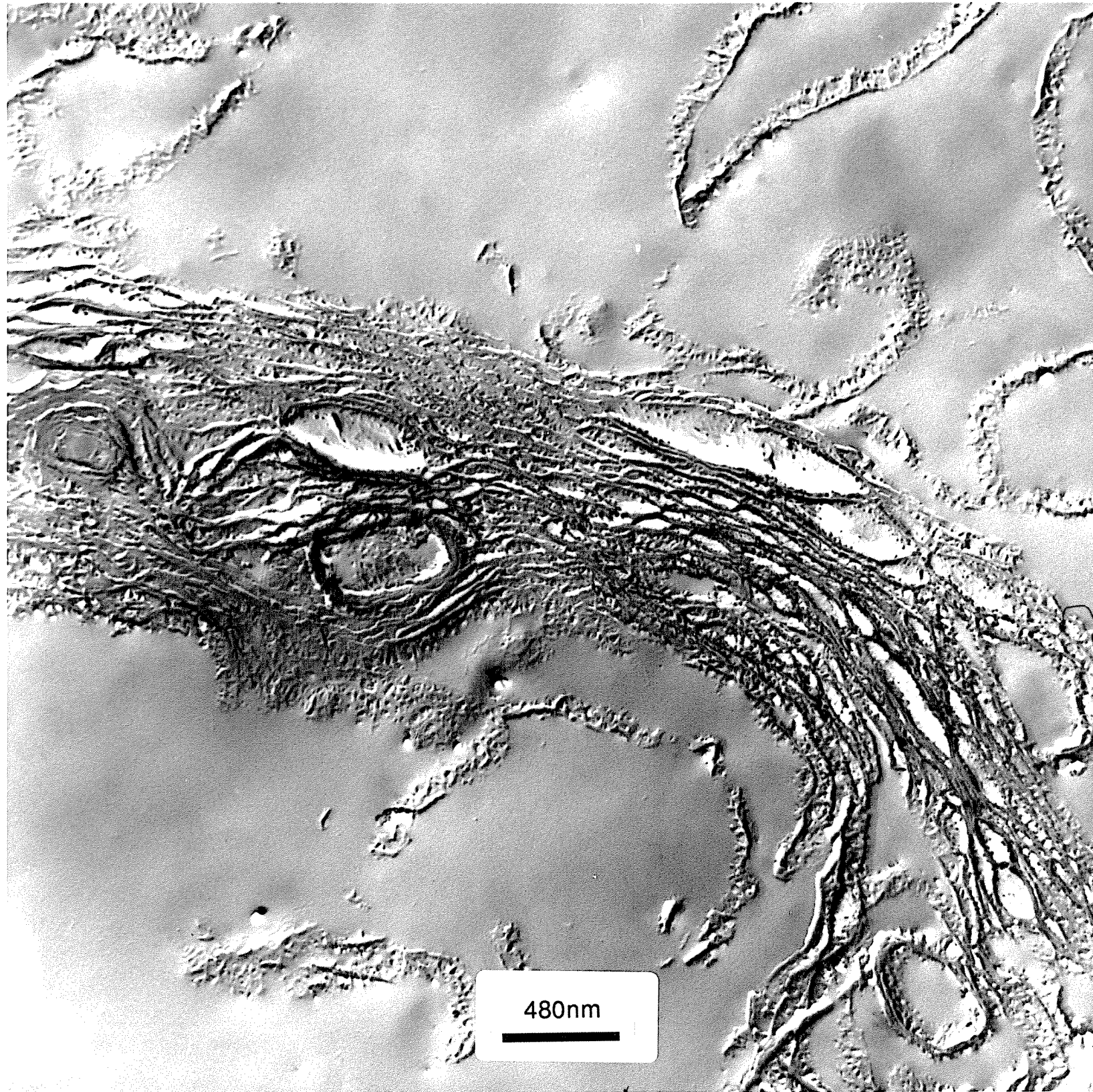
seemed quite similar to that of samples that had not been dehydrated. Sample clarification and gelation were generally observed for the rehydrated  $\omega$ -THIOLS (N=10-12) depending on the temperature and concentration of the sample. Turbid solutions were obtained for polymeric  $\omega$ -15 and  $\omega$ -16. In no case was entrapment of aqueous solutes possible either by hydration of the lyophilized polymers above the  $T_m$  in buffer containing carboxyfluorescein or by freezing and thawing. Also, DSC profile for polymeric  $\omega$ -15 samples with and without lyophilization were identical (data not shown). These data suggest that similar bilayer fragments are formed both by samples that have been lyophilized and those which have not.

To further establish the formation of bilayer fragments from hydrated polymers, samples were examined by electron microscopy. Using negative stain techniques, structures were observed, which were consistent with bilayer fragments and similar to that obtained for non-lyophilized samples. However, freeze fracture micrographs of polymeric  $\omega$ -15 MLVs show more definitively the onset of fragmentation (Figure 21). Whether the sizes of the fragments are similar in both lyophilized and non-lyophilized samples is not known. It is likely that fragment size or propensity for fragmentation may depend on a number of variables (i.e. concentration, temperature, sample history, polymerization conditions), in a way that has not yet been systematically characterized.

At this point, some consideration must be given for the inconsistencies between the data we report here for polymeric  $\omega$ -THIOLS and that reported by Regen in the original publication on the disulfide-polymerizable phosphatidylcholines. First, it should be noted that we have obtained identical-looking polymerized vesicles to that depicted in reference 23 by UV polymerization of  $\omega$ -THIOLS SUVs. However, both groups are now cognizant of the fact that the chemistry that occurs on photopolymerization is more complicated than disulfide formation. Proton NMR in fact

**Figure 21**

Freeze fracture electron micrographs of  $\omega$ -15 dispersions that had been polymerized,  
lyophilized and rehydrated.



indicated substantial loss of both thiol and disulfide groups. Most data from both groups, however, involved oxidatively polymerized lipids and it is here where the differences arise. Whereas Regen *et al.* report retention of morphology after polymerization of the  $\omega$ -THIOLS, our data is most consistent with structural reorganization. There are several possible explanations for our differing conclusions. The most likely, however, is differences in the polymerization conditions. We routinely polymerize at a 5-fold higher concentration (5 mg/ml vs 1 mg/ml). For reasons that are not clear, the morphological changes that we observe may not occur at 1 mg/ml. We have not investigated this point due to the greater amounts of material necessitated by most of our experiments. On the other hand, if the changes described in the text do occur even at 1 mg/ml, visually and by absorbance spectroscopy, they may go undetected at this low concentration. In this regard, the light scattering experiments described in this report were extremely useful in identifying the large size of the deceptively translucent polymeric  $\omega$ -11 "SUVS".

#### Morphology of $\omega$ -THIOL/Cholesterol Mixtures and Dimer-Forming $\omega$ -THIOLS.

Cholesterol was incorporated into monomeric  $\omega$ -THIOLS liposomes to examine the morphology of polymeric membranes "diluted" with a nonpolymerizable component. For these experiments, bath sonicated  $\omega$ -11/Chol SUVs were prepared and polymerized under the same conditions as the pure  $\omega$ -THIOLS. As shown in Table II, the turbidity of  $\omega$ -11/Chol SUVs was relatively unchanged before and after polymerization. Electron micrographs of polymerized  $\omega$ -11/Chol SUVs suspensions confirmed the presence of sealed liposomes (Figure 22). It is not clear whether the addition of cholesterol to prepolymerized lipid has the same effect.

**Figure 22**

Negative stain electron micrographs of polymerized 2:1  $\omega$ -11/CHOL SUVs

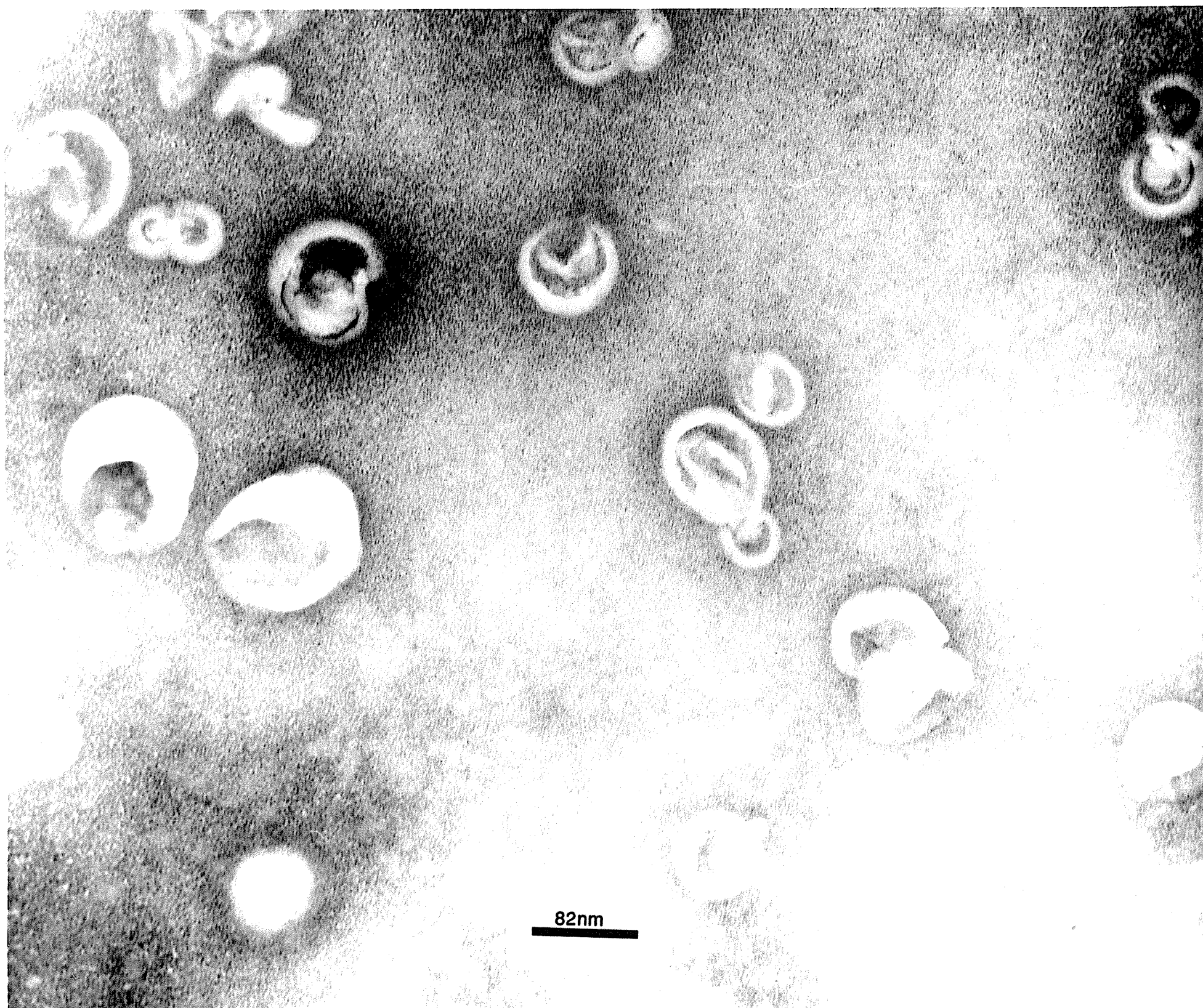
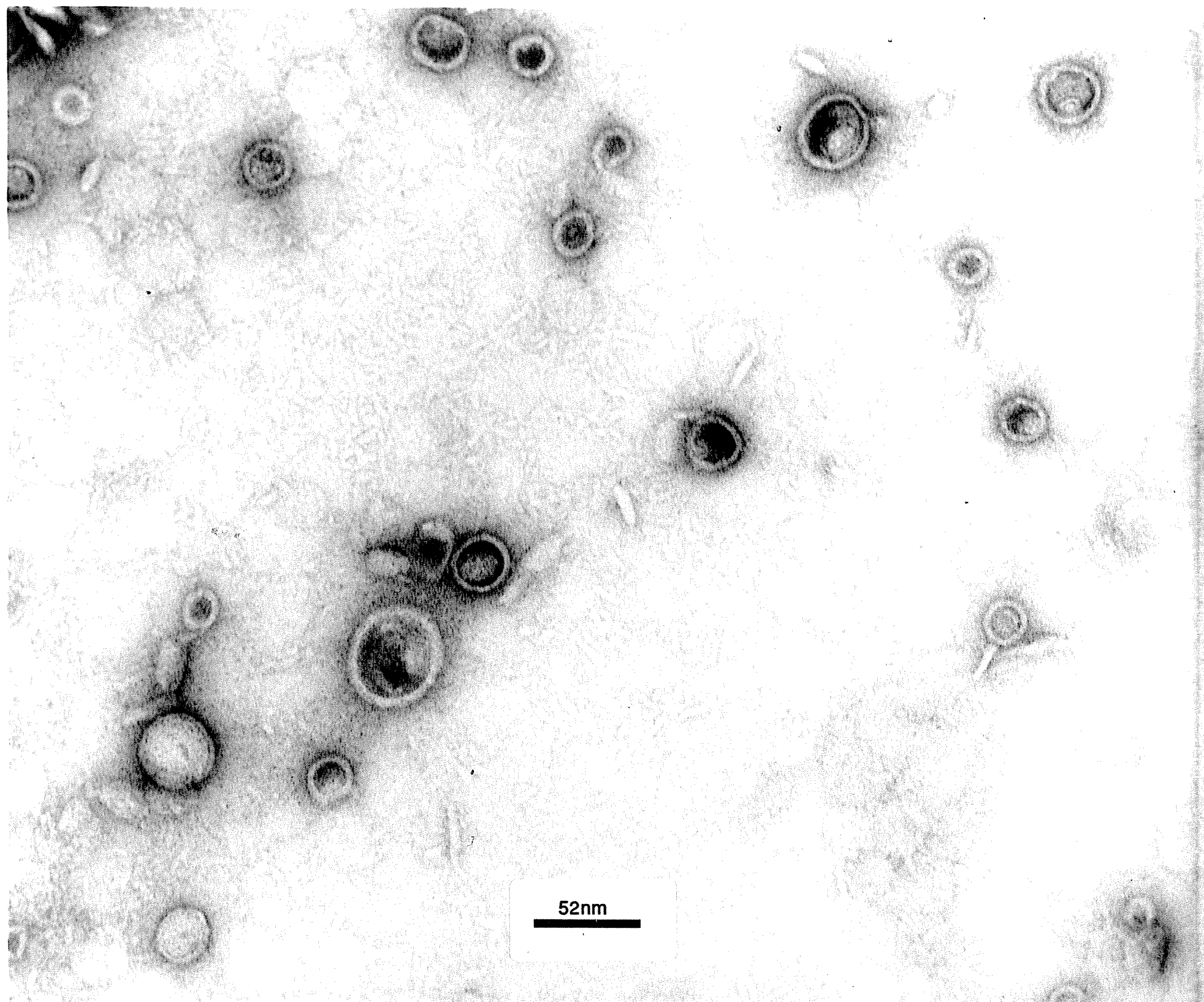
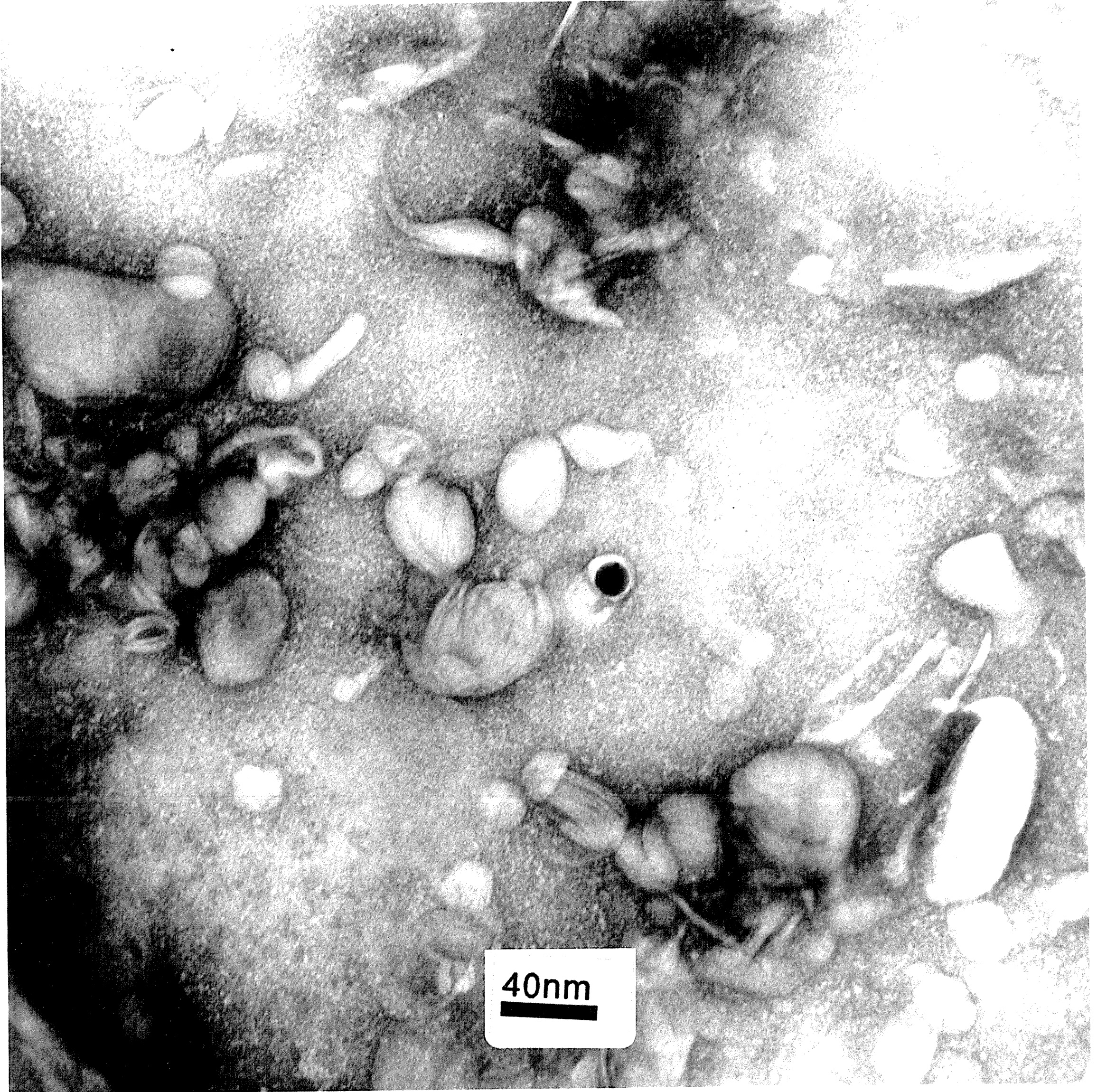


**Figure 23**

Negative stain electron micrographs of dimerized  $\omega$ 16-DPL dispersions.



Several possible explanations may explain the effects of cholesterol on the maintenance of sealed liposomes. First, it is very likely that cholesterol limits the size of the oligomer chains formed during polymerization. Smaller chains, if produced in the mixtures with cholesterol, may be able to organize more favorably into bilayer structures. Secondly, the presence of the mobile side chain on the steroid may provide enough mobility to the bilayer midplane to accommodate transient defects and thereby prevent fragmentation. For these reasons, mixed chain lipids were prepared, which have the thiol-containing fatty acid in the sn-2 chain and a nonpolymerizable saturated fatty acid in the sn-1 chain. (The notation used is sn2-sn1; i.e.  $\omega$ 16-DPL refers to 1-(hexadecanoyl)-2-(16-mercaptohexadecanoyl)-L- $\alpha$ -phosphatidylcholine and  $\alpha$ 18-DSL refers to 1-(octadecanoyl)-1-(2-mercaptooctadecanoyl)-L- $\alpha$ -phosphatidylcholine). These lipids are capable of forming dimers only. Furthermore, the nonpolymerizable fatty acid should contribute a fluid component to the hydrocarbon region of the bilayer. Various combinations of chain lengths were used to optimize the different depths of penetration of the two fatty acyl chains into the bilayer, known to occur for conventional phosphatidylcholines (38,39). In all cases, it was possible to entrap carboxyfluorescein from dispersions prepared from predimerized lipids. The presence of liposomes was also confirmed by negative stain electron microscopy (Figure 23), consistent with the work of Runquist, who showed liposome formation for DPL- $\omega$ 16 (which has the polymerizable moiety was in the sn-1 chain) (40).

## DISCUSSION

The results described in this chapter have shown drastically different behavior for thiol-containing phospholipids depending on the position of the polymerizable group. For monomeric  $\alpha$ -THIOLS (N=16-20), both multilamellar and small unilamellar

vesicles were readily formed. Consistent with earlier reports on  $\alpha$ -16, the gross morphology of SUVs was retained on polymerization, signifying a stable arrangement and minimal distortion of the lipid chains. It was also demonstrated that if the lipids were prepolymerized as multilamellar dispersions and subsequently lyophilized, they could be redispersed to form large liposomes or sonicated into SUVs. As shown in separate studies, this is likely due to the fact that the molecular structure of the polymer has internal motions that parallel those of nonpolymerizable phosphatidylcholines (mobile chains, a freely rotating headgroup and a rigid interfacial region). According to the work of Ringsdorf *et al.* on self-assembling polymeric lipids, the crucial element here is chain mobility (21,22). The short oligomeric chains estimated for the polymeric lipids are also likely to enhance the ease with which the lipids assemble into stable bilayers or can be reorganized by sonication into smaller structures.

It is interesting to note that formation of SUVs from the  $\alpha$ -THIOLS (both monomeric and polymeric, N=16-20) proceeds much more readily than nonpolymerizable analogues. Furthermore, they are much less subject to aggregation with time on standing at temperatures below the phase transition. By contrast, DSPC SUVs have been found difficult to make due to rapid flocculation, and diarachidoyl (N=20) SUVs have never been reported, to our knowledge. This seems to imply that the headgroups are slightly more hydrated, and the chains, less crystalline, at least in the gel state. Reduction in the temperature and enthalpy of the phase transition for the  $\alpha$ -THIOLS compared to conventional phosphatidylcholine analogues corroborates this interpretation (shown in the next chapter). Thus the presence of the sulfhydryl in the monomer and the disulfide in the polymer appears to reduce the packing density relative to phosphatidylcholine analogues. Several structural possibilities may be invoked to explain this, including (i) steric bulk of the sulfur atoms, (ii) increased hydration as a consequence of additional interfacial polarity, and/or (iii) a slightly different orientation

of the chains, which exposes the sulfhydryl/disulfide moiety more to the aqueous media and thereby increases the cross-sectional area per lipid molecule.

Contrary to *a priori* expectations, it was also noted that unsonicated dispersions prepared from prepolymerized  $\alpha$ -THIOLS were in general, smaller and more unilamellar than equivalent preparations of monomeric and particularly nonpolymerizable phosphatidylcholines.\* One way to rationalize this is to invoke the theoretical analysis of Israelachvili and others, which emphasizes the importance of molecular geometry (and entropy) on the morphology assumed by various amphiphiles (41-43). Without going into detail, it is sufficient to note that the fact that smaller liposomes are formed from polymeric  $\alpha$ -THIOLS suggests that the average headgroup area is larger than that for monomeric  $\alpha$ -THIOLS or nonpolymerizable phosphatidylcholines. In light of the above discussion on the effect of the presence of the sulfhydryl/disulfide moiety on chain packing, this is easy to comprehend for polymeric  $\alpha$ -THIOLS, compared to nonpolymerizable phosphatidylcholines. However, a larger headgroup area for polymeric versus monomeric  $\alpha$ -THIOLS is not intuitive unless it is assumed that the organization of the lipids in the membrane is somewhat different. In the case of monomeric  $\alpha$ -THIOLS, the lipids are free to pack in an energetically favorable manner. In the polymer, this must be restricted to some degree. Thus it is likely that while covalently-linked lipids are closely opposed, their conformational freedom to tightly pack with uncoupled neighboring lipids from a distant part of the same oligomer chain or from a different chain, will be inhibited. The net result of this should be formation of a corrugated or inhomogeneous interface with coupled lipids in tight juxtaposition but sequestered from other nonbonded lipids via surface defects. It is likely that in such defects, water can penetrate further into the interface. If this is the case, on average, the area per headgroup (including hydration)

---

\* Whether this reorganization to smaller sizes occurs during the polymerization or as a consequence of lyophilization and rehydration, is not yet known.

may be slightly larger than that of monomeric  $\alpha$ -THIOLS. Furthermore, this would account for their smaller size and facile hydration. Similar conclusions concerning the introduction of defects into the membrane interface as a consequence of polymerization have been described by Reed *et al.* (44).

In support of the above discussion, it has been determined from x-ray data (45) that the thickness of polymeric  $\alpha$ -16 bilayers is less than that reported for DPPC. This could arise from (i) chain tilting (ii) disordered chains or (iii) partial interdigitation of the chains, all of which may be the consequence of an increased headgroup area (41).

$\omega$ -THIOLS. Completely different properties were exhibited by the  $\omega$ -THIOLS where the sulfhydryl or disulfide is at the chain terminus. Monomeric  $\omega$ -THIOLS clearly formed liposomes as was shown by electron microscopy and entrapment of aqueous solutes. Surprisingly, bilayers were stable down to chain lengths of at least 11 carbons, and from preliminary data, it appeared that  $\omega$ -9 and  $\omega$ -10 could also form liposomes. This suggests that the polarity of the sulfhydryl group does not disrupt the packing of the chains. On the contrary, the sulfhydryl group appears to stabilize bilayers of even very short chain  $\omega$ -THIOLS. The basis for the stabilizing effect is not known but could be due to H-bonding between the sulfhydryls. Alternatively, by virtue of its higher molecular weight relative to the terminal methyl group, the "heavy" sulfhydryl could slow the frequency of off-axis excursions and internal motions of the chains, which tend to reduce intermolecular van der Waals attraction and thereby destabilize bilayer formation. Such a mechanism has been postulated for phosphatidylcholines with halogens substituted at the chain terminus (46).

On polymerization of the  $\omega$ -THIOLS, drastic alterations in the morphology of the unpolymerized liposomes take place. Short-chain  $\omega$ -THIOLS (N=9(?),10,11) that have been sonicated into SUVs form clear to opalescent viscous gels upon

polymerization at concentrations as low as 5 mg/ml. The clarity, viscosity and apparent size is concentration dependent in a manner inconsistent with retention of the SUV structure. MLVs of longer chain  $\omega$ -THIOLS (N=15,16) remain turbid, but the "texture" changes from opaque, nonviscous dispersions to more translucent but gelatinous particles, in many ways similar to the short-chain analogues. Whereas monomeric  $\omega$ -11 to  $\omega$ -16 encapsulated aqueous solutes, polymeric  $\omega$ -THIOLS did not. Taken together, these data suggest formation of nonliposomal structures as was corroborated by the observation of bilayer fragments in the electron micrographs of  $\omega$ -15 and  $\omega$ -16. In the limit of very short chains, (i.e. N=8,9), polymeric micelles or small fragments are likely formed.

The physical basis for the fragmentation of polymeric  $\omega$ -THIOLS is not yet understood. However, it seems very likely to be related to the fact that the bilayer midplane is rigidified, a physical state that may be detrimental to the ability of the lipids to respond to transient defects. In normal bilayers, a fluidity gradient extends from the interface to the membrane interior such that the chain terminus is the most fluid portion (25,47). Potential "voids" that might arise in a given region of the bilayer as a consequence of either small temporal chain fluctuations or gross changes brought about by passage through the phase transition can therefore be obviated by lateral expansion or segmental isomerization of the chains. If the mobility is considerably reduced by polymerization, there may be insufficient elasticity to compensate for the defects, thereby leading to fragmentation. In this regard, it is important to note that in a separate chapter, it is shown by  $^{13}\text{C}$  NMR relaxation and other techniques, that the polymeric  $\alpha$ -THIOLS that maintain a closed bilayer structure have a mobility profile similar to that of nonpolymerizable phosphatidylcholines. By contrast, similar experiments with polymeric  $\omega$ -THIOLS verify the absence of a mobility gradient.

The presence of cholesterol in the membrane prior to polymerization was shown to inhibit the transformation from closed liposomes to bilayer fragments. There are several possible explanations for this behavior. If we assume for the present that the above explanation provides a reasonable basis for fragmentation of the  $\omega$ -THIOL bilayers, then: (i) it is possible that at the mole ratios used (2:1  $\omega$ -11/Chol), the steroid alkyl chain adds sufficient mobility to the bilayer interior to allow for adjustments in the hydrocarbon organization to take place without fragmentation. (ii) Secondly and perhaps more importantly, it is well recognized that the phase transition is abolished in 2:1 mixtures of PC/Chol (i.e. DPPC/Chol) due to the interaction of the steroid with the PC component (58). Thus the extensive reorganizations of the bilayer that normally occur at the phase transition are inhibited. While this might be anticipated as an irrelevant point concerning polymeric  $\omega$ -THIOLS (since to date no chain-terminating polymeric lipids have been reported that retain their phase transition) it is shown in a later chapter that  $\omega$ -THIOLS in *both* the polymeric and monomeric states have gel to liquid-crystalline phase transitions. Thus the presence of cholesterol in the case of polymeric  $\omega$ -THIOLS may preserve the original liposome morphology by minimizing the temperature dependent fluctuations in the bilayer organization which, as described above, could conceivably lead to fragmentation in a rigid system. (iii) A final possibility is that the presence of the cholesterol restricts the degree of polymerization to even smaller values than the reported 10-30 units/chain for bilayers composed exclusively of disulfide phosphatidylcholines. Small fragments may, in fact, be able to organize more efficiently than large oligomers since the required motions would necessitate cooperativity among fewer coupled lipids.

In consideration of (i) and (iii) above, mixed-chain dimerizable lipids were also prepared. These lipids were able to form liposomes from a predimerized state. Whether

this is due to the unrestricted motion of 50% of the alkyl chains, the short oligomer size (DP=2), or both is unclear.

Having proposed some type of mechanism for the fragmentation, it is necessary to reconcile our observations on the  $\omega$ -THIOLS with that reported for other chain-terminating polymerizable phospholipids. As was mentioned in the introduction, several types of polymerizable phospholipids with the polymerizable moiety at the chain terminus have been synthesized and studied. These include methacryl, sorbyl and vinyl-based lipids. In all reported cases, liposomes were formed from the monomers and the original structures were retained on polymerization. To rationalize the differences between these lipids and the polymeric  $\omega$ -THIOLS, we must consider structural characteristics of the polymeric membranes that might distinguish liposome-forming from fragment-forming lipids. The double chain ( $\omega$ -DPL) and single chain ( $\alpha$ -MA and  $\omega$ -MA) methacryl-based phosphatidylcholines are useful as a point of comparison because their properties have been thoroughly examined (1-4,9,13). Figure 23 depicts the structures of  $\alpha$ -MA and  $\omega$ -MA and how polymerization is envisioned to occur for these lipids.  $\omega$ -DPL is similar to  $\omega$ -MA except that both chains contain polymerizable moieties.

First, it has been demonstrated that a high degree of polymerization (DP) can be achieved by methacryl phospholipids. For poly( $\alpha$ -MA) and poly( $\omega$ -MA) that have the polymerizable moiety in a single chain or the headgroup, the DP was estimated as approximately 500 units per chain (9). For the double chain lipid ( $\omega$ -DPL) the DP would be expected to be at least as high. Furthermore, membranes resulting from polymerization of these lipids may be highly crosslinked networks. By contrast, thiol-based phosphatidylcholines form short oligomers (DP=10-30) (24) and have the potential for forming linear polymer chains only. Intuitively, one would anticipate that for high molecular weight and certainly crosslinked polymeric membranes, it would be

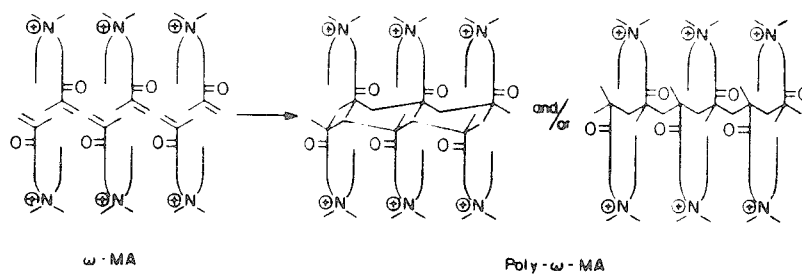
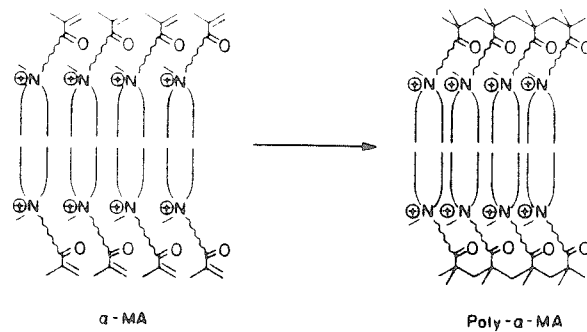
energetically prohibitive for the chains to reorganize into alternate morphologies following polymerization. By contrast, short uncrosslinked chains should be able to adopt different structures more readily.

A second difference between  $\omega$ -DPL and the  $\omega$ -THIOLS is that for  $\omega$ -DPL, the phase transition is abolished by polymerization (13). In the case of the  $\omega$ -THIOLS, it is retained and shifted to higher temperature (as described in Chapter III). Consequently, as a function of temperature, reorganizations of the chains within the  $\omega$ -DPL bilayer may be minimal so that temperature-induced defects are not created. By contrast, for  $\omega$ -THIOLS, membrane damage could be induced either at high temperature where the lipid chains are in a relatively disordered state, or by passage from high to low temperature where the chain rigidity may "freeze in" defects created in the liquid-crystalline state.

Finally, both  $\omega$ -DPL and the  $\omega$ -THIOLS have the potential for *intra-* as well as *inter-* leaflet coupling (13,24). All other things being equal, it would seem that fragmentation would be less probable if both halves of the bilayer were coupled. An appropriate model for fragmentation of bilayers polymerized by inter- and intra-leaflet coupling is hard to conceive. Thus if we assume that  $\omega$ -DPL is polymerized in both ways but the  $\omega$ -THIOLS are polymerized predominantly or exclusively within a given half of the bilayer, the susceptibility of  $\omega$ -THIOLS to fragmentation could be further rationalized on the basis of the coupling patterns. While we certainly have no proof of the polymerization patterns in either case, it would seem that the presence of a phase transition in polymeric  $\omega$ -THIOLS would argue for intra-leaflet coupling, at least if we assume that the changes that occur in the packing of the lipids at the  $T_m$  is similar to that of nonpolymerizable phosphatidylcholines. In such a case, we imagine the not so inconceivable possibility, that two linked chains from adjacent lipids would isomerize in some way as a coupled unit. Similar changes in chain packing that would lead to a

**Figure 23**

Schematic representation of the methacryloyl lipids  $\alpha$ -MA and  $\omega$ -MA in a bilayer arrangement before and after polymerization. Taken from reference (8).



substantial phase transition are difficult to envision for lipids polymerized across the bilayer.

### REFERENCES

1. Regen, S., Singh, A., Oehme, G. and Singh, M. (1981) *Biochem. Biophys. Res. Comm.* **101**, 131-136.
2. Juliano, R.L., Regen, S.L., Singh, M., Hsu, M.J. and Singh, A. (1983) *Biotechnology* 882-885.
3. Regen, S.L., Singh, A., Oehme, G. and Singh, M. (1982) *J. Am. Chem. Soc.* **104**, 791-795.
4. Regen, S. L., Czech, B. and Singh, A. (1980) *J. Am. Chem. Soc.* **102**, 6638-6640.
5. Akimoto, A., Dorn, K., Gros, L. Ringsdorf, H. and Schupp, H. (1981) *Angew. Chem. Int. Ed. Engl.* **20**, 90-91.
6. Hub, H., Hupfer, B., Koch, H. and Ringsdorf, H. (1980) *Angew. Chem. Int. Ed. Engl.* **19**, 938-940.
7. Hupfer, B., Ringsdorf, H. and Schupp, H. (1983) *Chem. Phys. Lipids* **33**, 355-374.
8. O'Brien, D.F., Whitesides, T., Klingbiel, R. (1981) *J. Polymer Sci.: Polymer Letters Ed.* **19**, 95-101.
9. Dorn, K., Patton, E., Klinkbiel, R. and O'Brien, D. (1983) *Makromol. Chem., Rapid Comm.* **4?**, 513-517.
10. O'Brien, D.F., Klingbiel, R.T., Specht, D.P. and Tyminski, P.N. (1985) *Ann. N.Y. Acad. Sci.* **446**, 282-295.

11. Lopez, E., O'Brien, D.F., Whitesides, T.H. (1982) *Biochim. Biophys. Acta.* **693**, 437-443.
12. Kusumi, A., Singh, M., Tirrell, D.A., Oehme, G., Singh, A., Samuel, N.K.P., Hyde, J.S. and Regen, S.L. (1983) *J. Am. Chem. Soc.* **105**, 2975-2980.
13. Liman, U., Frankel, D.A., O'Brien, D.F. (1988) *Biophys. J.* **53**, 325.
14. Bader, H., Jorn, K., Hupfer, B. and Ringsdorf, H. (1985) *Adv. Polm. Sci.* **64**, 1.
15. Gros, L., Ringsdorf, H. and Schupp, H. (1981) *Angew. Chem. Int. Ed. Engl.* **20**, 305.
16. Lelkes, P.I. and Friedman, P. (1984) *Biochim. Biophys. Acta.* **775**, 395-401.
17. Scherphof, G.L., Damen, J. and Wilshut, J. in: *Liposome Technology* ; Gregoriadis, G. (Ed.); Boca Raton: CRC Press, 1984; Vol. III, 205.
18. Scherphof, G. Roerdink, F., Hoekstra, D., Zborowski, J. and Wisse, E. in: *Liposomes in Biological Systems* ; Gregoriadis, G. and Allison A.C., (Eds); Chichester: John Wiley and Sons Ltd., 1980; 179-209.
19. Allen, T.M. (1981) *Biochim. Biophys. Acta.* **640**, 385-397.
20. Weinstein, J.N., Klausner, R.D., Innerarity, T., Ralston, E. and Blumenthal, R. (1981) *Biochim. Biophys. Acta.* **674**, 270-284.
21. Elbert, R., Lashewsky, A., and Ringsdorf, H. (1985) *J. Am. Chem. Soc.* **107**, 4134-4141.
22. Lashewsky, A., Ringsdorf, H. and Sneider, J. (1986) *Die Angewandte Makromol. Chem.* **145/146**, 1-17.
23. Regen, S.L., Yamaguchi, K., Samuel, N.K.P., and Singh, M. (1983) *J. Am. Chem. Soc.* **105**, 6354.

24. Samuel, N.K.P., Singh, M., Yamaguchi, K., and Regen, S.L. (1985) *J. Am. Chem. Soc.* **107**, 42-47.
25. Browning, J. in in : *Liposomes from Physical Structure to Therapeutic Applications* ; Knight, C.G. (Ed.); Elsevier: North Holland Biomedical Press, 1981; 189.
26. Wilshut, J., Ph.D. Thesis;
27. Chan, S.I., Bocian, D.F. and Petersen, N.O. in: *Membrane Spectroscopy* ; Grell, E. (Ed.); Springer-Verlag: Berlin Heidelberg, 1981; 1-50
28. Bocian, D.F. and Chan, S.I. (1978) *Ann, Rev. Phys. Chem.* **29**, 307-335.
29. Cullis, P.R., and De Kruijff, B. (1978) *Biochim. Biophys. Acta.* **553**, 31-42.
30. Seelig, J. and Seelig, A. (1980) *Quat. Rev. Biophys.* **13**, 19-61.
31. Seelig, J. (1978) *Biochim. Biophys. Acta.* **515**, 105-140.
32. Weinstein, J.N., Ralston, F., Leserman, L. D., Klausner, R.D., Dragsten, P., Henkart, P. and Blumenthal, R. in: *Liposome Technology* ; Gregoriadis, G. (Ed.); Boca Raton: CRC Press, 1984; Vol. III, 183.
33. Kobashi, K. (1968) *Biochim. Biophys. Acta.* **158**, 239-245.
34. Sheetz, M.P. and Chan, S.I. (1972) *Biochemistry* **11**, 4573-4581.
35. Schuh, J.R., Banerjee, U., Müller, L. and Chan, S.I. (1982) *Biochim. Biophys. Acta.* **687**, 219-225.
36. Tsuchida, K., Ohki, K., Sekiya, T., Yoshinori, N. and Hatto, Ichiro (1987) *Biochim. Biophys. Acta.* **898**, 53-58.
37. Horowitz, P. (1977) *j. Coll. Inter. Sci.* **61**, 197-198.
38. Pearson, R.H., Pascher, I. (1979) *Nature* **281**, 499-501.

39. Roberts, M.F., Bothner-By, A.A. and Dennis, E.A. (1978) *Biochemistry* **17**, 935-942.
40. Runquist, E. and Helmkamp, G.M. (1988) *Biochim. Biophys. Acta.* **940**, 10-20.
41. Israelachvilli, J.N., Marcelja, S. and Horn, R.G. (1980) *Q. Rev. Biophys.* **13**, 121-200.
42. Israelachvilli, J.N., Mitchell, J. and Ninham, B.W. (197) *Biochim. Biophys. Acta.* **470**, 185-201.
43. Mitchell, J. and Ninham, B.W. (1981) *J. Chem. Soc., Faraday Trans. 2* **77**, 601-629.
44. Reed, W., Lasic, D., Hauser, H., and Fendler, J. (1985) *Macromolecules* **18**, 2005-2012.
45. Dave Rhodes and T. Handel, unpublished results.
46. Lewis, R., private communications.
47. Burns, R. and Roberts, M.F. (1980) *Biochemistry* **19**, 3016-3013.

---

---

## Chapter III

---

---

### *Investigation of the Phase Transition Properties of Disulfide Polymerizable Phosphatidylcholine Bilayers by DSC, FT-IR and Fluorescence Polarization*

---

#### INTRODUCTION

In the previous chapter, we described the morphological behavior of two homologous series of thiol-containing phospholipids, the  $\alpha$ -THIOLS and the  $\omega$ -THIOLS. It was shown, for example, that the  $\alpha$ -THIOLS could be readily dispersed or sonicated into liposomes even from a prepolymerized state and for lipids with surprisingly long chain lengths (up to N=20) relative to saturated nonpolymerizable phosphatidylcholine analogues. Furthermore, polymeric  $\alpha$ -THIOL SUVs had a much lower tendency to aggregate (weeks) than nonpolymerizable analogues. By contrast,  $\omega$ -THIOLS with a wide range of chain lengths formed liposomes in the monomeric state but only short chain monomeric  $\omega$ -THIOLS (N= 10,11) could be sonicated into opalescent solutions of SUVs; sonicated long-chain  $\omega$ -THIOLS (N=15,16) aggregated rapidly. Furthermore, on polymerization, the  $\omega$ -THIOLS form what appear

to be bilayer fragments (or in the very least, highly aggregating, extremely leaky liposomes) rather than self-sealed liposomes. The disparity in the behavior of these two liposome types suggests major differences in the cohesive forces between the lipids in the bilayers composed of  $\alpha$ -THIOLS versus  $\omega$ -THIOLS.

To understand the structural details of such bilayers and the interactions between the constituent lipids, we have undertaken an investigation of their phase transition properties by DSC, FT-IR and fluorescence polarization. In particular, we were interested in the effect of the polymerizable moiety, the chain length, and whether the lipids are polymerized or not on the temperature and enthalpy of the phase transition, as well as the structural reorganizations that occur at the transition temperature at various depths within the bilayer. In addition, the temperature dependence of the release of an aqueous soluble fluorescent dye was monitored to examine whether the presence of thermal transitions in these polymerizable liposomes caused an abrupt increase in leakage rates as has been observed for nonpolymerizable phosphatidylcholines (1,2).

## MATERIALS AND METHODS

### MATERIALS.

Lipids were synthesized with minor modifications of the procedure established by Regen *et al.* (3,4) as described in Chapter VIII. Polymerization of monomeric phosphatidylcholines to the corresponding disulfide polymers was accomplished by the oxidation (20 equivalents  $H_2O_2$ ) of an aqueous dispersion of monomer (5 mg/ml in borate buffer, pH 8.5) for 4-8 h above the monomer phase transition as detailed in Chapter VIII. Polymeric dispersions were subsequently dialyzed, lyophilized and stored as dry powders until use. Carboxyfluorescein was purchased from Eastman Kodak and purified according to the protocol outlined in reference 5.

Diphenylhexatriene (DPH) was obtained from Aldrich. 2-(9-anthroyloxy)stearic acid (2-AS), 12-(9-anthroyloxy)stearic acid (12-AS) and 16-(9-anthroyloxy)palmitic acid (16-AP) were purchased from Molecular Probes and utilized without further purification. All other reagents were of analytical grade or better.

### Methods.

Differential Scanning Calorimetry (DSC). Calorimetric measurements were made on either a Microcal MC-2 or a Perkin Elmer scanning calorimeter at heating rates of 20°C/h and 30°C/h, respectively. Samples for measurements on the Microcal DSC were prepared by dispersing 2-5 mg of lipid in 2 ml Tris buffer (10 mM Tris, 150 mM NaCl, 0.2mM EDTA; pH 7.4) and equilibrating above the  $T_m$  for 15-30 min. For measurements with the Perkin Elmer calorimeter,  $\approx$  2-4 mg of lipid was placed in pans and hydrated in H<sub>2</sub>O for 30 min at 80 °C.

FT-IR. Lipid samples were hydrated in D<sub>2</sub>O for 30 min at 80 °C. Samples were then placed between CaF<sub>2</sub> windows and transferred to a rigorously thermostatted ( $\pm$  .1 °C) FT-IR mount containing Peltier thermoelectric modules (6). Automated data acquisition as a function of temperature was accomplished on a Mattson Sirius 100 FT-IR spectrometer under UNIX-based computer control.

Fluorescence Studies. Fluorescence measurements were carried out on an SLM-4000 spectrofluorimeter. For polarization measurements, the fluorimeter was configured in the T-format (7) with the monochromator in the path of the parallel-detected light and an appropriate band pass filter in the path of the perpendicularly polarized light. Excitation and emission wavelengths were 357 and 430 for DPH and 366 and 440 for the anthroyl probes, respectively. Samples were prepared by dispersing 3  $\mu$ moles lipid in Tris buffer, to which was added 3  $\mu$ l of a 2 mM solution of DPH in tetrahydrofuran or 2  $\mu$ ls of a 7.5 mM methanolic solution of 2-AS, 12-AS or 16-AP (the final lipid to dye

ratio was 750 for DPH and 150 for the anthroyl probes). Samples were warmed for 2 h at 5-10°C above the phase transition of the lipid and subsequently cooled to room-temperature. Polarization was calculated according to the equation:

$$(1) \quad P_s = \frac{I_{\parallel} - I_{\perp}}{I_{\parallel} + I_{\perp}}$$

where  $I_{\parallel}$  and  $I_{\perp}$  are the emission intensities of the light parallel and perpendicular to the polarization direction of the excitation beam, respectively. The contribution of scattered light to  $I_{\parallel}$  and  $I_{\perp}$  was checked routinely and found to be negligible.

Carboxyfluorescein Release. For carboxyfluorescein leakage experiments, 5 mg of lipid was hydrated with 1 ml of 50 mM carboxyfluorescein (in HEPES buffer) for 15 min above the phase transition temperature. SUVs were prepared by bath ( $\alpha$ -16) or probe ( $\alpha$ -18,  $\alpha$ -20) sonication with a Laboratory Supplies bath sonicator or a Heat Systems 350 W probe sonicator, respectively. During sonication, samples were placed under nitrogen and in a large room-temperature water bath to avoid excessive heating. In the case of MLVs, untrapped carboxyfluorescein was removed by pelleting the lipid 3-5 times from isotonic buffer by centrifugation at 2000 rpm (swinging bucket rotors, IEC Centra-8 centrifuge). SUVs were separated from untrapped solute by passage over G-25-50 spin columns (0.5-ml per 3-ml spin column). Due to the leakiness of  $\alpha$ -16 SUVs at ambient temperatures, aliquots were passed over spin columns immediately prior to each measurement at a new temperature. Typically, 50  $\mu$ l of liposomes were added to 2 ml of HEPES buffer equilibrated at a designated temperature in a thermostatted cell. Fluorescence intensity was monitored continuously for 15 min at excitation and emission wavelengths of 470 and 520 nm, respectively. The total amount of entrapped carboxyfluorescein was determined by the addition of 100  $\mu$ l 10% Triton X-100. Percent release was calculated as:

$$(2) \quad \% \text{ release} = \frac{I_{10} - I_0}{I_T - I_0}$$

where  $I_{10}$  is the intensity after 10 minutes,  $I_0$  is the initial intensity and  $I_T$  is the final intensity after the addition of Triton X-100. No correction was made for the temperature dependence of the carboxyfluorescein quantum yield.

## RESULTS

### Differential Scanning Calorimetry.

In studies of artificial and natural biomembranes, DSC has provided a wealth of information concerning the organization and interactions between the constituents of lipid bilayers (for reviews, see references 9-11). This is due to the fact that the thermodynamic parameters, which may be derived from calorimetric measurements ( $T_m$ ,  $\Delta H$  and cooperative units) are highly sensitive to the molecular structure of the lipids, the aggregate morphology and the addition of nonphospholipid components (i.e. cholesterol, proteins). Single component phospholipid membranes have been particularly well characterized as model membranes in terms of the effect of lipid structure on the  $T_m$  and  $\Delta H$ . For example, increasing the length of the acyl chains or decreasing the headgroup size (i.e PC versus PE) in saturated phospholipids causes an elevation in both the  $T_m$  and  $\Delta H$  for the gel to liquid crystalline phase transition. Unsaturated chains and bulky headgroups drastically decrease these parameters by reducing the ability of the chains to effectively pack in a tight crystalline array. These trends serve as a good reference point for understanding the effects of the polymerizable moiety and polymerization itself on the packing of the lipids in  $\alpha$ -THIOL and  $\omega$ -THIOLS bilayers.

Figure 1 shows typical DSC profiles for monomeric and polymeric  $\alpha$ -16 and  $\omega$ -16. As is generally observed for polymerized lipids, the transitions for both polymeric

$\alpha$ -16 and  $\omega$ -16 are severely broadened relative to the monomer, due to a reduction in the cooperativity of the lipids in the bilayer. The transitions corresponding to the polymers are also multicomponent, indicating a more complex behavior than that of the monomers or nonpolymerizable analogs. Relative to the 16-carbon saturated phosphatidylcholine DPPC, which has a phase transition of 41.7°C, the  $T_m$  is reduced in the case of monomeric and polymeric  $\alpha$ -16, and increased for  $\omega$ -16.

Table I summarizes the calorimetrically determined  $\Delta H$  and  $T_m$  data for the homologous series of  $\alpha$ - and  $\omega$ -THIOLS. It should be noted that for all polymeric lipids other than  $\alpha$ -16 and  $\omega$ -16, the main transitions are broadened but single component. The  $T_m$  and  $\Delta H$  for nonpolymerizable phosphatidylcholine analogues are tabulated in Table II for comparison. As can be seen, for all  $\alpha$ -THIOLS, monomeric and polymeric, the  $T_m$  (and  $\Delta H$  for polymeric  $\alpha$ -THIOLS) are reduced relative to that for the corresponding nonpolymerizable analogues. The depression in the  $T_m$  and  $\Delta H$  may be due to the additional bulkiness, polarity, and/or hydration at the interfacial region for these lipids. Compared to the monomeric  $\alpha$ -THIOLS, the  $T_m$  for the polymers are relatively broad and unshifted while the  $\Delta H$  is reduced. One possible explanation for the latter is a decreased interaction between the chains in the polymer relative to the monomer.

For monomeric  $\omega$ -THIOLS, the  $T_m$  is increased relative to the nonpolymerizable phosphatidylcholines indicating the terminal sulfhydryl has a stabilizing effect on membrane formation. This is somewhat surprising since these lipids have a polar group positioned in the low dielectric environment at the bilayer interior. However, the potential perturbation caused by this misplaced polarity may be completely offset by H-bonding interactions between sulfhydryls or the stabilizing affect of having a "heavy"

**Figure 1**

DSC profiles of polymeric and monomeric  $\alpha$ -16 and  $\omega$ -16.

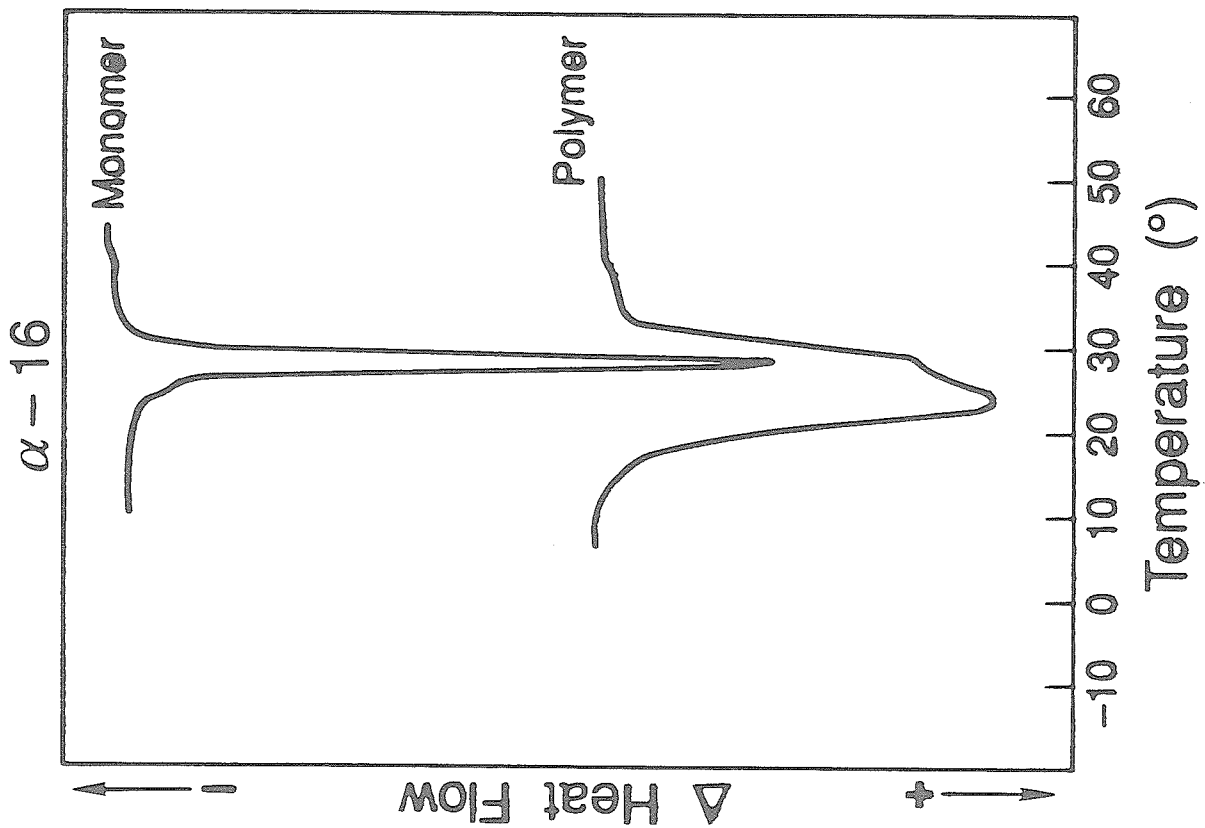
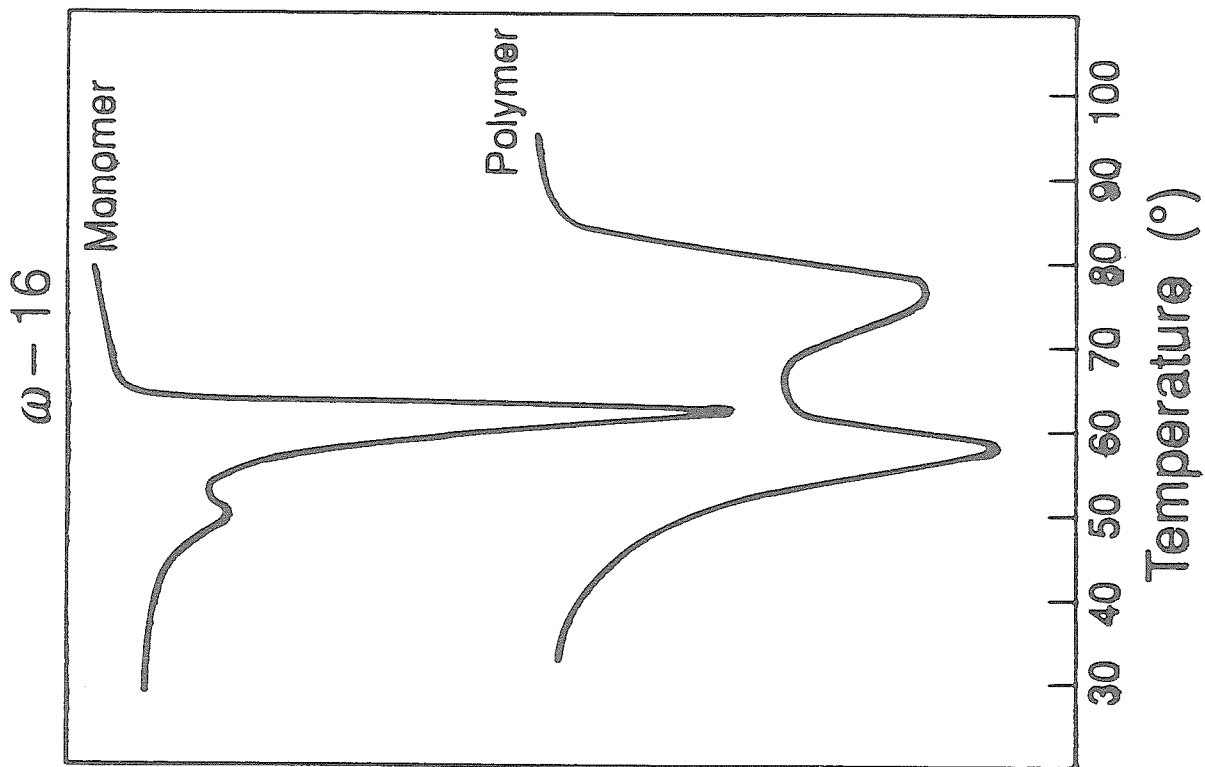


Table I

Summary of the phase transition temperatures ( $T_m$ ) and enthalpies ( $\Delta H$ ) for monomeric and polymeric  $\alpha$ -THIOLS and  $\omega$ -THIOLS as determined by DSC. The designations (M) and (P) refer to the monomer and polymer, respectively.

Lipid	T <sub>m</sub> (°C)	ΔH (kcal/mole)
<b>α-THIOLS</b>		
α-16 (M)	25.9 ± 0.5	7.8 ± 0.9
α-16 (P)	22.9 ± 3.0 <sup>a</sup>	5.6 ± 0.7
α-18 (M)	40.6 ± 0.3	11.7 ± 0.7
α-18 (P)	36.9 ± 0.9	8.7 ± 1.0
α-20 (M)	54.7	12.1
α-20 (P)	52.4 ± 0.5	10.2 ± 0.7
<b>ω-THIOLS</b>		
ω-10 (M)	< 5.0	
ω-10 (P)	19.5 ± 0.3	3.0
ω-11 (M)	< 5.0	
ω-11 (P)	33.6 ± 1.0	5.15 ± 0.4
ω-12 (M)	15.2 ± 0.3	5.0 ± 1.4
ω-12 (P)	38.9	
ω-15 (M)	49.6 ± 0.2	10.9
ω-15 (P)	60.3 ± 0.9	12.6 ± 2.0
ω-16 (M)	52.0 ± 3.0	10.1 ± 0.8
ω-16 (P)	64.5 ± 13.6 <sup>a</sup>	13.9 ± 2.1

<sup>a</sup>Mean of the high and low temperature components.

Table II

Summary of the phase transition temperatures ( $T_m$ ) and enthalpies ( $\Delta H$ ) for nonpolymerizeable phosphatidylcholines as determined by DSC.

<u># CARBONS (NAME)</u>	<u>T<sub>m</sub> (°C)<sup>a</sup></u>	<u>ΔH (kcal/mole)<sup>a</sup></u>
12 (DLPC)	-1.8	1.70
14 (DMPC)	23.9	5.44
16 (DPPC)	41.4	8.74
18 (DSPC)	54.9	10.6

<sup>a</sup>Taken from reference 11.

atom at the chain terminus. Regarding the latter postulate, it has been demonstrated that the presence of halogens at the chain terminus lead to a stabilization of the membrane (12). In any case, the increase in the  $T_m$  is consistent with the ability of short chain  $\omega$ -THIOLS (N=10 and possibly 9) to form stable bilayers as described in Chapter II. Polymerization of the  $\omega$ -THIOLS results in a further increase in the  $T_m$  indicating an enhancement of the interlipid interactions relative to both the monomer and nonpolymerizable species. In fact, while no transition is detected above 5°C for  $\omega$ -10 and  $\omega$ -11 monomeric dispersions, polymerization greatly increases the  $T_m$  to 20 and 38°C, respectively. The presence of the phase transition further confirms the fact that bilayers are formed down to even very short chain lengths (N=10 and possibly 9). For all  $\omega$ -THIOLS, the enthalpy follows the same trend as the  $T_m$  (polymer > monomer > nonpolymerizable PC).

In the above studies, our data concerning  $\alpha$ -16 dispersions is in agreement with reports by Regen on  $\alpha$ -16 SUVs (4). The slightly lower  $T_m$  (23° C) detected by this group is in keeping with the general reduction in the transition temperatures observed for SUVs compared to MLVs or LUVs (13,14,15). In the same study, however, no transition was detected for  $\omega$ -11 or  $\omega$ -16 monomers or polymers. This is presumably due to the low sensitivity of the technique used to detect the transition (absorbance spectrophotometry) and the fact that in the case of  $\omega$ -16 dispersions, an inadequate temperature range was scanned. Furthermore, it is not surprising that transitions for polymeric  $\omega$ -THIOLS would be overlooked because to date, all reports of chain terminating polymerizable lipids where the polymerizable moiety is in both chains, have indicated that polymerization abolishes the phase transition (reference 16 and 17 for reviews; also see 18 and 19). This is due to the general inhibitory effect of polymerization on the ability of the chain segments to undergo trans-gauche isomerizations. Thus, the results of the polymeric  $\omega$ -THIOLS were extremely

surprising.\* To clarify that the thermal measurements weren't due to some other process unrelated to the gel to liquid-crystalline (or other) phase transition, the temperature-dependent behavior was also investigated by FT-IR and fluorescence polarization, both of which allow us to probe more directly alterations occurring within the hydrocarbon region of the bilayers.

### FT-IR.

Fourier transform infrared spectroscopy has proven extremely useful in studies of synthetic and natural membranes because the tractable parameters (peak positions and bandwidths) are extremely sensitive to environmental changes, conformation, hydration and mobility (6,20-24). Furthermore, one can selectively monitor various positions within the bilayer by appropriate choice of the vibrational mode (methylene stretches for the hydrocarbon area, carbonyl stretches for the interfacial region, and the phosphate stretches for the headgroup). In this study, we were particularly interested in monitoring the behavior of the hydrocarbon region. In phospholipids, the CH<sub>2</sub> symmetric stretch is particularly informative in this regard as the peak position and bandwidth increase abruptly at the phase transition due to the increase in gauche conformations and mobility, respectively, in the chains.

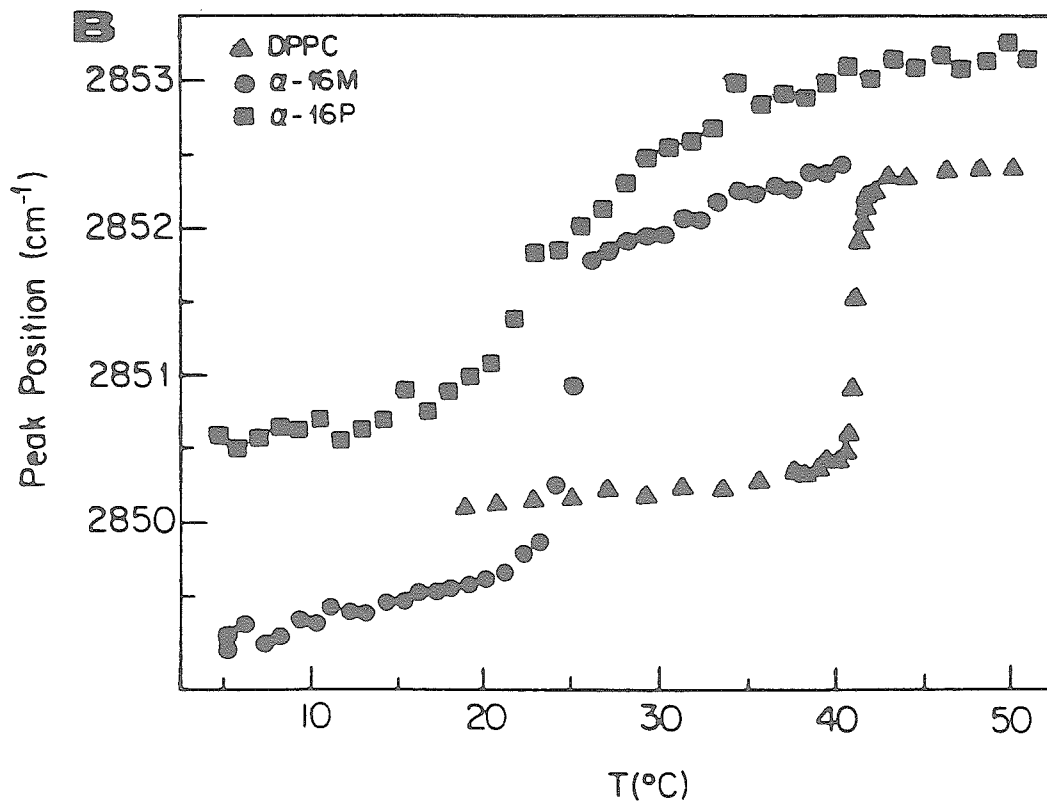
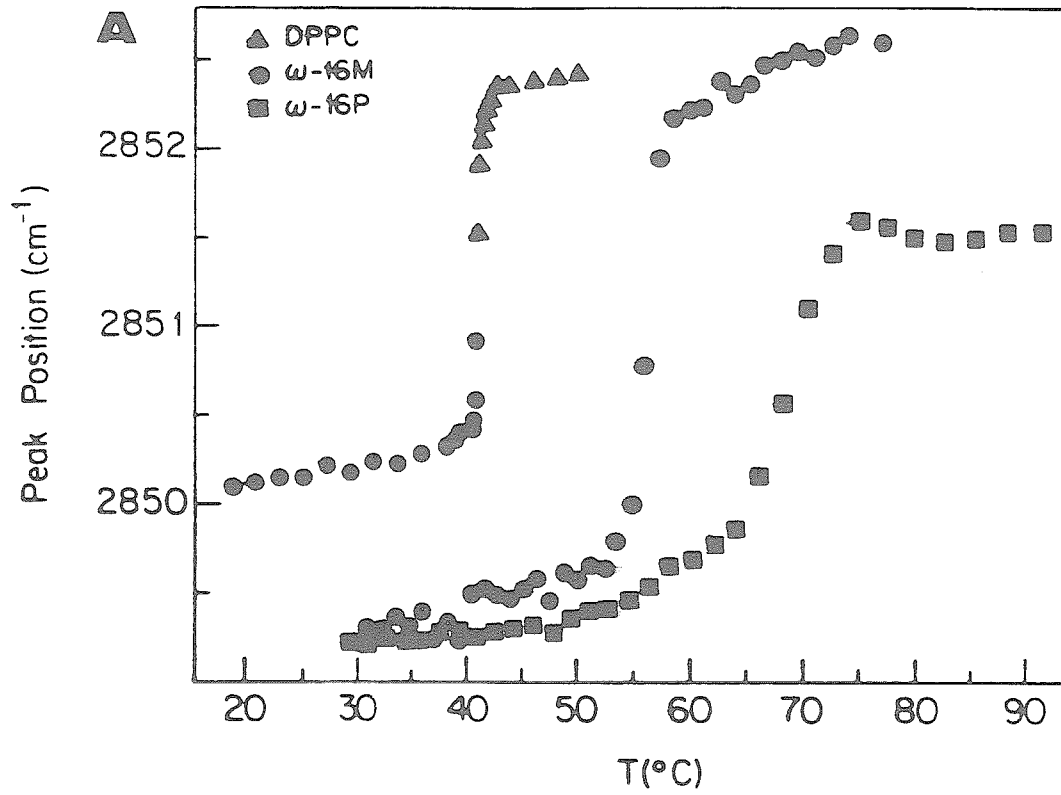
Figure 2 shows typical temperature-dependent profiles of peak position of the CH<sub>2</sub> symmetric stretch of polymeric and monomeric  $\alpha$ -16 and  $\omega$ -16. DPPC is included for reference. Both  $\alpha$ -16 and  $\omega$ -16 clearly show the presence of the T<sub>m</sub>. For the most part the data is consistent with that obtained from DSC measurements with the

---

\* It is important to note that the transitions are not due to residual monomer. Regen has reported greater than 95% conversion of  $\omega$ -11 and  $\omega$ -16 liposomes under slightly milder polymerizing conditions than used here. By NMR, we have found essentially complete oxidation of  $\omega$ -10 and  $\omega$ -11, and greater than 94% for  $\omega$ -15. The associated enthalpies are much too large to be due to a small percent of unpolymerized chains and therefore must correspond to structural changes associated with the polymers.

**Figure 2**

Peak position of the methylene symmetric stretching mode as a function of temperature for: A. monomeric  $\omega$ -16, polymeric  $\omega$ -16 and DPPC; B. monomeric  $\alpha$ -16, polymeric  $\alpha$ -16 and DPPC. The symbols are assigned in the figure legends.



exception that for polymeric  $\omega$ -16, the major component of the complex DSC trace that is sensed by the acyl chains is the high temperature component. The exact meaning of the initial component is therefore unclear but may be some sort of pretransition, perhaps largely involved with a headgroup reorientation. Clearly, however, the transitions are of a magnitude at least as great as that for DPPC and have the same characteristic trends confirming that this is truly a phase transition involving hydrocarbon disorder. Table III summarizes the  $T_m$  obtained from the midpoint in the break of the plots of peak position versus temperature for the series of  $\alpha$ -THIOLS and  $\omega$ -THIOLS. Also included is the empirical parameter  $\Delta PP$  (change in peak position between the gel and liquid crystalline state), which describes the magnitude of the change.

*Fluorescence Polarization of DPH.* In addition to the above techniques, fluorescence polarization of dyes imbedded in bilayers has also been a common method used for determining phase transitions as well as "fluidities" and apparent microviscosities (14,25-28). This is due to the fact that the polarization is sensitive to the dynamics and structural organization of the matrices in which the probe is solubilized. Diphenylhexatriene has been one of the most commonly used probes in this regard. Due to the hydrophobicity and rigid rod-like shape of this molecule, it is solubilized completely in the hydrocarbon region of the membrane and predominantly oriented with its long axis parallel to the lipid chains, at least in the gel state.\* Consequently, it is sensitive to the reorganizations and mobility of the chains averaged over the entire hydrocarbon region, making it ideal for reporting on phase transitions.

We also anticipated extracting information concerning membrane "fluidity" from the polarization data. However, the routine interpretation of steady state polarization in terms of fluidities and microviscosities has recently been called into question and

---

\* However, since it is not anchored to the membrane surface by a polar group, it can adopt other orientations such as parallel to the bilayer surface at the midplane of the membrane.

Table III

Summary of the phase transition temperatures ( $T_m$ ) and the magnitude of the change in the peak position between the gel and liquid-crystalline state ( $\Delta PP_{TM}$ ) for monomeric and polymeric  $\alpha$ -THIOLS and  $\omega$ -THIOLS. Measurements are based on the peak position of the methylene symmetric stretching mode in the infrared spectrum of the lipids. The designations (M) and (P) refer to the monomer and polymer, respectively.  $\Delta T$  (Gel-LC) is the temperature range over which  $\Delta PP_{TM}$  was determined.

Lipid	T <sub>m</sub> (°C)	ΔT (Gel-LC)	ΔPP <sub>TM</sub>
<b>α-THIOLS</b>			
α-16 (M)	25.5	5-40	3.25
α-16 (P)	24.0	5-40	2.65
α-18 (M)	39.0	15-50	2.75
α-18 (P)	38.5	15-40	2.95
α-20 (M)	53.5	30-70	2.88
α-20 (P)	51.5	30-70	3.22
<b>ω-THIOLS</b>			
ω-11 (M)	-4.0	-11-10	2.80
ω-11 (P)	33.5	4-44	1.64
ω-12 (M)	15.5	5-45	2.86
ω-12 (P)	39.0	5-55	2.50
ω-15 (M)	48.5	30-65	2.60
ω-15 (P)	61.0	30-75	2.50
ω-16 (M)	56.0	30-70	3.30
ω-16 (P)	69.0	30-90	2.3

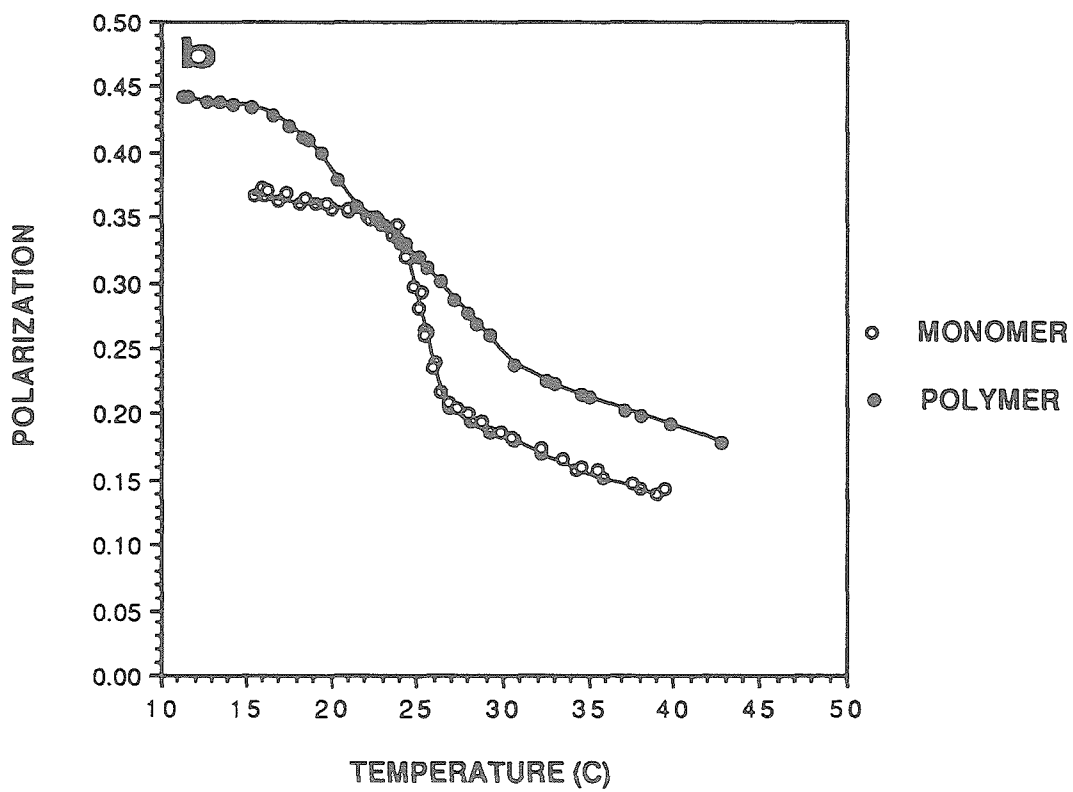
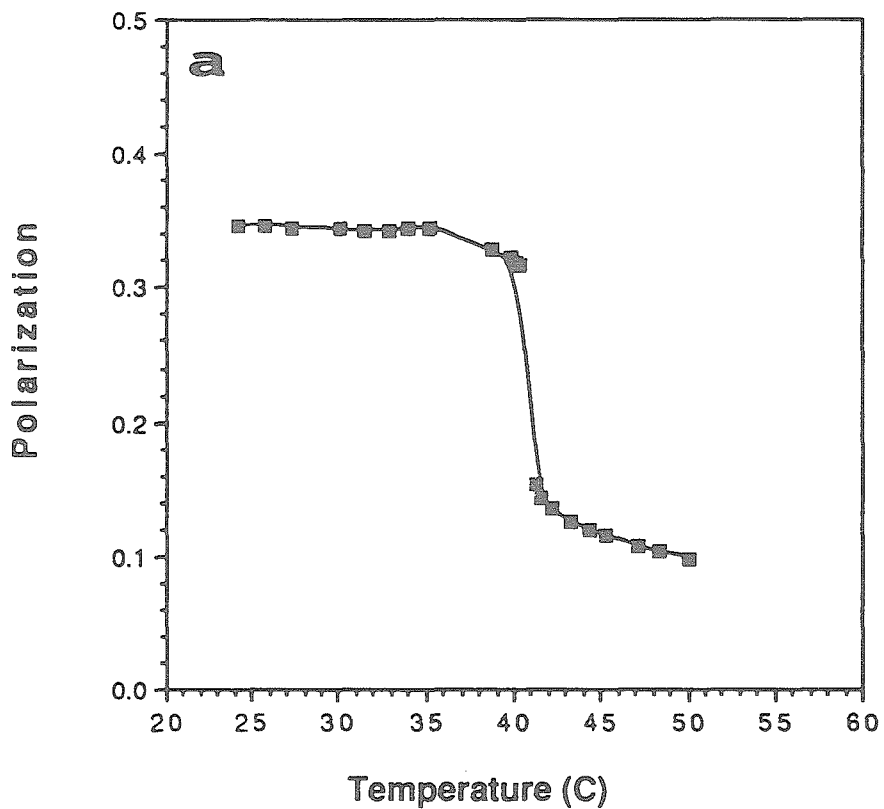
<sup>a</sup>The midpoint of the entire transition

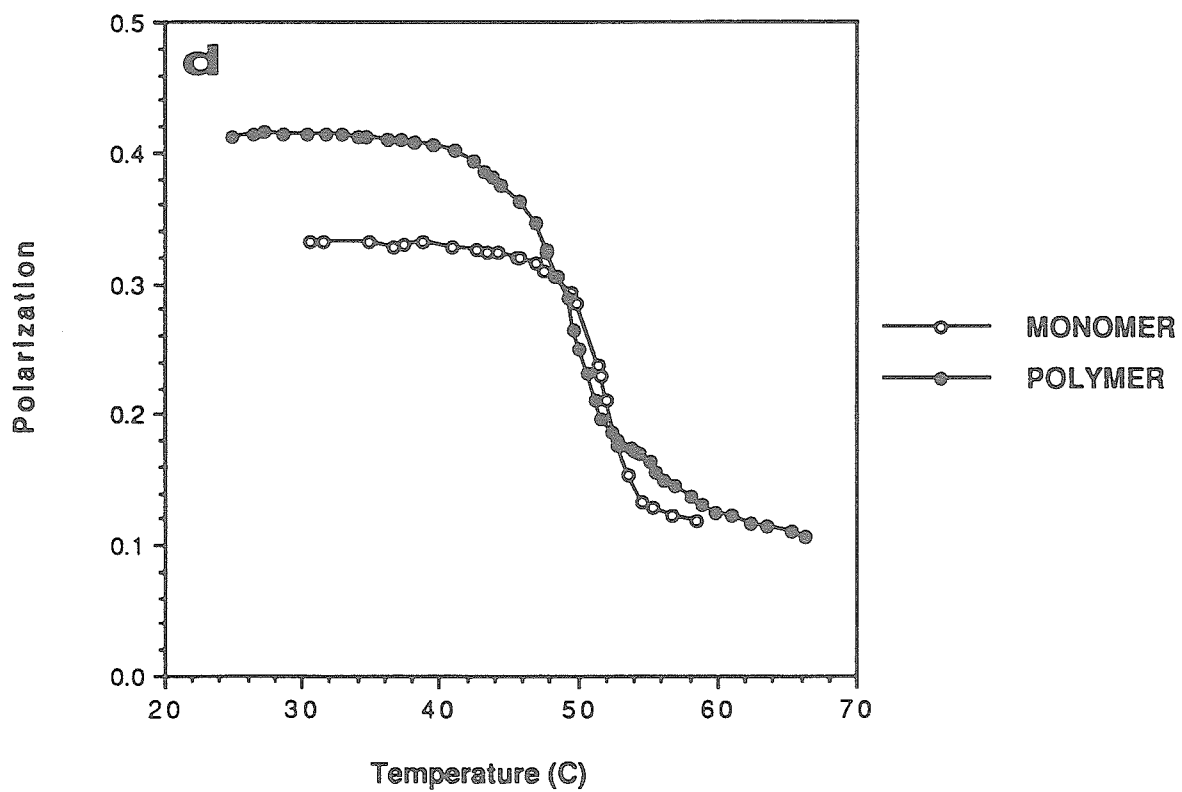
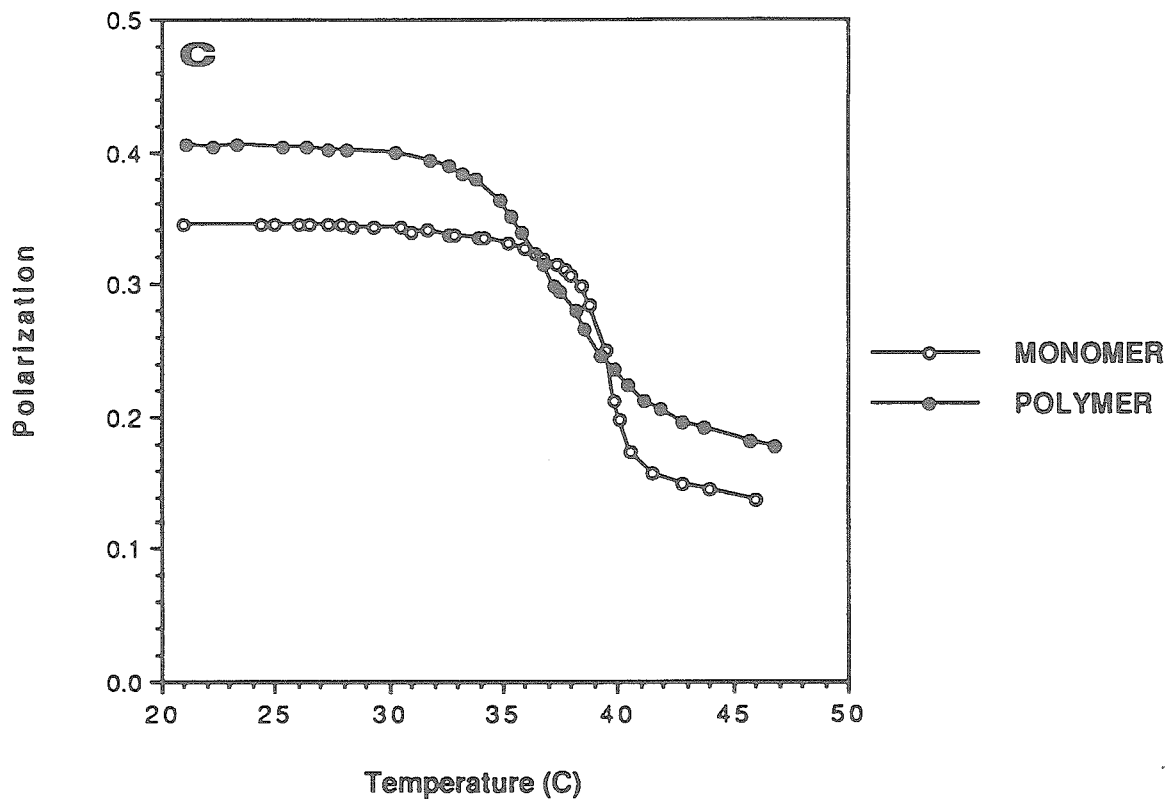
shown potentially misleading (29-32). This is due to the fact that the simple extrapolations from polarization to microviscosity are founded on the inappropriate assumptions of isotropic reorientation of the probes within an anisotropic matrix. Blitterswijk *et al.* have developed empirical relationships so that the contributions of chain ordering and motion may be extracted from these data without the need for time resolved experiments (29,30). Despite the value of such treatments for deriving "order parameters," one must always remember that the absolute value of the polarization may inaccurately reflect relative ordering from one system to another due to the differential perturbing effects of the probe on its microenvironment, the fact that the probe may reveal predominantly its own restricted motion rather than that of the membranes and the fact that the average location of certain probes may vary from one bilayer to another (33). For example, inconsistencies between results suggested by steady state polarization and NMR data have been reported by Seelig *et al.* concerning the effect of protein on lipid fluidity (34). Other spectroscopic data for corroborating interpretations made on the basis of fluorescence polarization are consequently useful. We therefore defer discussion of the absolute values of the polarization to a later chapter where they can be presented in light of data from other nonperturbing spectroscopic techniques. In the following results we consider only the information concerning the position of the phase transition and the extent of the change sensed by the probe on passing through the transition.

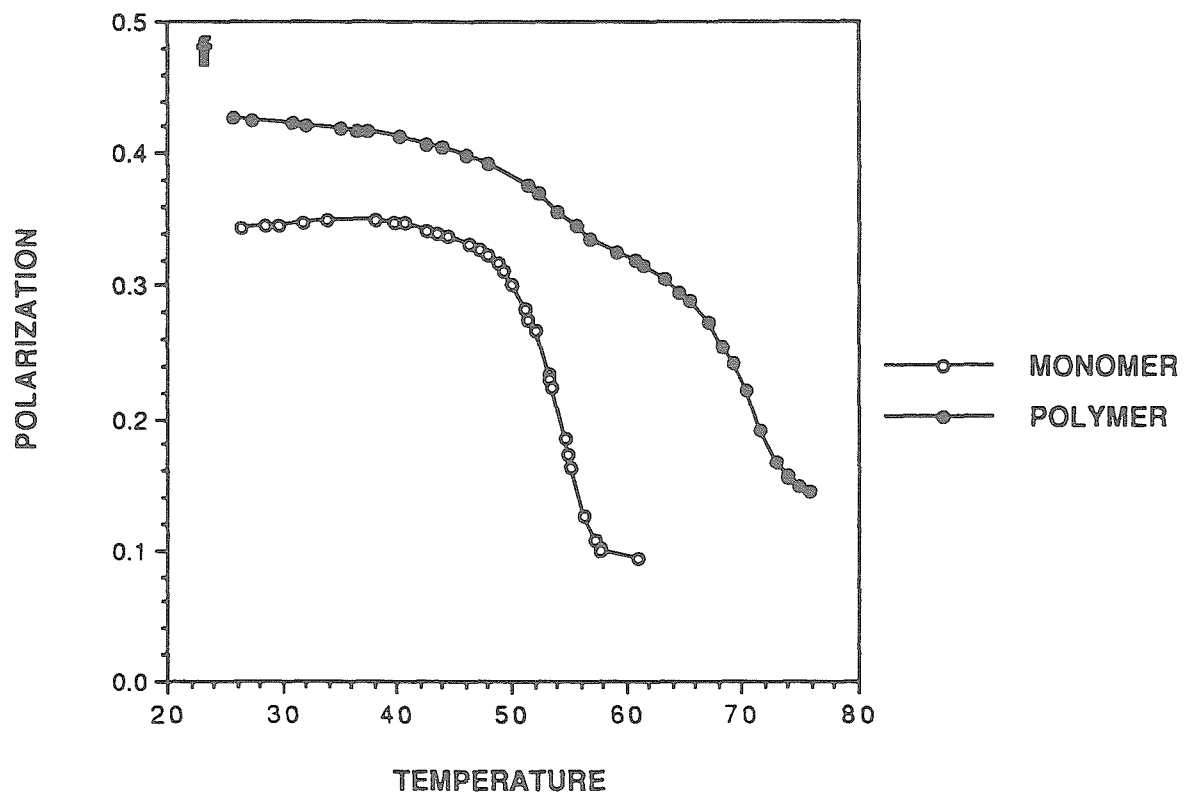
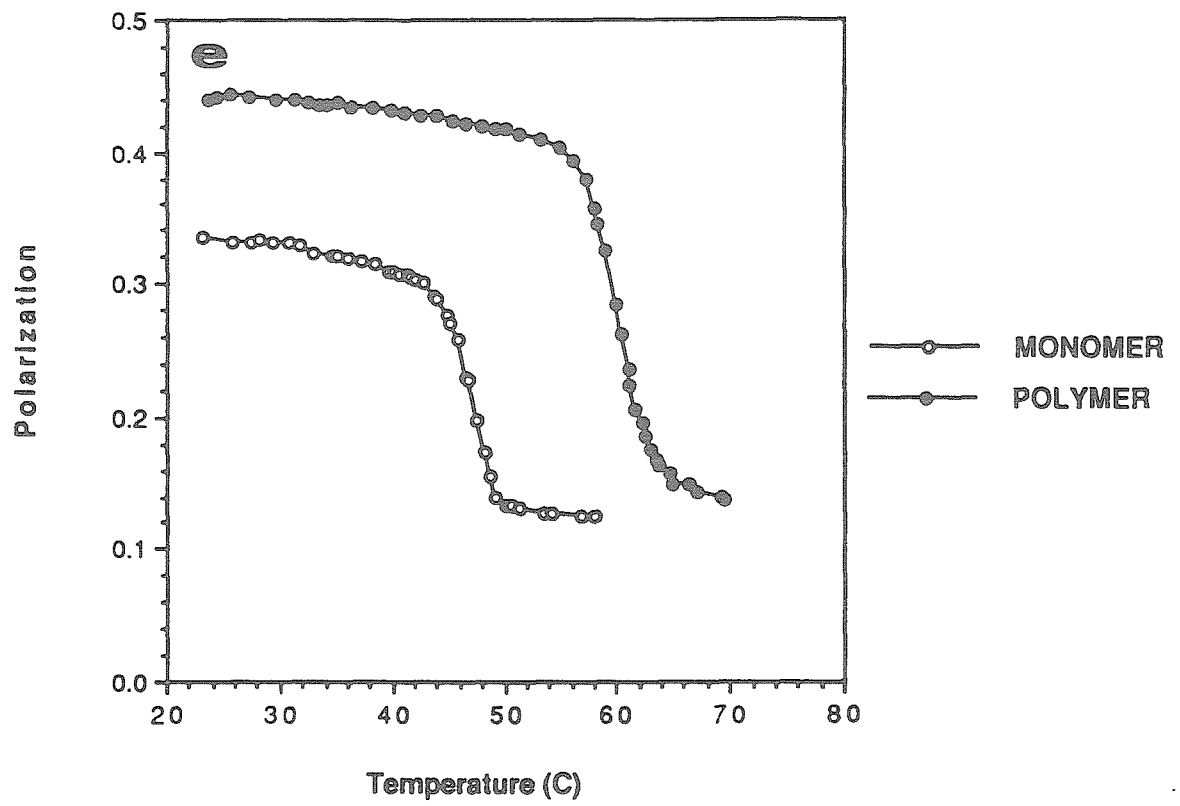
In Figure 3, typical plots of the the fluorescence polarization of DPH as a function of temperature is shown for several monomeric and polymeric  $\alpha$ -THIOLS and  $\omega$ -THIOLS. In general, data corroborate the DSC and FT-IR results in the presence and position of an order-disorder transition. In Table IV, the  $T_m$  and the extent of the change in polarization on passing through the transition ( $\Delta POL_{TM}$ ) is summarized for several  $\alpha$ - and  $\omega$ -THIOLS. It is interesting to note that as in the FT-IR detected

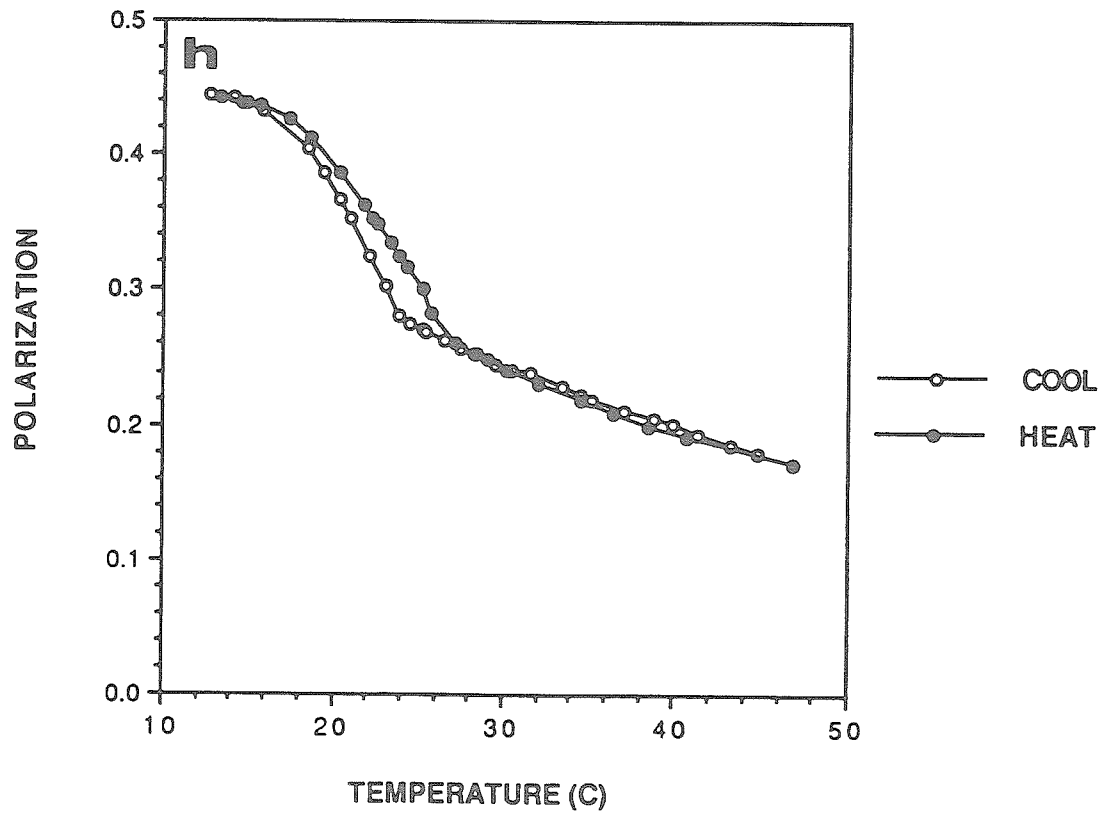
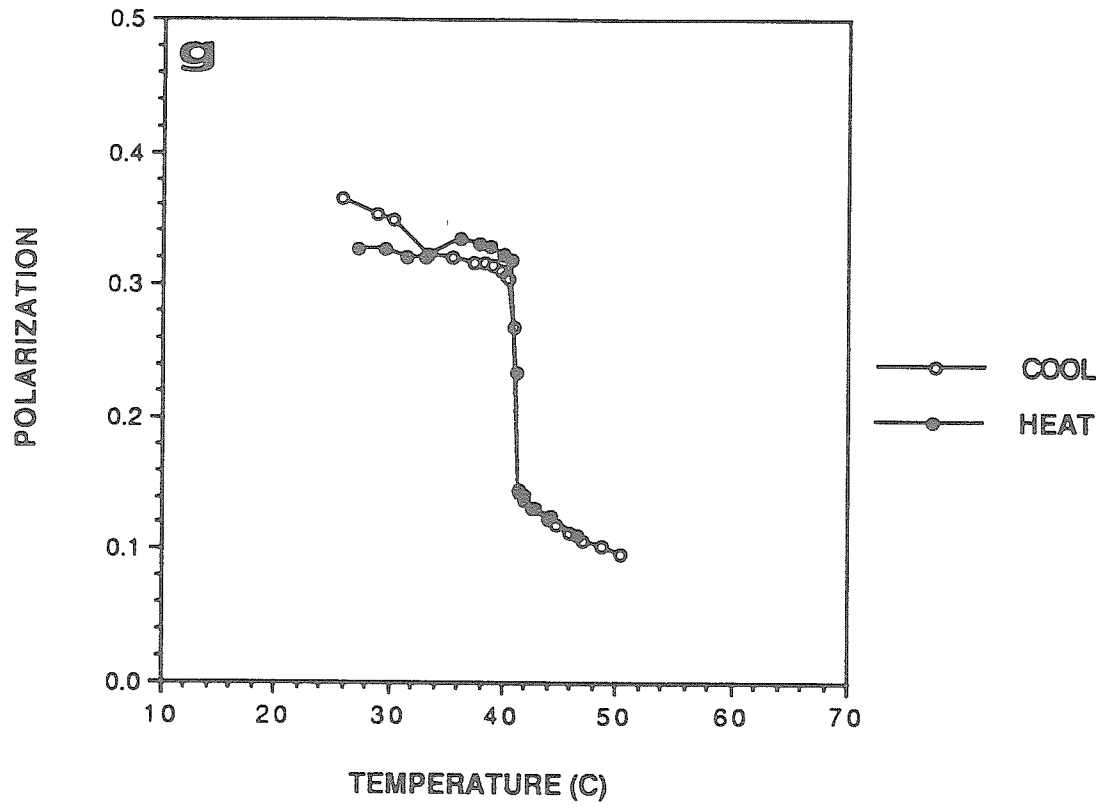
**Figure 3**

Typical plots of the fluorescence polarization of DPH as a function of temperature in various lipid bilayers: A. DPPC; B. monomeric and polymeric  $\alpha$ -16; C. monomeric and polymeric  $\alpha$ -18; D. monomeric and polymeric  $\alpha$ -20; E. monomeric and polymeric  $\omega$ -15; F. monomeric and polymeric  $\omega$ -16. Heating and cooling scans for DPH in bilayers of: G. DPPC; H. polymeric  $\alpha$ -16; I. polymeric  $\omega$ -11; J. polymeric  $\omega$ -15. All measurements (A-F) were made with heating scans. G-J demonstrate the hysteresis observed in the heating versus cooling scans of the  $\omega$ -THIOLS and the lack of hysteresis for DPPC and polymeric  $\alpha$ -16.









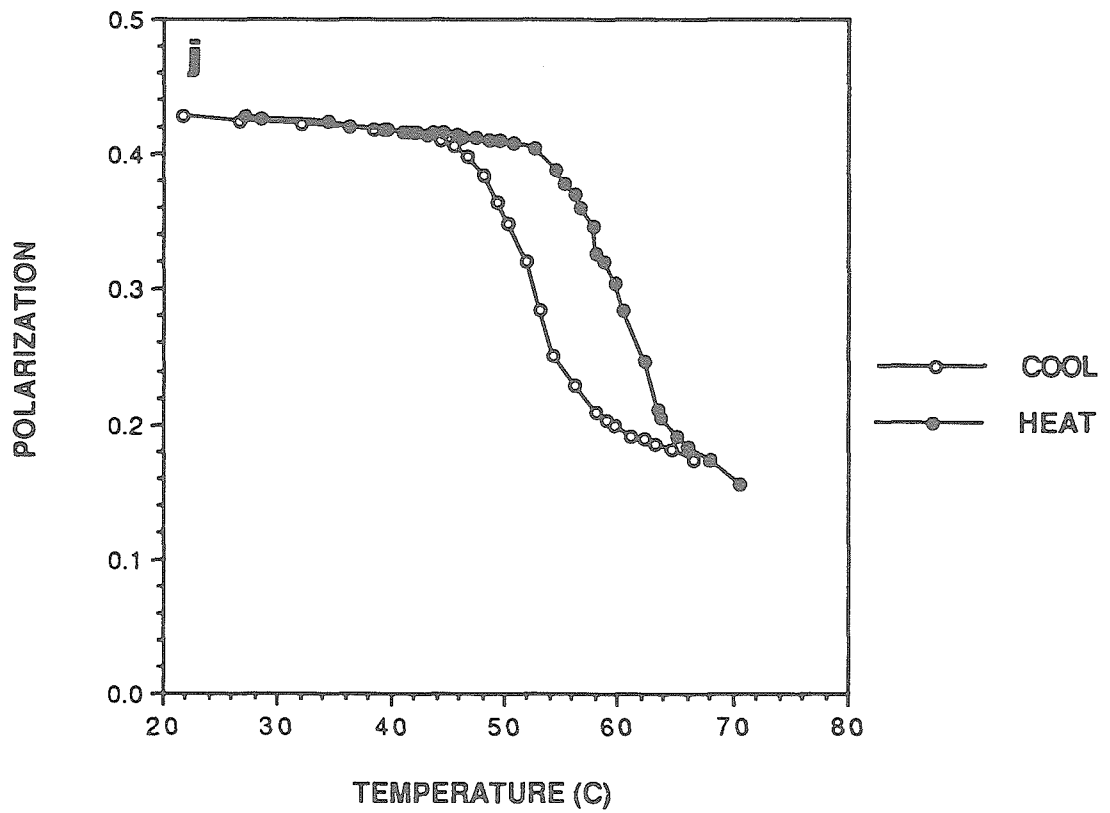
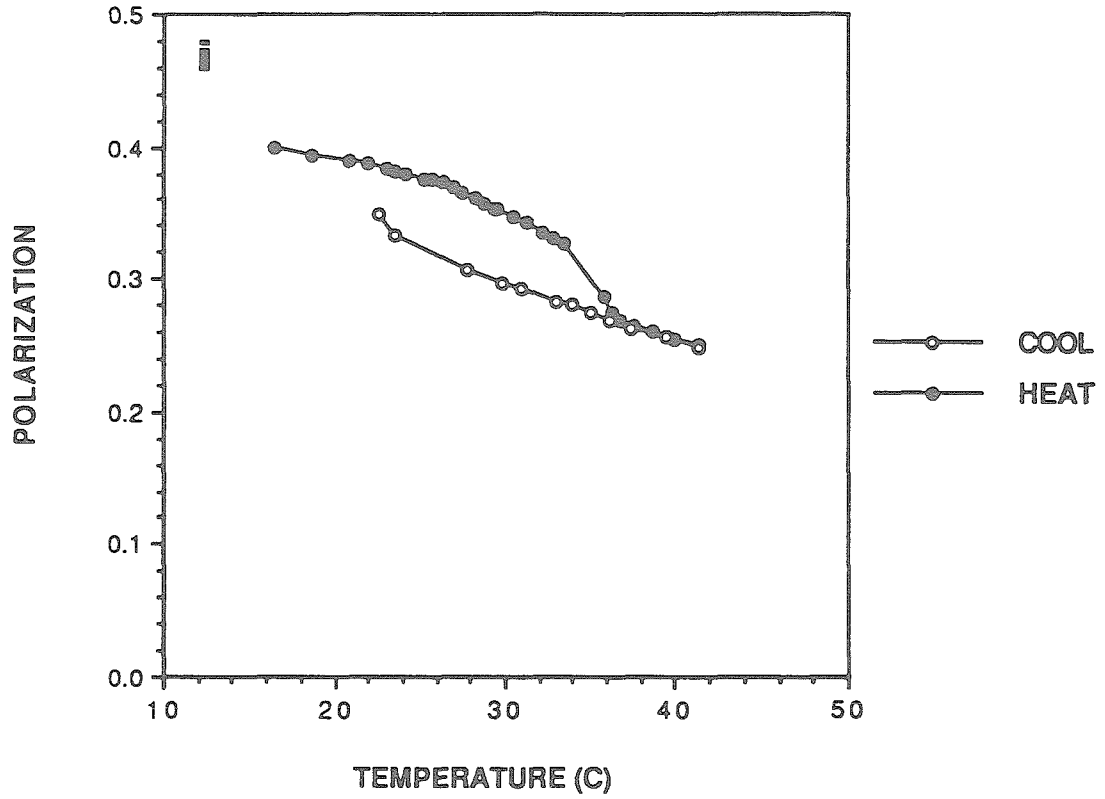


Table IV

Summary of the phase transition temperatures ( $T_m$ ) and the magnitude of the change in the fluorescence polarization between the gel and liquid-crystalline state ( $\Delta POL_{TM}$ ) for monomeric and polymeric  $\alpha$ -THIOLS and  $\omega$ -THIOLS and DPPC. Measurements are based on fluorescence polarization of DPH. The designations (M) and (P) refer to the monomer and polymer, respectively.  $\Delta T$  (Gel-LC) is the temperature range over which  $\Delta POL_{TM}$  was determined.

Lipid	$T_m$ (°C)	$\Delta T$ (Gel-LC)	$\Delta POL_{TM}$
<b><math>\alpha</math>-THIOLS</b>			
$\alpha$ -16 (M)	$25.5 \pm 1.4$	15-40	$0.146 \pm .020$
$\alpha$ -16 (P)	$22.4 \pm 1.4^a$	12.5-40	$0.241 \pm .020$
$\alpha$ -18 (M)	39.0	25-40	0.209
$\alpha$ -18 (P)	$36.5 \pm 0.5$	25-40	$0.217 \pm .020$
$\alpha$ -20 (M)	$52.0 \pm 1.0$	35-60	$0.195 \pm .020$
$\alpha$ -20 (P)	$50.1 \pm 1.3$	35-60	$0.292 \pm .020$
<b><math>\omega</math>-THIOLS</b>			
$\omega$ -11 (P)	35.0	20-40	$0.128 \pm .040$
$\omega$ -15 (M)	$47.0 \pm 0.2$	30-55	$0.213 \pm .020$
$\omega$ -15 (P)	$60.3 \pm 0.4$	40-70	$0.297 \pm .020$
$\omega$ -16 (M)	$53.0 \pm 0.3$	40-60	$0.352 \pm .010$
$\omega$ -16 (P)	$65.3 \pm 1.5^a$	35-80	$0.271 \pm .020$
<b>NONPOLYMERIZEABLE</b>			
DPPC	41.0	25-50	0.250

<sup>a</sup>The midpoint of the entire transition

transition for polymeric  $\omega$ -16, the restructuring that occurs at the first transition is not detected by polarization changes nearly as well as the second component. Thus it appears that the "main transition" of polymeric T-16 occurs at temperatures substantially higher than the monomer and DPPC. Furthermore,  $\Delta\text{POL}_{T_m}$  is also much larger for  $\omega$ -16, paralleling the relative enthalpies of these lipids. This reconfirms the unexpected result that despite polymerization at the chain terminus, membranes of polymeric  $\omega$ -THIOLS can undergo transitions involving major disordering of the hydrocarbon region. However, since steady state polarization is sensitive to both dynamic (mobility) and structural (packing) features of the membrane (29,35), it is not possible to determine the extent to which the  $T_m$ -induced reduction in polarization is due to structural disorder or increased chain motion. In the case of polymeric  $\omega$ -THIOLS, one could imagine, for example, a highly disorganized hydrocarbon interior that is nonetheless quite rigid compared to nonpolymerized lipids.

The average value of the  $T_m$  determined from DSC, FT-IR and fluorescence polarization is plotted as a function of carbon number in Figure 4. Similar plots of the enthalpy versus carbon number are shown in Figure 5. Data from nonpolymerizeable phosphatidylcholines are included in these figures for comparison. Relative to nonpolymerizeable phosphatidylcholines, the  $T_m$  for  $\alpha$ -THIOLS is reduced by  $\approx 16$   $^{\circ}\text{C}$  per  $\text{CH}_2$  group while it is increased by  $\approx 15$   $^{\circ}\text{C}$  and  $\approx 25$   $^{\circ}\text{C}$  for monomeric and polymeric  $\omega$ -THIOLS, respectively. Similar trends are exhibited by the enthalpies with the exception that the  $\Delta H$  for the monomeric  $\alpha$ -THIOLS is not substantially different from the nonpolymerizeable lipids. To summarize, the data presented thus far suggests the following:

Concerning the  $\alpha$ -THIOLS:

**Figure 4**

The average transition temperature ( $T_m$ ) determined from DSC, FT-IR and fluorescence polarization as a function of the number of carbons in the acyl chains of A. monomeric and polymeric  $\alpha$ -THIOLS and nonpolymerizable L- $\alpha$ -phosphatidylcholines (NONPOL.PC); B. monomeric and polymeric  $\omega$ -THIOLS and nonpolymerizable L- $\alpha$ -phosphatidylcholines.

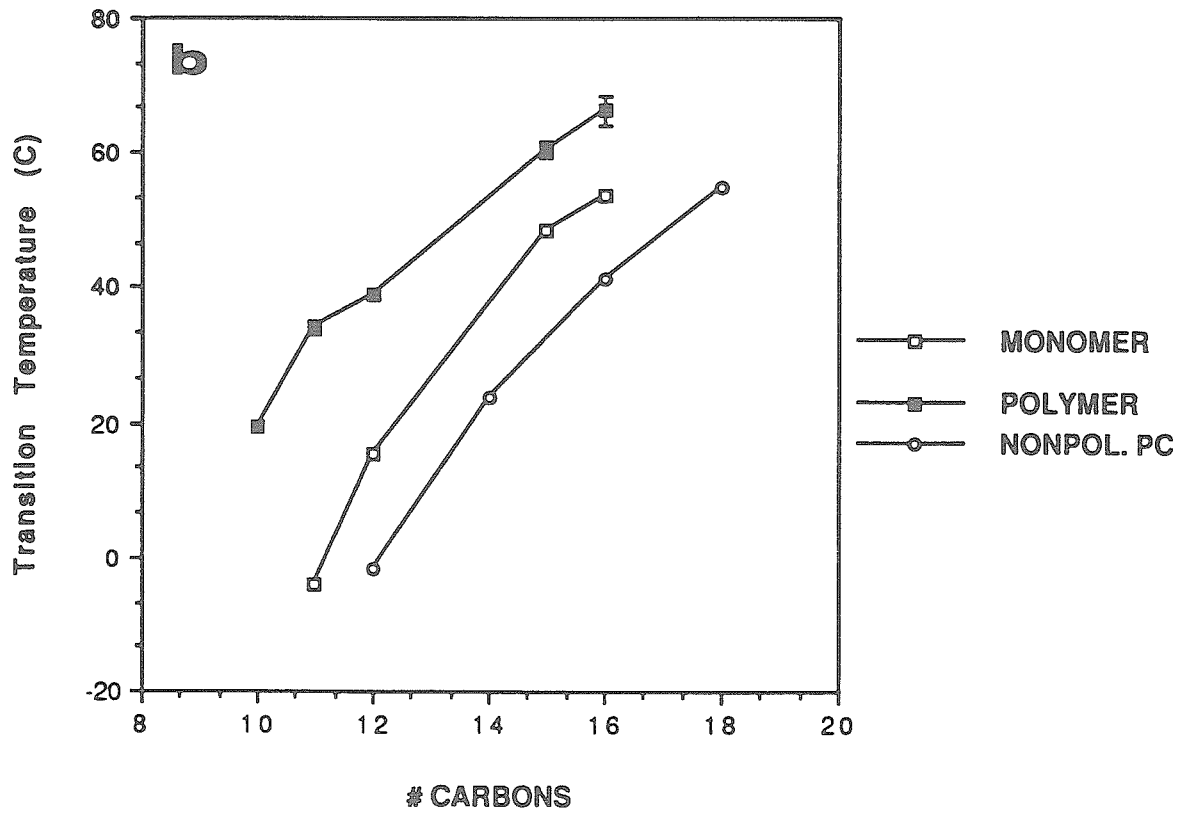
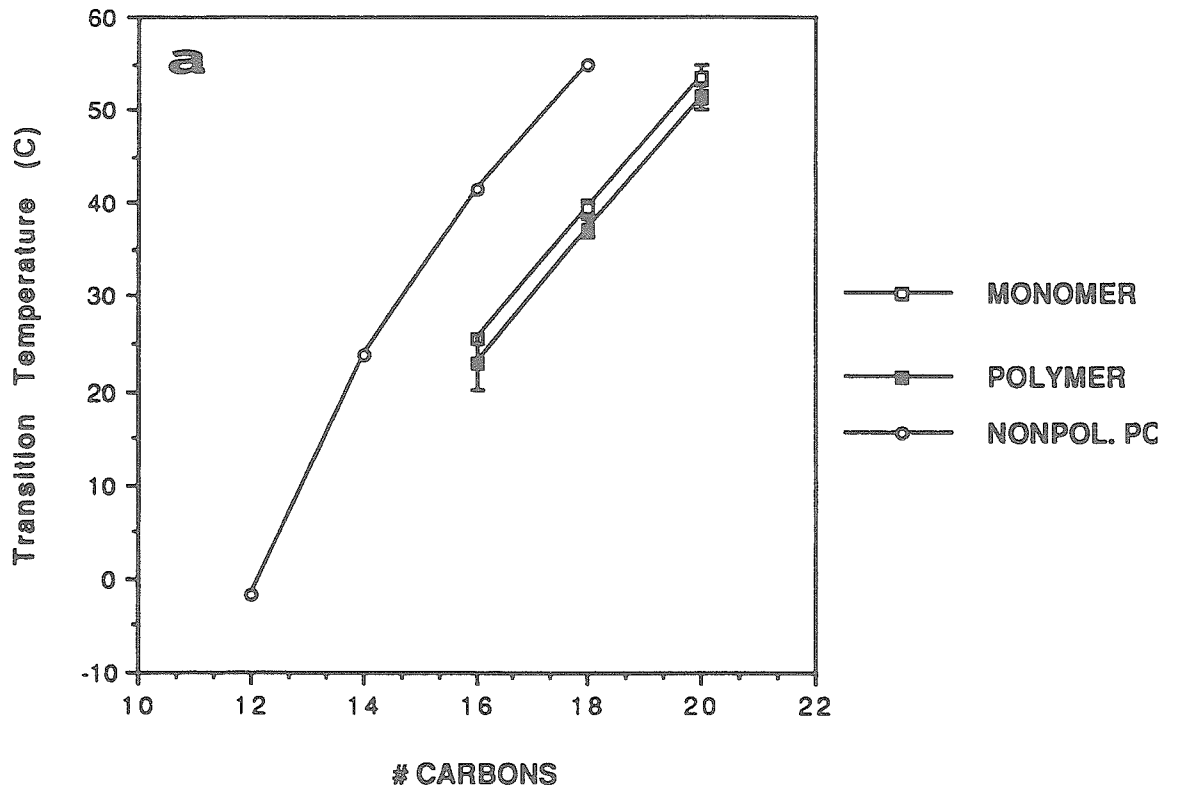
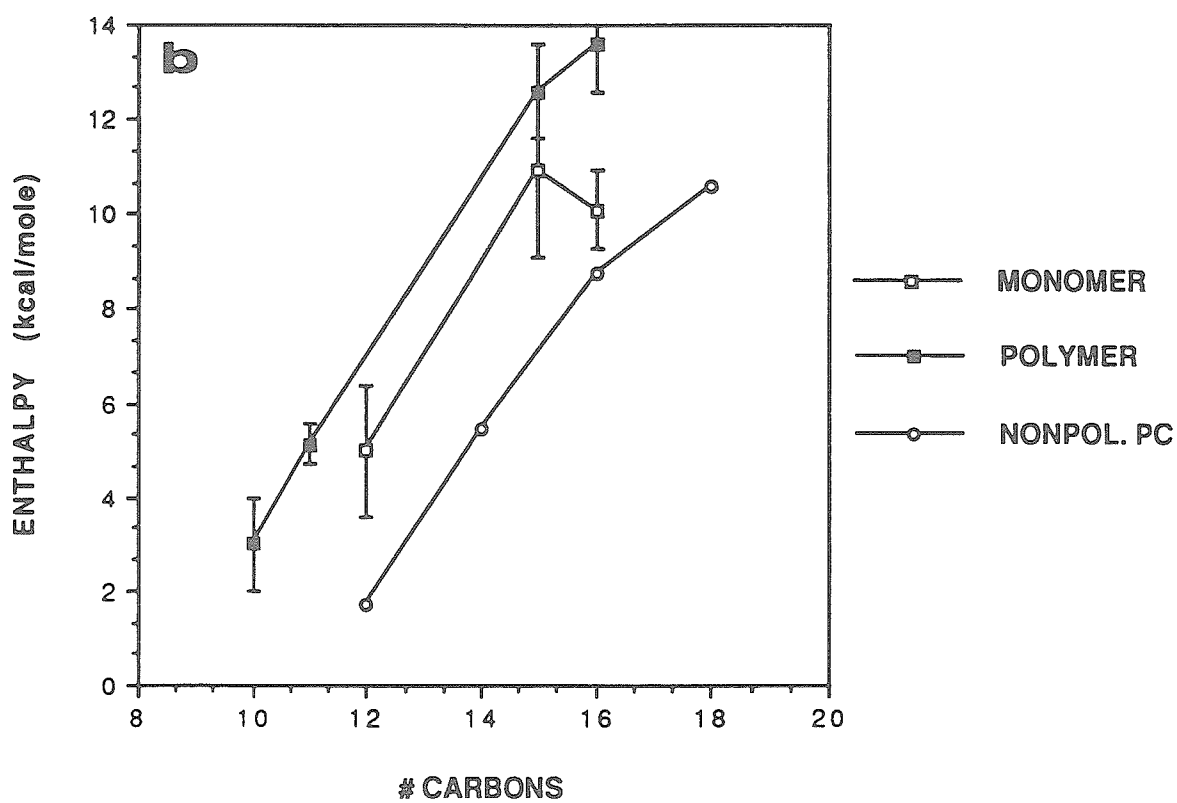
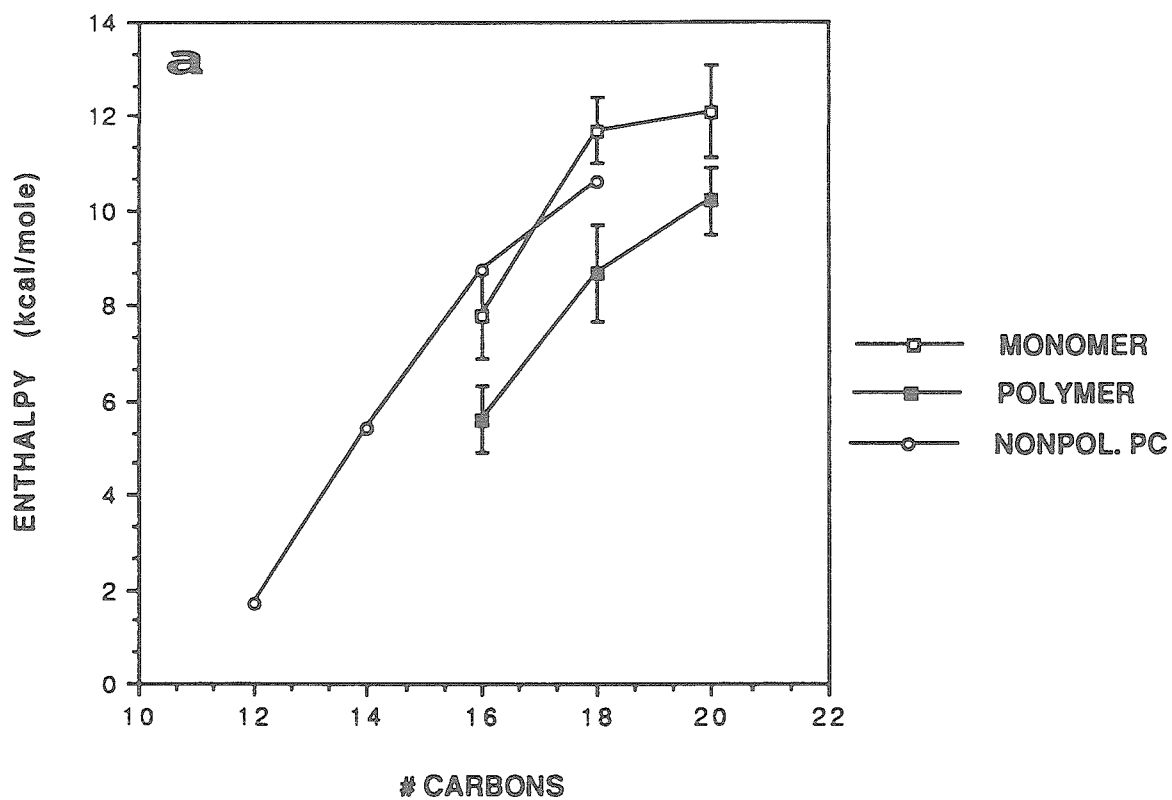


**Figure 5**

The enthalpy ( $\Delta H$ ) determined from DSC as a function of the number of carbons in the acyl chains of A. monomeric and polymeric  $\alpha$ -THIOLS and nonpolymerizeable L- $\alpha$ -phosphatidylcholines (NONPOL.PC); B. monomeric and polymeric  $\omega$ -THIOLS and nonpolymerizeable L- $\alpha$ -phosphatidylcholines.



(i) Based on the  $T_m$  data, the interactions between the  $\alpha$ -THIOLS are reduced relative to nonpolymerizable lipids. As mentioned earlier, this is likely due to the increased bulk and polarity as a consequence of the sulfhydryl or disulfide.

(ii) Polymerization results in a reduction of the enthalpy, which could be due to (a) increased chain disorder (as in the case of SUVs where a reduction in enthalpy and broadening of the transition is due to the disorder imposed by the packing constraints of a strongly curved bilayer (15)) and/or (b) fewer carbon chain segments that contribute fully to the transition. Regarding (a), we show in a later chapter by vibrational spectroscopy that in fact the hydrocarbon region of  $\alpha$ -THIOLS is more disordered than the monomeric lipids and nonpolymerizable analogues. Regarding (b), it seems quite probable that the first C-C segment close to the polymerizable moiety may be restricted in the extent to which reorientation can occur.

(iii) Polymerization results in an increased  $\Delta POL_{TM}$  for polymeric  $\alpha$ -THIOLS compared to the monomers and nonpolymerizable phosphatidylcholines. This may have some implications in terms of the physical structure of the bilayer, which is discussed in the last section. The important point to note is that polymerization does not inhibit major restructuring of the bilayer as might have been anticipated.

For the  $\omega$ -THIOLS:

(i)  $\omega$ -THIOLS in both the monomeric and the polymeric state undergo gel to liquid-crystalline phase transitions. The retention of a phase transition for polymeric T-THIOLS is unexpected and may have potential implications in terms of the structure of these membranes. This is discussed in the last section.

(ii) Both the  $T_m$  and  $\Delta H$  data suggest an increasing interaction between the chains in the order: polymer > monomer > nonpolymerizable analogue. As a consequence, bilayers are stabilized for even short-chain T-THIOLS.

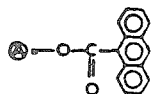
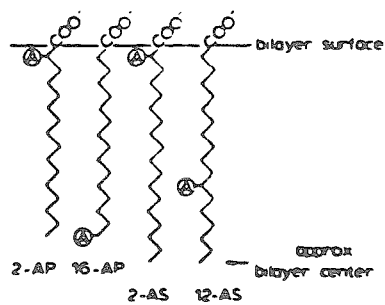
(iii) As for the  $\alpha$ -THIOLS,  $\Delta\text{POL}_{\text{TM}}$  is surprisingly greater for the polymeric lipids than for the monomers.

*Fluorescence Polarization of Depth-Dependent Anthroyl probes.* To further delineate if any gradients of reorganization occur through the phase transition as for conventional phosphatidylcholines, N-anthroyloxy fatty acid probes were used to examine the temperature dependence of the polarization at graded depths throughout the bilayer. These probes contain an anthroyl moiety at various positions along a stearic or palmitic acid chain (Figure 6). The polar carboxylate moiety tethers the probes to the membrane surface, therefore defining the position of the anthroyl moiety with respect to the bilayer interface. The correlation between depth of penetration into the bilayer and attachment position has been confirmed by quenching and resonance energy transfer experiments (35-37). This contrasts to DPH, which can adopt various positions and orientations (38).

Figure 7 shows typical polarization results for 2-AS, 12-AS and 16-AP as a function of temperature for various monomeric and polymeric matrices. Generally, in the gel state, the absolute polarization values do not follow the trend expected for a fluidity gradient (2-AS > 12-AS > 16-AP) (33). However, these values may reflect more the hindrance to depolarizing motions of the entire probe due to a portion of the membrane other than the microenvironment of the fluorophore. In the liquid-crystalline state, the expected order is observed suggesting a fluidity gradient extending from the bilayer interface to the membrane interior. Again it should be reiterated that the concept of fluidity encompasses both *mobility* and *acyl chain packing* (29,35). Thus the gradient may reflect a gradient of disordered packing in the bilayer, a gradient of motion, or both. In the case of the  $\alpha$ -THIOLS, both increased lipid chain mobility and decreased packing at the membrane interior would be expected to lead to a lower value

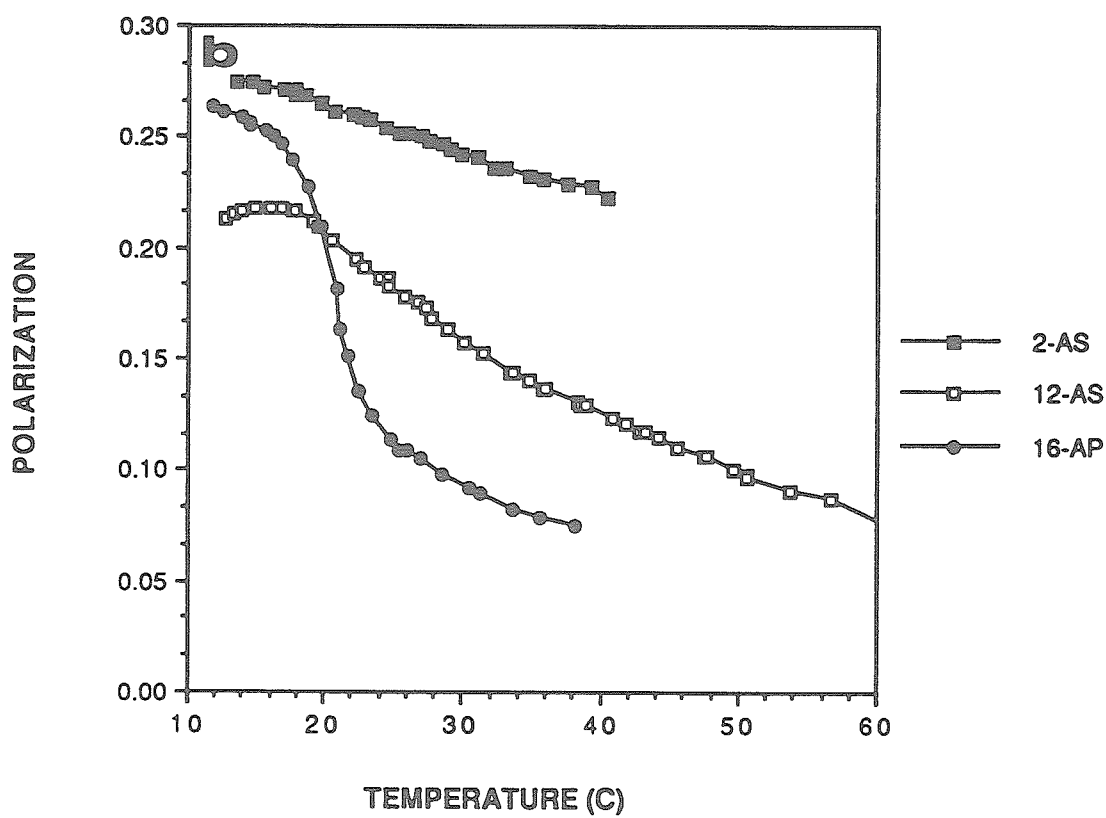
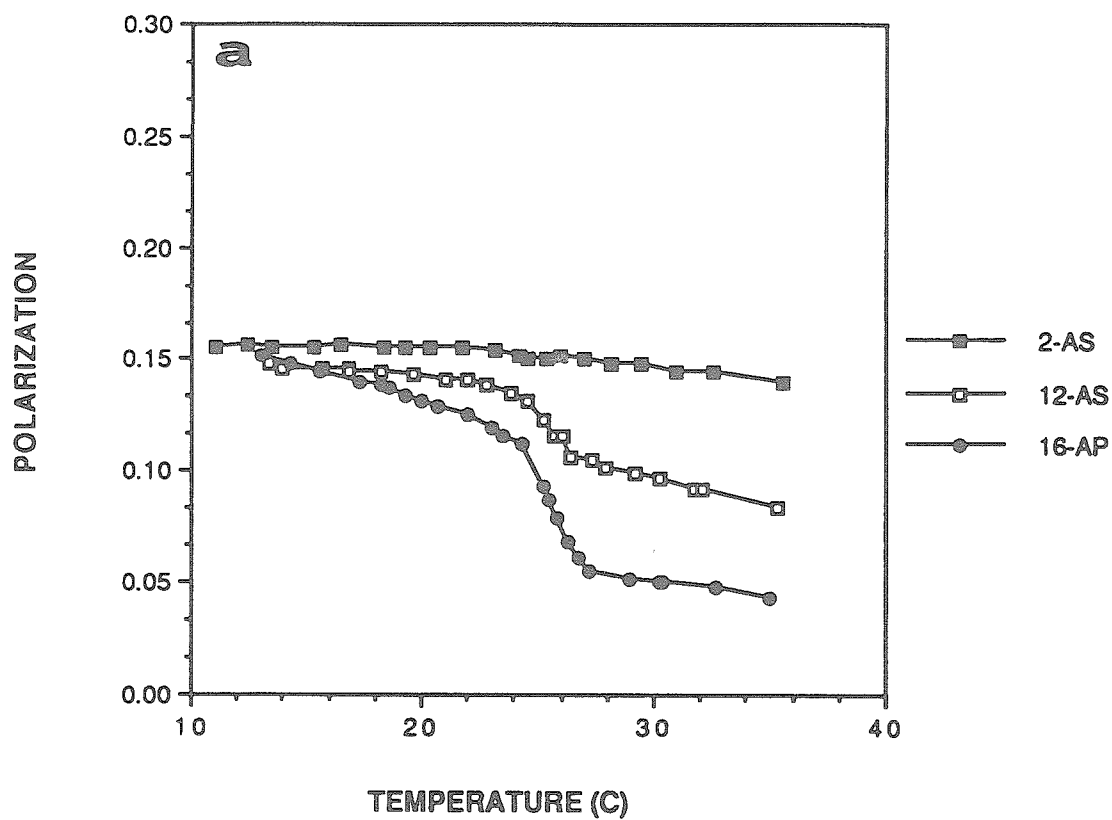
**Figure 6**

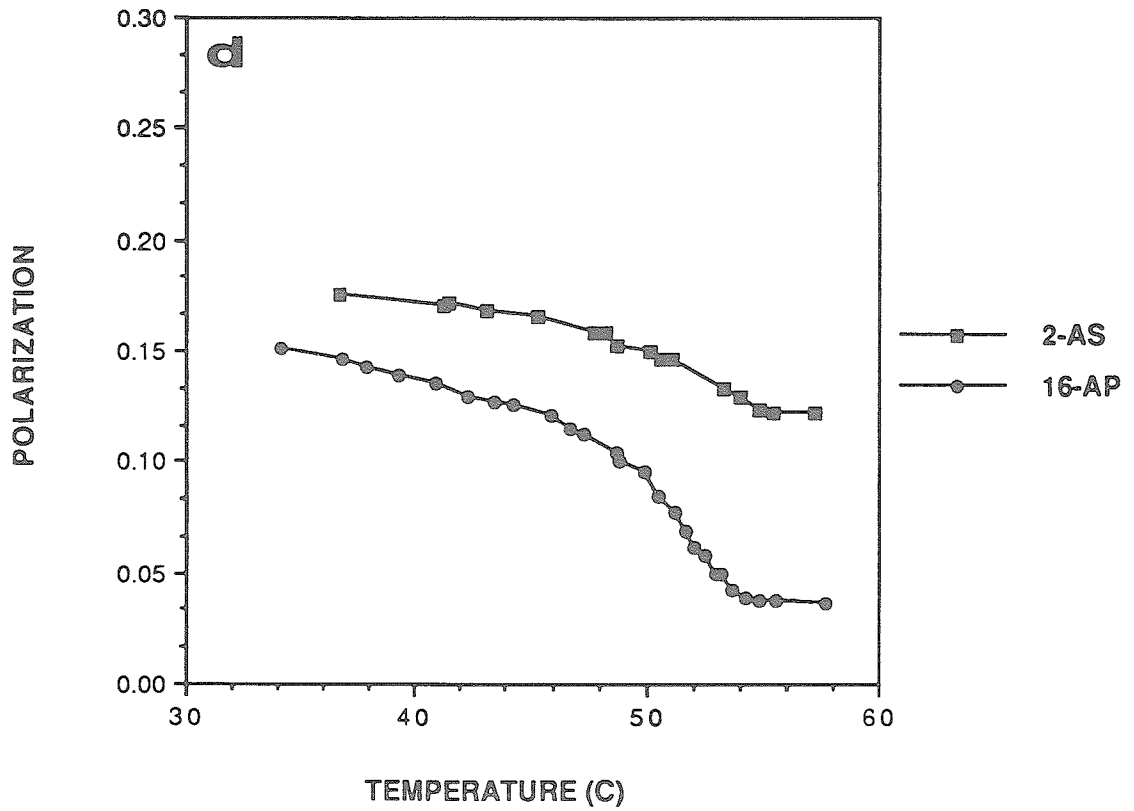
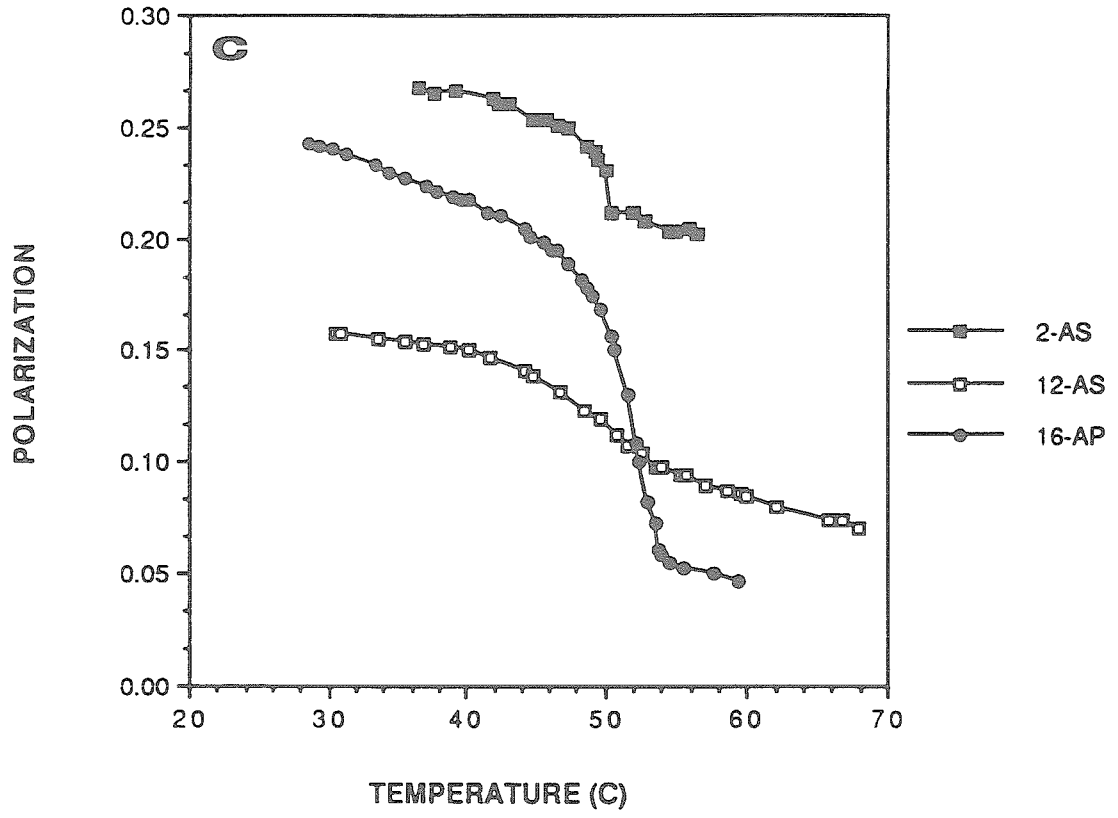
The orientation of n-anthroyloxy fluorescent probes in membranes. From reference (43).

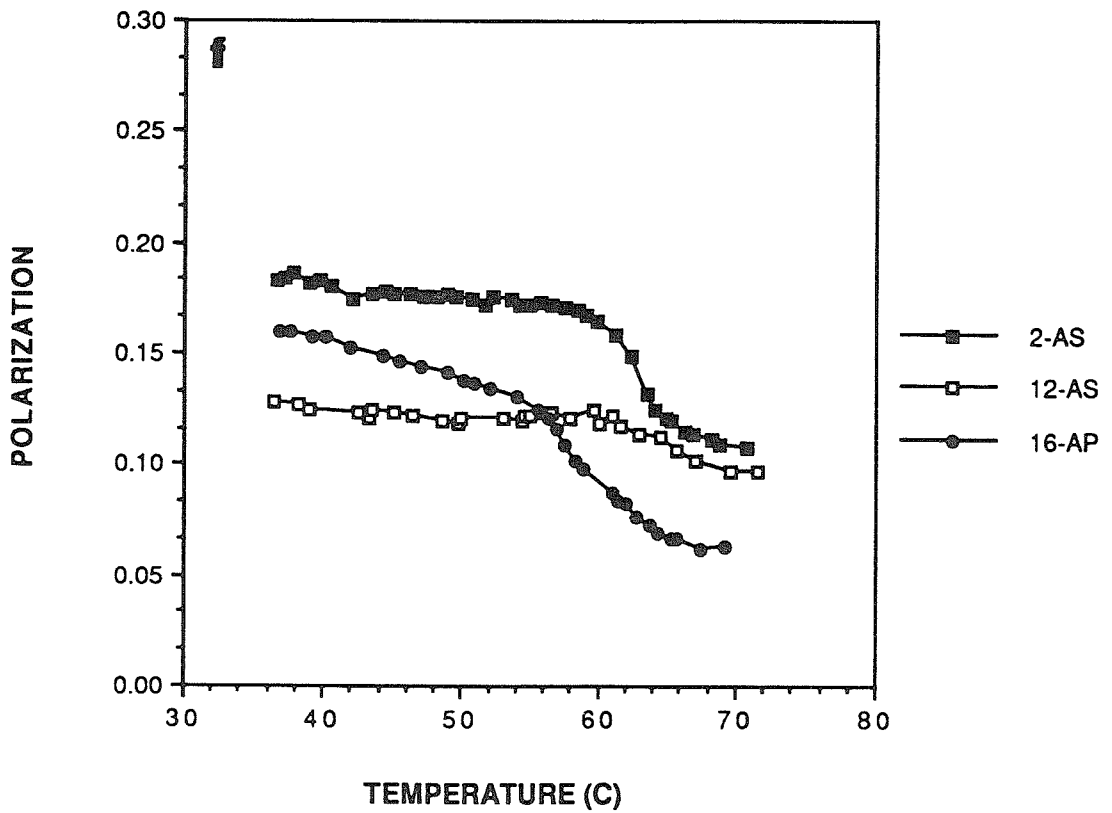
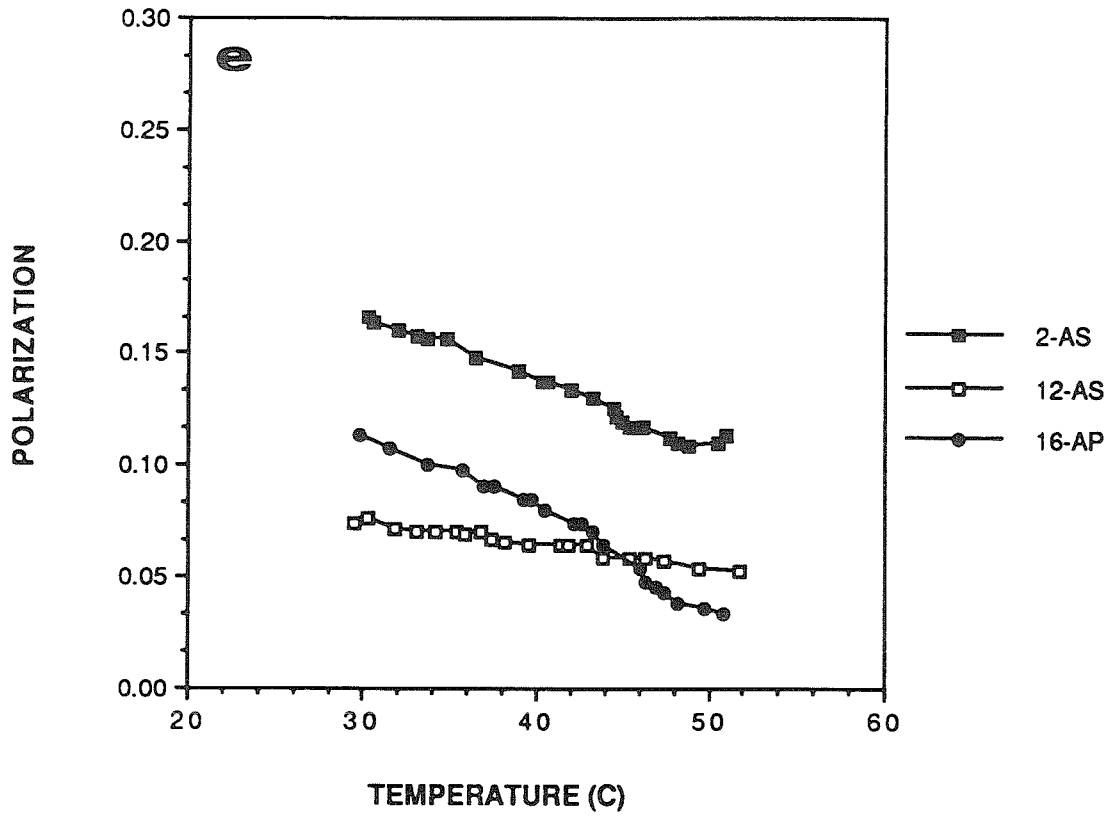


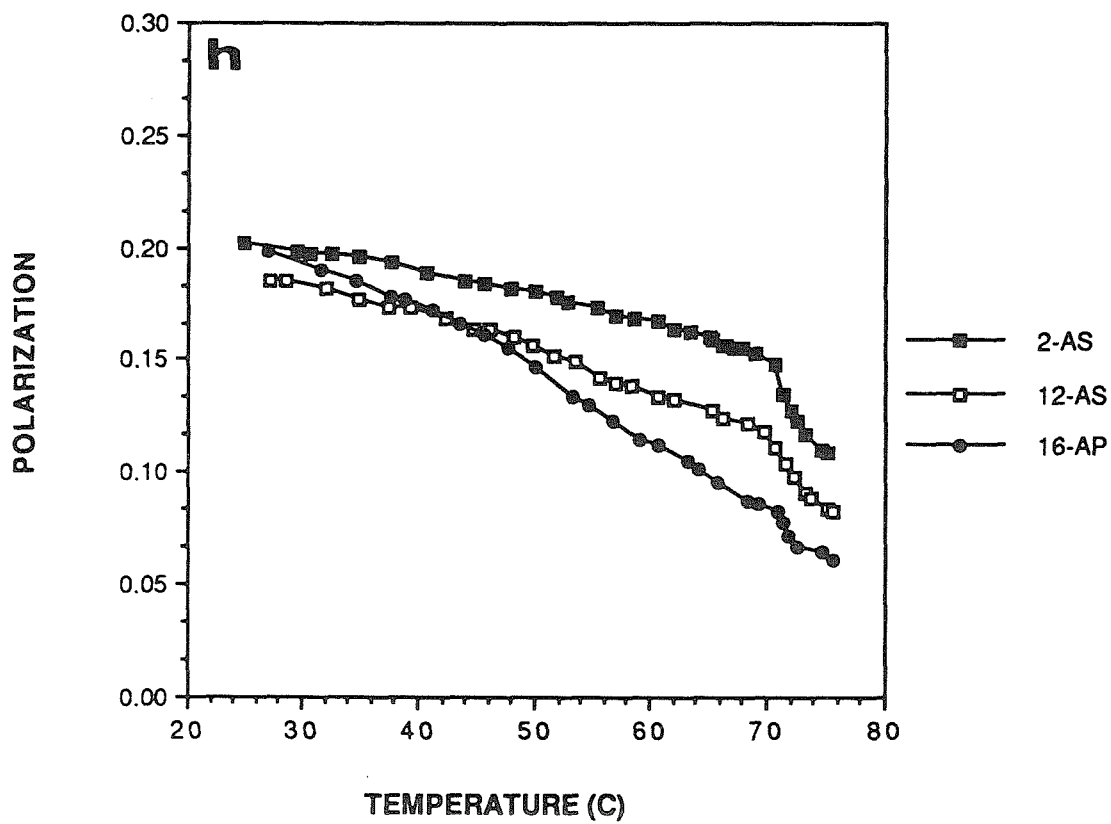
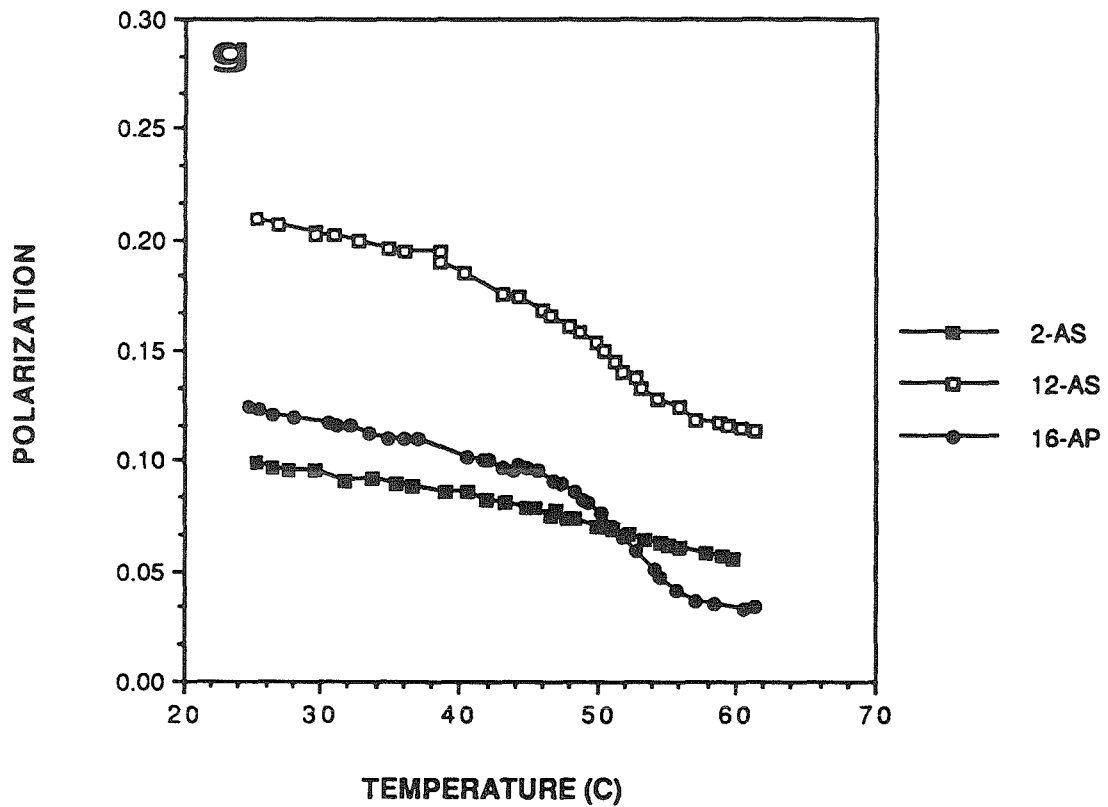
**Figure 7**

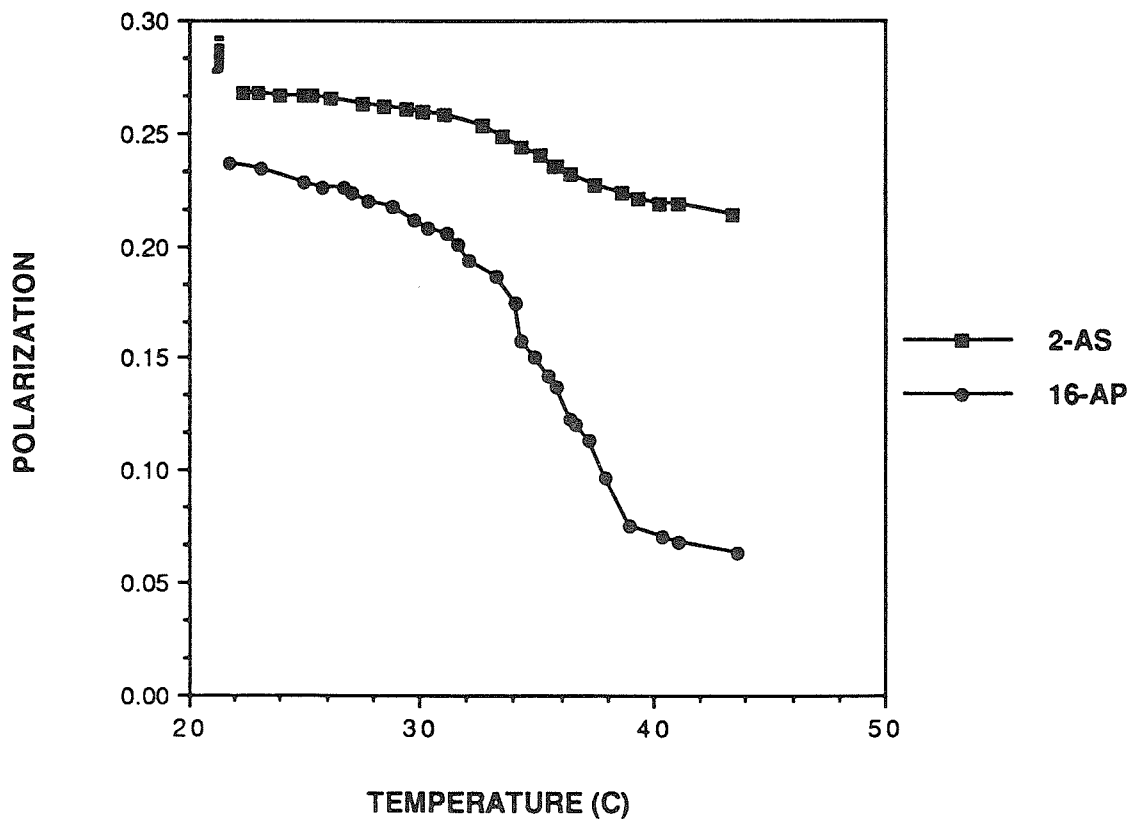
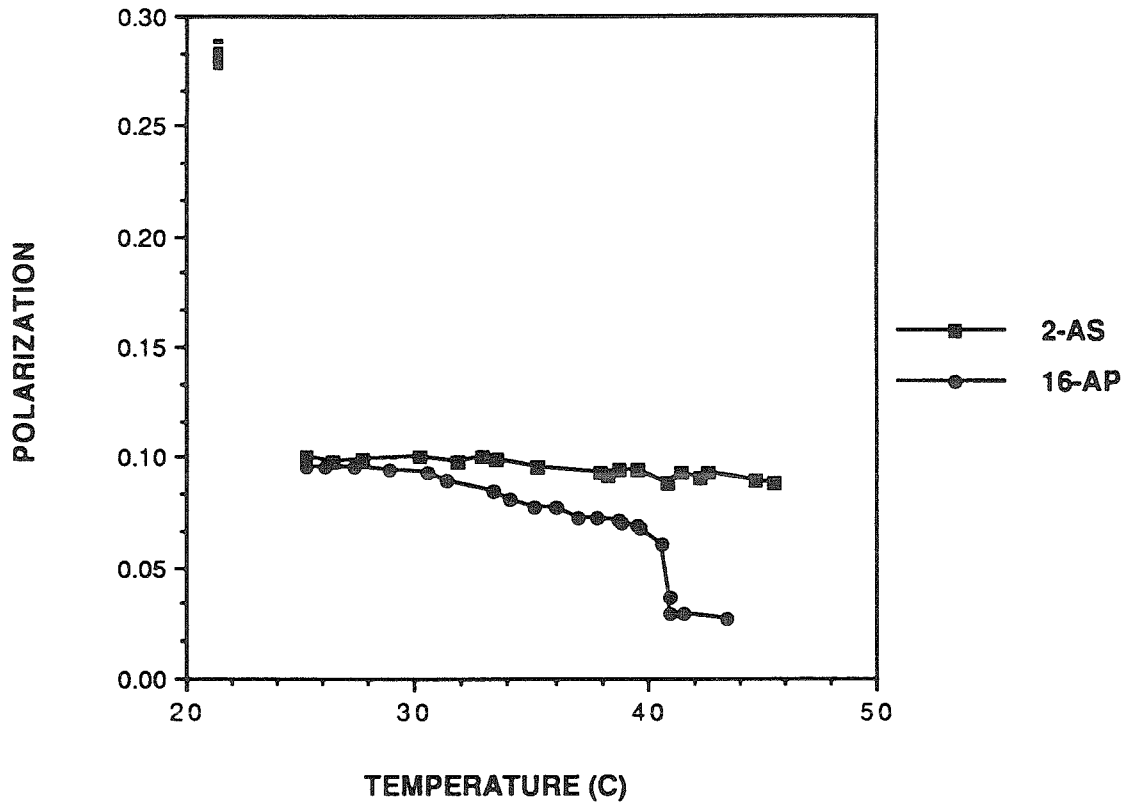
Gradients of "fluidity" as shown by typical plots of the fluorescence polarization of 2-AS, 12-AS and 16-AP as a function of temperature in various lipid bilayers: A. monomeric  $\alpha$ -16 ; B. polymeric  $\alpha$ -16; C. polymeric  $\alpha$ -20; D. monomeric  $\alpha$ -20; E. monomeric  $\omega$ -15; F. polymeric  $\omega$ -15; G. monomeric  $\omega$ -16; H. polymeric  $\omega$ -16; I. DPPC; J. polymeric  $\alpha$ -18. All measurements were made with heating scans. The symbols are assigned in the legends.











of the polarization for 16-AP compared to 12-AS and 2-AS. In the case of the polymerized  $\omega$ -THIOLS, the situation may be quite different, as is discussed below.

Table IV contains a summary of polarization values of the anthroyl probes solubilized in various monomeric and polymeric membranes in the liquid-crystalline state. Also included is the "apparent gradient" calculated as the difference in polarization between 2-AS and 16-AP (at temperatures above the  $T_m$  of each lipid). For the  $\alpha$ -THIOLS, it is interesting to note that the difference in polarization between 2-AS and 16-AP (the "apparent gradient") is greater for polymeric  $\alpha$ -THIOLS than for the monomers indicating that a similar "fluidity" profile is present in the polymeric membranes as in conventional bilayers. It is most likely the effect of the interfacial polymerization on the restricted motions of 2-AS that enhances the difference in the polarization between 2-AS and 16-AP for the polymeric membranes compared to the monomers. As with DPH, the changes in polarization of the anthroyl probes on passing through the phase transition ( $\Delta POL_{TM}$ ) is also greatest for the polymeric  $\alpha$ -THIOLS (see Figure 7).

For the  $\omega$ -THIOLS, the extent of phase transition-induced changes in polarization,  $\Delta POL_{TM}$ , were not as distinctly different between the monomers and polymers (Figure 7). More importantly, in contrast to the greater "gradient" of polymeric  $\alpha$ -THIOLS compared to the  $\alpha$ -THIOL monomers, the gradient for polymeric  $\omega$ -THIOLS was approximately *half* that of the corresponding monomers (Table IV). However, one would not expect as large a gradient for the polymeric  $\omega$ -THIOLS due to the conformational and dynamic restrictions imposed by the terminal disulfide on the chains. In fact, we were initially surprised by the observation of any gradient at all. There are two possible explanations for the observation of even a small gradient:

**Table V**

Summary of the values of the fluorescence polarization of 2-AS, 12-AS, and 16-AP in the liquid-crystalline state of various monomeric and polymeric  $\alpha$ -THIOLS and  $\omega$ -THIOLS. The "gradient," defined as the difference in the polarization of 2-AS and 16-AP, is also tabulated in the fourth column. The temperature in parenthesis is the temperature at which the polarization values were recorded and where the polarization becomes relatively constant with temperature. (M) and (P) refer to the monomeric and polymeric form of the lipid.

POLARIZATION

Lipid	2-AS	12-AS	16-AP	Gradient (T °C)
<b><math>\alpha</math>-THIOLS</b>				
$\alpha$ -16 (M)	0.133	0.072	0.042	0.091 (40)
$\alpha$ -16 (P)	0.219	0.122	0.073	0.160 (40)
$\alpha$ -18 (P)	0.214		0.131	0.150 (45)
$\alpha$ -20 (M)	0.124		0.033	0.091 (60)
$\alpha$ -20 (P)	0.208	0.078	0.043	0.165 (60)
<b><math>\omega</math>-THIOLS</b>				
$\omega$ -15 (M)	0.114		0.415	0.076 (55)
$\omega$ -15 (P)	0.105		0.071	0.034 (70)
$\omega$ -16 (M)	0.127	0.067	0.042	0.085 (60)
$\omega$ -16 (P)	0.106	0.059	0.065	0.041 (75)

<sup>a</sup>The midpoint of the entire transition

(i) The mobility of 16-AP is inherently higher than that of 2-AS. This is due to the attachment position at the chain terminus of the fatty acid, which provides greater motional freedom of the fluorophore compared to 2-AS and 12-AS. The latter two are motionally restricted by steric hindrance from the rest of the acyl chain. Thus the small gradient that is observed could be attributed exclusively to the inherent differences in the probe motions, without the need to assume any gradient is present in the bilayers of the polymeric  $\omega$ -THIOLS.

(ii) The gradient represents a small degree of disorder, which increases toward the bilayer interior. In this regard, it should be reiterated that the polarization values reflect both a combination of structural and dynamic characteristics of the membranes. Since polymerization decreases not only the translational and rotational mobility of the lipids as a whole, but in the case of the  $\omega$ -THIOLS, also the segmental motions, it is likely that whatever small gradient of disorder does exist is one of structural disorder and *not* due to increased motion and "fluidity" as is the conventional interpretation. In Chapter V, we show by  $^{13}\text{C}$  spin-lattice relaxation measurements ( $T_1$ ) that the relaxation rates of the carbons along the acyl chains of a polymeric  $\omega$ -THIOL are almost identical illustrating the lack of a mobility gradient. By contrast, a mobility gradient is observed for nonpolymerizable phosphatidylcholines and polymerized  $\alpha$ -THIOLS as indicated by the increase in the value of  $T_1$  from the  $\alpha$ -methylene to the chain terminus. Therefore if a gradient does exist, it is likely to be one of structural disorder only.

Carboxyfluorescein Release. Thus far, we have shown that these polymerizable membranes, monomeric and polymeric alike, undergo phase transitions involving major reorganizations of the membrane. In addition to the implications these data have

in terms of the membrane structure, knowledge of the phase transition is important for encapsulation technologies. For nonpolymerizable lipids, it has been shown that coincident with the phase transition is a maximal rate or abrupt increase in the leakage of entrapped solutes (1,2). To investigate whether similar phenomena occur for the THIOLE phosphatidylcholines, carboxyfluorescein release was examined as a function of temperature.

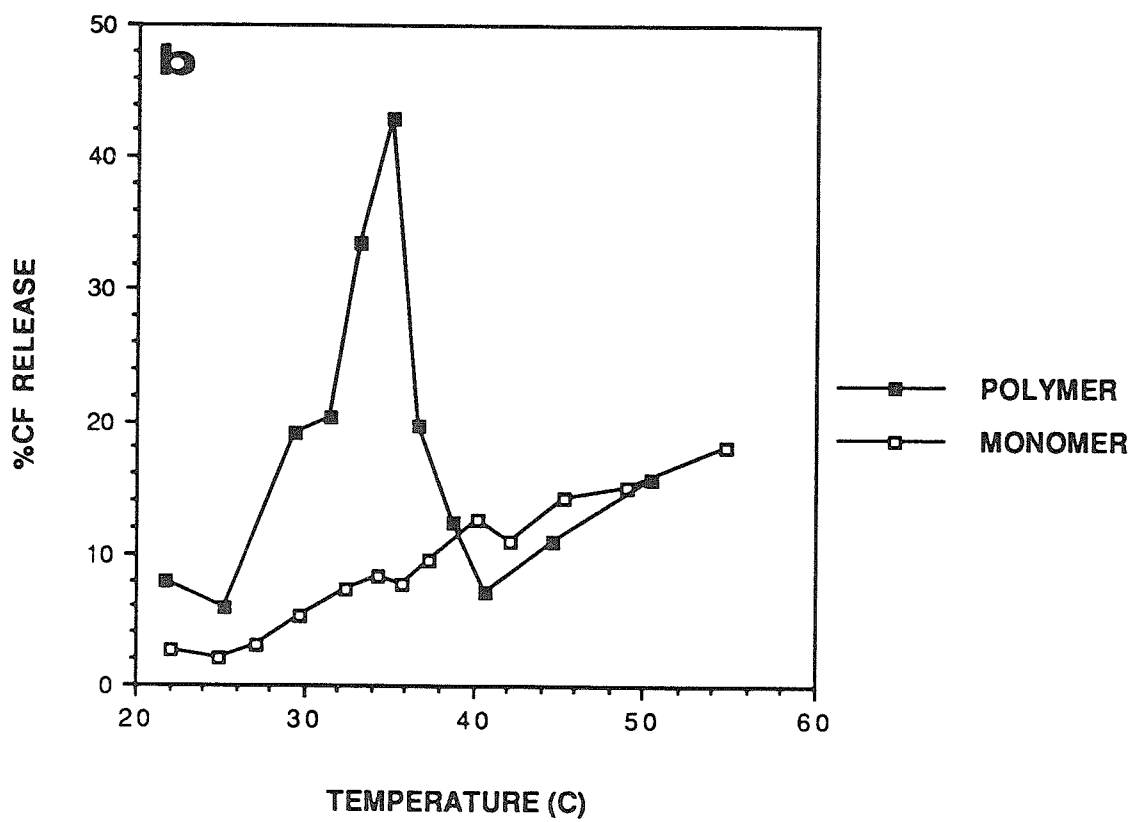
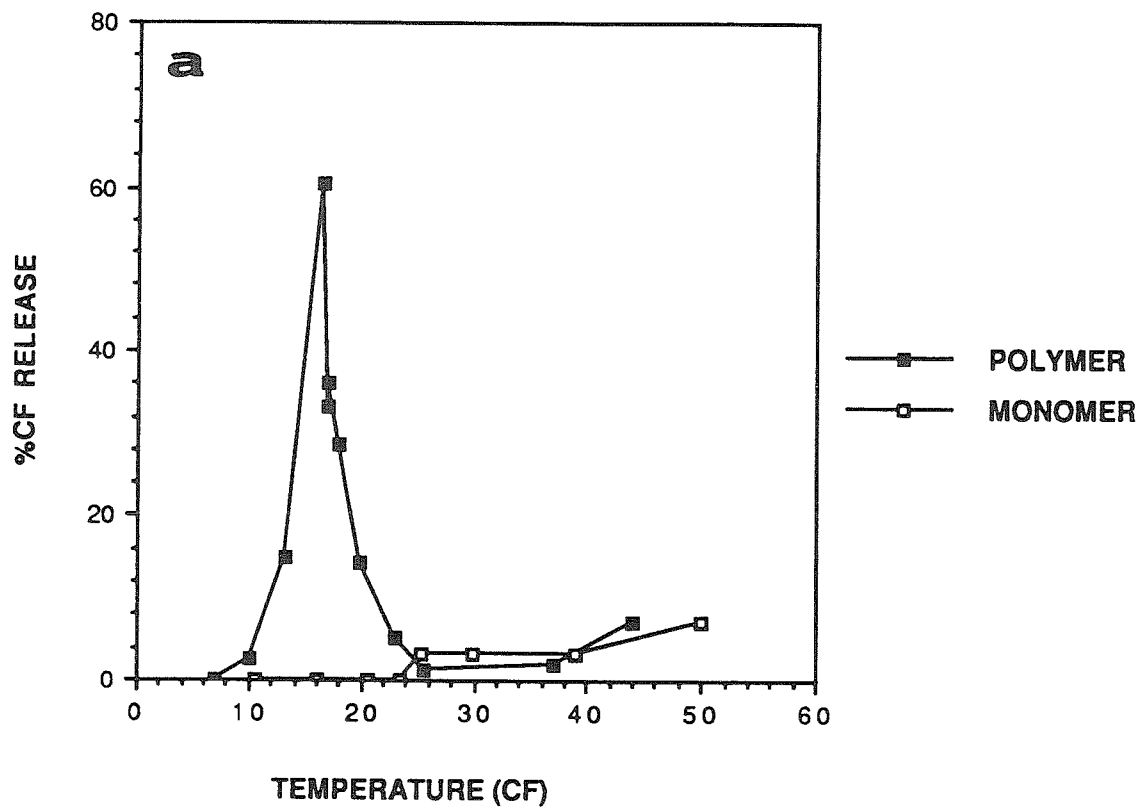
Figure 8 shows the release curves of sonicated dispersions of monomeric and polymeric  $\alpha$ -16 to  $\alpha$ -20. By comparison with the phase transition data, it is clear that for  $\alpha$ -18 and  $\alpha$ -20, maximal or increased leakage of carboxyfluorescein does in fact occur at the phase transition. For polymeric  $\alpha$ -16, maximal release occurs at the first component of the transition. This is demonstrated by the superposition of the DPH polarization curves with the carboxyfluorescein release profile in Figure 8 D. While the DPH is most sensitive to the second portion of the transition, 16-AP was found to be sensitive almost exclusively to the first portion (see Figure 7), which is also the part of the transition leading to carboxyfluorescein release. This suggests a reorganization predominantly localized to the bilayer midplane is responsible for the phase transition-induced leakage in polymeric  $\alpha$ -16. As a final point, it seems quite obvious that the increase in release at the  $T_m$  from polymeric  $\alpha$ -THIOLES exceeds that of the monomers.\* The physical basis for this is not clear but is consistent with the fact that the changes in membrane organization that occur on passing through the phase transition (as reflected by  $\Delta POL_{TM}$  in Table III) are generally greater for polymeric  $\alpha$ -THIOLES compared to their monomeric analogues. Furthermore, in the next chapter it is shown that the polymeric  $\alpha$ -THIOLES are more disordered than the monomers and nonpolymerizable analogues that would likely lead to enhanced solute release.

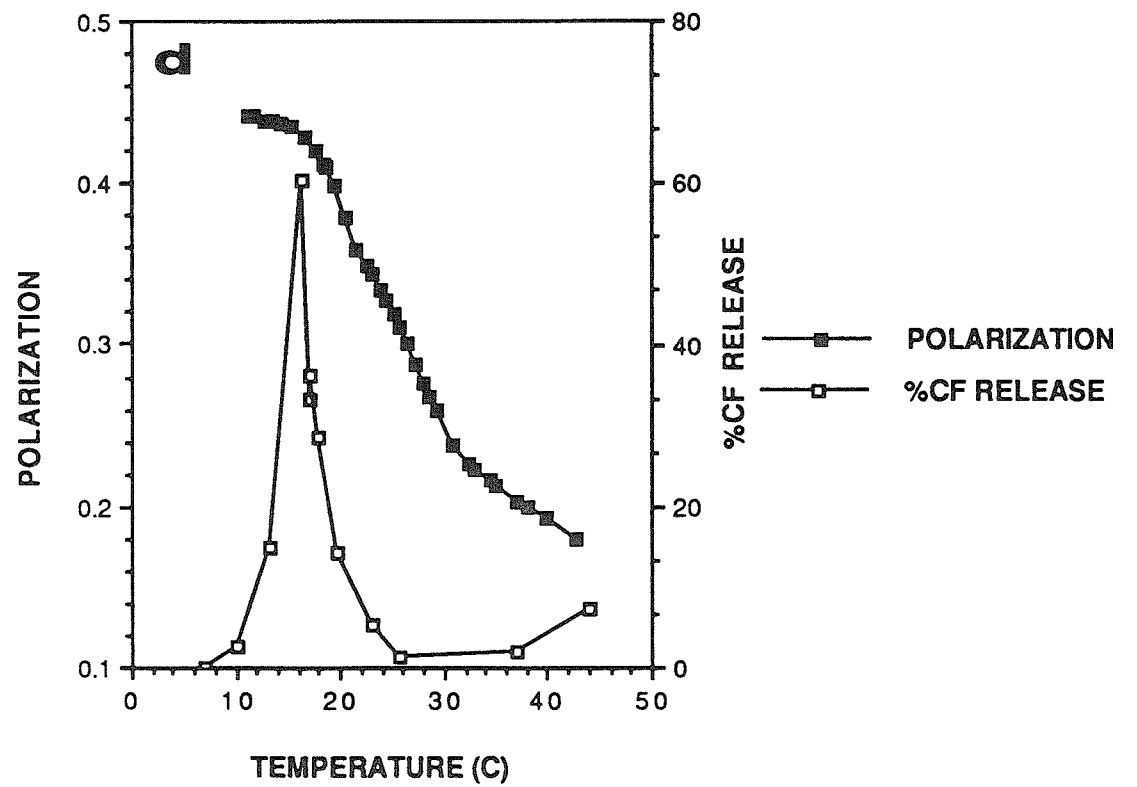
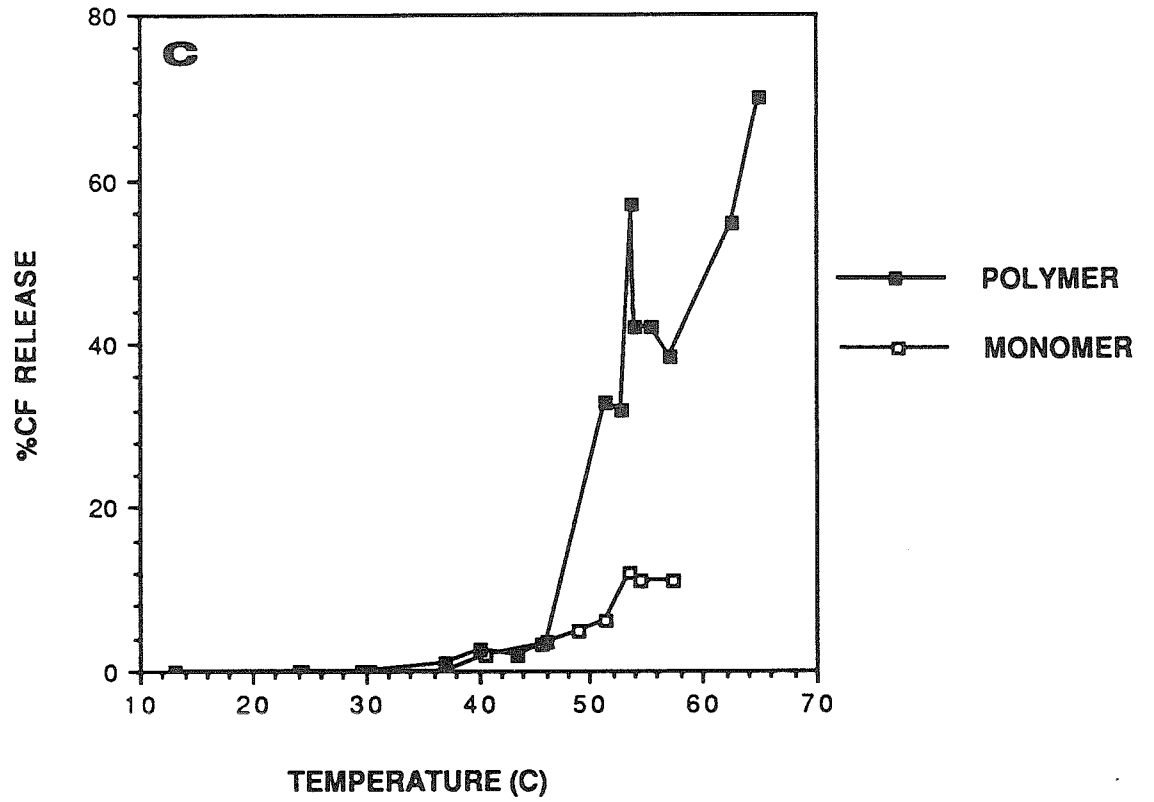
---

\* Some variation from run to run is observed but the trend of increased leakage for the polymers was reproducible.

**Figure 8**

Percent release of carboxyfluorescein as a function of temperature for monomeric and polymeric: **A.**  $\alpha$ -16 SUVs; **B.**  $\alpha$ -18 SUVs; **C.**  $\alpha$ -20 SUVs. The percent release was based on measurements of the carboxyfluorescein fluorescence after 10 min of incubation of the samples at the indicated temperatures. **D.** Superposition of the carboxyfluorescein release curve and DPH polarization curve of polymeric  $\alpha$ -16 SUVs to demonstrate the position of the maximum release rate with respect to the phase transition.





Polymeric  $\omega$ -THIOLS were not examined due to the fact that they appear to form bilayer fragments as described in Chapter II. Attempts to entrap carboxyfluorescein by hydration of lyophilized powders was predictably unsuccessful.

## DISCUSSION

In this study, we have examined the phase transition behavior of two series of polymerizable phosphatidylcholines in order to understand the molecular organization of the bilayer and how it is related to the molecular structure of the constituent lipids. Based on  $T_m$  and  $\Delta H$  data, it was concluded that the presence of the sulfhydryl or disulfide group at the interface ( $\alpha$ -THIOLS) reduces the packing density relative to phosphatidylcholine analogues lacking this pendant group. A combination of steric bulk, polarity and hydration most likely lead to a larger effective headgroup area and a reduced van der Waals interaction between the chains. Such structural features are consistent with the phenomenological observations described in Chapter II that these liposomes are readily hydrated and sonicated into SUVs. Using depth-dependant anthroyl probes, a gradient of structural disorder and/or increased motion extending from the interface to the bilayer midplane, was demonstrated for both polymeric and monomeric  $\alpha$ -THIOLS. In fact, it was even larger for polymeric  $\alpha$ -THIOLS than the monomers. This suggests retention of basic features of normal bilayers by polymerizing at a region of the bilayer normally quite rigid in nonpolymerizable membranes.

An unexpected result, however, was the fact that the differences in polarization between the gel and liquid crystalline state for all fluorescent probes was greater for polymeric than monomeric membranes. While somewhat speculative, this could be due to (i) increased immobilization of the probe in the gel state and/or (ii) increased

mobility of the probe in the liquid crystalline state, relative to nonpolymerized lipids. Results from vibrational spectroscopy described in the next chapter suggest that the lipid chains of polymeric  $\alpha$ -THIOLS are actually more disordered in the gel state than that of the nonpolymerized lipids. Therefore, while counterintuitive, we favor the argument that the mobility of the probes in the liquid-crystalline state is actually quite high, despite polymerization of the matrix. A possible mechanism for this could be the creation of interfacial defects between unlinked polymer segments or different polymer chains where the probe may be preferentially admitted. The available space within such defects for depolarizing motions should be greater than that within homogeneously-packed monomeric membranes. Similar reports of "cleft" formation have been described by Fendler *et al.* based on the greater mobility of spin probes in certain polymerized membranes, compared to their monomeric analogues (39). Finally, such a mechanism provides a rational physical basis for several other experimental observations pertaining to these lipids including morphology (Chapter II), the vibrational spectra (Chapter IV) and the *in vivo* clearance rates (Chapter VII).

As a final point concerning the  $\alpha$ -THIOLS, carboxyfluorescein release experiments revealed that leakage was greatly enhanced at the phase transition. In consideration of the thermal data, the implications of this are that long-chain (N=20)  $\alpha$ -THIOLS are necessary to optimize encapsulation efficiencies since the transition temperatures are such that polymeric  $\alpha$ -16 has a maximal leakage rate near room-temperature and polymeric  $\alpha$ -18, at 37°C (physiological temperature).

$\omega$ -THIOLS show very different behavior than the  $\alpha$ -THIOLS. For monomeric lipids, the  $T_m$  and  $\Delta H$  was increased relative to phosphatidylcholines of the same chain but lacking the sulfhydryl. The increased interaction between the lipids implied by these data is consistent with their morphological behavior: very short chain  $\omega$ -THIOLS (N=10 and possibly 9) form stable bilayers and long chain  $\omega$ -THIOLS have a high

propensity for aggregation. On polymerization, the enthalpy and transition temperature are increased even further. Using anthroyl probes, only small gradients of "fluidity" reflecting depth-dependent changes in mobility and/or structural disorder were detected in polymeric  $\omega$ -THIOLS compared to monomeric or nonpolymerizable analogues. The decreased magnitude of the gradient in the polymers is a consequence of the restricted motion imposed by the chain terminal polymerizable moiety. Furthermore, whatever gradient may be present is most likely a reflection of increased structural disorder from the interface to the bilayer midplane and not to increased mobility. Finally, it should be pointed out that polarity and fluidity gradients have also been reported for methacroyl-based phosphatidylcholines using ESR depth-dependent nitroxide spin labels, even for chain-terminating cross-linkable methacrylates (18). It is possible that the "fluidity gradients" detected in these experiments are predominantly gradients of structural disorder rather than segmental mobility of the chains.

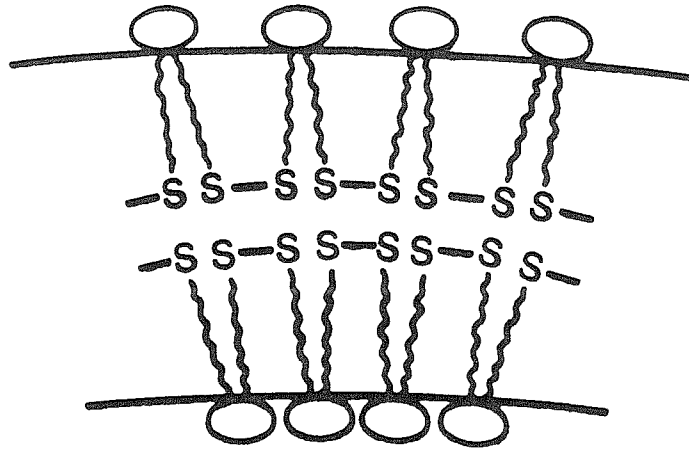
The most surprising of the above results concerning the polymeric  $\omega$ -THIOLS was the retention of the phase transition. For all reported double-chain phospholipids polymerizable at the chain terminus, no transitions were detected subsequent to polymerization. We believe the presence of a substantial phase transition in these lipids may therefore have structural implications concerning whether polymerization is strictly intraleaflet, interleaflet or a combination of both. The two extreme possibilities are illustrated in Figure 9.

It seems quite unlikely that transbilayer crosslinking would lead to a thermal transition at all, since this would have to involve a major cooperative compression of the bilayer thickness. Furthermore, gauche conformations in a chain on one side of the bilayer would tend to oppose gauche conformations in the chain to which it is linked on the other side of the bilayer. Runquist has in fact shown by phospholipase susceptibility experiments, that a dimerizable lipid, DPL- $\omega$ 16 (sn2-sn1) containing

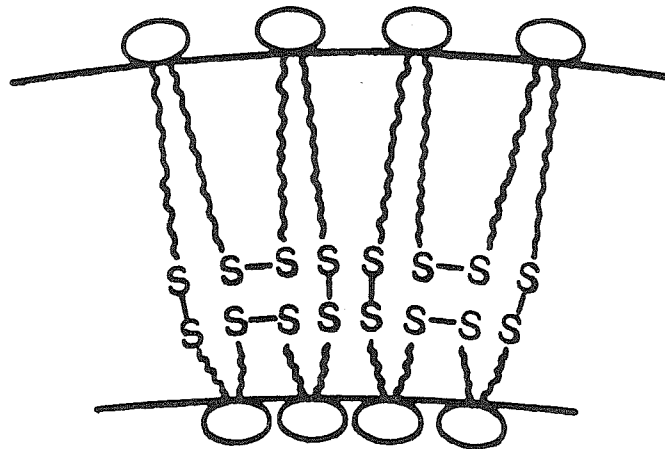
**Figure 9**

Possible modes of polymerization of  $\omega$ -THIOLS in lipid bilayers: **A.** Pure *intraleaflet* coupling; **B.** *Inter - and Intra-leaflet* coupling.

A



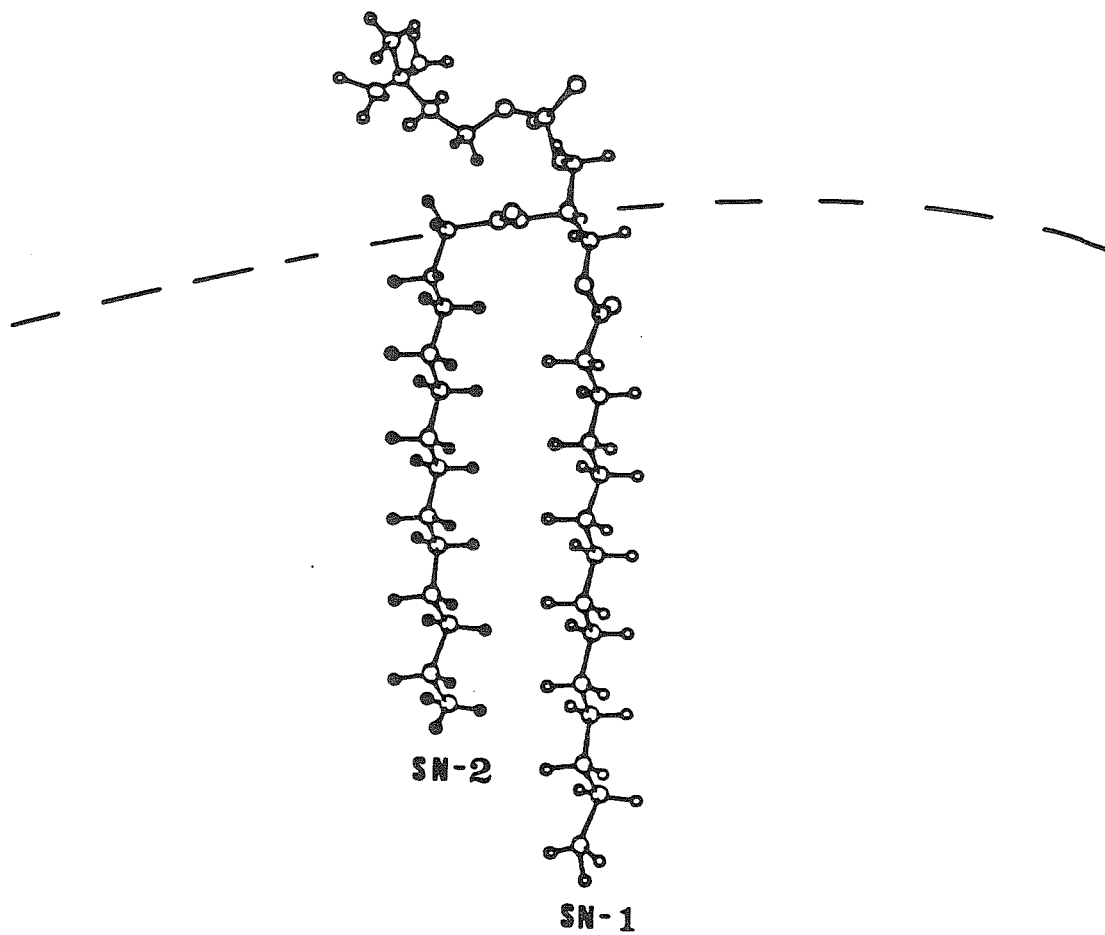
B



$\omega$ -16 in the sn-2 chain and DPL in the sn-1 chain, is crosslinked almost exclusively within a single leaflet of the bilayer (40). If we now consider the established orientation of the two acyl chains of DPPC in bilayers, we can further argue for predominantly intraleaflet coupling for the polymeric  $\omega$ -THIOLS. From NMR and X-ray studies it has been shown that the first few segments of the two chains have different conformations (41,42). The sn-1 chain is perpendicular to the bilayer along its entire length while the first two carbons of the sn-2 chain run parallel to the bilayer surface and the rest of the chain runs parallel to the sn-1 chain. The net result is a difference in the penetration lengths of the two chains into the bilayer as shown in Figure 10. The 2.5Å displacement of the sn-2 chain from the bilayer center should favor intraleaflet coupling. The sn-1 chain, on the other hand, may be more disposed to interleaflet coupling but as shown by Runquist, this is not the case. It is also important to note that polymerization of these lipids was carried out in the liquid crystalline state of the monomer where chain disorder should tend to promote intraleaflet coupling. If, on the other hand, the lipids had been polymerized in the gel state where the chains are highly trans in orientation, transbilayer polymerization might be more likely to occur. Finally, in the reports by Runquist, an enthalpy of 13 KCal/mole was measured for DPL- $\omega$ 16 which is interesting since it is slightly higher than the enthalpy of DPPC (8.7 kCal/mole) due to 1 intraleaflet coupled chain, and slightly less than the enthalpy of polymeric  $\omega$ -16, perhaps because  $\omega$ -16 has predominantly two intraleaflet coupled chains. Based on the presence of the phase transitions described in this chapter and the argument presented above, we believe that predominantly intraleaflet coupling is occurring in the  $\omega$ -THIOLS. A phase transition similar to that of nonpolymerizable lipids is then easily envisioned by two intraleaflet-coupled chains acting in concert. Disorder in one would promote cooperative disorder in the other.

**Figure 10**

Orientation of lecithins in bilayers. The dotted line represents the membrane surface and the chains are labeled as sn-1 and sn-2. It is clear from the figure that the sn-1 chain penetrates the bilayer to a greater extent than the sn-2 chain. From reference (42).



**REFERENCES**

1. Magin, R.L. and Weinstein, J.N. in: *Liposome Technology* ; Gregoriadis, G. (Ed.); Boca Raton: CRC Press, 1984; Vol. III,137-155.
2. Weinstein, J.N., Klausner, R.D., Innerarity, T., Ralston, E. and Blumenthal, R. (1981) *Biochim. Biophys. Acta.* **647**, 270-284.
3. Samuel, N.K.P., Singh, M., Yamaguchi, K. and Regen, S.L. (1985) *J. Am. Chem. Soc.* **107**, 42-47.
4. Regen, S.L., Yamaguchi, K., Samuel, N.K.P., and Singh, M. (1983) *J. Am. Chem. Soc.* **105**, 6354.
5. Weinstein, J.N., Ralston, F., Leserman, L. D., Klausner, R.D., Dragsten, P., Henkart, P. and Blumenthal, R. in: *Liposome Technology* ; Gregoriadis, G. (Ed.); Boca Raton: CRC Press, 1984; Vol. III, 183-204.
6. Blazyk, J. et al. (1987) *Applied Spectroscopy* **41**, 40.
7. Lakowicz, J.R. in: *Principles of Applied Spectroscopy* ; New York: Plenum Press, 1983, 128.
8. Biltonen, R.L. and Freire, E. (1978) *CRC Crit. Rev. Biochem.* 85-124.
9. Lee, A.G. (1977) *Biochim. Biophys. Acta.* **472**, 237.
10. Nagle, J.F. (1980) *Ann. Rev. Phys. Chem.* **31**, 157.
11. Mabrey-Gaud, S. in : in : *Liposomes from Physical Structure to Therapeutic Applications* ; Knight, C.G. (Ed.); Elsevier: North Holland Biomedical Press, 1981; 105.
12. Lewis, R., private communications.
13. Lentz, B.R., Barenholz, Y. and Thompson, T. (1976) *Biochemistry* **15**, 4521-4528.

14. Suurkuusk, J. Lentz, B.R., Barenholz, Y., Biltonen, R.L. and Thompson, T.E. (1976) *Biochemistry* **15**,1393-1401.
15. Gruenewald, B., Stankowski, S. and Blume, A. (1979) *FEBS Lett.* **102**, 227-229.
16. Fendler, J.H. (1984) *Science* **223**,888.
17. Bader, H., Dorn, K., Hupfer, B., Ringsdorf, H. (1985) *Adv. Polym. Sci.* **64**, 1.
18. Kusumi, A., Singh, M., Tirrell, D.A., Oehme, G., Singh, A., Samuel, N.K.P., Hyde, J. and Regen, S.L. (1983) *J. Am. Chem. Soc.* **105**, 2975-2980.
19. Leaver, J., Alonso, A., Durrani, A. and Chapman, D. (1983) *Biochim. Biophys. Acta.* **732**, 210-218.
20. Mantsch, H.H. (1984) *J. Mol. Struct.* **113**, 201-212.
21. Dluhy, R.A., Moffatt, D., Cameron, D.G., Mendelsohn, R. and Mantsch, H.H. (1985) *Can. J. Chem.* **63**, 1925.
22. Snyder, R.G., Hsu, S.L., Krimm, S. (1978) *Spectrochimica Acta.* **43A**, 395-406.
23. Casal, H.L. and Mantsch, H.H. (1984) *Biochim. Biophys. Acta.* **779**, 381-401.
24. Cameron, D.G., Casal, H.L., Gudgin, E.F. and Mantsch, H.H. (1980) *Biochim. Biophys. Acta.* **596**, 463-467.
25. Shinitzky, M., Dianoux, A.C., Gitler, C., and Weeber, G. (1971) *Biochemistry* **10**, 2106-2113.
26. Cogan, U., Shinitzky, M., Weber, G., Nishida, T. (1973) *Biochemistry* **12**, 521-528.
27. Shinitzky, M. and Barenholz, Y. (1978) *Biochim. Biophys. Acta.* **515**, 367-394.

28. Lentz, B.R., Barenholz, Y. and Thompson, T. (1976) *Biochemistry* **15** 4529-4537.
29. Van Blitterswijk, W.J., Van Hoeven, R.P. and Van der Meer, B.W. (1981) *Biochim. Biophys. Acta.* **644**,323-332.
30. Van der Meer, B.W., Van Hoeven, R.P. and Blitterswijk, W.J. (1986) *Biochim. Biophys. Acta.* **854**,38-44.
31. Heyn, M.P. (1979) *FEBS Lett.* **108**, 359-364.
32. Prendergast, F.G. (1981) *Periodicum Biologorum* **83**,69-79.
33. Cadenhead, D.A., Kellner, B.M., Jacobson, K. and Papahadjopoulos, D. (1977) *Biochemistry* **16**,5386-5392.
34. Seelig, J., Tamm, L., Hymel, L. and Feischer, S. (1981) *Biochemistry* **20**, 3922-3932.
35. Thulborn, K.R. and Sawyer, W.H. (1978) *Biochim. Biophys. Acta.* **511**, 125-140.
36. Chalpin, D.B. and Kleinfield, A.M. (1983) *Biochim. Biophys. Acta.* **731**, 465-474.
37. Haigh, E.A., Thulborn, K.R. and Sawyer, W.H. (1979) *Biochemistry* **18**, 3525-3532.
38. Chen, L., Dale, R., Roth, S. and Brand, L. (1977) *J. Biol. Chem.* **252**,2163.
39. Reed, W., Lasic, D. Huaser, H. and Fendler, J.H. (1985) *Macromolecules* **18**, 2005-2012.
40. Runquist, E.A. and Helmkamp, G.M. (1988) *Biochim. Biophys. Acta.* **940**, 10-20.
41. Roberts, M.F., Bothner-by, A.A. and Dennis, E.A. (1978) *Biochemistry* **17**, 935-942.

42. Pearson, R.H. and Pascher, I. (1979) *Nature* **281**, 499-501.

---

**Chapter IV**

---

*Investigations of the Acyl Chain Conformations and Membrane Packing  
Characteristics of Disulfide Polymerizable Phospholipids by  
Raman and FT-IR Spectroscopy.*

---

**Introduction**

To date, the majority of polymerizable lipids synthesized and described have the bilayer as their primary level of organization. This is in many cases due to the desire to imitate the compartmentalized nature of the cell for encapsulation technologies, or to prepare matrices conducive to reconstitution of functional proteins. To optimize the desirable membrane characteristics of such polymerized bilayers and establish structure-property relationships, a wide variety of physical studies have been carried out on a large library of polymeric lipids. For example, confirmation of the lamellar phase has been achieved primarily by freeze fracture and transmission electron microscopy (for a review of polymerized liposomes, see ref. 1 and 2; also see 3-5 for examples). The gel to liquid-crystalline phase transition, which reflects interactions between the components of the bilayer, is routinely measured for polymeric lipids by DSC. Finally, monolayer (6-7), permeability (8-12), fluidity (13), and diffusion studies (14) have also been carried out on a number of polymeric systems and compared to

similar studies of monomeric or nonpolymerizable analogues. As yet, however, there have only been a few studies concerned with the conformation of polymeric lipids on a molecular level (15). This is an important area for investigation since the physical properties of the bilayers are governed in large part by the conformation and packing of the constituent biomolecules.

In Chapters II and III, we examined the morphological and thermal properties of two classes of disulfide-polymerizable phospholipids. These studies revealed structural information pertaining to the macroscopic features of lipid aggregates and provided some insight into the nature of the packing of the lipids within the bilayer. In the present study, we examine more directly and on a molecular level, the conformational properties of the individual lipids and how they are organized within the bilayer. In particular, FT-IR and Raman spectroscopies are used to monitor vibrational modes sensitive to chain conformation, packing, and mobility. These include the C-H stretching vibrations in the IR and Raman spectra as well as the C-H bending and skeletal optical C-C stretching vibrations in Raman spectra. Changes in vibrational features as a function of chain length and position of the polymerizable moiety are used to establish general correlations between lipid structure and membrane organization for these two classes of polymerizable lipids. These data are further correlated to the macroscopic (bulk) physical properties of these lipids including morphology, leakage, and *in vivo* blood clearance, which are described in separate chapters.

## MATERIALS AND METHODS

### Materials.

The synthesis and polymerization of the disulfide polymerizable phosphatidylcholines was as described in Chapter VIII. Routinely the polymerized

form of the lipid was stored at 4°C until use. L- $\alpha$ -distearoylphosphatidylcholine (DSPC) and L- $\alpha$ -dipalmitoylphosphatidylcholine (DPPC) were purchased from Avanti Polar Lipids. All other reagents were of analytical grade and used without further purification.

### Methods.

FT-IR. Lipid samples were hydrated in D<sub>2</sub>O for 30 min at 80 °C. Samples were then placed between CaF<sub>2</sub> windows and transferred to a rigorously thermostated ( $\pm$  .1 °C) FT-IR mount containing Peltier thermoelectric modules (6). Automated data acquisition as a function of temperature was accomplished on a Mattson Sirius 100 FT-IR spectrometer under UNIX-based computer control.

Raman Spectroscopy. For hydrated samples, lipids were dispersed for 15-30 min above the phase transition and pelleted into 1 mm O.D. quartz capillaries. Dry samples were equilibrated for several hours at room temperature and placed in the capillaries as a plug. Data was recorded on a SPEX Raman spectrometer equipped with a Scamp microcomputer and a Spectra Physics 170 Argon ion laser using 500 mW of the 488-nm laser line. The slit width of the monochromator was set such that the accuracy of the band frequencies was  $\pm$  (3-4 cm<sup>-1</sup>). Data was transferred from the Scamp to the VAX mainframe computer where the data was baseline corrected using a least squares fit of a polynomial of up to order 15. A polynomial of 2 was generally sufficient to reproduce the baseline.

## RESULTS and DISCUSSION

Both FT-IR and Raman are nonperturbing techniques ideally suited for investigations of lipid conformation. This is due to the fact that many Raman- and

infrared-active modes characteristic of lipid molecules are extremely sensitive to changes in conformation and packing of the lipids, and may therefore be used to monitor even subtle changes in membrane organization induced by alteration of the lipid structure, temperature or the addition of non-phospholipid components (for a review, see 16-19; also see 20-28). Because of the dispersion of useful absorptions, one may also examine spectral features associated exclusively with the headgroup ( $\text{PO}_4^-$  and C-N stretching modes), the interfacial region (C=O stretching mode) and the acyl chains (skeletal C-C stretching and C-H stretching, twisting and deformation modes). Finally, because of the time scale of the experiment ( $\approx 10^{-12}$  s) most molecular motions are effectively frozen out, and therefore the interpretation of the data is not complicated by anisotropic motional averaging (17).

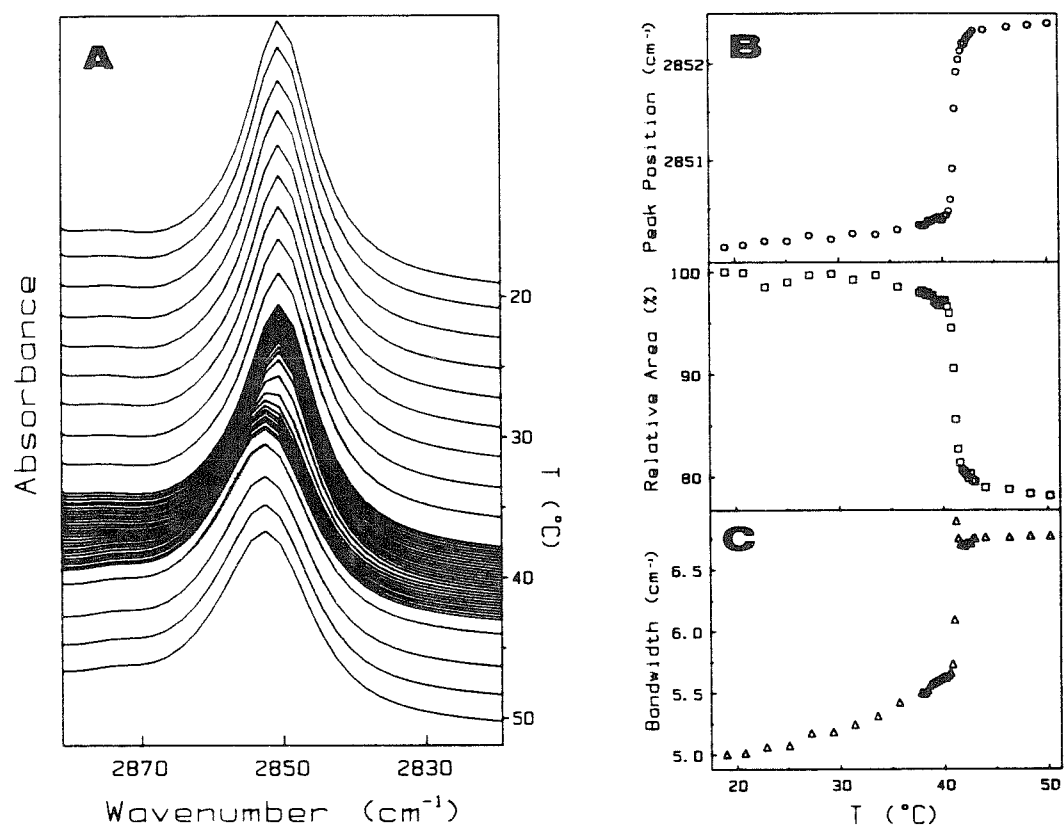
In the present study we have restricted ourselves to investigations of vibrational modes associated with the hydrocarbon region of polymerizable phospholipids, and for comparison, nonpolymerizable lipids. Data obtained from the C-H stretching region of the infrared spectrum are first described, followed by observations obtained from the Raman C-H stretching and skeletal C-C stretching vibrations.

### FT-IR.

As a preface to describing the results of the present study, it is useful to summarize salient features concerning the infrared spectra of nonpolymerizable saturated phosphatidylcholines that already been described in great detail. Figure 1 shows the C-H stretching region of DPPC as a function of temperature. The bands at 2850 and 2970  $\text{cm}^{-1}$  correspond to the C-H symmetric and asymmetric stretching modes, which are the strongest bands in the infrared spectra, while the less intense bands at 2956 and 2870  $\text{cm}^{-1}$  correspond to the asymmetric and symmetric stretches of the terminal methyl group (16,17). The frequencies and bandwidths of these modes are extremely sensitive to chain conformation and the amount of chain disorder, respectively. In

**Figure 1**

**A.** Temperature dependent changes in the C-H stretching region of DPPC bilayers; **B.** Changes in the peak position of the symmetric C-H stretching mode; **C.** Changes in the bandwidth of the symmetric methylene stretching mode.



particular, the introduction of gauche conformers in the chains and the onset of chain mobility causes an increase in the peak positions and bandwidth as shown in Figure 1 for the C-H symmetric stretching vibrations.\*

The change in peak position of  $\approx 2 \text{ cm}^{-1}$  at the  $T_m$  corresponds to the introduction of approximately 5 gauche conformers in the acyl chains of DPPC (16,29). Unfortunately, the relationship between frequency and/or change in frequency at  $T_m$ , and the number of gauche conformers is only semiquantitative (16). Bandwidths and the degree of chain disorder, on the other hand, have been reported to be more quantitatively related but this is complicated by the difficulty in establishing an accurate baseline from which to calculate bandwidths at a fractional peak height (16). Nonetheless, the general correlation of (i) decreased frequency and increased trans conformation and (ii) increased bandwidth and increased chain disorder are useful starting points for qualitatively describing the nature of membranes formed by polymerizable phospholipids.

The C-H stretching region for monomeric and polymeric 16-carbon  $\alpha$ - and  $\omega$ -THIOLS is shown in Figure 2. The most obvious difference between the spectra of the two classes of lipids is the absence of the methyl stretching modes at 2965 and 2870  $\text{cm}^{-1}$  in the case of the  $\omega$ -16. However, it is also apparent that at a given temperature above or below the  $T_m$ , the bandwidths of the  $\omega$ -16 are more narrow than that of the  $\alpha$ -16. Furthermore, the bandwidth of the  $\omega$ -16 decreases on polymerization while that of  $\alpha$ -16 increases, suggesting polymerization decreases the conformational disorder of  $\omega$ -16 bilayers, while it is increased on polymerization of  $\alpha$ -16. This also suggests that the  $\omega$ -16 bilayers as a class of lipids are more rigid and/or ordered than those of  $\alpha$ -16. These trends are better visualized in Figure 3, which

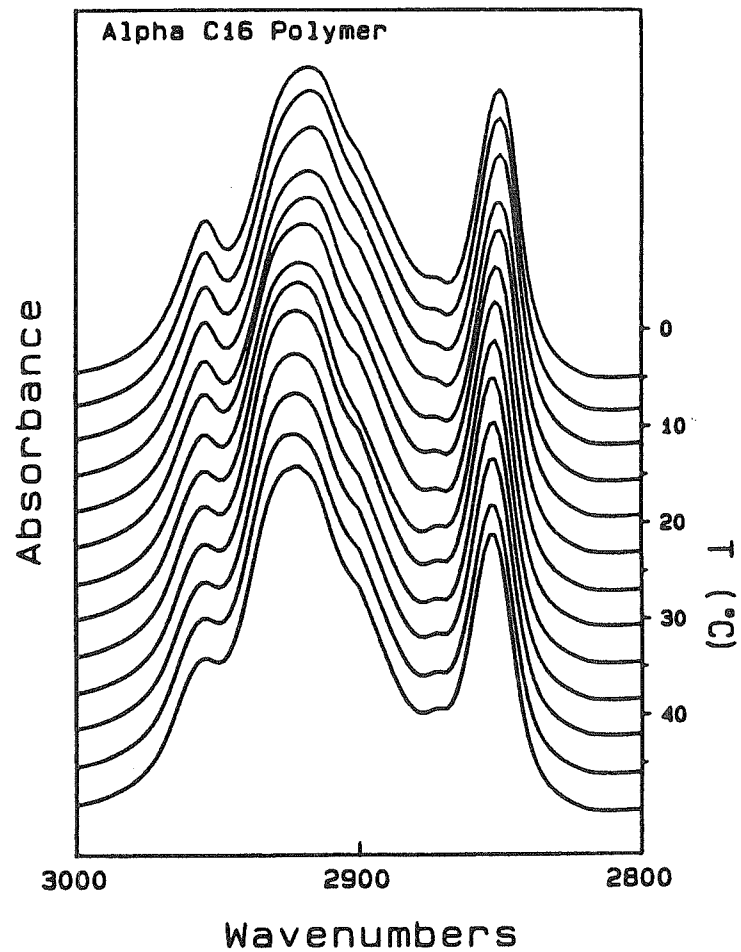
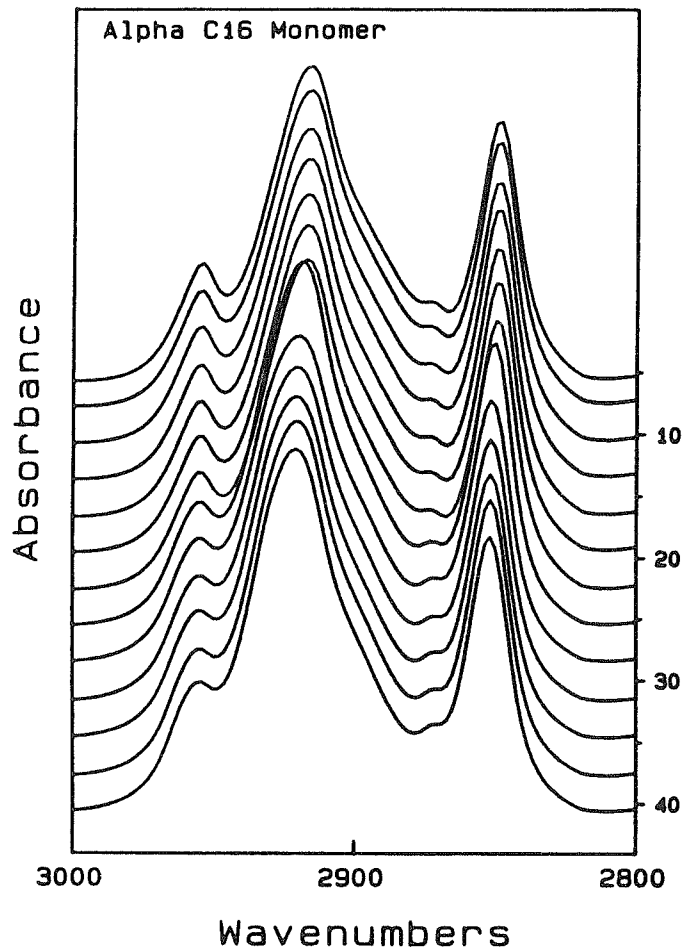
---

\* The symmetric stretching vibration is generally monitored in lieu of the more intense and sensitive asymmetric stretching mode, due to the fact that it is less overlapped by other vibrational modes.

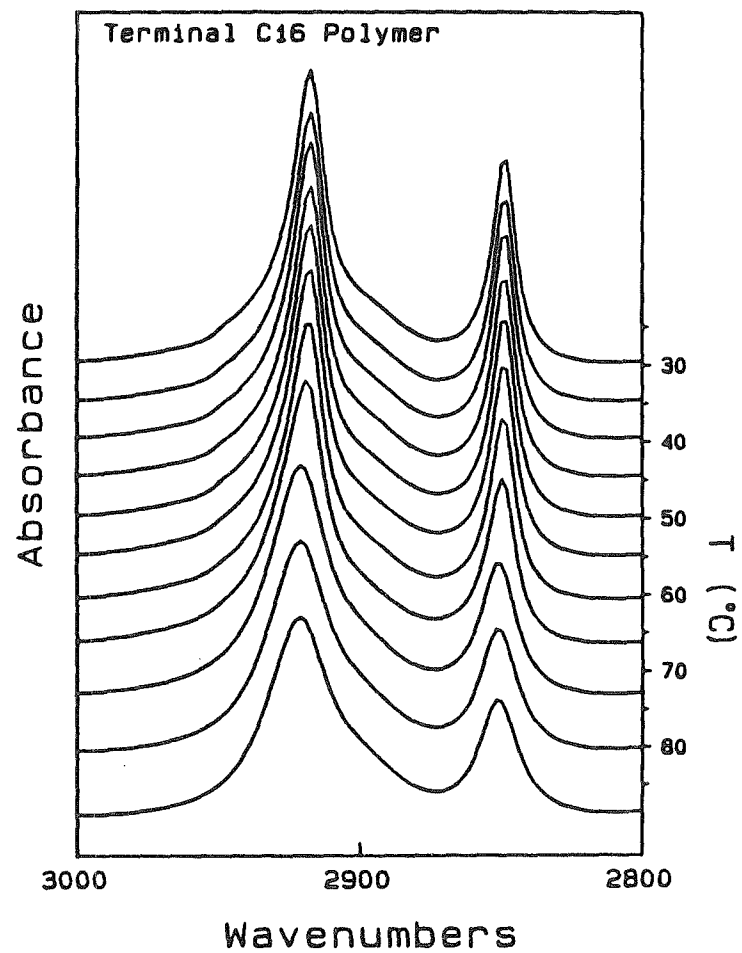
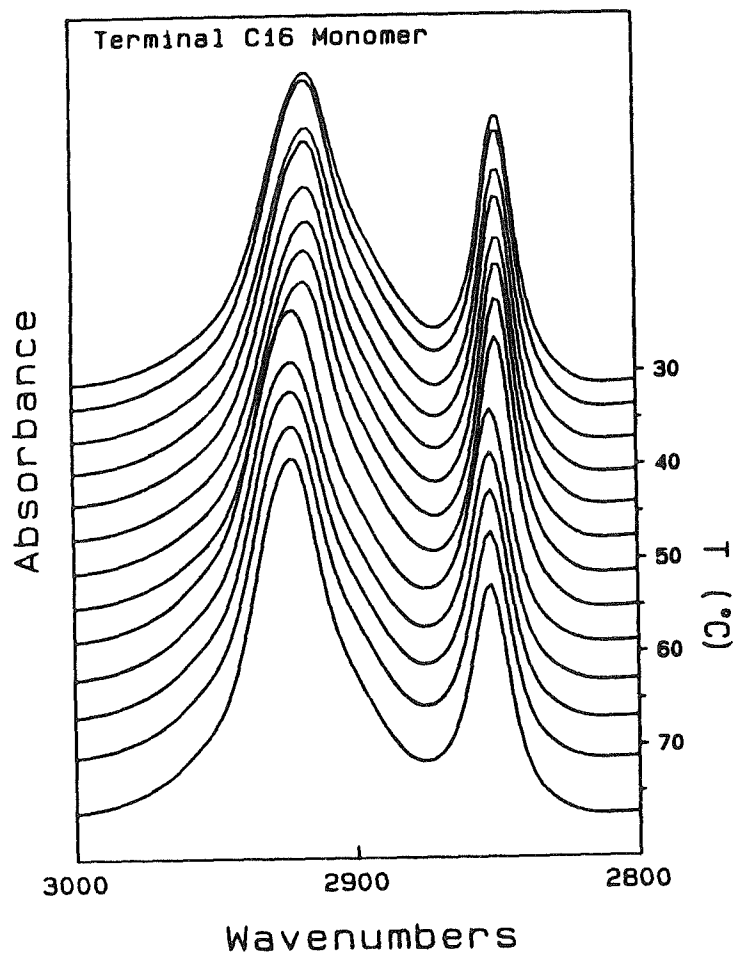
**Figure 2**

Temperature dependent changes in the C-H stretching region of: **A.**  $\alpha$ -16 monomeric and polymeric bilayers; **B.**  $\omega$ -16 monomeric and polymeric bilayers.

**A**

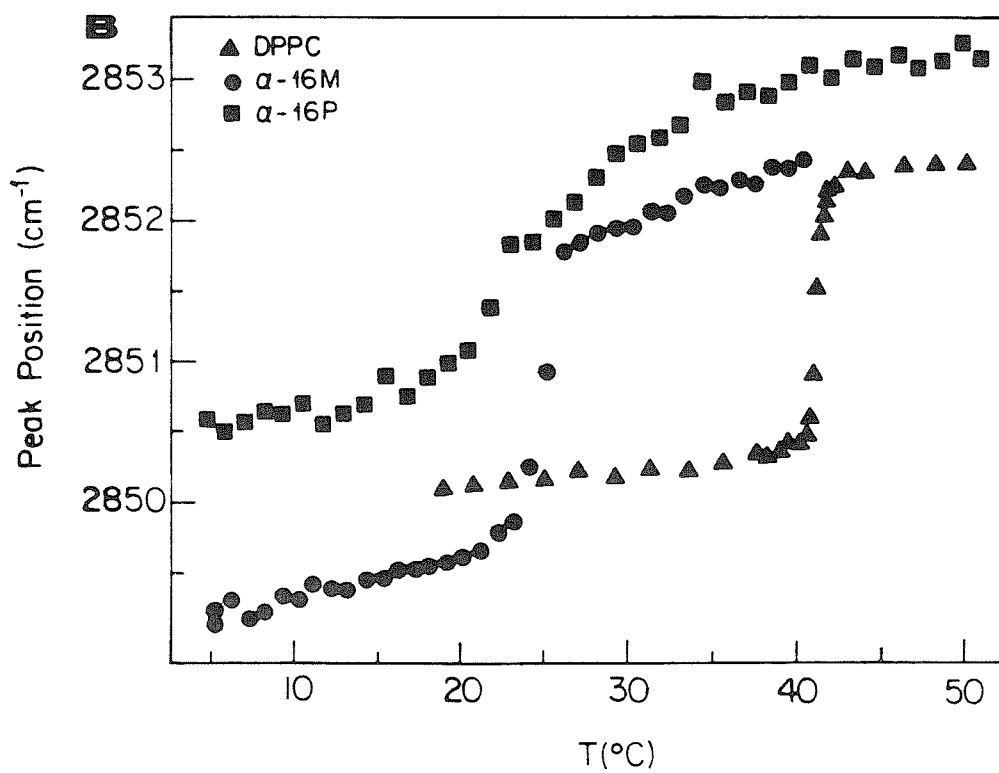
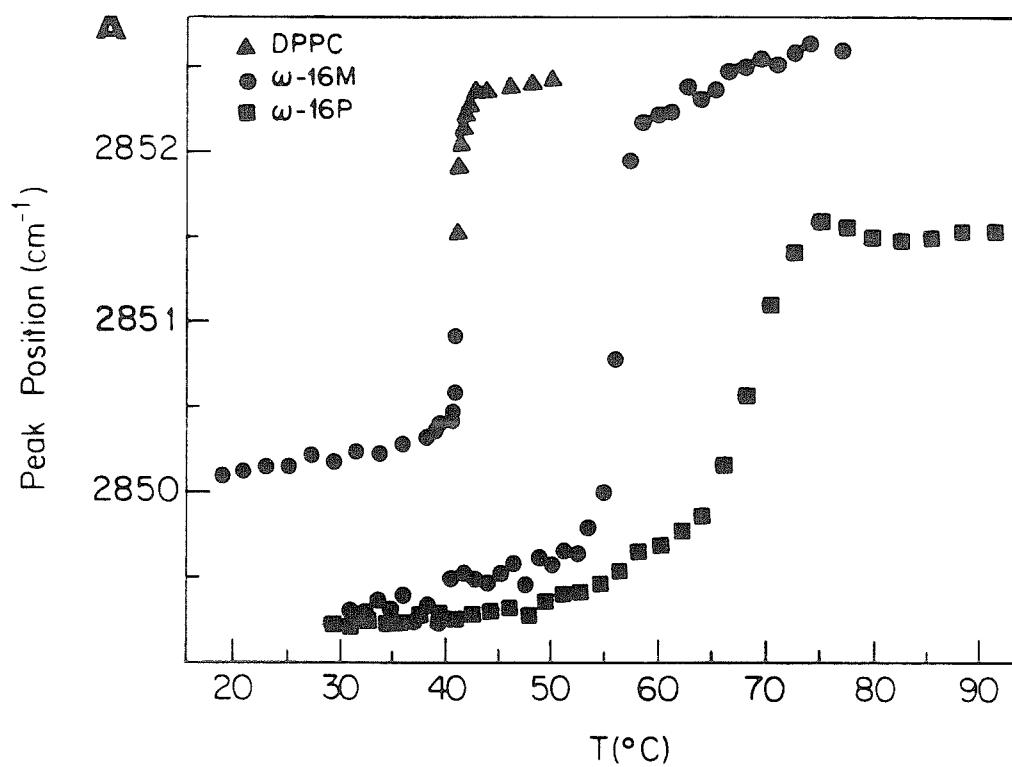


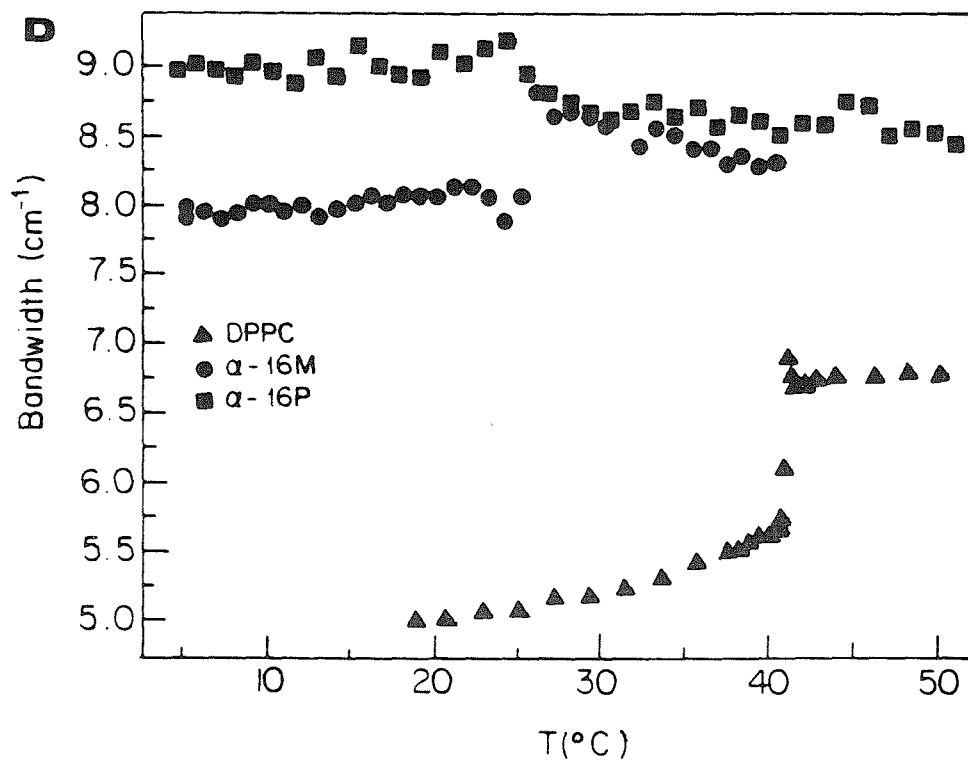
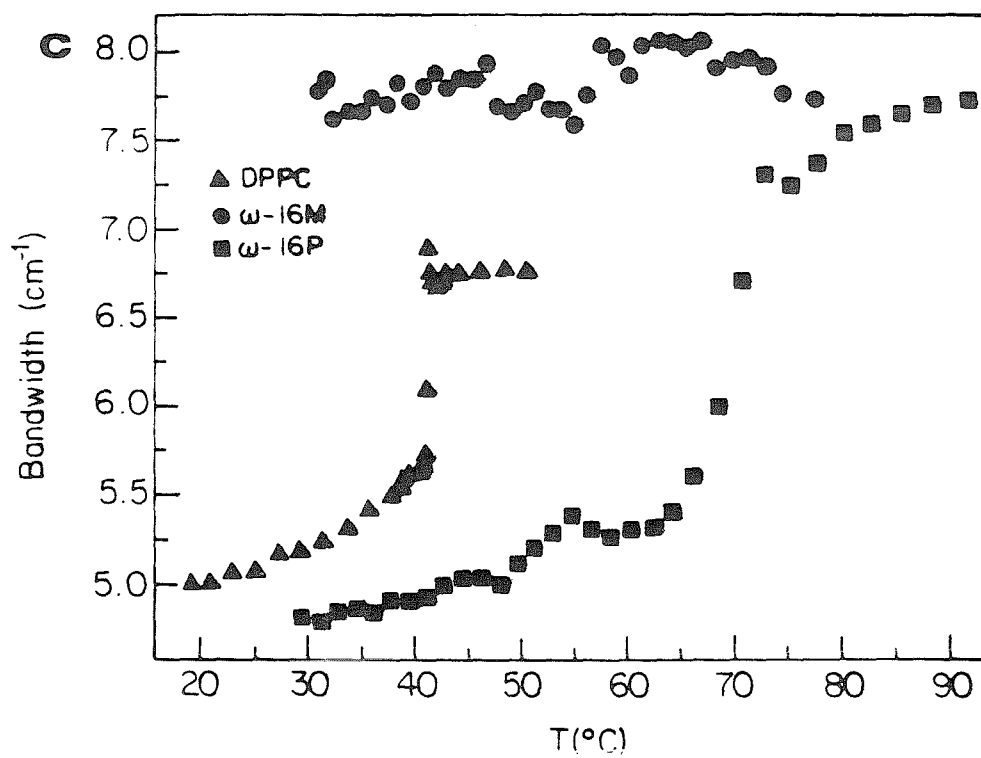
**B**



**Figure 3**

The peak position of the methylene symmetric stretching mode as a function of temperature for: **A.** monomeric and polymeric  $\omega$ -16 and DPPC bilayers; **B.** monomeric and polymeric  $\alpha$ -16 and DPPC bilayers. The half-height bandwidth of the methylene symmetric stretching mode as a function of temperature for: **C.** monomeric and polymeric  $\omega$ -16 and DPPC bilayers; **D.** monomeric and polymeric  $\alpha$ -16 and DPPC bilayers.





shows the half-height bandwidth versus temperature profiles for monomeric and polymeric  $\omega$ -16 and  $\alpha$ -16, as well as DPPC.

The plots of the frequency change as a function of temperature for  $\omega$ -16 and  $\alpha$ -16 bilayers are also shown in Figure 3. DPPC is again included for reference. The general reduction in the frequency of polymeric  $\omega$ -16 bilayers relative to the monomeric bilayers suggests a slightly higher trans-orientation of the chains. The difference between polymeric and monomeric  $\alpha$ -THIOLS is even greater but in the opposite direction: polymerization seems to increase the number of gauche conformers per chain. Similar effects of polymerization on band frequency are exhibited by  $\alpha$ - and  $\omega$ -THIOLS with different chain lengths as shown in Figure 4. In all cases, polymerization of  $\omega$ -THIOLS shifts the frequency of the CH<sub>2</sub> symmetric stretch to lower wavenumbers, while it shifts that for the  $\alpha$ -THIOLS to higher wavenumbers.\* While the results concerning the  $\omega$ -THIOLS are what is intuitively expected for polymeric versus monomeric lipids, the disordering effect of polymerization on the  $\alpha$ -THIOLS is not.

As for  $\omega$ -16, bandwidths for all  $\omega$ -THIOLS in the gel state are reduced on polymerization (Figure 4). Less consistent trends are shown for the  $\alpha$ -THIOLS (although it is not clear if this is simply the consequence of the establishment of a poor baseline) (Figure 4). However, in general, the bandwidths of the  $\alpha$ -THIOLS are notably higher than those of the  $\omega$ -THIOLS, particularly considering the fact that the  $\alpha$ -THIOLS have much longer chain lengths than the majority of  $\omega$ -THIOLS.\*\* Table I summarizes these data in terms of the peak position and bandwidth of the methylene

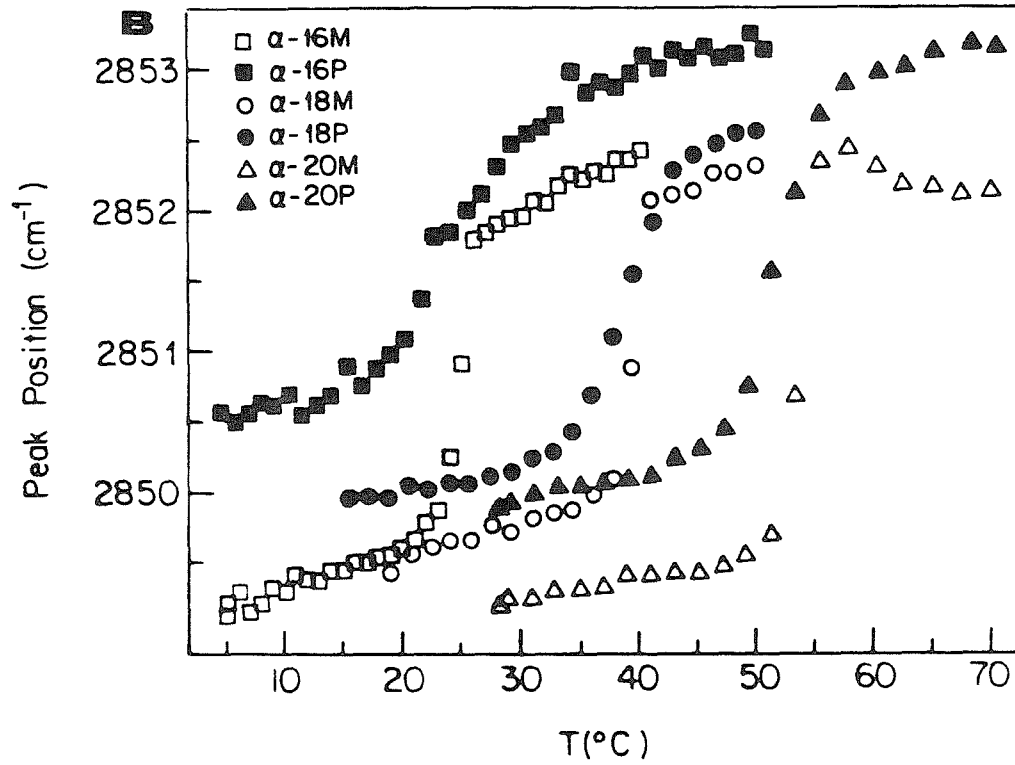
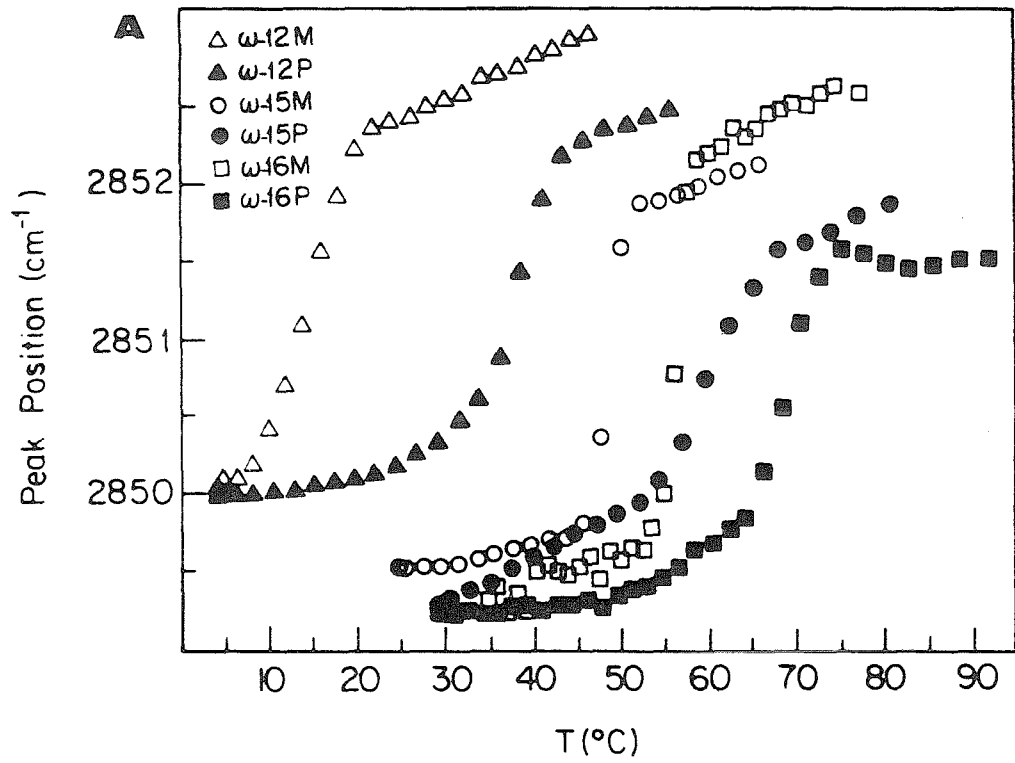
---

\* The exception to this is  $\omega$ -11. The reason for the anomalous band frequencies is not clear but may be the consequence of the morphological change exhibited by  $\omega$ -THIOLS on polymerization. For monomeric  $\omega$ -11, liposomes are formed on dispersion in water. In the case of the polymers, bilayer fragments/micelles are formed as described in chapter II.

\*\* Short chain lipids tend to be more disordered than long chain lipids, and therefore, the bandwidths shift to higher values.

**Figure 4**

The peak position of the methylene symmetric stretching mode as a function of temperature for: **A.** monomeric and polymeric  $\omega$ -THIOLS; **B.** monomeric and polymeric  $\alpha$ -THIOLS. The half-height bandwidth of the methylene symmetric stretching mode as a function of temperature for: **C.** monomeric and polymeric  $\omega$ -THIOLS; **D.** monomeric and polymeric  $\alpha$ -THIOLS.



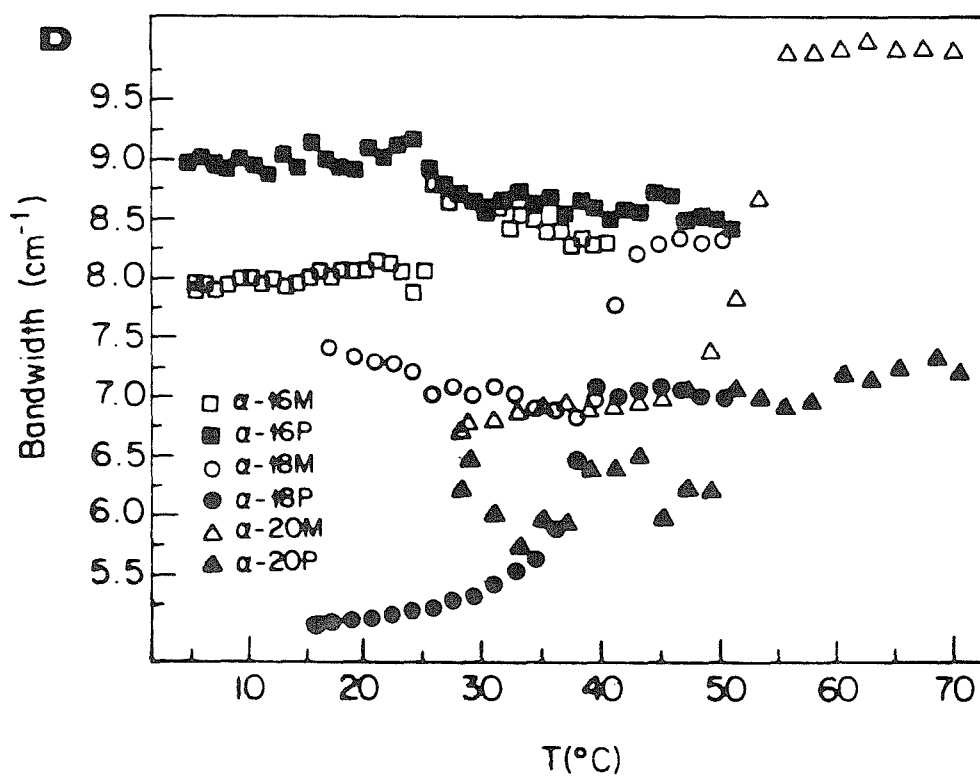
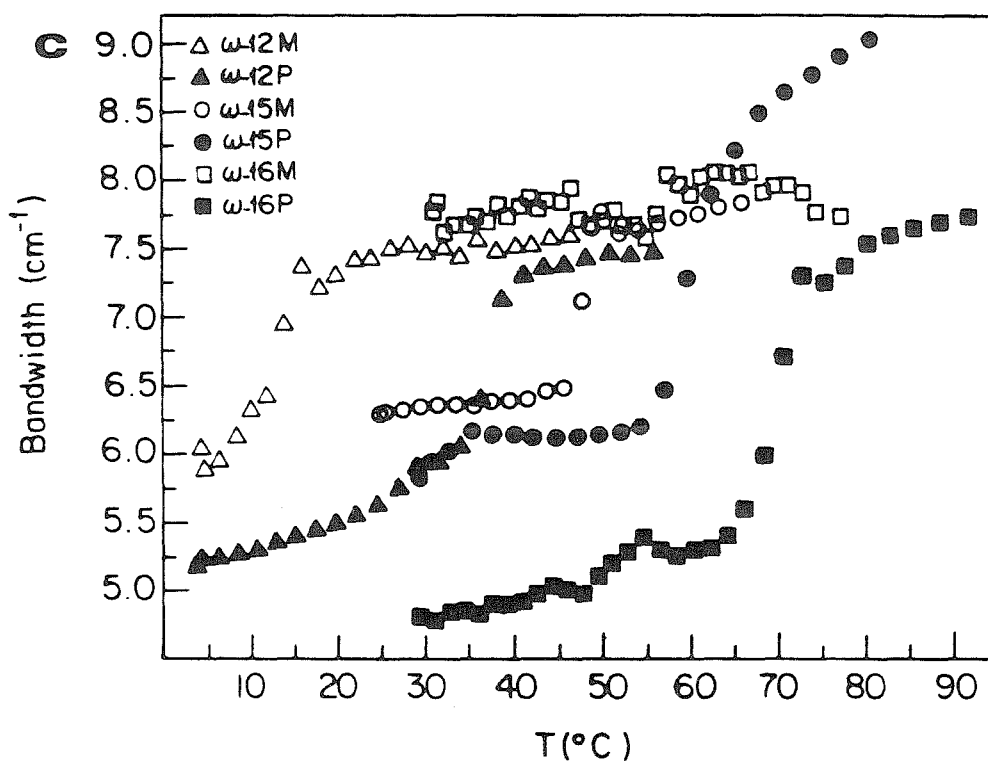


**Table I**

**A.** Summary of the peak positions of the symmetric C-H stretching mode for polymeric and monomeric  $\alpha$ -THIOLS and  $\omega$ -THIOLS in the gel ( $PP_{GEL}$ ) and liquid-crystalline ( $PP_{LC}$ ) state. Also included is the magnitude of the change  $\Delta PP$  and the temperatures at which the values for PP were extrapolated from the curve. **B.** Summary of the bandwidths of the symmetric C-H stretching mode for polymeric and monomeric  $\alpha$ -THIOLS and  $\omega$ -THIOLS in the gel ( $BW_{GEL}$ ) and liquid-crystalline ( $BW_{LC}$ ) state. Also included is the magnitude of the change  $\Delta BW$  and the temperatures at which the values for BW were extrapolated from the curve.

**A**

Lipid	Temperature (°C)		Peak Position (cm <sup>-1</sup> )		
	Gel-LC		PP <sub>GEL</sub> <sup>a</sup>	PP <sub>LC</sub> <sup>a</sup>	ΔPP <sup>a</sup>
<b>α-THIOLS</b>					
α-16 (M)	5-40		2849.2	2852.5	3.3
α-16 (P)	5-40		2850.5	2853.2	2.7
α-18 (M)	15-50		2849.5	2852.3	2.8
α-18 (P)	15-50		2850.0	2853.0	3.0
α-20 (M)	30-70		2849.3	2852.1	2.9
α-20 (P)	30-70		2845.0	2853.2	3.2
<b>ω-THIOLS</b>					
ω-11 (M)	-11.5-10		2848.6	2851.4	2.8
ω-11 (P)	4-44		2850.3	2852.0	1.7
ω-12 (M)	5-45		2850.1	2853.0	1.9
ω-12 (P)	5-55		2850.0	2852.5	2.5
ω-15 (M)	30-65		2849.5	2852.1	2.6
ω-15 (P)	30-75		2849.3	2851.8	2.5
ω-16 (M)	30-70		2849.3	2852.6	3.3
ω-16 (P)	30-90		2849.2	2851.5	2.3
<b>LECITHIN</b>					
DPPC	20-50		2850.1	2852.4	2.3

<sup>a</sup> Errors in the peak position are estimated to be  $\approx \pm 0.1 \text{ cm}^{-1}$ .

**B**

Lipid	Temperature ( $^{\circ}\text{C}$ )	Bandwidths ( $\text{cm}^{-1}$ )		
	Gel-LC	$\text{BW}_{\text{GEL}}^{\text{a}}$	$\text{BW}_{\text{LC}}^{\text{a}}$	$\Delta\text{BW}^{\text{a}}$
<b><math>\alpha</math>-THIOLS</b>				
$\alpha$ -16 (M)	5-40	7.9	8.4	0.5
$\alpha$ -16 (P)	5-40	9.0	8.8	-0.2
$\alpha$ -18 (M)	15-50	7.3	8.3	1.0
$\alpha$ -18 (P)	15-50	5.0	7.0	2.0
$\alpha$ -20 (M)	30-70	6.8	9.9	3.1
$\alpha$ -20 (P)	30-70	6.0	7.3	1.3
<b><math>\omega</math>-THIOLS</b>				
$\omega$ -11 (M)	-11.5-10	8.3	9.6	1.3
$\omega$ -11 (P)	4-44	5.3	7.9	2.6
$\omega$ -12 (M)	5-45	5.9	7.6	1.7
$\omega$ -12 (P)	5-55	5.2	7.5	2.3
$\omega$ -15 (M)	30-65	6.4	7.8	1.4
$\omega$ -15 (P)	30-75	5.9	8.9	3.0
$\omega$ -16 (M)	30-70	7.8	8.0	0.2
$\omega$ -16 (P)	30-90	4.8	7.7	2.9
<b>LECITHIN</b>				
DPPC	20-50	5.0	6.8	1.8

<sup>a</sup> Errors in the bandwidth are estimated to be less than  $\pm 0.2 \text{ cm}^{-1}$ .

symmetric stretch for the bilayers in the gel and liquid-crystalline states and the FT-IR determined phase transition.

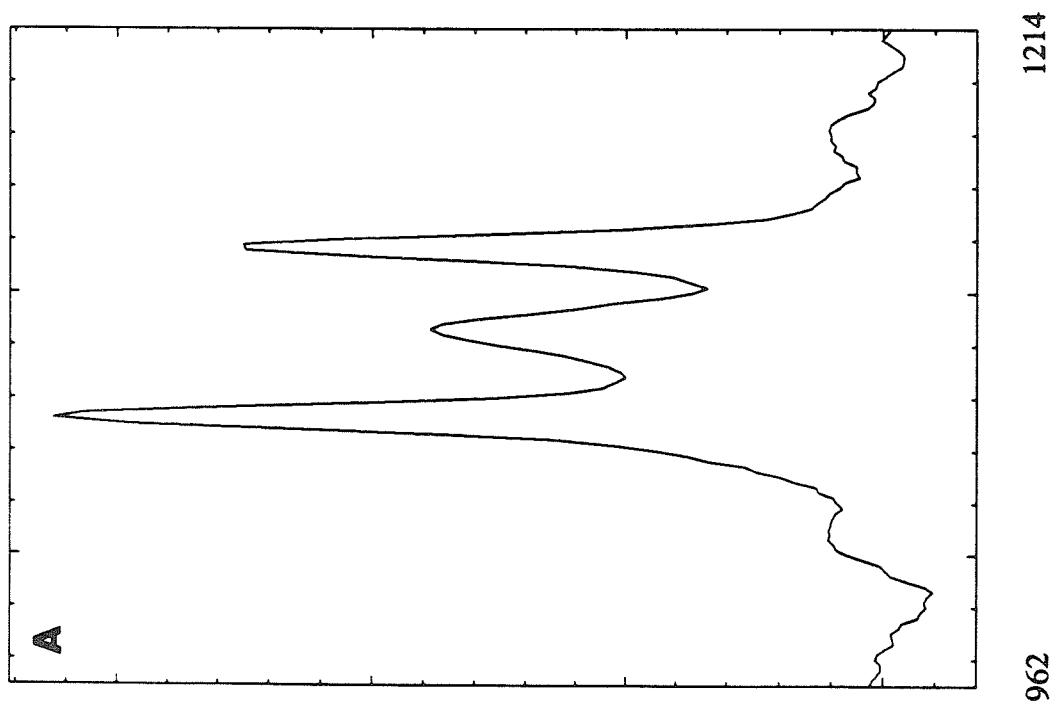
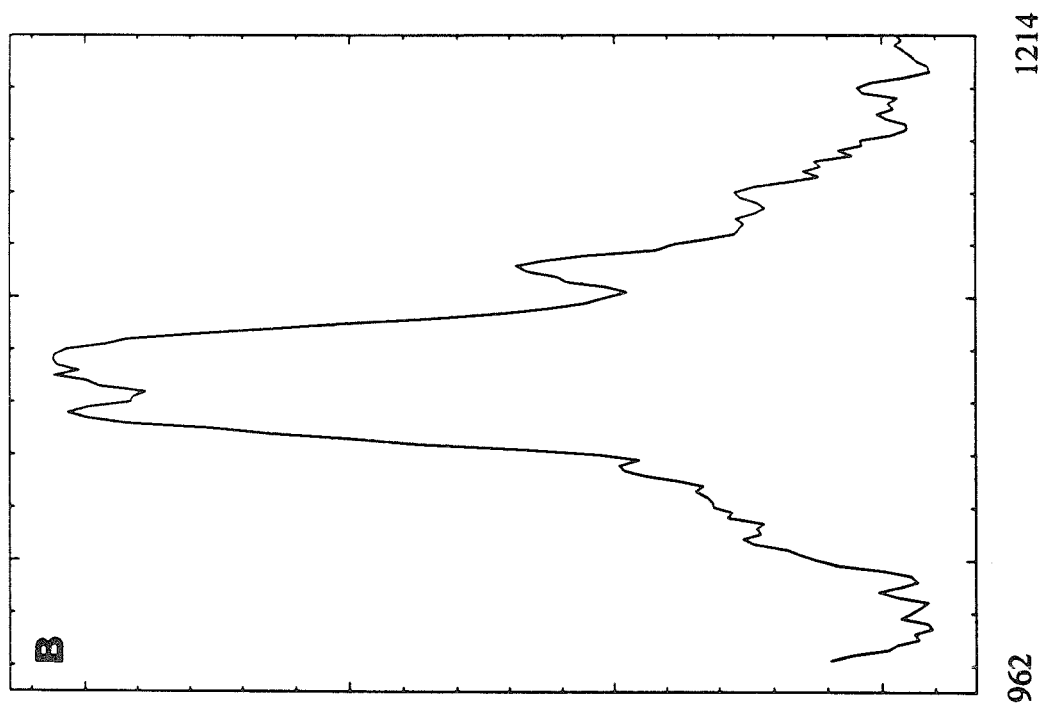
### RAMAN.

The Raman spectra of phospholipids is similar in many respects to the infrared spectra in that the modes of the hydrocarbon chains are the dominant features. Based on the analysis of the Raman spectra of polyethylene, long chain alkanes, and fatty acids, bands attributable to the hydrocarbon region of phospholipids have been readily assigned and evaluated in terms of their relationship to lipid acyl chain conformation and packing (18,19,23,30).

Particularly informative are the skeletal optical modes which appear between 1000-1200  $\text{cm}^{-1}$ . Although this region is vibrationally congested with C-C stretching modes of the acyl chains, the glycerol backbone, and the choline headgroup, three vibrations attributable to the acyl chains are the most intense features (23). The 1130 and 1065  $\text{cm}^{-1}$  vibrations are the in-phase and out-of-phase stretching modes for an ordered nearly all-trans chain conformation (21). The former is chain length and temperature sensitive while the latter is not (23). The 1090  $\text{cm}^{-1}$  vibration is diagnostic of C-C stretching modes of gauche rotamers (18,19,21,23). Thus as chain disorder increases by increasing the temperature, the intensity of the 1090  $\text{cm}^{-1}$  band increases while the band at 1130  $\text{cm}^{-1}$  decreases in intensity and shifts to lower frequency (21). This is illustrated in Figure 5, which shows the change in the skeletal optical mode region of DPPC with temperature from below to above the phase transition. The spectral features are often expressed in terms of the ratio of intensities of the 1090 to 1130 bands ( $I_{1090}/I_{1130}$ ). While there is no simple quantitative relationship between this ratio or the intensity of the 1130  $\text{cm}^{-1}$  vibration and the exact number of trans conformers in the chain (18) they do offer useful qualitative information concerning the lipid chain conformation.

**Figure 5**

The C-C stretching region for DPPC bilayers at: **A.** 25 °C and **B.** 56°C.

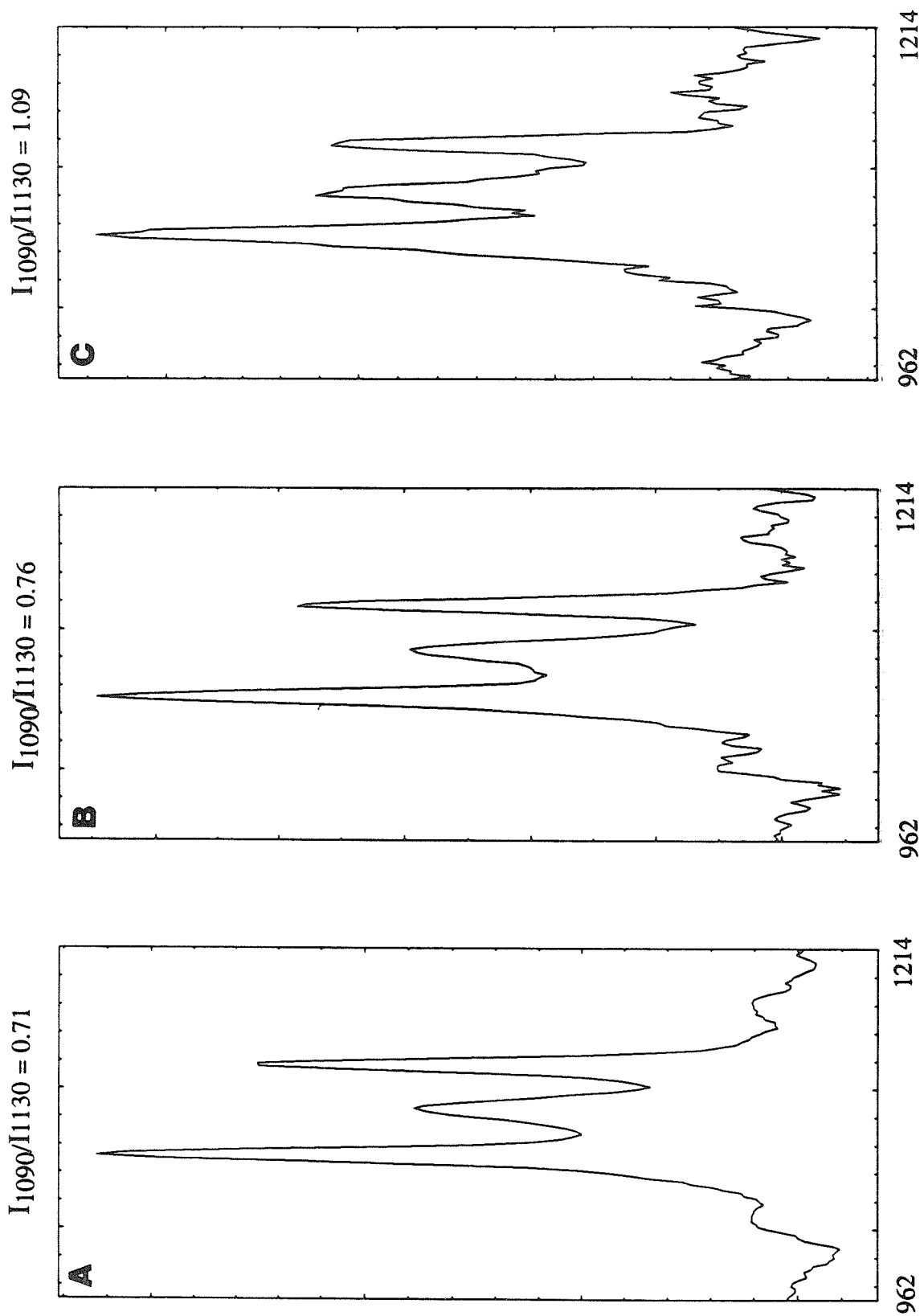


WAVENUMBERS (CM<sup>-1</sup>)

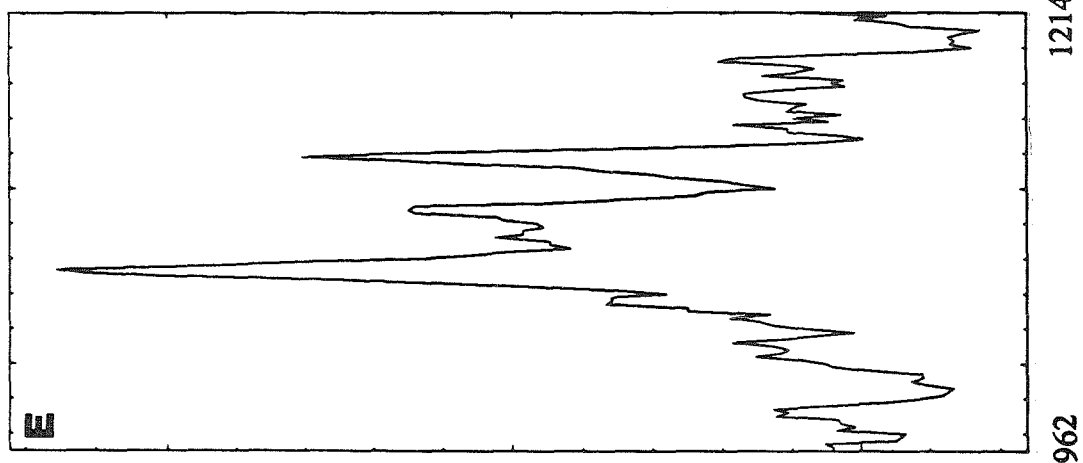
Figure 6 shows the 1100-1200 C-C stretching region for a variety of hydrated dispersions in the gel state. Corresponding  $I_{1090}/I_{1130}$  ratios and spectral frequencies are included on the graphs. From a cursory examination of the spectra and the ratios, it is clear that the 16- and 18-carbon saturated phosphatidylcholines (DPL and DSL, respectively) have a greater proportion of trans to gauche conformers than the corresponding 18- and 16-carbon  $\alpha$ -THIOLS in either the monomeric or polymeric state. Furthermore, a comparison of monomeric  $\alpha$ -16 to polymeric  $\alpha$ -16 suggests that polymerization has a disordering effect. (Similar conclusions were arrived at on the basis of FT-IR spectra.) In Figure 7, similar data are shown for powders of DSL, DPL, and polymeric  $\alpha$ -THIOLS. These samples were simply equilibrated at ambient humidity and therefore hydrated to some extent but not in excess. Bush et al. has shown that after four molecules of water are added to DPPC, spectral features do not change in either the acyl chain or headgroup region with further hydration (23). Furthermore, at a hydration level of two to four molecules of  $H_2O$  per lipid, the carbonyl vibration collapses from two vibrational modes at 1720 and 1738  $cm^{-1}$  corresponding to the sn-2 and the sn-1 chain, respectively, to a single broad vibration centered at 1738  $cm^{-1}$ . Powder samples of DPL showed only a single unsplit vibration at 1738  $cm^{-1}$  as did all other powder samples with the exception of DSL. Thus the differences observed in the  $I_{1090}/I_{1130}$  ratios between powder and dispersed samples of DPL and the fact that the carbonyl mode is singular indicates that between two and four water molecules are associated with the powders. While some samples may differ in the amount of associated water due to differences in the hygroscopic nature of the lipid, the data shows the same trends in that the nonpolymerizable phosphatidylcholines are more highly ordered than the polymeric systems. The very

**Figure 6**

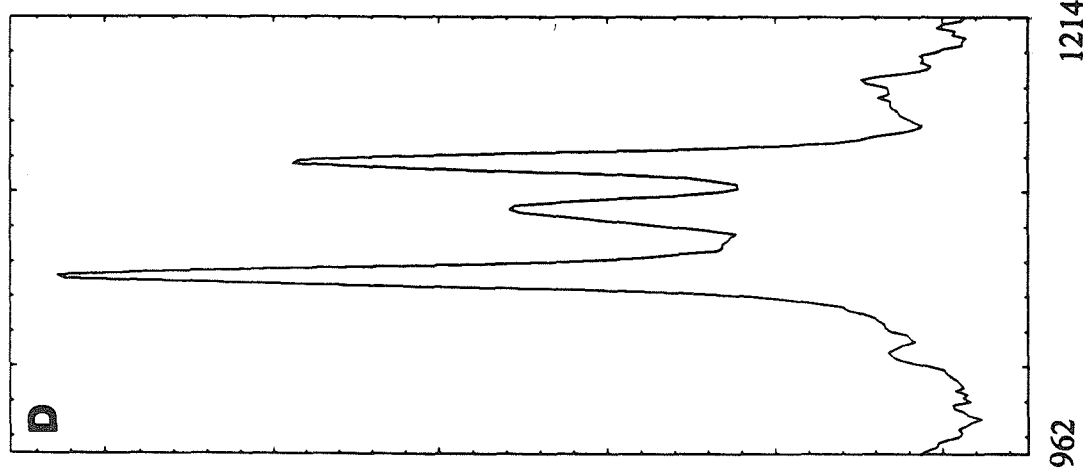
The C-C stretching region for hydrated bilayers of: **A.** DPPC (25 °C); **B.** monomeric  $\alpha$ -16 (10 °C); **C.** polymeric  $\alpha$ -16 (8.5 °C); **D.** DSPC (30.5 °C); **E.** polymeric  $\alpha$ -18 (19 °C).  $I_{1090}/I_{1130}$  ratios are included above the figures.



$I_{1090}/I_{1130} = 0.82$



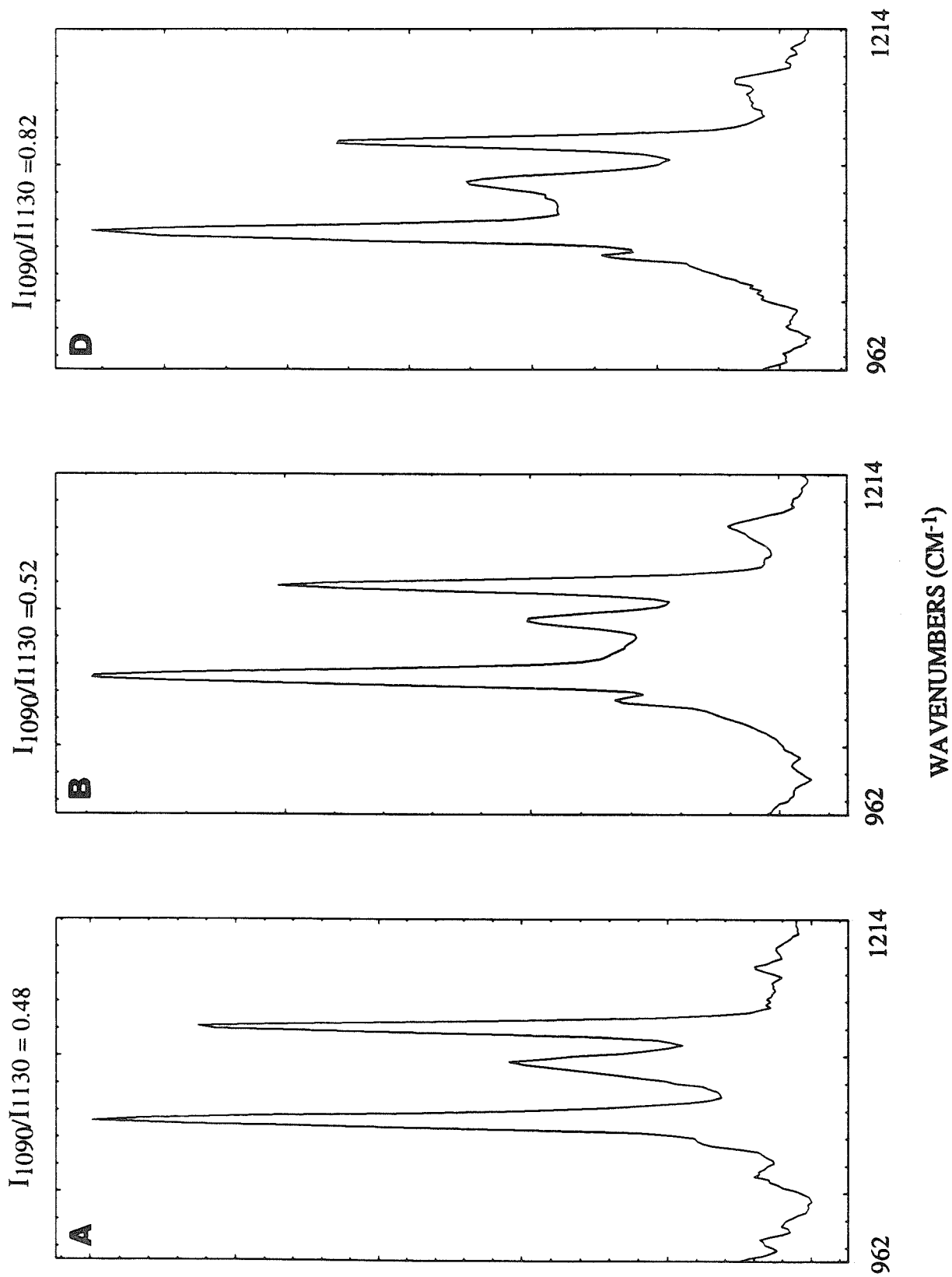
$I_{1090}/I_{1130} = 0.67$

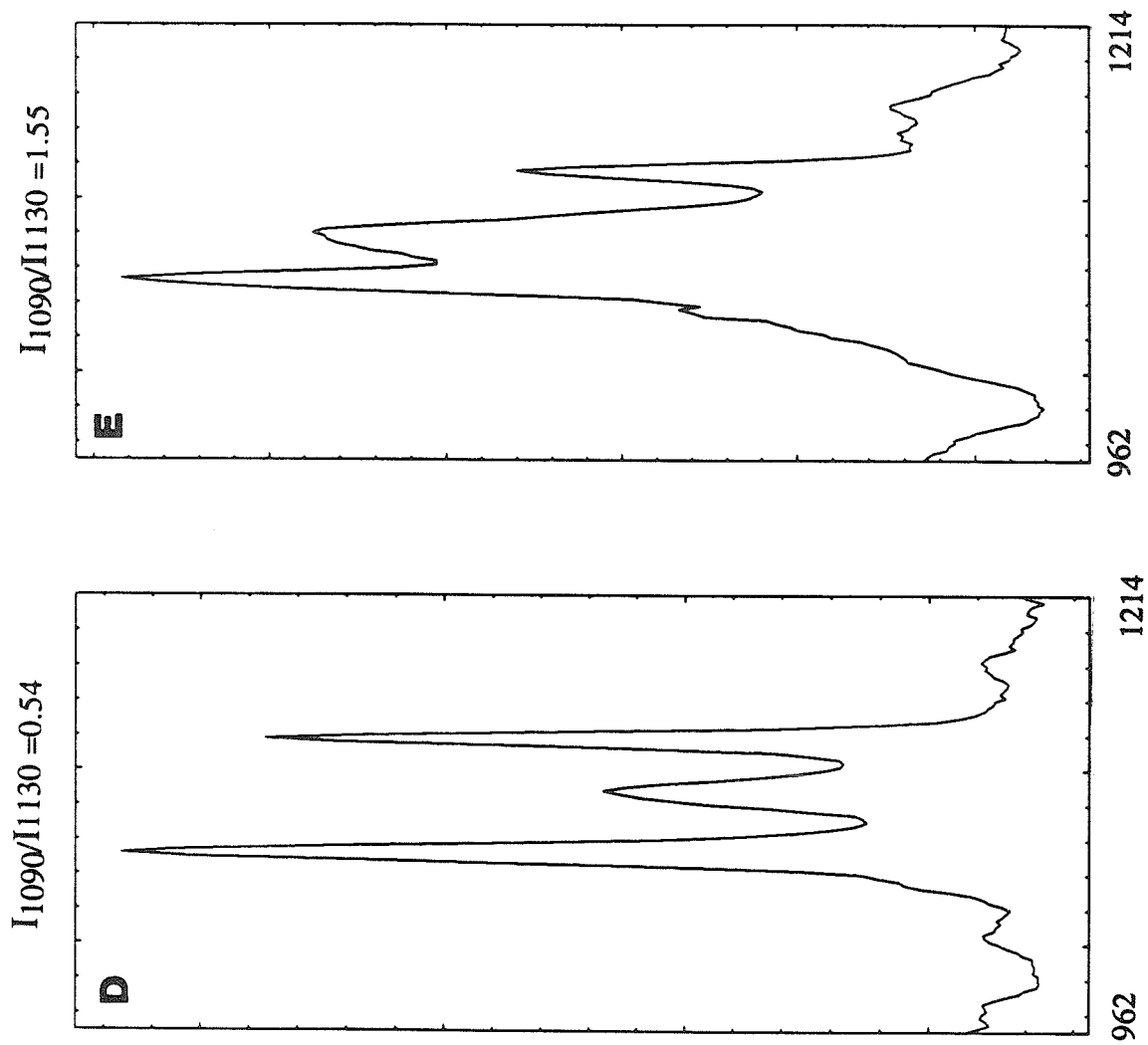


WAVENUMBERS (CM-1)

**Figure 7**

The C-C stretching region for unhydrated bilayers of: **A.** DSPC; **B.** polymeric  $\alpha$ -20; **C.** polymeric  $\alpha$ -18; **D.** DPPC; **E.** polymeric  $\alpha$ -16.  $I_{1090}/I_{1130}$  ratios are included above the figures. Measurements were made at 23 °C.

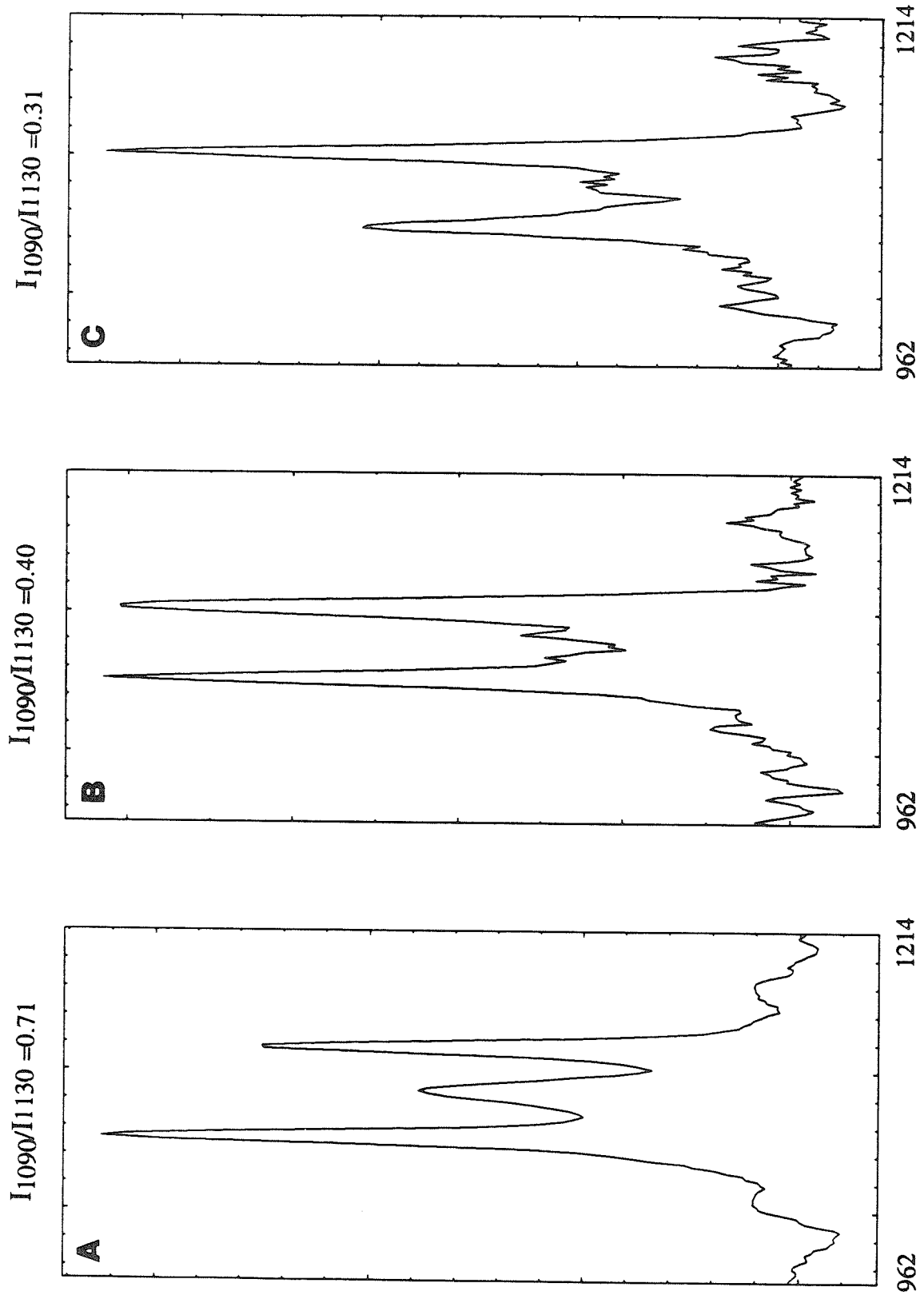


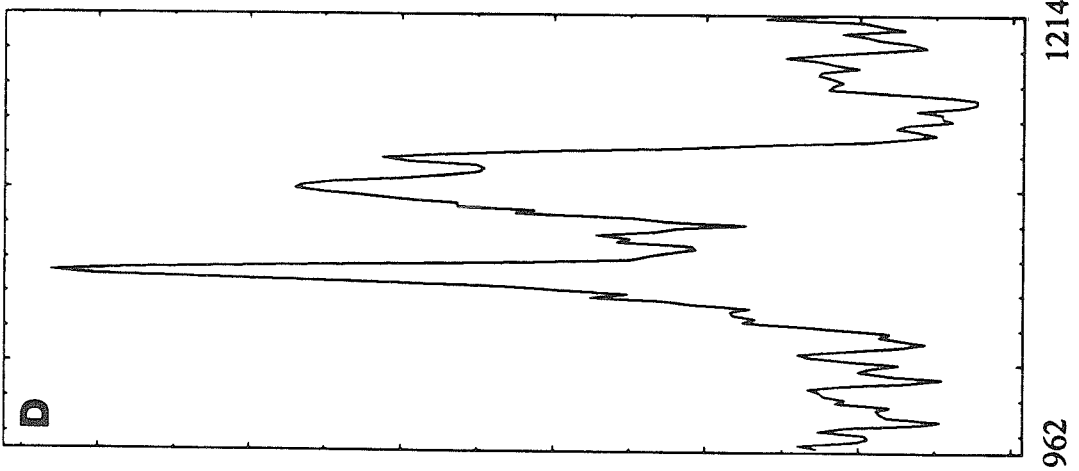
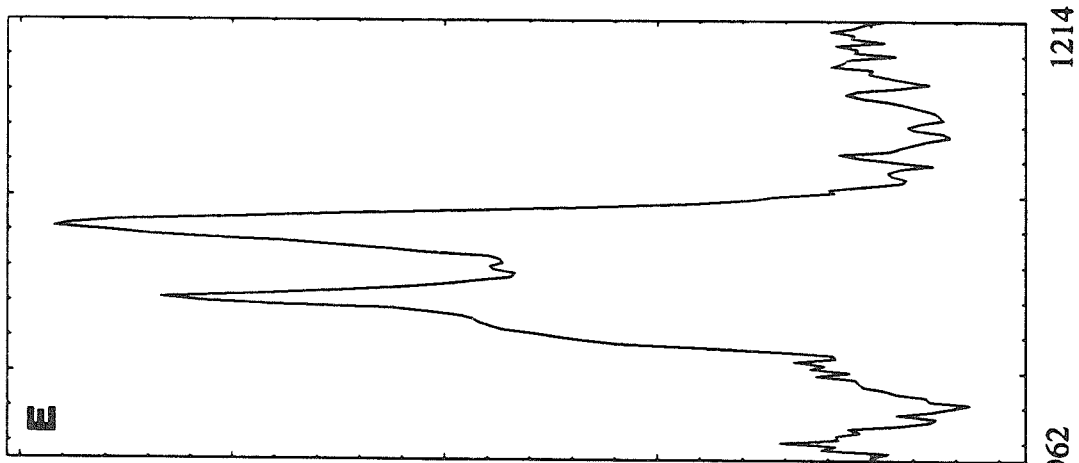


WAVENUMBERS (CM<sup>-1</sup>)

**Figure 8**

The C-C stretching region for hydrated bilayers of: **A.** DPPC (25 °C); **B.** monomeric  $\omega$ -16 (20 °C); **C.** polymeric  $\omega$ -16 (20 °C); **D.** dimeric  $\omega$ 16-DPL (20 °C); **E.** polymeric  $\omega$ -12 (26 °C).  $I_{1090}/I_{1130}$  ratios are included above the figures.





WAVENUMBERS (CM-1)

high  $I_{1090}/I_{1130}$  of polymeric  $\alpha$ -16 is due to the room temperature phase transition of the hydrated form of this lipid.

The C-C stretching regions of several  $\omega$ -THIOLS are shown in Figure 8 along with DPPC for comparison.  $I_{1090}/I_{1130}$  ratios and frequencies are included in the graphs. In contrast to the  $\alpha$ -THIOLS, the 1090  $\text{cm}^{-1}$  band diagnostic of gauche conformations is very low in intensity compared to DPPC for all  $\omega$ -THIOLS, even those with short 12-carbon acyl chains (however, the 1090  $\text{cm}^{-1}$  band in polymeric  $\omega$ -12 may be somewhat obscured). This would seem to indicate that the chains of the  $\omega$ -THIOLS are highly ordered and mostly trans. A second noteworthy feature of the  $\omega$ -THIOL spectra is the fact that the frequencies of the 1130  $\text{cm}^{-1}$  are shifted to lower wavenumber. This is the general trend observed for increased disorder and shorter chain lengths, but such an analysis of the data would be inconsistent with the low intensity of the 1090  $\text{cm}^{-1}$  band. Furthermore, the high relative intensity of the "1130  $\text{cm}^{-1}$ " band is greatly increased, which would imply an increased trans orientation. An alternative explanation compatible with a highly ordered chain conformation is that the acyl chains of  $\omega$ -THIOLS do not have only one "fixed end" as for fatty acids and lipids, but rather two, due to the presence of the disulfide linkage or the sulfhydryl group. Early work by Lippert and Peticolas have in fact attempted to address the question of what effects end groups have on carbon skeletal vibrations. An alteration of the band frequency is predicted theoretically (32).

In order to test this, a mixed chain  $\omega$ -THIOL was prepared that has a 16-carbon polymerizeable acyl chain in the sn-2 position and a nonpolymerizeable 16-carbon saturated fatty acid in the sn-1 position ( $\omega$ 16-DPL). On oxidation of this lipid, only dimers are formed by crosslinking adjacent sn-2 chains. Figure 8D shows the C-C stretching region for oxidized  $\omega$ 16-DPL. Four vibrational modes are visible: (i) the 1065  $\text{cm}^{-1}$  band which, being temperature and chain length insensitive, is unsplit (ii)

the 1090  $\text{cm}^{-1}$  band indicative of gauche conformations (iii) 1117  $\text{cm}^{-1}$  band attributable to the acyl chains of the dimer in a trans conformation (a two fixed-end vibration) and (iv) the 1131  $\text{cm}^{-1}$  band corresponding to trans conformations of the sn-1 nonpolymerizable (one fixed-end) chain. Whether or not the 1090  $\text{cm}^{-1}$  band arises from gauche conformers in the sn-1 chain, the sn-2 chain, or both is unclear. However, these data corroborate the conclusion that the spectra of monomeric and polymeric  $\omega$ -THIOLS correspond to that of carbon chains which are highly trans in orientation. Figure 9 shows spectra of "powders" of DPPC, polymeric  $\omega$ -15 and dimeric  $\omega$ 16-DPL, further confirming the highly ordered state of polymeric  $\omega$ -THIOLS compared to nonpolymerizable analogs.

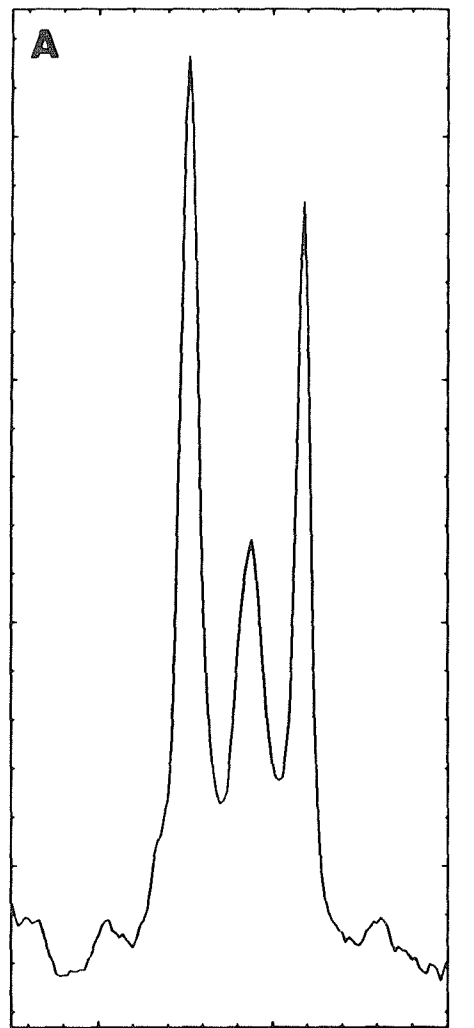
It would be expected that the C-C stretching region of the  $\alpha$ -THIOLS would change with temperature in a manner similar to DPPC since the polymerizable moiety is restricted to the rigid bilayer interface. On the other hand, it is not so obvious what would happen for the  $\omega$ -THIOLS. Figure 10 shows the change in the C-C stretching region for polymeric  $\omega$ -12 as a function of temperature. The area between the two trans-marker vibrations (1065 and 1107  $\text{cm}^{-1}$ ) does fill in as the temperature is elevated, indicating the induction of conformational disorder. Nonetheless, the spectra differ from that of DPL or polymeric  $\alpha$ -THIOLS in that a single distinctive broad vibration at 1090  $\text{cm}^{-1}$  is absent. The physical basis for this is unclear but may be related to the restriction at the chain terminus in the nature of gauche conformers formed or a different distribution of gauche kinks along the chain. (For nonpolymerizable and polymeric  $\alpha$ -THIOLS, gauche rotamers are formed predominantly toward the chain terminus).

*Raman C-H Stretching Region.* In addition to the C-C stretching vibrations, other interesting and informative spectral features for phospholipid molecules are the C-H

**Figure 9**

The C-C stretching region for unhydrated bilayers of: **A.** DPPC ; **B.** polymeric  $\omega$ -15; **C.** dimeric  $\omega$ 16-DPL.  $I_{1090}/I_{1130}$  ratios are included above the figures. Measurements were made at 23 °C.

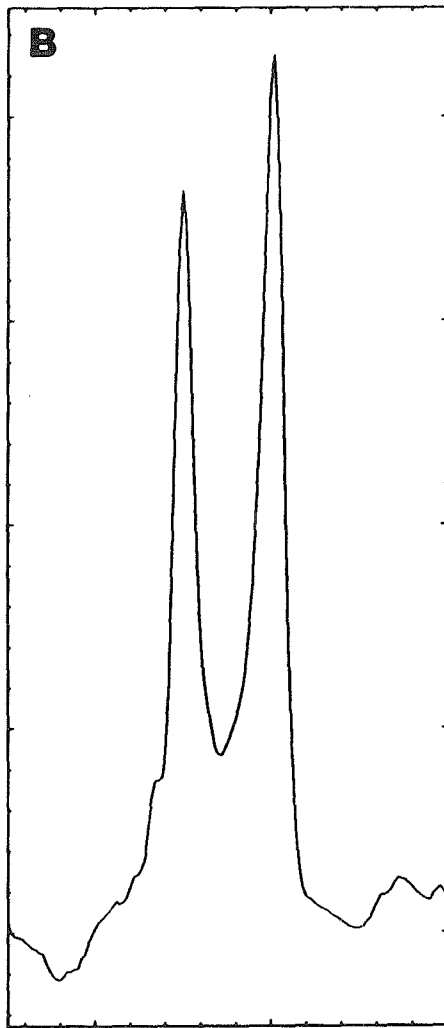
$I_{1090}/I_{1130} = 0.54$



962

1214

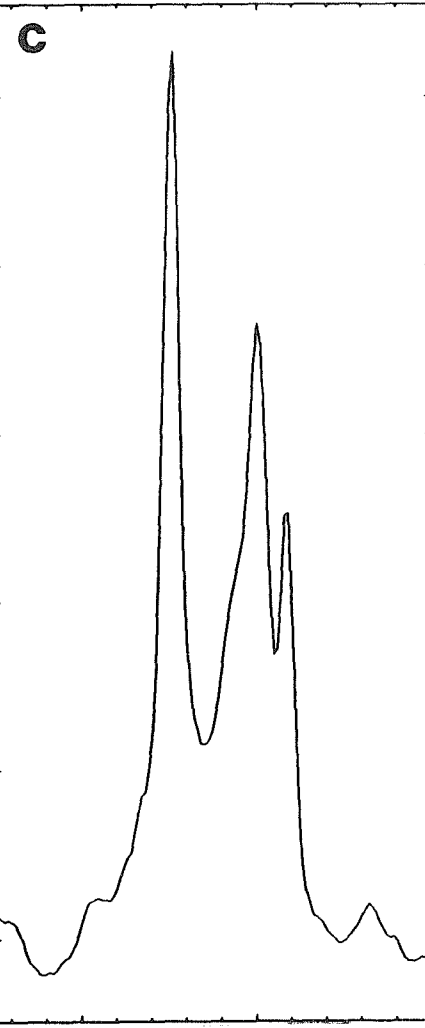
$I_{1090}/I_{1130} = 0.25?$



962

1214

WAVENUMBERS (CM<sup>-1</sup>)



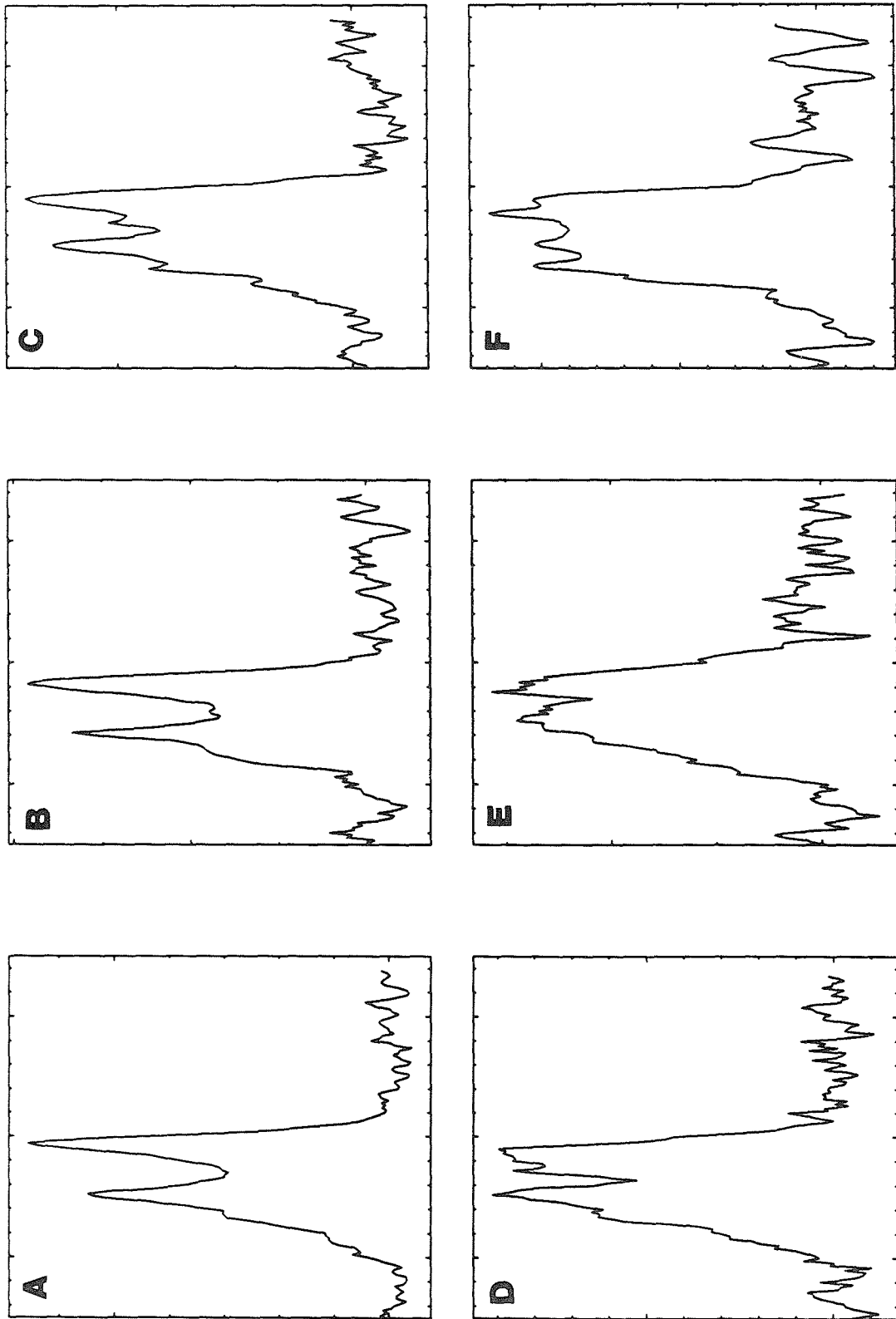
962

1214

**Figure 10**

Effect of temperature on the C-C stretching region of polymeric  $\omega$ -12 bilayers:

A. 26°C ; B 36 °C; C. 41 °C; D. 44.5 °C; E. 50 °C ; F. 54 °C.

WAVENUMBERS (CM<sup>-1</sup>)

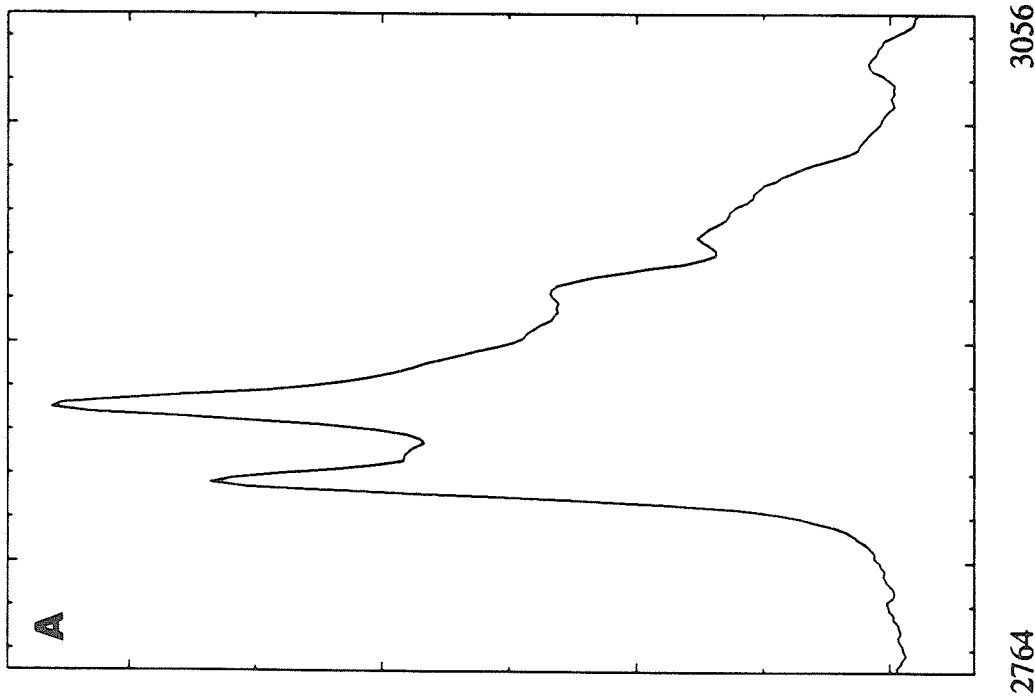
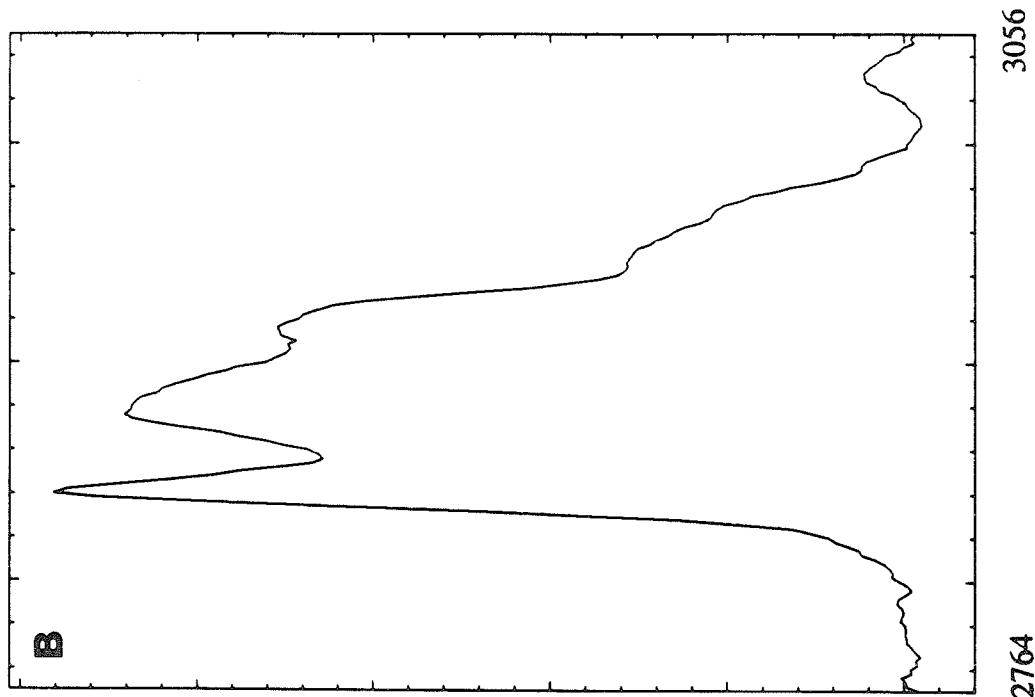
stretching vibrations between 2800 and 3100  $\text{cm}^{-1}$ . The vibrational modes in this region are sensitive to both lateral packing characteristics of the bilayer as well as intramolecular disorder (18,19,21,23,31). Figure 11 demonstrates the temperature-induced changes in the C-H stretching region of DPPC. On increasing the temperature, the intensity of the methylene C-H symmetric stretching mode (2850  $\text{cm}^{-1}$ ) increases while that of the C-H asymmetric stretching mode (2885  $\text{cm}^{-1}$ ) decreases. Thus the ratio of the methylene C-H symmetric stretching mode to the asymmetric stretching mode ( $I_{2885}/I_{2850}$ ) provides a qualitative measure of the packing density of the lipid chains and their conformational disorder.

Representative spectra for DPL, DSL and several monomeric and polymeric  $\alpha$ -THIOLS are displayed in Figure 12. As expected based on the conclusions drawn from the C-C stretching region, the data suggests the lipid chain lateral packing and conformational order is reduced for hydrated polymeric  $\alpha$ -THIOLS relative to both the monomeric  $\alpha$ -THIOLS and nonpolymerizable analogues. Similar trends are shown by the powder samples in Figure 13. These points are best illustrated by comparison of lipids with similar chain lengths (i.e., DSL versus polymeric  $\alpha$ -18, DPL and monomeric  $\alpha$ -16 versus polymeric  $\alpha$ -16, and monomeric  $\alpha$ -20 versus polymeric  $\alpha$ -20).

For the  $\omega$ -THIOLS, somewhat opposite trends were observed as shown in Figure 14 and 15 for hydrated and powder samples, respectively. By comparison to fully hydrated DPPC, the  $I_{2880}/I_{2850}$  ratio of monomeric and polymeric  $\omega$ -16 and dimeric  $\omega$ 16-DPL are slightly greater. In the powder samples, polymeric  $\omega$ -15 also has a slightly higher ratio and that of polymeric  $\omega$ -12 is only slightly less, despite the much shorter carbon chain of this lipid. Finally, it is interesting to note that the  $I_{2880}/I_{2850}$  ratio for polymeric  $\omega$ -12 (hydrated, Figure 14) is approximately the same as that for polymeric  $\alpha$ -20 (hydrated, Figure 12) despite the large difference in chain lengths

**Figure 11**

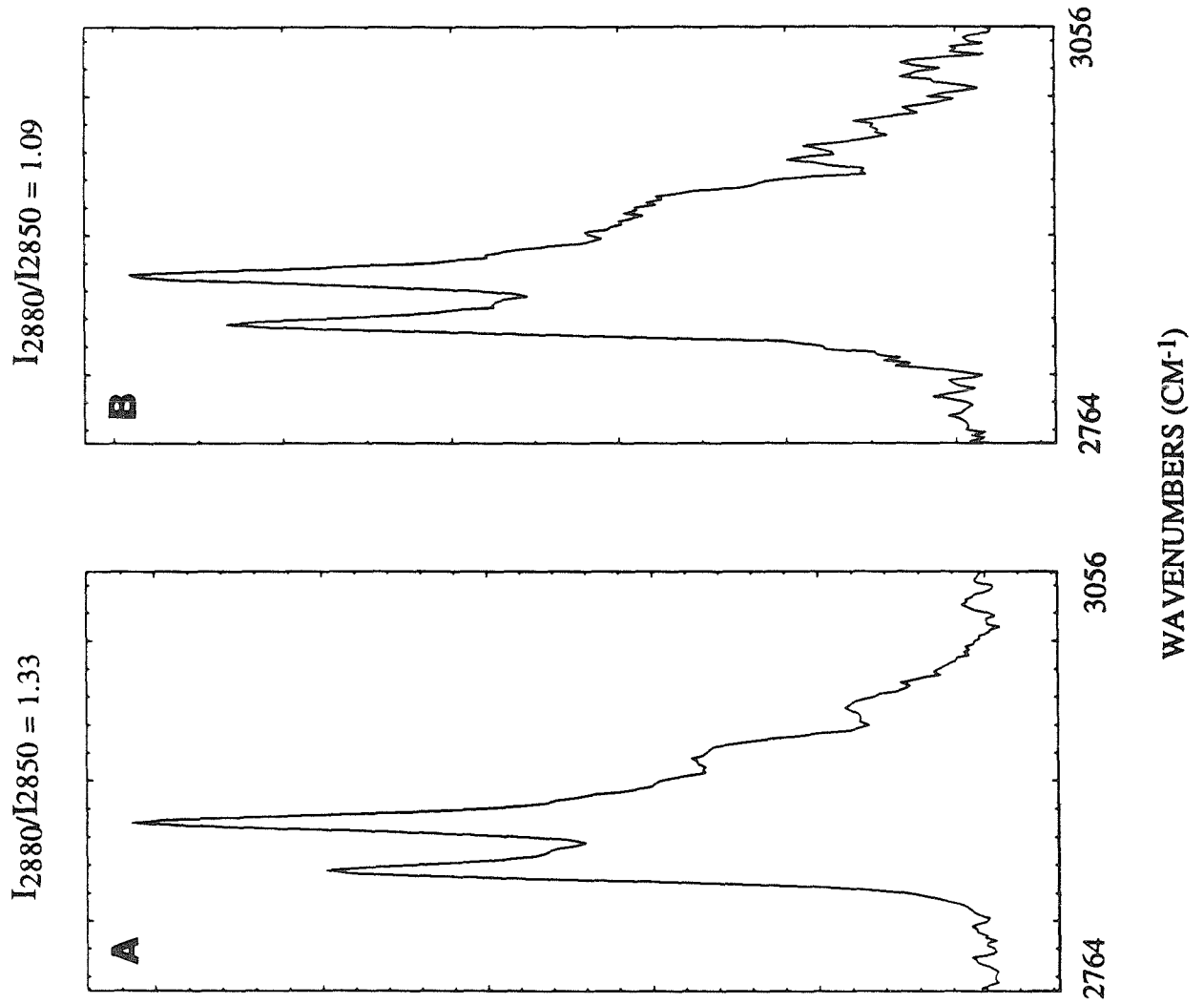
Raman C-H stretching region for DPPC bilayers at **A.** 25 °C and **B.** 56 °C.

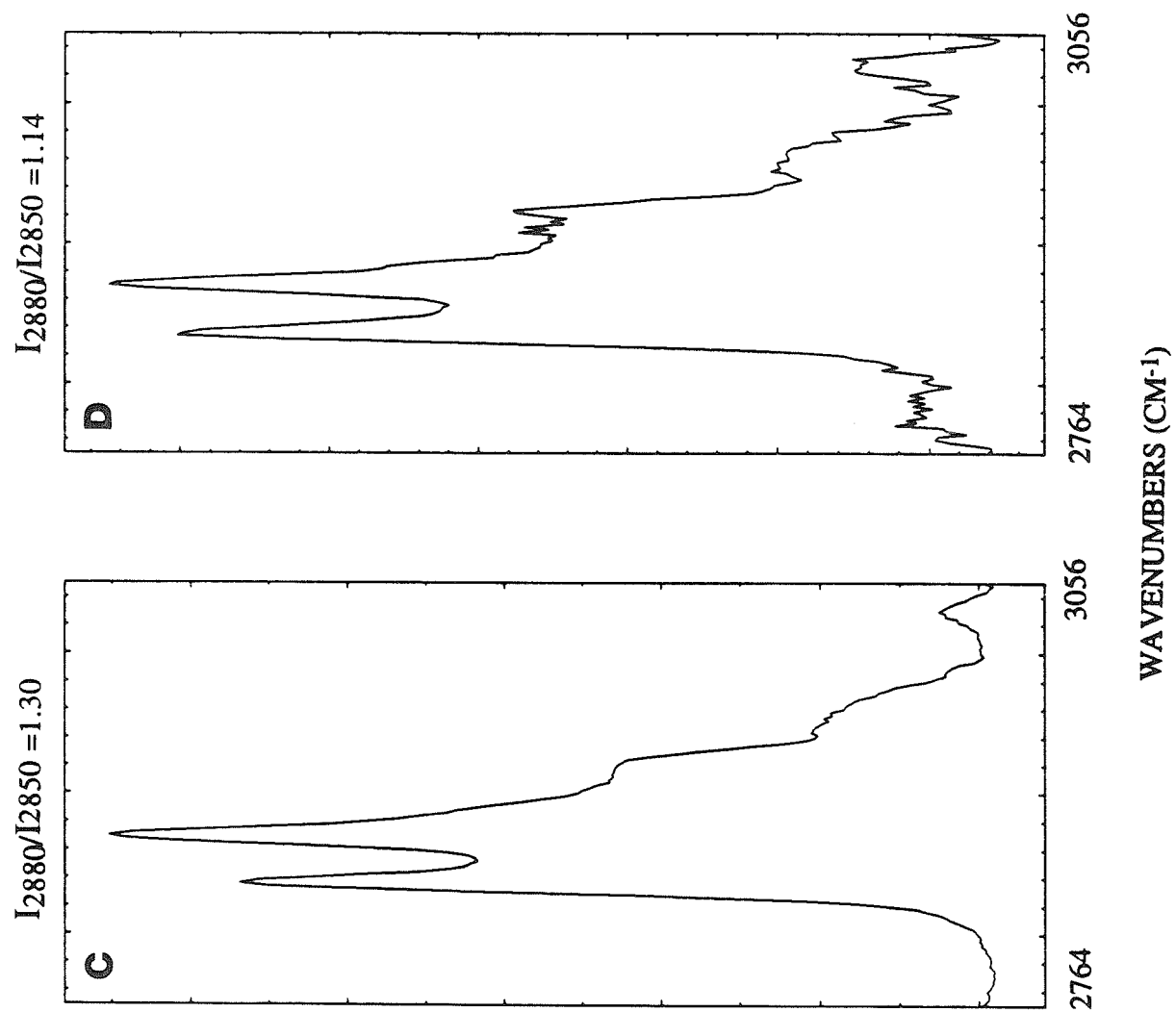


WAVENUMBERS (CM<sup>-1</sup>)

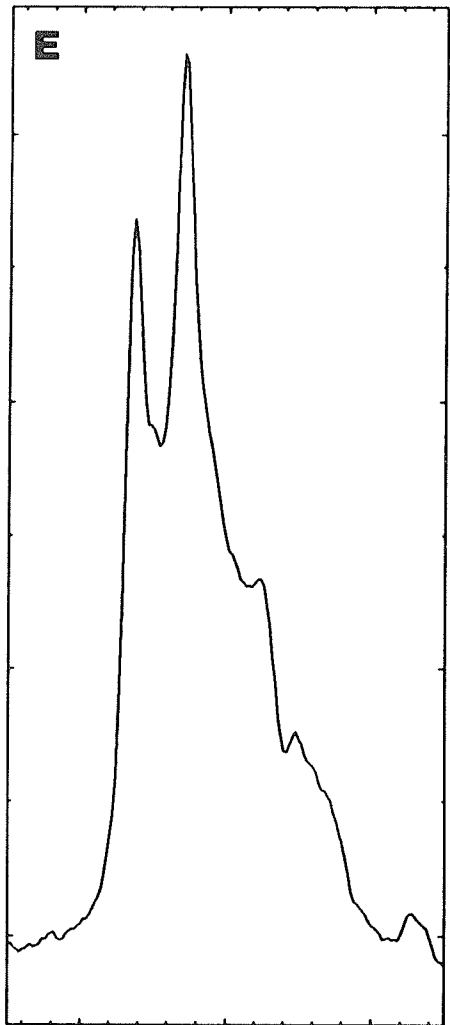
**Figure 12**

Raman C-H stretching region for hydrated bilayers of: **A.** DSPC (20.5); **B.** polymeric  $\alpha$ -18 (19 °C); **C** monomeric  $\alpha$ -20 (25 °C); **D.** polymeric  $\alpha$ -20 (22 °C); **E.** DPPC (25 °C); **F.** monomeric  $\alpha$ -16 (10 °C); **G.** polymeric  $\alpha$ -16 (8.5 °C).  $I_{2880}/I_{2850}$  ratios are included above the figures.





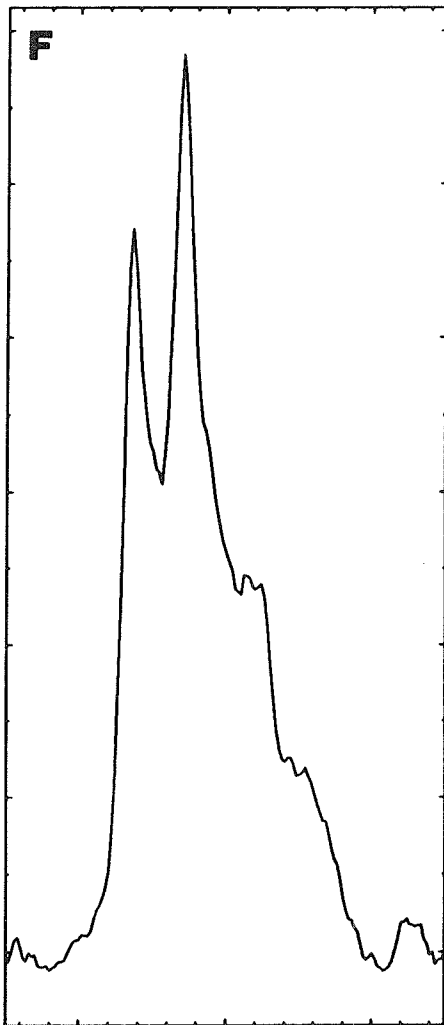
$I_{2880}/I_{2850} = 1.22$



2764

3056

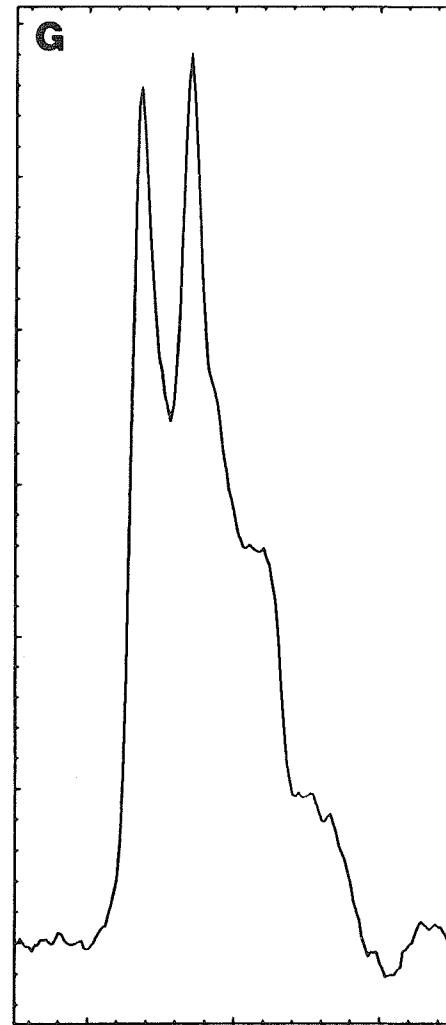
$I_{2880}/I_{2850} = 1.22$



2764

3056

$I_{2880}/I_{2850} = 1.04$



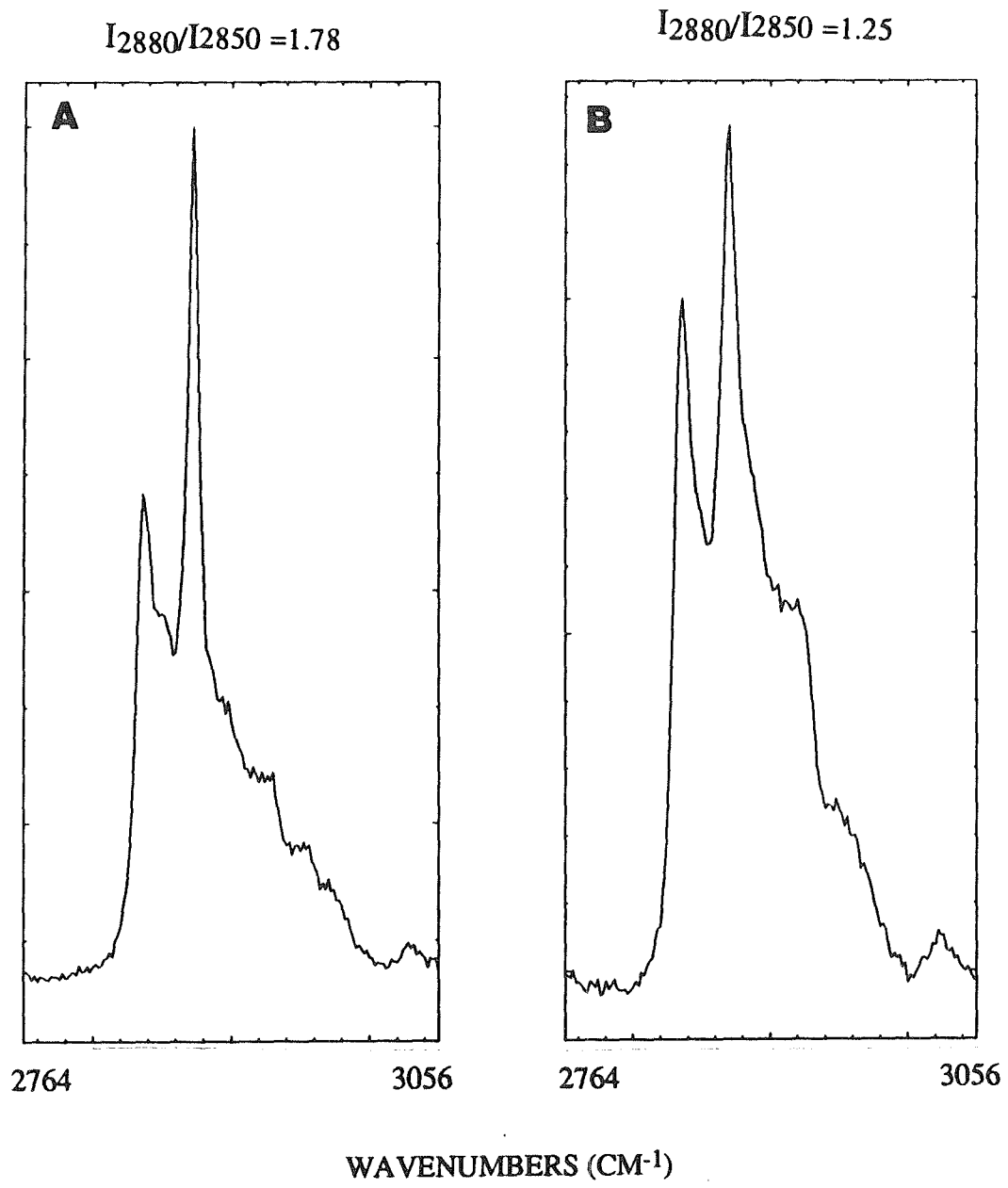
2764

3056

WAVENUMBERS (CM<sup>-1</sup>)

**Figure 13**

Raman C-H stretching region for unhydrated bilayers of : **A.** DSPC ; **B.** polymeric  $\alpha$ -18; **C.** DPPC ; **D.** polymeric  $\alpha$ -16.  $I_{2880}/I_{2850}$  ratios are included above the figures. Measurements were made at 23 °C.



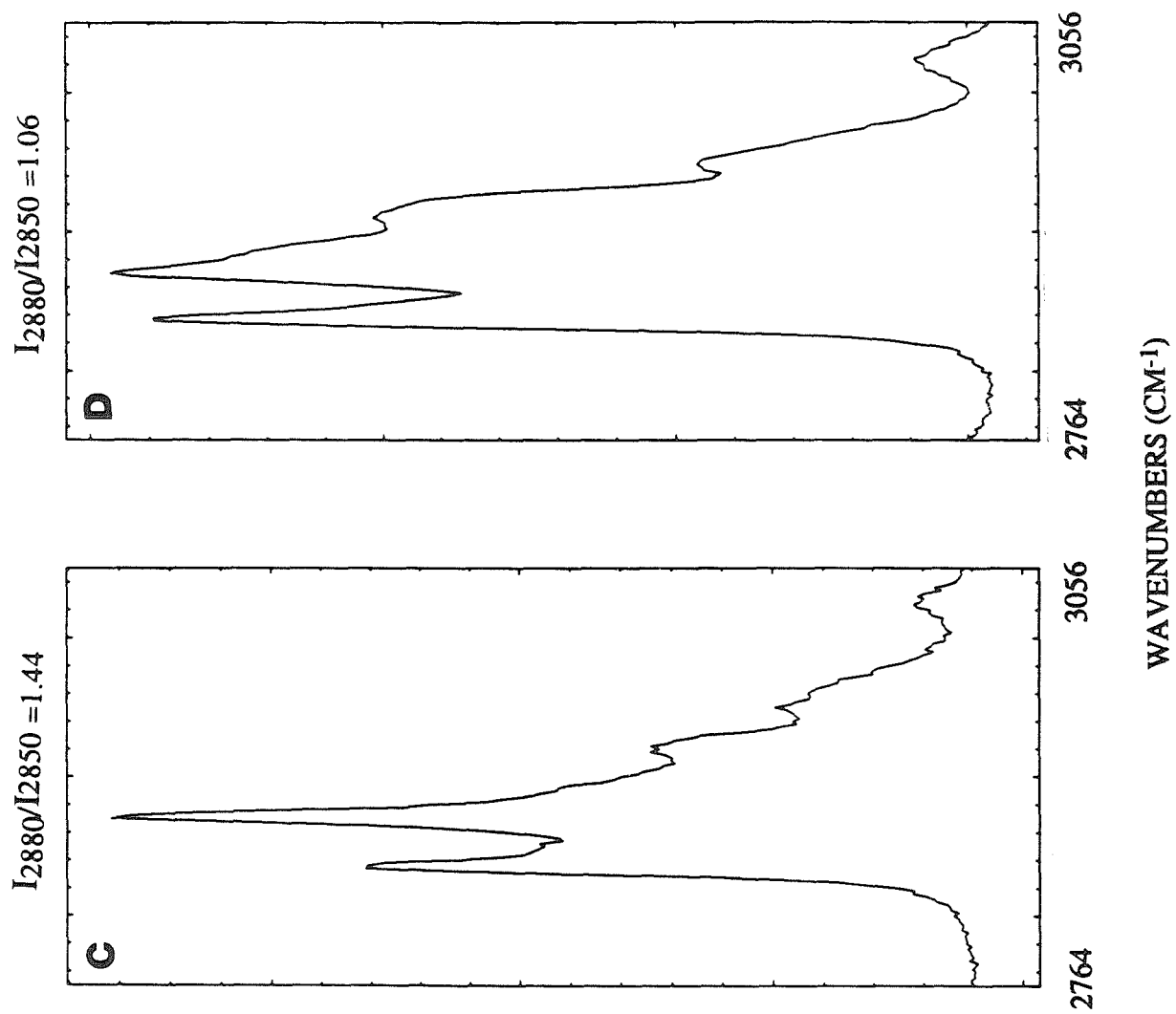
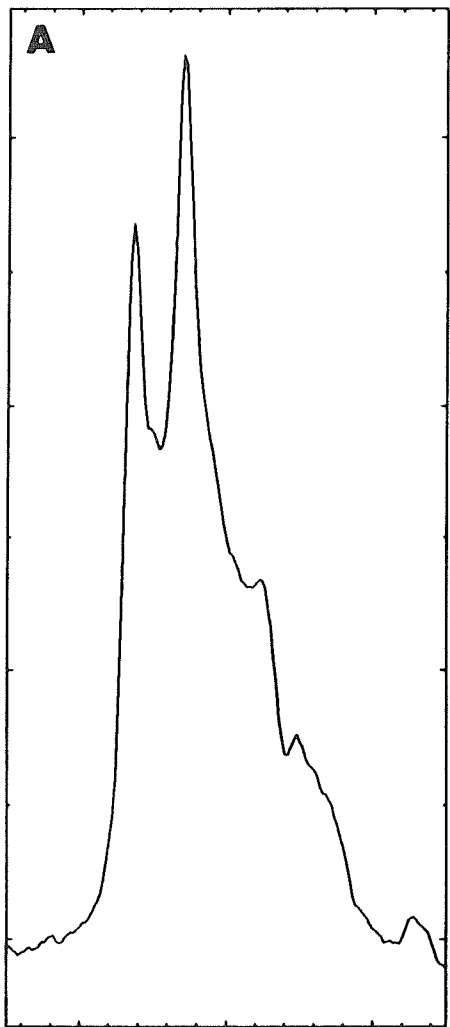


**Figure 14**

Raman C-H stretching region for hydrated bilayers of: **A.** DPPC (25.0 °C) ; **B.** monomeric  $\omega$ -16 (21 °C) ; **C** polymeric  $\omega$ -16 (20 °C) ; **D.** polymeric  $\omega$ -12 (26 °C) ; **E.**  $\omega$ 16-DPL (20 °C).  $I_{2880}/I_{2850}$  ratios are included above the figures.

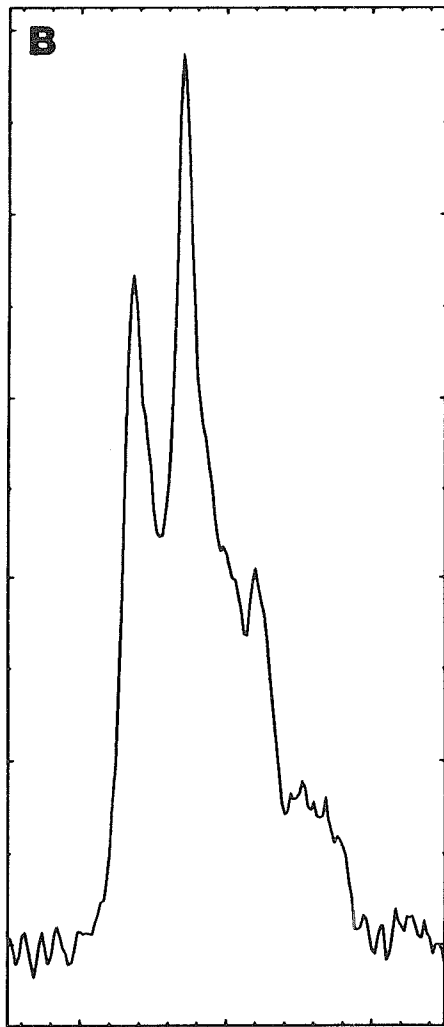
$I_{2880}/I_{2850} = 1.22$



2764

3056

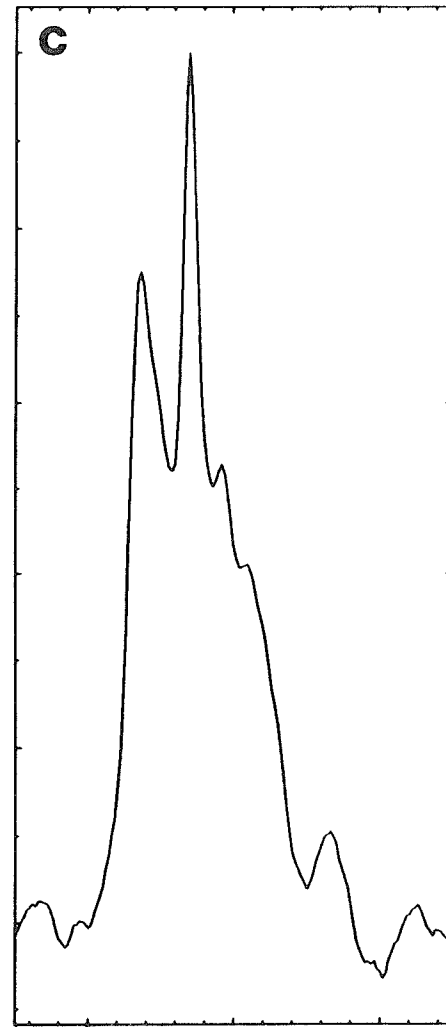
$I_{2880}/I_{2850} = 1.34$



2764

3056

$I_{2880}/I_{2850} = 1.33$

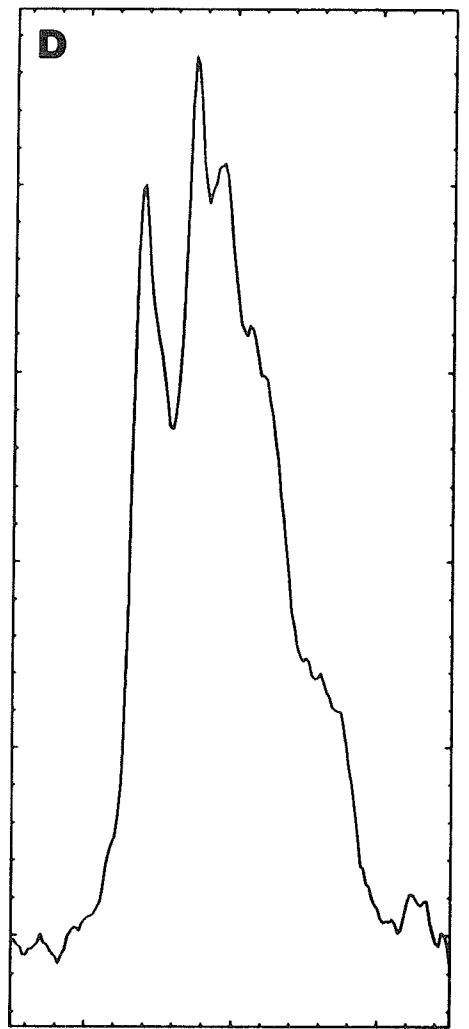


2764

3056

WAVENUMBERS (CM<sup>-1</sup>)

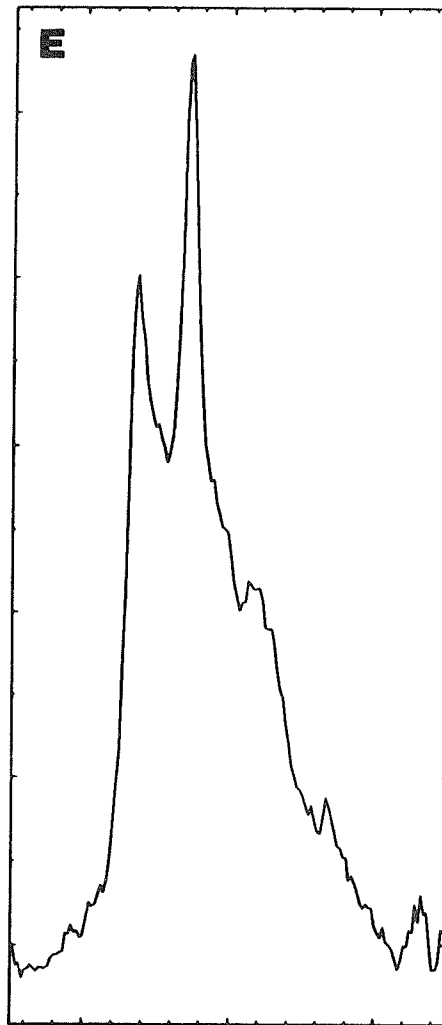
$I_{2880}/I_{2850} = 1.17$



2764

3056

$I_{2880}/I_{2850} = 1.32$



2764

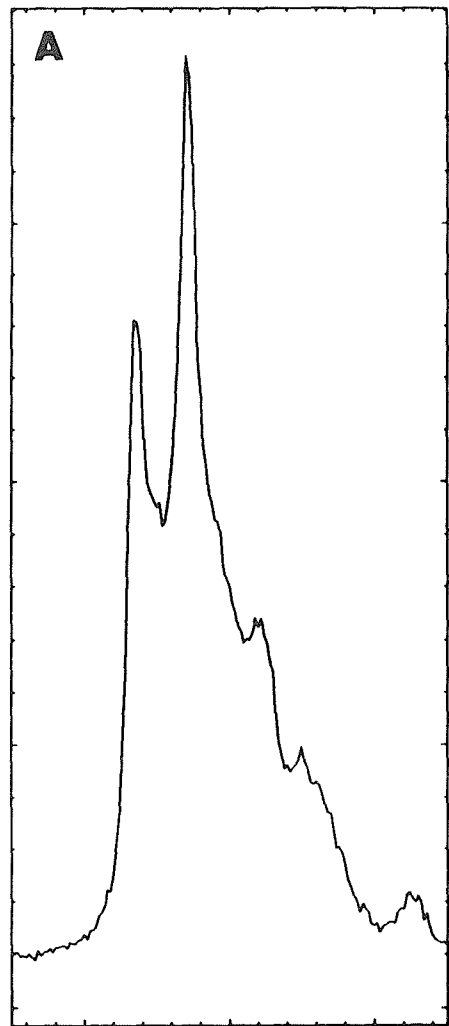
3056

WAVENUMBERS (CM<sup>-1</sup>)

**Figure 15**

The Raman C-H stretching region for unhydrated bilayers of: **A.** DPPC ; **B.** polymeric  $\omega$ -15; **C.** polymeric  $\omega$ -12.  $I_{2880}/I_{2850}$  ratios are included above the figures. Measurements were made at 23 °C.

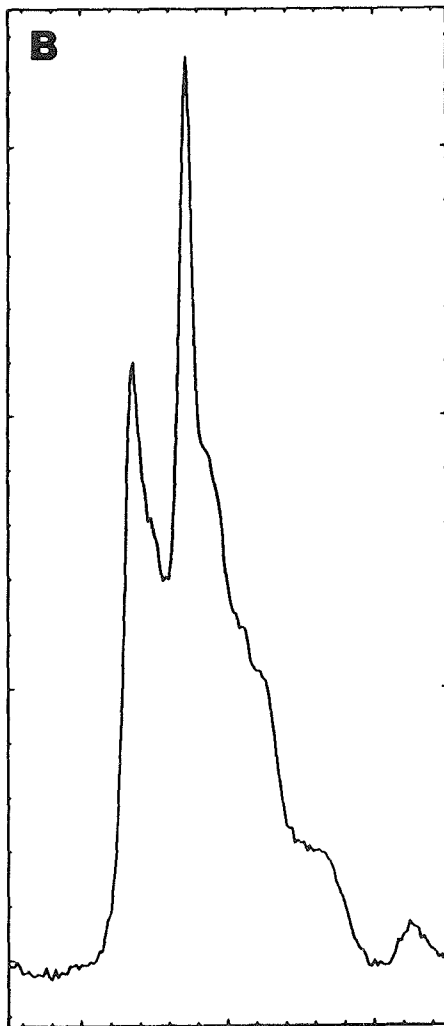
$I_{2880}/I_{2850} = 1.44$



2764

3056

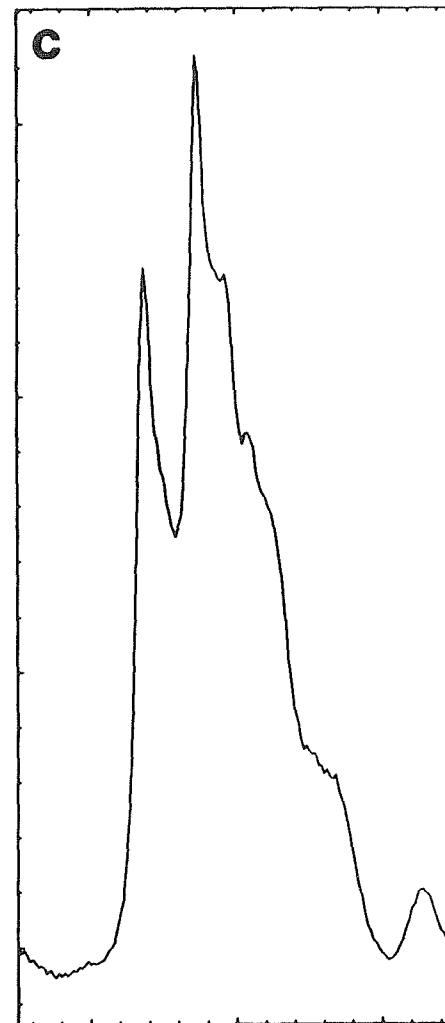
$I_{2880}/I_{2850} = 1.52$



2764

3056

$I_{2880}/I_{2850} = 1.32$



2764

3056

WAVENUMBERS (CM<sup>-1</sup>)

between these two lipid types. Thus, the data is in agreement with conclusions drawn from the C-C stretching region in that the  $\omega$ -THIOLS appear to be fairly ordered.

### CONCLUSION

The results described in this chapter have demonstrated that the position of the polymerizable moiety in disulfide polymerizable phosphatidylcholines has a marked effect on the conformational order and packing of these lipids in a bilayer. In the gel state, the acyl chains of monomeric  $\omega$ -THIOLS appears to be highly trans and fairly rigid as demonstrated by the bandwidth and peak positions of the symmetric C-H stretching modes in the infrared spectra and the intensity of trans versus gauche vibrational modes in the Raman C-C stretching region. The nature of the Raman C-H stretching region also implies that the  $\omega$ -THIOLS have a lateral packing similar to that of nonpolymerizable phosphatidylcholines. Thus the presence of a polar sulfhydryl group in the low dielectric medium at the bilayer midplane does not disrupt the bilayer organization. The results are in agreement with previous studies (Chapter III) of the position of the phase transition by DSC, FT-IR, and fluorescence polarization, which suggested that in fact the sulfhydryl group has a stabilizing effect. On polymerization, these trends are enhanced even further in the direction of greater ordering and chain immobilization.

The presence of a thiol or disulfide at the interfacial region of phosphatidylcholines has markedly different effects on the structural properties of the bilayer. In contrast to  $\omega$ -THIOLS, monomeric  $\alpha$ -THIOLS have a more disordered hydrocarbon interior than that of phosphatidylcholine analogues. This is not surprising due to the added bulk and hydration of the sulfhydryl group at the interface, which should increase the average area per molecule and therefore decrease the intermolecular chain-chain interactions. The consequences of polymerization of the  $\alpha$ -THIOLS is rather unintuitive, however.

Generally, when one thinks of polymerized lipids, the connotation is that of a rigid, stabilized bilayer. However, the FT-IR and Raman studies indicated quite clearly that the interfacial disulfide linkage actually increased the average number of gauche conformers in the chain and reduced the intramolecular packing. In fact, the  $I_{2880}/I_{2850}$  ratio of gel state polymeric  $\alpha$ -20 was similar to that of a polymerized 12-carbon  $\omega$ -THIOL, indicating a rather disordered bilayer for such a long chain lipid. It seems unlikely that the intramolecular interactions between adjacent covalently-linked lipids would be severely compromised (especially in comparison to monomeric analogues) since the presence of the disulfide bond should force the lipid chains together and restrict the extent to which they can move apart. However, the reduced conformational freedom of polymerized lipids must inhibit their ability to optimally pack *with lipids to which they are not directly bonded*, thus creating defects in the membranes between polymer chain segments. Disorder most likely arises within these regions of the bilayer.

The results presented in this study provide a physical basis for a variety of quantitative and phenomenological results observed in studies described in the other chapters. For example, in the case of the  $\omega$ -THIOLS, the high degree of order bestowed by the presence of the polymerizable moiety causes an increase in the transition temperature relative to the nonpolymerizable analogues, and promotes stable bilayer formation for even short chain ( $N < 12$ ) lipids. On the other hand, it was shown in Chapter II that polymerization of  $\omega$ -THIOLS transforms them from liposomes to bilayer fragments. Thus the degree of order and rigidity in the case of polymeric  $\omega$ -THIOLS may be incompatible with their ability to form curved, self-sealed bilayer structures, or to respond to transient defects created, on passing through the phase transition, for example.

Concerning the  $\alpha$ -THIOLS, it was shown in the previous chapter that the polymeric lipids have a reduced enthalpy relative to monomeric analogues and that they are prone to leakage of entrapped materials. Furthermore, polymeric  $\alpha$ -THIOLS readily disperse into relatively small liposomes (200-300 nm) or sonicate into SUVs even in the gel state and from the prepolymerized form of the lipids, consistent with a disordered hydrocarbon interior. Finally, in Chapter 7, *in vivo* studies are described, which illustrate the rapid blood clearance and degradation of polymeric SUVs. This is likely a reflection of the rapid adsorption of opsonizing and degradative proteins onto the liposome surface as a consequence of the fact that the hydrocarbon region is disordered and corrugated with surface defects.

#### REFERENCES

1. Gros, L., Ringsdorf, H. and Scupp, H. (1981) *Angew. Chem. Int. Ed. Engl.* **20**, 305-325.
2. Büschl, R., Folda, T. and Ringsdorf, H. (1984) *Macromol. Chem., Suppl.* **6**, 245-258.
3. Neumann, R., Ringsdorf, H. (1986) *J. Am. Chem. Soc.* **108**, 487-490.
4. Wagner, N., Dose, K., Koch, H. and Ringsdorf, H. (1981) *FEBS Lett.* **2**, 132.
5. Juliano, R., Regen, S.L., Singh, M., and Singh, A. (1983) *Biotechnology* 882-885.
6. Laschewsky, A., Ringsdorf, H., and Schneider, J. (1986) *Die Angewandte Makromolekulare Chemie* **145/146**, 1-17.
7. Elbert, R., Laschewsky, A. and Ringsdorf, H. (1985) *J. Am. Chem. Soc.* **107**, 4134-4141.

8. O'Brien, D.F., Klingbiel, R.T., Specht, D.P. and Tyminski, P.N. (1985) *Ann. N.Y. Acad. Sci.* **446**, 283-295.
9. Ringsdorf, H., Schlarb, B., Tyminski, P.N. and O'Brien, D, F. (1988) *Macromolecules* **21**, 671-677.
10. Dorn, K., Klingbiel, R.T., Specht, D.P., Tyminski, P.N., Ringsdorf, H. and O'Brien, D.F. (1984) *J. Am. Chem. Soc.* **106**, 1627-1633.
11. Regen, S.L., Singh, A., Oehme, G. and Singh, M. (1982) *J. Am. Chem. Soc.* **104**, 791-795.
12. Juliano, R.L., Hsu, S.L., Regen, S.L. and Singh, M. (1984) *Biochim. Biophys. Acta.* **770**, 109-114.
13. Kusumi, A., Singh, M., Tirrell, D.A., Oehme, G., Singh, A., Samuel, N.K.P., Hyde, J.S. and Regen, S.L. (1983) *J. Am. Chem. Soc.* **105**, 2975-2980.
14. Gaub, H., and Sackmann E., Büschl, R. and Ringsdorf, H. (1984) *Biophys. J.* **45**, 725-731.
15. Schoen, P. E., Yager, P. and Priest, R. G. (1985) *Polydiacetylenes : NATO Advanced Study Institute, Stratford on Avon, 1984.*
16. Casal, H.L., Mantsch, H.H. (1984) *Biochim. Biophys. Acta.* **779**, 381-401.
17. Cameron, D.G. and Dluhy, R.A. in: *Spectroscopy in the Biomedical Sciences* 53-85.
18. Carrey, P. in: *Biochim. Applications of Raman Spectroscopy* ; Spiro, T.G. (Ed.)
19. Levin, I.W. in: *Advances in Infrared and Raman Spectroscopy* ; Clark, J.H. and Hester, R.E. (Eds.) Wiley: Heyden; 1984.
20. Mantsch, H.H. (1984) *J. Mol. Structure* **1113**, 201-212.
21. Mushayakarara, E. and Levin, I.W. (1984) *Biochim. Biophys. Acta.* **769**, 585-595.

22. Knoll, W. (1986) *Biochim. Biophys. Acta.* **863**, 329-331.
23. Bush, S.F., Adams, R.G., Levin, I.W. (1980) *Biochemistry* **19**, 4429-4436.
24. Lafleur, M., Dasseux, J., Pigeon, M., Dufourcq, J. and Pérolet, M. (1987) *Biochemistry* **26**, 1173-1179.
25. Huang, C., Mason, J.T., Levin, I.W. (1983) *Biochemistry* **22**, 2275-2780.
26. Cameron, D.G., Casal, H.L., Gudgin, E.F. and Mantsch, H.H. (1980) *Biochim. Biophys. Acta.* **596**, 463-467.
27. Snyder, R.G., Scherer, J.R., and Gaber, B.P. (1980) *Biochim. Biophys. Acta.* **601**, 47-53.
28. Mantsch, H.H., Martin, A., and Cameron, D.G. (1981) *Biochemistry* **20**, 3138-3145.
29. Nagle, J.F. and Wilkinson, D.A. (1978) *Biophys. J.* **23**, 159-175.
30. Snyder, R.G., Hsu, S.L., and Krimm, S. (1978) *Spectrochimica Acta* **34A**, 395-406.
31. Benow, M.R., and Levin, I.W. (1977) *Biochim. Biophys. Acta.* **487**, 388-394.
32. Lippert, J. and Peticolas, W. (1972) *Biochim. Biophys. Acta.* **282**, 8-17.

## APPENDIX

In this chapter, data has been presented that clearly illustrates in a qualitative manner the ordering of the lipid chains in monomeric and polymeric  $\alpha$ - and  $\omega$ -THIOLS. Steady state fluorescence anisotropy  $r_s$  (or polarization  $P_s$ ) measurements have also

been widely used as indicators of membrane organization (1,2). Therefore it is now useful to recall the fluorescence anisotropy results of the previous chapter to evaluate their meaning in light of the conclusions drawn from the vibrational spectroscopy. It was shown using DPH as a fluorescent probe that upon polymerization of both lipid types, the anisotropy values uniformly increased at all temperatures and for all chain lengths evaluated. The temperature dependence of the DPH anisotropies for monomeric and polymeric  $\alpha$ -16 and  $\omega$ -16 is shown in Figure 3 of Chapter III.

Steady state anisotropies ( $r_s$ ) or polarization ( $P_s$ ) are based on the components of the emitted light perpendicular and parallel to the direction of excitation according to:

$$(1) \quad r_s = \frac{I_{\parallel} - I_{\perp}}{I_{\parallel} + 2I_{\perp}} \quad P_s = \frac{I_{\parallel} - I_{\perp}}{I_{\parallel} + I_{\perp}} \quad r_s = \frac{2P_s}{3 - P_s}$$

(see 1 and 2 for reviews as well as 3). Depolarization occurs if a reorientation (i.e. wobbling or rotational diffusion) of the fluorophore takes place during its fluorescence lifetime such that the emitting dipoles are randomly oriented relative to the initial direction of polarization (1-3). Thus, steady-state anisotropies should yield information concerning membrane structure and dynamics. In the past the steady state anisotropies have been routinely interpreted in terms of membrane fluidities and microviscosities whereby an increasing anisotropy was correlated with a decrease in membrane fluidity (1-4). Quantitatively, the Perrin equation was used to convert anisotropies into apparent microviscosities. However, more recently, such a simplified analysis has been called into question and shown inappropriate (3,5-7). This is due to the fact that the extrapolations of anisotropy to microviscosity were founded on the incorrect assumptions of isotropic reorientation of the probe within an anisotropic lipid matrix. Time resolved anisotropy measurements have revealed that the decay curve can be resolved into (i) an infinitely slowly decaying (static) part  $r_{\infty}$  which depends on the degree to which the fluorophore depolarizing rotations are restricted by molecular

packing and other interferences and (ii) a fast decaying (dynamic) factor  $r_f$ , which depends on the rate of probe rotation (5,6). (Analysis via the Perrin equation assumes only the latter contribution (3)). The decay curve can be expressed as:

$$(2) \quad r(t) = (r_0 - r_\infty)e^{-\frac{t}{\phi}} + r_\infty$$

where  $r_0$  is the fluorescence anisotropy in the absence of depolarizing rotational motion (0.4 for DPH),  $r_\infty$  is the static component representing the hindered motion of the probe,  $\phi$  is the rotational correlation time for rotation about the long molecular axis of DPH and  $r_s$  is the measured steady state anisotropy.\* Assuming a simple exponential decay of the total fluorescence intensity, the following expression is obtained, which resolves the steady state anisotropy into dynamic and static components (3):

$$(3) \quad r_s = \frac{r_0 - r_\infty}{1 + \frac{\tau}{\phi}} + r_\infty = r_f + r_\infty$$

where  $\tau$  is the lifetime of the fluorescent probe. Based on experimental data from steady state fluorescence anisotropy experiments ( $r_s$ ) and the limiting anisotropy ( $r_\infty$ ) obtained from time-resolved experiments, Blitterswijk *et al.* have derived empirical relationships from which one can estimate the value of  $r_\infty$  directly from  $r_s$  (3). The conversion between  $r_s$  and  $r_\infty$  is given by the equation:

$$(4) \quad r_\infty = \frac{4}{3}r_s - .10 \quad \text{for } .13 < r_s < .28$$

$$(5) \quad r_\infty \approx r_s \quad \text{for } r_s > .3$$

---

\* Alternative expressions have been applied to fit the decay curve. Eqn. (2) is based on a model for hindered motion. Lakowicz has also shown that the anisotropy decay of DPH can be fit by a model for an anisotropic rotator with two correlation times perhaps slightly better than the model for hindered motion (8,9). In the case of the two correlation time rotator model, the appropriate equation is:

$$r(t) = r_0 \left( g_1 e^{-\frac{t}{\phi_1}} + g_2 e^{-\frac{t}{\phi_2}} \right)$$

where  $\phi_1$  and  $\phi_2$  are the two correlation times and  $g_1 + g_2 = 1$ .

It is noteworthy that these relations between  $r_\infty$  and  $r_s$  were shown to be in good agreement with theoretical predictions based on the rotational dynamics in liquid crystals. The significance of this relation is that from  $r_s$ , the limiting anisotropy  $r_\infty$  can be determined without the need for time-resolved experiments, and from  $r_\infty$  a fluorescence order parameter can be calculated according to (1,3,5,6):

$$(6) \quad \frac{r_\infty}{r_0} = S_{DPH}^2$$

The order parameter describes the average static distribution of the probe orientation averaged over the length of the entire molecule and therefore reflects in some way restrictions to probe motion and therefore features of the bilayer structure (1,3). It is, however, not quantitatively comparable to order parameters obtained by for example  $^2\text{H-NMR}$ , which are dependent on the particular segment of the acyl chain which is deuterated. As one example of the meaning of the order parameter  $S_{DPH}$ , Kinoshita has adopted a cone model that assumes that the relevant motion executed by the rigid rod DPH structure is that of a wobble within an opening angle  $\varnothing$  where (10):

$$(7) \quad S = \frac{1}{2} \cos \varnothing (1 + \cos \varnothing)$$

While this model offers a visual description of the meaning of the order parameter it may or may not be an accurate description of the origin of  $r_\infty$  from one system to another. However, it must reflect in some way restrictions to probe motion such as those imposed by the addition of cholesterol, proteins or due to polymerization. By comparison of calculated order parameters obtained from fluorescence data in the previous chapter with the results obtained from the vibrational spectroscopy in this chapter, it may be possible to sort out what are the important structural and motional features of the polymeric bilayers that lead to the observed anisotropies.

Using the approach of Blitterswijk, we have calculated the order parameters and  $\Theta$  for polymeric/monomeric  $\alpha$ - and  $\omega$ -THIOLS, and DPPC. These are tabulated in Table II for a variety of chain lengths at temperatures below the  $T_m$ . As can be seen, in all cases of  $\alpha$ - and  $\omega$ -THIOLS, the value of  $S_{DPH}$  is increased on polymerization (values range between 0 and 1.0 where 1.0 is complete ordering) and the "cone angle"  $\Theta$  is decreased. Similar increases in  $S_{DPH}$  have been observed with increasing cholesterol or sphingomyelin content in biological membranes and correlated with increasing structural order in the membranes or the formation of rigid domains where DPH is preferentially solubilized (3). For  $\omega$ -THIOLS, the data confirmed conclusions drawn from DSC and vibrational spectroscopy that polymerization increases the membrane order. For the  $\alpha$ -THIOLS, however, while it would seem intuitive that polymerization would increase the order parameter, these data are inconsistent with all other results, particularly the vibrational spectroscopy in this chapter, which clearly suggested that polymerization had a disordering effect.

There are several possible explanations for the apparent disagreement between the fluorescence anisotropy and vibrational spectroscopy data for monomeric versus polymeric  $\alpha$ -THIOLS. Variations in the lifetime of the fluorescent probe between different membrane types may be excluded as a potential source of the discrepancy since the lifetimes are taken into account due to the empirical nature of the relationship. However it is possible that the position of the probe in the bilayer might lead to misleading conclusions (11). If, for example, DPH were solubilized more toward the bilayer midplane, the order parameter would be predictably lower due to the increased fluidity of the lipids toward the acyl chain methyl group as demonstrated by NMR and EPR results (12-14). This appears to be the case when one compares the  $S_{DPH}$  for monomeric (or polymeric)  $\alpha$ -20 versus  $\alpha$ -18 versus  $\alpha$ -16 dispersions; the lower  $S_{DPH}$  for monomeric  $\alpha$ -20 compared to  $\alpha$ -16 is inconsistent with the greater structural

**Table II**

Calculation of the fluorescence order parameter  $S_{DPH}$  and the cone angle for wobbling diffusion  $\Theta$  according to the empirical relations of Blitterswijk (Eqns. 4-7) for various polymeric and monomeric  $\alpha$ -THIOLS and  $\omega$ -THIOLS.

Lipid	Temperature (°C) <sup>a</sup>	r <sub>s</sub>	S <sub>DPH</sub> <sup>b</sup>	Θ
<b>α-THIOLS</b>				
α-16 (M)	15	0.286	0.85 ± .04	26.7
α-16 (P)	12.5	0.310	0.87 ± .02	19.8
α-18 (M)	25	0.256	0.78 ± .05	32.5
α-18 (P)	25	0.310	0.87 ± .02	24.2
α-20 (M)	35	0.226	0.71 ± .07	37.7
α-20 (P)	35	0.321	0.89 ± .02	22.2
<b>ω-THIOLS</b>				
ω-15 (M)	30	0.247	0.76 ± .06	34.0
ω-15 (P)	40	0.330	0.90 ± .02	21.0
ω-16 (M)	40	0.266	0.80 ± .05	30.7
ω-16 (P)	35	0.314	0.88 ± .02	23.5
<b>LECITHIN</b>				
DPPC	25	0.264	0.79 ± .05	31.5

<sup>a</sup> Anisotropies are taken at temperatures where the value of the anisotropy varies little with temperature. <sup>b</sup> Errors in S<sub>DPH</sub> are estimated from the following equation (3):

$$\text{Error} = 50 \left( 1 - \frac{5}{2} r_s \right)^2 \%$$

order of the long chain lipid  $\alpha$ -20 as demonstrated by DSC, Raman and FT-IR. This therefore suggests that the DPH is solubilized deeper into the bilayer and is less affected by the rigid interfacial region as the length of the acyl chain is increased. The effect of chain length and the consequence of a close proximity of DPH to the interface is also reflected in the relatively high order parameter of polymeric  $\omega$ -11. However, for polymeric versus monomeric  $\alpha$ -THIOLS of the same chain length (i.e. polymeric versus monomeric  $\alpha$ -16), the results would suggest that the DPH is buried deeper in the membranes of the monomeric lipids. While we cannot exclude this as the basis for the apparent increased structural order of polymeric versus monomeric  $\alpha$ -THIOLS, intuitively, one would anticipate the opposite behavior --- the polymerized membranes should force the probe into deeper solubilization sites due to the steric hindrance of the disulfide group.

An alternate and perhaps more likely explanation for the relative order parameters of monomeric versus polymeric  $\alpha$ -THIOLS invokes different modes of motion of the lipids within the membrane, which may be important to depolarizing rotations of DPH. While the order parameter describes the average static distribution of the orientation of the probe and not the probe dynamics, the motions of the bilayer must in some way contribute to the motional freedom of the fluorophore. In particular, the relevant fluctuations must be those with time scales longer than the fluorescent lifetime of DPH ( $> 1-10$  ns) such that they effectively produce an average static distribution of the fluorophores within the bilayer. Lakowicz has in fact shown by multifrequency phase-modulation fluorometry that the anisotropy of DPH in DPPC multilayers is best modelled by two correlation times where one correlation time is much longer (50-200 ns) than the other (1-5 ns) (8).

The correlation times of lipids in multilayers have been assessed primarily via NMR and ESR experiments. On the basis of  $^1\text{H}$  and  $^2\text{H}$  NMR spin lattice relaxation studies,

it has been shown shown that the time scale for chain isomerization and rotational reorientation in lecithin multilayers are approximately  $10^{-10}$  to  $10^{-11}$  s and  $10^{-7}$  s, respectively (15-18). Segmental isomerizations would not be expected to greatly contribute to  $r_{\infty}$  due to (1) the short correlation time and (2) the fact that DPH is probably too rigid to respond to these motions. Rotational reorientation, off-axis wobbling and even slower motions such as cooperative fluctuations perpendicular to the bilayer normal (i.e. lateral wave-like motions) and translational diffusion may, however, be important. If we now consider the motional differences in the nonpolymerizable or monomeric multilayers versus polymerized multilayers, potential sources for the elevated order parameters and decreased cone angles in polymeric bilayers become apparent. Clearly the rotational and translational diffusion of the polymeric lipids will be much slower than that of nonpolymerized analogues. In addition, whereas monomeric lipids may undergo lateral wave motions or wobbling rotational diffusion thereby "creating space" or a larger cone angle for similar motions by the probe, the polymeric lipids most likely vibrate only with rapid small amplitude motions that do not appreciably change the available space of the probe. Thus, despite the structural disorder and fast segmental isomerizations (see Chapter V) of the alkyl chains of polymeric  $\alpha$ -THIOLS, the slower collective motions of the polymeric lipids may be inhibited or slowed substantially such that they are effectively a rigid wall to the depolarizing motions of the probe.

In summary, the fluorescence polarization results show an increase in the order parameters for polymeric versus monomeric  $\alpha$ - and  $\omega$ -THIOLS. In light of calorimetric and vibrational spectroscopic data concerning the chain conformation and packing of  $\omega$ -THIOLS, this was anticipated. In the case of  $\alpha$ -THIOLS, however, since Raman, FT-IR and DSC experiments indicated polymeric  $\alpha$ -THIOLS membranes were characterized by a disordered hydrocarbon region and loose packing density, a

decrease in the order parameter was expected. Assuming that the position of DPH is similar in monomeric versus polymeric  $\alpha$ -THIOLS, the best explanation for these results is that the slow motions ( $\gg$  fluorescent lifetime of DPH) of the bilayers are the important determinants in the value of  $r_{\infty}$  and therefore the fluorescence order parameter. In other words, motions such as translational/rotational diffusion and off-axis wobbling of the lipids in monomeric and nonpolymerizable membranes are more rapid than in nonpolymerizable membranes. This results in a larger angular distribution of fluorescent probes and therefore a lower anisotropy/order parameter in the nonpolymerizable membranes, despite the fact the polymeric  $\alpha$ -THIOL membranes are disordered.\*

The same types of arguments may be applicable to the increased steady state anisotropy of DPH observed for reconstituted sarcoplasmic membrane vesicles compared to analogous pure lipid vesicles as observed by Seelig *et al.* (20). These results were contradictory to  $^2\text{H}$  and  $^{31}\text{P}$  NMR studies on the same systems, which indicated that the addition of protein had a disordering effect (the chemical shift anisotropy,  $\Delta\sigma$ , and the quadrupole splitting,  $\Delta\nu$ , were 10-20% *smaller* in the protein-containing vesicles). The authors concluded that the fast internal modes of motion of a phospholipid are less influenced by protein than translocation and reorientation of the entire molecule. Thus by comparison, it seems that similar mechanisms (reduction in translational, rotational and gross cooperative motions) are operative in increasing  $S_{\text{DPH}}$  for both protein-containing vesicles and polymeric membranes. Finally, in agreement Seelig *et al.*, the present study illustrates the caveats of steady state polarization measurements and how, in the absence of other spectroscopic data, steady state fluorescence measurements may be ambiguous and misleading. In the absence of the vibrational data, we might have concluded from the the polarization experiments that

---

\* Motion and order are not necessarily correlated.

the hydrocarbon chains of polymeric  $\alpha$ -THIOLS had a high degree of structural order and therefore were probably highly trans in conformation.

### REFERENCES

1. Prendergast, F.G. (1981) *Period. biol.* **83**, 69-79.
2. Lakowicz, J.R. in: *Principles of Fluorescence Spectroscopy* ; Plenum Press: New York; 1983.
3. Van Blitterswijk, W.J., Van Hoeven, R.P., and Van Der Meer, B.W. (1981) *Biochim. Biophys. Acta.* **644**, 323-332.
4. Shinitzky, M. and Barenholz, Y. (1978) *Biochim. Biophys. Acta.* **515**, 367-394.
5. Heyn, M.P. (1979) *FEBS Lett.* **108**, 359-364.
6. Jähnig, F. (1979) *Proc. Natl. Acad. Sci. U.S.A.* **76**, 6361-6365.
7. Veatch, W.R. and Stryer, L. (1977) *J. Mol. Biol.* **117**, 1109-1113.
8. Lakowicz, J.R., Cherek, H., Maliwal, B.P., and Gratton, E. (1985) *Biochemistry* **24**, 376-383.
9. Lakowicz, J.R., Prendergast, F.G. and Hogen, D. (1979) *Biochemistry* **18**, 508-519.
10. Kinoshita, K., Kawato, S. and Ikegami, A. (1977) *Biophys. J.* **20**, 289-305.
11. Cadenhead, D.A. Kellner, B.M., Jacobson, K. and Papahadjopoulos, D. (1977) *Biochemistry* **16**, 5386-5392.
12. Smith, I. in: *Nuclear Magnetic Resonance of Liquid Crystals* ; Emsley, J.W. (Ed.) ; Reidel Publishing, 1985; 533-566.
13. Burns, R. and Roberts, M.F. (1980) *Biochemistry* **19**, 3106-3113.

14. Jacobs, R. E., Oldfield, E. (1981) *Progress in NMR Spec.* **14**, 113-136.
15. Peterson, N.O. and Chan S.I. (1977) *Biochemistry* **16**, 2657-2667.
16. Feigenson, G.W. and Chan S.I. (1974) *J. Am. Chem. Soc.* **96**, 1312-1319.
17. Seiter, C.H.A. and Chan, S.I. (1973) *J. Am. Chem. Soc.* **95**, 7541-7553.
18. Chan, S.I., Bocian, D.F, and Peterson, N.O. in: *Membrane Spectroscopy* ; Springer-Verlag: Berlin Heidelberg; 1981; 1-50.

---

---

**Chapter V**

---

---

*Investigations of the Dynamic Properties of Polymerized Phosphatidylcholines by  
 $^{13}\text{C}$  and  $^1\text{H}$  NMR*

---

**INTRODUCTION**

Numerous studies on phospholipid membranes of both synthetic and natural origin have revealed a close correlation between the molecular mobility of the constituent phospholipids and a variety of physical and biological properties (*for reviews, see 1-5*). This has prompted investigation of the effects of lipid structure (headgroup size and charge, chain length and degree of unsaturation) on lipid mobility as well as the motional and structural consequences of the addition of cholesterol, anaesthetics, proteins and carbohydrates (*6-17*). Polymeric lipid aggregates have been recently recognized as a new and important class of synthetic membranes due to their potential as diagnostic or therapeutic drug delivery systems, for reactivity control, and in a wide variety of other applications (*18-22*). However, relatively few studies have been directed toward delineating their motional behavior and correlating these motions with their physical properties (*23,24*). In the last several chapters, polymerizeable  $\alpha$ - and  $\omega$ -THIOLS have been shown to have drastically different thermal and morphological

properties as a consequence of the difference in the position of the polymerizable moiety (at the chain terminus ( $\omega$ -THIOLS) or at the methylene alpha to the carbonyl ( $\alpha$ -THIOLS)). Whereas  $\alpha$ -THIOLS have a behavior resembling most closely that of conventional phospholipid bilayers,  $\omega$ -THIOLS, by contrast, exhibit unusual behavior including fragmentation, elevated thermal properties and a propensity for extensive aggregation. Thus a detailed study of the motional properties may shed some light on the interrelationship between lipid structure, lipid mobility, and membrane function.

NMR has been a particularly useful technique for delineating the motional properties of lipids due to the dependence of various parameters (such as spin-lattice relaxation times and linewidths) on the correlation times of the molecular motion. In this chapter, we use  $^1\text{H}$  and  $^{13}\text{C}$  NMR to evaluate the presence or absence of a mobility gradient (which is characteristic of most synthetic and biological membranes) and the extent of motional restriction imposed by the polymerizable moieties. Furthermore, in the polymeric systems, the dynamical constraints introduced via polymerization are useful for further examination of theories concerning the relevant motions that determine the relaxation behavior in membranes. For example  $^{13}\text{C}$  spin-lattice relaxation times ( $T_1$ ) in micelles and liposomes have been shown to be informative in studying motions of the alkyl chains because the spin-lattice relaxation time is sensitive to both fast segmental isomerizations ( $\tau_c \approx 10^{-11}$  s) about carbon-carbon bonds in the chains as well as to slow and/or cooperative fluctuations ( $\tau_c > \omega_0^{-1}$  where  $\omega_0$  is the Larmor frequency) (25-31). The latter may be "rigid body" motions of the entire phospholipid (translational or collective wave-like motions of the whole molecule) or cooperative motions of the acyl chains alone decoupled from the backbone and headgroup (26). In the case of  $\alpha$ -THIOLS where the polymeric moiety is at the rigid interfacial region, the construction of the polymerized bilayer is such that the translational and rotational motions of the lipids as a whole will be severely hindered whereas the fast segmental

motions and low frequency motions of the acyl chains may be relatively unaffected. By contrast, one might expect that for  $\omega$ -THIOLS, the polymerizeable moiety at the chain terminus should drastically alter the rate and nature of the fast segmental and slow hydrocarbon chain fluctuations in addition to the rotational and translational diffusion of entire phospholipid units. Thus, investigations of the spin-lattice relaxation times of the polymeric lipids and comparison to nonpolymerizeable analogs may help to further delineate the motions sensed by the relaxation rates and to elucidate the motional state of polymerized bilayers and how it is correlated to the physical properties of these artificial membranes.

While the bulk of the investigation to be described concerns high resolution studies of sonicated vesicles and micelles,  $^{13}\text{C}$  solid state magic angle spinning is also employed to examine the spectra and relaxation properties of unsonicated lipid dispersions. The following study therefore covers three topics:

(i) High resolution  $^{13}\text{C}$  NMR spectra and spin-lattice relaxation investigations of (a) polymeric  $\alpha$ -16 versus DMPC SUVs and (b) polymeric  $\omega$ -8 versus D8PC micelles. The reason for using the short chain lipids in (b) is that long-chain  $\omega$ -THIOLS form bilayer fragments that aggregate extensively and cannot be sonicated into particles small enough to be visible by NMR without resorting to magic angle spinning techniques. Nonetheless, they serve as useful models of the motional behavior expected from the long chain analogues.

(ii)  $^1\text{H}$  NMR of sonicated and unsonicated lipid dispersions.

(iii)  $^{13}\text{C}$  MASS spectra and relaxation properties of a variety of nonpolymerizeable and polymeric lipids. Since these experiments are as yet incomplete, they are only briefly discussed at the end.

## MATERIALS AND METHODS

### Materials.

The synthesis and polymerization of the disulfide polymerizable phosphatidylcholines was as described in Chapter VIII. Routinely the polymerized form of the lipid was stored at 4°C until use. L- $\alpha$ -dipalmitoylphosphatidylcholine (DPPC), L- $\alpha$ -dimyristoylphosphatidylcholine (DMPC), egg phosphatidylcholine (EPC) and L- $\alpha$ -dioctanoylphosphatidylcholine (D8PC) were purchased from Avanti Polar Lipids. All other reagents were of analytical grade and used without further purification.

### Methods.

Liposome Preparation. For high resolution  $^{13}\text{C}$  NMR studies, small unilamellar vesicles (30-75 mg/ml) were prepared by hydrating nonpolymerizable phosphatidylcholines or prepolymerized  $\alpha$ -THIOLS in phosphate buffer (10 mM sodium phosphate, 5 mM EDTA; pH 7.4) above the phase transition for  $\approx$  15 min. Sonication was subsequently carried out using a Heat Systems 350 W probe sonicator until a constant level of optical clarity was achieved. During sonication, the samples were placed under a stream of nitrogen and in a room temperature water bath to avoid lipid degradation. Titanium particles and large liposomes were removed from the SUVs by centrifugation at 12000  $\times g$  for 5 minutes in an eppendorf centrifuge. For micelle-forming D8PC and polymeric  $\omega$ -8 lipids, samples were hydrated in phosphate buffer and warmed at 45°C for  $\approx$  15 to 30 minutes with intermittent vortexing. In the case of D8PC micelles, 0.2M KSCN was added to the buffer to stabilize the micellar phase (40). Sample concentrations were 50-75 mg/ml (above cmc) and 35-75 mg/ml for D8PC and polymeric  $\omega$ -8, respectively.

For  $^{13}\text{C}$  MASS studies, lipids were hydrated with excess  $\text{H}_2\text{O}$  or  $\text{D}_2\text{O}$  containing .2 mM EDTA to form a paste. These were centrifuged into ultra-high spinning keflar rotors and sealed with o-ring-containing macor caps (Doty Scientific).

For high resolution  $^1\text{H}$  NMR studies, lipid dispersions were prepared by hydrating the lipids with  $\text{D}_2\text{O}$  or  $\text{D}_2\text{O}/.15\text{NaCl}$  (pH 6.8) above the phase transition for approximately 30 min. Sonicated samples were prepared in an analogous fashion but subsequently probe sonicated until translucent solutions were obtained (as described above). Sample concentrations were generally 5 mg/ml. In some cases sodium acetate (0.625  $\mu\text{moles}$ ) was added as an internal standard.

*NMR Measurements.* High resolution  $^{13}\text{C}$  and  $^{13}\text{C}$  MASS spectra were acquired at 125 MHz with a Bruker AM-500. Chemical shifts are reported with respect to the choline methyl peak assumed to resonate at 54.3 ppm (40). All high resolution and MASS spectra are processed with 20 Hz (liposomes) and 2 Hz (micelles) linebroadening. Spin-lattice relaxation times were measured using the inversion recovery sequence (180 -  $\tau$  - 90) (32), a 90 degree pulse width of 16-18  $\mu\text{s}$  and a recycle delay of at least 3-5 times  $T_1$  for all carbons with the exception of the terminal methyl groups. Spectra were recorded with the nuclear Overhauser enhancement (NOE). Composite pulse decoupling was used at 305°C to minimize sample heating. Bilevel decoupling (1 and 10W for NOE and complete proton decoupling during aquisition, respectively) was used at 320°C and 335°C. For MASS samples,  $T_1$  measurements were made in an analogous fashion but with 10 W decoupling (no NOE), a 90 degree pulse width of 4.5  $\mu\text{s}$  and at ambient temperature. For all measurements,  $T_1$  values were determined by a least squares fit to the three parameter equation using standard Bruker software:

$$(1) \quad S(t) = A + B \exp\left(\frac{-\tau}{T_1}\right)$$

where A, B, and  $T_1$  are adjustable parameters. Figure 1 shows a typical fit of the data. The utility of the three parameter fit compared to the two parameter equation is that Eqn. 1 is less sensitive to systematic errors including misset pulse angles, the frequency offset between the carrier and resonance line in question and truncated waiting periods (33). At least two long  $\tau$  values (longer than  $T_1$ ) were included in the data set so the inaccuracy of the methyl  $T_1$ 's should be quite small as shown by Kowalewski *et al.* The exception to this is for the chain methyls in experiments run at 335°C. Reported values are the average of 2-4 measurements.

NOE factors were measured using gated broadband proton decoupling. Approximately 10 W decoupling power was used during spectral acquisition. For spectra recorded with the NOE, samples were irradiated with 1 W decoupling power during the 10 s (305°C) or 15 s (320°C) recycle delay. Calculation of the NOE was made by comparison of the intensities of samples recorded with and without irradiation during the recycle delay.

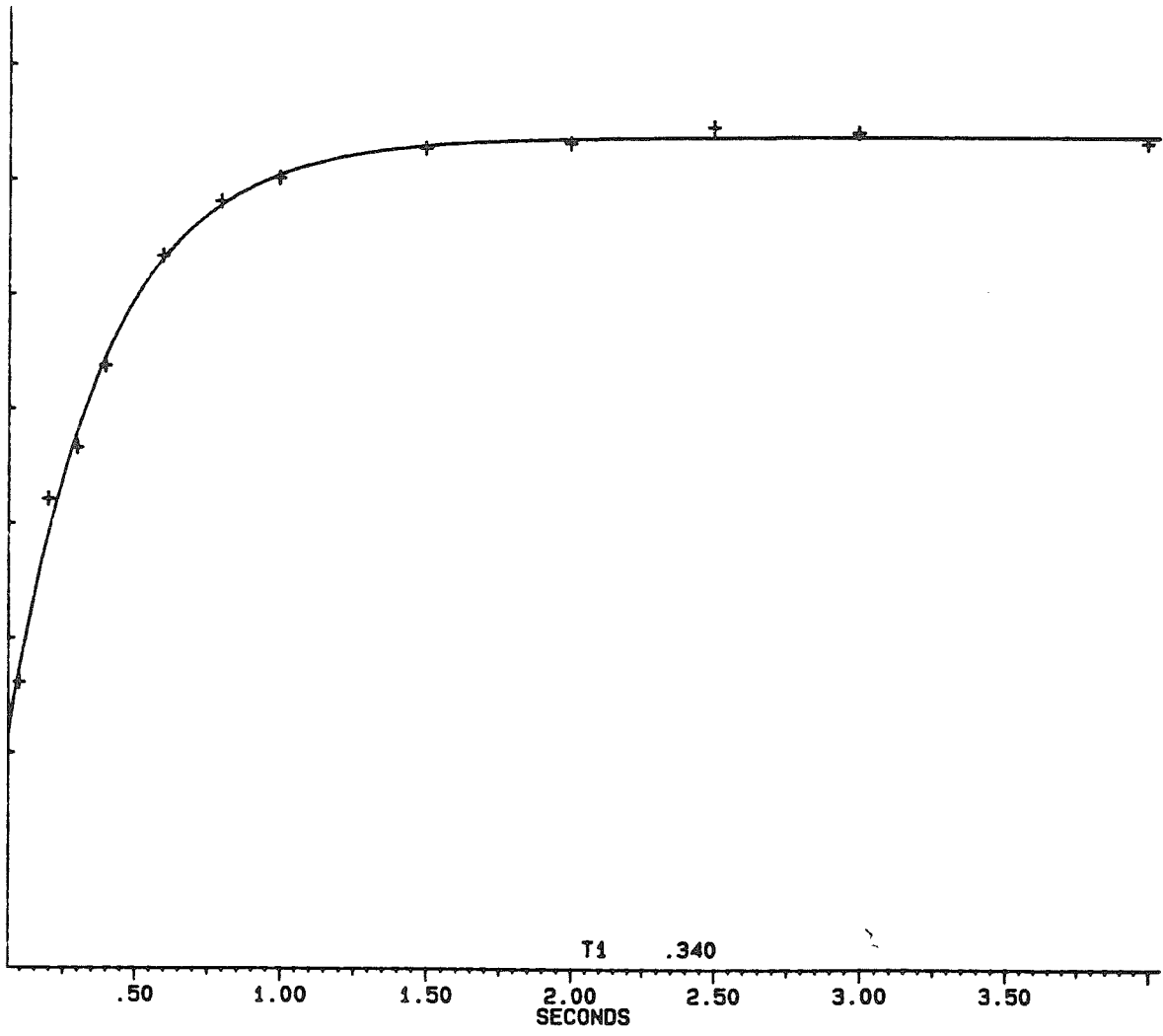
High resolution  $^1\text{H}$  spectra were recorded at 500 MHz using a 45° excitation pulse ( $\approx 3 \mu\text{s}$ ) and a 2.5 s repetition rate. When necessary, the HOD resonance was presaturated.

### Light Scattering.

Determination of particle sizes and diffusion coefficients was accomplished via dynamic light scattering using a Malvern 4700 light scattering system equipped with a goniometer, a 128 channel correlator and a 3 W Spectra Physics argon ion laser. 488 nm incident laser light was used with the detector placed at 90 degrees relative to the incoming beam. Calculations of the particle size were based on the Stokes-Einstein

**Figure 1**

Representative fit of the relaxation data to Eqn. (1).



equation using monomodal analysis with the software supplied by Malvern. Measurements are the average of three determinations on the samples whose linewidths are tabulated in Table II.

## **BACKGROUND**

In this chapter is described  $^{13}\text{C}$  and  $^1\text{H}$  NMR studies of polymerizeable phospholipid liposomes as a first step in an investigation to analyze the dynamic nature of these bilayers. While our experiments are restricted to a single spectrometer frequency which limits to a small extent the conclusions which may be extracted from the  $^{13}\text{C}$  relaxation data, consideration of the treatments and results of others who have carried out measurements at up to seven spectrometer frequencies provides some basic principles useful in understanding our results. Thus as a preface to a discussion of the data, in the present section we summarize some of the basic concepts concerning  $^{13}\text{C}$  NMR relaxation and the dynamics of phospholipid bilayers, and general approaches and results that have been described in the literature to analyze  $^{13}\text{C}$  relaxation in lipid aggregates, in terms of their motional properties.

The  $^1\text{H}$  NMR studies described here involve analysis of the linewidths in terms of the motional state of the lipids.\* For simplicity, we therefore postpone discussion of the origin of the  $^1\text{H}$  NMR linewidths until the results and discussion section.

### **Motions in Bilayers.**

First it is necessary to consider the wide variety of motions that characterize the phospholipid bilayer and contribute to the spectra and relaxation properties of various

---

\*  $^1\text{H}$  NMR spin lattice relaxation measurements were not carried out for the lipid systems under study due to the well-recognized complications in the interpretation of the data. These complications arise from the difficulty in separating intramolecular versus intermolecular dipolar interactions and the presence of spin diffusion along the acyl chains. Furthermore, the spectra contain much less detail than  $^{13}\text{C}$  spectra, even at the high (11.7 Tesla) magnetic fields used in the present study.

nuclei. These motions include the overall tumbling of the liposome, lateral diffusion over the surface of the liposome, rotational diffusion of the phospholipid about the long molecular axis, trans-gauche isomerizations of the acyl chain segments and slow cooperative fluctuations of domains of phospholipids in a direction perpendicular to the bilayer normal (1,25). The time scales of these motions encompass a wide range and are important determinants in their effective contribution to the relaxation properties (1-5). For example, the overall tumbling of a vesicle is calculated according to:

$$(2) \quad \tau_v = \frac{4 \pi r^3 \eta}{3 k T}$$

where  $r$  is the radius of the liposome,  $\eta$  is the viscosity of the suspending medium and  $T$  is the temperature. Thus for MLVs 5  $\mu\text{m}$  in size,  $\tau_v$  is on the order of 16 s whereas for 250  $\text{\AA}$  SUVs, it is  $2 \times 10^{-6}$  s. The lateral diffusion coefficient ( $D_{LD}$ ) of phospholipids in the plane of liquid-crystalline bilayers has been estimated to be  $\approx 10^{-8}$   $\text{cm}^2/\text{s}$ . This makes the time for complete traversal over the surface of a 5  $\mu\text{m}$  and 250  $\text{\AA}$  liposome to be  $\approx 1.5$  s and  $4 \times 10^{-5}$  s, respectively, as given by the equation (1):

$$(3) \quad \tau_{LD} = \frac{r^2}{4 D_{LD}}$$

The *effective* correlation time ( $\tau_e$ ) for the diffusion of a phospholipid over the surface of a liposome of radius  $r$  is then given by (29):

$$(4) \quad \frac{1}{\tau_e} = \frac{1}{\tau_{LD}} + \frac{1}{\tau_v}$$

which for 5  $\mu\text{m}$  sized MLVs and 250  $\text{\AA}$  SUVs would be 1.4 s and  $2 \times 10^{-6}$  s, respectively. Thus the particle size can greatly influence certain motional time scales.

In addition to these intermediate to slow global motions of the individual phospholipids, slow cooperative motions of collective groups of molecules have been

modelled by a continuous distribution of timescales less than  $\omega_0^{-1}$  (where  $\omega_0$  is the larmor frequency and is in the range of MHz) (25-27,34,35). Finally, fast local motions such as trans-gauche isomerizations of the lipid chains have been reported to fluctuate on a time scale of approximately  $10^{-10}$  to  $10^{-11}$  s, similar to that measured for liquid paraffins (25-27,34-36).

All of the above motions are in reference to nonpolymerizeable phospholipids in the liquid-crystalline state. Lowering the temperature below the phase transition markedly increases the correlation times and decreases the amplitude of most or all of these motions (5). For example, the lateral diffusion coefficient for a gel state phospholipid is on the order of  $10^{-10}$  to  $10^{-11}$  cm<sup>2</sup>/s. Relatively few dynamic studies, however, have been devoted to determining the dynamic behavior of gel state phospholipids. Polymerization of phospholipids should also greatly reduce the motions to an extent depending on the position of the polymerizeable moiety and the degree of polymerization. For all polymerizeable lipids described in this thesis, the rotational and lateral diffusion of the lipids will obviously be slowed, while the effect on cooperative fluctuations is less predictable. Segmental motions should be greatly hindered in the case of the  $\omega$ -THIOLS whereas in the case of the  $\alpha$ -THIOLS, one might anticipate that they are unaltered or only modulated in amplitude relative to nonpolymerizeable analogues.

### NMR Relaxation in General.

Relaxation and in particular, the spin-lattice relaxation can provide much insight into the dynamic nature of the molecules in question. It is therefore useful to consider what is being measured in a relaxation experiment. The spin-lattice relaxation rate ( $T_1^{-1}$ ) of a given nucleus is a measurement of the return of the z magnetization to its equilibrium value following perturbation by a radiofrequency pulse (37). In the case of the spin-

spin relaxation rate ( $T_2^{-1}$ ) that governs the homogeneous part of the linewidth, one measures the return of x,y magnetization (perpendicular to the field direction) to its equilibrium value of zero (37). For  $^{13}\text{C}$  and  $^1\text{H}$  nuclei, the rates are dominated by modulation of the  $^{13}\text{C}$ - $^1\text{H}$  and  $^1\text{H}$ - $^1\text{H}$  dipolar interactions, respectively, due to molecular reorientation (26-29,38). This is the link between the relaxation rate and molecular motion.

$^{13}\text{C}$  NMR is especially useful for measurements of spin-lattice relaxation times due to (i) the large chemical shift range and subsequent dispersion of the resonances, (ii) the fact that the  $^{13}\text{C}$ - $^1\text{H}$  dipolar interactions are purely intramolecular and because (iii)  $^{13}\text{C}$ - $^{13}\text{C}$  coupling can be ignored due to the intermediate ( $\approx 1\%$ ) natural abundance of the  $^{13}\text{C}$  nucleus (26). Nonetheless, as should be clear from the above description of the possible motions of phospholipids in membranes, the motional state is anisotropic and highly complex. Since the experimental relaxation rates are dependent not only on the time scales of the motion but on their amplitudes as well, the interpretation of the measured relaxation rates is nontrivial. Despite these difficulties much insight has been gained by studies attempting to unify the relaxation behavior of various nuclei, their temperature and frequency dependence, and their dependence on membrane ordering. The following represents some basic concepts necessary for understanding  $^{13}\text{C}$ - $^1\text{H}$  NMR relaxation and some of the approaches taken to model the dynamic behavior of micelles, microemulsions and phospholipids. This provides a useful basis from which to interpret the results of the experiments presented in this chapter.

### $^{13}\text{C}$ Relaxation.

The spin-lattice relaxation of  $^{13}\text{C}$  nuclei is due predominantly to fluctuations in the  $^{13}\text{C}$ - $^1\text{H}$  dipolar interaction as expressed by the equation (39):

$$(5) \quad \frac{1}{T_1} = \frac{N_i}{20} \left( \frac{\gamma_H^2 \gamma_C^2 \hbar^2}{r_{CH}^6} \right) [J(\omega_H - \omega_C) + 3J(\omega_C) + 6J(\omega_H + \omega_C)]$$

which, in the extreme narrowing limit reduces to (26):

$$(6) \quad \frac{1}{T_1} = \frac{(\gamma_H^2 \gamma_C^2 \hbar^2)}{r_{CH}^6} \tau_c$$

The corresponding equations for the spin-spin relaxation rate  $R_2 = T_2^{-1}$  is given by (39):

$$(7) \quad \frac{1}{T_2} = \frac{(\gamma_H^2 \gamma_C^2 \hbar^2)}{40 r_{CH}^6} [J(\omega_H - \omega_C) + 3J(\omega_C) + 6J(\omega_H + \omega_C) + 4J(0) + 6J(\omega_H)]$$

where the presence of spectral density at zero frequency, denoted by  $J(0)$ , accounts for the greater sensitivity to slow motions of  $T_2^{-1}$  relative to  $T_1^{-1}$  (37). The nuclear Overhauser enhancement ( $\text{NOE} = 1 + \eta_{CH}$ ) is given by (39):

$$(8) \quad \text{NOE} = 1 + \frac{\gamma_H}{\gamma_C} \left[ \frac{6J(\omega_H + \omega_C) - J(\omega_H - \omega_C)}{J(\omega_H - \omega_C) + 3J(\omega_C) + 6J(\omega_H + \omega_C)} \right]$$

In the above equations,  $\omega_H$  and  $\omega_C$  are the larmor frequencies of proton and carbon-13 nuclei, respectively where  $\omega_i = \gamma_i B_0$ ,  $\gamma_H$  and  $\gamma_C$  are the magnetogyric ratios of proton and carbon nuclei,  $r_{CH}$  is the carbon proton internuclear distance (1.09 Å) and  $\tau_c$  is the correlation time.  $J(\omega)$  is the spectral density function given as the fourier inverse of the autocorrelation function  $G(\tau)$  (37):

$$(9) \quad J(\omega) = \int_{-\infty}^{\infty} \tilde{G}(\tau) e^{-i\omega\tau} d\tau$$

where  $J(\omega)$  describes the frequency distribution and magnitude of fluctuations in the Hamiltonian (in this case the dipolar Hamiltonian) being modulated by the motion. The

autocorrelation function  $G(\tau)$  describes the time scale for the decay of the motional order between time  $t = 0$  and  $t = \tau$  and is therefore given as :

$$(10) \quad G(\tau) = \langle H_{loc}(0) \cdot H_{loc}(\tau) \rangle$$

where  $H_{loc}$  is the local (dipolar) fluctuating field (37). Thus to properly interpret relaxation data, one must derive appropriate expressions for the autocorrelation function based on various motional models. These are then used to calculate spectral densities and on substitution into equations (5), (7) and (8) allow calculation of  $^{13}\text{C}$  relaxation rates and NOEs.

For isotropically reorienting systems with one effective correlation time ( $\tau_c$ ) in the extreme narrowing limit, the single exponentially decaying autocorrelation function (37):

$$(11) \quad G(\tau) = \langle H_{loc}^2(0) \rangle_0 e^{-\frac{\tau}{\tau_c}}$$

leads to spectral densities of the form (28):

$$(12) \quad J(\omega_C) = \frac{\tau_c}{1 + \omega_C^2 \tau_c^2}$$

$$(13) \quad J(\omega_H - \omega_C) = \frac{\tau_c}{1 + (\omega_H - \omega_C)^2 \tau_c^2}$$

$$(14) \quad J(\omega_H + \omega_C) = \frac{\tau_c}{1 + (\omega_H + \omega_C)^2 \tau_c^2}$$

Substitution of the spectral density expressions into Eqn. (5) leads to :

$$(15) \quad \frac{1}{N_H T_1} = \left( \frac{\gamma_H^2 \gamma_C^2 h^2}{r_{CH}^6} \right) \left[ \frac{3}{10} \left( \frac{\tau_c}{1 + \omega_C^2 \tau_c^2} \right) + \frac{1}{10} \left( \frac{\tau_c}{1 + (\omega_H^2 - \omega_C^2) \tau_c^2} \right) \right] + \frac{3}{5} \left( \frac{\tau_c}{1 + (\omega_H^2 + \omega_C^2) \tau_c^2} \right)$$

Eqn. (15) has been used extensively in the past for the analysis of micelles and phospholipid dynamic behavior, where  $T_1$  is thus ascribed solely to the effect of fast local motions in the extreme narrowing regime (26,40). However, it has become clear in the last several years that the assumption of isotropic reorientation and a single effective correlation time is a major oversimplification of phospholipid motions in micelles and membranes. If fast motions (correlation time  $< \omega_0^{-1}$ ) were the only contribution to  $T_1^{-1}$ , then one would expect (i) an increase in  $T_1$  with temperature and (ii) the invariance of  $T_1$  with magnetic field strength (25,26). The increase of  $T_1$  with temperature has been clearly demonstrated for both micelles and phospholipid vesicles (25-27,40). Brown, however, has conducted an extensive investigation of  $^{13}\text{C}$  spin-lattice relaxation times of liquid-crystalline DPPC SUVs and has shown that despite the temperature dependence that would seem to imply fast correlation regime behavior, there is also a substantial frequency dependence (26,27). Quantitatively  $T_1$  varies by greater than a factor of two over the range of field strengths from 1.4 to 11.7 Tesla suggesting, by contrast, the applicability of the slow motion regime. Frequency dependencies have also been observed in  $^{13}\text{C}$   $T_1^{-1}$  studies of micelles and microemulsions (28-31).

In order to resolve the apparent dilemma it has been hypothesized that in addition to fast local segmental motions that would account for the temperature dependence, slow motions ( $\tau_c > \omega_0^{-1}$ ) must also be invoked to explain the frequency dependence (25-27).

For micelles, microemulsions and vesicles, this has been treated as described in the following two sections.

### Micelles and Microemulsions.

In the case of micelles and microemulsions, the frequency dependence has been taken into account by assuming that slow global motions (the isotropic tumbling of the entire particle and the diffusion of monomers over the surface of the sphere) contribute to the relaxation in addition to fast segmental motions. To incorporate slow motions into the relaxation expression for microemulsions, Tricot *et al.* assumed a distribution of correlation times expressed by a suitable probability function instead of a unique value of  $\tau_c$  (28). The spectral density for the distribution was expressed by:

$$(16) \quad J(\omega_i) = \int_0^{\infty} \frac{H(\tau_c)\tau_c}{1 + \omega_i^2\tau_c^2}$$

where  $H(\tau_c)$  is a normalized probability density function characterized by a width of correlation times and  $\omega_i$  stands for  $(\omega_H - \omega_C)$ ,  $\omega_C$ , or  $(\omega_C + \omega_H)$ . In doing so, an upper limit to the correlation times to be considered was set by the correlation time for rotation of the microsphere as calculated by the Stokes Einstein equation (Eqn. 2).

As an alternative to the above approach, a number of groups have developed a two-step model to interpret the relaxation data of micelles (29-31). In these studies, two correlation times, each described by a single exponential decay, are considered in deriving the autocorrelation function: one corresponds to fast segmental motions and the other corresponds to slow tumbling and translational diffusion of the monomers over the surface of the sphere. Due to the disparity in the approximate time scales for each motion, these motions are assumed to be uncorrelated. In the work of Söderman,

the final form of the spectral density function for the two-step model was given as (30,31):

$$(17) \quad J(\omega) = (1 - S^2) J^f(\omega) + S^2 J^s(\omega)$$

where:

$$(18) \quad J^{f,s}(\omega) = \frac{2\tau_c^{f,s}}{[1 + (\omega\tau_c^{f,s})^2]}$$

In these equations,  $\tau_c^{f,s}$  and  $J^{f,s}$  are the correlation times or spectral densities, respectively, for fast (f) slightly anisotropic motion or a slow (s) isotropic motion,  $S_{CH}$  is the order parameter averaged over the fast motions:

$$(19) \quad S_{CH} = \left(\frac{1}{2}\right) \langle 3 \cos^2 \theta - 1 \rangle_f$$

and  $\theta$  is the angle between the C-H vector and the director axis.

Qualitatively, similar results were obtained from both the model involving a distribution of correlation times and from the two-step model (28,30,31). Furthermore, the results unequivocally demonstrated the contribution of slow motions to the relaxation rate and illustrated that the assumption of a single exponential correlation in the extreme narrowing regime results in the underestimation of the rate of segmental motions of the constituent surfactants (28).

### Vesicles.

In the case of  $^{13}\text{C}$  relaxation in *vesicles*, Brown and co-workers have carried out an extensive study at seven different field strengths and examined several motional models (26,27). These included:

(i) A single correlation time model based on the assumption of fast restricted rotational diffusion. This model is essentially that used to describe segmental motions in simple fluids but modified to include the presence of an ordering potential.

(ii) Two correlation time models involving a fast motion of limited amplitude as in (i) superimposed on a slower motion. The fast and slow motions are considered to be statistically independent such that:

$$(20) \quad \frac{1}{T_1} = \frac{1}{T_{1f}} + \frac{1}{T_{1s}}$$

where  $T_{1f}^{-1}$  and  $T_{1s}^{-1}$  are the relaxation times for the fast and slow motions, respectively. In regards to the slow component, two paradigms were envisioned: a noncollective process involving a single correlation time or a collective process described by a continuous distribution of correlation times in analogy to models applied to the relaxation behavior of smectic and nematic liquid crystals.

In the work by Brown, it was demonstrated that the relaxation behavior of liquid-crystalline DPPC was not at all consistent with the restricted anisotropic diffusional model (i). In particular, even assuming highly ordered and extremely anisotropic systems,  $T_1^{-1}$  was predicted to be frequency independent in contrast to the experimental results. On the other hand, introduction of a slow component (the noncollective or collective model (ii)) allowed for an accurate description of the data. The  $T_1$  expressions for the slow component of the collective and noncollective models are given as follows (26):

*Collective:*

$$(21) \quad \left\langle \frac{1}{T_1} \right\rangle_{\Omega'''} = \frac{3}{20} \left( \frac{\gamma_H \gamma_C h}{r^3} \right)^2 \left[ \left( \frac{\gamma_H}{\gamma_C} + 1 \right)^{\frac{-1}{2}} + 3 + 6 \left( \frac{\gamma_H}{\gamma_C} + 1 \right)^{\frac{-1}{2}} \right] \\ \times \langle d_{00}(\beta'''; t) \rangle^2 C \omega_C^{\frac{-1}{2}}$$

*Noncollective:*

$$(22) \quad \left\langle \frac{1}{T_1} \right\rangle_{\Omega''} = \frac{1}{10} \left( \frac{\gamma_H \gamma_C h}{r^3} \right)^2 \left[ \left( \frac{\gamma_H}{\gamma_C} - 1 \right)^{-2} + 3 + 6 \left( \frac{\gamma_H}{\gamma_C} + 1 \right)^{-2} \right] \\ \times \langle d_{00}(\beta'''; t) \rangle^2 \left[ 1 - \langle d_{00}(\beta''; t) \rangle^2 \right] \frac{1}{\tau_s \omega_C^2}$$

where  $\langle \rangle_{\Omega'''}$  denotes that the relaxation rate is averaged over all orientations of the bilayer with respect to the field direction,  $d_{pn}(\beta)$  are the Wigner rotation elements describing the bilayer orientation,  $\beta$  is a generalized Euler angle and  $\langle d_{00}(\beta'''; t) \rangle \equiv (S_{CH})_{\Omega'}$  is the order parameter averaged over the fast motions. The above equations for the collective model can be more simply written as :

$$(23) \quad \frac{1}{T_{1s}} = B S_{CH}^2 \omega_C^{\frac{-1}{2}}$$

where B is a collection of constants. The full expression for  $T_1^{-1}$  is then:

$$(24) \quad \frac{1}{T_1} = A \tau_f + B S_{CH}^2 \omega_C^{\frac{-1}{2}}$$

For the noncollective model, analogous expressions are:

$$(25) \quad \frac{1}{T_{1s}} = CS_{CH}^2 \omega_C^{-2}$$

and

$$(26) \quad \frac{1}{T_1} = A\tau_i + CS_{CH}^2 \omega_C^{-2}$$

The first term in the expressions for  $T_1^{-1}$  (Eqn. 24 and 26) represent the  $T_1$  due to fast local motions in the extreme narrowing regime such as trans-gauche segment isomerizations. The correlation time for these fast motions can be abstracted from the  $T_1^{-1}$  data by extrapolation to infinite frequency. The second term that is proportional to  $(S_{CH})^2$  is due to the contribution from the slow motions. Unfortunately, because the coefficient of the frequency dependent (slow) term is the product of several parameters, it is not possible to estimate the order parameter. Nonetheless, one may still evaluate the relative importance of fast diffusive versus slow collective/noncollective motions.

For the noncollective versus collective model, the distinguishing features are the  $\omega_C^{-2}$  versus  $\omega_C^{-1/2}$  frequency dependence (26). Although based on the available data it was not possible to completely rule out either model, it was tentatively concluded that the results were most consistent with a collective model. Regardless, the important point was that as with micelles and microemulsions, the slow motions, albeit of a different nature, make a substantial contribution to  $T_1^{-1}$  in vesicles. The differences in the origin of the slow motions of vesicles versus micelles and microemulsions arises from the differences in the sizes and construction of these two types of aggregates. In the case of the micelles/microemulsions, the sizes are sufficiently small that the effective diffusion time of the individual phospholipids (Eqn.4) is shorter than that of vesicles and therefore its overall effect on  $T_1^{-1}$  may be more substantial. On the other hand, the

micellar dimensions may be too small to support sizeable collective-like motions envisioned for the bilayers.

Dependence of  $T_1^{-1}$  on Order Parameters and Temperature in Vesicles. To further test the type of motional model most completely representing the relaxation data in vesicles, the empirical dependence of the  $^{13}\text{C}$   $T_1^{-1}$  rates on the order parameter  $S_{\text{CD}}$  (see Eqn. 24 and 26) were examined by Brown using a power law of the form (26):

$$(27) \quad \frac{1}{N_{\text{H}}T_1} = \gamma_1(S_{\text{CD}})^{\gamma_2} + \gamma_3$$

In this equation,  $\gamma_i$  are adjustable parameters and  $S_{\text{CD}}$  ( $=S_{\text{CH}}$ ) is the deuterium order parameter obtained from  $^2\text{H}$  NMR studies. Within experimental error, a value of  $\gamma_2 = 2$  was obtained, reemphasizing the importance of slow motions that characteristically show a  $(S_{\text{CD}})^2$  dependence of  $T_1^{-1}$ . An additional observation was that the temperature dependence of  $T_1$  and  $(S_{\text{CD}})^2$  were correlated; for all temperatures above the phase transition of DPPC, the  $(N_{\text{H}}T_1)^{-1}$  versus  $(S_{\text{CD}})^2$  data were superimposable on a single straight line. In the past, measurements of the temperature dependence of  $T_1^{-1}$  have been evaluated by Arrhenius-type expressions and interpreted in terms of activation energies (contained in the A term of Eqn. 24 and 26) for effective motions of the lipid chain segments or headgroups (41-43). Because of the proportionality between  $T_1^{-1}$  and  $(S_{\text{CD}})^2$ , an alternative explanation has been offered, which suggests that  $T_1^{-1}$  could be influenced, in addition or exclusively, by the temperature dependence of the order parameter through the B and C term in Eqn. 24 and Eqn. 26 (26).

Physically, the temperature dependence of  $S_{\text{CD}}$  has been ascribed to the coefficient of thermal expansion or elastic constant of the bilayer (26,41,44,45). One could imagine that these equilibrium properties might be somewhat different for polymerizeable versus nonpolymerizeable phospholipids. In the case of polymeric membranes, intervening

covalent linkages should inhibit expansion along the direction of the polymer chain (but not between unlinked segments) whereas the thermal expansion and elasticity of nonpolymerizable membranes are determined exclusively from thermodynamic properties. This idea will be reiterated in the discussion section of the temperature dependence of  $T_1^{-1}$  for the lipid systems under consideration.

Calculation of the NOE. On the basis of the spectral densities derived for the collective, noncollective, and anisotropic diffusion models, values for the NOE have been calculated in the work by Brown (26). For all three models, the anisotropic diffusion model, the collective model and the noncollective model, the NOE could be much less than the maximum value calculated from Eqn. (27) :

$$(28) \quad \eta_{CH} = \frac{1}{2} \frac{\gamma_H}{\gamma_C}$$

which is the well-known equation for the calculation of the maximum NOE for isotropically reorienting molecules in the extreme narrowing regime. The point is that a reduction in the NOE from the maximal value is not necessarily an indication that other competing relaxation mechanisms (i.e. chemical shift anisotropy) contribute to the relaxation rate but may be a consequence of the fact that the motional state of the bilayer does not fulfill extreme narrowing, isotropically reorienting conditions; ordering and slow motion may be important.

#### Analysis of Spin-lattice Relaxation Rates at a Single Frequency.

As described in the last few sections, the most complete analysis of relaxation data requires measurements at several spectrometer frequencies in order to delineate the relative contribution of fast and slow motions. However, this is sometimes not possible due to the fact that it is extremely time consuming and presupposes sufficient access to a number of spectrometers at a variety of field strengths. This is generally not

the case and therefore most analyses are carried out at a single frequency. To alleviate this difficulty, Söderman and Stilbs have demonstrated that one can obtain the order parameter  $S_{CH}$  for a given surfactant system from measurements of the  $^{13}C$   $T_1$  and nuclear Overhauser enhancements at a single magnetic field strength (46). The derivation involves insertion of the two-step spectral density equation (Eqn. 17) into equations for  $T_1^{-1}$  and  $\eta_{CH}$  (written under the assumption of broad-band decoupling) and subtracting them. The resulting equation is then:

$$(29) \quad \frac{1}{T_1} \left( 1 - 2\eta_{CH} \left( \frac{\gamma_C}{\gamma_H} \right) \right) \left( \frac{1}{N} \right) = \left( \frac{1}{20} \right) \left[ \frac{\gamma_H \gamma_C \mu_0 h}{4 \pi r_{CH}^3} \right]^2 f(J(\omega)) S^2$$

where  $f(J(\omega))$  is a function of the various spectral densities in the equations for  $T_1^{-1}$  and  $\eta_{CH}$ . The square root of the left hand side of the equation then gives the order parameter to within a constant of proportionality and is independent of the form of  $J(\omega)^s$  chosen to evaluate the system (46). Thus one can determine the relative internal ordering of the carbons within the system under study.\*

In the following section is a description of the  $^{13}C$  spin-lattice relaxation rates and NOE data for the polymeric and nonpolymerizable lipid systems described in the introduction. Although we do not have the necessary frequency dependence of  $T_1^{-1}$  to be able to evaluate the relative contribution of fast and slow motions, the above discussion should provide a basis for qualitatively interpreting the data nonetheless. Furthermore, we can examine (i) the presence or absence of a mobility gradient in the polymeric systems, (ii) use the simplified methodology of Söderman and Stilbs (expressed in Eqn. 28) to examine the relative ordering of the lipid systems in question, and (iii) evaluate the temperature dependence of the relaxation data. The  $^{13}C$  data is

---

\* In this regard, however, it should be noted that for phospholipid bilayers, the  $^{13}C$   $T_1^{-1}$  and  $^2H$  order parameters  $S_{CD}$  have been found to exhibit similar profiles with distance along the lipid chains (25).

followed by a presentation of the  $^1\text{H}$  spectra for polymeric versus nonpolymerizable lipids.

## RESULTS and DISCUSSION

### $^{13}\text{C}$ NMR of SUVs and Micelles.

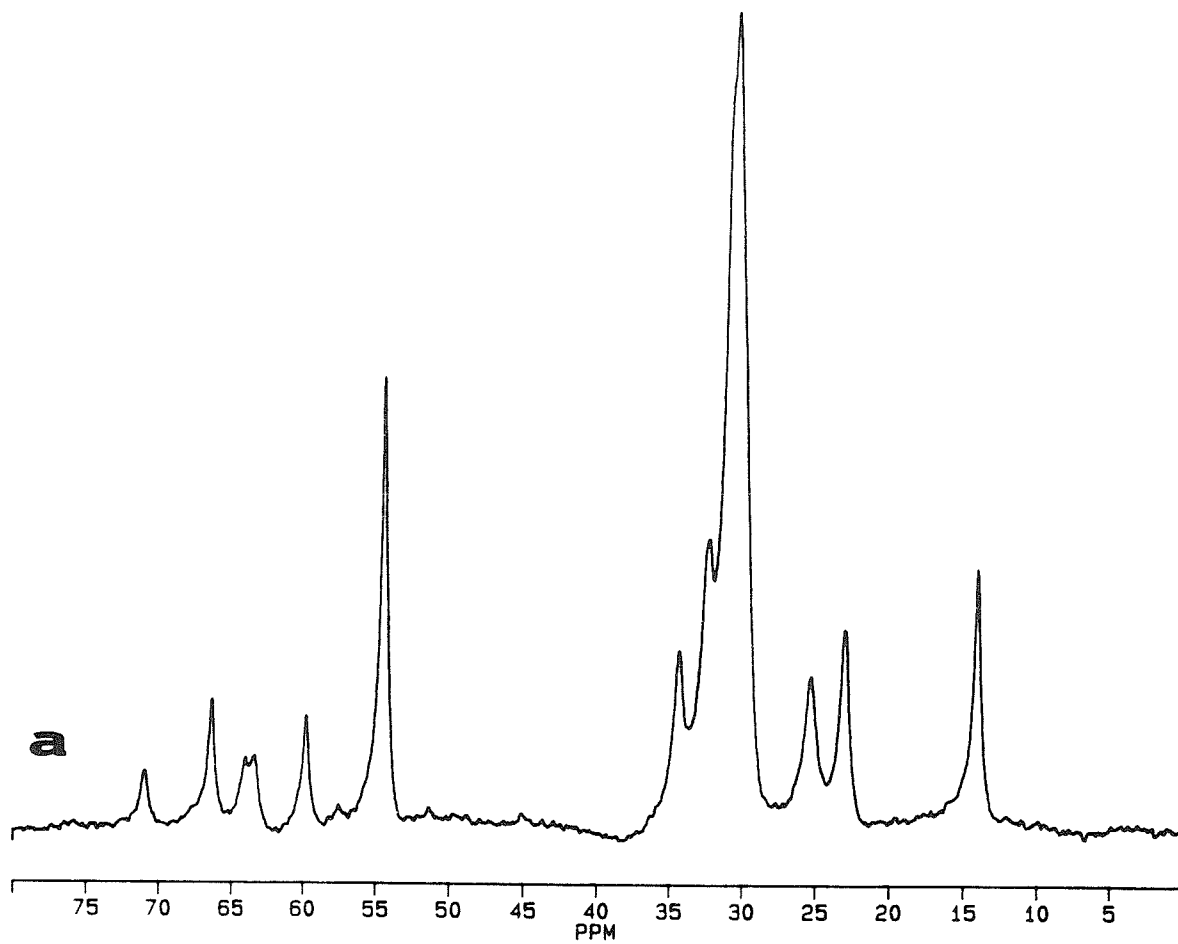
*Linewidth and Resonance Assignments of DMPC and  $\alpha$ -16 SUVs.* In this first section, we describe the  $^{13}\text{C}$  NMR spectra and relaxation behavior of a variety of liposome types. Figure II shows the spectra of (A) DMPC and (B) polymeric  $\alpha$ -16 at 305°C. Assignments are tabulated in Table I and are based on those previously reported for phosphatidylcholine liposomes and micelles (40) as well as on the spectra of fatty acids and the relaxation behavior of the resonances in question. DMPC was chosen for comparison to  $\alpha$ -16 rather than the 16 carbon analogue (DPPC) due to the similarities between the phase transition temperatures of these two lipids ( $\approx 23$  °C). The most obvious difference between the spectra of the two liposome types is the broadness of some of the resonances in the polymeric SUVs. In some cases, the spin-spin relaxation rate appears to be sufficiently fast that certain spectral resonances apparent in the spectra of DMPC are absent in that of the polymeric  $\alpha$ -16. These include the barely detectable single carbon resonances belonging to the glycerol backbone at 62-64 ppm and 70 ppm. The carbonyl resonance apparent in the spectra of DMPC at  $\approx 174$  ppm, is also completely missing in the spectra of  $\alpha$ -16 (region not shown). As anticipated, due to the rigidification by attachment to the polymerizable disulfide moiety, the  $\alpha$ -carbon expected to arise at  $\approx 53$  ppm is not visible.\* Finally, the  $\beta$ -carbon is broadened and shifted from  $\approx 25$  ppm (as in the spectra of DMPC) to  $\approx 27$  ppm due to the deshielding affects of the disulfide.

---

\* Based on the resonance position of the  $\alpha$ -methylene in the protected fatty acid (CHSS). It is possible, however, that it is buried underneath the choline resonance.

**Figure II**

$^{13}\text{C}$  Spectra (125 MHz) of: **A.** DMPC SUVs and **B.** Polymeric  $\alpha$ -16 SUVs. Spectra were recorded at 305°K and apodized with 20 Hz line broadening prior to fourier transformation.



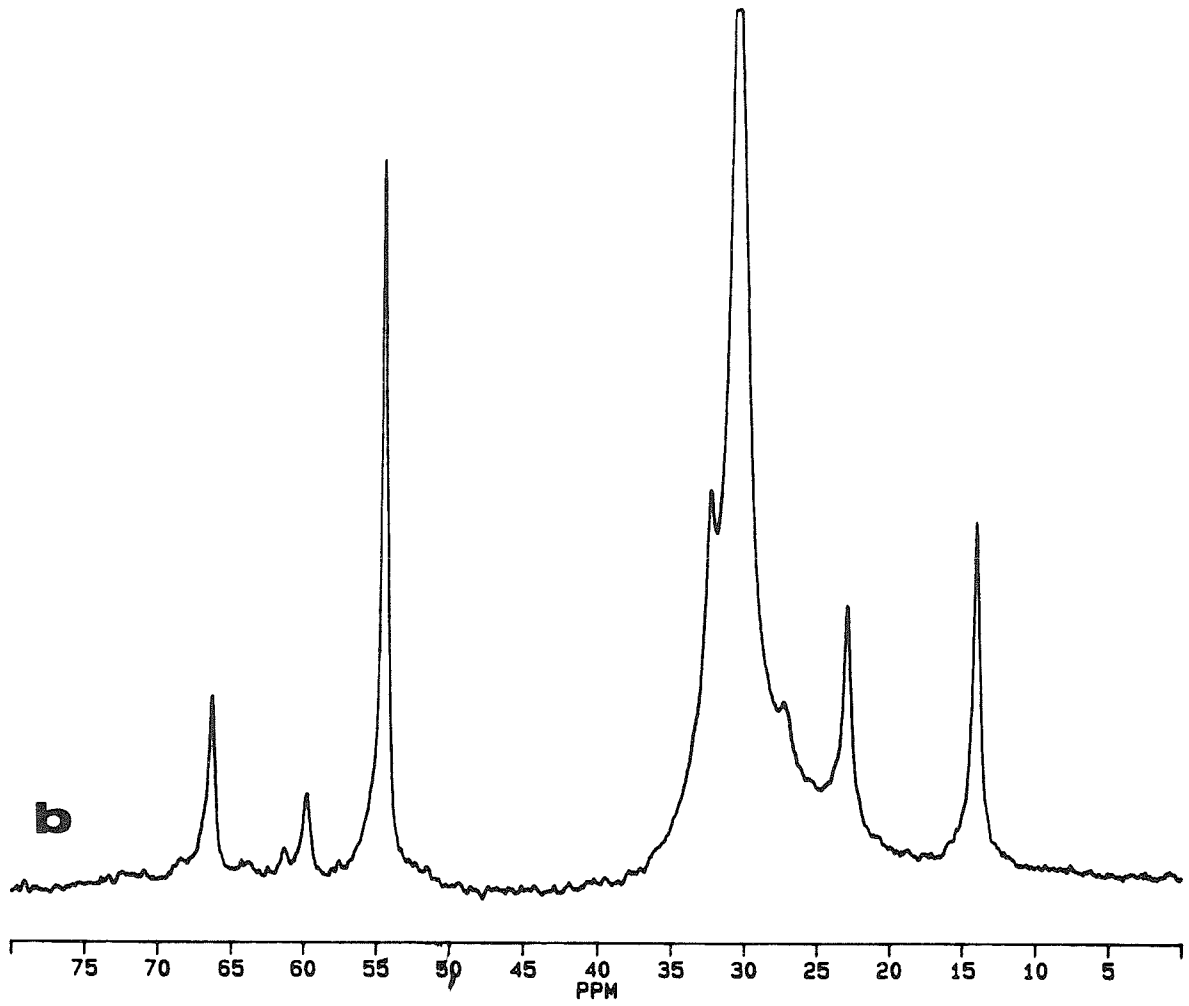


**Table I**

Resonance Assignments, spin-lattice relaxation times ( $T_1$ ) and NOEs for: **A.** DMPC SUVs and **B.** Polymeric  $\alpha$ -16 SUVs. Chemical shifts are reported in ppm relative to the choline methyls at 54.3 ppm. Numbers in parentheses denote the temperature of the experiment.

<b>A</b>	<b>Carbon Atom</b>	<b>Chemical Shift</b>	<b>T1 (305 °K)</b>	<b>T1 (320 °K)</b>	<b>T1 (335 °K)</b>	<b>NOE (305 °K)</b>
	<b>Backbone</b>					
	CH <sub>2</sub> O	70.9	.26 ± .02	.28 ± .01	.22 ± .04	1.57
	CH <sub>2</sub> OP	63.9	.15 ± .02	.21 ± .03		1.02
	CH <sub>2</sub> O	63.3	.13 ± .01	.17 ± .01	.15 ± .03	1.03
	<b>Head group</b>					
	CH <sub>2</sub> N	66.2	.42 ± .03	.65 ± .02	.78 ± .15	2.69
	CH <sub>2</sub> OP	59.7	.41 ± .05	.58 ± .01	.73 ± .04	2.17
	N(CH <sub>3</sub> ) <sub>3</sub>	54.3	.56 ± .05	.87 ± .08	1.35 ± .08	2.70
	<b>Acyl chains</b>					
	α	34.2	.38 ± .04	.46 ± .01	.583 ± .04	2.06
	β	25.1	.48 ± .05	.60 ± .02	.86 ± .05	2.14
	Bulk CH <sub>2</sub>	30.1	.72 ± .05	.911 ± .05	1.23 ± .03	2.39
	ε	32.2	1.23 ± .03	1.78 ± .10	2.05 ± .15	2.37
	ω-1	22.8	1.86 ± .23	2.59 ± .05	3.89 ± .16	2.37
	ω-CH <sub>3</sub>	13.9	3.17 ± .23	4.86 ± .05	7.43 ± .49	2.58

<b>B</b>	<b>Carbon Atom</b>	<b>Chemical Shift</b>	<b>T1 (305 °K)</b>	<b>T1 (320 °K)</b>	<b>T1 (335 °K)</b>	<b>NOE (305 °K)</b>
	<b>Backbone</b>					
	CH <sub>2</sub> O					
	CH <sub>2</sub> OP					
	CH <sub>2</sub> O					
	<b>Head group</b>					
	CH <sub>2</sub> N	66.23	.41 ± .02	.44 ± .08	.44 ± .03	2.34 ± .44
	CH <sub>2</sub> OP	59.65	.46 ± .04	.45 ± .20	.58 ± .04	1.68 ± .21
	N(CH <sub>3</sub> ) <sub>3</sub>	54.30	.52 ± .02	.65 ± .02	1.10 ± .16	2.61 ± .10
	<b>Acyl chains</b>					
	α					
	β	27.00			.435 ± .04	
	Bulk CH <sub>2</sub>	30.20	.61 ± .01	.71 ± .06	.84 ± .06	2.26 ± .01
	ε	32.15	1.12 ± .15	1.09 ± .05	1.27 ± .03	2.36 ± .11
	ω-1	22.76	1.66 ± .09	1.86 ± .22	2.96 ± .65	2.59 ± .11
	ω-CH <sub>3</sub>	13.9	3.20 ± .10	3.90 ± .56	5.62	2.45 ± .28

**Table II**

Estimated linewidths at half height for: DMPC SUVs, polymeric  $\alpha$ -16 SUVs, D8PC micelles and  $\omega$ -8 "micelles." Values are reported in Hz ( $\pm 5$ ).

---

 LINEWIDTH
 

---

<u>Carbon Atom</u>	<u>DMPC</u>	<u><math>\alpha</math>-16</u>	<u>D8PC</u>	<u><math>\omega</math>-8</u>
<b>Backbone</b>				
CH <sub>2</sub> O			14	58
<b>Head group</b>				
CH <sub>2</sub> N	45	49	14	26
CH <sub>2</sub> OP			12	23
N(CH <sub>3</sub> ) <sub>3</sub>	45	38	19	28
<b>Acyl chains</b>				
$\omega$ -1	75	74		
$\omega$ -CH <sub>3</sub>	45	55		

By contrast to the broadened resonances described above, a number of other resonances do not have significantly different linewidths. These include, for example, the headgroup methylenes, the choline methyls, the  $\omega$ -1 methylene and the terminal methyl. The estimated half height linewidths of these groups are tabulated in Table II. No conclusion concerning the breadth of the resonance corresponding to the bulk methylenes can be drawn due to the differences in the chemical shifts of the carbons contributing to the envelope.

The  $^{13}\text{C}$  linewidths are sensitive not only to fast motions, but also to slow motions with  $\tau_c > \omega_0^{-1}$  (5). The importance of slow motions is predicted in Eqn. (7) by the dependence of  $T_2^{-1}$  on the spectral density at zero frequency ( $J(0)$ ) (37). These slow motions can include isotropic tumbling of the vesicles, lateral diffusion and slow cooperative motions. To examine whether differences in particle size might be the exclusive source of the spectral broadening in the case of  $\alpha$ -16 SUVs, the particle sizes were measured by dynamic light scattering. The similarity of the sizes as shown in Table III indicates that different vesicle tumbling rates does *not* contribute to the linebroadening. If it did, one would expect a uniform increase in the linewidths rather than the selective broadening observed in the spectra of the  $\alpha$ -16 SUVs. One would also expect all resonances to broaden if the slowed rotational and lateral diffusion of the  $\alpha$ -16 phospholipids *as a whole* had a substantial effect. Thus the disappearance or broadening of certain spectral features encompassing the glycerol backbone and polymerizable moiety reflects the selective rigidification of that portion of the membrane.

*Linewidth and Resonance Assignments of D8PC and Polymeric  $\omega$ -8 Micelles.* In Figure III  $^{13}\text{C}$  spectra are shown for D8PC micelles and polymeric  $\omega$ -8 "micelles." Linewidth

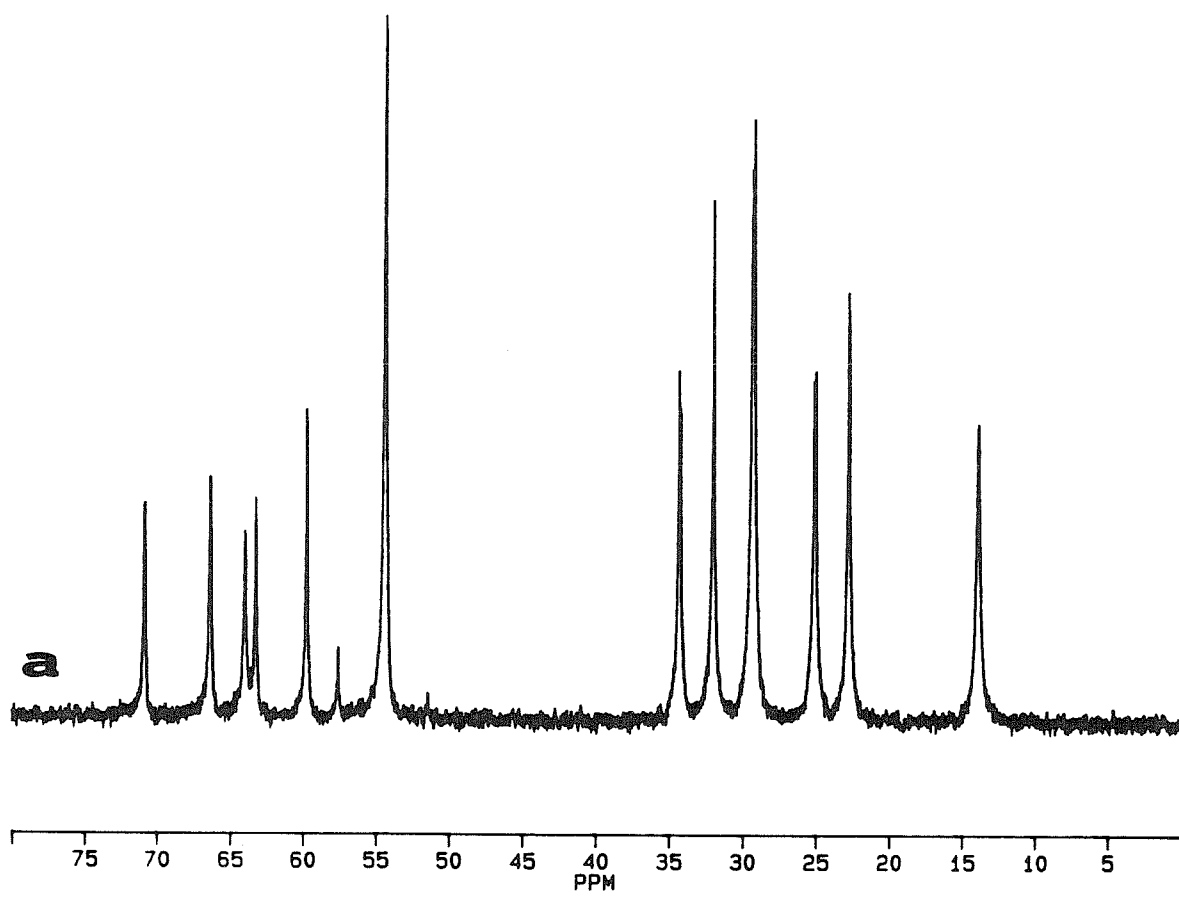
**Table III**

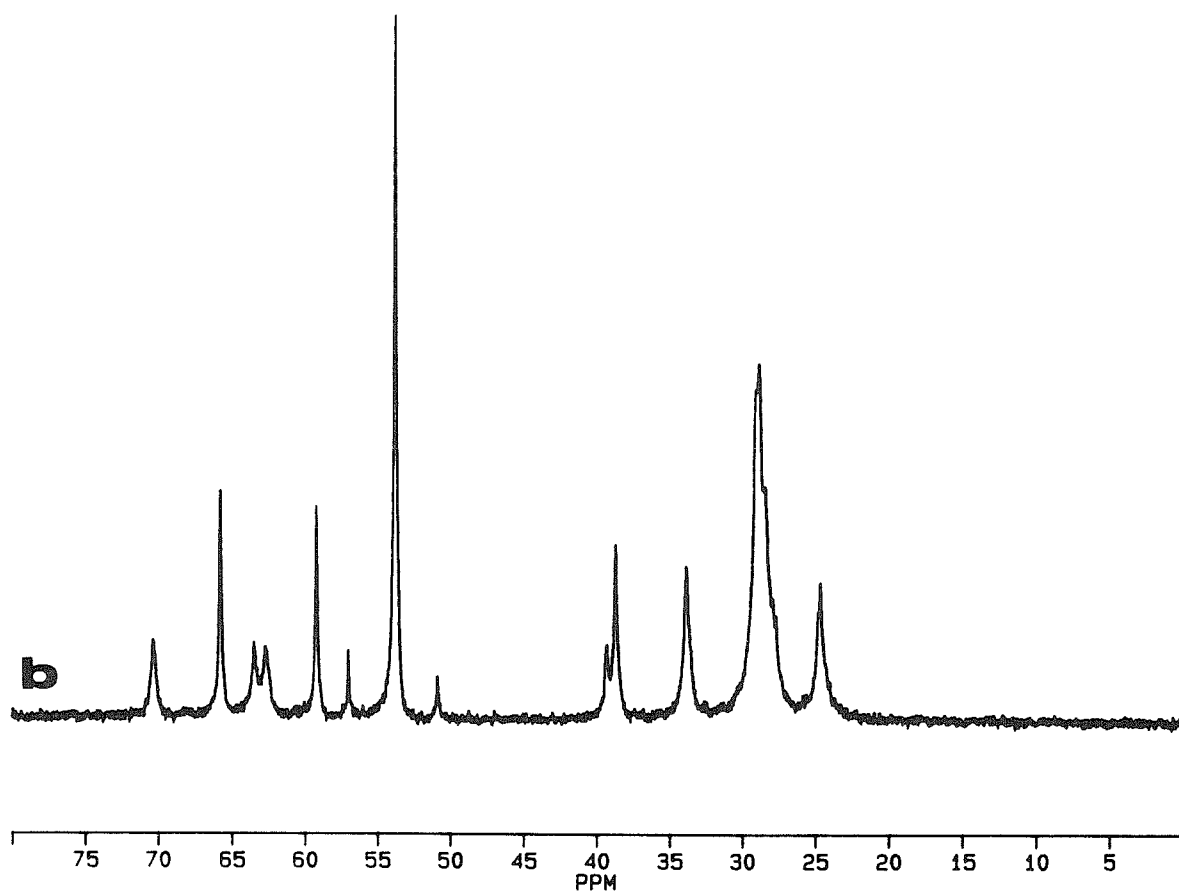
Z average particle sizes as measured by dynamic light scattering for the lipid preparations whose linewidths are reported in Table II. Measurements are the average of three determinations. Errors are reported as the standard deviation from the mean of triplicate measurements and do not represent the polydispersity.

<u>LIPID</u>	<u>SIZE (nm)</u>
DMPC SUV's	$37 \pm 1$
a-16 SUV's	$36 \pm 1$
D8PC micelles	$< 10$
$\omega$ -8 "micelles"	$192 \pm 2$

**Figure III**

$^{13}\text{C}$  Spectra (125 MHz) of: A. D8PC micelles and B. Polymeric  $\omega$ -8 "micelles."  
Spectra were recorded at 305°K and apodized with 2 Hz line broadening prior to  
fourier transformation.





differences are not obvious from the spectra but as shown in Table II, the linewidths of polymeric  $\omega$ -8 are measurably larger than that for D8PC micelles. In the case of the D8PC micelles, the linewidths are sharp enough that it is possible to detect splitting of certain resonances (the  $\alpha$ ,  $\beta$  and  $\omega$ -1 carbons) as a consequence of the nonequivalence of the sn-1 and sn-2 chains.

The basis of the broadness of the lines in polymeric  $\omega$ -8 micelles is most likely due to the extremely large effective aggregate size as measured by dynamic light scattering (Table III). At the concentrations used for acquisition of the spectra in Figure III ( $\approx$  60-75 mg/ml) the solutions of polymeric  $\omega$ -8 are extremely viscous, which is a characteristic of all the short chain  $\omega$ -THIOLS. The large size is due to the general tendency of the  $\omega$ -THIOLS to form bilayer fragments and to aggregate extensively. In fact, the term "micelle" is used loosely here since a detailed picture of the shape and size of polymeric  $\omega$ -8 dispersions is unknown with the exception that (i) it is non-vesicular and (ii) the effective size is highly concentration dependent (see chapter II). Considering the differences in the effective size for these gelatinous "micelles" compared to the D8PC micelles, DMPC SUVs and polymeric  $\alpha$ -16 SUVs, one might expect the linewidths to be much broader. The fact that they are comparable to that measured for  $\alpha$ -16 and DMPC liposomes suggests the fact that the measured sizes are due to simple aggregation and that there may be a high degree of disorder or a dynamical nature to the gross morphology of these polymeric aggregates.

Resonance assignments of polymeric  $\omega$ -8 and D8PC micelles are tabulated in Table III. In contrast to the polymeric  $\alpha$ -16 SUVs, all carbon resonances are visible including those of the rigid glycerol backbone and the carbonyl (not shown). This is despite the fact that the size of the  $\alpha$ -16 SUVs are smaller than that of the polymeric  $\omega$ -8 "micelles." The differences between the spectra of D8PC and polymeric  $\omega$ -8 are due to chemically-induced shifts of certain carbon segments on account of the deshielding

effect of the disulfide. The  $\gamma$ ,  $\delta$ ,  $\epsilon$ , and  $\omega-1$  resonances are shifted into a broad envelope at  $\approx 29$  ppm. The  $\underline{C}H_2S-S$ , which in the monomeric state ( $\underline{C}H_2-SH$ ) is superimposed on the  $\alpha$ -methylene, is shifted to 34 ppm on oxidation. Thus the resonance at 14 ppm in D8PC corresponding to the  $\omega$ -carbon is absent.

*Spin-lattice Relaxation and NOE Measurements of DMPC and  $\alpha$ -16 SUVs.* Table I summarizes the spin-lattice relaxation and NOE data for the resolvable carbons of DMPC and polymeric  $\alpha$ -16 SUVs at various temperatures. Examination of the data at 305°C indicates that the  $T_1$ s are only slightly smaller for the polymer but by no more than 10%, which is just above the accuracy of the  $T_1$  determination. This would seem to suggest that the motional properties that dominate the relaxation behavior of the visible resonances are similar in both cases. We cannot resolve sufficiently the  $\alpha$ - and  $\beta$ -methylene carbons of the  $\alpha$ -16 acyl chains in order to accurately assess the effect of polymerization near the interface. However, it is clear from the complete absence of the  $\alpha$ -methylene that it must be fairly rigid. With increasing distance from the polymerizable moiety, however, the relaxation behavior of the carbon segments are less distinguishable from those of DMPC and therefore the fast local motions of the acyl chains become less affected by the polymerization. Apparently the presence of the polymerizable moiety only significantly restricts the fast segmental motions of the carbons in the vicinity of the disulfide group. Thus a motional gradient extending from the backbone to the terminal methyl group is retained similar to that observed in nonpolymerizable phospholipids (26,27,40). This is shown in Figure 4. Although the individual carbons contributing to the bulk methylene resonance at  $\approx 29$  ppm are not resolved, the value of  $T_1$  across the envelope was found to be relatively constant and therefore we assume for the time being that, as for DPPC, a plateau of relatively constant values of  $T_1^{-1}$  exist in the center of the acyl chain followed by an increase

**Table IV**

Resonance Assignments, spin-lattice relaxation times ( $T_1$ ) and NOEs for : **A.** D8PC micelles and **B.** Polymeric  $\omega$ -8 micelles. Chemical shifts are reported in ppm relative to the choline methyls at 54.3 ppm. Numbers in parentheses denote the temperature of the experiment.

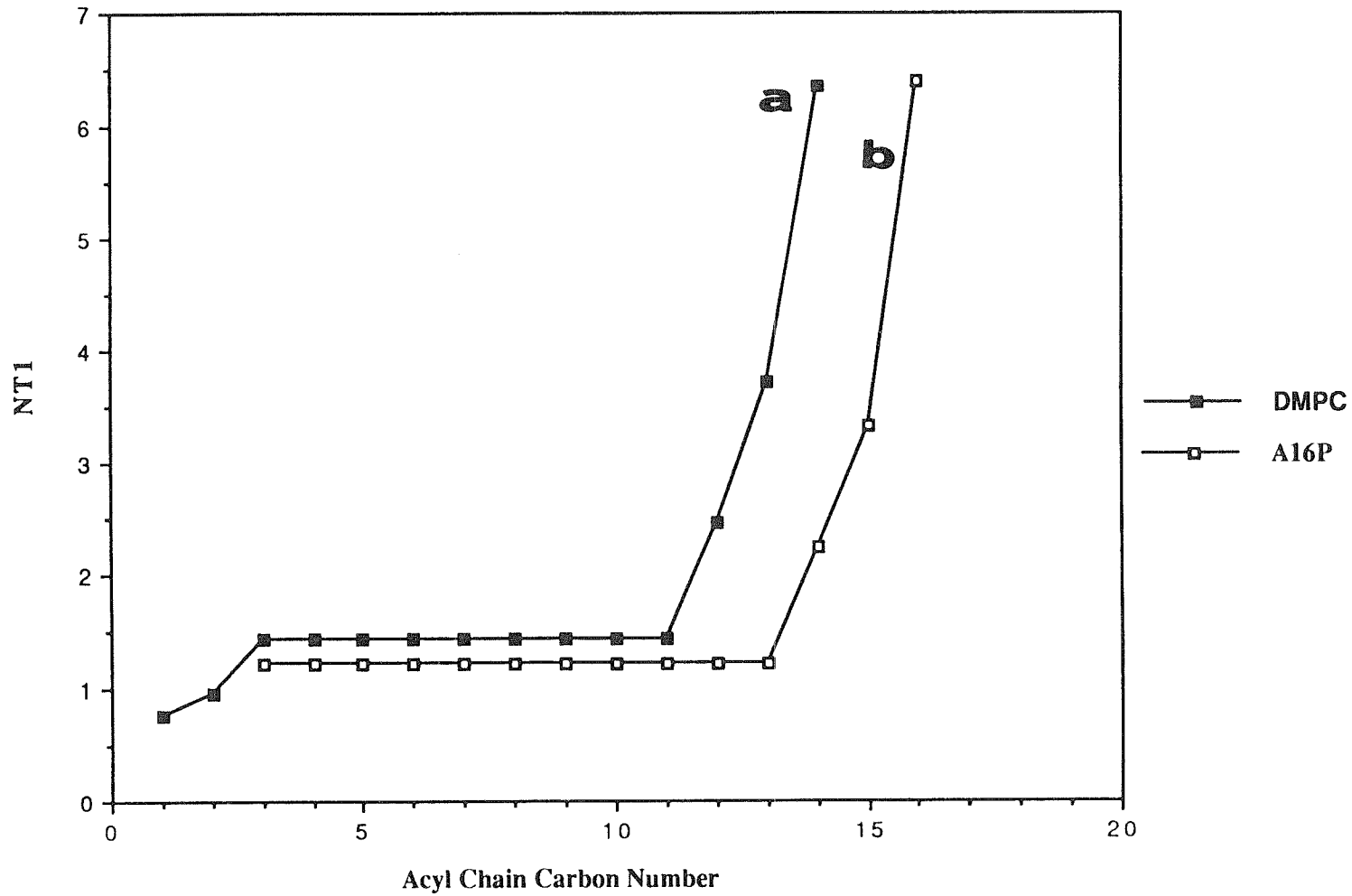
Carbon Atom	Chemical Shift	T1 (305 °K)	T1 (320 °K)	NOE (305 °K)
<b>Backbone</b>				
CH <sub>2</sub> O	70.8	.32 ± .04	.43 ± .03	1.75 ± .13
CH <sub>2</sub> OP	63.9	.20 ± .01	.28 ± .02	2.08 ± .25
CH <sub>2</sub> O	63.2	.17 ± .01	.23 ± .01	1.7 ± .21
<b>Head group</b>				
CH <sub>2</sub> N	66.3	.64 ± .02	.96 ± .05	2.51 ± .28
CH <sub>2</sub> OP	59.7	.63 ± .02	.90 ± .03	2.33 ± .08
N(CH <sub>3</sub> ) <sub>3</sub>	54.3	.82 ± .02	1.2 ± .04	2.7 ± .02
<b>Acyl chains</b>				
α	34.3	.50 ± .01	.60 ± .01	2.23 ± .13
β	25.1	.70 ± .03	.86 ± .02	2.36 ± .16
γ and δ	29.3	.90 ± .01	1.19 ± .01	2.45 ± .12
ε	32.0	1.31 ± .03	1.80 ± .04	2.53 ± .22
ω-1	22.7	1.96 ± .05	2.46 ± .09	2.63 ± .02
ω-CH <sub>3</sub>	13.9	3.76 ± .66	4.48 ± .26	2.84 ± .23

Carbon Atom	Chemical Shift	T1 (305 °K)	T1 (320 °K)	NOE (305 °K)
<b>Backbone</b>				
CH <sub>2</sub> O	70.8	.27 ± .01	.38 ± .04	1.25
CH <sub>2</sub> OP	63.9	.19 ± .01	.15 ± .05	1.63
CH <sub>2</sub> O	63.1	.17 ± .07		
<b>Head group</b>				
CH <sub>2</sub> N	66.2	.67 ± .03	.87 ± .07	2.04
CH <sub>2</sub> OP	59.7	.60 ± .01	.82 ± .18	22.28
N(CH <sub>3</sub> ) <sub>3</sub>	54.3	.77 ± .03	1.11 ± .07	2.75
<b>Acyl chains</b>				
α	34.3	.36 ± .03	.48 ± .12	2.10
β	25.1	.39 ± .02	.55 ± .14	2.53
Bulk CH <sub>2</sub>	29.4	.38 ± .01	.52 ± .08	2.12
ω-CH <sub>2</sub> SS	39.3	.292 ± .02	.44 ± .15	2.26

**Figure 4.**

$^{13}\text{C}$  spin-lattice relaxation times for the acyl chain carbons of: **A.** DMPC and **B.** Polymeric  $\alpha$ -16 SUVs. The data are taken from Table I and plotted as  $N_{\text{H}}T_1$ , where  $N_{\text{H}}$  denotes the number of directly bonded  $^1\text{H}$  nuclei. The flat plateau region corresponds to the bulk methylene protons, which have a fairly uniform  $T_1$  across the broad methylene envelope. However, in reality, it is expected that the plateau region should have some slope.

Mobility Gradient for DMPC  
versus A16P at 305 K



toward the center of the bilayer. (For DPPC, the plateau extends from  $\approx$  C-4 to  $\approx$  C-12 (26,27).

The values of the NOE at 305°C (Table I) were also only slightly smaller for polymeric  $\alpha$ -16 compared to DMPC SUVs. Of the resolvable resonances, the only one with a significant ( $\approx$ 23%) difference was that of the headgroup CH<sub>2</sub>OP, which may reflect either (i) slower motion of this moiety due to its proximity to the disulfide and glycerol backbone or possibly (ii) a different orientation of the headgroup.

The value of the NOE is often interpreted in terms of the percentage of the relaxation due to the dipolar interaction. For an isotropically reorienting system in the extreme narrowing regime, an NOE of 2.99 would indicate the C-H dipolar interaction is the exclusive mechanism for relaxation (26,37,40). Interpreted in this way, with the exception of carbons associated with the glycerol backbone (and carbonyl carbon), one can conclude that the C-H dipolar interaction is the primary pathway for relaxation. In fact, the values are not substantially lower than the average values of  $2.6 \pm .2$  reported for micelles at approximately half the field strength (40). Therefore, since the competing relaxation mechanism (chemical shift anisotropy) increases with the square of the field strength, it cannot have a substantial contribution. This is in agreement with the contention of others that chemical shift anisotropy has little effect on the relaxation of protonated <sup>13</sup>C nuclei, even at the field strength employed in these experiments (26,33).

The question then arises as to why the NOE is not the full value of 2.99. This is most likely due to the fact that the motions in liposomes do not fulfill the assumption of extreme narrowing rates and isotropic reorientation necessary for application of Eqn. (28). As was discussed in the background section, Brown has shown that for motions characterized by rotational diffusion in the presence of an ordering potential (extreme narrowing regime) or by models involving both fast ( $< \omega_0^{-1}$ ) and slow ( $> \omega_0^{-1}$ )

motional components, the NOE for pure dipolar interactions can be much less than 2.99 (26).

Based on the similarities of  $T_1^{-1}$  and NOE data for the two lipid systems described above, we conclude that, at least at 305°C (just above the phase transition of DMPC and polymeric  $\alpha$ -16) the motions in the bilayers of DMPC and  $\alpha$ -16 that contribute to  $T_1^{-1}$  may not be that different. In particular, fast segmental motions and slow cooperative fluctuations of the acyl chains may have similar magnitudes. The exception to this is that the rotational and lateral diffusion of the lipids as a whole in  $\alpha$ -16 SUVs must be much slower than in DMPC, but these motions may have little bearing on  $T_1^{-1}$ .

Temperature Dependence of the Spin-Lattice Relaxation Rates for DMPC and Polymeric  $\alpha$ -16 SUVs. Differences in the relaxation behavior of  $\alpha$ -16 compared to DPPC SUVs start to become more apparent as the temperature is raised. In both cases, an increase in temperature results in an increase in  $T_1$  as shown in Table I. However, the ratio of the  $T_1$ s at 320°C versus 305°C ( $T_1$  320/305) and 335°C versus 305°C ( $T_1$  335/305) range from 1.3 to 1.5 ( $T_1$  320/305) and 1.1- 2.4 ( $T_1$  335/305) for DMPC compared to .98 - 1.3 ( $T_1$  320/305) and 1.1 - 2.0 ( $T_1$  335/305) for  $\alpha$ -16. Thus the presence of the polymerizable moiety inhibits the temperature dependent changes in the rates or amplitudes of the motions sensed by the spin-lattice relaxation. The enhancement factors ( $T_1$  320/305 and  $T_1$  335/305) are tabulated in Table V and indicate that the enhancement is greatest for the choline headgroup and for the carbons associated with the chain terminus.

In the past, the increase in  $T_1$  with temperature was taken as evidence that extreme narrowing conditions apply and thus that the  $T_1$  reflects predominantly the fast segmental motions of the chains. Arrhenius-type expressions were consequently

**Table V**

Summary of the ratio of the spin-lattice relaxation rates at 320 °K and 335 °K relative to the rates at 305 °K ( $T_1$  320/305 and  $T_1$  335/305) (taken from Table I). Also included are the relative order parameters  $S_{rel}$  calculated according to Eqn. (29). In these calculations  $\eta_{CH}$  at 305 °K was used since within experimental error, little difference in  $\eta_{CH}$  was observed for DMPC and D8PC at 320 °K versus 305 °K. The numbers in parentheses denote the temperature (°K) of the relaxation experiment. **A.** Values for DMPC SUVs and **B.** Values for polymeric  $\alpha$ -16 SUVs.

**A**

Carbon Atom	T1 (320/305)	T1 (335/305)	S <sub>rel</sub> (305)	S <sub>rel</sub> (320)	S <sub>rel</sub> (335)
<b>Backbone</b>					
CHO	1.09	.87	1.82	1.74	1.95
CH <sub>2</sub> OP	1.42		1.85	1.55	
CH <sub>2</sub> O	1.42	1.51	1.96	1.66	1.81
<b>Head group</b>					
CH <sub>2</sub> N	1.55	1.85	.42	.34	.31
CH <sub>2</sub> OP	1.42	1.79	.71	.72	.53
N(CH <sub>3</sub> ) <sub>3</sub>	1.56	2.41	.29	.24	.19
<b>Acyl chains</b>					
α	1.21	1.55	.79	.77	.63
β	1.26	1.78	.67	.60	.50
Bulk CH <sub>2</sub>	1.27	1.78	.46	.41	.35
ε	1.45	1.67	.35	.30	.28
ω-1	1.39	2.09	.29	.26	.20
ω-CH <sub>3</sub>	1.53	2.34	.16	.13	.11

<b>B</b> Carbon Atom	T1 (320/305)	T1 (335/305)	S <sub>rel</sub> (305)	S <sub>rel</sub> (320)	S <sub>rel</sub> (335)
<b>Backbone</b>					
CHO					
CH <sub>2</sub> OP					
CH <sub>2</sub> O					
<b>Head group</b>					
CH <sub>2</sub> N	1.09	1.07	.61	.61	.61
CH <sub>2</sub> OP	.987	1.27	.85	.85	.75
N(CH <sub>3</sub> ) <sub>3</sub>	1.26	1.96	.31	.31	.25
<b>Acyl chains</b>					
α					
β					
Bulk CH <sub>2</sub>	1.18	1.39	.62	.62	.57
ε	.98	1.13	.38	.38	.35
ω-1	1.12	1.78	.32	.31	.25
ω-CH <sub>3</sub>	1.22	1.76	.15	.15	.13

utilized to yield activation energies for these fast local motions. As described in the background section, however, it is now clear from the observed frequency dependences of  $T_1$  that slow motions *also* contribute to the relaxation and thus that the dynamic behavior of phospholipids is best described as the sum of a frequency-independent fast motion term and frequency-dependent and order parameter-dependent slow motion term. Using these models, an alternative interpretation for the temperature dependence of  $T_1^{-1}$  was proposed: it was shown that the temperature dependence of  $T_1^{-1}$  could in fact be due to the temperature dependence of the *order parameter*, which is in turn related to the coefficient of thermal expansion and bilayer elasticity (26,41).

We should consider both of the above explanations for the temperature dependence of  $T_1^{-1}$  to explain the data, which shows that  $T_1^{-1}$  ( $\alpha$ -16) changes less with temperature than  $T_1^{-1}$  (DMPC):

(i) Based on Arrhenius behavior alone, the data suggests that the activation energy for the fast segmental motions of polymeric  $\alpha$ -16 is *less* than that of DMPC in the liquid-crystalline state. The lower value for polymeric  $\alpha$ -16 is somewhat counterintuitive, however. One would expect, by contrast, that polymerization would actually effect a greater barrier to fast segmental motions thus leading to a higher activation energy than that for a nonpolymerized lipid. Using the Arrhenius model, however, the data implies that indeed the fast segmental motions are less hindered in the polymer. We know by FT-IR and Raman studies that at least *in the the gel state*, the hydrocarbon region of the  $\alpha$ -THIOLS is more disordered and less densely packed than polymerizeable analogues and thus a lower activation energy for the polymer would seem reasonable (see Chapter IV). Whether or not this is true for polymeric  $\alpha$ -16 *in the liquid-crystalline state* is unclear. If it is true, it is likely that the polymeric lipids will be more disordered than the nonpolymerizeable analogues only up to a certain temperature since the presence of intrachain covalent linkages should put a limit on the

lateral expansion of the bilayer. Faster segmental motions for  $\alpha$ -16 compared to DMPC in the liquid-crystalline state does not seem like a satisfying conclusion, however.

(ii) If we assume as an alternative, that the temperature dependence of  $T_1^{-1}$  could in fact be related to the order parameter, the relaxation rates for DMPC versus  $\alpha$ -16 make more intuitive sense. The order parameter is defined as the ensemble time average of Eqn. (19). Thus it provides a quantitative description of the degree of organization in the bilayer via the time average of the angular ( $\theta$ ) fluctuations of a given coordinate axis (i.e., a C-D or C-H bond segment) with respect to the director axis.\* For phospholipid membranes, the director axis is the normal to the bilayer surface. Values of  $S_{CD}$  ( $=S_{CH}$ ) equal to 1 and 0 reflect completely ordered and disordered bilayers, respectively (4).

Physically, what the temperature dependence of the order parameter reflects is the elasticity of the bilayer and the change in the thermal expansion coefficient ( $\alpha$ ) defined by (44):

$$(30) \quad \alpha = \frac{\Delta d}{d\Delta T}$$

where  $d$  is the bilayer thickness. Seelig *et al.* has shown that a segmental expansion coefficient ( $\alpha_i$ ) can be written in terms of the molecular order parameter  $\Delta S_{mol}$  as follows (44):

$$(31) \quad \alpha_i = \frac{\Delta S_{mol}}{2.25\Delta T}$$

In this equation,  $S_{mol} = 2S_{CD}$  (4,44). Thus these equations reflect the fact that a relatively small change in the order parameter with temperature reflects a *reduced* value of the thermal expansion coefficient. The temperature dependence of  $T_1$  and the

---

\* It should be noted, however, that the order parameter does *not* provide insight into the rates of motion.

enhancement ratios in Tables I and V therefore imply that DMPC has a higher thermal expansion coefficient than  $\alpha$ -16. This is also shown by the temperature dependence of the relative order parameters ( $S_{rel}$ ) (Table V), which allow one to very roughly estimate that  $\alpha_i(\text{DMPC})$  is greater than  $\alpha_i(\alpha\text{-16})$  by a factor of 2 based on the  $S_{rel}$  for the bulk methylene and terminal methyl group.\* It should be noted that the relative order parameters in Table V are those described in the background section as calculated according to the method of Sölderma Eqn. (29) (46).

From a physical and structural standpoint, a reduction in the thermal expansion coefficient of the bilayer upon interfacial polymerization is actually quite appealing. As shown by Eqn. (30), this implies that the bilayer thickness  $\Delta d$  changes little with temperature. For nonpolymerizable lipids, it has been demonstrated that a reduction in  $\Delta d$  upon increasing the temperature, is by necessity compensated by a decrease in the lateral packing density of the lipids. These dimensional alterations are the consequence of introduction of chain disorder via the introduction of gauche conformers. For polymerized  $\alpha$ -THIOLS, the presence of the disulfide linkage between adjacent lipids within a polymer chain should put an upper limit on the degree of lateral expansion, which can occur along the direction of the polymer chain and therefore the extent to which the bilayer thickness can change. As described in earlier chapters, only between unlinked lipids is there the possibility for unrestricted lateral expansion. The net effect, however, should be that the thermal expansion coefficient of the bilayer is reduced in polymerized  $\alpha$ -16 compared to DMPC, which is consistent with the data. (Preliminary

---

\* Since  $S_{rel}$  is not equivalent to  $S_{mol}$  and also may not be strictly comparable for DMPC versus  $\alpha$ -16, the ratio of the segmental thermal expansion coefficients for DMPC versus  $\alpha$ -16 is only a crude and perhaps empirical approximation estimated as :

$$\frac{\alpha_{DMPC}}{\alpha_{\alpha-16}} = \frac{\frac{\Delta S_{rel}(DMPC)}{\Delta T}}{\frac{\Delta S_{rel}(\alpha-16)}{\Delta T}}$$

x-ray diffraction studies have in fact suggested that there is not a great change in the bilayer thickness with temperature) (49).

*Spin-lattice Relaxation and NOE Measurements of  $\Omega$ -8 and D8PC Micelles.* The data for polymeric  $\Omega$ -8 micelles compared to D8PC micelles shows some distinctly different behavior. Examination of the relaxation data and calculated relative order parameters in Tables IV and VI indicates that while the  $T_1$ 's associated with the backbone and headgroup are only slightly reduced compared to those of the nonpolymerized micelles, the  $T_1$ 's associated with the chains are much smaller. This is not the consequence of the differences in the sizes of the two lecithin species: It has been clearly demonstrated that while the spin-spin relaxation rate (which contributes to the linewidth of the resonances) is dependent on aggregate size and morphology, the spin-lattice relaxation rate is not (29). Furthermore an effect of aggregate size would cause a uniform  $T_1$  decrease in all carbons of  $\Omega$ -8 whereas the data shows it is predominantly the chain methylenes that are influenced by the polymerization.

The simplest and most logical interpretation of the data is that polymerization restricts the rate and/or amplitude of the fast segmental motions. Since we do not have the appropriate frequency dependence of  $T_1^{-1}$  to extrapolate out the correlation times for the fast motions, we can calculate an effective correlation time according to Eqn. (15). As was described in the background section, this analysis has been widely used in the past and although strictly valid only for isotropic motion, is useful for qualitatively comparing the motions of the same carbons in different lipid systems (40). The effective correlation times calculated for the acyl chains of polymeric  $\Omega$ -8 and D8PC micelles at 305°C (Table VII) indicate a substantial reduction in the motion of the chain methylenes for the polymeric  $\Omega$ -8 relative to D8PC and that the difference between the two lipid systems is most notable towards the chain terminus.

**Table VI**

Summary of the ratio of the spin-lattice relaxation rates at 320 °K relative to the rates at 305 °K ( $T_1$  320/305) (taken from Table IV). Also included are the relative order parameters  $S_{rel}$  calculated according to Eqn. (29). In these calculations  $\eta_{CH}$  at 305 °K was used because within experimental error, little difference in  $\eta_{CH}$  was observed for DMPC and D8PC at 320 °K versus 305 °K. The numbers in parentheses denote the temperature (°K) of the relaxation experiment. **A.** Values for D8PC micelles and **B.** Values for polymeric  $\omega$ -8 micelles.

D8PC

<b>A</b>	<u>Carbon Atom</u>	<u>T1 (320/305)</u>	<u>S<sub>rel</sub> (305)</u>	<u>S<sub>rel</sub>(320)</u>
	<b>Backbone</b>			
	CHO	1.34	1.40	.75
	CH <sub>2</sub> OP	1.44	1.28	.7
	CH <sub>2</sub> O	1.32	1.15	1.0
	<b>Head group</b>			
	CH <sub>2</sub> N	1.49	.43	.35
	CH <sub>2</sub> OP	1.43	.51	.43
	N(CH <sub>3</sub> ) <sub>3</sub>	1.46	.24	.20
	<b>Acyl chains</b>			
	α	1.19	.62	.57
	β	1.23	.47	.43
	γ and δ	1.32	.39	.34
	ε	1.37	.30	.25
	ω-1	1.26	.21	.19
	ω-CH <sub>3</sub>	1.28	.08	.07

Polymeric  $\omega$ -8

<b>B</b>	<u>Carbon Atom</u>	<u>T1 (320/305)</u>	<u>S<sub>rel</sub> (305)</u>	<u>S<sub>rel</sub>(320)</u>
	<b>Backbone</b>			
	CHO	1.43	1.81	1.51
	CH <sub>2</sub> OP	1.26	1.36	1.52
	CH <sub>2</sub> O			
	<b>Head group</b>			
	CH <sub>2</sub> N	1.29	.60	.52
	CH <sub>2</sub> OP	1.38	1.36	1.52
	N(CH <sub>3</sub> ) <sub>3</sub>	1.44	.23	.19
	<b>Acyl chains</b>			
	$\alpha$	1.33	.77	.68
	$\beta$	1.42	.55	.46
	Bulk CH <sub>2</sub>	1.36	.76	.65
	$\omega$ -CHSS	1.49	.80	.67

**Table VII**

Effective correlation times for the resolvable carbons of the acyl chains in D8PC and polymeric  $\omega$ -8 micelles calculated according to equation 15. Values are given in picoseconds.

Effective Correlation Time (ps)

<u>Carbon Atom</u>	<u>D8PC</u>	<u><math>\omega</math>-8</u>
<b>Acyl Chains</b>		
$\alpha$	48	65
$\beta$	34	66
Bulk CH <sub>2</sub>	28	63
$\omega$ -CH <sub>3</sub> / $\omega$ -SS	4	81

Figure 5 illustrates an additional interesting distinction between the motional behavior of polymeric  $\omega$ -8 compared to D8PC. In the case of the nonpolymerized lipid, there is a motional gradient (indicated by the increasing values of  $NT_1$ ), which increases from the glycerol backbone towards the chain terminus with a plateau region of relatively constant  $T_1$ 's in the center of the chain. This is similar to  $T_1$  profiles for liposomal-forming lecithins as shown in Figure 4 for polymeric  $\alpha$ -16 and DMPC, and is in agreement with work reported from other groups (40). By contrast, Figure 5 also illustrates the apparent lack of a mobility gradient in polymeric  $\omega$ -8 due to the disulfide coupling at the chain terminus. In fact there appears to be a slight elevation in the  $T_1$ 's of the carbons in the middle of the chain rather than the typical increase towards the end of the chain exhibited by D8PC and most phospholipid bilayers. These effects hold true at both 305°C and 320°C and suggest that polymerization at the chain terminus greatly reduces the rates and/or amplitudes of the fast segmental motions of the chains.

It is interesting to note that in Chapter IV what is usually referred to as a "fluidity gradient" was detected for liquid-crystalline polymeric  $\omega$ -15 and  $\omega$ -16 using depth-dependent fluorescent probes. It was pointed out that this gradient could reflect increasing motion *or* structural disorder with depth within the bilayer. If the lack of a motional gradient exhibited by the  $^{13}\text{C}$   $T_1$  results for polymeric  $\omega$ -8 micelles can be extrapolated to long 15- or 16-carbon chain analogues, then it appears that the fluorescence-detected gradient is one of structural disorder only.

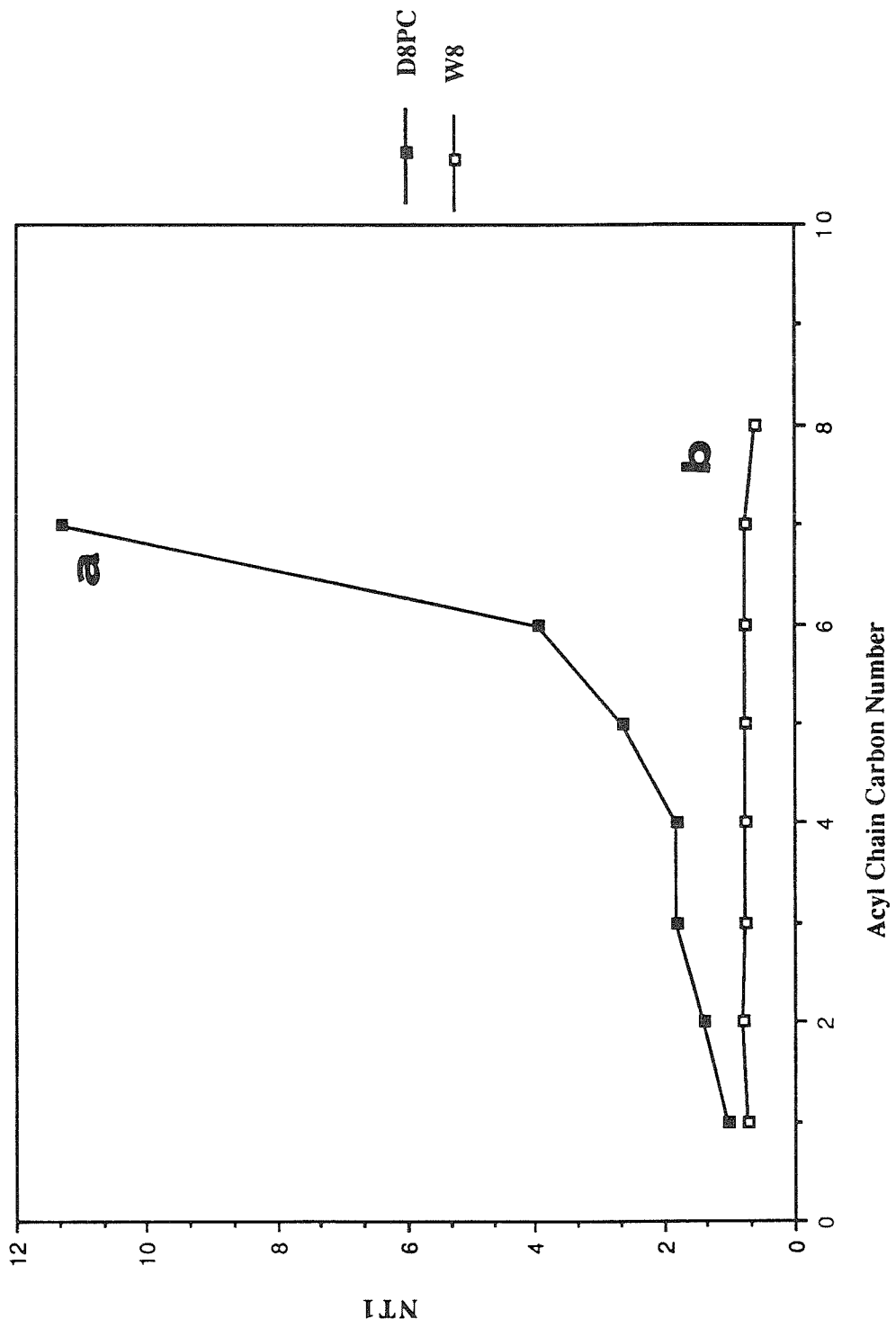
*Temperature Dependence of the Spin-Lattice Relaxation Rates for D8PC and Polymeric  $\omega$ -8 Micelles.* Upon raising the temperature, the  $T_1$  increases for both D8PC and polymeric  $\omega$ -8 micelles.\* However, in contrast to the reduced temperature dependence of  $T_1$  for

---

\* In the simplest interpretation of such data, this would imply that extreme narrowing conditions apply. However as already described, this is an oversimplification of the data.

**Figure 5**

$^{13}\text{C}$  spin-lattice relaxation times for the acyl chain carbons of : **A.** D8PC micelles and **B.** Polymeric  $\omega$ -8 micelles. The data are taken from Table IV (305 °K) and plotted as  $N_{\text{H}}T_1$  where  $N_{\text{H}}$  denotes the number of directly bonded  $^1\text{H}$  nuclei. The nonresolvable carbons of  $\omega$ -8 and D8PC, which contribute to the bulk methylene envelope were arbitrarily given the same value.



the  $T_1$ 's of polymeric  $\alpha$ -16 SUVs compared to DMPC, the enhancements are similar for  $\omega$ -8 and D8PC micelles ( $T_1$  320/305 = 1.3-1.5) at least over the temperature range investigated\* (Table IV and Table VI). This is a surprising result. If we once again consider the Arrhenius treatment of the relaxation data, this would imply a similar activation energy for segmental isomerization in both systems. Such a conclusion is difficult to imagine since gauche conformers are known to concentrate and propagate at the chain terminus (2,25). If the chain terminus is coupled by polymerization, however, the distribution of the gauche conformers as well as the rates and amplitudes of these isomerizations should decrease. If we consider the data in terms of the temperature dependence of the order parameter (relative order parameters are tabulated in Table VI) we find that the change in  $S_{rel}$  with temperature ( $\Delta S_{rel}/\Delta T$ ) is at least as great for  $\omega$ -8 as for D8PC (in fact it is larger). These results suggest that:

(i) The thermal expansion coefficient of the two systems is not measurably different over the temperature range examined. This is in contrast to the  $\alpha$ -THIOLS and implies that polymerization at the chain terminus does not inhibit the temperature-induced lateral expansion of the lipid bilayer to the extent that interfacial polymerization does. It should be noted, however, that if the lipids were highly crosslinked, the results might be quite different.

(ii) Despite polymerization at the chain terminus and the lack of a mobility gradient, the hydrocarbon region of these lipids can become quite disordered in the liquid-crystalline state. If this were not the case, the  $T_1$  would not be expected to change much with temperature.\*\*

### $^1H$ NMR.

---

\*It is possible that at higher temperatures, greater differences would be observed.

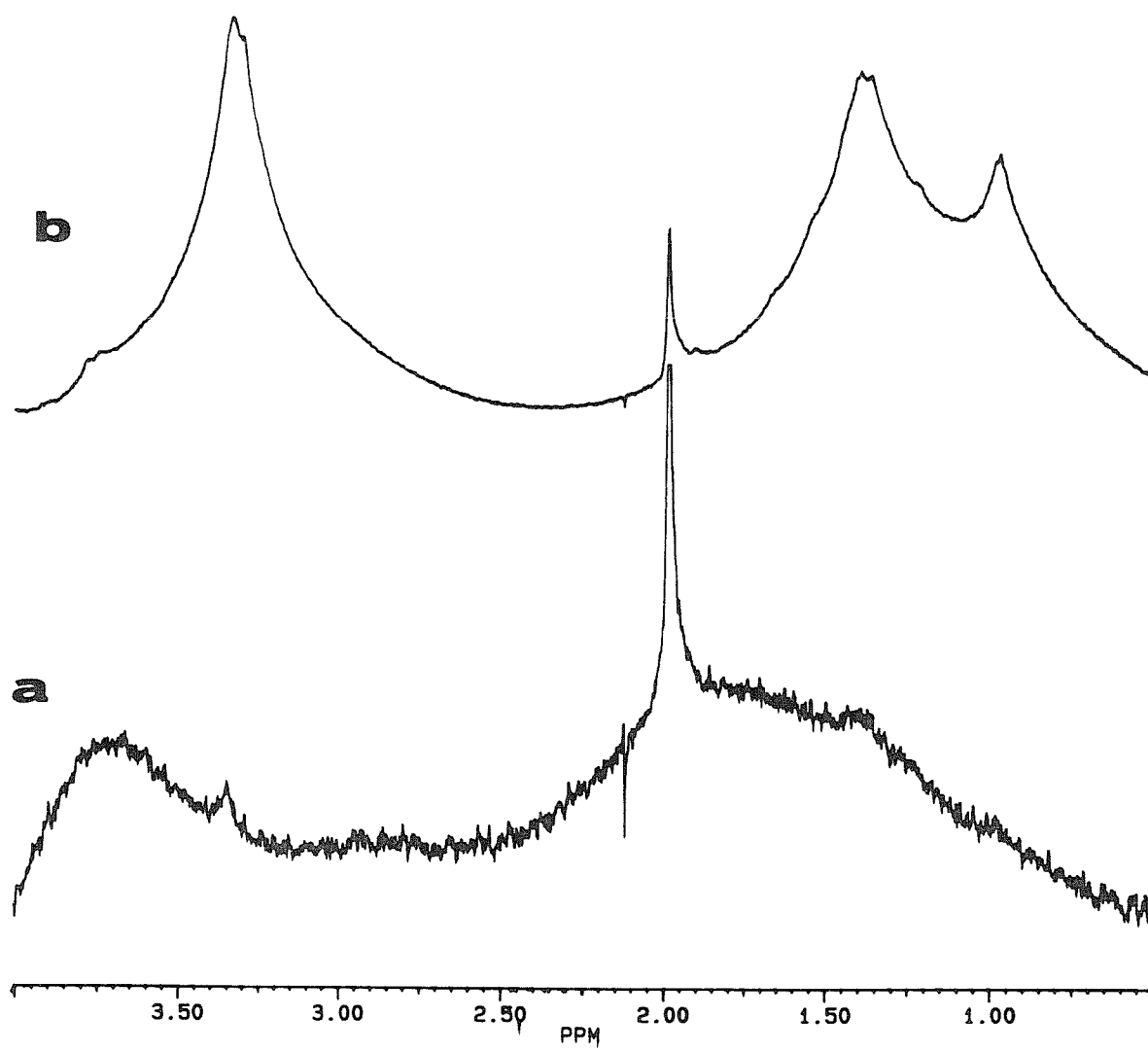
\*\*It should be reiterated that disorder and mobility can be, but are not necessarily concomitant.

$^1\text{H}$  NMR serves as an informative adjunct to  $^{13}\text{C}$  NMR data for determining the motional state of lipids in bilayers. As with  $^{13}\text{C}$  NMR, the  $^1\text{H}$  spectra and relaxation properties of phospholipids are sensitive to the anisotropic motions of the individual molecules and the isotropic motion of the liposome as a whole. For large unsonicated dispersions of most lecithins, the proton spectra consists of very broad unresolved features. The tumbling rate of these dispersions and the lateral diffusion of lipids in the plane of the bilayer is on the order of seconds and therefore is much too long to average the dipolar interactions (1,2). For large ( $\approx 5\ \mu\text{m}$ ) liposomal particles, therefore, any motional averaging that occurs must be the consequence of local motions of the phospholipids (1,2). Figure 6A shows a "high resolution"  $^1\text{H}$  spectra of an unsonicated DPPC dispersion at  $47^\circ\text{C}$  (above  $T_m$ ). Very little is visible under the acquisition conditions used with the exception of minor contributions from the choline methyls ( $\approx 3.1\ \text{ppm}$ ) and the methylene/methyls ( $1.2\ \text{ppm}$ ). This is due to the slow motions of the bilayer, which promotes effective spin-spin relaxation.

Figure 6 B also shows an analogous spectrum (same concentration of lipid and NaAc) for polymeric  $\alpha$ -18 at  $47^\circ\text{C}$ . In contrast to DPPC, which shows very little intensity, approximately 30% of the total protons are observed in the spectra based on an analysis of absolute intensities using NaAc as an internal standard. (The exact percentage is dependent on the length and temperature of the hydration conditions of the lipid in a manner that has not yet been systematically characterized.) Since both lipids have similar phase transition temperatures ( $41.7^\circ$  and  $37^\circ\text{C}$ , respectively) the differences in the spectra are not the consequences of differences in the reduced temperatures at which the spectra were taken. The spin-spin relaxation ( $T_2$ ), which contributes to the linewidth, is caused by both rapid molecular motions and by motions near zero frequency. Thus, both the overall motion of the vesicles and local segmental fluctuations can contribute to spectral narrowing (1,2,7,48-50). The more highly

**Figure 6**

<sup>1</sup>H NMR spectra of A. DPPC and B.  $\alpha$ -18 MLVs at 47 °C. Both samples contain 5.6  $\mu$ moles lipid and .31  $\mu$ moles NaAc.



resolved features of the  $\alpha$ -18 dispersion can therefore arise from several sources: (i) faster lateral diffusion of the lipids over the surface of the liposome, (ii) a faster rate or amplitude of local motions such as chain tilting, chain reorientation, or segmental motions or (iii) a smaller liposome size or a heterogeneous population of liposomes in which the small components can tumble rapidly enough to partially average the interproton dipolar interactions. Each of these reasons should be considered:

(i) Because the lipids in  $\alpha$ -18 are polymerized, a faster lateral diffusion (i) can be excluded. For monomers, this is estimated to be on the order of  $4 \times 10^{-5}$  s for 250 Å vesicles but seconds for 5  $\mu$ m MLVs. For oligomers diffusing over the surface of even 200-300 nm liposomes, the lateral diffusion rate should be several orders of magnitude larger than  $10^{-5}$  and insufficient to average the motion.\*

(ii) Local chain fluctuations (ii) may possibly contribute to the spectral features since these are much faster motions. However, since the motions of the lipid as a whole (rotational diffusion and perhaps cooperative tilting or swaying) will be hindered by polymerization, only reorientation and off axis excursions of the acyl chains (from the director axis) could possibly be viable sources of local motional averaging. However the  $^{13}\text{C}$  relaxation results showed that in the liquid-crystalline state, the relaxation time of polymeric  $\alpha$ -16 was shorter than that of DMPC, which could suggest (a) more effective slow motions or (b) reduced rates and amplitudes of fast motions for the polymer. Consequently, while it cannot be ruled out, faster local motions of the chains of liquid-crystalline polymeric  $\alpha$ -18 are unlikely to contribute to spectral narrowing.

(iii) The primary reason for the enhanced resolution of  $\alpha$ -18 dispersions is likely to arise from isotropic vesicle tumbling. Many studies have demonstrated the

---

\* For monomeric lipids the  $\tau_{\text{LD}}$  would be 3-6 msec for 200-300nm liposomes. Oligomers should have a much longer correlation time.

tremendous sensitivity of  $^1\text{H}$  linewidths to vesicle tumbling rates (1,2,51,52). Thus it is useful to recall the results of Chapter II where it was shown by EM and light scattering that prepolymerized  $\alpha$ -THIOLS form a polydisperse and generally smaller distribution of liposomes than their nonpolymerizable analogues. Furthermore, addition of  $\text{MnCl}_2$  to relax externally oriented cholines indicated that the  $^1\text{H}$  NMR-visible liposomes were unilamellar.

Even in the gel state,  $\alpha$ -THIOLS tend to be more highly resolved than DPPC in the liquid-crystalline state. This is demonstrated quite clearly by the spectra of gel and liquid-crystalline polymeric  $\alpha$ -16 and  $\alpha$ -20 MLVs in Figures 7 and 8. For liquid-crystalline  $\alpha$ -16 and  $\alpha$ -20, the generally smaller size and faster vesicle tumbling rates of  $\approx 30\%$  of the liposomes is the major source of motional averaging. However, for the gel state dispersions, faster local motions may also be important. Conceptually one would not expect a polymerized lipid to give rise to greater segmental motion than a nonpolymerized analogue. However, in Chapter IV it was shown by vibrational spectroscopy that in fact polymeric  $\alpha$ -THIOLS are more disordered in the gel state than the corresponding monomers or nonpolymerizable analogues. Although this does not necessarily confirm that the local motions are faster for gel state  $\alpha$ -THIOLS, it cannot be ruled out (more disordered systems do often exhibit faster motions).

SUVs. Sonication of the vesicles into 250-500 Å sized particles results in a significant transformation of the  $^1\text{H}$  spectra. Figure 9 shows the high resolution features of DPPC SUVs at various temperatures. Above the phase transition temperature (Figure 8 A), the choline methyls ( $\approx 3.1\text{ppm}$ ), the bulk methylenes ( $\approx 1.2\text{ppm}$ ), the terminal methyls ( $\approx .85\text{ppm}$ ), the headgroup methylenes ( $\approx 3.75$  and  $4.35\text{ppm}$ ) and even the  $\alpha$ -carbonyl methylene ( $2.5\text{ppm}$ ) are extremely well resolved. This is due to the fact that reduction of the particle size to 250-500 Å is accompanied by a

**Figure 7**

$^1\text{H}$  NMR spectra of polymeric  $\alpha$ -16 MLVs in  $\text{D}_2\text{O}$  at A.  $7^\circ\text{C}$  and B.  $32^\circ\text{C}$

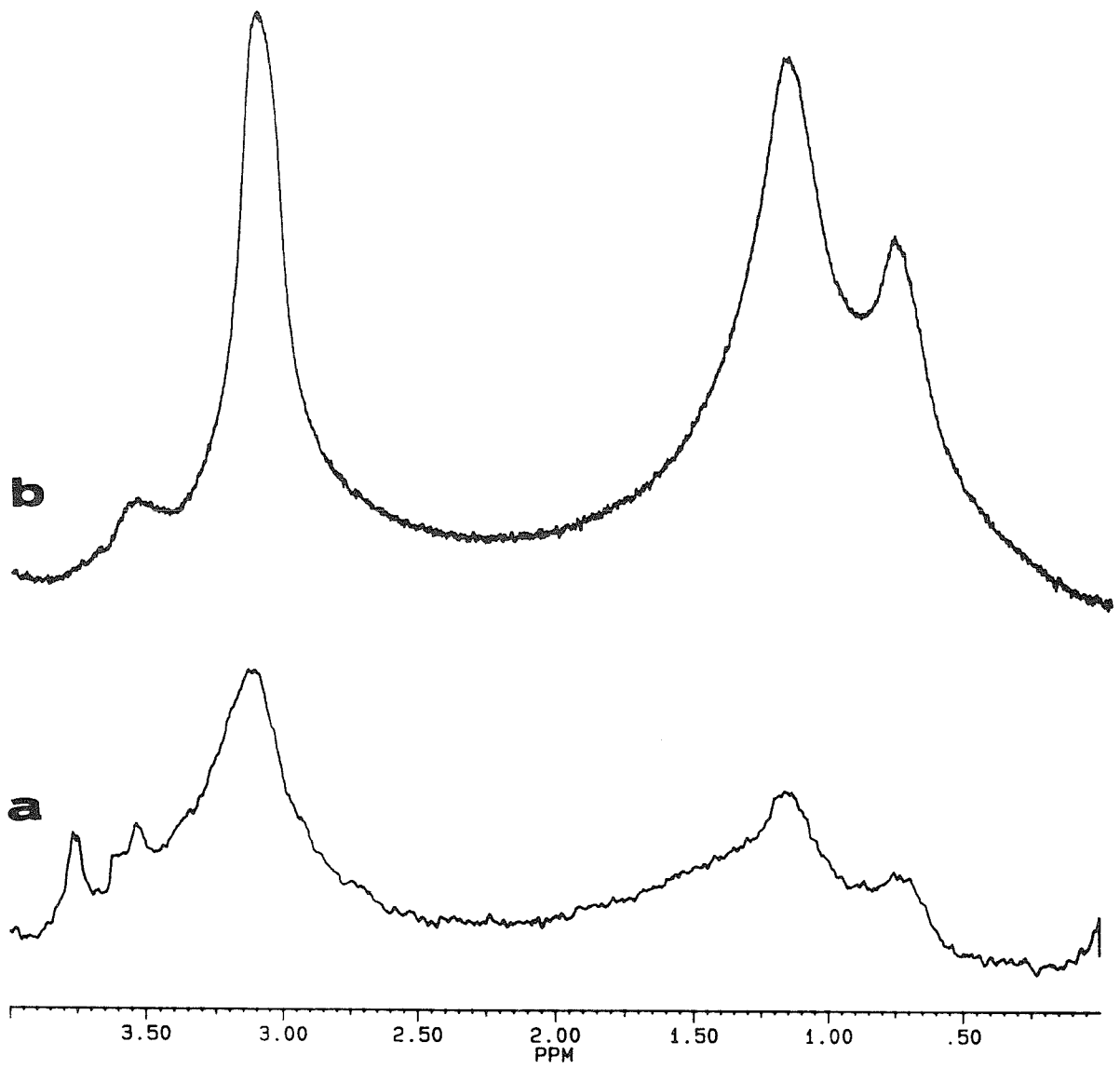


**Figure 8**

$^1\text{H}$  NMR spectra of polymeric  $\alpha$ -20 MLVs in  $\text{D}_2\text{O}$  at **A.** 25°C and **B.** 45 °C and **C.** 60 °C

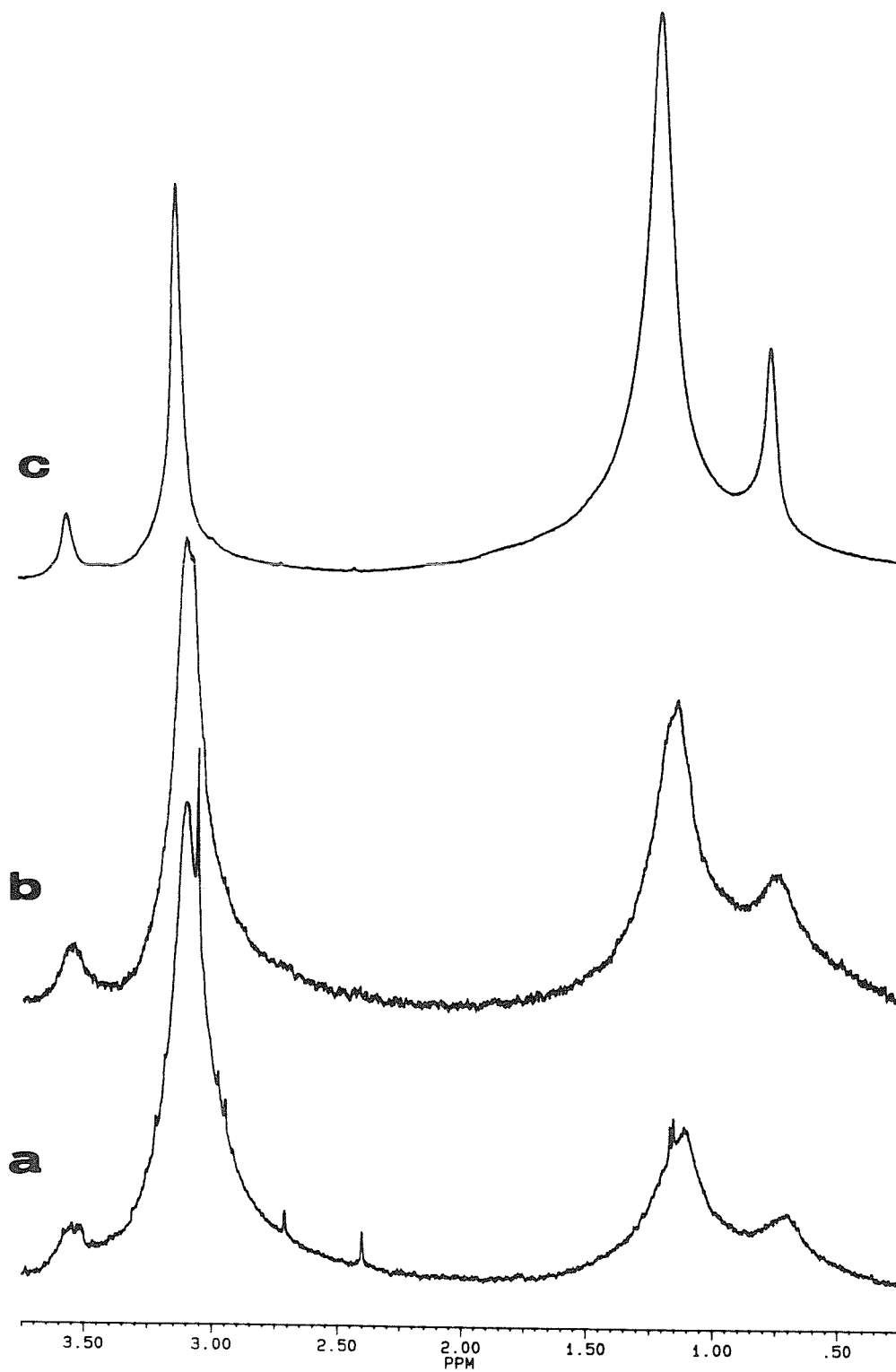
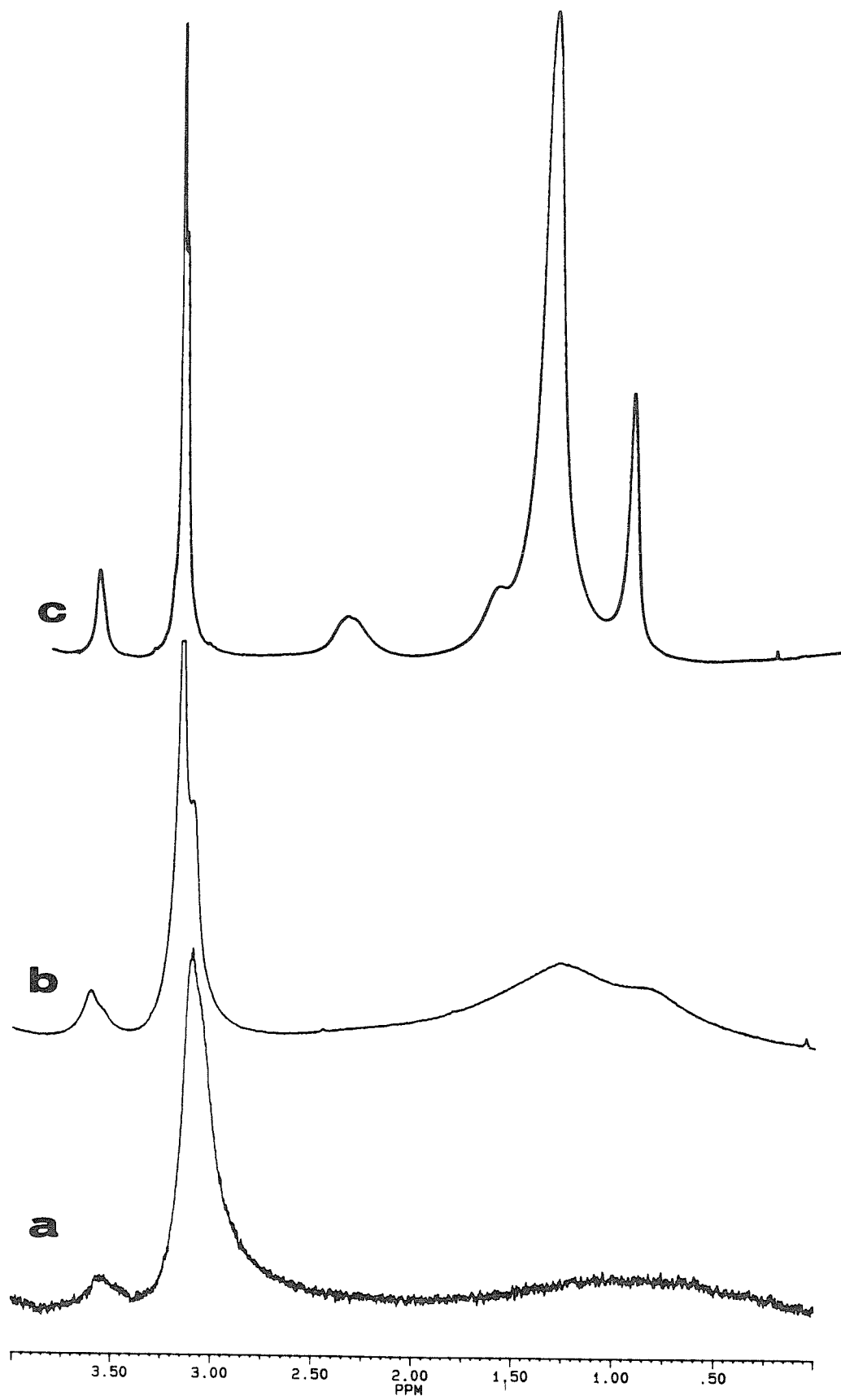


**Figure 9**

$^1\text{H}$  NMR spectra of DPPC SUVs in  $\text{D}_2\text{O}$  at A. 25°C and B. 30 °C and C. 50 °C



concomitant decrease in the tumbling rate  $\tau_v$  of the liposomes to  $\approx 2 \times 10^{-6}$  (for 250 Å vesicles) as given by Eqn. (1). Furthermore, lateral diffusion  $\tau_{LD}$  of the lipids over the surface of the liposomes is on the order of  $4 \times 10^{-5}$  s as calculated by Eqn. (2). The effective averaging time scale of  $10^{-6}$  s is sufficient to partially average the dipolar interaction, and thus the spectra of SUVs are more highly resolved than that of MLVs (1,2). Seiter and Chan and Horwitz *et al.* (1,49,53) have argued, however, that this degree of motional averaging is not fast enough to account for the degree to which the  $^1\text{H}$  spectra of SUVs are narrowed and that additional sources of motion must be invoked. Thus it has been concluded and shown by the insensitivity of the linewidth of SUVs to viscosity, that below a certain size,  $^1\text{H}$  linewidths are independent of the vesicle tumbling rate (54). The additional modes of motion that contribute to spectral narrowing have been attributed to the local fluctuations of the phospholipid molecule including chain reorientation (55).

In the liquid-crystalline spectra of DPPC SUVs it is also possible to distinguish the inward (high field shoulder) and outward facing choline-methyls (low field shoulder). Shuh *et al.* have shown that for even smaller vesicles, all visible resonances with the exception of the  $\alpha$ -carbonyl methylene are split into those belonging to the inward and outward facing leaflets (56). These effects have been ascribed to the differences in packing constraints between the two halves of the bilayer imposed by the small radius of curvature.

As the temperature is lowered through the phase transition, all resonances are broadened considerably due to the crystallization of the lipids, the slowing of local chain fluctuations, lateral diffusion (and perhaps reduction in the tumbling rate due to aggregation). A proportionately larger contribution of the choline methyls are retained (Chan *et al.* have reported 100% of the intensity to be visible) relative to the fatty acids,

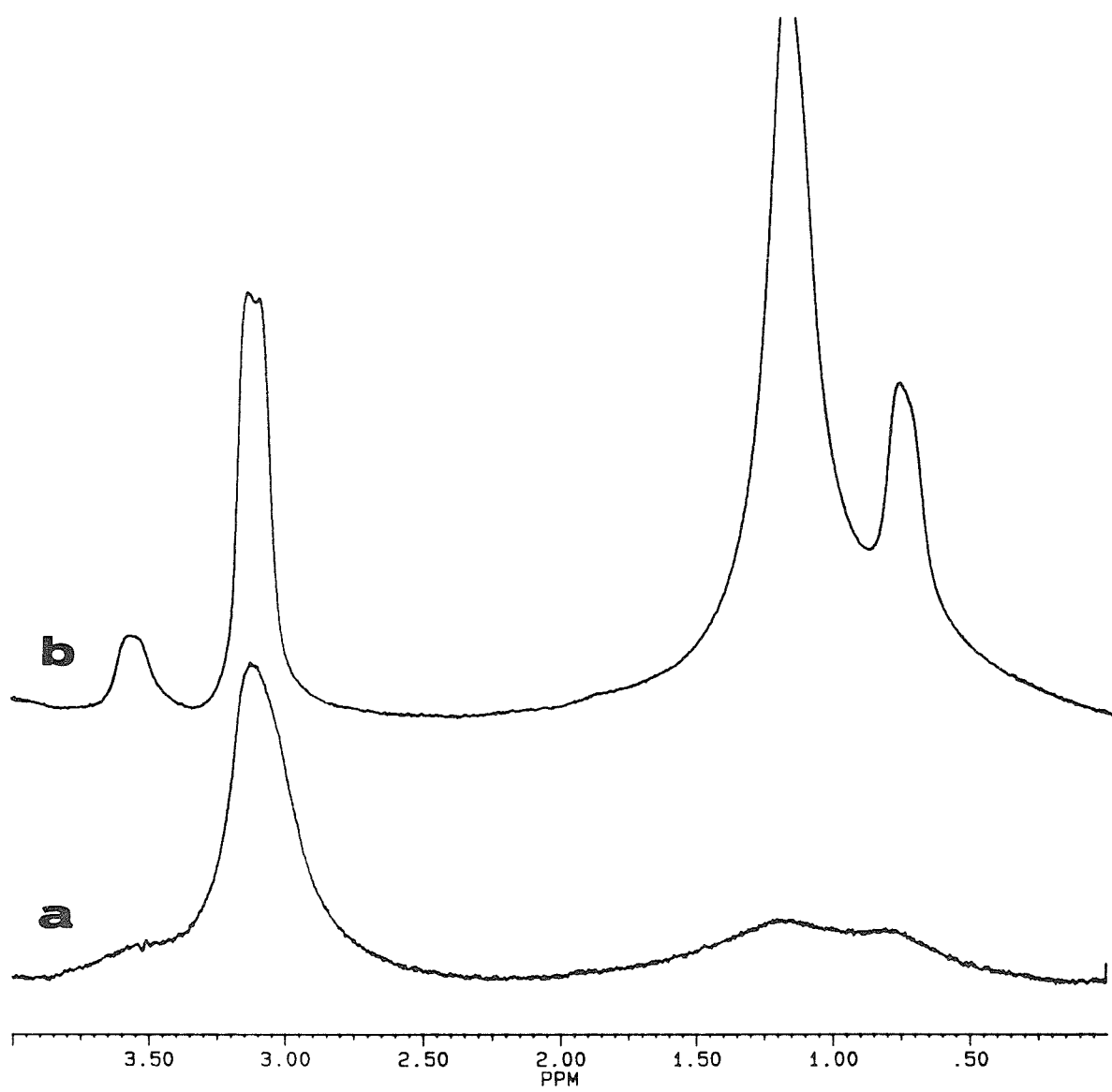
which are almost undetected at 298°C. This indicates a relatively higher mobility for the headgroup relative to the chains.

Figure 10 shows the  $^1\text{H}$  NMR spectra of sonicated  $\alpha$ -16 and  $\alpha$ -18 liposomes in the gel and liquid-crystalline state. In contrast to liquid-crystalline MLVs, which show more highly resolved spectra compared to DPPC MLVs, the liquid-crystalline SUVs are less well resolved. In particular there is no distinction between the inside and outside choline resonances despite the fact that these vesicles were found to be approximately the same size in repeated preparations. The increase in breadth is due to the restricted bilayer expansion and subsequent restricted rates of lateral diffusion and local motions (rotational diffusion, chain tilting) relative to nonpolymerizable lipids in the liquid-crystalline state. In the gel state, by contrast, there appears to be at least as much or a greater contribution from the chains despite the motional constraints imposed by polymerization on the motions of the lipids as a whole. These results are consistent with the analysis of the  $^1\text{H}$  linewidths in the MLVs. We therefore suggest that polymerization inhibits crystalline chain packing in the gel state to the extent achieved by nonpolymerizable analogues and that the increased volume available allows for greater rates or amplitudes of local fluctuations in the hydrocarbon portion of the chain. Furthermore, these fast local motions must more than compensate for the necessarily slow rotational and lateral diffusion of the polymerized phospholipids such that the effective motion of the polymeric acyl chains is greater than that of the nonpolymerizable analogues. This is not an intuitive result.

$^1\text{H}$  NMR of  $\omega$ -THIOLS. For completeness, Figure 11 shows the  $^1\text{H}$  NMR of bath-sonicated polymeric  $\omega$ -16 at 25°C and 66°C. Bath sonication was used in lieu of probe sonication since the latter results in immediate precipitation of the bilayers. Successful sample preparation is more the exception than the rule. The difficulty in preparing NMR-visible particles is due to the fact that the  $\omega$ -THIOLS form bilayer

**Figure 10**

$^1\text{H}$  NMR of  $\alpha$ -16 SUVs in  $\text{D}_2\text{O}$  at : **A.** 7 °C, **B.** 32 °C and  $\alpha$ -18 SUVs in  $\text{D}_2\text{O}$  at **C.** 29 °C; **D.** 50 °C



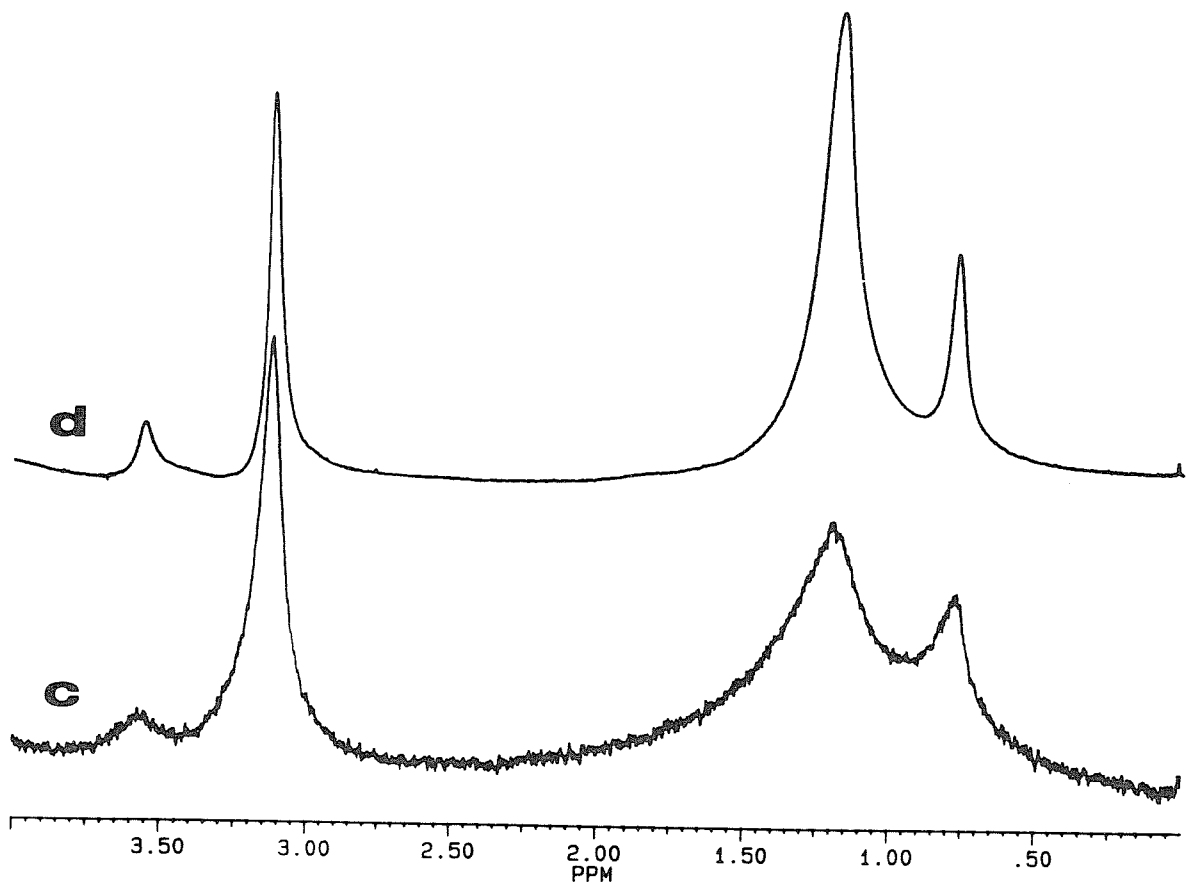
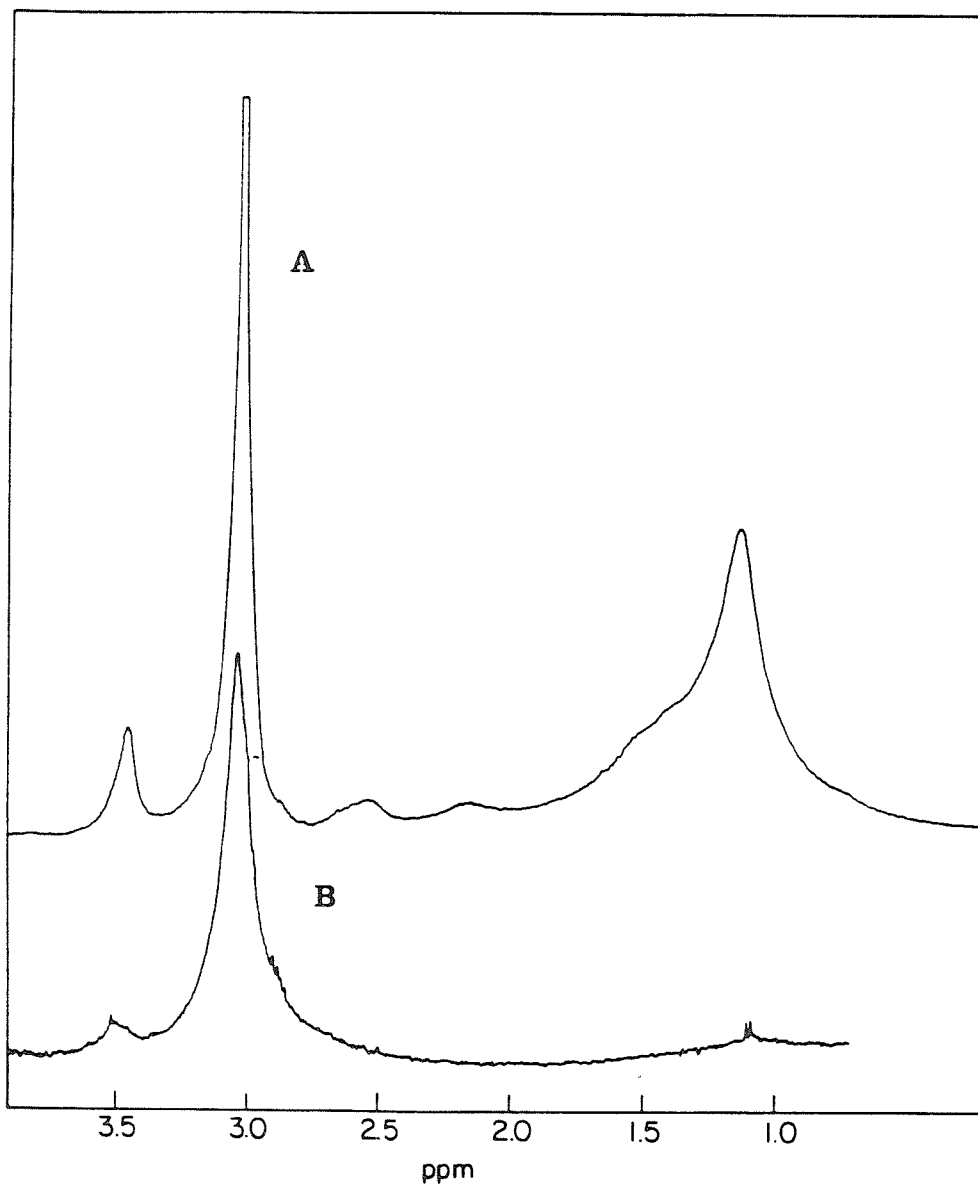


**Figure 11**

$^1\text{H}$  NMR of bath sonicated  $\omega$ -16 bilayer fragments in  $\text{D}_2\text{O}$  at **A.** 60°C and **B.** 25 °C



fragments, not closed liposomes. Therefore the bath sonication most likely temporarily disaggregates or reduces the size of the fragments. The spectra, which were taken immediately after sample preparation, broadened very quickly with time due to aggregation. Nonetheless, it is clear that upon raising the temperature the acyl chains acquire greater mobility despite the fact that they are polymerized at the chain terminus.\* On the other hand, compared to the  $\alpha$ -THIOLS or nonpolymerizable analogues, the contribution of chain protons relative to the choline headgroup is relatively small, indicating restricted motion.

## CONCLUSIONS

In this study,  $^{13}\text{C}$  spin-lattice relaxation and  $^1\text{H}$  NMR experiments were carried out to evaluate the dynamic behavior of polymerized  $\alpha$ - and  $\omega$ -THIOLS. In particular, we were interested in (i) making a comparison of polymerizable versus nonpolymerizable lipids and (ii) in elucidating the effect of the position of the polymerizable moiety on the motional state of the bilayer. The following is a précis of the major conclusions:

### $\alpha$ -16 versus DMPC Liposomes.

(i) Comparison of the spectral features of DMPC liposomes to polymerized  $\alpha$ -16 liposomes indicated that the polymerization-induced rigidification of the membrane is primarily localized to the interfacial region including the glycerol backbone and the first few segments of the acyl chains. With progressive distance towards the methyl terminus of the acyl chains, the effect of the disulfide linkage is less obvious; spectral linewidths and  $T_1^{-1}$  become less distinguishable between the polymerized versus nonpolymerized aggregates, at least at temperatures just above the

---

\* An alternative possibility which cannot be completely ruled out is that the temperature causes disruption of the bilayer fragments into smaller particles. The faster tumbling rate of the smaller fragments could then lead to more effective motional averaging of the dipolar interactions.

phase transition temperature. In fact, based on spin-lattice relaxation times, polymerized  $\alpha$ -THIOLS were shown to maintain one of the characteristic features of conventional phospholipid bilayers - that of a mobility (or fluidity) gradient. This is due to the fact that the position of the polymerizable moiety is at the interfacial region, which is the most rigid portion of a normal bilayer.

(ii) The temperature dependences of the  $^{13}\text{C}$  relaxation rates in polymeric  $\alpha$ -16 SUVs were less pronounced than those of DMPC. Based on current theories, this can be interpreted in one of two ways: (A) that the activation energies for segmental isomerization is less for polymeric  $\alpha$ -THIOLS (Arrhenius model) or (B) that the temperature dependence of the order parameter (and therefore the bilayer expansion coefficient) is less.

A is difficult to rationalize. One would expect that segmental isomerizations would be more difficult for the polymer, which is not what the data implies based on an Arrhenius interpretation. While we have no data to suggest one explanation is better than the other, a reduction of the temperature dependence of the order parameter (B) implying a lower thermal expansion coefficient is conceptually appealing. The intervening covalent linkages between phospholipids should inhibit (i) the lateral expansion of the bilayer along the direction of the polymer chains and (ii) the extent to which the rates of rotational diffusion, off axis wobbling and a number of other motions can increase with temperature. In other words, with increasing temperature in the liquid-crystalline state, polymerized  $\alpha$ -THIOLS cannot achieve the degree of disorder attained by nonpolymerizable lipids.

(iii)  $^1\text{H}$  NMR studies of polymerized  $\alpha$ -THIOL MLVs reconfirm the fact that the  $\alpha$ -THIOLS tend to form a heterogeneous but generally smaller distribution of liposomes. However, spectra of SUVs in the liquid-crystalline state are much broader

than those of nonpolymerizable analogues. This is most likely due to the restricted rotational diffusion and other local motions of the polymerized lipids, which have been shown to be important determinants of the proton linewidth (5,49,52). By contrast, it appears that certain local motions (segmental isomerization or reorientation of the *acyl chains*) may be more rapid or of greater amplitude in gel state polymeric SUVs and MLVs than gel state nonpolymerizable analogues. The latter is consistent with Raman and FT-IR studies, which show that the hydrocarbon region of polymeric  $\alpha$ -THIOLS are more disordered than in the monomers or nonpolymerizable lipids.

(iv) In conclusion, the  $^{13}\text{C}$  and  $^1\text{H}$  NMR studies suggest that in the gel state, the hydrocarbon chains of polymeric  $\alpha$ -THIOLS are more disordered and have faster local motions. This is because polymerization adds steric bulk and reduces the conformational freedom of the lipids to pack into tight crystalline arrays. By contrast, in the liquid-crystalline state, the extent to which the membranes can become disordered is limited by the reduced rotational and lateral diffusion of the phospholipids as a whole, as well as the reduced thermal expansion coefficient of the bilayer.

#### Polymeric $\omega$ -8 and DBPC Micelles.

(i) In contrast to  $\alpha$ -16 SUVs, all resonances of polymeric  $\omega$ -8 "micelles" were resolvable. Based on the effective sizes as measured by dynamic light scattering, this was actually contradictory to what would have been anticipated since the spin-spin relaxation rates are sensitive to the slow motions of the lipid aggregates (i.e., vesicle and micelle tumbling). Since the size of polymeric  $\omega$ -8 was substantially greater than that of  $\alpha$ -16 liposomes, much broader spectral features were expected. However, the light scattering measurement is sensitive to *macroscopic* viscosity of the sample and not to the *microscopic* viscosity. It therefore seems quite likely that the spectral narrowing stems from the fact that there is a high dynamic nature to the gross

aggregate structure and that the particles are effectively tumbling at a much more rapid rate than that expected for a thick gelatinous suspension.

(ii)  $^{13}\text{C}$  spin-lattice relaxation measurements of polymeric  $\omega$ -8 relative to D8PC micelles indicated substantially reduced motions in the acyl chains of the polymer whereas the effect on the headgroup carbons was less pronounced. This suggests that the motions sensed by the relaxation measurements are *primarily* fast segmental motions. Rotational and lateral diffusion of the individual phospholipids in the polymer *must* be slowed, but these motions should uniformly affect all the carbons in the phospholipid.

(iii) Since the polymerized  $\omega$ -8 lipids are effectively tethered by the polar group at the interface as well as by the disulfide group at the chain terminus, no mobility gradient was observed along the acyl chains. This contrasts sharply to the polymeric  $\alpha$ -16 SUVs as well as nonpolymerizable phospholipid aggregates, which have mobility gradients, and illustrates the importance of the position of the polymerizable moiety in determining the dynamic properties of micelles and bilayers. Furthermore, this implies that the gradients observed in  $\omega$ -THIOLS using depth dependent anthroyloxy probes (Chapter III) are gradients of structural disorder, not mobility.

(iv) Although only two temperatures were examined, the similarity in the temperature dependence of  $T_1^{-1}$  for D8PC and  $\omega$ -8 micelles suggests that the lateral expansion coefficient of the aggregates are more comparable than that of  $\alpha$ -16 versus DMPC. Furthermore, despite the disulfide linkage at the chain terminus of  $\omega$ -8, the hydrocarbon region can become quite disordered. This is most easily visualized if

intraleaflet coupling\* is assumed, as discussed in Chapters II and III, since that construction should allow a greater amount of gauche conformers to be introduced into the chain segments.

### Implications in Terms of Other Membrane Properties.

As has been described in the last several chapters, the physical properties of polymeric  $\alpha$ -THIOLS, especially with respect to morphology, more nearly resemble those of nonpolymerizable phospholipids than the  $\omega$ -THIOLS.  $\alpha$ -THIOLS have been shown to retain a liposomal structure upon polymerization and even to form self-sealed bilayers from a prepolymerized state. By contrast, the  $\omega$ -THIOLS form liposomes in the unpolymerized state, but upon polymerization, these closed structures break up into bilayer fragments with no identifiable aqueous compartment. The basis of this behavior may be due to the dynamic properties of the two types of phospholipids. In the case of polymeric  $\alpha$ -THIOLS, a fluidity/mobility gradient is retained, and thus defects that are formed in the hydrocarbon region by, e.g., thermal alterations, can be compensated for by a rearrangement of the chain conformation, similar to what occurs in nonpolymerizable phospholipids. In the case of  $\omega$ -THIOLS, however, no mobility gradient was detected and therefore the introduction of membrane defects or structural disorder may be more difficult to amend, thereby causing fragmentation. On the basis of fluorescence polarization experiments, it now seems quite clear that there is indeed a gradient of structural disorder introduced in the liquid-crystalline state of these lipids which may ultimately lead to loss of liposomal integrity.

---

\* Intraleaflet coupling is not a strictly valid term for a micelle (although these may actually be small bilayer fragments). In any case, the implication is that polymerization occurs between neighboring lipids whose chains and headgroups are oriented essentially in the same direction.

### Future Experiments and Solid State $^{13}\text{C}$ NMR.

Based on the discussion presented in the background and theory section, it would clearly be interesting to examine the frequency dependence of the spin-lattice relaxation rates of the lipids described in this chapter in order to abstract the correlation times of the fast motions, the relative contribution of fast and slow motions to  $T_1^{-1}$ , and whether or not the cooperative (collective) slow motions demonstrated for DPPC liposomes are maintained in polymerized membranes. Furthermore, since polymerization undoubtedly reduces certain slow motions of the lipid as a whole (i.e., rotational and lateral diffusion), rotating-frame spin-lattice relaxation experiments, which are sensitive to slow motions intermediate between  $T_1$  and  $T_2$ , should provide substantial insight into the modulation of the dynamic behavior of phospholipids as a consequence of polymerization (5, 26). Finally, solid state magic angle sample spinning (MASS) techniques could be employed to carry out such experiments without the necessity of sonication or the need for the samples to be in the liquid-crystalline state. In the studies reported in this chapter, it was not possible to examine the relaxation behavior of long chain polymeric  $\omega$ -THIOLS due to the fact that they aggregate and form fragments that cannot be sonicated into particles small enough to be visible by conventional high resolution techniques. However, using solid state techniques these systems should be amenable to study. The following briefly describes our initial results and the potential utility of solid state MASS for studying liposomes:

Preliminary Solid State MASS Spectra We have already initiated some solid state  $^{13}\text{C}$  MASS experiments and although they are not complete, some results are included here to demonstrate the utility of the approach. Figure 11 shows spectra of a variety of *unsonicated* lipid dispersions taken at room temperature with magic angle sample

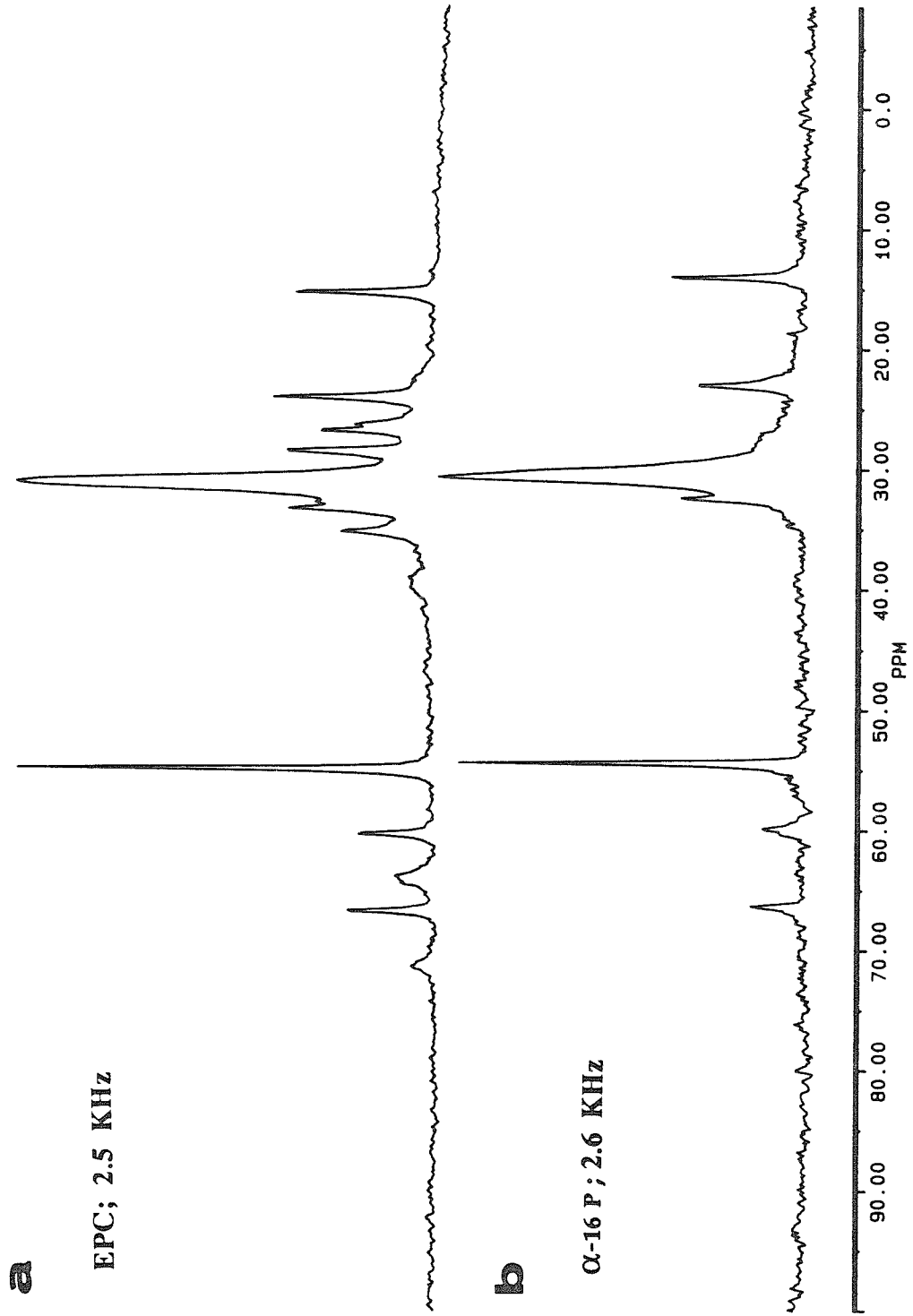
spinning (the spinning frequencies are noted in the spectra and legend). The differences in the resolution from sample to sample is a function primarily of the phase transition temperatures of the lipids: EPC is in the liquid-crystalline state at room temperature; polymeric  $\alpha$ -16 is neither completely in the gel state or completely in the liquid-crystalline state as it has a broad transition with a maximum approximately at room temperature; DPPC has a transition slightly above room-temperature (41.7°C) and polymeric  $\omega$ -15 has a phase transition well above 50°C. The greatest resolution is therefore achieved for EPC, which has a fair degree of mobility due to its phase state, whereas polymeric  $\omega$ -15 and  $\alpha$ -20 have much less resolution of the acyl chains. With higher spinning rates it should be possible to obtain a comparable degree of resolution as was obtained for EPC using lipids that have transition temperatures well above room temperature. This, however, raises one of the current difficulties that was encountered in these exploratory studies: the difficulty in achieving rapid, homogeneous spinning rates. The speed and stability that could be obtained varied from sample to sample and while it seems to be due to problems with the rotor design, it is clearly not an insurmountable problem. Given improved rotors, higher rates should be easily achieved (dry samples depending on their density may be currently spun at 14 kHz). Furthermore, thermal control will allow examination of samples in both the gel state as well as in the liquid-crystalline state.\*

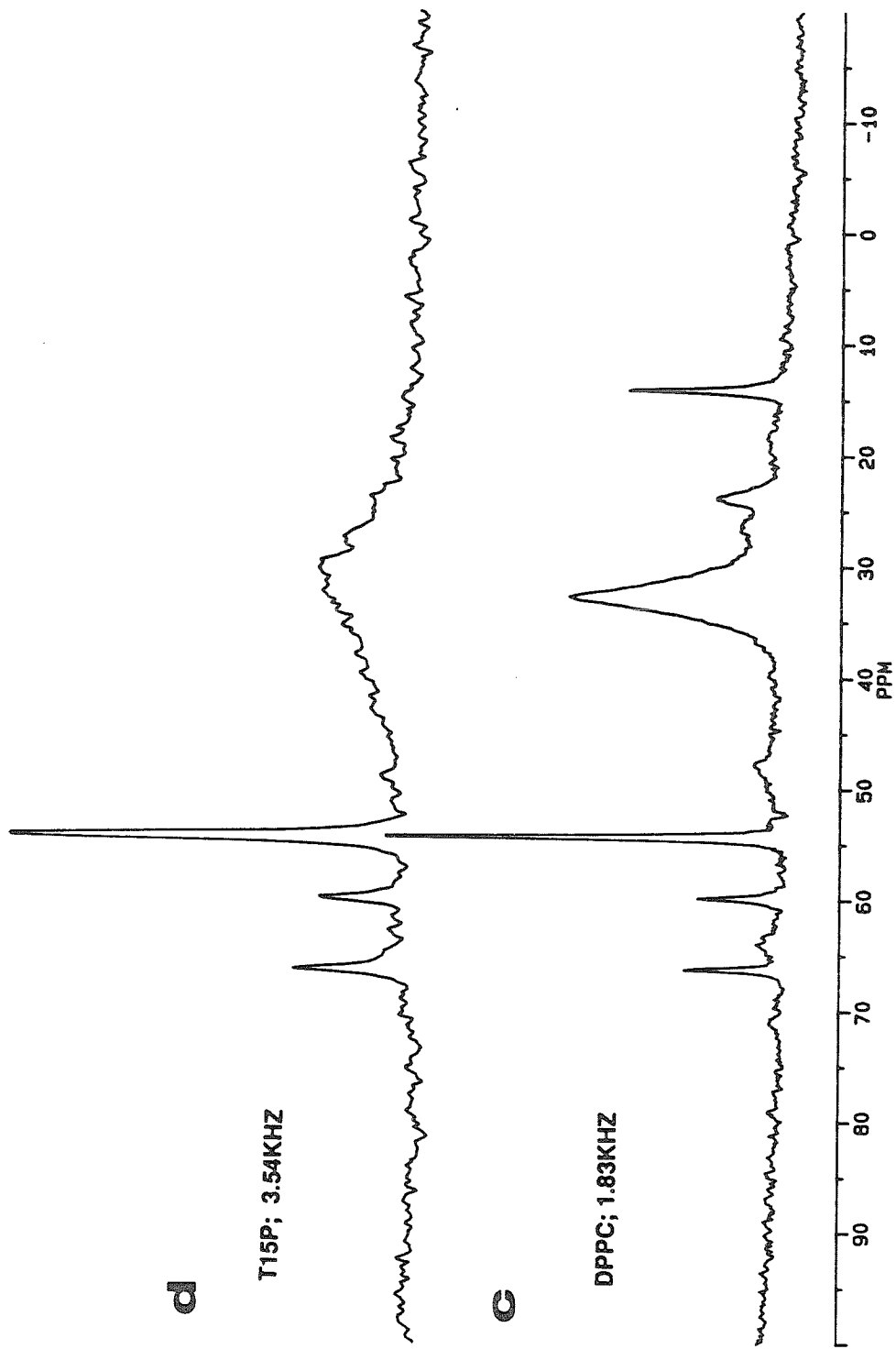
---

\* Studies of sonicated liposomes using high resolution techniques have been predominantly devoted to lipids in the liquid crystalline state due to the relatively featureless spectra obtained for sonicated gel state lipids. Oldfield *et al.* have shown that one can even observe cholesterol in lipid dispersions using MASS. Thus these experiments should greatly increase the variety of lipid systems that can be examined and the conditions under which the experiments can be carried out.

**Figure 11**

$^{13}\text{C}$  MASS spectra of lipid dispersions in  $\text{H}_2\text{O}$  containing .5 mM EDTA. Measurements were made at ambient temperature and at the spinning frequencies indicated in the spectra: **A.** EPC ; **B.** Polymeric  $\alpha$ -16 **C.** DPPC ; **D.** Polymeric  $\omega$ -15.





**d**

T15P; 3.54KHZ

**c**

DPPC; 1.83KHZ

### REFERENCES

1. Chan, S.I, Bocian, D.F. and Petersen, N.O. in: *Membrane Spectroscopy* ; Grell, E. (Ed.); Berlin Heidelberg: Springer Verlag, 1981; 1-50.
2. Bocian, D.F., Chan S.I. (1978) *Ann. Rev. Phys. Chem.* **29**, 307-335.
3. Marsh, D. in : *Liposomes from Physical Structure to Therapeutic Applications* ; Knight, C.G. (Ed.); Elsevier: North Holland Biomedical Press, 1981; 139-188.
4. Browning, J.L. in : *Liposomes from Physical Structure to Therapeutic Applications* ; Knight, C.G. (Ed.); Elsevier: North Holland Biomedical Press, 1981; 223-258.
5. Davies, J.L. (1986) *Chem. Phys. Lipids* **40**, 223-258.
6. Browning, J. L. (1981) *Biochemistry* **20**, 7123-7151.
7. Kainosho, M., Kroon, P.A., Lawaczeck, R., Petersen, N.O. and Chan, S.I. (1978) *Chem. Phys. Lipids* **21**, 59-68.
8. Banerjee, U., Zidovetzki, R., Birge, R., Chan, S.I. (1985) *Biochemistry* **24**, 7621-7627.
9. Ellena, J., Pates, R. and Brown, M.F. (1986) *Biochemistry* **25**, 3742-3748.
10. Killan, J.A., Borle, F., De Kruiff, B. and Seelig, J. (1986) *Biochim. Biophys. Acta.* **854**, 133-142.
11. Lewis, B. A., Das Gupta, S.K. and Griffin, R.G. (1984) *Biochemistry* **23**, 1988-1993.
12. Urbina, J. and Waugh, J.S. (1974) *Proc. Natl. Acad. Sci. U.S.A.* **71**, 5062-5067.
13. Cornell, B.A., Hiller, R.G., Raison, J., Separovic, F., Smith, R., Vary, J.C. and Morris, C. (1983) *Biochim. Biophys. Acta.* **732**, 473-478.

14. Lee, C.W.B., Waugh, J.S. and Griffin, R.G. (1986) *Biochemistry* **25**, 3737-3741.
15. Forbes, J., Husted, C. and Oldfield, E. (1988) *J. Am. Chem. Soc.* **110**, 1059-1065.
16. Cornell, B.A., Davenport, J.B. and Separovic, F. (1982) *Biochim. Biophys. Acta.* **689**, 337-345.
17. Lee, C.W., Waugh, J.S. and Griffin, R.G. (1986) *Biochemistry* **25** , 3737-3741.
18. Laschewsky, A., Ringsdorf, H. and Sneider, J. (1986) *Die Angewandte Makromolekulare Chemie* **145/146** ,1-17.
19. O'Brien, D.F., Klingbiel, R.T., Specht, D.P. and Tyminski, P.N. (1985) *Ann. N.Y. Acad. Sci.* **446**, 282-295.
20. Hupfer, B., Ringsdorf, H. and Schupp, H. (1983) *Chem. Phys. Lipids* **33**, 355-374.
21. Regen, S.L., Yamaguchi, K., Samuel, N.K.P., and Singh, M. (1983) *J. Am. Chem. Soc.* **105**, 6354.
22. Samuel, N.K.P., Singh, M., Yamaguchi, K. and Regen, S.L. (1985) *J. Am. Chem. Soc.* **107**, 42-47.
23. Ebelhäuser, R. and Fahmy, T. (1984) *Makromol. Chem., Rapid Comm.* **5**, 333-336.
24. Pons, M., Villaverde, C. and Chapman, D. (1983) *Biochim. Biophys. Acta.* **730**, 306-312.
25. Brown, M.F., and Williams, G.D. (1985) *J. Biochem and Biophys. Methods* **11**, 71-81.
26. Brown, M.F., (1984) *J. Chem Phys.* **80**, 2808-2836.

27. Brown, M.F., Ribiero, A.F., Williams, G.D. (1983) *Proc. Natl. Acad. Sci. U.S.A.* **80**, 4325-4329.
28. Tricot, Y., Kiwi, J., Niederberger, W. and Grätzel, M. (1981) *J. Chem Phys.* **85**, 862-870.
29. Wennerström, H., Lindman, B., Söderman, O., Torbjörn, D. and Rosenholm, J.B. (1979) *J. Am. Chem. Soc.* **101**, 6860-6864.
30. Söderman, O., Walderhaug, H., Henriksson, U. and Stilbs, P. (1985) *J. Phys. Chem.* **89**, 3693-3701.
31. Söderman, O., Henriksson, U. and Olson, U. (1987) *J. Phys. Chem.* **91**, 116-120.
32. Vold, R.L., Waugh, J.S., Klein, M.P. and Phelps, D.E. (1968) *J. Chem. Physics* **48**, 3831.
33. Kowalewski, J., Levy, G.G., Johnson, L.F. and Palmer, M.F. (1977) *J. Magn. Res.* **26**, 533-536.
34. Brown, M.F., Seelig, J. and Habèrlin, U. (1979) *J. Chem. Phys.* **70**, 5045-5053.
35. Brown, M.F. (1982) *J. Chem Phys.* **77**, 1576-1599.
36. Lee, A.G., Birdsall, J.M., Metcalfe, J.C., Warren, G.B. and Roberts, G.C. (1976) *Proc. R. Soc. Lond. B.* **193**, 253-274.
37. Levy, G.C. in: *Topics in Carbon-13 NMR Spectroscopy* ; New York: John Wiley and Sons, 1974.
38. Kuhlmann, K.F., Grant, D.M. and Harris, R.K. (1970) *J. Chem. Phys.* **52**, 3439.
39. Doddrell, D., Glushko, U. and Allerhand, A. (1972) *J. Chem. Phys.* **56**, 3683-3689.
40. Burns, R. A., and Roberts, M.F. (1980) *Biochemistry* **19**, 3100-3106.

41. Brown, M.F. (1982) *J. Chem. Phys.* **77**, 1576-1599.
42. Brown, M.F., Seelig, J. and Häberlen, U. (1979) *J. Chem. Phys.* **70**, 5045.
43. Milburn, M.P. and Jeffrey, K.R. (1987) *Biophys. J.* **52**, 791-799.
44. Seelig, A. and Seelig, J. (1974) *Biochemistry* **13**, 4839.
45. Seelig, J. (1977) *Quat. Rev. Biophys.* **10**, 353.
46. Sölderman, O. and Stilbs, P. (1986) *Chem. Phys. Lipids* **41**, 117-122.
47. Rhodes, D. and Handel, T.M., unpublished results.
48. Petersen, N.O. and Chan, S.I. (1977) *Biochemistry* **16**, 2657-2667.
49. Seiter, C.H.A., and Chan, S.I. (1973) *J. Am. Chem. Soc.* **95**, 7541-7553.
50. Feigenson, G.W. and Chan, S.I. (1974) *J. Am. Chem. Soc.* **96**, 1312-1319.
51. Finer, E.G. (1974) *J. Magn. Res.* **13**, 76-86.
52. Sheetz, M.P. and Chan, S.I. (1972) *Biochemistry* **11**, 4573-4581.
53. Horwitz, A.F., Michaelson, D. and Klein, M.P. (1973) *Biochim. Biophys. Acta.* **298**, 1-7.
54. Chan, S.I., Sheetz, M.P., Seiter, C. H. A., Feigenson, G. W., Hsu, M., Lau, A., and Yau, A. (1973) *Ann. N.Y. Acad. Sci.* **222**, 499-522.
55. Kainosho, M., Kroon, P.A., Lawaczeck, R. and Petersen, N.O. (1978) *Chem. Phys. Lipids.* **21**, 59-68.
56. Schuh, J.R., Banerjee, U., Müller, L. and Chan, S.I. (1982) *Biochim. Biophys. Acta.* **687**, 219-225.

---

## Chapter VI

---

### *Investigations of the Dynamics and Conformation of the Headgroup of Polymerized Phospholipid Membranes by $^{31}\text{P}$ NMR*

---

#### Introduction

The effects of polymerization on the bulk properties of disulfide polymerized phospholipids was examined in Chapter II (morphological properties) and Chapter III (thermal properties). In Chapters IV and V, vibrational spectroscopy and  $^{13}\text{C}$  NMR was employed to examine the conformation and dynamics of the hydrocarbon region of the bilayer. Equally important as the hydrocarbon region, however, is the lipid headgroup. Many studies have demonstrated the importance of headgroup size, charge and the addition of ions on the thermal properties of the lipids as well as the macroscopic morphologies they assume (1-5). For example, phosphatidylethanolamine (PE) and phosphatidylserine (PS) are lipids well known for their propensity to form hexagonal phase tubules upon lowering the pH (PE) or upon addition of  $\text{Ca}^{+2}$  (PS) (6). Secondly, it is the headgroup region that first comes into contact with the components of the surrounding medium such as serum proteins and cell surfaces. From the standpoint of *in vivo* uses of liposomes, the interfacial properties may largely be

involved with the subsequent fate of the phospholipid membrane. As an example, Scherphof and others have demonstrated the effect of headgroup charge on their clearance rates of liposomes from the circulatory system (7).

$^{31}\text{P}$  NMR has proven a useful technique for studying the behavior of phospholipid headgroups in pure lipid systems, in membranes reconstituted with proteins and for studies of the interactions of phospholipids with cholesterol, proteins and ions (8-10). In this chapter is described an investigation of the effect of polymerization on the dynamics and conformational properties of phosphatidylcholine membranes. In particular, we were interested in whether immobilization of the lipid molecules at the interfacial region or chain terminus of the phospholipids had an effect on the conformational and motional properties of the headgroup. Studies in the past have demonstrated that the headgroup reorientation rate is on the order of nanoseconds and largely uncorrelated with the dynamics of the rest of the lipid molecule (11). Based on these data, one might expect that polymerization in either fashion would leave the interfacial properties of the membrane unaltered. On the other hand, in previous chapters we have shown that the packing of the lipids in the membrane is modified by polymerization, which may in turn cause changes in the orientation and motional properties of the headgroup. To examine these possibilities,  $^{31}\text{P}$  spin-lattice relaxation times ( $T_1$ ) and cross polarization measurements were carried out to examine the *dynamic* behavior of polymerized versus unpolymerized membranes. To obtain information concerning the *conformational* properties of the headgroup, the chemical shift anisotropy and its temperature dependence are also evaluated.

## MATERIALS AND METHODS

### Materials.

The synthesis and polymerization of the disulfide polymerizable phosphatidylcholines was as described in Chapter VIII. Routinely the polymerized form of the lipid was stored at 4°C until used. L- $\alpha$ -dipalmitoylphosphatidylcholine (DPPC) and L- $\alpha$ -dimyristoylphosphatidylcholine (DMPC), were purchased from Avanti Polar Lipids. All other reagents were of analytical grade and used without further purification.

### **Methods.**

*Liposome Preparation.* For  $^{31}\text{P}$  spin-lattice relaxation studies, small unilamellar vesicles (30-75 mg/ml) were prepared by hydrating nonpolymerizable phosphatidylcholines or prepolymerized  $\alpha$ -THIOLS in Tris buffer (10 mM Tris, 0.2 mM EDTA; pH 7.4) above the phase transition for  $\approx$  15 min. Sonication was subsequently carried out using a Heat Systems 350 W probe sonicator until a constant level of optical clarity was achieved. During sonication, the samples were placed under a stream of nitrogen and in a room temperature water bath to avoid lipid degradation. Titanium particles and large liposomes were removed from the SUVs by centrifugation at 12000 x g for 5 minutes in an eppendorf centrifuge.

For CSA studies of unsonicated bilayers, lipids were hydrated in Tris buffer (10 mM Tris, 0.2 mM EDTA; pH 7.4) for 15-30 minutes above the phase transition temperature. Samples for cross polarization experiments were hydrated with excess  $\text{H}_2\text{O}$  containing 0.2 mM EDTA to form a paste. These were centrifuged into ultra-high spinning keflar rotors and sealed with o-ring-containing macor caps (Doty Scientific).

*NMR Measurements.*  $^{31}\text{P}$  MASS spectra were acquired at 202 MHz with a Bruker AM-500.  $^{31}\text{P}$  NMR CSA and relaxation measurements were acquired on either a Bruker AM-500 or a Varian XL200 at frequencies of 202MHz and 80 MHz, respectively.  $^{31}\text{P}$  Chemical shifts are reported with respect to 85% phosphoric acid. All powder spectra

were apodized with 200Hz linebroadening prior to fourier transformation. Spectra were recorded with inverse gated decoupling. During the aquisition time, 10 W broad band or 40 W CW decoupling was applied for sonicated and unsonicated samples, respectively. Spin-lattice relaxation times were measured using the inversion recovery sequence  $(180 - \tau - 90)$ , a 90 degree pulse width of 23  $\mu$ s and a recycle delay of at least 3-5 times  $T_1$ . For all measurements,  $T_1$  values were determined by a least squares fit to the three parameter Eqn. (1) as described in Chapter V:

$$(1) \quad S(t) = A + B \exp\left(\frac{-t}{T_1}\right)$$

Cross polarization magic angle spinning (CP MASS) was used to determine the rate of  $^1\text{H}$ - $^{31}\text{P}$  cross polarization  $(T_{\text{PH}})^{-1}$  and the return to equilibrium of the proton magnetization  $(T_{1\rho})^{-1}$ . The intensity of the phosphorous signal as a function of contact time was fit to a double exponential rise and decay similar to that used for studies of  $^{13}\text{C}$  CP experiments (12):

$$(2) \quad I = A \exp\left(\frac{-t_m}{T_{1\rho}}\right) \left[ 1 - \exp\left(\frac{-t_m}{T_{\text{CH}}}\right) \right]$$

where A is a constant, I is the intensity of the phosphorous signal and  $t_m$  is the contact time.

## RESULTS

### Spin Lattice Relaxation Measurements

*Background.* In this first section, we describe the results of spin-lattice relaxation measurements ( $T_1$ ) of polymeric and nonpolymerizable phospholipid membranes.  $T_1$  measurements provide information concerning the rate and amplitudes motions. As described in the last chapter, however, quantitative analysis of the relaxation times to

derive correlation times for molecular reorientation can be quite complicated in anisotropic systems. Interpretation of the data can be further aggravated if the nucleus under study can relax by more than one relaxation mechanism. In the case of  $^2\text{H}$  and  $^{13}\text{C}$  NMR, the relaxation rates are governed by the quadrupolar and dipolar interactions, respectively. However, in the case of  $^{31}\text{P}$  NMR, relaxation can occur by a combination of both dipolar and chemical shift anisotropy (CSA) such that:

$$(3) \quad \frac{1}{T_1} = \frac{1}{T_{1D}} + \frac{1}{T_{1\text{CSA}}}$$

where  $T_{1D}$  and  $T_{1\text{CSA}}$  are the relaxation times due to the dipolar and CSA, respectively. The relative contribution of either mechanism depends on the field strength: the contribution from chemical shift anisotropy increases with field strength while the dipolar contribution decreases. Milburn and Jeffrey have evaluated the relative contribution of the two mechanisms at various field strengths and have demonstrated the predominance of CSA at 145 MHz (11). Consequently, at the magnetic field strengths employed in this study (202 MHz), the CSA should be the exclusive relaxation pathway.

For isotropically reorienting systems, the relaxation rate due to chemical shift anisotropy is given by the expression (12):

$$(4) \quad \frac{1}{T_{1\text{CSA}}} = \alpha \omega_p^2 (\Delta\sigma)^2 J(\omega) = \alpha \omega_p^2 (\Delta\sigma)^2 \frac{\tau_c}{1 + \omega_p^2 \tau_c^2}$$

where  $\omega_p$  is the Larmor frequency,  $\Delta\sigma$  is the chemical shielding anisotropy that is averaged by the molecular motion,  $\tau_c$  is the correlation and  $\alpha$  is an empirical constant. This equation is based on the spectral density  $J(\omega)$  for a *single* effective correlation time and has been used by a number of investigators to abstract correlation times and activation energies for the phosphate group reorientation (11,13). Whether or not this is

a correct model is, however, controversial. In the last chapter we summarized the current approach for modeling  $^{13}\text{C}$  relaxation rates in terms of a two correlation time model. Nonetheless, without invoking a model or even having any knowledge about the relative contribution of the chemical shift anisotropy versus dipolar relaxation pathways, one can still obtain useful semi-quantitative information from the temperature dependence of the  $T_1$  if a minimum in the relaxation time can be observed. This is due to the fact that at the  $T_1$  minimum, the correlation time is equal to the reciprocal of the larmor frequency of the phosphorous nucleus (i.e.,  $\omega_{\text{P}}^{-1} \approx \tau_{\text{c}}$ ) (12). This is the approach we have taken in this study.

*The Validity of Studying Sonicated Liposomes.* Before presenting the data, a few points should be made concerning the differences in our experimental approach compared to that taken by other investigators who have also examined the temperature dependence of  $T_1$  to obtain the  $T_1$  minimum (11,13). In these earlier studies, multilamellar vesicles (MLVs) rather than sonicated vesicles (SUVs) have been used in order not to complicate the interpretation of the data by the possible contribution of the motion due to the vesicle tumbling. Using the Stokes-Einstein relation, for 500 Å SUVs the tumbling rate can be calculated to be  $1.6 \times 10^{-6}$  s compared to 1.5 s for a 5 µm MLV. However, the observation of the  $T_1$  minimum is a result of selecting for motion of the phosphate group at  $\omega_{\text{O}}^{-1}$  which is  $5 \times 10^{-9}$  s at the operating frequency of the experiments described here, and much shorter than the vesicle tumbling rate even for the SUVs. Consequently, vesicle tumbling of SUVs should not affect the  $T_1$  minimum. On the other hand, use of multilamellar dispersions which give rise to powder spectra due to the orientational dependence of the chemical shielding effect, may be complicated by the orientational dependence of  $T_1$ .\* In the experiments carried out by Milburn (11), Seelig (14) and Ghosh (13), the lipids under study were unsaturated and

---

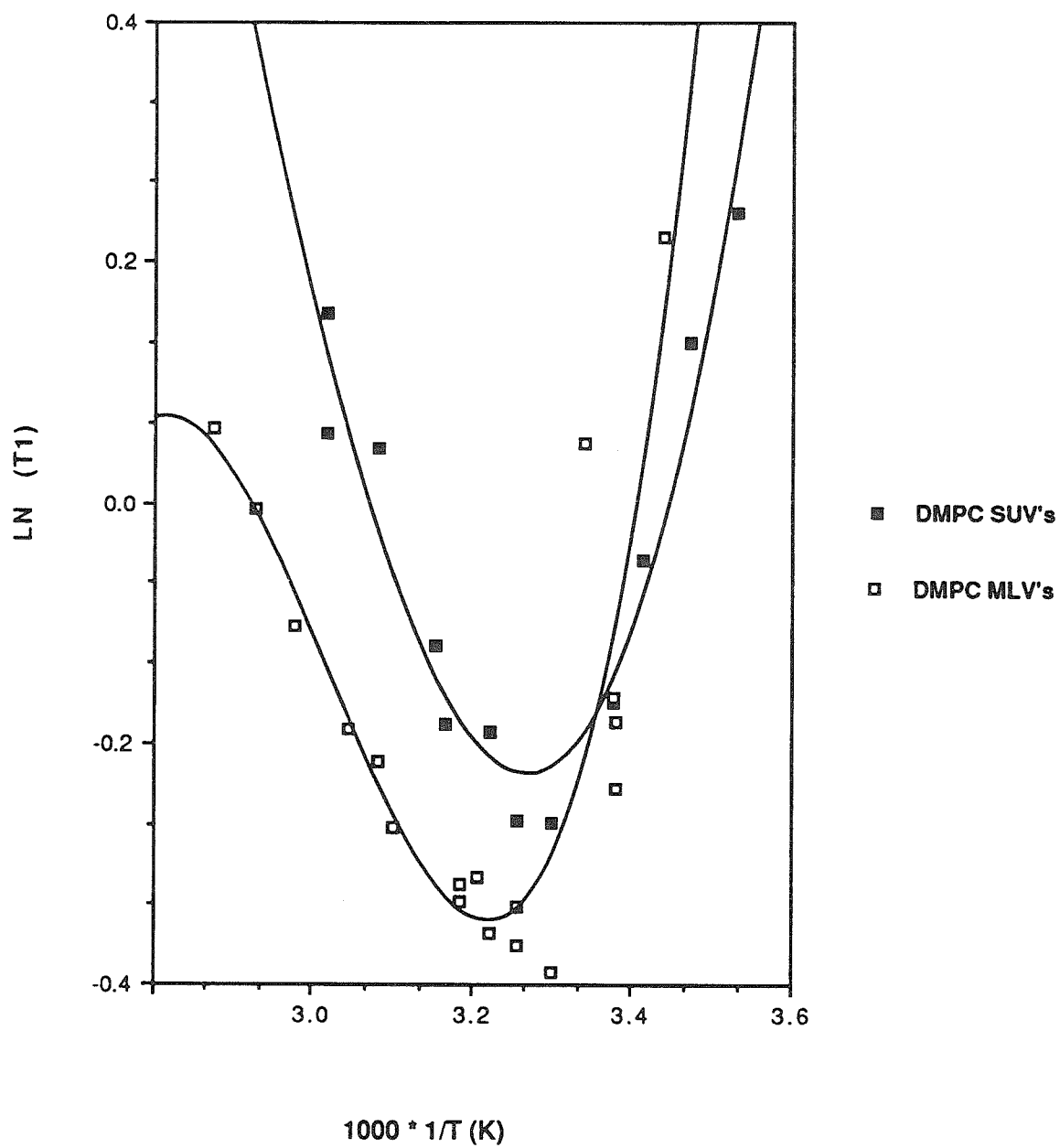
\*A typical powder spectra for an unsonicated MLV is shown in Figure 7.

in the *liquid-crystalline* state throughout the temperature range of the study. It was shown that there was no orientational dependence to the relaxation rate: all portions of the powder spectra recovered with the same time constant presumably due to the rapid diffusion of the phospholipids over the surface of the liposome. In the present study, however, the lipids under investigation are (i) in the *gel* state and (ii) *polymerized* in some cases. Regarding (ii): Comparison of the data obtained from polymerized versus nonpolymerized MLVs might be complicated by the slow diffusion rates of the polymers in the plane of the bilayer relative to the diffusion of nonpolymerized liposomes. Regarding (i): We examined the temperature dependence of DMPC multilamellar vesicles and found that in the *gel* state, there *was* an orientational dependence. The  $T_1$  was highest for the low field "foot" of the powder spectra and decreased in value across the powder pattern towards the high field edge. For these reasons as well as limitations in the quantity of the polymerizable lipids, experiments in this study were carried out using sonicated vesicles.

Figure 1 shows a  $T_1$  versus temperature profile for DMPC multilamellar vesicles versus sonicated vesicles. As can be seen, the position of the  $T_1$  minimum is almost identical in the two preparations. The minimum for the SUVs occurs at approximately 33 °C whereas for the MLVs, it occurs at 36.5 °C. This slight shifting to lower temperature for the SUVs is indicative of a slightly faster rate of reorientation of the phosphate segment. This is *expected* on the basis of the greater disorder in sonicated versus unsonicated liposomes due to the packing constraints imposed by the small radius of curvature. The major difference arises in the absolute value of the  $T_1$ : the values of the SUVs are elevated with respect to the MLVs. The  $T_1$ s for the MLVs, however, were based on the relaxation rate of the "peak" at the high field edge of the spectra. As mentioned above, we consistently found that this point of the powder spectra gave the lowest values of  $T_1$ . At the point where the isotropic signal should arise (1/3 of the way

**Figure 1**

$^{31}\text{P}$  spin-lattice relaxation time (202 MHz) as a function of temperature for DMPC MLVs and SUVs. The symbols are assigned in the legend.



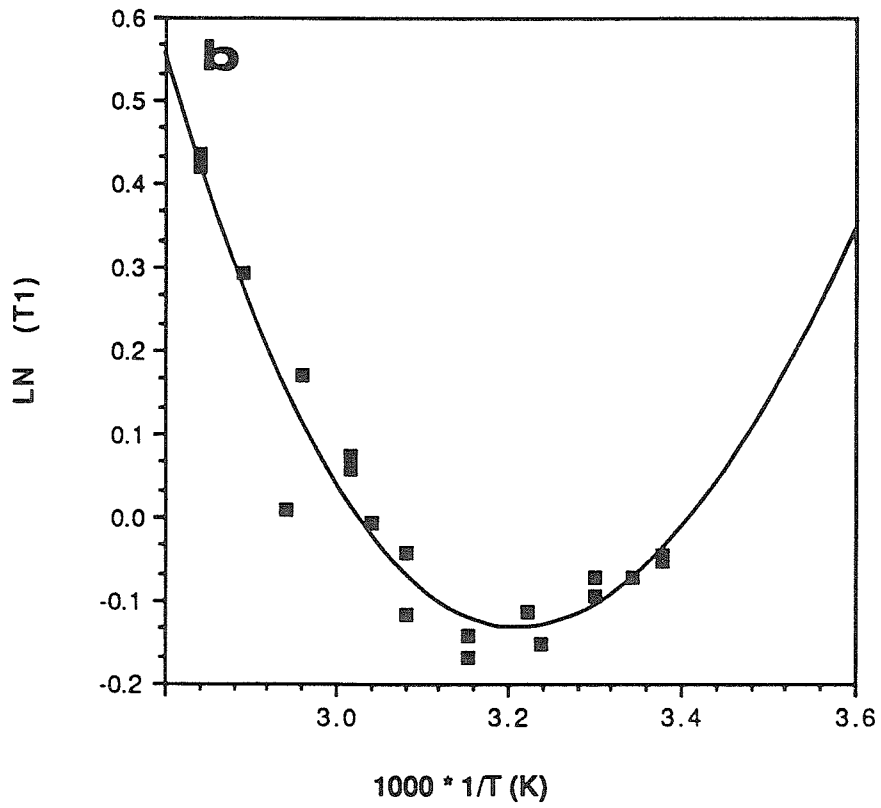
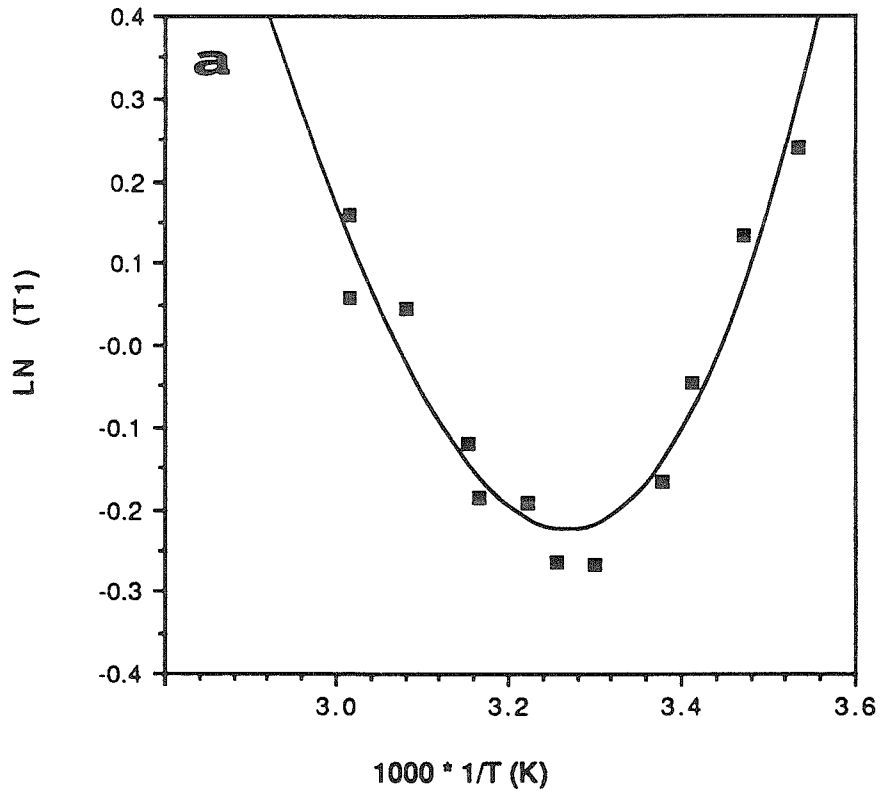
between the left and right edge of the spectra), the  $T_1$ s were higher, and higher still at the low field foot. Consequently, we suspect that the differences in the absolute value of the  $T_1$  for SUVs versus MLVs is a reflection of the orientational dependence in the MLVs. Nonetheless, the important point is that the position of the  $T_1$  minimum, which is the parameter of interest, can be accurately determined using either sonicated or unsonicated liposomes.

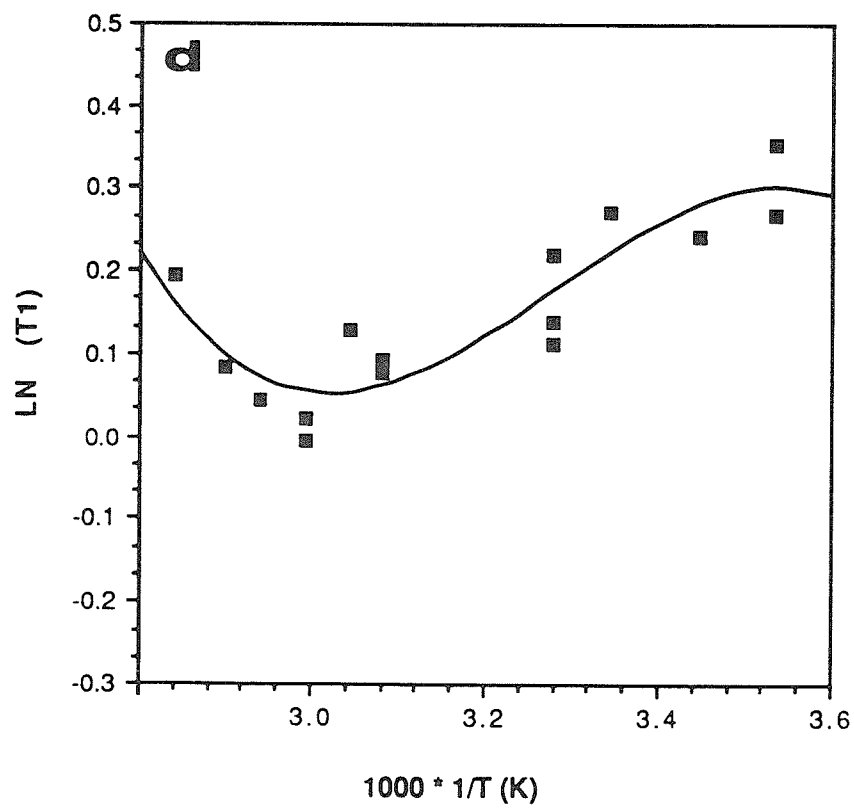
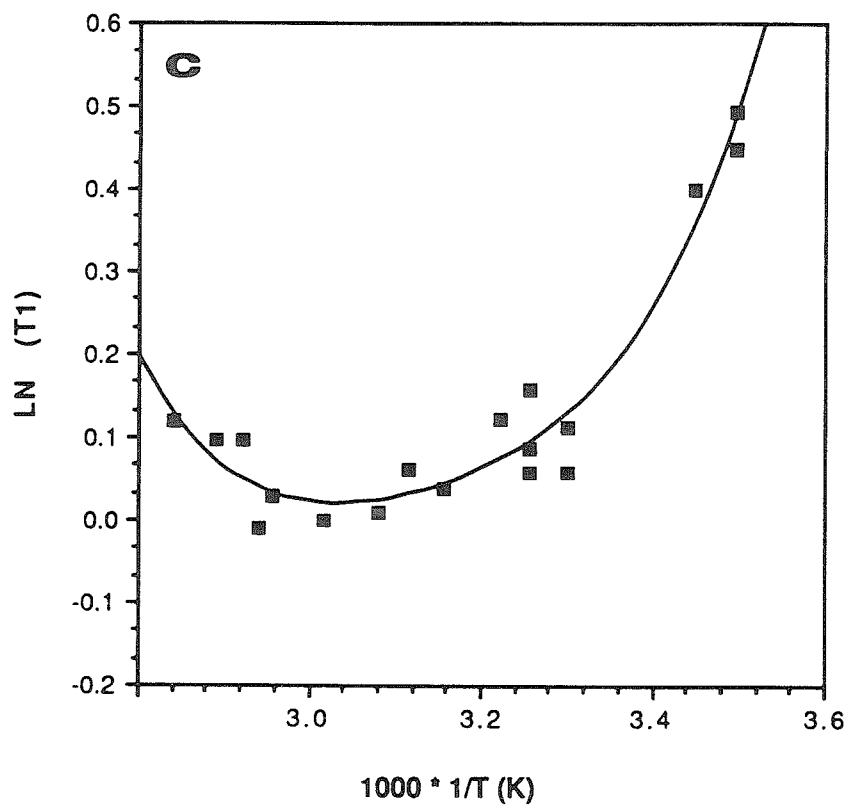
Temperature Dependence of the  $T_1$ ; the Position of the  $T_1$  Minimum. Figure 2 shows plots of the  $T_1$  (202 MHz) versus temperature for SUVs prepared from the nonpolymerizable lipids : (1) DPPC and (2) DMPC as well as the polymerized lipids: (3)  $\alpha$ -16, and (4)  $\alpha$ -20 . In all cases, a minimum in the  $T_1$  was observed. For DPPC, this occurred at  $\approx 40$  °C. While it may be initially tempting to conclude that this is due to the effect of the phase transition, which occurs at  $\approx 40$  °C for this lipid, other liposome types did not show a minimum at their respective phase transition temperatures. Furthermore, if the transition was the source of the minimum, we would expect to see a similar break at 40 °C regardless of the field strength of the measurement. However, at 80 MHz, the minimum appears close to room temperature. Consequently we can conclude that the presence of the minimum near the  $T_m$  of DPPC is purely coincidental.

For DMPC, the  $T_1$  minimum occurs at  $\approx 30$  °C, which is 7 °C above the phase transition of the lipid. The shift of the  $T_1$  minimum to lower temperature for DMPC versus DPPC indicates that the rate of head group reorientation is slightly faster. This is what is expected due to the shorter chain length (14 carbons) of DMPC compared to DPPC (16 carbons). By contrast, the  $T_1$  for the two polymeric  $\alpha$ -THIOLS are shifted to very high temperatures. For  $\alpha$ -16, which has a  $T_m$  near that of DMPC ( $\approx 23$  °C), the minimum occurs at 57 °C. This indicates that the rate and/or amplitude of the motion of the phosphate segment in the polymeric lipid is slower than that of the

**Figure 2**

$^{31}\text{P}$  spin-lattice relaxation times (202 MHz) as a function of temperature for SUVs prepared from: A. DMPC; B. DPPC; C.  $\alpha$ -16; D.  $\alpha$ -20.





nonpolymerizeable liposome. Interestingly, the minimum for polymeric  $\alpha$ -20 is  $\approx 60$  °C which is virtually the same as that for  $\alpha$ -16 within experimental error. This is despite the fact that  $\alpha$ -20 has a 20 carbon chain length and a gel to liquid-crystalline phase transition, which occurs at  $\approx 51$  °C. This suggests that the presence of the disulfide moiety fixes the distance between adjacent phospholipid and reduces the effects of chain length on headgroup packing. (Assuming both polymeric  $\alpha$ -THIOLS adopt the same headgroup conformation, one would then expect the same headgroup packing to give rise to similar reorientation rates in both lipid types).

Apriori, we did not expect to see a reduction in the rate of headgroup motion for the polymers compared to the nonpolymerizeable phospholipid. The basis for our expectations is that it is generally believed that the effective correlation time determined from the phosphorous data does not describe the motion of the molecule as a whole, but rather the motion of the phosphate group relative to the glycerol backbone. More specifically, it has in fact been suggested that the reorientation occurs predominantly about the P-O bond adjacent to the glycerol backbone (11). Therefore we expected that the lipid packing would largely determine the relaxation rates. As described in the previous chapter, we believe the polymeric  $\alpha$ -THIOLS to be more disordered and less tightly packed (in the gel state) than nonpolymerizeable phospholipids. Consequently, a faster rate of motion was anticipated but this is clearly not what the data show.

The question then arises as to why the correlation time of the phosphate moiety is actually slower. There are several possible explanations including:

(i) The slower rotational motion of the polymerized phospholipid molecule as a whole contributes somewhat to the relaxation rate.

(ii) The headgroup has a slightly different conformation, which induces a slower motion or a reduction in the *amplitude* of the fluctuations.

To investigate whether the reorientation of the lipid as a whole might be influential,  $T_1$  measurements were carried out on a polymeric  $\omega$ -THIOL ( $\omega$ -10) which has a 10-carbon acyl chain and the polymerizable moiety at the chain terminus. The  $\omega$ -THIOLS cannot be sonicated into SUVs due to the fact that they form bilayer fragments and therefore the linewidths of the spectra were much broader. However, this does not preclude the determination of the temperature of the  $T_1$  minimum. Furthermore, as shown by a comparison of DMPC  $T_1$ s for MLVs versus SUVs, the gross morphology should also not influence the position of the minimum to a large extent.

As shown in Figure 3, the temperature of the minimum corresponds to approximately 30 °C, which is slightly less than that for DMPC. The transition temperature for  $\omega$ -10 is  $\approx$  19 °C, also slightly less than that of DMPC. Thus, by comparison to  $\alpha$ -16, ( $T_m \approx$  23 °C), the correlation time does not seem to be affected significantly by polymerization. In agreement with other studies, this further suggests that the rotational reorientation of the lipid as a whole does not largely influence the  $T_1$ . We therefore suspect that in the case of polymeric  $\alpha$ -THIOLS, a conformational change of the headgroup may be at least partially responsible for the slower motion of the phosphate moiety.

As a final point, Figure 4 shows the linewidths of  $\alpha$ -20 versus DMPC SUVs at 80 MHz as a function of temperature. Consistent with the slower motion described above for the polymeric  $\alpha$ -THIOLS, the linewidths are broader reflecting a faster spin-spin relaxation rate. In contrast to the  $T_1$  measurements, which are sensitive to fast motions on the order of the Larmor frequency, however, the spin-spin relaxation rates are sensitive to slow motions. The increased linewidths for the polymeric lipids is therefore likely a consequence of the reduced translational and rotational diffusion of the lipids as a whole, rather than the segmental motions associated with the headgroup.

**Figure 3**

$^{31}\text{P}$  spin-lattice relaxation times (202 MHz) as a function of temperature for bilayer fragments prepared from polymeric  $\omega$ -10.

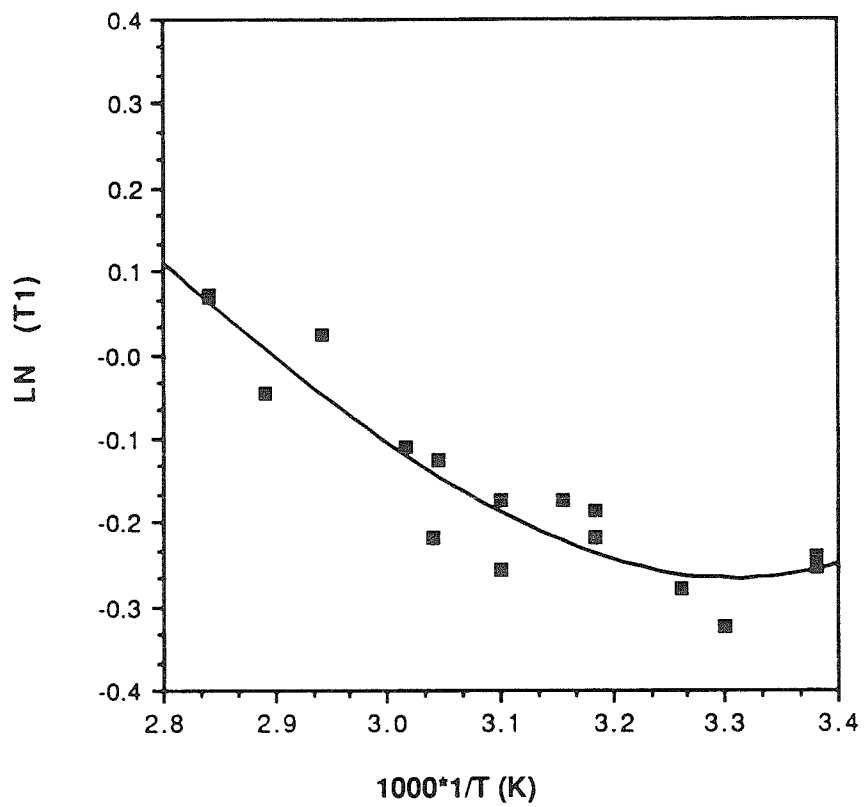
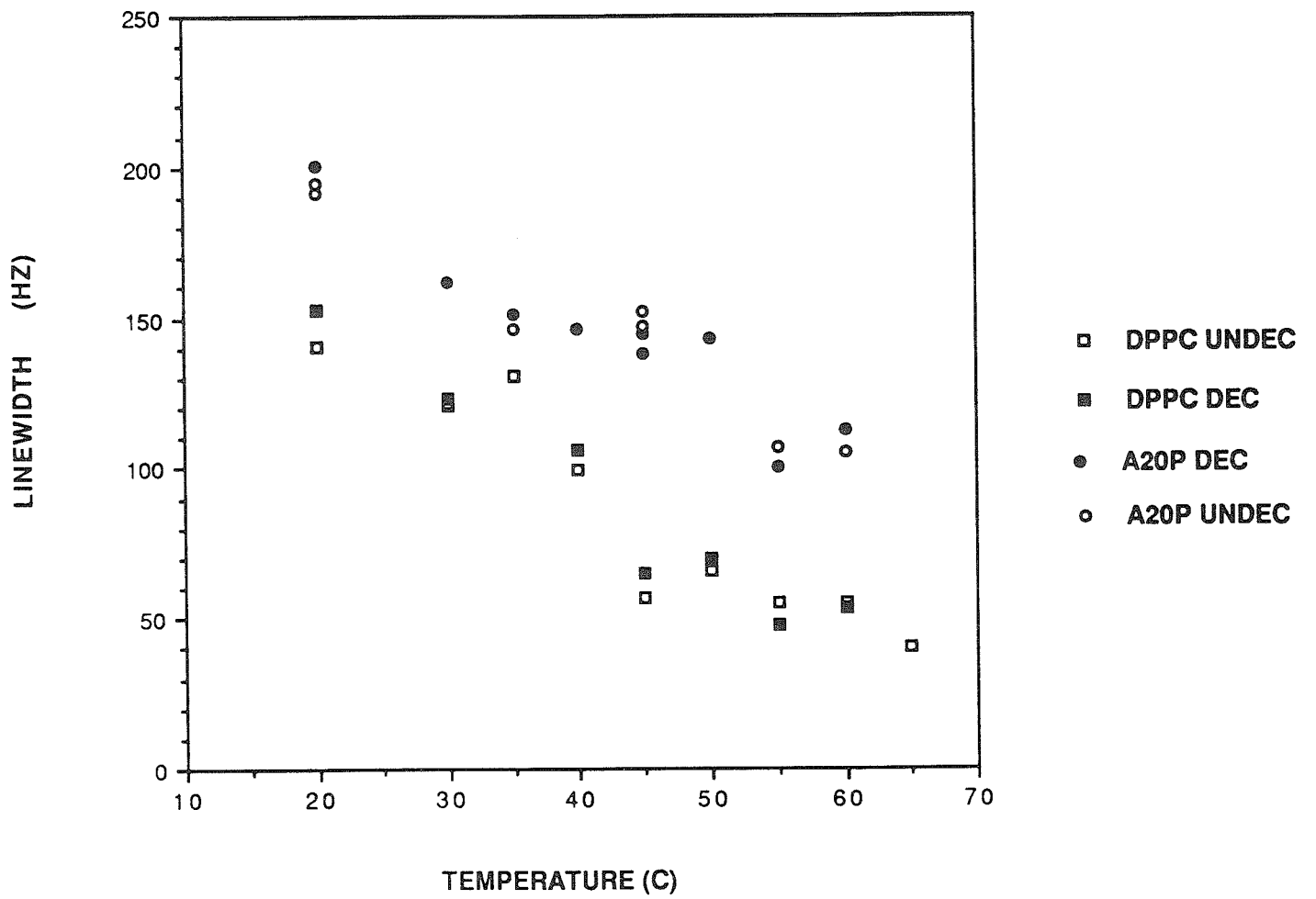


**Figure 4**

Linewidths (80 MHz) of SUVs prepared from  $\alpha$ -20 SUVs versus DPPC SUVs. Symbols are assigned in the legend. Dec and undec refer to decoupled and undecoupled spectra.



Temperature Dependence of the  $T_1$ ; the Breadth of the Minimum and Slope of the Profile.

In addition to the position of the  $T_1$  minimum, the magnitude of the change in  $T_1$  over a given temperature range and the breadth of the  $T_1$  minimum are quite different for the polymeric versus the monomeric lipids. For both  $\alpha$ -20 and  $\alpha$ -16, the minimum is quite broad suggesting perhaps a distribution of correlation times rather than a single effective correlation time as has been assumed in studies to model the  $T_1$  data. Secondly, the slopes of the  $T_1$  plots are much more shallow in the case of the polymeric lipids than the monomeric lipids. This is particularly evident in the  $T_1$  profiles for  $\alpha$ -16 versus DPPC SUVs at 80 MHz (Figure 5 ).\* In previous studies, the slopes have been evaluated in terms of activation energies for headgroup reorientation (11). In the work by Milburn and Jeffrey, for example, the  $T_1$  data was fit using combined expressions for dipolar and chemical shift anisotropy rates, into which was substituted a spectral density equation appropriate for a single effective correlation time. The correlation time was then modelled by an Arrhenius relationship to derive the activation energy:

$$(5) \quad \tau_c = \tau_o \exp\left(\frac{E_a}{kT}\right)$$

where  $\tau_o$  is the correlation time at infinite temperature and  $E_a$  is the activation energy.

If we assume that the slopes of the plots are related to the activation energy for reorientation of the phosphate segment, the data would imply that the activation energy for the  $\alpha$ -THIOLS is *lower* than that for the nonpolymerizeable phospholipids, even though the headgroup reorientation is slower. Whether this is the case or not is unknown but would be consistent with our initial expectations that the lipids are not as

---

\* The position of the minimum is shifted to lower temperatures in both cases since the larmor frequency is lower. Thus the  $T_1$  selects for motions with  $\tau_c = 10^{-8}$  s.

tightly packed as nonpolymerizable lipids, at least in the gel state and perhaps for temperatures slightly above the  $T_m$ . An alternative explanation has been suggested by Brown, however, to describe the temperature dependence of the relaxation rates of  $^{13}\text{C}$  and  $^2\text{H}$  nuclei. As discussed in the last chapter, it has been suggested that the temperature dependence of the  $T_1$  reflects the temperature dependence of the order parameter rather than the activation energy for the motion. If we assume that this is also a viable explanation for the  $^{31}\text{P}$  NMR data presented here, then qualitatively, the data suggests that while the motion of the headgroup is generally slower, the reorientation rate does not change with temperature to the extent that occurs in nonpolymerizable lipids. This is due to the fact that the phospholipids in polymerized membranes are limited in the rate of motions that can be achieved and the extent to which the bilayer can become disordered on account of the intervening covalent linkages between the phospholipids.

#### $^1\text{H}$ - $^{31}\text{P}$ Cross Polarization Experiments.

To further investigate the motional properties of the membranes, the rate of transfer of magnetization from vicinal protons to the phosphorous nuclei was measured by CP MASS. In contrast to the spin-lattice relaxation rates, the parameters derived from these experiments,  $T_{1\rho}$  and  $T_{\rho\text{H}}$ , are sensitive to slow motions of the bilayer (12). Because we have a very limited data set for these experiments, further discussion of the theoretical background will not be given.

Table I summarizes the data obtained for polymeric  $\alpha$ -16 compared to DPPC. The shorter values of both  $T_{\rho\text{H}}$  and  $T_{1\rho}$  for  $\alpha$ -16 is indicative of the slower motions of the polymeric lipid relative to DPPC. This is despite the fact that the temperature of the measurement was room temperature or perhaps slightly higher due to sample

**Figure 5**

<sup>31</sup>P spin-lattice relaxation times (80 MHz) as a function of temperature for bilayer fragments prepared from **A.** DPPC SUVs and **B.** polymeric  $\alpha$ -16 SUVs.

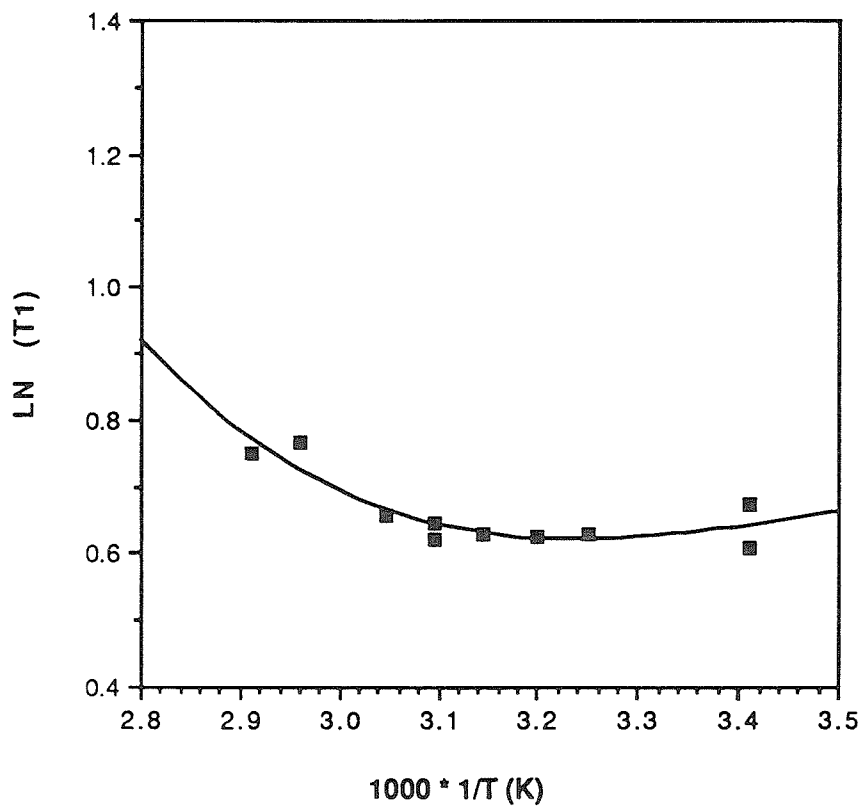
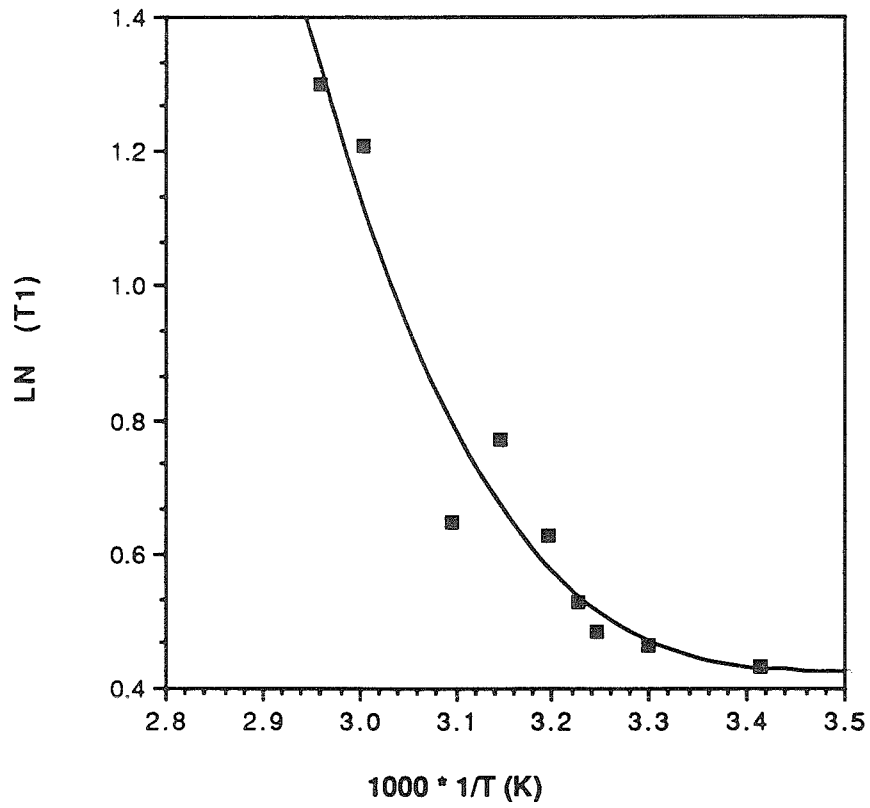


**Table I**

Summary of  $T_{PH}$  and  $T_{1\rho}$  values for DPPC and  $\alpha$ -16 as determined by cross polarization magic angle sample spinning (CP MASS) experiments.

Lipid	$T_{1\rho}$	$T_{PH}$
$\alpha$ -16 (P)	$14.2 \pm 4.0$	$0.63 \pm .10$
$\omega$ -15 (P)	22.4	1.29
DPPC	$27.7 \pm 5.7$	$1.67 \pm .27$

heating. Consequently,  $\alpha$ -16 is in the liquid-crystalline state while DPPC is in the gel state at the measuring temperature. If the temperature of the measurement was such that  $\alpha$ -16 was also in the gel state, the disparity in the relaxation times would be even greater. These data confirm the results of the spin-lattice relaxation rates, which show a slowing of the motion for  $\alpha$ -16 relative to the nonpolymerizable phospholipids.

By contrast, the  $T_{1\rho}$  and  $T_{PH}$  for polymeric  $\omega$ -15 is only slightly lower than that of DPPC. The reduction may be due to some degree of motional restriction due to the polymerization. Alternatively, it could be argued that the reduction in the relaxation times is due to the fact that  $\omega$ -15 is at a lower reduced temperature at the temperature of the experiment on account of the high phase transition of this lipid.

### Investigation of the Chemical Shift Anisotropy and Lineshapes of Polymerized versus Nonpolymerized Phospholipid Dispersions.

In the above two sections, the dynamic behavior of the polymeric and nonpolymerizable lipids was described. The present section is concerned with investigations of the chemical shift anisotropy, which provides information concerning both the motion as well as the average orientation of the phosphate segment. As a preface to the data, a brief introduction to the theory is first described:

For dry phospholipid samples, the  $^{31}\text{P}$  NMR spectra are very broad as a consequence of the incomplete motional averaging of the chemical shift and dipolar terms of the spin Hamiltonian (14). It is possible to remove the dipolar broadening by high power proton decoupling or cross polarization in which case the resulting powder spectra give information concerning the residual chemical shift anisotropy (CSA). For a given spin  $i$ , the observed chemical shift is related to the principle components of the chemical shift tensor by:

$$(6) \quad \sigma_{zz} = \lambda_{i1}^2 \sigma_{11} + \lambda_{i2}^2 \sigma_{22} + \lambda_{i3}^2 \sigma_{33}$$

where the  $\lambda$ s are the direction cosines of the principle axes of the chemical shift tensors  $\sigma_{ii}$  with respect to the magnetic field direction (16). In powder samples, the random orientation of the nuclei combined with the dependence of the chemical shift on the orientation with respect to the magnetic field results in broad axially asymmetric spectra as shown in Figure 6A (15). Upon hydration, the onset of continuous uniaxial motion about the long molecular axis of the lipid results in a narrowing of the powder spectra, the breadth of which is related to the static chemical shielding tensors by (3):

$$(7) \quad \Delta\sigma = S_{11}(\sigma_{xx} - \sigma_{yy}) + S_{33}(\sigma_{zz} - \sigma_{yy})$$

where :

$$(8) \quad S_{ii} = \frac{1}{2}(3 \cos^2 \theta_{ii} - 1)$$

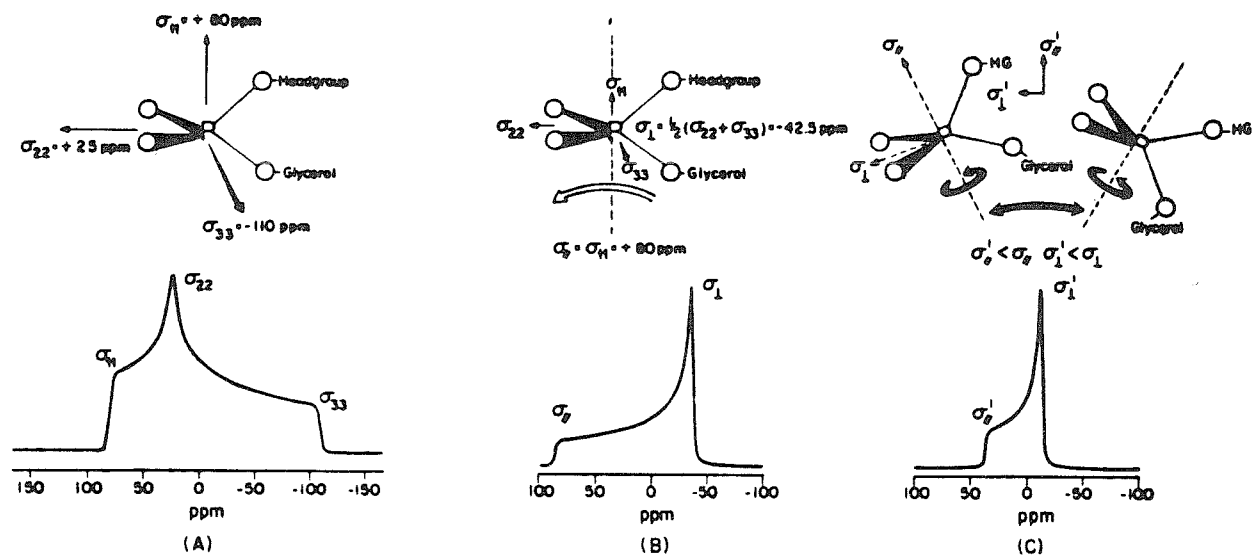
Here, the  $S_{ii}$  are order parameters, which essentially describe the averaging motion and  $\theta_{ii}$  are the angles between the molecular reorientation axis and the shielding directions of the tensors. Two order parameters are necessary to describe the spectrum because of the nonaxiality of the static chemical shielding tensors. The effect of such axial motion on the appearance of the spectrum is illustrated in Figure 6B and Figure 7. Figure 7 shows a typical axially symmetric powder spectrum for phosphatidylcholine in the liquid-crystalline state. The residual chemical shift anisotropy  $\Delta\sigma$  can also be expressed as (3):

$$(9) \quad \Delta\sigma = \sigma_{||} - \sigma_{\perp}$$

This quantity is experimentally measured as the splitting between the two edges of the spectrum at the half-height of the low frequency foot.

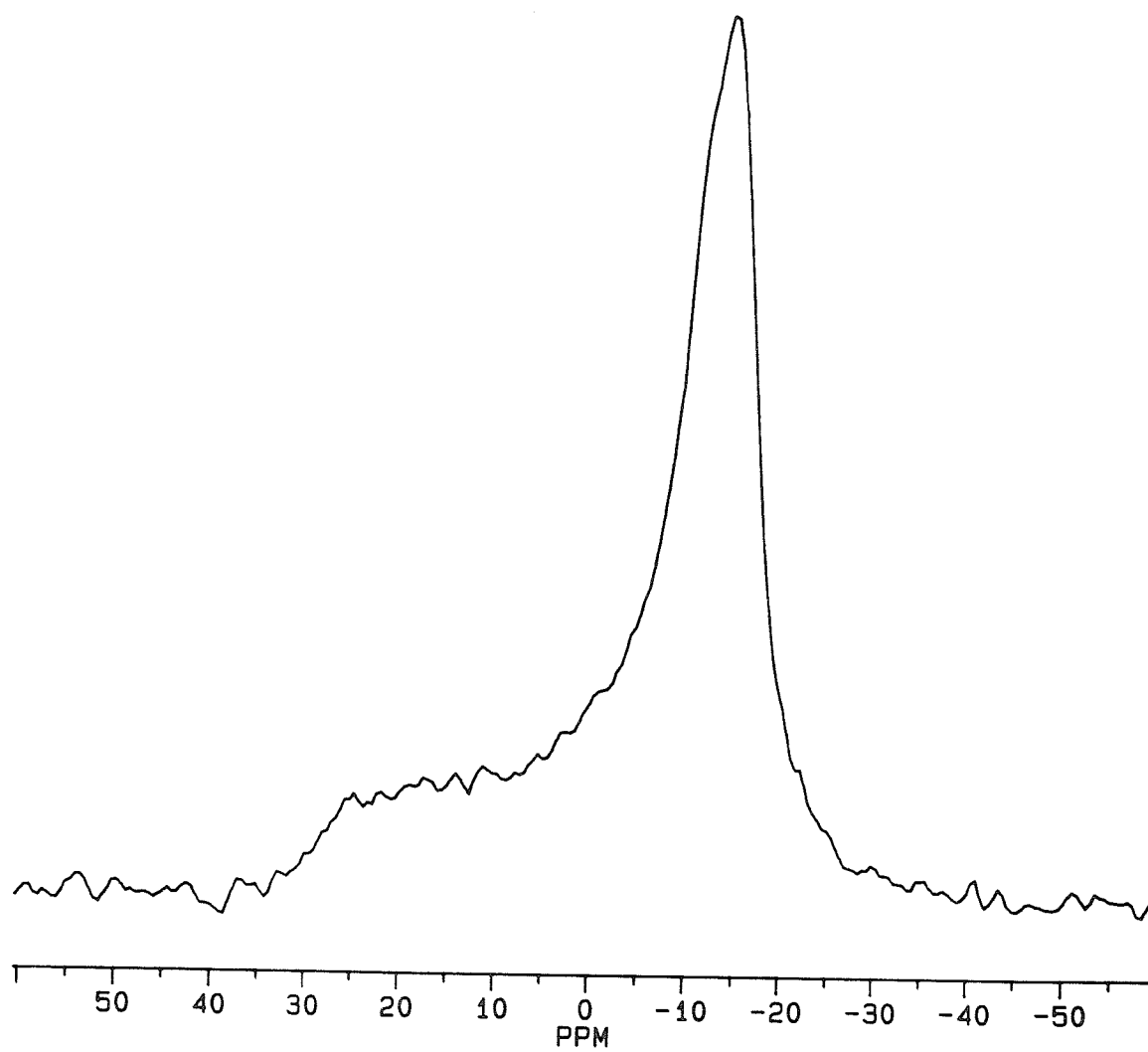
**Figure 6**

Illustration of the various possible motional states of the phosphodiester moiety of a membrane phospholipid and the resulting  $^{31}\text{P}$  NMR spectra : **A.** static, anhydrous phospholipid; **B** ordered, hydrated phospholipid; **C** disordered hydrated phospholipid. Taken from reference (15).



**Figure 7**

A typical powder spectra for a phosphatidylcholine. The spectra in this case is  $\alpha$ -16 at 313 °C. The spectra was acquired at 202 MHz with 10 W BB decoupling.



From the chemical shift anisotropy, one can derive information concerning the motions and orientation of the headgroup. Figure 6C illustrates how increased disorder and motion in the headgroup of a phospholipid might lead to a further reduction in the  $\Delta\sigma$ . As an example of the reduction in  $\Delta\sigma$  with increased motion, the powder spectra of hydrated lipid dispersions are drastically altered upon passing through the gel to liquid-crystalline phase transition. This is illustrated by the spectra in Figure 8 for DMPC at various temperatures. The increased breadth of the spectra at low temperatures is due to a reduction in the rate of motion of the phospholipid headgroup.

In addition to the rate of motion, it has also been shown that the value of  $\Delta\sigma$  is strongly dependent on the tilt angles of the headgroup (16). The tilt angles are the angles that relate the chemical shift tensor to the axis of motional averaging and are contained in the order parameters of Eqns. (7) and (8). Thus by examination of the chemical shift anisotropy it is possible to abstract information concerning the mobility and order parameters of the headgroup. While separation of the conformational information contained in the order parameter from the dynamic properties of the headgroup are difficult, combined with the motional information derived from the spin-lattice relaxation studies described earlier we should be able to make reasonable interpretations of changes associated with  $\Delta\sigma$ .

*The Temperature Dependence of the CSA for Polymerized and Nonpolymerizable Phospholipids.* The spectra for DMPC MLVs as a function of temperature was shown in Figure 8. Analogous spectra are shown in Figure 9 for DPPC, polymeric  $\alpha$ -16, and polymeric  $\alpha$ -20. The spectral changes in DPPC are similar to those for DMPC. For the polymeric lipids, the spectra in the liquid-crystalline state resemble those of the nonpolymerizable lipids in the presence of an axially symmetric powder spectrum.

**Figure 8**

Temperature dependent changes in the powder spectrum of DMPC. Spectra were recorded at 202 MHz with 10 W BB decoupling: **A** 290 °K; **B** 295 °K; **C**.300 °K; **D**. 310 °K.

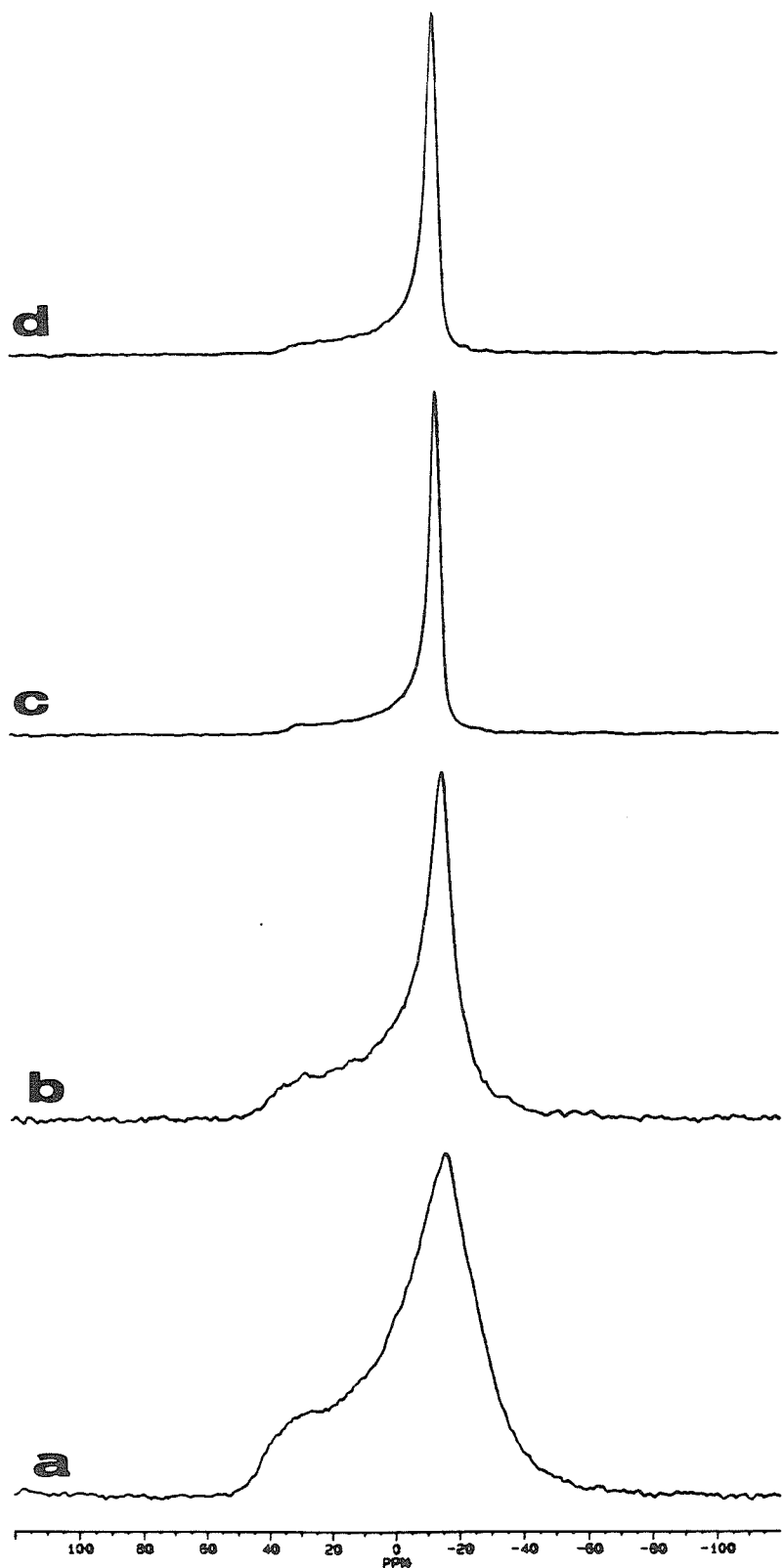
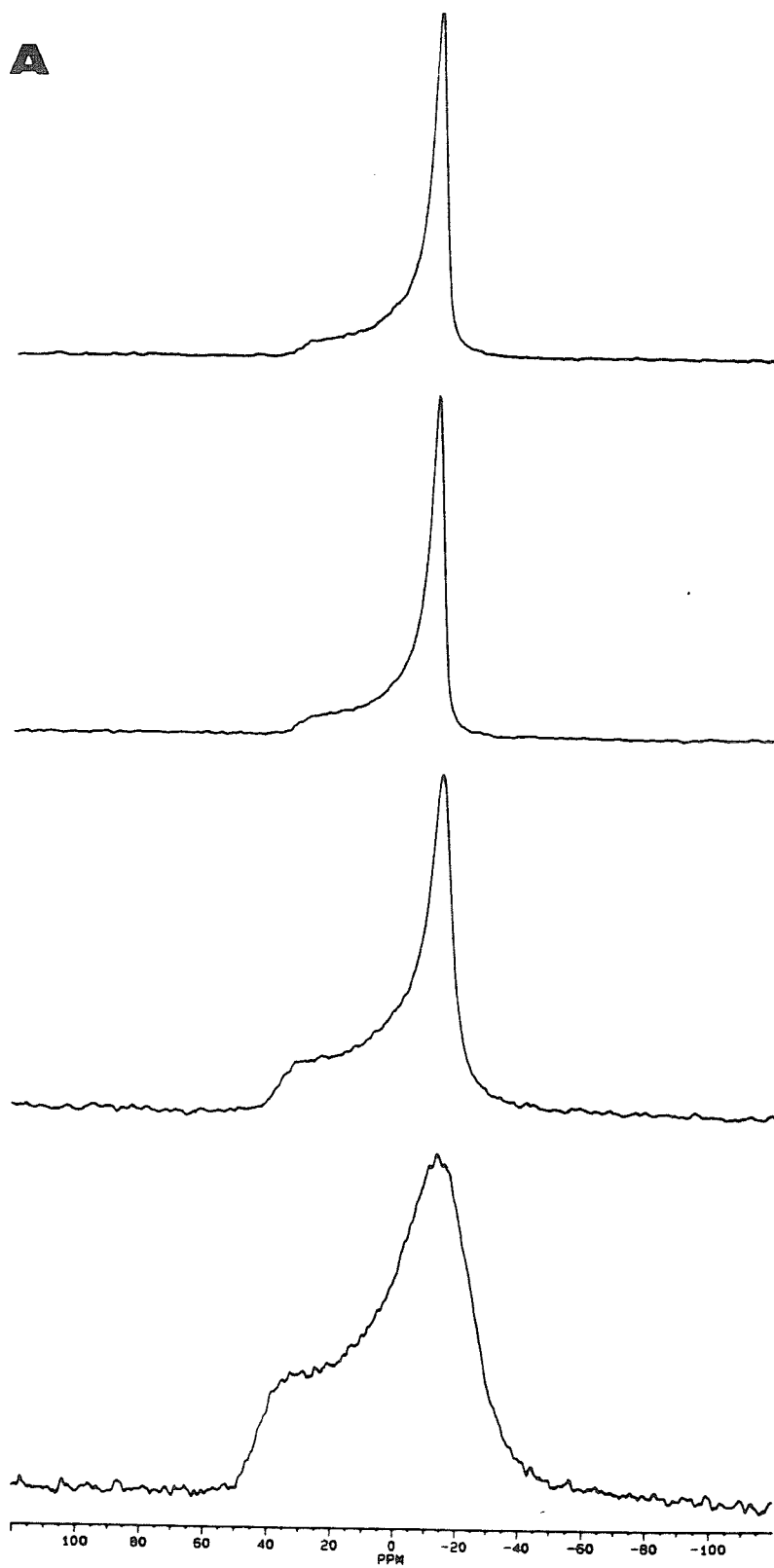
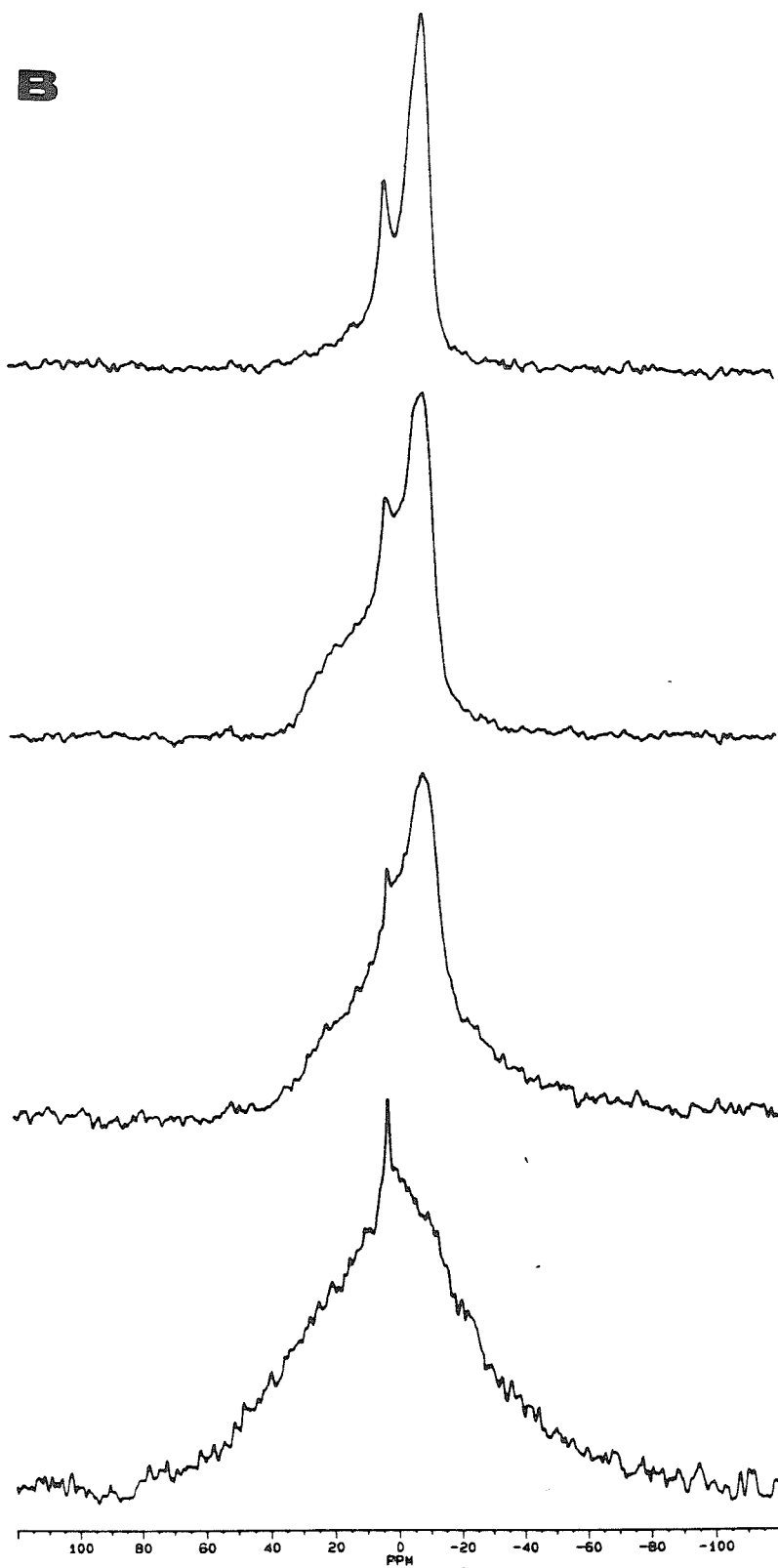


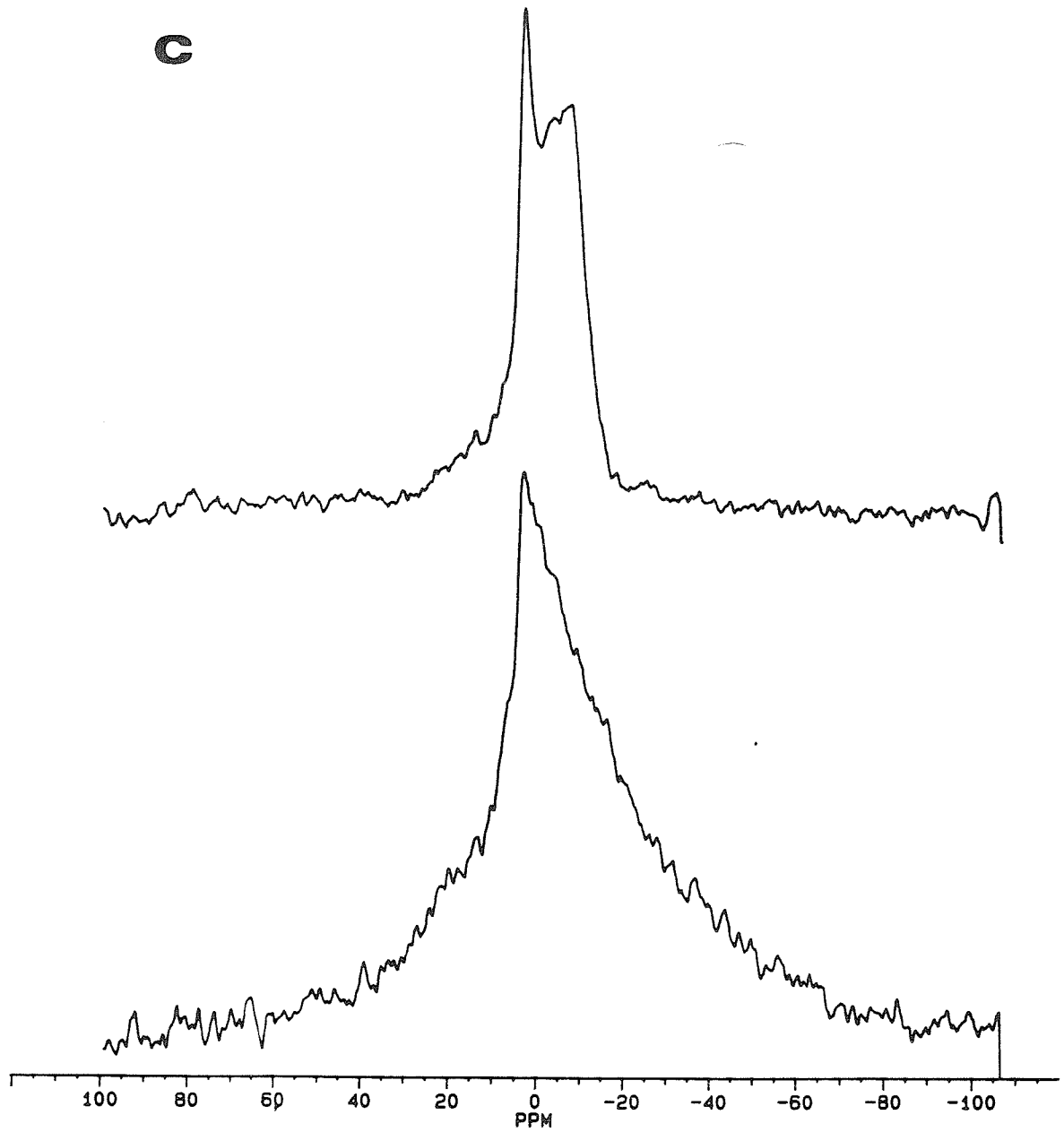
**Figure 9**

Temperature dependent changes in the powder spectrum of **A**. DPPC (300 °K, 308 °K, 316 °K and 321 °K); **B** polymeric  $\alpha$ -16 (297 °K, 300 °K, 304 °K and 315 °K); **C**. polymeric  $\alpha$ -20 (298 °K, 330 °K) . Spectra were recorded at 202 MHz with 10 W BB decoupling. Temperatures are given in the order of spectra from bottom to top.



**B**





However, upon reduction of the temperature to just below the phase transition, the spectra of both  $\alpha$ -16 and  $\alpha$ -20 are no longer axially symmetric but have the characteristics associated with a slowing of the headgroup reorientation. This is consistent with the fact that the spin-lattice relaxation rates indicated a slower motion of the polymeric  $\alpha$ -THIOLS. It cannot be ruled out, however, that the observed features are due to a conformational change of the headgroup.

By contrast to the polymeric  $\alpha$ -THIOLS, polymeric  $\omega$ -16 which is polymerized at the chain terminus and has a much higher phase transition temperature than either of the  $\alpha$ -THIOLS, has spectral features above and below the phase transition temperature similar to that of the nonpolymerizable phospholipids (Figure 10). This was a surprising result since the higher transition temperature of this lipid compared to the  $\alpha$ -THIOLS implies an increased interaction between the lipid chains, which should reduce the available space for the headgroup motion. However, these results are consistent with the fact that the effective correlation time determined for another polymeric  $\omega$ -THIOL,  $\omega$ -10, was not unusually different than that of the nonpolymerizable phosphatidylcholines.

The change in the CSA can be observed more quantitatively by a plot of  $\Delta\sigma$  versus temperature. This is shown in Figure 11 for DPPC, DMPC and  $\alpha$ -16. For both the nonpolymerizable phospholipids, the value of  $\Delta\sigma$  is similar in the liquid-crystalline state ( $\approx 50$  ppm). On the other hand, the  $\Delta\sigma$  of the polymeric  $\alpha$ -THIOL is  $\approx 7$ -10 ppm *smaller* than that of the nonpolymerizable lipids in the liquid-crystalline state. This is shown more clearly by a comparison of an enlarged spectrum of DMPC versus polymeric  $\alpha$ -16 in Figure 12.

Generally the reduction in  $\Delta\sigma$  has been associated with increased disorder and motion in the headgroup as was illustrated in Figure 6C (15). However, spectral

**Figure 10**

Temperature dependent changes in the powder spectrum of  $\omega$ -16. Spectra were recorded at 202 MHz with 10 W BB decoupling: A 298 °K; B 340 °K.

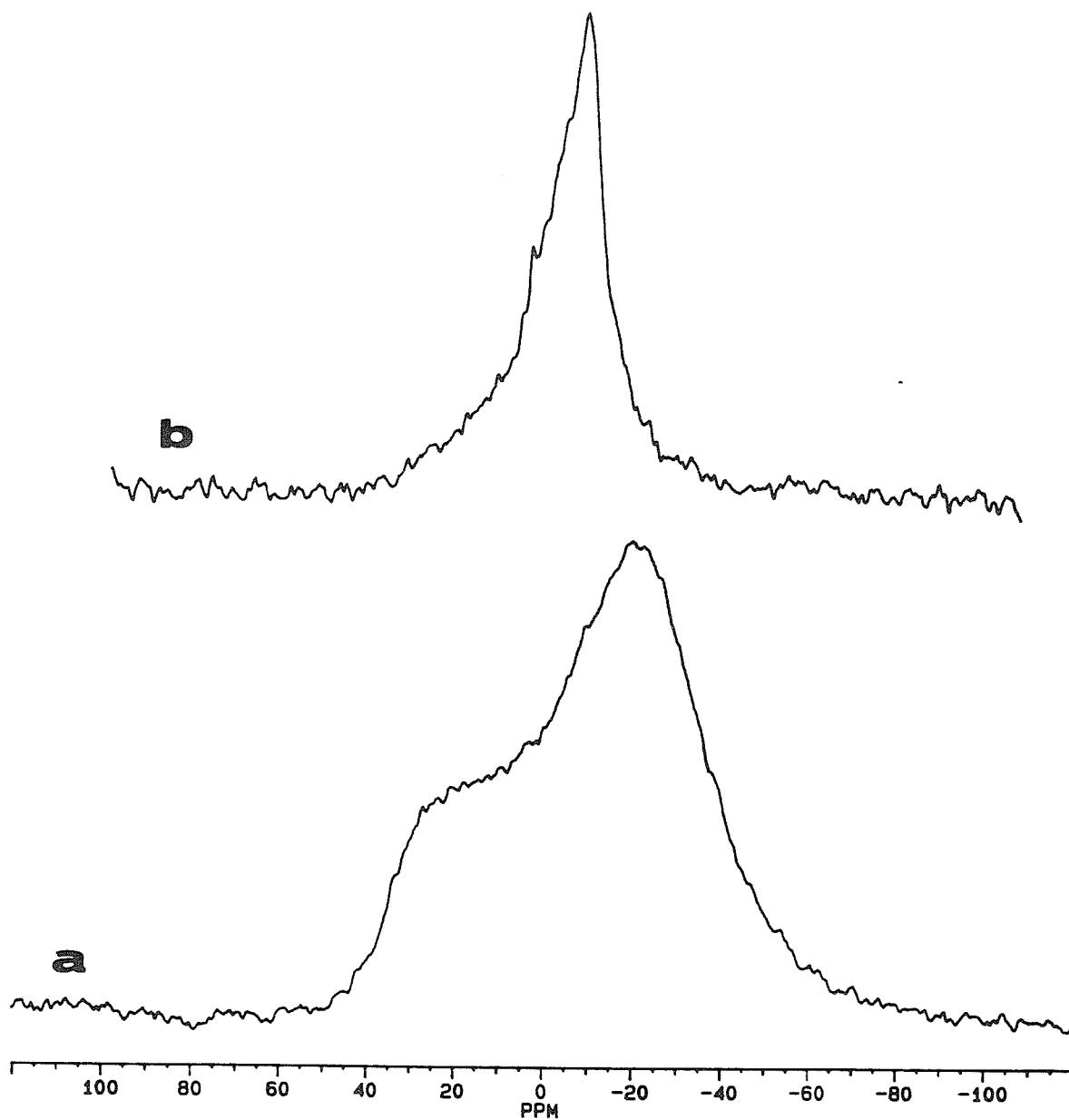
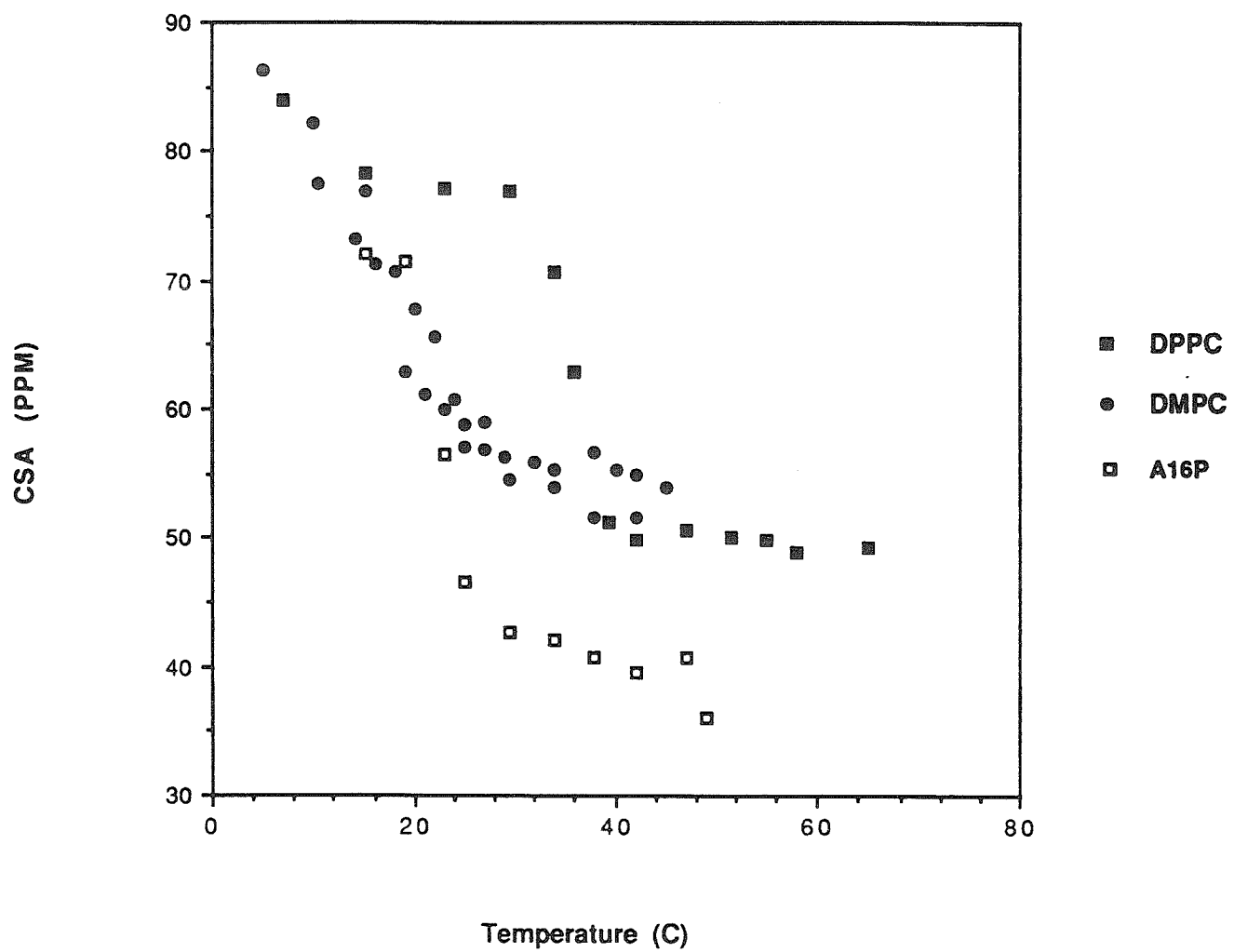


**Figure 11**

Plot of the CSA versus temperature for DMPC, DPPC and  $\alpha$ -16 MLVs. Symbols are assigned in the figure legend.



simulations carried out by Banerjee *et al.* have shown that changes in  $\Delta\sigma$  is sensitive primarily to the orientation of the phospholipid headgroups with respect to the axis of motional averaging (16). By contrast, changes in the rate of axial rotation was shown to be much less influential on value  $\Delta\sigma$  as was  $T_2^{-1}$ .\* If we consider the CSA data in light of the  $T_1$  and cross polarization data we can fairly confidently rule out increased motion as the source of the reduction in the value of  $\Delta\sigma$  for the polymeric  $\alpha$ -THIOLS. Both the  $T_1$  and cross polarization results indicated that the motions of the headgroup were in fact slowed relative to the nonpolymerizable membranes. Any change in  $\Delta\sigma$  due to motion for the  $\alpha$ -THIOLS relative to DPPC and DMPC should have resulted in an increased value of  $\Delta\sigma$ . Thus we conclude that the headgroup *orientation* of the  $\alpha$ -THIOLS is perturbed as a consequence of polymerization at the interfacial region. Such a conformational change may in fact be the basis for the reduced rates and/or amplitudes of the motions relative to the nonpolymerizable lipids. Simulations are currently in progress to substantiate this even further.

### Conclusions

In this study the dynamic and conformational properties of polymeric and nonpolymerizable lipids were examined by a combination of relaxation measurements and the analysis of the residual chemical shift anisotropy. The results once again illustrate the very different properties of polymerizable lipids depending on whether the polymerizable moiety is at the chain terminus or the interfacial region. In the case of the  $\omega$ -THIOLS, the relaxation properties and CSA were not substantially different in comparison to nonpolymerizable phosphatidylcholines. In the case of the  $\alpha$ -THIOLS, relaxation measurements indicated that the reorientation rate of the headgroup was slowed relative to nonpolymerizable analogs. This is despite the fact that at least in the

---

\*  $T_2^{-1}$  is determined by the residual  $^1\text{H}$ - $^{31}\text{P}$  dipolar interaction.

gel state, the hydrocarbon chains of the  $\alpha$ -THIOLS are more disordered. The basis for the slower effective correlation time is not clear. However, analysis of the chemical shift anisotropy as a function of temperature in the polymeric  $\alpha$ -THIOLS was most consistent with the assumption of a head group conformational change relative to nonpolymerizable phospholipids. This could result in a lower correlation time either sterically or as a consequence of a decreased amplitude of the headgroup fluctuations.

It is interesting to note that the phenomenological properties of the  $\alpha$ -THIOLS also suggest a headgroup conformational change. Hydration of these lipids proceeds very readily even in the gel state of long 20-carbon chain phospholipids. Furthermore, as shown in Chapter II, SUVs prepared from polymeric  $\alpha$ -THIOLS are stable for extended periods below the phase transition temperature, in contrast to nonpolymerizable analogues, which aggregate rapidly in the gel state. Since these lipids are zwitterionic, small changes in the orientation of the headgroup could modulate the electrostatic properties of the membrane surface. It would seem on the basis of the phenomenological data that the charge of the headgroup is not as effectively screened by interaction with neighboring lipids. Alteration of the headgroup conformation and effective surface charge could also result in a different behavior of these lipids *in vivo* compared to their nonpolymerizable analogues. This is in fact shown to be the case in the next section.

### References

1. Mabrey-Gaud, S. in : *Liposomes from Physical Structure to Therapeutic Applications* ; Knight, C.G. (Ed.); Elsevier: North Holland Biomedical Press, 1981; 105.
2. Cullis, P.R., and De Kruijff, B. (1978) *Biochim. Biophys. Acta.* **513** , 31-42.
3. Seelig, J. (1978) *Biochim. Biophys. Acta.* **515**, 105-140.

4. Seelig, J. and Seelig, A. (1980) *Quat. Rev. Biophys.* **13**, 19-61.
5. Gruner, S. M., Cullis, P. R., Hope, M. J. and Tilcock, C. P. S. (1985) *Ann. Rev. Biophys Biophys Chem.* **14**, 211-238.
6. Pahapadjoupolous, D., Portis, A. and Pangborn, W. *Annals New York Acad. Sci.* **50**, 308
7. Dijkstra, J., Van Galen, M., and Scherphof, G. L. (1985) *Biochim. Biophys. Acta* **813**, 287-297.
8. Boulanger, Y., Schreier, S. and Smith, I. (1981) *Biochemistry* **20**, 6824-6830.
9. Yaegle, P., Hutton, W.C., Huang, C., and Martin, R.B. (1977) *Biochemistry* **16**, 4344-4349.
10. Ellena, J., Pates, R., and Brown, M. (1986) *Biochemistry* **25**, 3742-3748.
11. Milburn, M. and Jeffrey, K. (1987) *Biophys. J.* **52**, 791-799.
12. Cornell, B.A., Davenport, J.B. and Separovic, F. (1982) *Biochim. Biophys. Acta.* **689**, 337-345.
13. Ghosh, R. (1988) *Biochemistry* **27**, 7750-7758.
14. Seelig, J. , Lukas, T., Hymel, L. and Fleischer, S. (1981) *Biochemistry* **20**,3922-3932.
15. Smith, I . and Eikel, I.H. in: *Phosphorous -31 NMR*; ; Academic Press; 1984, 447-475.
16. Griffin, R. (1981) *Methods in Enzymology* **72**, 109-175.

---

---

## Chapter VII

---

---

### *In Vitro and In Vivo Investigations of the Stability, Blood Clearance Rates and Biodistributions of Disulfide Polymerized Phosphatidylcholine Liposomes*

---

#### INTRODUCTION

The interest in phospholipid vesicles as potential drug delivery systems has inspired a large research effort over the past several years to demonstrate the viability of this concept. Several strategies with diagnostic or therapeutic implications have been envisioned and include (i) passive delivery via unmodified liposomes, particularly to malignant tissue (1) (ii) targeted delivery via liposomes modified with specific recognizable determinants on their surface (i.e., carbohydrates, antibodies, and peptides) (2-8) and (iii) slow release systems either residing in a particular organ such as the liver, or circulating in the blood (9,10). In all cases, one or all of the following have presented frustrating impediments to the practical implementation of these ideas : (i) liposome stability (solute leakage and lipid degradation) in the presence of serum and cellular components such as phospholipases and HDL (ii) rapid accumulation in the reticuloendothelial system (RES, i.e., liver and spleen) and (iii) difficulty in exiting the microcirculation to reach extravascular tissue (11-24).

Serum induced leakage of aqueous solutes has been adequately resolved primarily with lipid mixtures containing cholesterol to "solidify" the membrane, inhibit protein and HDL interaction, and abolish the phase transition (18,19,22-24). Chemical stability

with respect to phospholipases and other enzymes in serum or cells has also been improved by the addition of cholesterol (16) as well as by the synthesis of more chemically inert lipids such as those containing carbamyl, ether or alkyl linkages (10, 25-29). Construction of liposomes with a prolonged residence in the blood (slow RES accumulation) and the capacity to exit the microcirculation is a more complex problem than membrane stability, however. A long circulation time is a demonstrated prerequisite for extravascular tissue accumulation, and has been shown to be promoted by liposomes which are small, neutral and solid\* (1,19,20,30). The requirement for a small size and neutral surface charge is due to the fact that large and/or negatively charged liposomes are more rapidly endocytosed than small neutral liposomes, particularly via phagocytic Kupffer cells in the case of large particles (16,32,35). The necessity for very solid, well-packed liposomes is more subtle but appears to be related to the reduced capacity of certain plasma proteins such as macroglobulin to penetrate the membrane interface and accelerate RES uptake in a process referred to as opsonization (24,26).

Consideration of the strict requirements outlined above for the use of liposomes for *in vivo* (and other) applications has prompted several groups to investigate the use of *polymerizeable* lipids as membrane substitutes (37-52). Conceptually, one might expect that certain polymeric membranes could meet the criterion described above and surpass the chemical stability, permeability, and impenetrability of nonpolymerizeable liposomes. In reality, however, just as for nonpolymerizeable lipids, the success of polymeric lipids has turned out to be very structure dependent. Certain polymeric lipids have been shown to be very mechanically stable, resistant to dissolution by organic solvents and detergents, and impermeable, while others are not. With the accumulating knowledge of the interrelationships between lipid structure and

---

\* "Solid" refers to liposomes containing lipids, which have a high gel to liquid crystalline phase transition temperature ( $T_m$ ) and/or cholesterol.

membrane physical properties, however, polymeric membranes with desirable characteristics are becoming much more predictable. The behavior of polymeric membranes *in vivo* will also eventually reach the current level of understanding of nonpolymerizable liposomes. But to date, few *in vivo* studies have been reported. In this chapter we therefore describe *in vitro* and *in vivo* investigations of liposomes prepared from the disulfide-polymerized lipids discussed in the previous chapters. This class of polymerizable lipids was in fact originally chosen because of their biodegradable linkages and potential utilization for *in vivo* applications. Furthermore, we hoped that by crosslinking the membrane via disulfide groups, we would create liposomes that were very stable and solid and therefore had the potential for slow degradation and a long half life in the blood.

In this study, Perturbed Angular Correlation Spectroscopy (PAC) has been utilized to:

(1) Examine the serum induced leakage of solutes ( $^{111}\text{In}^{+3}$ ) entrapped in MLVs and SUVs.

(2) Determine the tissue distribution and blood clearance rate, primarily of SUVs for passive targeting applications.

(3) Determine the degradation rate in the liver and spleen, primarily of MLVs for slow release systems.

The data is analyzed in terms of what we know about the physical properties of these polymeric lipids (i.e., phase transition behavior, lipid packing, hydrocarbon order, and morphology). For certain applications such as slow release, the data suggests polymeric lipids have great promise. For other applications, while the studies do not demonstrate the impressive results initially envisioned for polymerized liposomes, taken in combination with the physical characterization described in earlier chapters they allow us to suggest how we must modify the polymerized membranes in order to achieve the desired results.

## Materials and Methods

### Materials

The synthesis and polymerization of the disulfide polymerized phosphatidylcholine was as described in Chapter VIII. Routinely, the polymerized form of the phosphatidylcholine was stored at 4°C as a lyophilized powder until use. L- $\alpha$ -distearoylphosphatidylcholine (DSPC), L- $\alpha$ -dipalmitoylphosphatidylcholine (DPPC), egg phosphatidylcholine (EPC), and bovine brain phosphatidyl serine (BPS) (>99% purity) were purchased from Avanti Polar Lipids. Cholesterol (> 99% purity) was obtained from Sigma. Carrier free  $^{111}\text{In}^{+3}$  (chloride form in .1M HCL) was obtained from Amersham. A23187 was obtained from Calbiochem. Defined fetal calf serum was obtained from HyClone, aliquoted and frozen in 1 ml volumes and used within 24 hours of thawing.\* All other reagents were of analytical grade and used without further purification.

### Preparation and Loading of Liposomes

#### **A. SUVs :**

(i) *Preparation of Sonicated Vesicles.* Sonicated vesicles were routinely prepared by cosolubilization of the lipids in chloroform, evaporation of the chloroform under nitrogen to form a thin film, and vacuum drying overnight to remove residual solvent. The lipids were then hydrated with HEPES buffer (10 mM HEPES, 135 mM NaCl; pH 7.4) containing 1 or 10 mM nitrilotriacetic acid (NTA) above the phase transition and subsequently probe sonicated for 10-20 min under nitrogen with a Heat Systems 350 W sonicator. During sonication, the solutions were placed in a room temperature water bath to avoid excessive sample heating. Titanium particles and large liposomes were

---

\* Aged serum or repeated freezing and thawing of the serum apparently denatures the binding proteins as reduced chelation of  $^{111}\text{In}^{+3}$  is often observed under these circumstances.

removed from the SUVs by centrifugation at 12000 x g for 5 min in an eppendorf centrifuge.

(ii) *Encapsulation of  $^{111}\text{In}^{+3}$* . The protocol utilized to load  $^{111}\text{In}^{+3}$  into the SUVs is a modification of the procedure developed by K. Hwang *et al.* (53). This procedure, which utilizes acetylacetone (ACAC) as the carrier, was employed in lieu of other methods that involve the ionophore A23187, hydroxyquinoline, or oxine, as unpredictable amounts of these materials may be left in the bilayer after chromatography\* (54,55). More importantly, this method does not require the elevated temperatures necessary for loading by A23187 and therefore minimizes heat induced lipid degradation.

Liposomes (12.5  $\mu\text{moles}$  in 2 ml Hepes containing NTA) prepared as in (i) were passed over Sephadex G-25-50 spin columns equilibrated with HEPES buffer to remove untrapped NTA. Typically, 0.5 ml were applied per 3 ml spin column and spun at 500 rpm (swinging bucket rotors) (10 min) to load the column and allow permeation of the resin by the chelate, followed by 2000 rpm (3min) to spin out the liposomes. A freshly prepared  $^{111}\text{In}^{+3}$  loading solution (0.25 ml, see (iii) below) was then added to 1ml of the liposome solution and incubated for 1 hour at 5-10° below the lipid phase transition temperature. The sample was then passed over G-25-50 spin columns as described above to remove untrapped  $^{111}\text{In}^{+3}$  and ACAC. The liposomes were then diluted to 5 ml with HEPES buffer plus the remaining 1 ml of liposomes. The final lipid concentration was 2  $\mu\text{M}$  assuming a 25% loss on the spin columns.

(iii) *Preparation of the loading solution.* The loading solution described above was prepared as follows: 3 mCi  $^{111}\text{In}^{+3}$  was aliquoted into plastic eppendorf vials and dried under an IR lamp. Immediately prior to incubation with the liposomes, the dried

---

\* Most or all of the ACAC appears to be removed according to UV spectra of the liposomes before and after size exclusion chromatography (Gero Decher, unpublished results).

$^{111}\text{In}^{+3}$  was solubilized first with 10- $\mu\text{l}$  3mM HCl followed by addition of 0.25 ml Tris Buffer (10 mM Tris, 135 mM NaCl; pH 7.8 ) and 3-4  $\mu\text{l}$  ACAC.

**B. MLVS.** For the preparation and loading of multilamellar vesicles, three separate protocols were evaluated in an attempt to load the individual lamellae as completely as possible. Two involved loading via carriers (1) ACAC and (2) A23187 using slight modifications of the procedure described above. The third employed no carrier and involved freezing and thawing (FAT) of a very concentrated liposome suspension following the procedures outlined by Mayer *et al.* (56). In order to keep the liposomes as structurally similar as possible, regardless of the loading procedure, freezing and thawing were always used in the preparation of all MLVs. In this regard, it is recognized that the extrusion procedure used by Scherphof and others results (32,63) in more homogeneous and reproducibly sized liposomes, but this was not a viable addition or alternative to freezing and thawing for complete loading of all the lamellae of MLVs.

In the results section , it should be noted that in the MLV *serum stability* studies, all three loading protocols were utilized as is designated in the figures. In most cases where a given liposome type was loaded by more than one method, little difference was observed, presumably because little degradation occurred during the course of the experiment.\* For the *in vivo* animal studies, however, MLVs were loaded almost exclusively via the carrier-free FAT method because the time scale for complete intracellular release of  $^{111}\text{In}^{+3}$  is much shorter than in serum and therefore should depend very strongly on the distribution  $^{111}\text{In}^{+3}$  throughout the lamellae. The

---

\* In some cases where stability was dependent on the loading protocol (Fig. 15 ), those loaded by the FAT method were found to be more stable as would be expected if the  $^{111}\text{In}^{+3}$  was more completely distributed among the lamellae. Loading by A23187 resulted in the least stable liposomes, presumably because of all three protocols, the A23187 is least efficient in loading  $^{111}\text{In}^{+3}$  beyond the first lamellae. This is not surprising because very high temperatures are normally required to load liposomes by the A23187 protocol.

limitations of carrier-loading procedures (ACAC or A23187) for obtaining complete loading of  $^{111}\text{In}^{+3}$  throughout the lamellae is that the  $^{111}\text{In}^{+3}$  (and the carrier for the ACAC method) is added externally to the liposomes. Since the affinity of NTA for the  $^{111}\text{In}^{+3}$  is higher than that of the carrier, it is not likely that much  $^{111}\text{In}^{+3}$  would be loaded beyond the first or second lamellae because this would likely involve several transfers of  $^{111}\text{In}^{+3}$  between carrier and the chelate where the rate of back-transfer from the chelate to the carrier is predictably slow. It has been shown by NMR experiments, however, that  $\text{Mn}^{+2}$  can be effectively entrapped throughout the lamellae of MLVs by successive freeze-thaw cycles, making this the method of choice (56).

(i) *Loading of MLVs with carriers A23187 or ACAC.* The general methodology for the preparation and loading (via ACAC or A23187) of MLVs was as follows: Lipids were cosolubilized in chloroform (in the case of A23187 loading, .025  $\mu\text{moles}$  of A23187 was cosolubilized in chloroform with the lipid; ratio of lipid to A23187 = 500), the chloroform was evaporated with a stream of nitrogen to form a thin film, and the residual solvent was removed under vacuum overnight. The lipid ( 12.5  $\mu\text{moles}$ ) was then hydrated with 1 ml of HEPES buffer containing 10 mM NTA and hydrated above the lipid phase transition 1 min followed by vortexing 30 s. The heat/ vortex cycle was repeated 10 times. The sample was then frozen in liquid nitrogen and allowed to thaw at room temperature; the cycle was repeated 10 times. Unentrapped NTA was removed by pelleting the lipid at 12000 x g for 5 min., hydrating the pellet with HEPES and repeating the procedure a total of three times. To 1 ml of resuspended MLVs, 0.25 ml of loading buffer was added. The loading buffer was prepared as described above for ACAC loading of SUVs, except without ACAC when A23187 was being utilized as the carrier. For ACAC loading, the liposomes were incubated 2 hours 5-10 degrees below the lipid phase transition temperature. The incubation conditions were 2 hours 5-10 degrees above the transition temperature for loading with

A23187. Unentrapped  $^{111}\text{In}^{+3}$  was removed by successively pelleting and resuspending the liposomes in HEPES containing 10 mM EDTA (3 times) followed by pelleting from HEPES (no EDTA) twice at 2000 rpm for 5-10 min. The sample was then hydrated to 5 ml for a final concentration of 2  $\mu\text{M}$  (assuming 25% loss during the centrifugation). Measurement of the value of  $G_{22}(\infty)$  of the liposomes before and after addition of calf serum confirmed complete removal of unentrapped  $^{111}\text{In}^{+3}$ .

(ii) *Loading of MLVs by freezing and thawing.* Using  $\text{MnCl}_2$  as a relaxation agent to relax the phosphorous nuclei of phosphatidylcholine MLVs and monitoring the  $^{31}\text{P}$  NMR spectra, it has been shown that one can entrap a solute throughout the lamellae of MLVs by several cycles of freezing and thawing (56). The freeze-thaw method (FAT) was therefore utilized as a carrier-free loading procedure as follows: A chloroform solution of the lipids was added to a dried aliquot of  $^{111}\text{In}^{+3}$  (in glass test tubes) and the solvent removed under nitrogen followed by vacuum drying overnight. The lipid (12.5  $\mu\text{moles}$ ) was hydrated with a minimum (50  $\mu\text{l}$ ) of HEPES buffer containing 10 mM NTA and hydrated above the phase transition temperature for 15 min with intermittent vortexing. Freezing and thawing of the sample followed by removal of unentrapped  $^{111}\text{In}^{+3}$  was as described above in (i). The sample was diluted to 5 ml with HEPES (2  $\mu\text{M}$  final concentration assuming 25% loss of lipid).

### Animal Experiments, Serum Stability, and PAC Measurements.

(i) *Serum Stability.* The serum stability of the liposomes was assessed by incubating a small aliquot (50-100  $\mu\text{l}$ ) of a liposome suspension in a 50:50 mixture of serum and HEPES buffer to which was added a few  $\mu\text{l}$  of gentomycin. Samples (0.5 ml total volume) were placed in 4 ml omni vials, incubated at 23°C or 37°C, and periodically measured for the value of  $G_{22}(\infty)$  over the course of several days. Only those liposome compositions found to have reasonable stabilities ( $\geq 80\%$  intact over a

24 hour period at 37°C in serum) were utilized in the animal experiments. The stability data presented in the results section are the combined results of at least two separate experiments.

(ii) *Animal Experiments.* For each experiment, sixteen to twenty Balb/c mice (18-22gms) were injected via tail vein with 0.2ml of a 2  $\mu$ M suspension of liposomes (.4  $\mu$ moles per 20 gm body weight). At various times post injection, the mice were lightly anaesthetized with ether and sacrificed via cardiac puncture. Organs were excised, fragmented, and rinsed thoroughly with phosphate buffered saline (PBS) to remove residual blood. For the PAC measurements, tissue and blood samples (maximal volume  $\approx$ .75 ml) were placed in 4 ml plastic omni vials. Coincidence counting rates of the liver, spleen, and blood were measured immediately although it was found that the  $G_{22}(\infty)$  samples remained unchanged for several hours after their removal. Measurement of the total radioactivity associated with the samples was measured using the absolute mode of the spectrometer and generally postponed until the end of the experiment to normalize for the decay of  $^{111}\text{In}^{+3}$ . In initial experiments, due to the rapid clearance of liposomes from the blood, no account was made for the decay of  $^{111}\text{In}^{+3}$ . Each time point represents the average of two mice. Preliminary experiments (data not included) were consistent with those presented here.

(iii) *Data Analysis.* The percentage of intact liposomes in serum or tissues was calculated according to Eqn. 11. In these calculations, the  $G_{22}(\infty)$  for  $^{111}\text{In}^{+3}$ -NTA entrapped inside the liposomes ( $G_c$ ) was measured prior to each experiment and ranged between .5 and .71, depending on the liposome composition.  $G_b$ , the  $G_{22}(\infty)$  for  $^{111}\text{In}^{+3}$  in bovine serum, was measured regularly and found to be  $.2 \pm .02$ . In these calculations,  $G_c$  and  $G_b$  were assumed to represent 100% and 0% intact liposomes, respectively.

Calculation of the percentage of the injected dose of liposomes associated with each tissue was made assuming the sum of the recovered dose in the tissues excised in

the SUV experiments (liver, blood, spleen, heart, lung, kidney, intestines and stomach) represents 85% of the injected dose. For the MLV studies, only the spleen, liver and blood were removed and assumed to account for 75% of the injected dose.\* This was done in order to normalize for variations in the amount injected, and was found to agree fairly well with the calculated values of the % injected dose at early time points (< 8 hours). Furthermore, we were primarily concerned with the clearance rate of the SUVs from the blood rather than their absolute distribution in other tissues because for healthy animals, the ultimate distributions do not have a strong dependence on liposome composition (with the exceptions mentioned in the text).

(iv) *Perturbed Angular Correlation Spectrometer.* The instrument used for the PAC measurements was a home-built four detector slow coincidence spectrometer similar to that previously described. The basic set up involved (4) 5x 5 cm NaI(Tl) crystal detectors placed in a square array with opposing crystals A vs B and C vs D at a distance of approximately 7.5 cm. Four combination single channel analyzer/amplifier units were obtained from Ortec, each of which was set via approximately 2V windows to select for the high energy gamma (C and D) or the low energy (A and B) gamma rays. Distances between the detectors and the window settings were optimized to match the scalar counts of A to B and C to D. A coincidence interface unit was used to determine the total counts (absolute mode) as well as the rate at which the detection of a low energy gamma ray was followed within 600 nsecs, by the detection of a high energy gamma ray (coincidence mode). Thus, two measurements of the coincidence counting rates at 180° and 90° are made simultaneously and can be related to  $G_{22}(\infty)$ . The program for the calculation of  $G_{22}(\infty)$  and statistics was written by Gero Decher based on the thesis of C. Meares (58).

---

\* These values were based on the complete distribution analysis of sphingomyelin/cholesterol liposomes as determined by Hwang *et al.* (58).

**Light Scattering Measurements.** Determination of liposome size (SUVs) was accomplished via dynamic light scattering using a Malvern 4700 light scattering system equipped with a goniometer, a 128 channel correlator and a 3 W Spectra Physics argon ion laser. 488 nm incident light was used with the detector placed at 90 degrees relative to the incoming beam. Calculations of the particle size were based on the Stokes-Einstein equation using the software supplied by Malvern. Measurements are the average of three determinations.

### **Perturbed Angular Correlation Spectroscopy : Background and Theory**

In this study, perturbed angular correlation spectroscopy (PAC) was the technique utilized to study the biodistribution and stability of liposomes both *in vitro* and *in vivo*. The ability to apply PAC in these investigations arises from the fact that one can monitor the rotational reorientation of molecules to which is bound a radioactive nucleus undergoing nuclear relaxation by emission of a gamma-ray cascade. Among the laboratories employing this technique,  $^{111}\text{In}^{3+}$  has been most frequently utilized as the radioactive "probe" since it emits a 173-247 keV gamma-ray cascade whose intermediate lifetime is appropriate for monitoring changes in the motions of interest. Because it is a relatively uncommon spectroscopy, a description of the basic theory (summarized from the thesis of C. Meares (58)) and how the technique can be utilized in the present investigations of liposomes, is discussed in this section.

**Theory.** When radioactive nuclei decay by emitting two gamma-rays in succession, there may be a correlation between the directions of propagation of  $\gamma_1$  and  $\gamma_2$  as a consequence of the conservation of angular momentum. The coincidence counting rate or probability  $\omega(\theta, t)$  that a nucleus will emit a radiation  $\gamma_2$  at an angle  $\theta$  with respect to the first gamma-ray is given by the equation:

$$(1) \quad \omega(\theta, t) = \frac{1}{\tau_n} \exp\left(-\frac{t}{\tau_n}\right) [1 + A_{22} G_{22}(t) P_2 \cos(\theta)]$$

where  $P_2 \cos\theta$  is the second Legendre polynomial ( $1/2 (3\cos^2\theta - 1)$ ) and  $\theta$  is the angle between the two gamma-rays,  $\tau_n$  is the mean lifetime of the 247 keV intermediate state ( $1.22 \times 10^{-7}$  sec for  $^{111}\text{In}^{+3}$ ) and  $A_{22}$  (-0.18) is a constant dependent on the spin and multipolarities of the nucleus.  $G_{22}(t)$  is the perturbation factor that completely describes the interactions of the nucleus with its environment. This is also the experimentally measured quantity determined by the anisotropy of the  $180^\circ$  and  $90^\circ$  coincidence counting rates.

If the lifetime of the intermediate state is so short that the nucleus has no time to interact with the environment, a situation corresponding to the "unperturbed" state, then  $G_{22} = 1$ . This is not normally the case for  $^{111}\text{In}^{+3}$  and the major perturbing influence is caused by the interaction of the nuclear quadropole moment with the external electric or magnetic field gradients. The consequence of this is an attenuation of the correlated gamma emission and  $G_{22} < 1$ . The actual form of  $G_{22}$  depends on the nature of the perturbation as well as the tumbling rate of the nucleus. Assuming the predominance of the nuclear quadropole interaction, the three important cases corresponding to no motion, slow motion, and fast motion are as follows:

(i) *No Motion* : In the static case  $G_{22}(t)$  is related to a time dependent Hamiltonian describing an axially symmetric field. The resulting equation which relates  $G_{22}(t)$  to the quadropole interaction is given by :

$$(2) \quad G_{22}(t) = \frac{1}{5} \left( 1 + \frac{13}{7} \cos \omega_o t + \frac{10}{7} \cos 2\omega_o t + \frac{5}{7} \cos 3\omega_o t \right)$$

Here  $\omega_o$  is the characteristic interaction frequency related to the quadropole frequency  $\omega_Q$  by:

$$(3) \quad \omega_o = \frac{2\pi e |QV_{zz}|}{4hI(2I-1)}$$

where  $\omega_o = 3\omega_Q$  for integral I,  $\omega_o = 6\omega_Q$  for half integral I,  $V_{zz}$  is the axially

symmetric electric field gradient,  $e$  is the electric charge, and  $Q$ , the quadrupole moment. This case would apply for polycrystalline samples.

(ii) *Slow Motion* : The case of slow rotational diffusion where  $\tau_c > \tau_n$  would be pertinent for very large molecules in solution (such as liposomes or proteins), small molecules in viscous solution, and solids in the molten state. The derivation of the expression for  $G_{22}(t)$  is based on the above expression for the static situation with the introduction of time dependence into the transformation between the microcrystal principal axis system and the laboratory frame.  $G_{22}(t)$  has the same form as in the static situation but is multiplied by a decay constant related to the rotational correlation time  $\tau_c$  of the molecule to which  $^{111}\text{In}^{+3}$  is bound. Thus:

$$(4) \quad G_{22}(t) = \exp\left(-\frac{t}{\tau_c}\right) \left[ \frac{1}{5} \left( 1 + \frac{13}{7} \cos \omega_o t + \frac{10}{7} \cos 2\omega_o t + \frac{5}{7} \cos 3\omega_o t \right) \right]$$

(iii) *Rapid Motion* : For the other extreme of rapid rotational reorientation,  $\tau_c \ll \tau_n$ , the perturbation is caused by fluctuating electric field gradients and time dependent perturbation theory is used to derive the expression:

$$(5) \quad G_{22}(t) = \exp(-\lambda t)$$

Here  $\lambda = 1/T_1$  is essentially a relaxation time related to the quadrupole interaction and rotational correlation time by :

$$(6) \quad \lambda = \frac{1}{T_1} = \frac{63}{1000} \left[ \frac{(e^2 q Q)^2}{h^2} \right] \tau_c$$

assuming an axially symmetric electric field gradient and  $I = 5/2$ . This expression would apply for liquid samples in which the rotational correlation time of the molecule to which  $^{111}\text{In}^{+3}$  is bound is short compared to  $\tau_n$ , such as in the case for aqueous  $^{111}\text{In}^{+3}$ -chelate complexes.

For situations such as in our laboratory where one has an instrumental set up in which the resolving time of the coincidence circuitry is longer than the mean lifetime of the intermediate nuclear state, one can use the time integrated perturbation factor rather than the differential perturbation factor defined as:

$$(7) \quad \overline{G_{22}(\infty)} = \frac{1}{\tau_n} \int_0^{\infty} e^{-\frac{t}{\tau_n}} G_{22}(t) dt$$

The two cases appropriate to the work here are the fast and slow motion situations. For the fast motion case, the integrated perturbation factor is given as :

$$(8) \quad \overline{G_{22}(\infty)} = \frac{1}{1 + \lambda\tau_n} = \frac{1}{1 + \frac{\tau_n}{T_1}}$$

For large quadrupole moments,  $G_{22}(\infty)$  exhibits a strong dependence on  $\tau_c$  in the fast motion regime ( $\tau_c = 10^{-11}$  to  $10^{-8}$  sec). Thus one can easily distinguish interactions between  $^{111}\text{In}^{+3}$  bound to small molecules vs macromolecules. This is the fundamental principal upon which the serum stability and tissue degradation studies are based, as will be shown .

For the slow motion region :

$$(9) \quad \overline{G_{22}(\infty)} = \frac{1}{5}\tau_n \left[ \frac{1}{C} + \frac{13}{7} \left( \frac{C}{C^2 + \omega_o^2} \right) + \frac{10}{7} \left( \frac{C}{C^2 + 4\omega_o^2} \right) + \left( \frac{C}{C^2 + 9\omega_o^2} \right) \right]$$

where  $C = (1/\tau_n + 1/\tau_c)$ . For quadrupole interactions on the order of  $10^9$  Hz, which is common for metal complexes, this approximation should hold for rotational correlation

times  $> 10^{-8}$  s. Furthermore, if  $\omega_0^2 \gg (1/\tau_n + 1/\tau_c)^2$ , then  $G_{22}(\infty)$  is independent of the quadrupole interaction and gives  $\tau_c$  directly from the relation:

$$(10) \quad \overline{G_{22}(\infty)} = \frac{1}{5} \left( \frac{1}{1 + \frac{\tau_n}{\tau_c}} \right)$$

This equation should be true for vesicles if one can assume  $\omega_0 \approx 10^9$  Hz. Based on this equation, one would expect a low  $G_{22} (\approx 0.2)$  for  $^{111}\text{In}^{+3}$  bound to a vesicle where  $\tau_c = 10^{-6}$  to  $10^{-4}$ . Furthermore, one can calculate that if  $^{111}\text{In}^{+3}$  is completely immobilized by the vesicle, the  $G_{22}(\infty)$  should also be relatively insensitive to vesicle size.

**Use of PAC for Stability Studies of Liposomes in Serum and Tissue.** The way in which this technique can be used to monitor liposome stability follows a strategy which has been adopted by several groups and is based on the differences in the rotational correlation time (reflected by different values of  $G_{22}(\infty)$ ) for  $^{111}\text{In}^{+3}$  bound to small molecules vs macromolecules. For example, if  $^{111}\text{In}^{+3}$  is bound to a weak chelator such as nitrilotriacetic acid (NTA) inside a liposome, it will exhibit a rapid rotational rate and therefore a high  $G_{22}(\infty)$ . On the other hand, if the structural integrity of the liposome is compromised by components of the serum in which it is suspended, the  $^{111}\text{In}^{+3}$ -chelate complex will be released to the external medium and the  $^{111}\text{In}^{+3}$  transferred to the more strongly binding proteins (reported to be transferrin). The lower rotational correlation time of  $^{111}\text{In}^{+3}$  bound to the proteins will be reflected by a low  $G_{22}(\infty)$ . Upon disruption of a liposome, the internal aqueous contents are diluted into a much larger external volume of serum. Therefore slow exchange (compared to  $1/\tau_n$ ) from the protein-bound form of  $^{111}\text{In}^{+3}$  to chelated  $^{111}\text{In}^{+3}$  can be assumed due to the low concentration and weaker affinity of the chelate compared to competing proteins. Under these conditions, two populations

of  $^{111}\text{In}^{+3}$  exist ; a population bound to small chelators inside intact liposomes, and a population bound to serum proteins from disrupted liposomes. One can therefore calculate the percentage of intact liposomes in serum or in tissues from the following equation :

$$(1) \quad G_o = \chi_b G_b + \chi_c G_c$$

Here  $G_o$ , the observed  $G_{22}(\infty)$ , is the weighted average of the values of  $G_{22}(\infty)$  for protein-bound  $^{111}\text{In}^{+3}$  ( $G_b$ ) and chelated  $^{111}\text{In}^{+3}$  ( $G_c$ ).  $\chi_b$  and  $\chi_c$  are the mole fractions of  $^{111}\text{In}^{+3}$  bound to protein and bound to chelate, respectively, and therefore represent the mole fractions of disrupted ( $\chi_b$ ) and intact ( $\chi_c$ ) liposomes (7,59). This equation was used to calculate the percent of intact liposomes in the experiments described later in this chapter. It should be stressed that the most unique capability of this technique is that one can make such measurements on fluids (i.e., serum), tissue samples, or even whole animals since it is based on the emission of gamma-rays.

***Additional Information from the Absolute Value of  $G_{22}$ .*** The absolute value of  $G_{22}(\infty)$  for  $^{111}\text{In}^{+3}$ -chelate complexes encapsulated in liposomes does not seem to have been exploited beyond evaluating the stability and permeability of the liposomes as was described above. However, it appears that one can derive some additional information about the microenvironment at the membrane interface from this measurement alone, as it represents the competition for binding to  $^{111}\text{In}^{+3}$  between the chelate and interactive groups of the lipids (such as the phosphate group of natural phospholipids). For certain types of liposomes, a given concentration or type of chelate may not be completely effective in competing with the membrane lipids for the  $^{111}\text{In}^{+3}$ , resulting in an intermediate or low value for the measured  $G_{22}(\infty)$ ,

depending on the extent of membrane-immobilization. Similar to Eqn. (11) and for binary systems in general, if the exchange rate between the chelate and membrane binding sites is slow compared to  $1/\tau_n$ , the observed  $G_{22}(\infty)$  will be a weighted average of *vesicle-bound* and chelated  $^{111}\text{In}^{3+}$ :

$$(12) \quad G_o = \chi_v G_v + \chi_c G_c$$

Characteristics of the membrane, which could result in additional binding of  $^{111}\text{In}^{3+}$ , include surface charge, hydration, head group packing and orientation, or additional binding sites. In the case of the polymerized liposomes, one might anticipate some effect from the disulfide or sulfhydryl group on the value of  $G_{22}(\infty)$  for  $^{111}\text{In}^{3+}$  in the liposomes. This is discussed in the next section concerning loading of  $^{111}\text{In}^{3+}$  into liposomes.

## RESULTS and DISCUSSION

This section is divided into five topics: (1) loading of liposomes (2) serum stability of SUVs (3) *in vivo* blood clearance, biodistributions and stability of SUVs (4) serum stability of MLVs and (5) *in vivo* blood clearance, biodistributions and stability of MLVs.

### Loading of Liposomes.

The stability of disulfide polymerized liposomes in serum and at physiological temperatures has not been established. The initial focus of this study was therefore to examine the leakage of various liposome compositions in order to (1) correlate these results with the structural investigations described in earlier chapters and (2) determine liposome compositions that were stable and therefore worthwhile investigating in terms of their biodistribution and *in vivo* stability. In preparation of these serum stability

studies, the conditions for loading  $^{111}\text{In}^{+3}$  into liposomes were investigated with some interesting results, which are described in this section.

Table I lists the values of  $G_{22}(\infty)$  obtained for  $^{111}\text{In}^{+3}$  in various chelated environments. The high value obtained for  $^{111}\text{In}^{+3}$ -NTA is indicative of a rapid tumbling rate for  $^{111}\text{In}^{+3}$  whereas the low  $G_{22}(\infty)$  of  $^{111}\text{In}^{+3}$  in serum indicates a slow correlation time. In the case of  $^{111}\text{In}^{+3}$ -NTA entrapped in DPPC/Chol vesicles, the  $G_{22}(\infty)$  is similar to that for  $^{111}\text{In}^{+3}$ -NTA alone indicating that the NTA effectively competes with the lipid headgroups (the phosphates) for complexation to  $^{111}\text{In}^{+3}$ . For pure DPPC liposomes, however, the  $G_{22}(\infty)$  is slightly lower, due to some immobilization of  $^{111}\text{In}^{+3}$  at the membrane surface. These results are consistent with the previously reported work of K. Hwang (7).

In Table II, values for  $G_{22}(\infty)$  and the percent loading are tabulated for  $^{111}\text{In}^{+3}$ -NTA encapsulated in monomeric and polymeric  $\alpha$ -16 SUVs. In contrast to the relatively high  $G_{22}(\infty)$  values obtained for DPPC and DPPC/Chol (Table I), low values are obtained for monomeric  $\alpha$ -16 and  $\alpha$ -16/Chol SUVs (Table II; A and B) consistent with that expected for  $^{111}\text{In}^{+3}$  completely immobilized by the liposome. If NTA is not removed from the outside of the liposomes prior to the addition of the loading buffer, it would be anticipated that there would be no driving force for loading of  $^{111}\text{In}^{+3}$  into the liposome interior, and the amount of encapsulated  $^{111}\text{In}^{+3}$  should therefore correspond to the captured volume (0.1-2% for the size and concentration of liposomes used). Table II (A and B), however, shows almost complete loading of  $^{111}\text{In}^{+3}$ . This contrasts with the negligible entrapment by DPPC/Chol when external NTA is not removed prior to loading (Table II, E). The most probable explanation for these results are (i) there is binding of the  $^{111}\text{In}^{+3}$  to the thiol groups of the lipid or (ii) there is a strong interaction between  $^{111}\text{In}^{+3}$  and the phosphate of the phospholipid headgroup. To distinguish between these possibilities,  $\alpha$ -16 SUVs were

**Table I**

$G_{22}(\infty)$  for  $^{111}\text{In}^{+3}$  in various chelate environments. For all chelates, the  $G_{22}(\infty)$  is high, indicative of a rapid tumbling rate. The addition of 50 % serum results in a reduction of  $G_{22}(\infty)$  due to the immobilization of the  $^{111}\text{In}^{+3}$  by serum proteins.

**$G_{22}(\infty)$  for  $^{111}\text{In}^{+3}$  in Various Environments**

Solution Composition	Reported $G_{22}(\infty)^a$	Measured $G_{22}(\infty)$
1 mM NTA $^{111}\text{In}^{+3}$	0.68	0.68
1 mM Citrate $^{111}\text{In}^{+3}$	0.71	0.86
1 mM EDTA - $^{111}\text{In}^{+3}$	0.75	0.82
NTA- $^{111}\text{In}^{+3}$ in 50% serum	0.18	0.20
DPPC/Chol + 1 mM NTA- $^{111}\text{In}^{+3}$		0.67
DPPC + 1 mM NTA- $^{111}\text{In}^{+3}$		0.48

<sup>a</sup>Taken from reference (7)

**Table II**

Encapsulation efficiency and value of  $G_{22}(\infty)$  for  $^{111}\text{In}^{+3}$  entrapped in various sonicated liposome preparations. The percentage of entrapment varies depending on the loading protocol. However, in all cases the  $G_{22}(\infty)$  of monomeric  $\alpha$ -16 liposomes is low while that of polymeric  $\alpha$ -16 liposomes is high, even when 10 mM NTA is used.

### Encapsulation Efficiency and $G_{22}(\infty)$ for Various Liposomes

Lipid	$G_{22}(\infty)$	Percent Entrapped
A. Monomeric $\alpha$ -16; 1mM NTA on the exterior and interior of the SUV <sup>a</sup> .	0.16	$\approx 100\%$
B. Monomeric 2:1 $\alpha$ -16/Chol	0.23	$\approx 100\%$
C. Polymeric $\alpha$ -16	0.54	$\approx 62\%$
D. Polymeric $\alpha$ -16; 1mM NTA on the exterior and interior of the SUV <sup>a</sup> .		$< 1\%$
E. 2:1 DPPC/Chol ; 1 mM NTA on the exterior and interior of the SUV <sup>a</sup>		$< 1\%$

<sup>a</sup>Unless noted otherwise, NTA is only retained on the internal compartment of the SUV.

polymerized.\* The  $G_{22}(\infty)$  values and percentage of encapsulation for polymerized  $\alpha$ -16 SUVs (Table II; C) are consistent with competition but not complete immobilization of  $^{111}\text{In}^{+3}$ -NTA, as was the case for DPPC SUVs. Furthermore, when NTA is not removed from the liposome exterior prior to loading, almost no  $^{111}\text{In}^{+3}$  is associated with the liposomes, as shown in Table II,D. Finally, the elution profiles in Figure 1 show virtually complete loading for monomeric  $\alpha$ -16 and a much smaller percentage for the polymeric SUVs. This supports the conclusion that  $^{111}\text{In}^{+3}$  is binding to the thiol groups in the unpolymerized liposomes. As an alternative explanation of the data, it might be argued that in the monomeric  $\alpha$ -thiols, the head groups are packed more tightly than in DPPC liposomes resulting in a higher surface concentration of phosphates and that polymerization somehow negates this affect. Based on the phase transition properties of the  $\alpha$ -thiols, however, this seems unlikely since the  $T_m$ s of these lipids are considerably lower than their nonpolymerizable analogs (i.e.,  $T_m \approx 23^\circ\text{C}$  for  $\alpha$ -16 and  $41^\circ\text{C}$  for DPPC) and relatively unshifted upon polymerization, which would suggest the opposite result : (1) a decreased headgroup interaction for the  $\alpha$ -thiols relative to DPPC and (2) little difference between monomeric and polymeric liposomes. Furthermore, if a headgroup interaction was the cause of the binding, an effect of cholesterol (a headgroup spacer) might be expected, but as is shown in Table II (A and B ), this is not the case.\*\*

To further corroborate these effects, the  $\omega$ -THIOLS were also examined. In Table III, the  $G_{22}(\infty)$  values and percent entrapment are shown for unpolymerized  $\omega$ -11 and 2:1  $\omega$ -11/Chol SUVs. As for the unpolymerized  $\alpha$ -THIOLS , the  $G_{22}(\infty)$  is low

---

\* In these experiments, liposomes were polymerized after sonication in contrast to those used in the serum stability and *in vivo* experiments, which were polymerized prior to liposome formation and stored as lyophilized powders.

\*\* One explanation that cannot be ruled out at this point, however, is a different headgroup orientation for monomeric  $\alpha$ -thiols, which result in more effective binding of  $^{111}\text{In}^{+3}$  to the phospholipid phosphate or a synergistic effect between the sulfhydryl and phosphate groups.

**Figure 1**

Elution profiles for  $\alpha$ -16 SUVs containing 1mM NTA after loading with  $^{111}\text{In}^{+3}$  by the ACAC protocol. **A.** Unpolymerized  $\alpha$ -16 SUVs; **B.** Polymerized  $\alpha$ -16 SUVs. The initial peaks eluted from the column correspond to that of the liposomes (solid lines) and entrapped  $^{111}\text{In}^{+3}$  (dotted lines) whereas the later peaks correspond to absorbance due to the buffer and ACAC (solid line) and unentrapped  $^{111}\text{In}^{+3}$  (dotted lines). The separation was carried out on a 30 x 1.2 cm Sepharose 4BCL column to which was added 0.5 -1.0 mls of a liposome solution. The presence of lipid in the fractions eluted from the column was monitored using a UV detector ( $\lambda = 280$  nm). Radioactivity associated with the fractions was measured using the absolute mode of the PAC spectrometer.

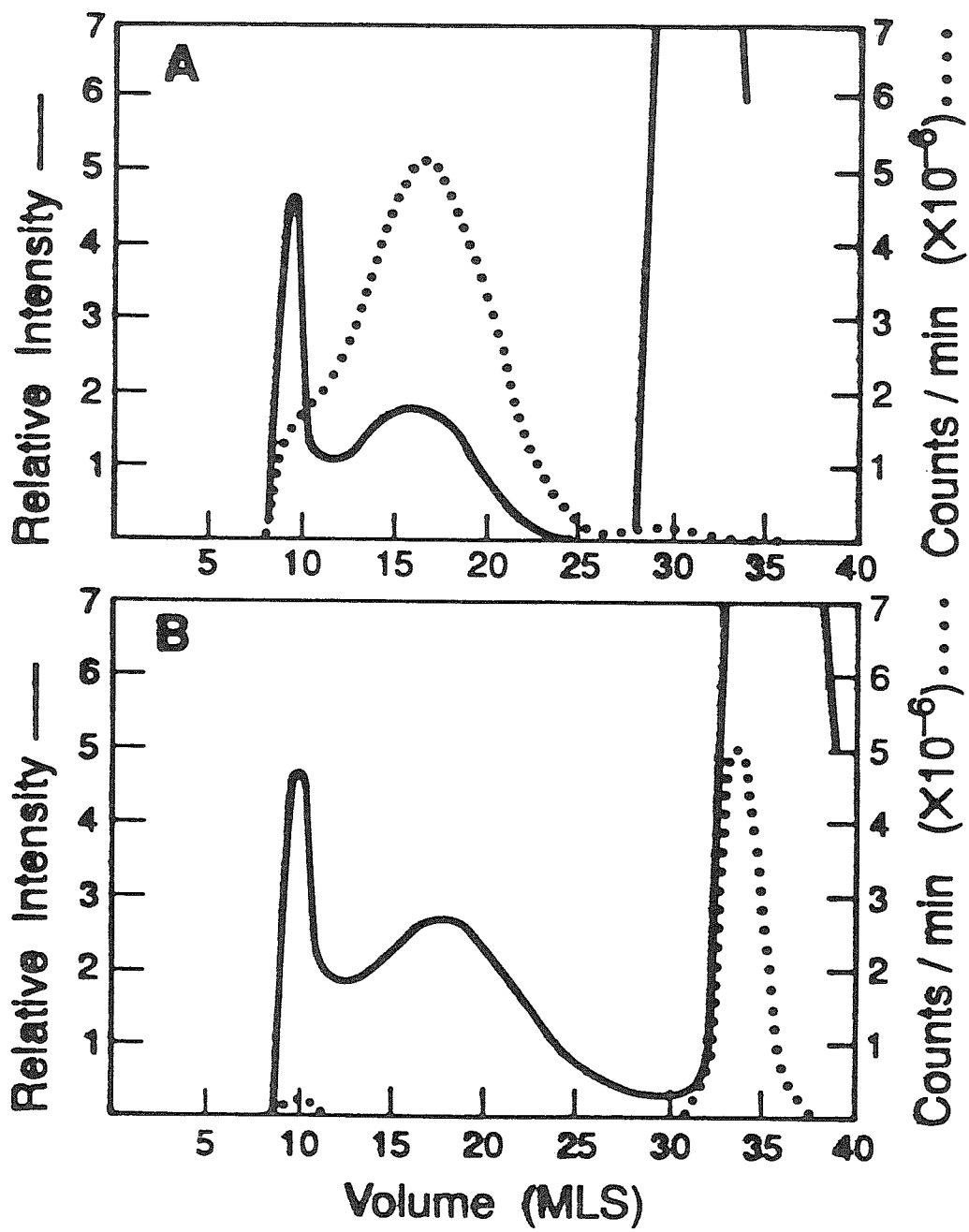


**Table III**

Encapsulation efficiency and value of  $G_{22}(\infty)$  for  $^{111}\text{In}^{+3}$  entrapped in sonicated  $\omega$ -11 liposomes containing 1mM NTA. Liposomes were loaded by the ACAC loading protocol .

**Encapsulation Efficiency and  $G_{22}(\infty)$  for  $\omega$ -11 Liposomes**

<u>Lipid</u>	<u><math>G_{22}(\infty)</math></u>	<u>Percent Entrapped</u>
A. Monomeric $\omega$ -11; 1mM NTA on the exterior and interior of the SUV <sup>a</sup> .	0.15	$\approx 93\%$
B. Monomeric 2:1 $\omega$ -11/Chol	0.14	$\approx 100\%$
C. Polymeric $\omega$ -11	0.22	$\approx 22\%$

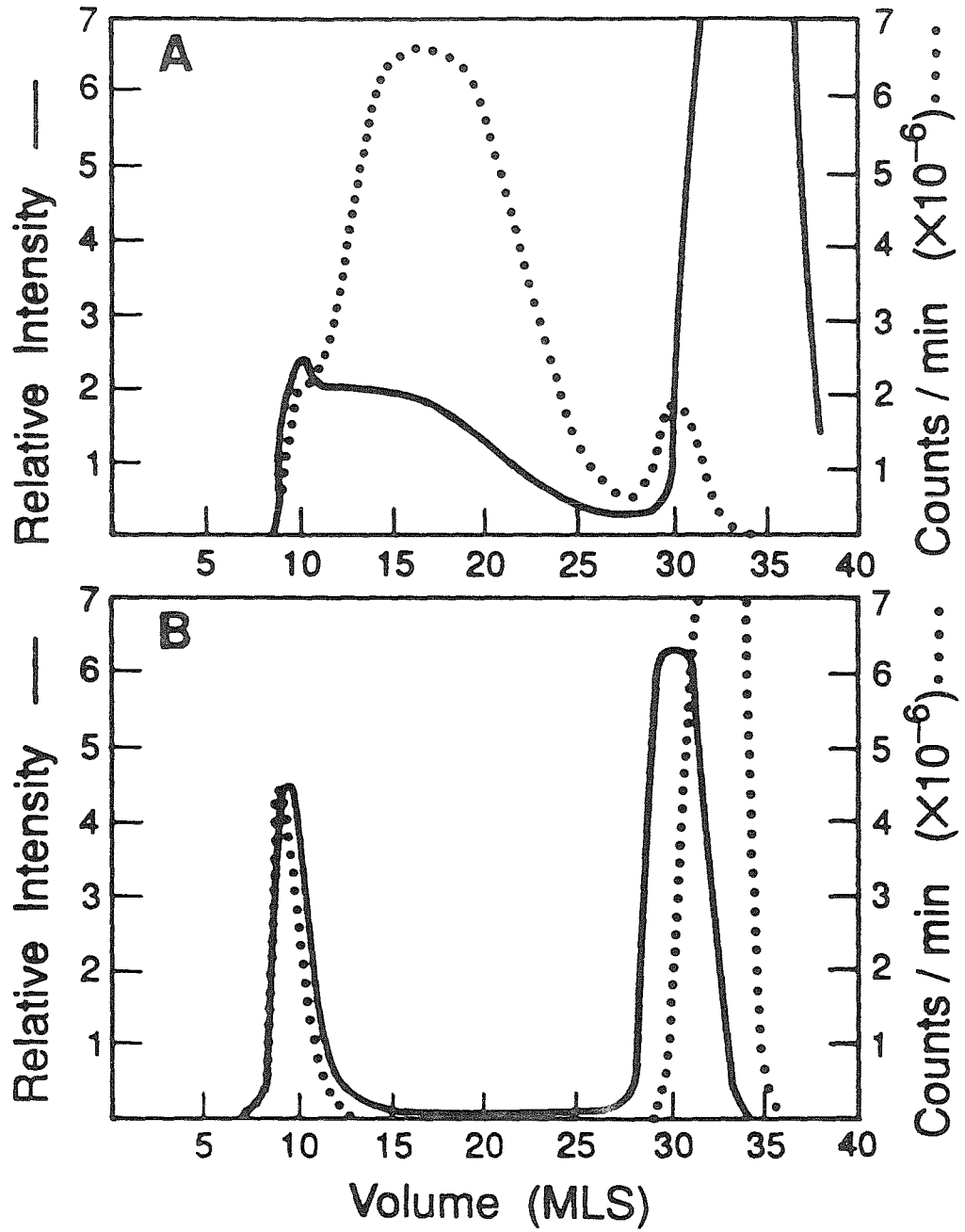
<sup>a</sup>Unless noted otherwise, NTA is only retained on the internal compartment of the SUV.

and the entrapment virtually complete for unpolymerized  $\omega$ -11 (Table III; A and B and Figure 2A) indicating liposome immobilization of  $^{111}\text{In}^{+3}$ . Also noteworthy is the almost complete loading of  $^{111}\text{In}^{+3}$  even when NTA is equally distributed on both sides of the membrane prior to loading, and the negligible effects of cholesterol. Upon polymerization, the  $G_{22}(\infty)$  remains relatively low in contrast to the polymerized  $\alpha$ -THIOLS but the encapsulation is far less than the 100% observed for monomeric  $\alpha$ -THIOLS and  $\omega$ -THIOLS (Table III C and Figure II B). The reasons for this difference may be related to the fact that  $\omega$ -THIOLS form micelles or bilayer fragments upon polymerization (see Chapter II) and therefore have no aqueous compartment for entrapping  $^{111}\text{In}^{+3}$ -NTA. In this regard it should be reiterated that pure DPPC and pure polymerized  $\alpha$ -16 SUVs have slightly lower values of  $G_{22}(\infty)$  compared to  $^{111}\text{In}^{+3}$ -NTA alone, which in the simplest case can be interpreted according to Eqn. 12 as resulting from two populations of  $^{111}\text{In}^{+3}$ : (1) a fraction bound to the liposomes and (2) a fraction of encapsulated, NTA-chelated  $^{111}\text{In}^{+3}$ . Since the polymerized  $\omega$ -THIOLS have no internal aqueous space, only population (1) will contribute to the observed  $G_{22}(\infty)$ , which would account for the low value and the low encapsulation. Similar results were consistently observed for polymerized  $\omega$ -16 and  $\omega$ -15 bilayer fragments. In all cases, whether or not the liposome binding is due to the phosphate groups or the high concentration of disulfides in the membrane interior is difficult to assess. However, in preliminary investigations, we have observed that the addition of 2-10 mM EDTA to the membranes results in the removal of  $^{111}\text{In}^{+3}$  from the polymerized  $\omega$ -THIOLS at a slower rate than from DPPC liposomes (DPPC to which no NTA is added so all the  $^{111}\text{In}^{+3}$  is phosphate bound). This would be expected if at least some of the  $^{111}\text{In}^{+3}$  binding was due to the highly concentrated disulfides in the membrane interior.

While a slight digression from the main objective of the work described in this chapter, the above results of  $^{111}\text{In}^{+3}$  loading indicated some interesting and possibly

**Figure 2**

Elution profiles for  $\omega$ -11 SUVs containing 1 mM NTA after loading with  $^{111}\text{In}^{3+}$  by the ACAC protocol. **A.** Unpolymerized  $\omega$ -11 SUVs; **B.** Polymerized  $\omega$ -11 SUVs. The initial peaks eluted from the column correspond to that of the liposomes (solid lines) and entrapped  $^{111}\text{In}^{3+}$  (dotted lines) whereas the later peaks correspond to absorbance due to the buffer and ACAC (solid line) and unentrapped  $^{111}\text{In}^{3+}$  (dotted line). The separation was carried out on a 30 x 1.2 cm Sepharose 4BCL column to which was added 0.5 -1.0 mls of a liposome solution. The presence of lipid in the fractions eluted from the column was monitored using a UV detector ( $\lambda = 280$  nm). Radioactivity associated with the fractions was measured using the absolute mode of the PAC spectrometer. It is noteworthy that upon polymerization, the polymerized lipid elutes exclusively in the void volume corresponding to a large increase in the particle size in comparison to the unpolymerized  $\omega$ -11 SUVs, which elute almost completely within the fractionation range of the column.



useful peculiarities of the thiol-containing liposomes. Thiol-containing lipid-metal binding is in fact currently under study by several groups for various applications. From a practical standpoint, however, it presents a technical difficulty in the current investigation in that complete immobilization of  $^{111}\text{In}^{+3}$  by the monomeric  $\alpha$ -THIOLS and  $\omega$ -THIOLS precludes the use of PAC for biodistribution and stability studies of these systems. This is due to the fact that it is not possible to entrap  $^{111}\text{In}^{+3}$ -NTA in the aqueous interior of these liposomes, even when 10 mM NTA is used to compete the  $^{111}\text{In}^{+3}$  off the liposome surface\* . Similarly, for the polymeric  $\omega$ -THIOLS, PAC cannot be used because the assay relies on the presence of an internal compartment.\*\* Therefore, in the remainder of the chapter concerning the serum stability, tissue distributions, and degradation of liposomes in the liver, only the polymerized  $\alpha$ -THIOLS, nonpolymerizable lipids, and their mixtures with cholesterol will be discussed. The exception to this is a mixed chain  $\omega$ -THIOL composed of a polymerizable chain (N=16) and a nonpolymerizable chain (N=16) in the sn-1 and sn-2 positions, respectively ( $\omega$ 16-DPL). In contrast to the identical chain  $\omega$ -THIOLS , mixed chain thiols were found to form liposomes upon oxidation to dimers, for all chain lengths investigated (see Chapter II). A final point to note is that for all remaining experiments described in this chapter, 10 mM NTA was utilized as the internal chelate concentration in order to eliminate as much as possible  $^{111}\text{In}^{+3}$ -liposome binding, elevate the value of  $G_c$  ( $G_{22}(\infty)$ ), and thereby increase the dynamic range and sensitivity of the experiment.\*\*\*

---

\* The  $G_{22}(\infty)$  is still low with 10mM NTA.

\*\* Conceptually, biodistribution studies could be done since  $^{111}\text{In}^{+3}$  is associated with the membranes, but the results would be complicated by possible dissociation of  $^{111}\text{In}^{+3}$  prior to deposition in target tissues.

\*\*\* We have observed that at this chelate concentration,  $^{111}\text{In}^{+3}$  is still readily transferred from NTA to serum and cellular proteins. By contrast, EDTA, which has a much higher affinity for  $^{111}\text{In}^{+3}$  than NTA, remains bound to  $^{111}\text{In}^{+3}$  *in vivo* and therefore cannot be used in these studies.

## 1. SUVs

### SERUM STABILITY OF SUVs

Having established the basic loading protocol and determining which lipids could be evaluated by the PAC technique, the stabilities of liposomes having various compositions were evaluated. In particular, we were interested in the  $\alpha$ -THIOLS (N=16-20) as we have found they form SUVs very readily, presumably as a consequence of their slightly disordered chains, well hydrated headgroups, and the tendency to form unilamellar vesicles (see Chapter II). It has already been shown in earlier chapters, however, that the  $\alpha$ -THIOLS have broad phase transitions centered around 23°, 38°, and 52°C for N=16,18, and 20, respectively, and that leakage is maximal at these temperatures. This is illustrated in Figure 3 for  $\alpha$ -16 SUVs which have a  $T_m$  at approximately room temperature, and a correspondingly higher leakage rate at 23°C than at 37°C. Pure  $\alpha$ -16 and especially  $\alpha$ -18 liposomes are therefore unsuitable for physiological studies as all contents would be released, especially in serum, which generally accelerates the leakage. This is similar to the behavior of nonpolymerizable lipids, which are most permeable in the vicinity of the phase transition (60). For nonpolymerizable phospholipids, leakage has been greatly minimized by the addition of cholesterol to both condense the bilayer and abolish the phase transition temperature (e.g., for DPPC/Chol, SPH/Chol, and EPC/Chol). The same strategy was attempted with  $\alpha$ -16 and  $\alpha$ -18 SUVs, and as illustrated in Figures 4 and 5, the addition of cholesterol does enhance the stability. For  $\alpha$ -16/Chol SUVs, it is difficult to say what stoichiometry of the two components is most stable as there is a fair amount of scatter in the data and there is not an exact correlation between mole fraction of cholesterol and stability. Nonetheless, above a 2:1 ratio, the liposomes appear quite resistant to leakage of  $^{111}\text{In}^{3+}$  (80% on average for  $\approx$  100 h in serum). For  $\alpha$ -18, increasing concentrations of cholesterol in the membrane clearly promote stability, at least up to a ratio of 3:2 ( $\alpha$ -18:Chol). At physiological temperatures,  $\alpha$ -18

**Figure 3**

Leakage of  $^{111}\text{In}^{+3}$  from polymerized  $\alpha$ -16 SUVs at 23 °C and 37°C in serum. The decreased rate of leakage at the higher temperature is due to the room temperature phase transition of polymerized  $\alpha$ -16. Temperatures are noted in the legend of the figure.

### A16P SUVs; LEAKAGE AT 37 versus 22

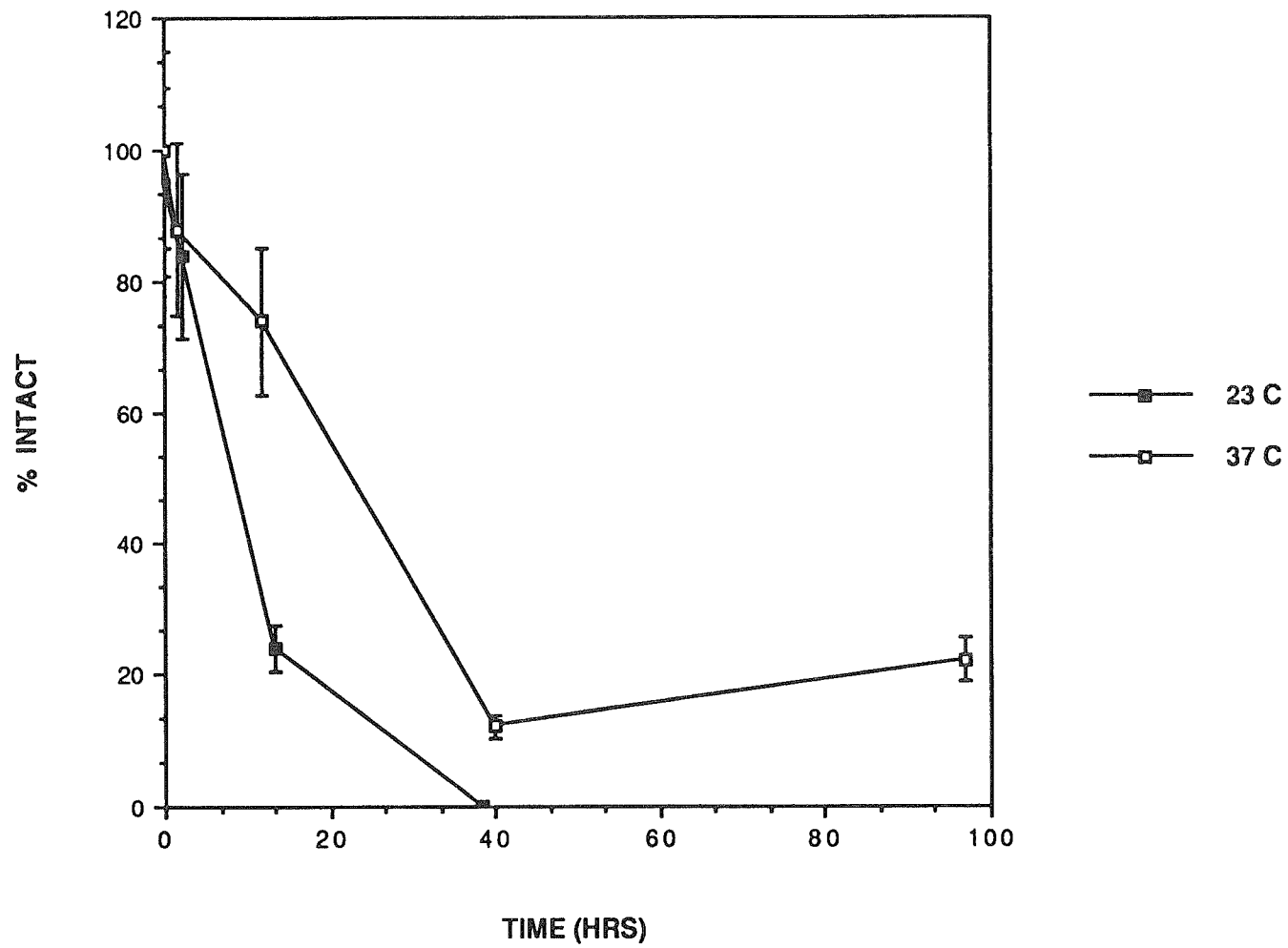


**Figure 4**

Leakage of  $^{111}\text{In}^{3+}$  from polymerized  $\alpha$ -16/Chol SUVs at **A.** 37°C and **B.** 23 °C in serum. The  $\alpha$ -16/Chol mole ratios are indicated in the legend of the figures.

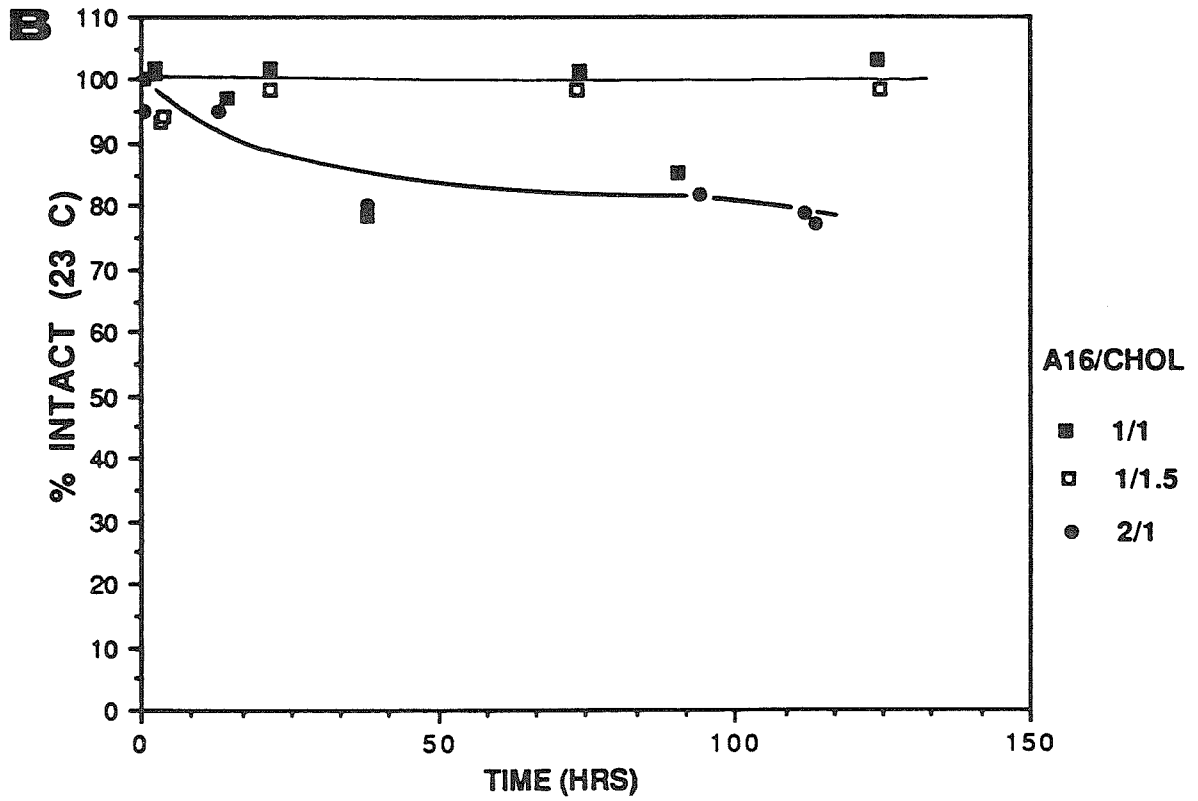
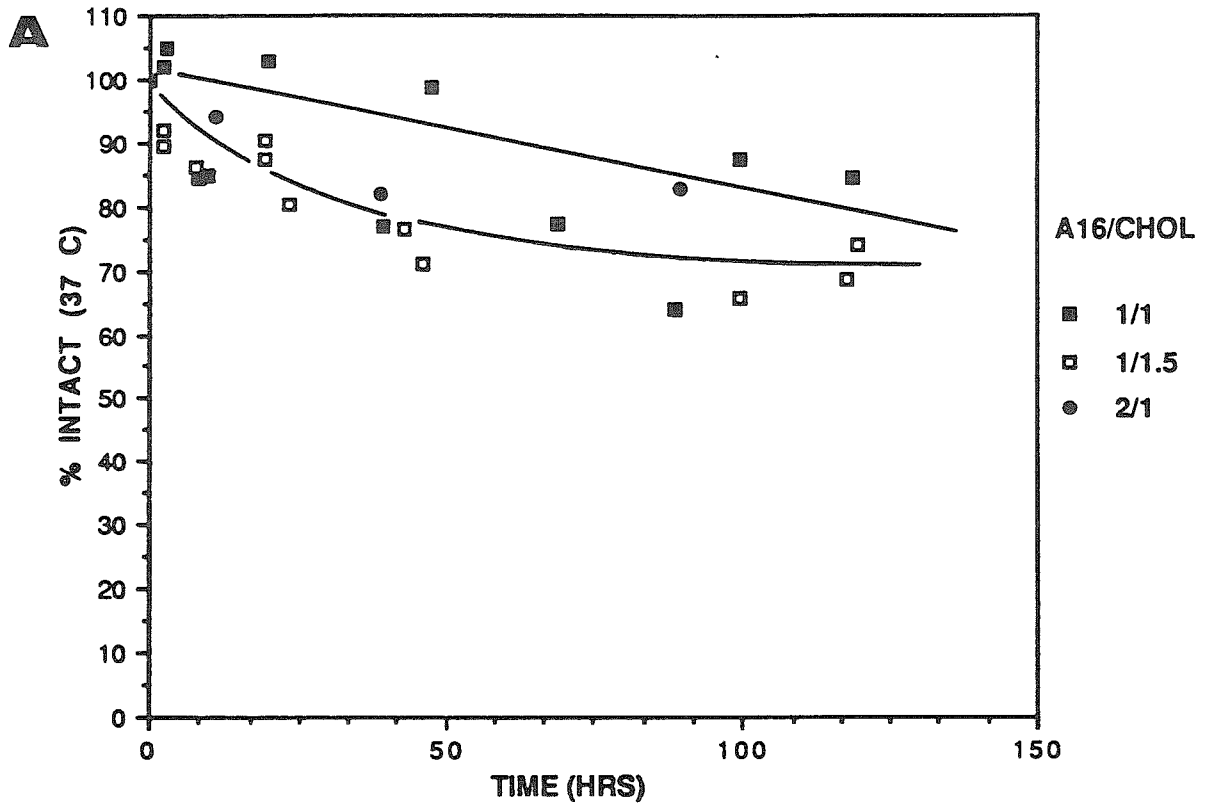
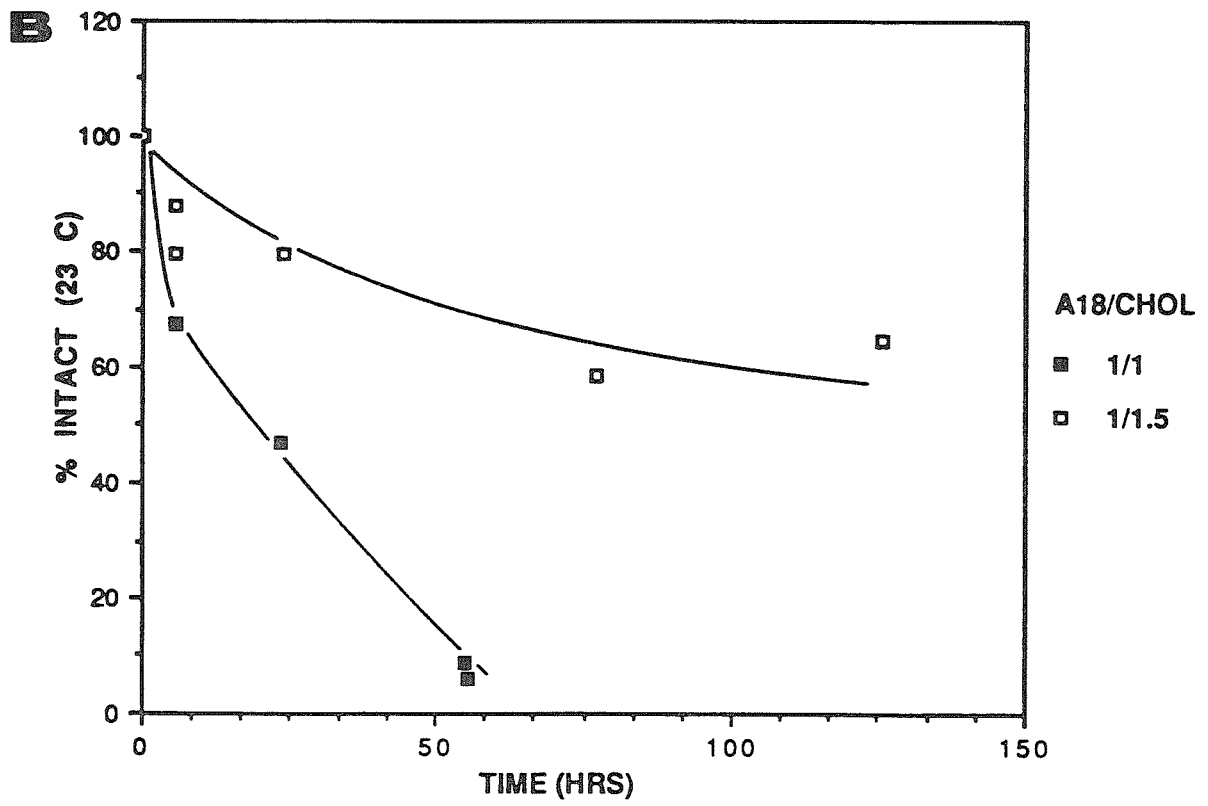
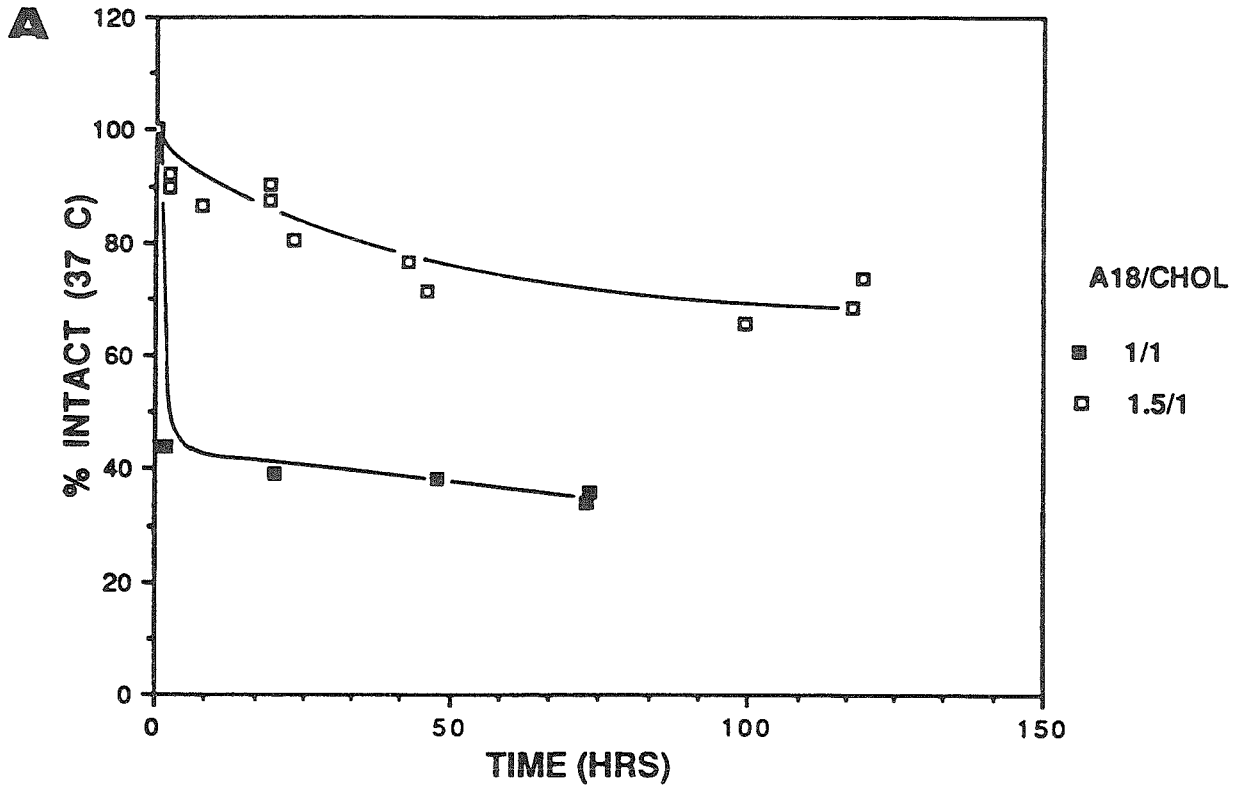


**Figure 5**

Leakage of  $^{111}\text{In}^{3+}$  from polymerized  $\alpha$ -18/Chol SUVs at **A.** 37°C and **B.** 23 °C in serum. The  $\alpha$ -18/Chol mole ratios are indicated in the legend of the figures.



liposomes release contents virtually instantaneously.

It is interesting to note that these polymeric liposomes can accommodate so much cholesterol in the bilayer and still readily form SUVs. For saturated phosphatidylcholines, the addition of such large amounts (> 50%) precludes SUV formation. In fact equimolar DSPC/Chol liposomes are often difficult to prepare (20). The apparent disorder in the polymeric membranes described in Chapters III and IV indicates that these membranes are not as tightly packed as their saturated nonpolymerizeable phosphatidylcholine analogues and the additional "space" may be fundamentally important for the cholesterol solubility.\* An additional interesting point is the fact that  $\alpha$ -16/Chol 1:1 is more stable than  $\alpha$ -18/Chol 1:1 at 37°C in serum, despite the longer chain length of the phospholipid in the latter. This may be an effect of the phase transition of  $\alpha$ -18. Due to the polymeric nature of the lipids, some degree of phase separation of the cholesterol and  $\alpha$ -THIOL may occur with the result that the transition is not completely eliminated. DSC of 2:1  $\alpha$ -THIOL/Chol mixtures did in fact show that the transition was not completely abolished as it is for many nonpolymerizeable phospholipids at this stoichiometry. Furthermore, the percentage of residual transition after cholesterol incorporation (2:1  $\alpha$ -THIOL/Chol) increased with increasing chain length, consistent with the leakage data. Whether or not there is any detectable transition at a 1:1 ratio has yet to be ascertained. On the other hand, it is not known whether phase-separated domains, which give rise to transitions and alterations of the membrane sizeable enough to have an effect on serum-induced leakage, must have a transition detectable by DSC.

$\alpha$ -20 was originally synthesized in order to circumvent the phase transition-induced leakage exhibited by the other  $\alpha$ -THIOLS at the two temperatures most relevant to

---

\* Partitioning studies of propranolol in  $\alpha$ -16 dispersions also indicates a higher solubility of these neuro compared to DPPC (D. Rhodes, unpublished results).

these studies (room temperature ( $\alpha$ -16) and physiological temperature ( $\alpha$ -18)). In contrast to  $\alpha$ -16 and  $\alpha$ -18 (both liquid-crystalline at 37°C),  $\alpha$ -20 not only has a transition well away from these critical temperatures ( $\approx$ 52°C), but it is in the gel state, which would be expected to minimize leakage, in analogy to the behavior of nonpolymerizable phospholipids. The stability of SUVs in serum shows that this is indeed the case. On average,  $\approx$  90% of the contents are retained at 150 h at both room temperature and 37°. This is shown in Figure 6A. In contrast to  $\alpha$ -16 and  $\alpha$ -18 SUVs, however, the addition of cholesterol to  $\alpha$ -20 SUVs is destabilizing (Figure 6B). It has been shown that for certain lipids (i.e., DPPC), cholesterol increases leakage in the gel state by fluidizing the membrane, whereas it decreases leakage in the liquid crystalline state by condensing the membrane (61). These data, however, were demonstrated for leakage *in buffer* and the effects of serum proteins on leakage were not considered. Furthermore, liposomes prepared from DSPC/Chol 2:1 (an 18-carbon saturated phospholipid) have been found to be extremely stable in serum towards leakage of  $^{111}\text{In}^{3+}$  despite the fact that the phospholipid component is a gel state lipid ( $T_m \approx 57^\circ\text{C}$ ) (data not shown). It therefore seems a more likely explanation is hydrophobic mismatch between the cholesterol and long 20 carbon chains of  $\alpha$ -20, which could promote bilayer defects and subsequent solute leakage. This explanation would also be consistent with the correspondence between the residual enthalpy with chain length for 2:1  $\alpha$ -THIOL/Chol mixtures described above.

### *IN VIVO* STUDIES OF SUVs

*Tissue Distributions of SUVs.* The results from the last section indicated  $\alpha$ -20,  $\alpha$ -16/Chol, and  $\alpha$ -18/Chol SUVs were reasonably stable in serum (37°C) and therefore suitable for studying the *in vivo* behavior of this class of polymerizable lipids. The tissue distributions of these liposome types was of interest to see if the presence of the polymerizable group near the interface altered the distribution profile in any way.

**Figure 6**

Leakage of  $^{111}\text{In}^{+3}$  from polymerized **A.**  $\alpha$ -20 SUVs at 37°C and 23 °C in serum and **B.**  $\alpha$ -20/Chol SUVs at 37 °C in serum. The  $\alpha$ -20/Chol mole ratios are indicated in the legend of the figures.

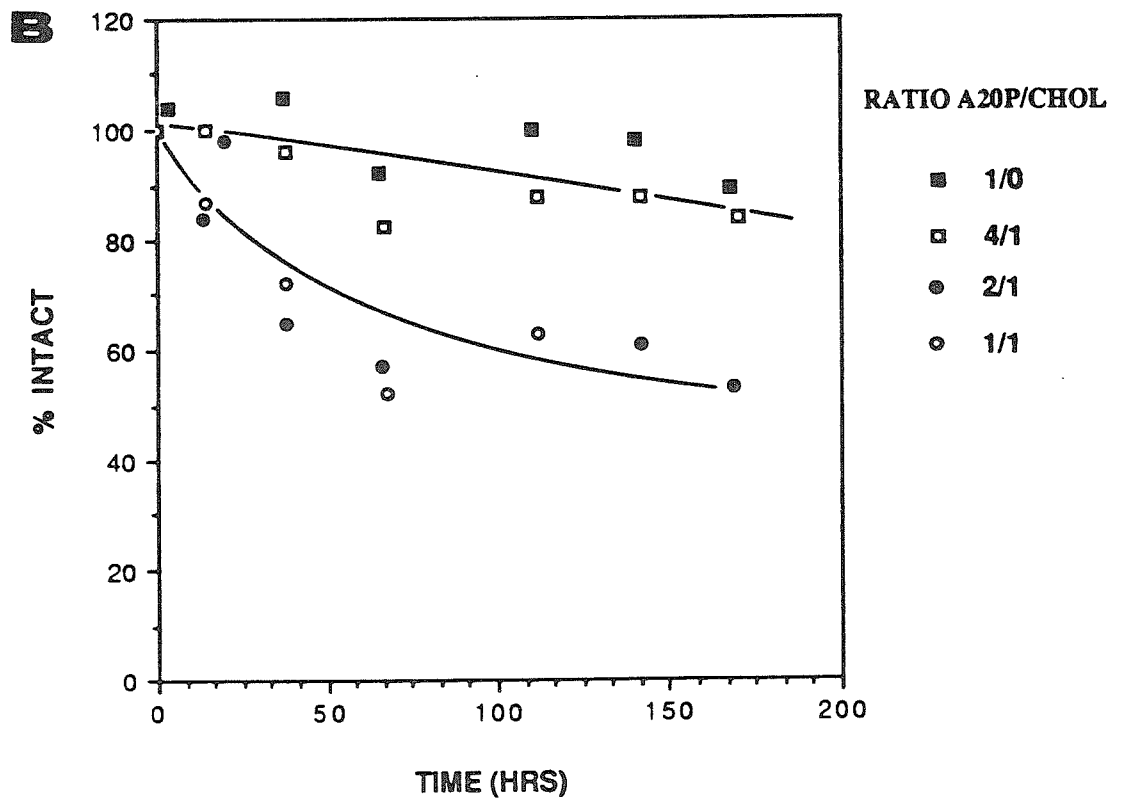
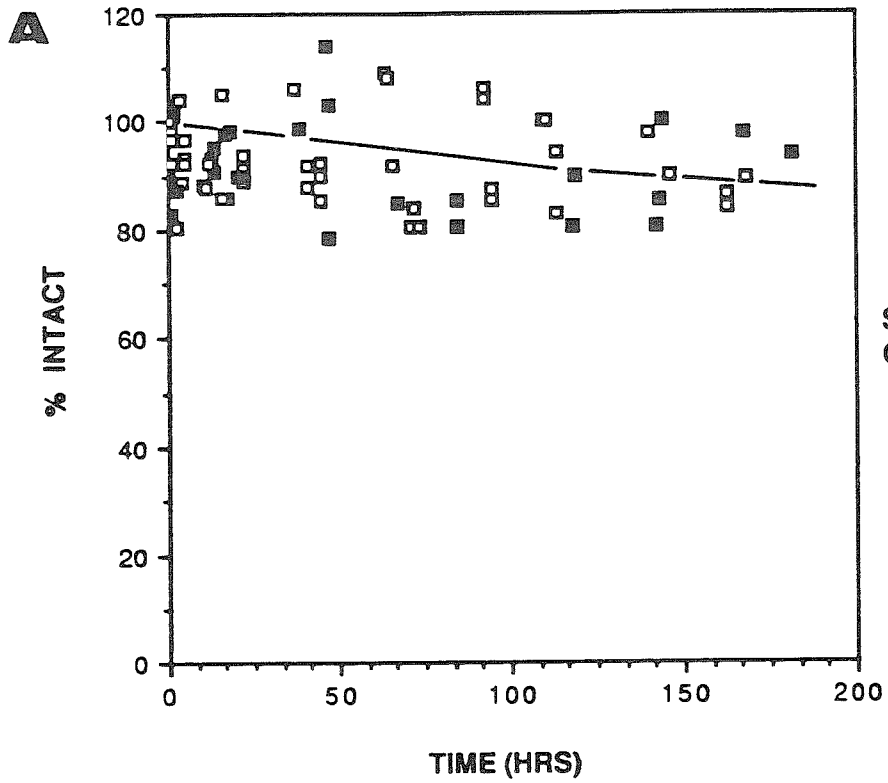


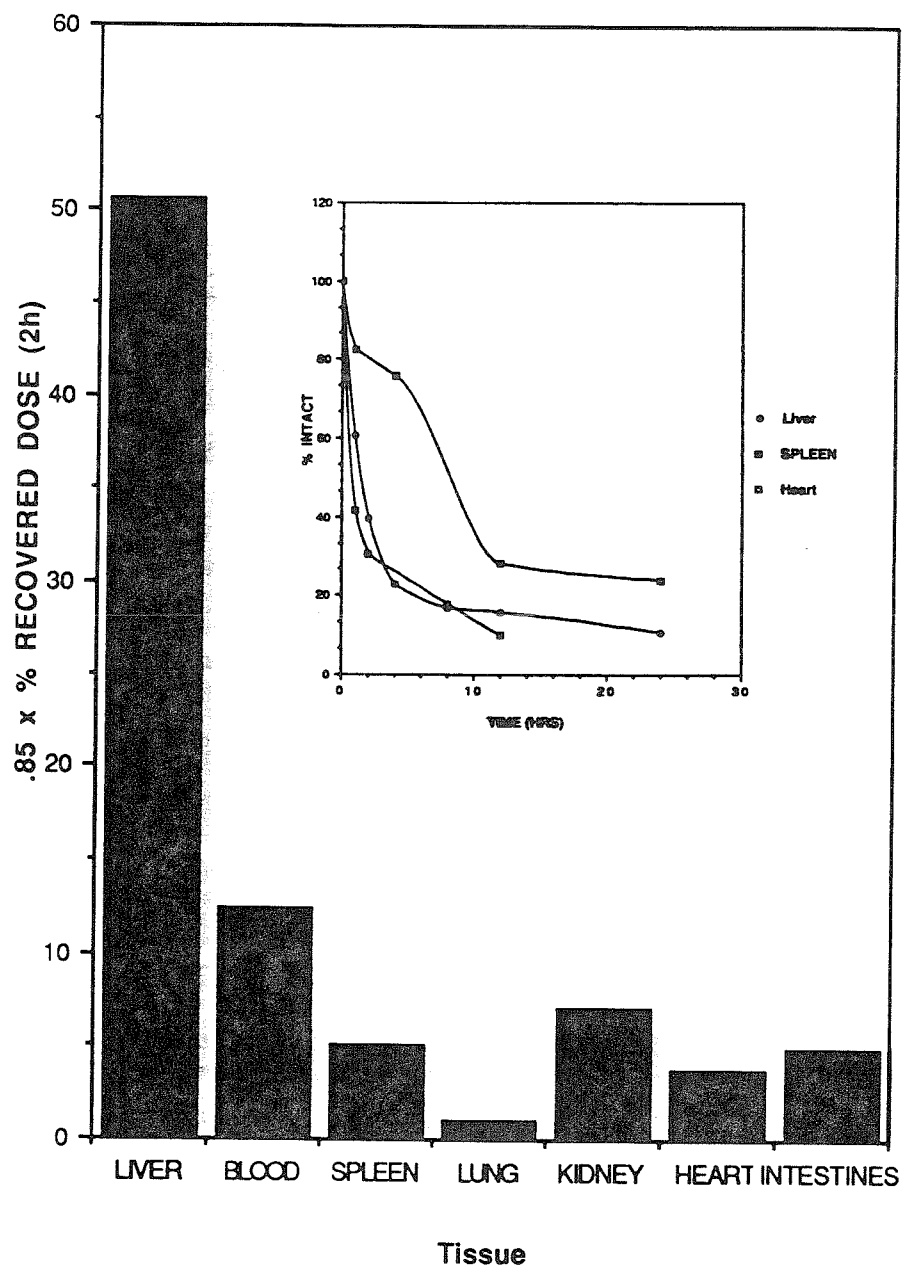
Figure 7 shows a typical distribution following clearance of the  $\alpha$ -20 liposomes from the blood (2 h). For the most part, the distribution resembles that of many other phosphatidylcholine-based liposomes in that the majority go to the liver, and on a gram basis, to the spleen (1,10,57). An interesting exception to this in the case of  $\alpha$ -20 liposomes was a small but reproducible 2-4 fold higher percentage (3-4%) associated with the heart that could not be accounted for by residual blood. In fact, the percent injected dose was higher in the heart than the lung whereas the opposite is generally observed in nonpolymerized liposomes. Analysis of the  $G_{22}(\infty)$  of the heart indicated that these liposomes were intact and the degradation rate quite slow relative to the liver and spleen (see insert). It seems very likely, considering the endothelial barriers between the blood and cardiac cells, that the liposomes are adhering to the vessel walls but are not being internalized by the cells. This would also be consistent with the slow degradation.

Radioactivity associated with both the intestines and kidneys is common to all liposome types studied, as is a low  $G_{22}(\infty)$  indicating protein-bound  $^{111}\text{In}^{+3}$ . Since the percent injected dose in these tissues increases with time after blood clearance, the radioactivity most likely originates from degraded liposomes in the liver (and spleen) and is subsequently translocated via macromolecular carriers either back into the blood and finally to the kidneys or from the liver into the intestines. In the kidneys, the  $^{111}\text{In}^{+3}$  is stripped of binding proteins and passed into the urine bound to a small chelate as evidenced by extremely high values of the  $G_{22}(\infty)$ . The latter result is consistent with recent observations by Derksen *et al.* (10).

*Blood Clearance of  $\alpha$ -20 SUVs.* As shown above, a major percentage of intravenously injected liposomes ultimately accumulate in the RES, regardless of liposome

**Figure 7**

Tissue distribution of  $\alpha$ -20 SUVs 2 h after intravenous injection into Balb/c mice.  
The insert shows the intracellular degradation rates for the heart, liver and spleen.



composition.\* What does depend drastically on composition is the *rate* of blood clearance. Furthermore, as explained in the introduction, a reasonably long circulation time is necessary for extravasation of the liposomes from the circulatory system into extravascular tissues or tumors. We therefore were interested in the rate of blood clearance of polymerized SUVs and how it compares to that of long-circulating nonpolymerizable liposomes. The basic structural question we wished to address with these experiments was : Can one mimic the solid membrane surface exhibited by, e.g., DSPC/Chol and SPH/Chol liposomes with interfacial disulfide polymerization? Because  $\alpha$ -20 SUVs were stable without the addition of other constituents, they were studied first to examine the effect of polymerization without the complication of added cholesterol.

Figure 8A shows the percentage of  $\alpha$ -20 SUVs in the blood, liver and spleen with time. As can be seen, the liposomes are cleared extremely rapidly (< 1 hour) with a concomitant accumulation in the liver. As a point of reference, similar data is shown for DSPC/Chol liposomes in Figure 8B. Clearly there is a great disparity in the clearance rates. The slow clearance for DSPC/Chol liposomes is however largely due to the presence of the cholesterol component as has been shown by Gregoriadis *et al.*, and in that sense the comparison is unfair (20). Unfortunately, we have not done similar experiments with pure DSPC or more appropriately, DAPC (diarachidoylphosphatidylcholine, N = 20)\*\* . However, a longer circulation half life in mice (2.1 hours) for DSPC SUVs of approximately the same size as the  $\alpha$ -20 liposomes has been reported. Furthermore, the clearance profile of the DSPC liposomes showed a biphasic, *gradual* removal over the course of hours rather than an *immediate*

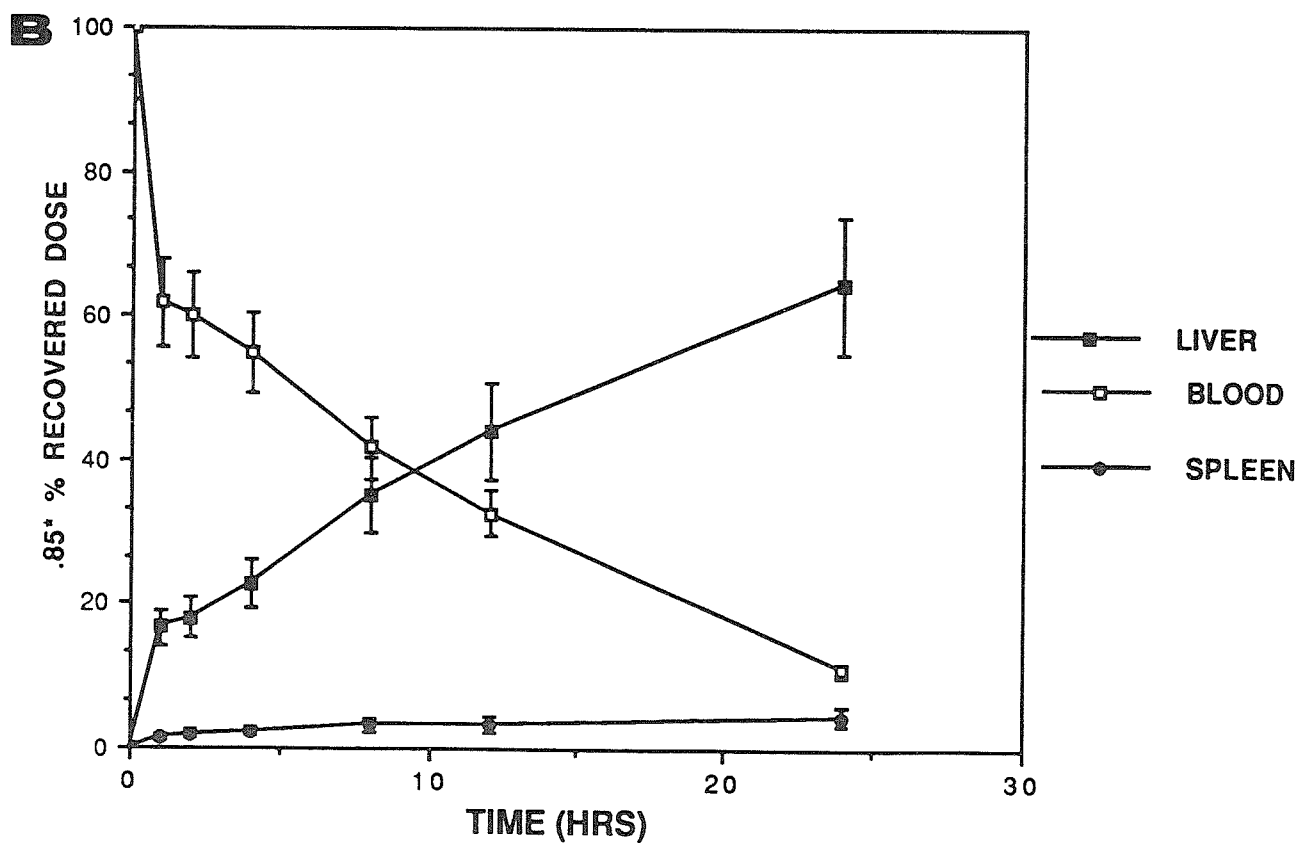
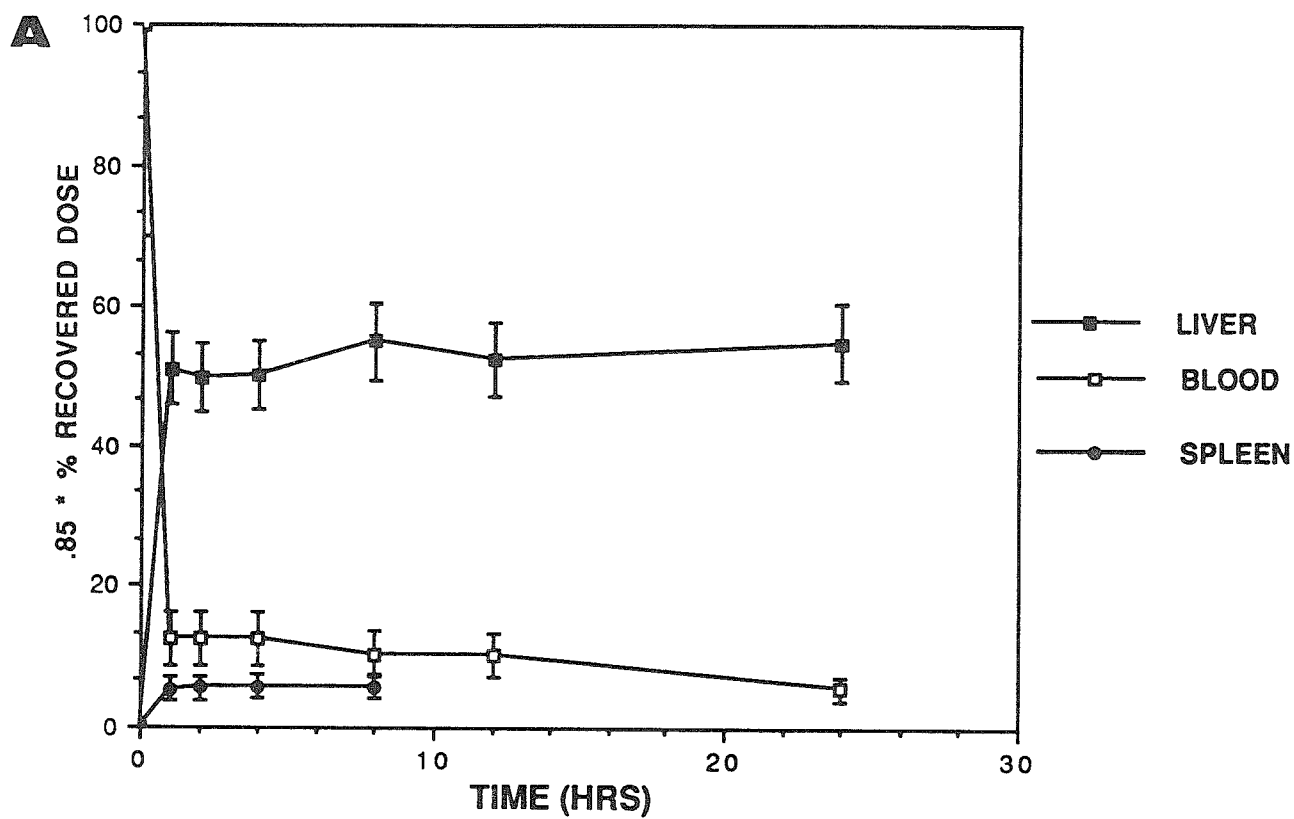
---

\* In some cases, accumulation in the bone has also been observed for very long circulating liposomes. As for the liver and spleen, the bone marrow has fenestrations in the endothelial barrier which can allow passage of SUVs. We have not examined the carcass for radioactivity, but considering the relatively short life time of the liposomes in the blood, significant accumulation is unlikely.

\*\* It is not even clear that DAPC SUV's can be formed, due to the extreme crystallinity of bilayers formed from these lipids. This contrasts with  $\alpha$ -20 SUV's, which are very readily formed.

**Figure 8**

The percentage of liposomes recovered in the blood, liver and spleen with time for: A. Polymeric  $\alpha$ -20 liposomes and B. 2:1 DSPC/Chol. The symbol designations are indicated in the figure legend.



*clearance* as in the case of  $\alpha$ -20 SUVs.\* These data indicate polymerization in this manner has not had the intended effect of solidifying the interface and retarding protein absorption, and in fact, seems to have been detrimental to prolonged blood circulation.

*Intracellular Degradation of  $\alpha$ -20 SUVs.* It has been shown that for many nonpolymerizable SUVs, there is a correlation between *stability* in the blood and *longevity* in the blood ; liposomes of low stability tend to be cleared at a rapid rate (20). Although it has not been demonstrated, it might be expected that stability of liposomes *in cells* would also have a correlation with the circulation time in the blood. The degradation of liposomes in the liver and spleen was therefore examined. Figure 9 shows the percentage of intact liposomes in these tissues for  $\alpha$ -20 and DSPC/Chol SUVs. As predicted above, the rapidly cleared  $\alpha$ -20 SUVs are also more quickly degraded than the DSPC/Chol liposomes in these organs, despite the fact that the initial intracellular concentration of  $\alpha$ -20 liposomes is higher than that of DSPC/Chol\*\*. It should be pointed out, however, that because of the nature of the PAC assay, the percent intact refers collectively to the consequences of both (i) liposome leakage and (ii) liposome degradation. For SUVs, lipid degradation is not necessary to release all contents ; a single "hole" or defect in the bilayer induced by protein penetration is sufficient. Therefore, in Figure 9 the more rapid degradation for  $\alpha$ -20 SUVs may be a consequence of accelerated chemical degradation, mechanical disruption by, e.g., protein absorption , or a combination of both. An additional possibility is that the two liposome types access different cell populations in the liver. Accumulation of the  $\alpha$ -20 SUVs in the catabolically very active Kupffer cells versus endocytosis of the

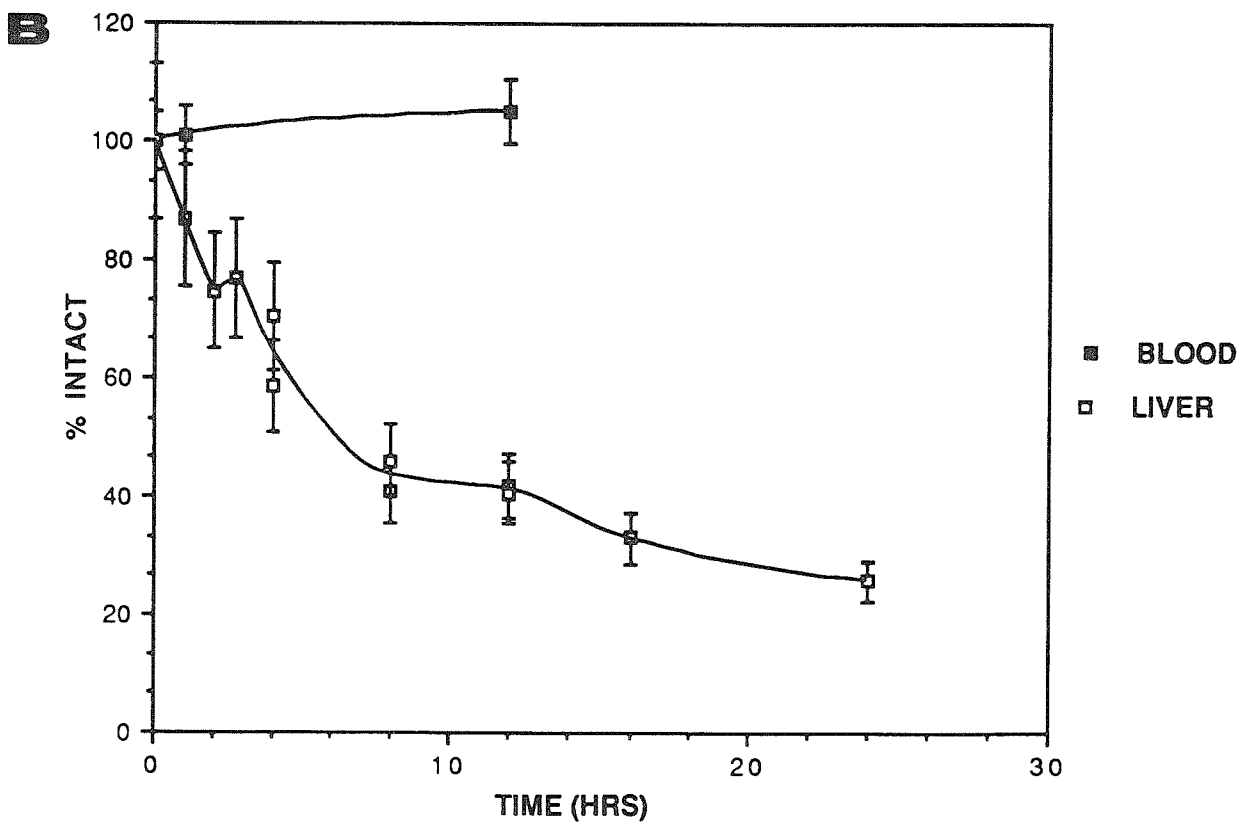
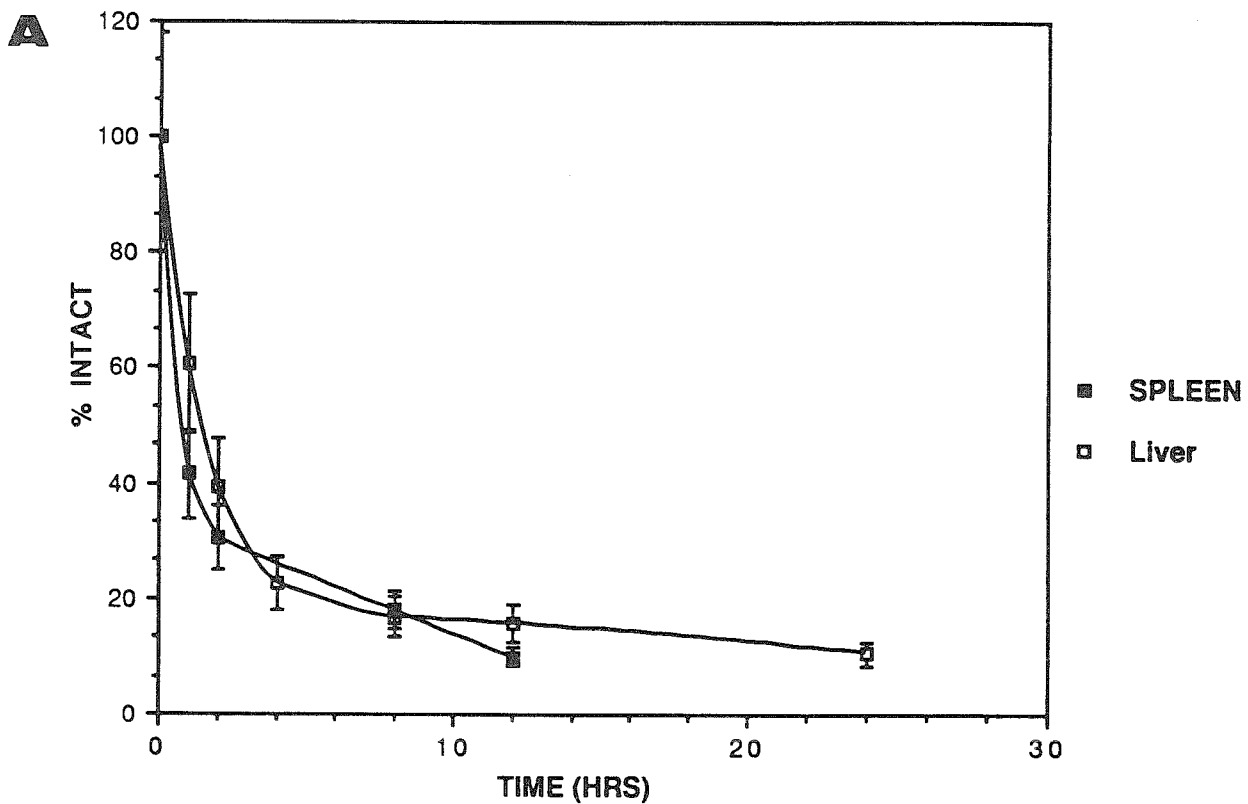
---

\* The biphasic clearance pattern of the DSPC/Chol liposomes is generally observed for SUV' s and has been ascribed to a combination of effects including heterogeneity in the size distribution of the liposomes, saturation of the endocytic machinery, and depletion of opsonizing proteins (36).

\*\* A dependence of the degradation rate of liposomes on the injected dose is well documented and indicates a faster rate at lower liposome concentrations and saturation at very high concentrations. In these experiments, the injected dose is far below the saturation limit.

**Figure 9**

Percentage of intact liposomes remaining in the liver, spleen and blood for **A.** Polymeric  $\alpha$ -20 SUVs and **B.** 2:1 DSPC/Chol SUVs at various times following intravenous injection in Balb/c mice. Symbol designations are indicated in the figure legend.



DSPC/Chol liposomes by the more numerous but less active hepatocytes could explain the difference. While we cannot distinguish the intrahepatic distribution on the basis of our data, one could rationalize Kupffer cell uptake of  $\alpha$ -20 SUVs based on what is known about the distribution of liposomes between parenchymal and non-parenchymal cells. MLVs are known to be rapidly phagocytosed almost exclusively by the Kupffer cells while SUVs have additional access to the hepatocytes via the 30-200 nm fenestrations in the liver sinusoids (32). Long lived phosphatidylcholine-based SUVs have been shown to accumulate primarily in the hepatocytes, but upon addition of negative charge (i.e., phosphatidyl serine (PS)), the hepatic distribution is shifted towards the Kupffer cells (32). Thus Kupffer cell uptake of  $\alpha$ -20 SUVs could occur, particularly if these liposomes absorbed proteins that bestowed a net negative charge to the membrane surface, as is known to occur for many colloidal systems (36). Regardless of the details whereby the  $\alpha$ -20 SUVs are rapidly cleared and permeabilized, the fundamental reason must arise from the different physical properties of the membranes in question. This is discussed next.

*Analysis of Blood Clearance and Degradation in Terms of the Membrane Organization of  $\alpha$ -20 SUVs.* Given the characterization of the membrane physical properties described in the last several chapters, we are in a position to speculate as to the *structural basis* for the rapid blood clearance and intracellular degradation of the  $\alpha$ -20 SUVs. Ample evidence has demonstrated that blood clearance and stability can be manipulated by the choice of the phospholipid (and proportion of cholesterol) in the membrane (20,24,28). Fluid lipids such as EPC are cleared and degraded rapidly due to the susceptibility of such membranes to disruption by HDL, phospholipases and the absorption of other proteins (16,24). The  $\alpha$ -THIOLS as a general class of phospholipids, have been shown by a variety of physical techniques to have a more disordered hydrocarbon region in the gel state than nonpolymerizable lipid analogues. In fact, the acyl chains

appear to be in a state somewhere intermediate to the gel and liquid-crystalline state of nonpolymerizable lipids. On the other hand, the glycerol backbone and headgroup region have been shown by NMR to be more rigid as a consequence of the polymerization. This latter fact we hoped implied that these liposomes had an effectively solid interface with properties similar to DSPC/Chol and SPH/Chol, despite the disorder in the chains. The *in vivo* data does not support this anticipation, however. In retrospect, it is clear that rigidity is not necessarily a reflection of tight interfacial packing. In fact, the polymerization-induced rigidity at the interface most likely restricts the conformational freedom of the lipids and inhibits their ability to pack into well-organized crystalline arrays. Particularly in light of the two-dimensional structure of the polymer in question, which is that of a *linear chain* rather than an *infinitely crosslinked network*. the consequence of this could be the induction of interfacial defects and the observed disorder in the lipid chains.\* This appears to be the most viable explanation for the behavior of  $\alpha$ -20 SUVs *in vivo* ; despite the fact that these lipids are in the gel state and polymerized, the membrane is in fact relatively disordered and therefore accessible to interaction with serum and cellular proteins. The result of this is the observed rapid rate of blood clearance and intracellular degradation.

*In Vivo Studies of  $\alpha$ -THIOL/Chol SUVs.* As described above, the clearance and degradation rates for  $\alpha$ -20 SUVs were unusually rapid, especially considering that the lipid is a saturated gel state phospholipid with unusually long hydrocarbon chains. However, the rates for SUVs composed exclusively of phospholipids generally tend to be rapid, and only upon addition of cholesterol are long half lives obtained. For example, Gregoriadis demonstrated a 2.1 hour half life for DSPC SUVs, but upon addition of equimolar cholesterol, this was extended to  $\approx 7.5$  hours (8,20). Likewise, Hwang has measured a 16.5 half life for 1:1 SPH/Chol SUVs (58). That for SPH

---

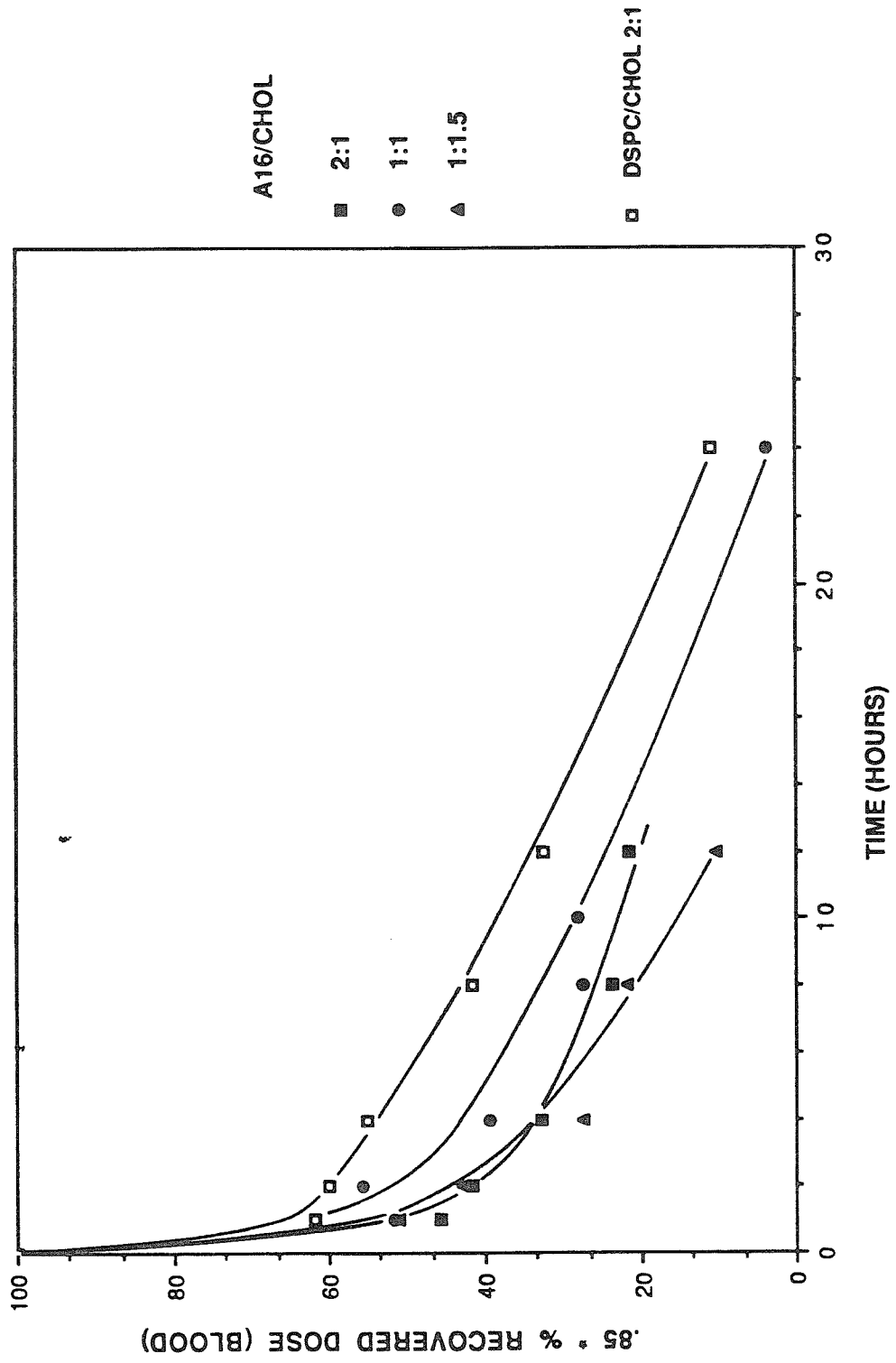
\* This was also mentioned as a possible explanation for spectroscopic and phenomenological data described in earlier chapters.

alone has not been reported, presumably because the phase transition is 37°C and contents would be released immediately upon injection. SPH differs only slightly from the structure of a basic phosphatidylcholine by the presence of a rigid linkage in the sn-2 position. Nonetheless, this simple modification allows the formation of well packed bilayers with equimolar cholesterol, accounting for the exceptionally long blood half lives.  $\alpha$ -THIOLS are also modified at the interfacial region in a manner that imposes rigidity, and since large quantities of cholesterol are readily accommodated in the bilayer, it was of interest to see if upon addition of cholesterol, solid SPH/Chol-like liposomes could be formed. (In this regard, the PAC experiments may be viewed as a qualitative assay of the nature of the interface presented by liposomes). Since  $\alpha$ -16/Chol SUVs were found to be more stable in serum than those prepared from either  $\alpha$ -18/Chol or  $\alpha$ -20/Chol, SUVs composed of  $\alpha$ -16/Chol in the ratios 2:1, 1:1 and 1:1.5 were examined for blood clearance.

Figure 10 shows the blood clearance of 2:1, 1:1 and 1:1.5  $\alpha$ -16/Chol SUVs. Within experimental error (which includes the effect of slight differences in liposome size), the rate is notably similar to 2:1 DSPC/Chol. Compared to  $\alpha$ -20 SUVs the clearance rates are much slower due to the solidifying effect of the sterol. Unfortunately, the ability of these liposome types to accommodate so much cholesterol in the bilayer does not prolong the blood circulation time beyond a certain point, which is somewhat surprising. From light scattering measurements of the  $\alpha$ -16/Chol SUVs, it is clear that the lack of additional effects from cholesterol is not due to an increase in the average size of the liposomes with increasing cholesterol content; all liposomes were found to have approximately the same size ( $50 \pm 5$  nm). A more likely explanation would therefore seem to be differences in the interaction of the phospholipid and cholesterol, possibly due to polymerization-induced restrictions of the orientation of cholesterol in the bilayer.

**Figure 10**

Percentage of liposomes remaining in the blood at various times post-injection for polymeric  $\alpha$ -16/Chol SUVs with mole ratios: 2:1, 1:1 and 1:1.5. The figure legend indicates the corresponding symbols and mole ratios.



*Blood Clearance of Additional  $\alpha$ -THIOL-Containing SUVs.* Several other types of SUVs composed of mixtures of polymeric and non-polymeric components were examined in an effort to further explore the possibility that the  $\alpha$ -THIOLS might provide important constituents of SUVs with long blood half-lives. Among these,  $\alpha$ 18-DSL/Chol 2:1 SUVs were studied since the phospholipid component forms dimers which should have greater conformational flexibility than polymeric analogues, and therefore may be able to pack more favorably in bilayers than the polymers.\* This expectation is consistent with serum stability data since the leakage of  $^{111}\text{In}^{+3}$  from 2:1  $\alpha$ 18-DSL/Chol was found to be less than from both 1:1 and 2:1  $\alpha$ -18/Chol SUVs, despite the fact that both  $\alpha$ -THIOLS have broad phase transitions encompassing 37°C. Unfortunately, the blood clearance rate of  $\alpha$ 18-DSL/Chol 2:1 SUVs were similar but not better than that of  $\alpha$ -16/Chol and 2:1 DSPC/Chol (Figure 11A). The effect of GM<sub>1</sub> as an additional component to polymeric SUVs was also examined since it has been shown to dramatically extend the circulation times of LUVs. (depending on the other membrane constituents) (9,62). As shown in Figure 11B, the addition of 15 mole % of GM<sub>1</sub> to  $\alpha$ -20 SUVs did not retard the blood clearance rate or accumulation in the liver. The above results reiterate the fact that because these polymeric lipids disorder rather than order the membrane, they do not have the proper interfacial and hydrocarbon properties conducive to long circulation times in the blood. Furthermore, implicit in their polymeric nature is a restriction of the conformational possibilities of the monomeric units compared to nonpolymerizable phospholipids. This could limit the interaction of the polymeric lipids with added amphiphiles (i.e., cholesterol) and perhaps induce some degree of phase separation such that the nominally stabilizing

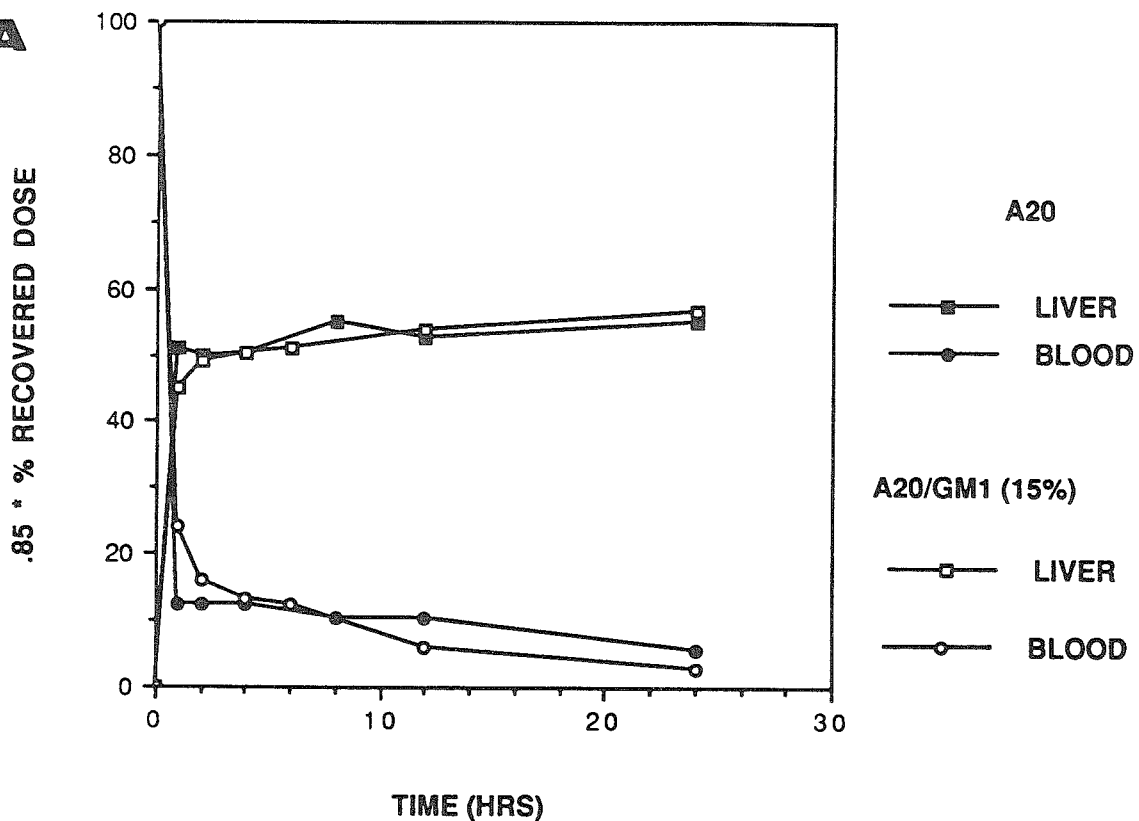
---

\*  $\alpha$ 18-DSL consists of a polymerized 18-carbon chain in the sn-1 position and an 18-carbon saturated chain in the sn-2 position.

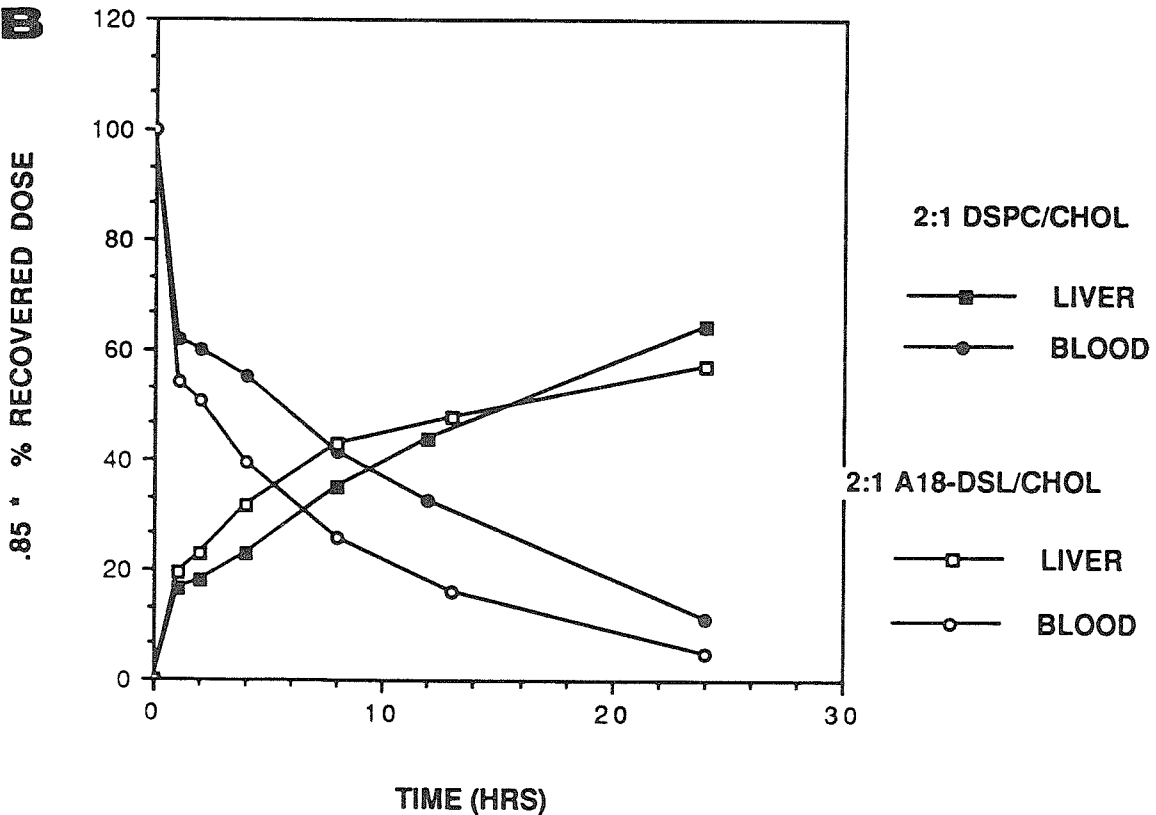
**Figure 11**

Percentage of liposome recovered in the blood and the liver with time for : **A.** Polymeric  $\alpha$ -20 versus polymeric  $\alpha$ -20/GM<sub>1</sub> (85:15) SUVs and **B.** 2:1 DSPC/Chol versus 2:1  $\alpha$ 18-DSL/Chol SUVs .

**A**



**B**



effect of added components might be reduced. Thus, the intracellular degradation and blood clearance of this class of polymerizable lipids is rapid.

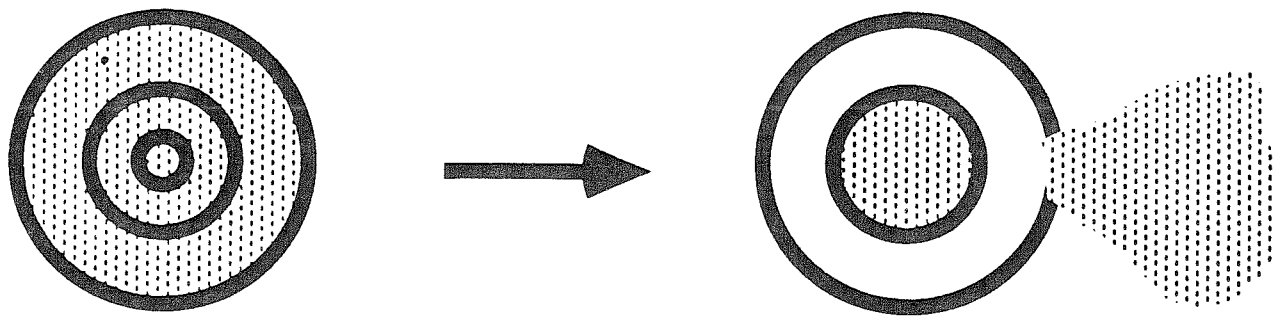
## 11. MLVS

*Motivation for Study.* The results presented above seem best interpreted in terms of the *mechanical* caveats (i.e., packing constraints) of the  $\alpha$ -THIOL polymerizable phospholipids. Unfortunately, one of the predictable advantages of polymerized liposomes, *chemical* stability, could not be explicitly examined in the SUV studies. As was mentioned earlier, this is due to the fact that the PAC assay monitors leakage rather than lipid degradation, and for SUVs, leakage may be completely independent of chemical stability. A single defect in the membrane of an SUV could in fact cause complete release of the internal contents. This is not likely the case for MLVs which have  $^{111}\text{In}^{+3}$  equally distributed throughout the lamellae. The outermost lamella would be subject to the same mechanisms for solute release as SUVs. However, for the release from internal lamellae to occur by anything other than passive leakage, each lamellae must be successively degraded and removed, thereby exposing those on the MLV interior. This is illustrated in Figure 12. Therefore, if polymeric lipids were incorporated into the membrane, one might expect that the rate of lipid degradation would be slower than that of nonpolymeric MLVs. From a technological standpoint, one could envision a very useful role of polymeric MLVs as intracellular slow release systems (from the liver and spleen where they tend to rapidly accumulate). *In vitro* and *in vivo* studies of MLVs containing the  $\alpha$ -THIOLS were therefore designed to examine these possibilities.

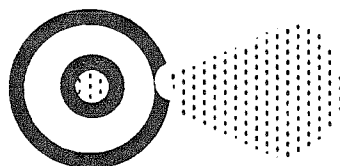
**Figure 12**

Schematic representation of the degradation process for MLVs versus SUVs. **A.** In the case of MLVs, assuming the degradation rate is faster than passive leakage, the first lamellae may release contents rapidly (like SUVs) simply as a consequence of protein absorption. In order to release  $^{111}\text{In}^{+3}$  entrapped in the lamellae more interior to the liposome, however, each layer must be successively degraded; **B.** By contrast, for SUVs, all contents may be released if a defect is created in the bilayer by protein absorption. No chemical degradation need be invoked.

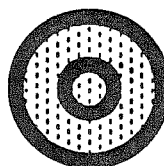
### MLV RELEASE



Degrade

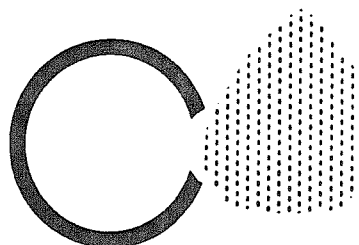
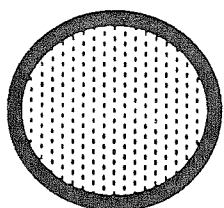


Degrade



---

### SUV RELEASE



### Serum Stability of MLVs.

As for the studies involving SUVs, it was first necessary to establish what compositions of MLVs are stable in serum. Because the organization of lipids in MLVs and SUVs can be quite different due to variations in the radius of curvature between the two liposome types, one cannot assume that lipid compositions, which give rise to stable SUVs necessarily produce stable MLVs. This is demonstrated in Figure 13, which shows a greater stability for  $\alpha$ -20 SUVs compared to MLVs. In general, however, the opposite trend is observed; MLVs tend to be more stable than SUVs due to the curvature of the SUV surface, which induces membrane disorder (16). While the relative stabilities of the  $\alpha$ -20 MLVs and SUVs are difficult to explain, it should be recalled that  $\alpha$ -20 phospholipids have a propensity to form largely unilamellar structures upon dispersion in water, and these tend to be significantly smaller than those of nonpolymerizable phosphatidylcholines (see Chapter II). Thus, the production of larger liposomes by freezing and thawing may in fact cause an unfavorable packing of the lipids in the bilayer and a subsequently more permeable membrane.  $\alpha$ -20 MLVs were therefore not examined with respect to their *in vivo* degradation rates because they were not sufficiently stable.

The addition of cholesterol to  $\alpha$ -20/Chol SUVs (2:1 mole ratio) was not effective in increasing the membrane stability as shown in Figure 13. This is consistent with the fact that for  $\alpha$ -20/Chol SUVs, cholesterol has a destabilizing effect. For MLVs containing  $\alpha$ -16 or  $\alpha$ -18 polymeric lipids, however, cholesterol was a necessary addition in order to suppress the phase transition and inhibit rapid leakage at room temperature and 37°C, respectively. As shown in Figure 14, 2:1  $\alpha$ -16/Chol MLVs are reasonably stable at 37°C, but at room temperature they are quite leaky presumably due to the phase transition. At a higher (1:1) mole fraction of cholesterol, leakage at room temperature and 37°C is similar, but there is no further increase in the stability

**Figure 13**

Percentage of  $^{111}\text{In}^{+3}$  retained within liposomes of 2:1  $\alpha$ -20 MLVs versus 2:1  $\alpha$ -20/Chol MLVs in 50 % serum at 23 °C and 37 °C. The figure legends indicate the temperatures and liposomes used.

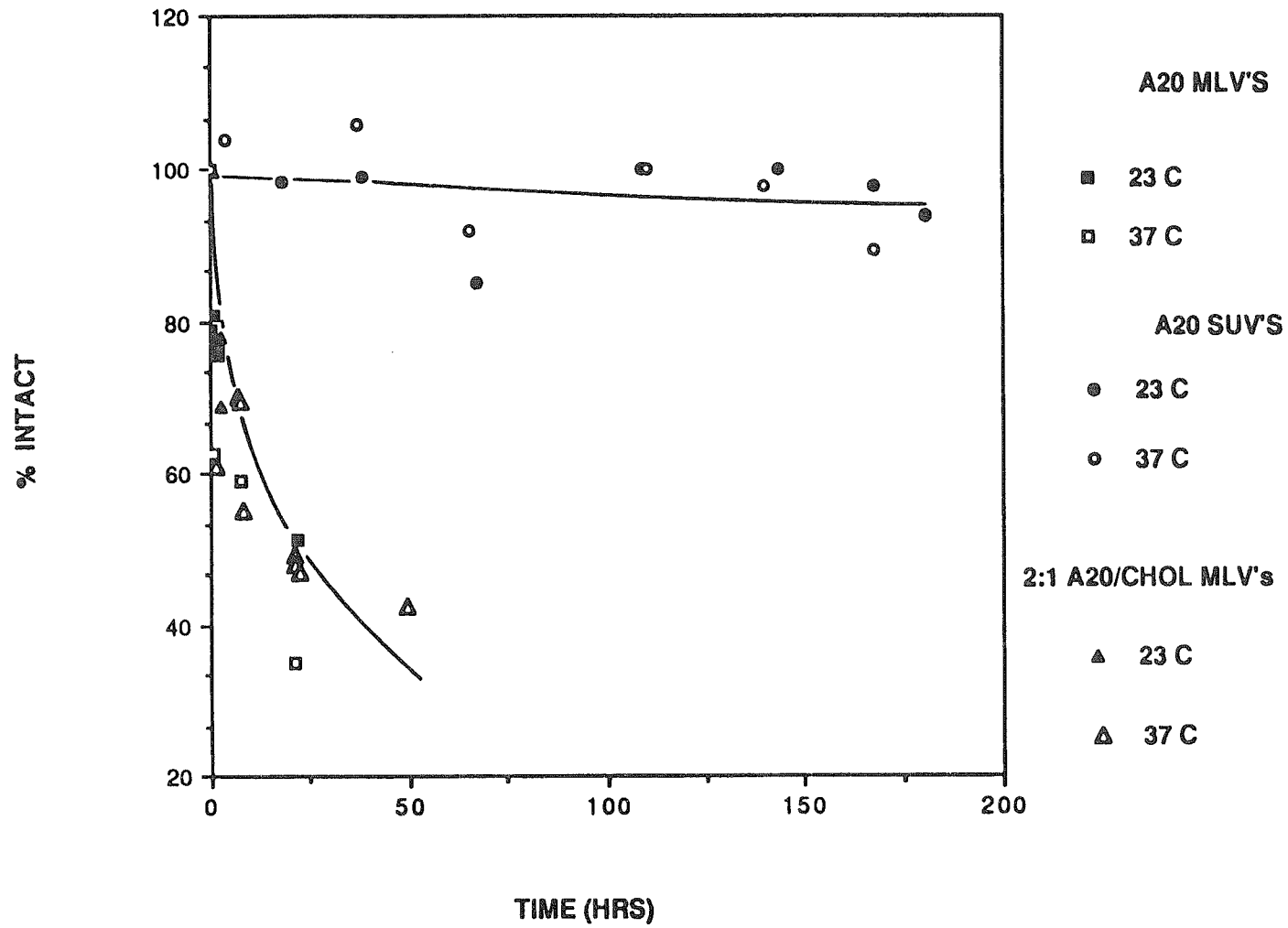
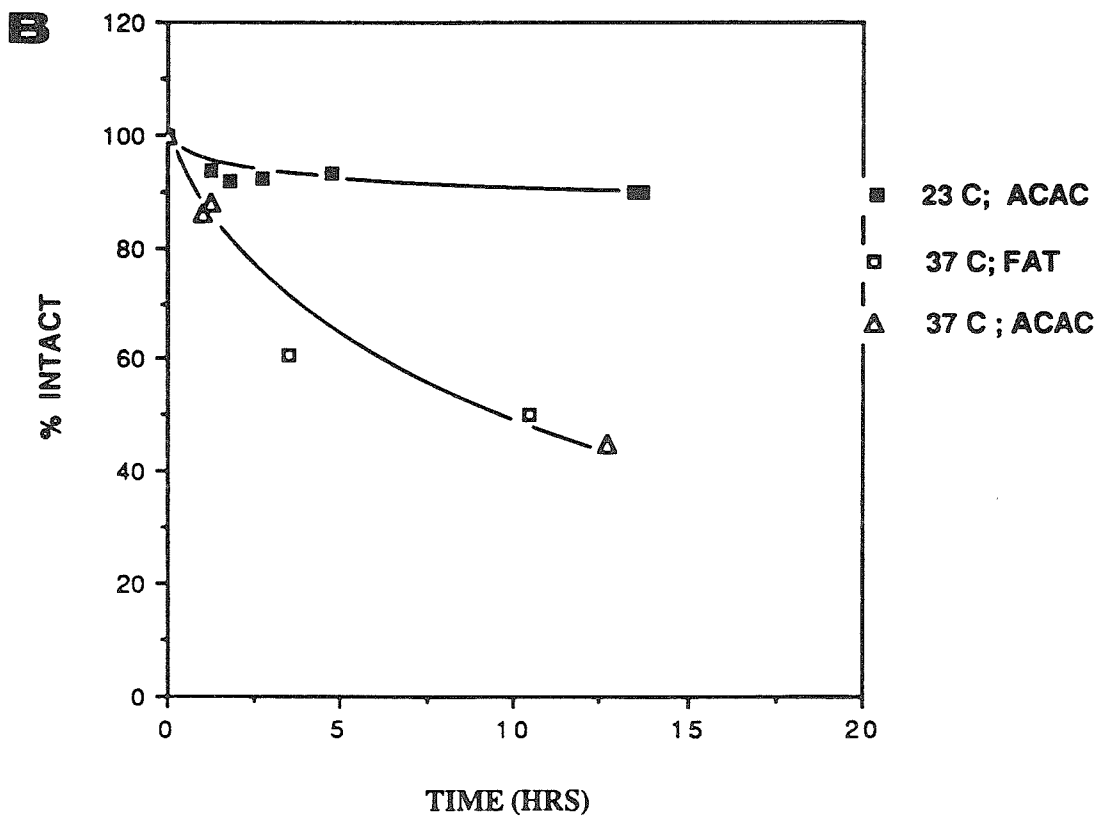
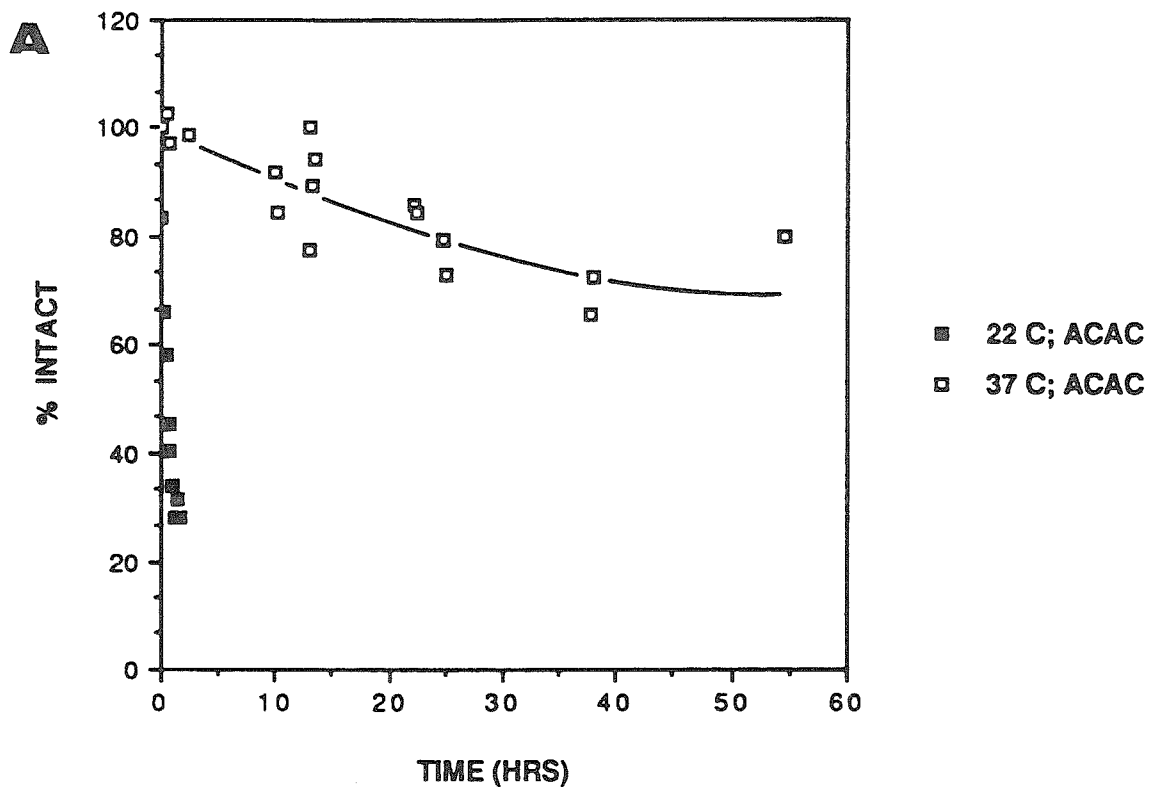


**Figure 14**

Percentage of  $^{111}\text{In}^{+3}$  retained within liposomes of: **A.** 2:1  $\alpha$ -16/Chol MLVs and **B.** 1:1  $\alpha$ -18/Chol MLV', in 50 % serum at 23 °C and 37 °C. The figure legends indicate the temperatures and loading protocols used.



over that observed for 2:1  $\alpha$ -16/Chol at 37°C. Likewise, for 1:1  $\alpha$ -18/Chol, leakage is predictably greater at 37°C than at room temperature and also greater than that of 2:1  $\alpha$ -16/Chol MLVs despite the lower cholesterol content of the latter. These results are consistent with the leakage behavior of  $\alpha$ -16/Chol and  $\alpha$ -18/Chol SUVs.

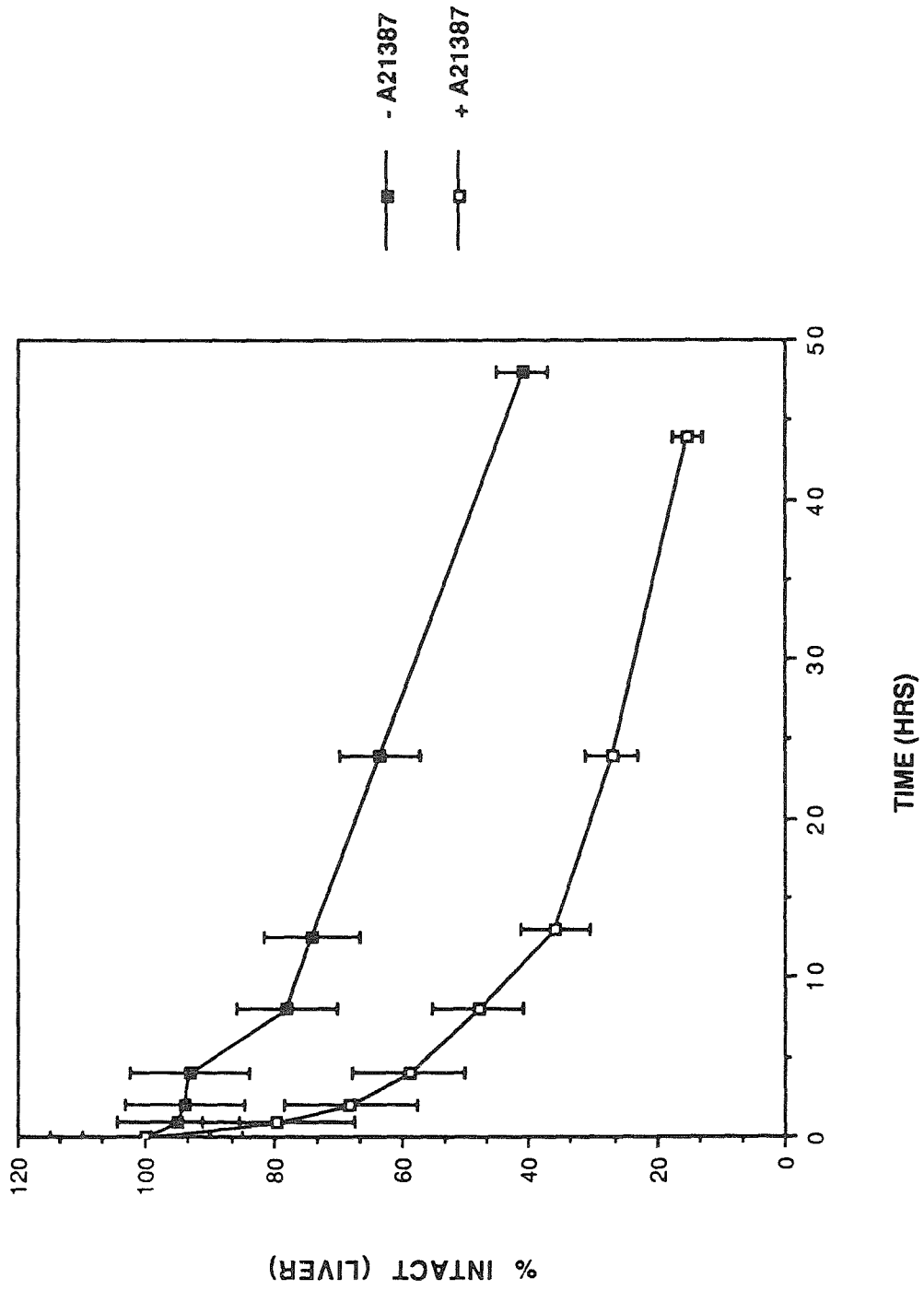
Several other MLV compositions were examined and found to be stable including 4:5:1  $\alpha$ -18/Chol/PS and  $\omega$ 16P-DPL/Chol (data not shown). The  $\alpha$ -18/Chol/PS MLVs were chosen for comparison to the stable nonpolymerizeable analogues, EPC/Chol/PS and DSPC/Chol/PS, which have been extensively characterized by Scherphof and Spanger *et al.* (32,63). The 2:1  $\omega$ 16P-DPL/Chol MLVs were examined in comparison to 2:1 DSPC/Chol MLVs.

### IN VIVO STUDIES OF MLVs.

*Intracellular Liver Degradation of MLVs.* Based on the results of the serum stability studies, *in vivo* investigations were carried out with polymeric MLVs composed of  $\alpha$ -16/Chol,  $\omega$ 16P-DPL/Chol and  $\alpha$ -18/Chol/PS, and the nonpolymerizeable control MLVs; DSPC/Chol, EPC/Chol/PS and DSPC/Chol/PS. The main objective of the studies with the MLVs was to examine if the incorporation of polymeric components retarded the degradation rate of the liposomes in the liver as a consequence of increased chemical stability. To do this, an alternate loading strategy (Freeze and Thaw) was developed in order to distribute the  $^{111}\text{In}^{+3}$  throughout the lamellae of the MLV. Our basic assumption in these experiments is that if the distribution of  $^{111}\text{In}^{+3}$  is uniform throughout the MLV, then the rate of  $^{111}\text{In}^{+3}$  release should reflect the liposome composition and susceptibility to chemical degradation. (This contrasts to release from SUVs or release from the external lamellae of MLVs where degradation may not be necessary.) Figure 15 shows a slower  $^{111}\text{In}^{+3}$  release rate from FAT-loaded (no

**Figure 15**

Percentage of intact liposomes in the liver at various times after intravenous injection of 2:1 DSPC/Chol MLVs loaded by (i) the A23187 loading protocol or (ii) the freeze and thaw (FAT) loading protocol. The slower rate of degradation for the FAT (-A23187) liposomes is presumably a consequence of the fact that the internal lamellae of the MLV are more completely loaded with  $^{111}\text{In}^{3+}$ .



A23187) than A23187-loaded 2:1 DSPC/Chol MLVs in the liver. This is consistent with (1) loading of FAT MLVs beyond just the first lamellae and (2) a dependence of leakage on lipid degradation for FAT MLVs. Other liposome types loaded by the FAT method were therefore examined. In all these PS-containing liposomes that were studied (4:5:1 EPC/Chol/PS; DSPC/Chol/PS; and  $\alpha$ -18/Chol/PS), the phosphatidylcholine (PC) component has eighteen-carbon acyl chains.\* Thus, the intracellular (liver) degradation rates may be analyzed in terms of the effect of having as the phosphatidylcholine component, an unsaturated liquid-crystalline phosphatidylcholine (EPC), a saturated gel state phosphatidylcholine (DSPC), or a polymeric phosphatidylcholine at its phase transition ( $\alpha$ -18). Figure 16A shows the percentage of intact liposomes at various times post injection in the liver for the three compositions. As expected, the most fluid liposomes, EPC/Chol/PS, are degraded very rapidly. Substitution of EPC by gel state DSPC results in liposomes that are more slowly degraded. The rate is slowed even further when the polymeric  $\alpha$ -18 is the PC component, despite the fact that the  $T_m$  of this lipid is approximately physiological temperature. Finally, when the PC component is completely polymeric as in 1:1  $\alpha$ -16/Chol (i.e., still equimolar PC/Chol but no PS) the degradation rate is the slowest of the four compositions, despite the fact that the polymer is fluid at 37°C.

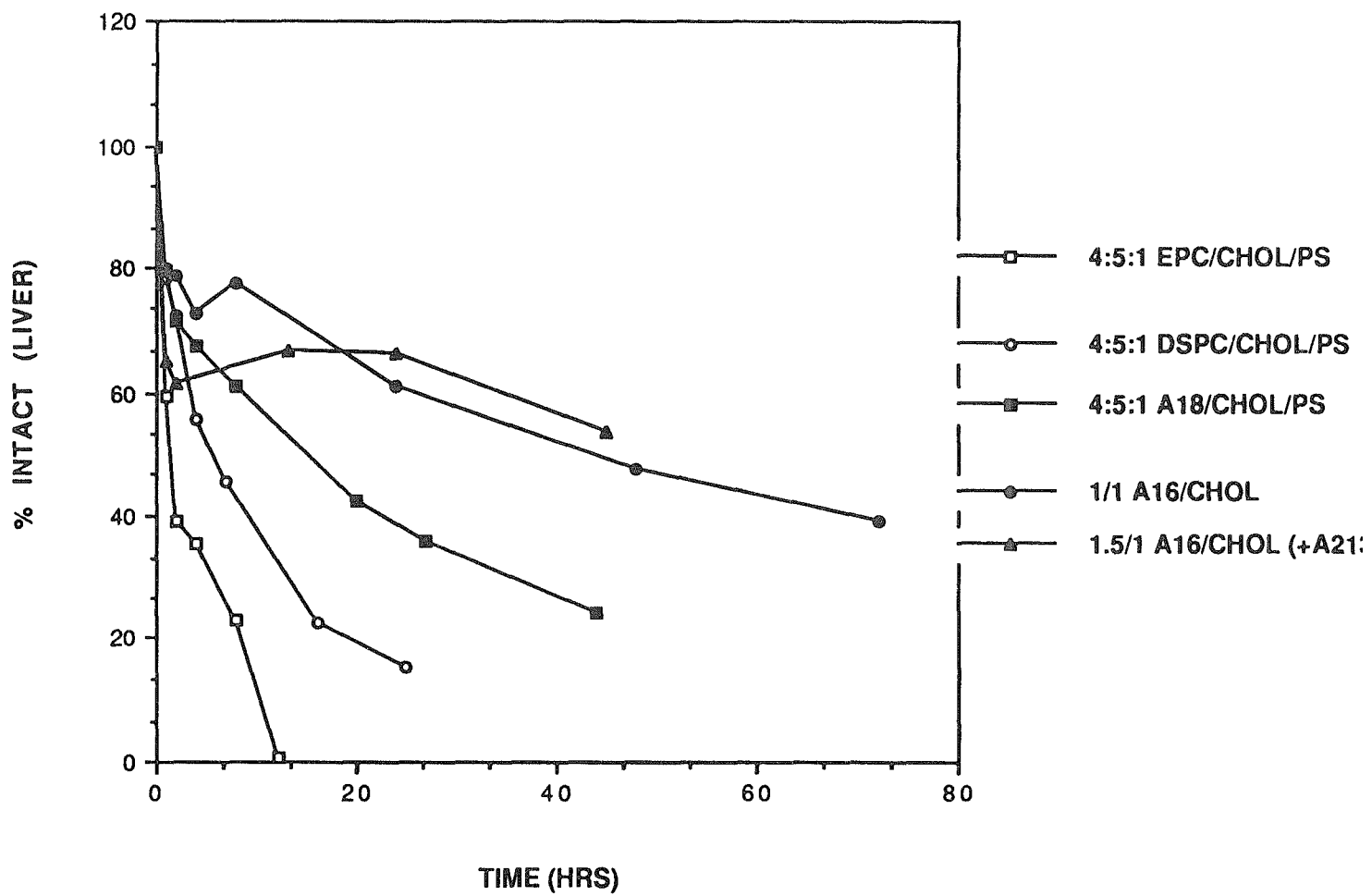
In the above examples, it was noted that the more stable polymer-containing liposomes were in the fluid state. The reasons for emphasizing this point is due to the fact that in addition to the presence of extra polymeric linkages, which should make the lipids more chemically stable, the physical packing of the lipids in the bilayer should also influence the rate of lipid degradation. Fluid lipids are known to be more susceptible to interaction with enzymes such as phospholipases, as well as to detergent and acidic environments such as those found in intracellular lysosomal compartments.

---

\* EPC has predominantly eighteen carbon unsaturated fatty acyl chains.

**Figure 16**

Percentage of intact liposomes in the liver at various times after intravenous injection of : **A.** 4:5:1 EPC/Chol/PS, 4:5:1 DSPC/Chol/PS, 4:5:1  $\alpha$ -18/Chol/PS, 1:1  $\alpha$ -16/Chol and 1.5/1  $\alpha$ -16/Chol MLVs ; **B.** 2:1 DSPC/Chol and 2:1  $\omega$ 16P-DPL/Chol MLVs. The symbols corresponding to the liposome types are indicated in the figure legend.



Therefore, the fact that the polymeric liposomes composed of fluid lipids (1:1  $\alpha$ -16/Chol and 4:5:1  $\alpha$ -18/Chol/PS) were more stable than DSPC/Chol/PS containing a *gel state* phosphatidylcholine emphasizes the effectiveness of polymerization. On the other hand, equally impressive rates as  $\alpha$ -16/Chol can be achieved by the *monomeric* but *solid* liposomes 2:1 DSPC/Chol (Figure 16B). Similarly, liposomes composed of 2:1 T16P-DPL/Chol are also very stable. The latter contain only dimeric rather than polymeric phosphatidylcholines but appear to be fairly solid based on the physical characterization and serum stability studies. It therefore appears that polymerization may enhance the intracellular lifetime of multilamellar vesicles due to the presence of extra bonds, which should slow the lipid degradation. However, the lipid packing in the membrane is also an important factor in the rate of degradation because this controls the access of phospholipases and degrading cellular components to the lipids in the membrane. Thus the design of polymeric liposomes, which have additional stable chemical linkages and yet retain a tight packing of the lipids, should result in even more slowly degraded liposomes than those described here.

*Tissue Distributions of MLVs.* In contrast to the rate of blood clearance of SUVs, which shows a marked dependence on the liposome composition, that for all MLVs studied was very rapid with the majority accumulating in the liver and spleen in approximately 2 hours or less. An effect of liposome composition was observed, however, in the relative accumulation of MLVs in the spleen versus the liver. These results are summarized in Table IV. For most liposomes, there is more than a 9-fold greater accumulation in the liver (similar to that observed for the SUVs studied). For other compositions such as the  $\alpha$ -18/Chol and  $\alpha$ -16/Chol samples, however, a very large percentage goes to the spleen, especially when evaluated in terms of the percent injected dose per gram of tissue. The reasons for such a large spleen accumulation is not known but has been observed by others for certain liposomes containing large

**Table IV**

Percentage of recovered dose in the liver and spleen 4 h following intravenous injection of various multilamellar liposome preparations. Noteworthy is the high (> 9) liver to spleen (L/S) ratio for some liposome types and the very low ratio for others. The low values indicate a tremendous accumulation in the spleen on the basis of liposome accumulation per gram of tissue.

.75 \* % Recovered Dose<sup>a</sup>

<u>MLV Composition</u>	<u>Loading Protocol</u>	<u>LIVER</u>	<u>SPLEEN</u>	<u>Ratio L/S<sup>b</sup></u>
2:1 DSPC/CHOL	FAT + A21387	67.9	2.6	26.1
4:5:1 DSPC/CHOL/PS	FAT	68.1	6.9	9.9
4:5:1 $\alpha$ -18/CHOL/PS	FAT	68.5	6.5	10.5
1.5:1 $\alpha$ -18/CHOL	FAT + A21387	52.0	18.1	1.5
2:1 $\alpha$ -16/CHOL	FAT + ACAC	42.2	29.2	2.9
1:1 $\alpha$ -16/CHOL	FAT	35.3	27.9	1.3

<sup>a</sup>Measurements are the average values from two mice. <sup>b</sup>Ratio of the % recovered in the liver versus the spleen.

amounts of cholesterol (64). Therefore, the presence of the polymeric component in these liposomes may not be the cause of this rather unusual behavior. Regardless of the cause, because such a large percent goes to the spleen for these MLVs, they may offer a possible mode for targeting drugs to T-cells, which could potentially be of great utility especially in view of the current AIDS crisis.

### CONCLUSION

In this study we have examined the *in vitro* and *in vivo* behavior of disulfide polymerized liposomes in regards to tissue distribution, vascular clearance rates, and intracellular degradation. SUVs were examined with the anticipation that polymerization might slow blood clearance and retard *in vivo* degradation. The opposite results were observed.

Scherphof *et al.* have demonstrated that structural irregularities at the interface or reduced cohesive forces between lipids have a profound effect on susceptibility to the degrading activity of phospholipases and lipoproteins (16). It also seems clear that similar features of the membrane surface are conducive to absorption of opsonizing proteins, which accelerate endocytosis, particularly by phagocytic Kupffer cells. Thus, the extremely rapid clearance of  $\alpha$ -20 SUVs from the blood and intracellular release of  $^{111}\text{In}^{+3}$  would seem to confirm that the  $\alpha$ -THIOLS are characterized by disturbances in the acyl chain packing, consistent with the spectroscopic evidence presented in earlier chapters. The interfacial and headgroup regions, on the other hand were found in earlier NMR studies to be quite rigid, but on the basis of the *in vivo* data, it is apparent that this does not preclude the presence of a faceted membrane surface. Addition of large amounts of cholesterol to "patch up" the defects and solidify the membrane did slow clearance, but not to the extent achievable by certain non-polymerizable phospholipid mixtures.

*In vivo* studies have also been carried out on polymerized and nonpolymerized SUVs and MLVs of bis{12-(methacroyloxy)dodecanoyl-L- $\alpha$ -phosphatidylcholine where the polymerizeable moiety is at the chain terminus (65). Similar rapid clearance and degradation rates were observed in these systems, and in fact, the polymeric lipids were removed from the blood more rapidly than the nonpolymerizeable analogues. The explanation offered for these results was (i) differences in the absorption behavior of polymerized liposomes for serum and other opsonizing proteins and (ii) the differences in the ability of the polymerized liposomes to interact with the reticuloendothelial cells. While the physical basis for these results was not discussed, in consideration of the lipid structure, which is that of a short 12 carbon chain terminated with a somewhat polar methacroyl group, it seems likely that the membrane may in fact be less tightly packed than some nonpolymerizeable gel state phospholipids and therefore subject to similar clearance mechanisms as the  $\alpha$ -THIOLS and fluid lipids in general. This is *despite* the structural framework of these liposomes, which has been shown to be extremely resistant to disintegration by organic solvents and detergents due to the fact that the membrane can form a crosslinked network (66). An insoluble matrix does not necessarily mean it is resistant to protein absorption.

The structural basis for the membrane disorder of the  $\alpha$ -THIOLS has been discussed in previous chapters. However, it is instructive to compare these lipids to other classes of polymeric lipids and in particular to another class of polymeric lipids (amino acid amphiphiles), which have rigid amide linkages in the headgroup. These have also been found to be fairly permeable to solutes despite having reasonably long 16-carbon chain lengths (67). In fact, as in the case of the  $\alpha$ -THIOLS studied here, permeability (and presumably hydrocarbon chain disorder) is actually increased upon polymerization. In these studies leakiness of the membranes was attributed to the short polymer chains formed by the condensation mechanism, the lengths ( $\leq 10$ ) of which

are similar to those estimated for the  $\alpha$ -THIOLS. An alternate or additional reason that we put forth to explain the disorder is the mere presence of the the *rigid* polymer linkage which (i) creates additional bulk that sterically inhibits maximal Van der waals interactions between the lipids and (ii) reduces the conformational freedom of the lipids to form close-packed membranes (especially when they are not crosslinked in three dimensional arrays), thereby introducing interfacial defects. To alleviate the disruptive effects of the polymerizeable moieties, headgroup polymerization has also been investigated where the polymerizeable group has been spaced at various distances from the membrane interface (68). In these studies, which involved ethylene oxide chains as spacers, effective decoupling of the effect of the polymerized headgroup from the acyl chain was in fact observed. As yet, *in vivo* studies have not been carried out but may provide further interesting clues as to what are the necessary structural features for creating polymerizeable liposomes that are superior to nonpolymerizeable liposomes for *in vivo* applications.

### REFERENCES

1. Proffitt, R.T., Williams, L.E., Presant, L.A., Tin, G.W., Uliana, J.A., Gamble, R.C. and Baldeschwieler, J.D. (1983) *Science* **29**, 502-505.
2. Baldeschwieler, J.D., (19 ) *Ann. N.Y. Acad. Sci.* **446**, 349-367.
3. Connor, J. and Huang, L. (1986) *Cancer Res.* **46**, 3431-3435.
4. Huang, A., Kennel, S.J. and Huang, L. (1983) *J. Biol. Chem.* **258**, 14034-14040.
5. Szoka, F.C. and Mayhew, E. (1983) *Biochem. Biophys. Res. Comm.* **110**, 140-146.
6. Leserman, L.D., Machy, P. and Barbet, J. in: *Liposome Technology* ; Gregoriadis, G. (Ed.); Boca Raton: CRC Press, 1984; Vol. III, 29-40.

7. Huang, L., Huang, A. and Kennel S. in: *Liposome Technology* ; Gregoriadis, G. (Ed.); Boca Raton: CRC Press, 1984; Vol. III, 51-62.
8. Ponpipom, M.M., Shen, T.Y., Baldeschwieler, J.D. and Wu, P. in: *Liposome Technology* ; Gregoriadis, G. (Ed.); Boca Raton: CRC Press, 1984; Vol. III, 95-116.
9. Allens, T.M. and Chonn, A. (1987) *Febs. Lett.* **223**, 42-46.
10. Derksen, J.T.P., Baldeschwieler, J.D. and Scherphof, G.L. (1989) *Proc. Natl. Acad. Sci. U.S.A.*
11. Abra, R.M. and Hunt, C.A. (1981) *Biochim. Biophys. Acta.* **666**, 493-503.
12. Poste, G., Bucana, C., Raz, A., Bugelski, P., Kirsh, R. and Fidler, I.J. (1982) *Cancer Res.* **42**, 1412-1422.
13. Papahadjopoulos, D. (1979) *Ann. Rep. Med. Chem.* **14**, 250-260.
14. Scherphof, G., Roerdink, F., Waite, M. and Parks, J. (1978) *Biochim. Biophys. Acta.* **542**, 296-307.
15. Scherphof, G., Van Leeuwen, B., Wilschut, J., and Damen, J. (1983) *Biochim. Biophys. Acta.* **732**, 595-599.
16. Scherphof, G., Damen, J. and Wilschut, J. in: *Liposome Technology* ; Gregoriadis, G. (Ed.); Boca Raton: CRC Press, 1984; Vol. III, 205-224.
17. Tall, A. (1980) *J. Lipid Res.* **21**, 354-363.
18. Allen, T.M. and Cleland, L.G. (1980) *Biochim. Biophys. Acta.* **597**, 418-426.
19. Senior, J., Crawley, J.C.W. and Gregoriadis, G. (1985) *Biochim. Biophys. Acta.* **839**, 1-8.
20. Senior, J. and Gregoriadis, G. (1982) *FEBS Lett.* **145**, 109-114.
21. Senior, J. and Gregoriadis, G. in: *Liposome Technology* ; Gregoriadis, G. (Ed.); Boca Raton: CRC Press, 1984; Vol. III, 263-282.

22. Kirby, C. Clarke, J. and Gregoriadis, G. (1980) *FEBS Lett.* **119**, 43-46.
23. Kirby, C. Clarke, J. and Gregoriadis, G. (1980) *Biochem J.* **186**, 591-598.
24. Gregoriadis, G. and Senior, J. (1980) *FEBS Lett.* **119**, 43-46.
25. Gupta, C.M. and Bali, A. (1981) *Biochim. Biophys. Acta.* **663**, 506-515.
26. Agarwal, K., Bali, A. and Gupta, C.M. (1986) *Biochim. Biophys. Acta.* **883**, 468-475.
27. Agarwal, K. and Gupta, C.M. (1984) *Chem. Phys. Lipids* **36**, 169-177.
28. Bali, A., Dhawan, S. and Gupta, C.M. (1983) *FEBS Lett.* **153**, 373-377.
29. Deshmukh, D.S., Bear, W.D., Wisniewski, H.M. and Brockerhoff, H. (1978) *Biochem. Biophys. Res. Comm.* **82**, 328,334.
30. Hwang, K.J., Luk, K. and Beaumier, P. (1982) *Life Sciences* **31**, 949-954.
31. Senior, J. and Gregoriadis, G. (1982) *Life Sciences* **30**, 2123-2136.
32. Spanjer, H.H., van Galen, M., Roerdink, F.H., Regts, J. and Scherphof, G. (1986) *Biochim. Biophys. Acta.* **863**, 224-230.
33. Roerdink, F.H., Regts, J., Van Leeuwen, B. and Scherphof, G. (1984) *Biochim. Biophys. Acta.* **770**, 195-202.
34. Nicholas, A.R. and Jones, M.N. (1986) *Biochim. Biophys. Acta.* **860**, 600-607.
35. Juliano, R.L. and Stamp, D. (1975) *Biochem. Biophys. Res. Comm.* **63**, 651-658.
36. Saba, T.M. (1970) *Arch. Inter. Med.* **126**, 1031-1052.
37. Akimoto, A., Klaus, D., Gros, L., Ringsdorf, H. and Schupp, H. (1981) *Angew. Chem. Int. Ed. Engl.* **20**, 90-91.

38. Gros, L., Ringsdorf, H. and Schupp, H. (1981) *Angew. Chem. Int. Ed. Engl.* **20**, 305-325.
39. Büschl, R., Folda, T. and Ringsdorf, H. (1984) *Makromol. Chem. Suppl.* **6**, 245-258.
40. Wagner, N., Dose, K., Koch, H. and Ringsdorf, H. (1981) *FEBS Lett.* **132**, 313-318.
41. Dorn, K., Klingbiel, R.T., Specht, D.P., Tyminski, P.N., Ringsdorf, H. and O'Brien, D.F. (1984) *J. Am. Chem. Soc.* **106**, 1627-1633.
42. Moellerfeld, J., Prass, W., Ringsdorf, H., Hamazaki, H. and Sunamoto, J. (1986) *Biochim. Biophys. Acta* **857**, 265-270.
43. Ringsdorf, H., Schlarb, B., Tyminski, P.N. and O'Brien, D.F. (1988) *Macromolecules* **21**, 671-677.
44. Kippenberg, D., Rosenquist, K., Odberg, L., Tundo, P. and Fendler, J. (1983) *J. Am. Chem. Soc.* **105**, 1129-1135.
45. Johnston, D.S., McLean, L.R., Wittan, M.A., Clark, A.D. and Chapman, D. (1983) *Biochemistry* **22**, 3194-3202.
46. Johnston, D.S., Sanghera, S., Pons, M. and Chapman, D. (1980) *Biochim. Biophys. Acta.* **602**, 57-59.
47. Freeman, F.J., Hayward, J.A. and Chapman, D. (1987) *Biochim. Biophys. Acta.* **924**, 341-351.
48. Weber, B., Dodrer, N. and Regen, S. (1987) *J. Am. Chem. Soc.* **109**, 4419,4421.
49. Sodownik, A., Stefely, J. and Regen, S.L. (1986) *J. Am. Chem. Soc.* **108**, 7789-7791.
50. Krause, H.L., Juliano, R.L. and Regen, S.L. (1987) *J. Pharm. Sci.* **76**, 1-5.
51. Regen, S.L. (1985) *Ann. N.Y. Acad. Sci.* **446**, 296-307.

52. Samuel, N.K.P., Singh, M., Yamaguchi, K. and Regen, S.L. (1985) *J. Am. Chem. Soc.* **107**, 42-47.
53. Beaumier, P. and Hwang, K. (1982) *J. Nuclear Med.* **23**, 810-815.
54. Hwang, K. (1978) *J. Nuclear Med.* **19**, 1162-1170.
55. Hwang, K., Merriam, J., Beaumier, P. and Luk, K.S. (1982) *Biochim. Biophys. Acta.* **716**, 101-109.
56. Mayer, L.D., Hope, M.J., Cullis, P.R. and Janoff, A.S. (1985) *Biochim. Biophys. Acta* **817**, 193-196.
57. Hwang, K.J., Kuen-Fai, S.L. and Beaumier, P. (1980) *Proc. Natl. Acad. Sci. U.S.A.* **77**, 4030-4034.
58. Meares, C., Ph.D. Dissertation, Stanford University, 19 .
59. Hwang, K. and Mauk, M. (1977) *Proc. Natl. Acad. Sci. U.S.A.* **74**, 4491-4995.
60. Weinstein, J.N., Klausner, R.D., Innerarity, T., Ralston, E. and Blumenthal, R. (1981) *Biophys. Biochim. Acta* **647**, 270-284.
61. Papahadjoupoulos, D., Jacobson, S., Nir, S. and Isac, T. (1973) *Biophys. Biochim. Acta* **311**, 330-348.
62. Allen, T.M., Williamson, P. and Schlegel, R. (1988) *Proc. Natl. Acad. Sci. U.S.A.* **85**, 8067-8071.
63. Scherphof, G., Roerdink, F., Dijkstra, J., Ellens, H., De Zanger, R. and Wisse, E. (1983) *Biol. Cell* **47**, 47-58.
64. Scherphof, G., private communications.
65. Krause, H.J., Juliano, R.L. and Regen, S. (1985) *J. Pharmaceutical Science* **76**, 1-5.
66. Juliano, R.L., Regen, S.L., Singh, M., Hsu, M.J. and Singh, A. (1983) *Biotechnology* **882-885**.

67. O'Brien, D.F. (1986) *Biophys. J.* ,438-439.
68. Elbert, R., Laschewsky, A. and Ringsdorf, H. (1985) . *Am. Chem. Soc.* **107**, 4134-4141.

I ain't often right but I've never been wrong.

it seldom turns out the way it does in the song

Once in a while you get shown the light.

in the strangest of places if you look at it right .

----R. Hunter

---

**Chapter VIII**

---

*SYNTHESIS AND POLYMERIZATION*

---

**Materials.**

All reagents used in the synthesis of the thiol-containing phosphatidylcholines were obtained from Aldrich with the following exceptions: 8-bromooctanoic acid, 9-bromooctanoic acid and 10-bromooctanoic acid were obtained from Chemicals Procurement Company. 2-bromoarachidic acid was obtained from Maxdem. The bromoacid starting materials were pure as determined by NMR (90 MHz) and TLC and therefore were used without further purification. 15-pentadecanolide and 16-hexadecanolide (purity > 99%) were purchased from Columbia organics. L- $\alpha$ -glycero-3-phosphorylcholine•cadmium chloride (GPC•CdCl<sub>2</sub>) (purity > 99%) was obtained from Sigma. Lysophospholipids (purity >99%) used in the synthesis of the mixed chain lipids were purchased from Avanti Polar Lipids. Dithiothreitol was obtained from Schwarz/Mann Biotech (Division of ICN) or Calbiochem. 5-5'-dithio-bis(2-nitrobenzoic acid) (DTNB) was obtained from Aldrich. The silica gel used for flash chromatography was purchased from Baker. Kieselgel 60 was purchased from EM Science. All other materials were of analytical grade and used without further purification.

**Methods.**

NMR. The  $^1\text{H}$  NMR spectra of all final products were recorded on a Bruker AM-500. Intermediate compounds were also examined at 500 MHz although a 90 MHz Jeol and 200 MHz Varian spectrometers were occasionally employed. Relevant acquisition parameters for proton spectra (500 MHz) include a  $45^\circ$  excitation pulse ( $\approx 3 \mu\text{s}$ ) and a 3.5 s repetition rate. For aqueous ( $\text{D}_2\text{O}$ ) solutions, the HOD resonance was presaturated when necessary. Spectra are referenced with respect to  $\text{CHCl}_3$  (7.24 ppm) or HOD (4.63 ppm).

High resolution  $^{13}\text{C}$  spectra were acquired at 125 MHz on a Bruker AM-500. Chemical shifts are reported with respect to the choline methyl peak assumed to resonate at 54.3 ppm. Spectra were recorded with the nuclear Overhauser enhancement (NOE) using bilevel decoupling (1W and 10W for NOE and complete decoupling, respectively). Samples were prepared in either  $\text{CDCl}_3$ ,  $\text{CDCl}_3/\text{MeOH}$ , or phosphate buffer (50 mM sodium phosphate, .5mM EDTA ; pH 7.4).

### Thiol Analysis

The procedure used for detection or quantitative analysis of residual thiol groups was identical to that described previously (1-3). Briefly, a solution of tris(hydroxymethylamino)methane (0.2 M Tris, 1% EDTA, pH 8.2) was prepared and diluted with an equal volume of ethanol. The thiol reagent (referred to as Ellman's reagent) was prepared by dissolving 40 mg (0.101 mmol) of 5-5'-dithio-bis(2-nitrobenzoic acid) (DTNB) in 10 ml of the Tris/EtOH buffer. For quantitative analysis, a small aliquot of sample ( $< 50 \mu\text{l}$ ) is added to 1.5 ml of Tris/EtOH buffer containing 0.1 ml of the Ellman's reagent. After 20 min, the concentration of thiols may be calculated from the absorbance at 412 nm using a molar extinction coefficient of  $1.36 \times 10^4$ . To qualitatively detect the presence of thiol or completion of the polymerization,

the reagent was used as a TLC spray (.1% solution of the reagent in Tris/Ethanol buffer).

### General Synthesis.

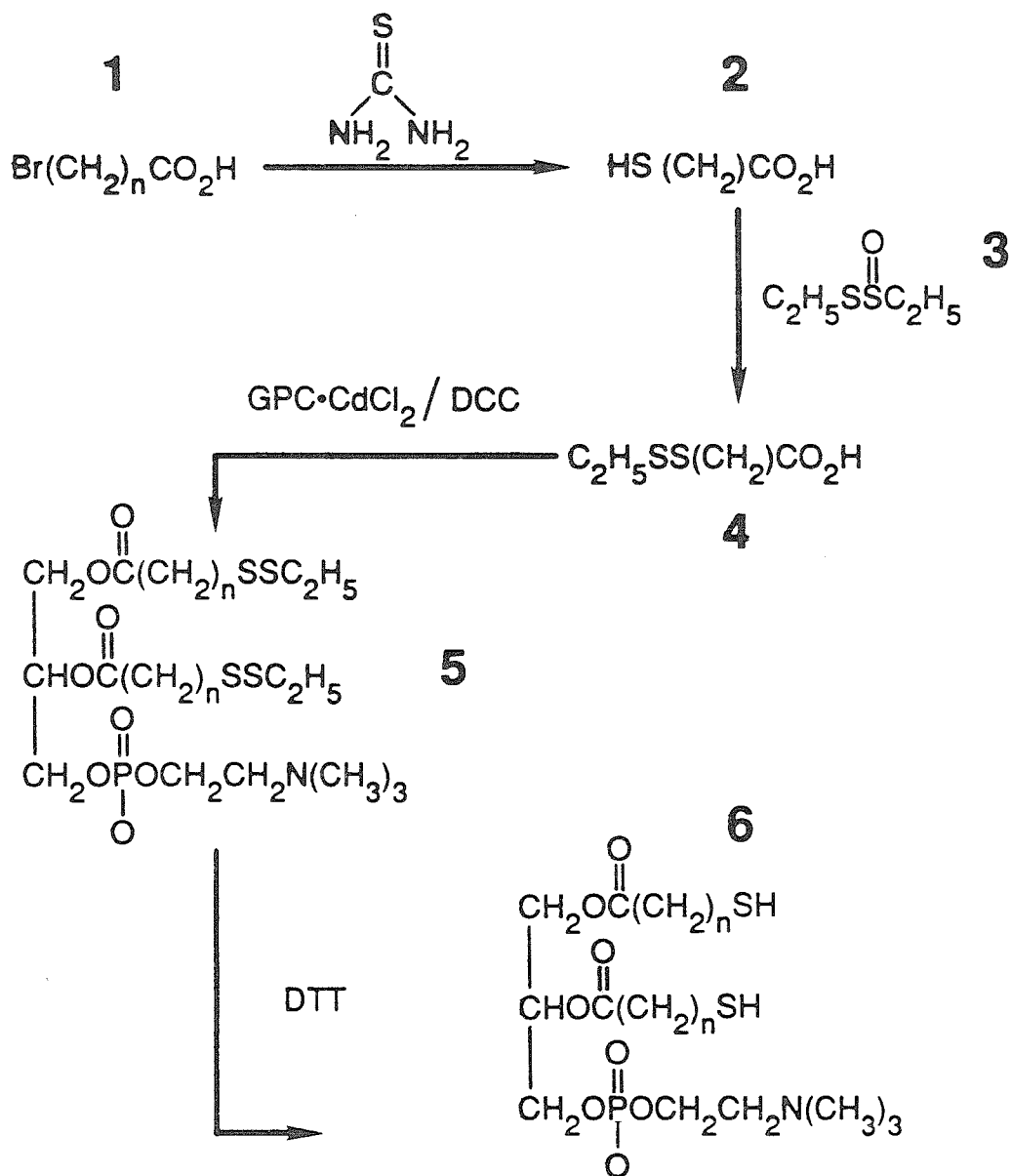
The general scheme for the synthesis of the monomeric  $\omega$ -THIOLS (i.e., 1,2-di(16-mercaptohexadecanoyl)-L- $\alpha$ -phosphatidylcholine) and monomeric  $\alpha$ -THIOLS (i.e., 1,2-di(2-mercaptohexadecanoyl)-L- $\alpha$ -phosphatidylcholine) are depicted in Figure 1. The reactions were carried out exactly as described by Regen *et al.* (1,4) with the exceptions of the general modifications described below. For each step of the synthesis, the compounds were isolated in pure form as monitored by TLC and  $^1\text{H}$  NMR. The only exceptions to this were (i) the protected fatty acids (structures 4 and 9 in Figure 1) and the protected phospholipids (structures 5 and 10 in Figure 1). In the case of the protected fatty acids, residual ethanethiosulfinate (ETS; 3) was difficult to remove without substantial loss of product recovery, despite a number of solvent systems used for chromatographic purification. Similar difficulties have been encountered in the Regen group (Bruce Weber, private communications). However, no difference in the  $^1\text{H}$  NMR (500 MHz) was found when the protected phospholipids were prepared from pure versus slightly impure protected acids as the contaminant appears to be unreactive and easily removed in the subsequent purification step. In the case of the protected phospholipids, lysolipid was occasionally observed by TLC but was removed in the final purification step.

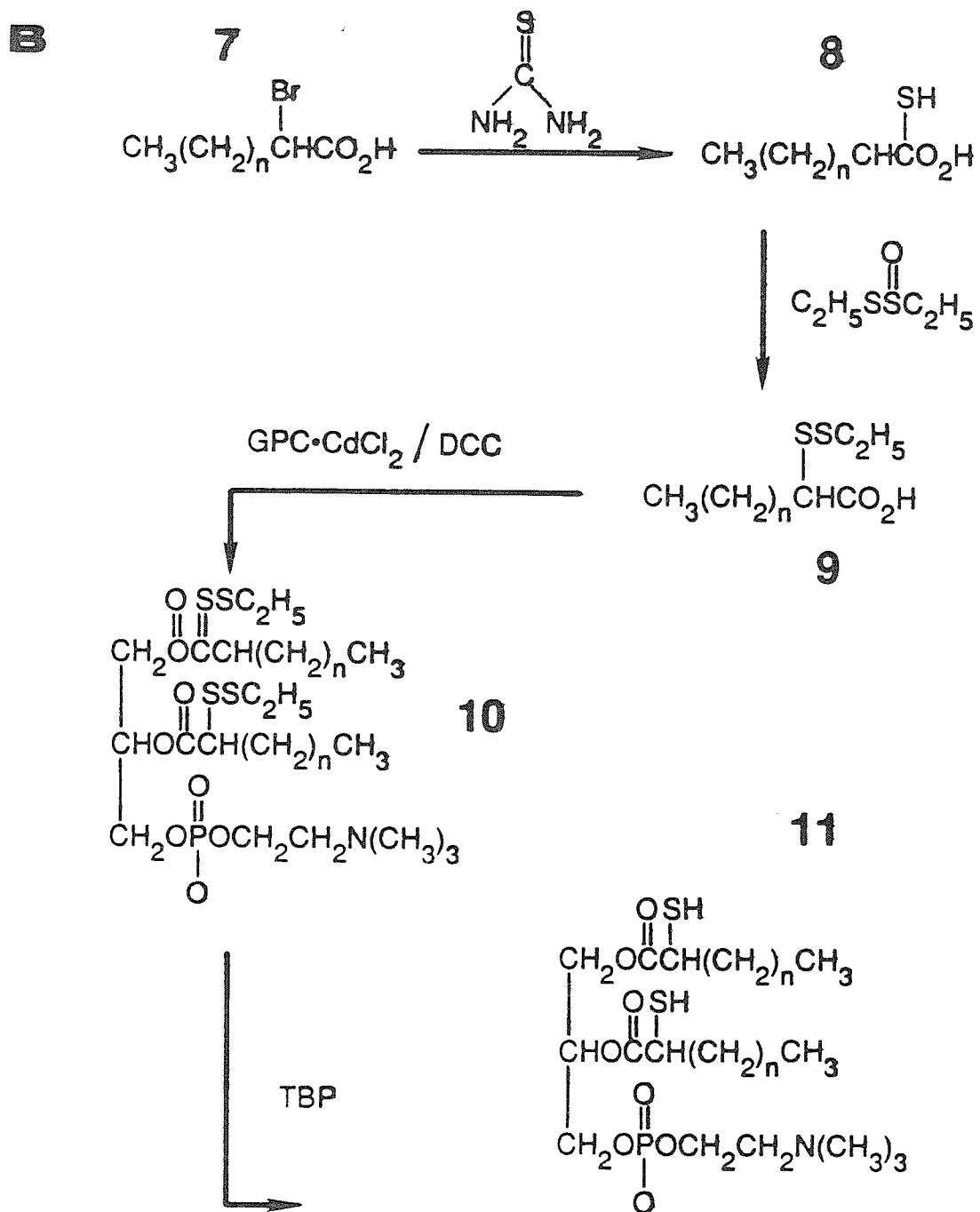
$\omega$ -THIOLS. For the monomeric  $\omega$ -THIOLS (Figure 1A) all steps in the synthesis were similar to the reported procedure with two exceptions:

(i) A 4-fold excess (versus protected acid) of dicylocarbohexyldiimide (DCC) was used to avoid problems with residual water in the reactants and solvent, and

**Figure 1**

Schematic diagram for the synthesis of: **A.** The  $\omega$ -THIOLS and **B.** The  $\alpha$ -THIOLS.

**A**



therefore to increase the yield. Typically 80-90% yields of compound **5** were obtained.

(ii) A different deprotection procedure was utilized. Using tributylphosphine (TBP) according to the methodology of Regen *et al.*, we consistently found a peak at  $\approx$  .87 ppm in the  $^1\text{H}$  spectrum of the monomeric  $\omega$ -THIOLS (Figure 1, compound **6**) corresponding to a terminal methyl group as determined from decoupling experiments and comparison to the spectra of DPPC. Integration of the peak intensities in the spectra indicated the amount of  $\text{CH}_2\text{-SH}$  to be low by 10-40% consistent with a high phosphorous to sulfur ratio. (Phosphorous and sulfur ratios were determined using standard procedures (1-3 and 5).) These results have since been confirmed by the Regen group (6). The proton spectra of the protected phospholipid, however, indicated the presence of the appropriate material. An example is shown in Figure 2. Consequently, it appears that TBP is not entirely selective for the sulfur of the leaving group, and in some cases both sulfurs are removed with the ultimate production of a terminal methyl group. The result is that a certain percentage of the lipids have one alkyl chain terminated with a thiol and one (or both) chain(s) terminated with a methyl group.

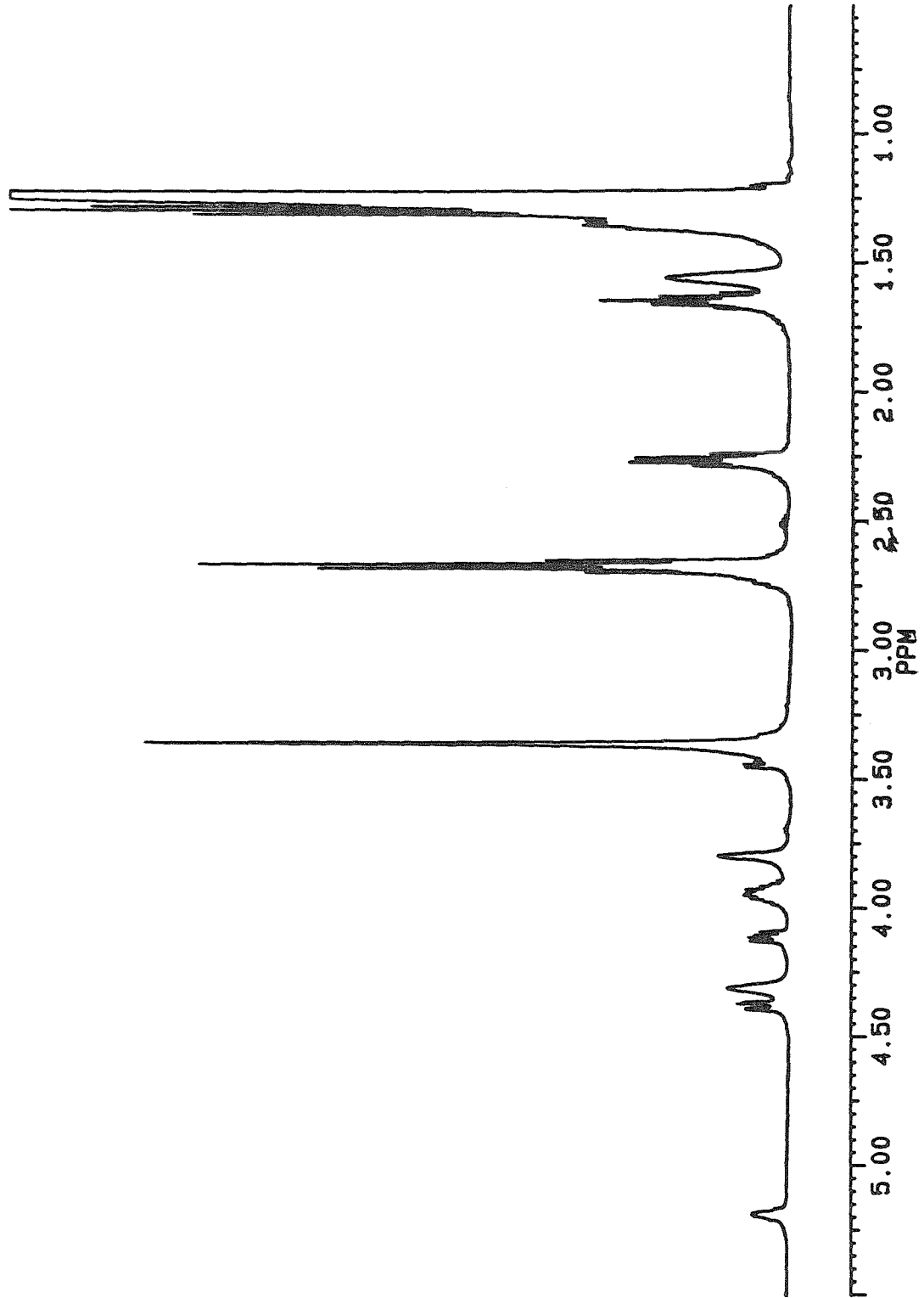
Since the reaction can be viewed essentially as a condensation reaction, small amounts of a chain terminating monomer (such as is a phospholipid with only one thiol) will severely reduce the theoretical degree of polymerization  $X_n$ .  $X_n$  is given by the following equation:

$$(1) \quad \bar{X}_n = \frac{1}{1-p}$$

where  $p$  is the extent of the reaction. It can be calculated that if 10% of the thiols are removed in the deprotection step, a maximum degree of polymerization  $X_n=10$  can only be obtained assuming 100% reaction of the remaining thiols.

**Figure 2**

<sup>1</sup>H NMR spectra of 1,2-di(16-diethyldithiohexadecanoyl)-L- $\alpha$ -phosphatidylcholine.



In order to alleviate this problem, dithiothreitol (DTT) was used as an alternative strategy to deprotect the phospholipids via a disulfide exchange reaction. The driving force in this case is cyclization of DTT into a six membered ring. The reaction conditions are described below but require optimization. Final products were always checked for complete deprotection by NMR (500 MHz) and it was sometimes necessary to repeat the exchange reaction. However, as will be demonstrated by representative spectra of the final products, it is possible to obtain complete deprotection of the lipids without loss of thiol groups by this method.

*α*-THIOLS. For the synthesis of the *α*-THIOLS, initially we followed the procedure of Regen (1) with the exception that  $\approx$  a 4-fold excess of DCC was utilized in the condensation step to form the protected phospholipid (Figure 1, compound **10**) as had been done in the synthesis of the  $\omega$ -THIOLS. Consistently, however, we obtained only a 10-15% yield of (**10**) compared to the reported value of 91% (1). Eventually, it was determined that utilizing an excess of DCC was the problem and that by using a 0.8 to 1.2 molar equivalent of DCC (versus the protected fatty acid), yields of 50-60% were obtainable.

The problem with utilizing excess DCC is believed to be a consequence of slower reaction kinetics for the formation of either the protected phospholipid or the activated ester of the fatty acid due to the large substituent adjacent to the carboxyl group. The competing reaction is the formation of dicyclohexylacylurea (DCAU) (7) which removes the protected fatty acid from the reactive pool, a reaction that may be driven by excess DCC. As described above, it is therefore necessary to employ near stoichiometric amounts of DCC and therefore to be particularly cautious about removing water from the solvent.

Deprotection of the  $\alpha$ -THIOLS was generally carried out using TBP as there appears to be no problem with loss of thiol groups. Steric hindrance probably makes TBP specific for the sulfur adjacent to the methylene group ( $\text{S}\underline{\text{S}}\text{CH}_2\text{CH}_3$ ) in the protected phospholipid. The DTT exchange reaction was also employed to determine if there were any visible differences in the final products. While the reaction does not proceed as quickly as with TBP, identical  $^1\text{H}$  NMR spectra and DSC traces were obtained for  $\alpha$ -16 prepared by both methods. Nonetheless, the original method of Regen was generally employed as it is more straightforward and optimal conditions for deprotection have been worked out.

*Mixed-Chain Phospholipids.* The synthesis of the mixed chain  $\omega$ -THIOLS and  $\alpha$ -THIOLS were carried out in exactly the same manner as depicted in Figure 1 with the exception that the fatty acids were condensed with a lysophosphatidylcholine (i.e., monopalmitoylphosphatidylcholine) rather than  $\text{GPC}\cdot\text{CdCl}_2$ . The final products therefore contain a nonpolymerizable fatty acid of the desired chain length in the sn-1 position and a thiol containing fatty acid in the sn-2 position as shown in Chapter I. The same procedures were used for the deprotection steps depending on whether the lipid was a mixed chain  $\omega$ -THIOL or mixed chain  $\alpha$ -THIOL.

#### General Synthetic Methods.

The synthesis of the compounds under study have already been thoroughly documented for chain lengths  $N=11,16$  ( $\omega$ -THIOLS) and  $N=16$  ( $\alpha$ -THIOLS) (1,4). For completeness, however, the synthetic procedures are reported below with the modifications described in the preceding section. Lipids with different chain lengths were synthesized but the methodology is the same as are the general NMR spectral features. Consequently, to avoid redundancy, we report only the synthesis of the 16-carbon lipids,  $\alpha$ -16 (1,2-di(2-mercaptohexadecanoyl)-L- $\alpha$ -phosphatidylcholine) and

$\omega$ -16 (1,2-di(16-mercaptohexadecanoyl)-L- $\alpha$ -phosphatidylcholine). In addition, the synthesis for a mixed-chain  $\omega$ -THIOL (1-(hexadecanoyl)-2-(16-mercaptohexadecanoyl)-L- $\alpha$ -phosphatidylcholine  $\omega$ 16-DPL\* ) and a mixed-chain  $\alpha$ -THIOL (1-(octadecanoyl)-1-(2-mercaptooctadecanoyl)-L- $\alpha$ -phosphatidylcholine); referred to as  $\alpha$ 18-DSL) are also reported. Again, the syntheses for the mixed-chain lipids having other chain lengths is generally the same as the procedures reported below.

*Ethylethanethiosulfinate (compound 3)* Diethyldisulfide (88 g, 0.721 mol) in 200 ml  $\text{CH}_2\text{Cl}_2$  was cooled to  $-20^\circ\text{C}$  in a  $\text{CCl}_4$ /dry ice bath. To this, m-chloroperbenzoic acid (162 g, 0.93 mol) was added slowly with continuous mechanical stirring over the course of one hour. The bath was subsequently removed and the reaction mixture allowed to stir for 6 h at room temperature. The product was then extracted from the solid with  $\text{CH}_2\text{Cl}_2$ . To the extract, 40 g of solid  $\text{Na}_2\text{CO}_3$  was added and the mixture stirred vigorously for 2 h. The solution was then cooled to  $\approx 4^\circ\text{C}$  and filtered (2X). Finally, the filtrate was concentrated and distilled under vacuum at .48 mm (b.p. =  $73^\circ\text{C}$  at .48mm) to yield the purified product.

$^1\text{H}$  NMR ( $\text{CDCl}_3$ ):  $\delta$  1.44 (t, 3H,  $\underline{\text{CH}_3\text{CH}_2\text{SSO}}$ );  $\delta$  1.45 (t, 3H,  $\underline{\text{CH}_3\text{CH}_2\text{SOS}}$ );  $\delta$  3.15 (q, 2H,  $\text{CH}_3\underline{\text{CH}_2\text{SSO}}$ );  $\delta$  3.30 (q, 2H,  $\text{CH}_3\underline{\text{CH}_2\text{SOS}}$ ).

*2-Mercaptohexadecanoic Acid (compound 8)*. 8.3 g (24.8 mmol) 2-bromohexadecanoic acid and thiourea (2.02 g, 26.5 mmol) in 50 ml EtOH were refluxed 4-6 h. Upon cooling the solution, 11 g NaOH (275 mmol) in 50 ml 50:50 EtOH/ $\text{H}_2\text{O}$  was added and the solution was allowed to reflux for another 48 h. The cooled solution was subsequently acidified with 75 ml 4N HCl, which initiated the precipitation of a white solid. After filtration of the solid, the solid was stirred in 100 ml boiling water for 10

---

\* The notation used is sn2-sn1; i.e.  $\omega$ 16-DPL refers to 1-(hexadecanoyl)-2-(16-mercaptohexadecanoyl)-L- $\alpha$ -phosphatidylcholine and  $\alpha$ 18-DSL refers to 1-(octadecanoyl)-1-(2-mercaptooctadecanoyl)-L- $\alpha$ -phosphatidylcholine).

min, cooled and filtered. The later process was repeated 3 to 4 times to purify the fatty acid from urea.

$^1\text{H}$  NMR ( $\text{CDCl}_3$ ):  $\delta$  .87 (t, 3H,  $\text{CH}_3$ ); 1.24 (br s, 24H,  $(\text{CH}_2)_n$ ); 1.71 and 1.90 (m, 1H,  $\text{CH}_2\text{CHSH}$ ); 2.05 (d, 1H, SH); 3.31 (q, 1H,  $\text{CHSH}$ ); 9.5 (s, 1H, COOH).

2-Ethylthiohexadecanoic Acid (compound 9). 2-Mercaptohexadecanoic acid (1.85 g, 6.42 mmol), ethylethanethiosulfinate (1.18 g, 8.55 mmol) and triethylamine (0.72 ml, 5.2 mmol) were dissolved in 16 ml chloroform and stirred under argon in the dark for 24 h. After removal of the solvent via rotary evaporation, the mixture was purified by passage over a 60 x 3.5 cm silica gel column using chloroform as the eluant. We found it difficult to isolate the protected acid in pure form without significant loss of the product unless the material was rechromatographed and a very large column was used. However, the presence of a small amount of the impurity, which runs ahead of the fatty acid on the column, did not seem to affect subsequent reaction steps.

$^1\text{H}$  NMR ( $\text{CDCl}_3$ ):  $\delta$  .87 (t, 3H,  $\text{CH}_3$ ); 1.24 (br s, 27H,  $(\text{CH}_2)_n$  and  $\text{SCH}_2\text{CH}_3$ ); 1.75 and 1.90 (m, 1H,  $\text{CH}_2\text{CHSS}$ ); 2.73 (q, 2H,  $\text{SSCH}_2\text{CH}_3$ ); 3.31 and 3.34 (t, 1H,  $\text{CHSS}$ ); 10.5 (s, 1H, COOH)

1,2-Di(2-ethylthiohexadecanoyl)-L- $\alpha$ -phosphatidylcholine (compound 10). GPC• $\text{CdCl}_2$  (89.6 mg, 0.196 mmol), 2-ethylthiohexadecanoic acid (348 mg, 1.0 mmol) and 4-dimethylaminopyridine (DMAP) (48.0 mg, 0.40 mmol) were dissolved in freshly distilled chloroform (distilled over  $\text{P}_2\text{O}_5$ ) to which was added dicyclohexylcarbodiimide (DCC) (165 mg, 0.80 mmol). The mixture was placed under argon and allowed to stir in the dark for 2-5 days. To remove DMAP, 7.5-10 g of AG 501-X8 (D) resin and sufficient chloroform were added to the mixture to form a thick slurry. The slurry was swirled intermittently for approximately 10 min and subsequently removed by filtration. After the filtrate was concentrated under reduced pressure, the residue was purified by

passage over a 1.5 inch diameter (24 cm of gel) flash chromatographic column by eluting with the following gradient of solvents:  $\text{CHCl}_3$ ; 50:50  $\text{CHCl}_3/\text{MeOH}$ ; 65:25:2  $\text{CHCl}_3/\text{MeOH}/\text{H}_2\text{O}$ ; and 65:25:4  $\text{CHCl}_3/\text{MeOH}/\text{H}_2\text{O}$ .

$^1\text{H}$  NMR ( $\text{CDCl}_3$ ):  $\delta$  .86 (t, 6H,  $\text{CH}_3$ ); 1.26 (br s, 54H,  $(\text{CH}_2)_n$  and  $\text{SCH}_2\text{CH}_3$ ); 1.74 and 1.85 (m, 2H,  $\text{CH}_2\text{CHSS}$ ); 2.69 (q, 4H,  $\text{SSCH}_2\text{CH}_3$ ); 3.31 and 3.34 (br s, 11H,  $\text{CHSS}$  and  $\text{N}(\text{CH}_3)_3$ ); 3.79 (br s, 2H,  $\text{CH}_2\text{N}$ ); 3.95-4.05 (br s, 2H,  $\text{CH}_2\text{OP}$  (glycerol backbone)); 4.22 and 4.52 (m, 2H,  $\text{CH}_2\text{O}$  (glycerol backbone sn-1 chain)); 4.35 (s, 2H,  $\text{CH}_2\text{OP}$  (headgroup)); 5.24 (s, 1H,  $\text{CH}$  (glycerol backbone, sn-2 chain)).

1,2-Di(2-mercaptohexadecanoyl)-L- $\alpha$ -phosphatidylcholine (compound 11). 75 mg (0.082 mmol) 1,2-di(2-ethylthiohexadecanoyl)-L- $\alpha$ -phosphatidylcholine was suspended in 1 ml of 50:50 EtOH/ $\text{H}_2\text{O}$  to which was added tributylphosphine (0.15 ml, 0.61 mmol). The reaction was placed under argon and stirred for 12-18 h in the dark. Subsequently, the solvent was removed in vacuo and the remaining residue was purified by flash chromatography as described above for 1,2-di(2-ethylthiohexadecanoyl)-L- $\alpha$ -phosphatidylcholine (compound 10).

$^1\text{H}$  NMR ( $\text{CDCl}_3$ ):  $^1\text{H}$  NMR ( $\text{CDCl}_3$ ):  $\delta$  .87 (t, 6H,  $\text{CH}_3$ ); 1.24 (br s, 48H,  $(\text{CH}_2)_n$ ); 1.65 and 1.85 (m, 2H,  $\text{CH}_2\text{CHSH}$ ); 2.12 and 2.25 (m and d, respectively, 2H,  $\text{SH}$ ); 3.29 and 3.36 (br s, 11H,  $\text{CHSH}$  and  $\text{N}(\text{CH}_3)_3$ ); 3.79 (br s, 2H,  $\text{CH}_2\text{N}$ ); 3.95-4.05 (br s, 2H,  $\text{CH}_2\text{OP}$  (glycerol backbone)); 4.20 and 4.52 (br m, 2H,  $\text{CH}_2\text{O}$  (glycerol backbone, sn-1 chain)); 4.35 (s, 2H,  $\text{CH}_2\text{OP}$  (headgroup)); 5.24 (s, 1H,  $\text{CH}$  (glycerol backbone, sn-2 chain)).

16-Bromohexadecanoic Acid (compound 1) Generally, it was possible to purchase the necessary bromoacids to make the mercapto fatty acid. However, in the case of the  $\omega$ -16 and  $\omega$ -15, it was necessary to prepare the bromoacid from the decanolate. 16-Hexadecanolate (5.4 g, 21.0 mmol) in 48% hydrobromic acid (7 ml, 62 mmol) and

glacial acetic acid (70 ml) was refluxed for 4 hrs. Upon cooling to room temperature, 50 ml H<sub>2</sub>O was added, which induced precipitation of the product. The white solid was filtered, washed several times with water and dried under vacuum.

<sup>1</sup>H NMR (CDCl<sub>3</sub>): δ 1.20-1.40 (br s, 22H, (CH<sub>2</sub>)<sub>n</sub>); 1.61 (m, 2H, β-CH<sub>2</sub>); 1.83 (m, 2H, ω-1 CH<sub>2</sub>); 3.39 (t, 2H, CH<sub>2</sub>Br).

16-Mercaptohexadecanoic Acid (compound 2) 16-Bromohexadecanoic acid (10.7g, 32 mmol) and thiourea (2.6 g, 34 mmol) in 26 ml absolute ethanol were refluxed 2-4 h. Upon cooling the solution, 3.4 g solid NaOH in 10.6 ml H<sub>2</sub>O was added and the solution was refluxed again for 3-6 h. The reaction mixture was then cooled and acidified with 3N HCl (ml-50 for 12.8 mmol) until a white precipitate formed. The precipitate was washed several times with 3N HCl followed by distilled water to remove urea, and subsequently dried under vacuum.

<sup>1</sup>H NMR (CDCl<sub>3</sub>): δ 1.29 (br s, 22H, (CH<sub>2</sub>)<sub>n</sub>); 1.60 (m, 4H, β-CH<sub>2</sub> and ω-1 CH<sub>2</sub>); 2.33 (t, 2H, CH<sub>2</sub>COOH); 2.50 (q, 2H, CH<sub>2</sub>SH); 11.7 (s, 1H, COOH).

16-Ethylthiohexadecanoic Acid (compound 4) 16-Mercaptohexadecanoic acid (1.85 g, 6.42), ethylethanethiosulfinate (1.18 g, 8.55 mmol) and triethylamine (0.72 ml, 5.22 mmol) were dissolved in 20 ml chloroform, placed under argon and allowed to stir at room temperature in the dark for 24 h. The solvent was then removed and the residue purified by passage over a silica gel column as described for 2-ethylthiohexadecanoic acid (compound 9).

<sup>1</sup>H NMR (CDCl<sub>3</sub>): δ 1.2–1.4 (br s, 25H, (CH<sub>2</sub>)<sub>n</sub> and SSCH<sub>2</sub>CH<sub>3</sub>); 1.63 (m, 4H, β-CH<sub>2</sub> and ω-1 CH<sub>2</sub>); 2.33 (t, 2H, CH<sub>2</sub>COOH); 2.68 (q, 4H, CH<sub>2</sub>SSCH<sub>2</sub>CH<sub>3</sub>); 10.5 (s, 1H, COOH).

1,2-Di(16-ethylthiohexadecanoyl)-L- $\alpha$ -phosphatidylcholine (compound 5). GPC•CdCl<sub>2</sub> (220.8 mg, 0.5 mmol), 16-ethylthiohexadecanoic acid (695 mg, 2 mmol) and 4-dimethylaminopyridine (120.0 mg, 1mmol) were dissolved in freshly distilled chloroform (distilled over P<sub>2</sub>O<sub>5</sub>) to which was added dicyclohexylcarbodiimide (DCC) (1.03 g or more , 5 mmol). The mixture was placed under argon and allowed to stir in the dark for 2-5 days. To remove DMAP, 7.5-10 g of AG 501-X8 (D) resin and sufficient chloroform were added to the mixture to form a thick slurry. The slurry was intermittantly swirled for approximately 10 min and subsequently removed by filtration. After the filtrate was concentrated under reduced pressure, the residue was purified by passage over a 1.5 inch diameter (24 cm of gel) flash chromatographic column by eluting with the following gradient of solvents: CHCl<sub>3</sub>; 50:50 CHCl<sub>3</sub>/MeOH; 65:25:2 CHCl<sub>3</sub>/MeOH/H<sub>2</sub>O; and 65:25:4 CHCl<sub>3</sub>/MeOH/H<sub>2</sub>O.

<sup>1</sup>H NMR (CDCl<sub>3</sub>):  $\delta$  1.2-1.40 (br s, 50H, (CH<sub>2</sub>)<sub>n</sub> and SCH<sub>2</sub>CH<sub>3</sub>); 1.43 (br s, 4H,  $\beta$ -CH<sub>2</sub>); 1.63 (m, 4H,  $\omega$ -1 CH<sub>2</sub>); 2.26 (m, 4H, CH<sub>2</sub>COO); 2.67 (m, 8H, CH<sub>2</sub>SSCH<sub>2</sub>CH<sub>3</sub>); 3.36 (s, 9H, N(CH<sub>3</sub>)<sub>3</sub>); 3.80 (br s, 2H, CH<sub>2</sub>N); 3.92 (s, 2H, CH<sub>2</sub>OP (glycerol backbone)); (4.11 and 4.37 (m, 2H, CH<sub>2</sub>O (glycerol backbone, sn-1 chain)); 4.36 (s, 2H, CH<sub>2</sub>OP (headgroup)); 5.19 (s, 1H, CH (glycerol backbone, sn-2 chain)).

1,2-Di(16-mercaptohexadecanoyl)-L- $\alpha$ -phosphatidylcholine. As described above, this step of the reaction requires optimization and therefore it is critical to examine the proton NMR of the product to be sure that complete deprotection has taken place. Sometimes a second reaction is necessary. Generally, the short chain lipids 1,2-di(-mercaptoundecanoyl)-L- $\alpha$ -phosphatidylcholine to 1,2-di(16-mercaptooctanoyl)-L- $\alpha$ -

phosphatidylcholine are much more readily deprotected and solubilized\* by the excess DTT than the long chain compounds.

Approximately 200 mg (0.22 mmol) 1,2-di(16-ethyldithiohexadecanoyl-L- $\alpha$ -phosphatidylcholine (compound **6**) and 1-1.5 g ( $\approx$  6.5 mmol) dithiothreitol were solubilized in 5 ml EtOH. The reaction mixture was placed under argon and allowed to stir for 2-3 days in the dark at 40°C. The solvent was subsequently removed by rotary evaporation and the final product purified by flash chromatography as described above for 1,2-di(16-ethyldithiohexadecanoyl-L- $\alpha$ -phosphatidylcholine (compound **11**).

$^1\text{H}$  NMR ( $\text{CDCl}_3$ ):  $\delta$  1.2-1.35 (br s, 44H,  $(\text{CH}_2)_n$ ); 1.56 (m, 8H,  $\beta$ - $\text{CH}_2$  and  $\omega$ -1  $\text{CH}_2$ ); 2.26 (m, 4H,  $\text{CH}_2\text{COO}$ ); 2.49 (m, 4H,  $\text{CH}_2\text{SH}$ ); 3.36 (s, 9H,  $\text{N}(\text{CH}_3)_3$ ); 3.79 (br s, 2H,  $\text{CH}_2\text{N}$ ); 3.92 (m, 2H,  $\text{CH}_2\text{OP}$  (glycerol backbone)); 4.11 and 4.37 (m, 2H,  $\text{CH}_2\text{O}$  (glycerol backbone, sn-1 chain)); 4.36 (br s, 2H,  $\text{CH}_2\text{OP}$  (headgroup)); 5.19 (s, 1H,  $\text{CH}$  (glycerol backbone, sn-2 chain)).

*1-hexadecanoyl-2-(16-Ethyldithiohexadecanoyl)-L- $\alpha$ -phosphatidylcholine* ( $\omega$ 16-DPL). L- $\alpha$ -mono-hexadecanoylphosphatidylcholine (lyso-DPL) (250 mg, 0.504 mmol), 16-ethyldithiohexadecanoic acid (347 mg, 1 mmol) and 4-dimethylaminopyridine (60 mg, .49 mmol) were dissolved in freshly distilled chloroform to which was added dicyclohexylcarbodiimide (246 mg, 1.26 mmol). The mixture was placed under argon and allowed to stir in the dark for 2 days. To remove DMAP, 7.5-10 g of AG 501-X8 (D) resin and sufficient chloroform were added to the mixture to form a thick slurry. The slurry was swirled intermittently for approximately 10 min and subsequently removed by filtration. After the filtrate was concentrated under reduced pressure, the residue was purified by passage over a 1.5 inch diameter (24 cm of gel)

---

\* Solubilization of the lipid was the primary reason for choosing such high concentrations of DTT and the elevated reaction temperatures.

flash chromatographic column by eluting with the following gradient of solvents:  $\text{CHCl}_3$ ; 50:50  $\text{CHCl}_3/\text{MeOH}$ ; 65:25:2  $\text{CHCl}_3/\text{MeOH}/\text{H}_2\text{O}$ ; and 65:25:4  $\text{CHCl}_3/\text{MeOH}/\text{H}_2\text{O}$ .

1-(hexadecanoyl)-2-(16-mercaptohexadecanoyl)-L- $\alpha$ -phosphatidylcholine. Approximately 200 mg (0.24 mmol) 1-hexadecanoyl-2-(16-ethylthiohexadecanoyl)-L- $\alpha$ -phosphatidylcholine and 1 g (6.5 mmol) dithiothreitol (DTT) were solubilized in 5 ml EtOH. The reaction mixture was placed under argon and allowed to stir for 2-3 days in the dark. The solvent was subsequently removed by rotary evaporation and the final product purified by flash chromatography as described above for 1,2-di(16-ethylthiohexadecanoyl)-L- $\alpha$ -phosphatidylcholine (compound 6).

$^1\text{H}$  NMR ( $\text{CDCl}_3$ ):  $\delta$  .85 (t, 3H  $\text{CH}_3$  sn-1); 1.2-1.35 (br s, 52H,  $(\text{CH}_2)_n$ ); 1.56 (m, 6H,  $\beta$ - $\text{CH}_2$  (sn-1 and sn-2) and  $\omega$ -1  $\text{CH}_2$  (sn-2)); 2.27 (m, 4H,  $\text{CH}_2\text{COO}$ ); 2.50 (m, 4H,  $\text{CH}_2\text{SH}$  (sn-2)) ; 3.36 (s, 9H,  $\text{N}(\text{CH}_3)_3$ ); 3.79 (br s, 2H,  $\text{CH}_2\text{N}$ ); 3.92 (m, 2H,  $\text{CH}_2\text{OP}$  (glycerol backbone)); 4.12 and 4.39 (m, 2H,  $\text{CH}_2\text{O}$  (glycerol backbone, sn-2 chain)); 4.36 (br s, 2H,  $\text{CH}_2\text{OP}$  (headgroup)); 5.19 (s, 1H,  $\text{CH}$  (glycerol backbone, sn-1 chain)).

1-octadecanoyl-2-(2-ethylthiooctadecanoyl)-L- $\alpha$ -phosphatidyl-choline. L- $\alpha$ -mono-octadecanoylphosphatidylcholine (lyso-DSL) (250 mg, .477 mmol), 16-ethylthiohexadecanoic acid (720 mg, 1.91 mmol) and 4-dimethylaminopyridine (60 mg, .49 mmol) were dissolved in freshly distilled chloroform to which was added dicyclohexylcarbodiimide (246 mg, 1.26 mmol). The mixture was placed under argon and allowed to stir in the dark for 2 days. To remove DMAP, 7.5-10 g of AG 501-X8 (D) resin and sufficient chloroform were added to the mixture to form a thick slurry. The slurry was swirled intermittently for approximately 10 min and subsequently removed by filtration. After the filtrate was concentrated under reduced pressure, the

residue was purified by passage over a 1.5 inch diameter (24 cm of gel) flash chromatographic column by eluting with the following gradient of solvents:  $\text{CHCl}_3$ ; 50:50  $\text{CHCl}_3/\text{MeOH}$ ; 65:25:2  $\text{CHCl}_3/\text{MeOH}/\text{H}_2\text{O}$ ; and 65:25:4  $\text{CHCl}_3/\text{MeOH}/\text{H}_2\text{O}$ .

1-octadecanoyl-2-(2-Mercaptooctadecanoyl)-L- $\alpha$ -phosphatidylcholine ( $\alpha$ 18-DSL) 1-octadecanoyl-2-(2-ethylthiooctadecanoyl)-L- $\alpha$ -phosphatidylcholine (75 mg, .082 mmol) was suspended in 1 ml of 50:50 EtOH/H<sub>2</sub>O to which was added tributylphosphine (0.15 ml, 0.61 mmol). The reaction was placed under argon and stirred for 12 h in the dark. Subsequently, the solvent was removed in vacuo and the remaining residue was purified by flash chromatography as described above for 1,2-di(2-ethylthiohexadecanoyl)-L- $\alpha$ -phosphatidylcholine (compound #). Alternatively, approximately 200 mg 1-(2-ethylthiooctadecanoyl)-2-octadecanoyl-L- $\alpha$ -phosphatidylcholine (.24 mmol) and 1 g ( $\approx$  6.5 mmol) dithiothreitol were solubilized in 5 ml EtOH. The reaction mixture was placed under argon and allowed to stir for 2-3 days in the dark. The solvent was subsequently removed by rotary evaporation and the final product purified by flash chromatography as described above for 1,2-di(2-ethylthiohexadecanoyl)-L- $\alpha$ -phosphatidylcholine.

<sup>1</sup>H NMR ( $\text{CDCl}_3$ ):  $\delta$  .87 (t, 6H,  $\text{CH}_3$ ); 1.24 -1.4 (br s, 56H,  $(\text{CH}_2)_n$ ); 1.56 (br s, 2H,  $\beta$ - $\text{CH}_2$  (sn-1)); 1.65 and 1.85 (m, 2H,  $\text{CH}_2\text{CHSH}$  (sn-2)); 2.15 (d, 2H,  $\text{SH}$  (sn-2)); 2.25 (m, 2H,  $\text{CH}_2\text{COO}$  (sn-1)) 3.29 (m, 1H,  $\text{CHSH}$  (sn-2)); 3.36 (br s, 9H,  $\text{N}(\text{CH}_3)_3$ ); 3.80 (br s, 2H,  $\text{CH}_2\text{N}$ ); 4.0 (br s, 2H,  $\text{CH}_2\text{OP}$  (glycerol backbone)); 4.13 and 4.41 (m, 2H,  $\text{CH}_2\text{O}$  (glycerol backbone, sn-2 chain)); 4.36 (s, 2H,  $\text{CH}_2\text{OP}$  (headgroup)); 5.24 (s, 1H,  $\text{CH}$  (glycerol backbone, sn-1 chain)).

### Representative Spectra.

Representative spectra of the monomeric  $\alpha$ -THIOLS and  $\omega$ -THIOLS and the mixed chain compounds are shown in Figures 3-6. Assignments are similar to those described above for the final products. The important features to note are:

(i). In the case of the  $\omega$ -THIOLS (Fig 3); (i.e., 1,2-di(16-mercaptohexadecanoyl)-L- $\alpha$ -phosphatidylcholine, 1,2-di(15-mercaptopentadecanoyl)-L- $\alpha$ -phosphatidylcholine, 1,2-di(12-mercaptododecanoyl)-L- $\alpha$ -phosphatidylcholine and 1,2-di(11-mercaptoundecanoyl)-L- $\alpha$ -phosphatidylcholine) there is no methyl group apparent in the spectra at .87 ppm indicating that the disulfide exchange reaction is a great improvement over deprotection with TBP.

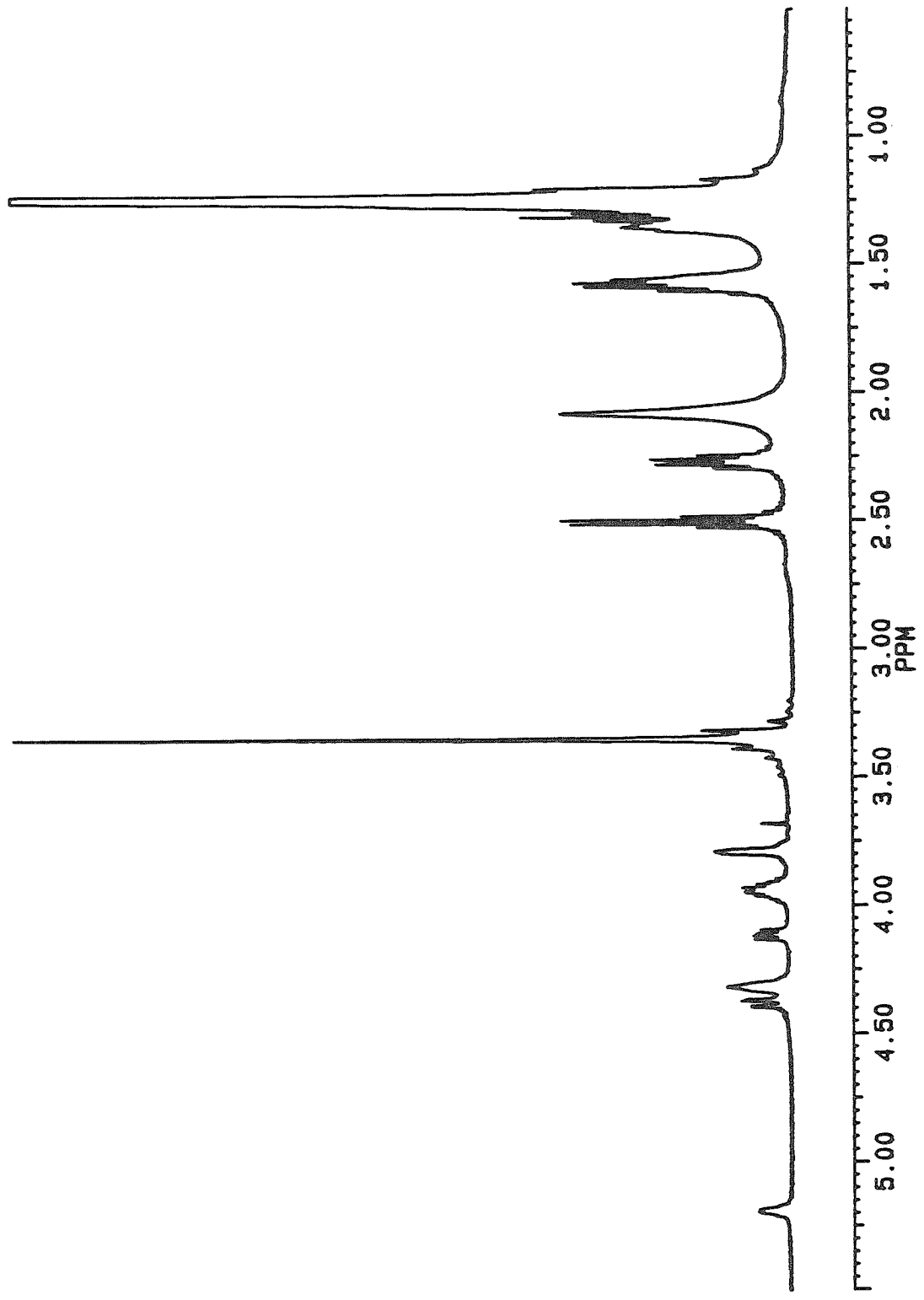
(ii). The spectra of monomeric  $\alpha$ -THIOLS (Figure 4); (i.e., 1,2-di(2-mercaptohexadecanoyl)-L- $\alpha$ -phosphatidylcholine, 1,2-di(2-mercaptooctadecanoyl)-L- $\alpha$ -phosphatidylcholine and 1,2-di(2-mercaptoarachidoyl)-L- $\alpha$ -phosphatidylcholine) are significantly broader than the spectra for the  $\omega$ -THIOLS. This is most likely due to the fact that the products are a mixture of stereoisomers due to the presence of the chiral CHSH group.

(iii). The synthesis of the mixed-chain lipids is known to occur with some percentage of acyl chain migration. We did not examine this analytically by GPC. However, for  $\alpha$ -THIOLS, the SH resonance from the sn-1 chain is distinct from that of the sn-2 chain in the  $^1\text{H}$  NMR spectra. The sn-1 SH appears as a downfield doublet whereas the SH from the sn-2 chain is shifted slightly upfield and appears as a multiplet (see Figure 4 for examples). In the  $^1\text{H}$  spectra of the mixed chain compounds (Figure 6), only a very small percentage of the SH groups may be assigned to the sn-2 chain, indicating only a small amount of acyl chain migration.

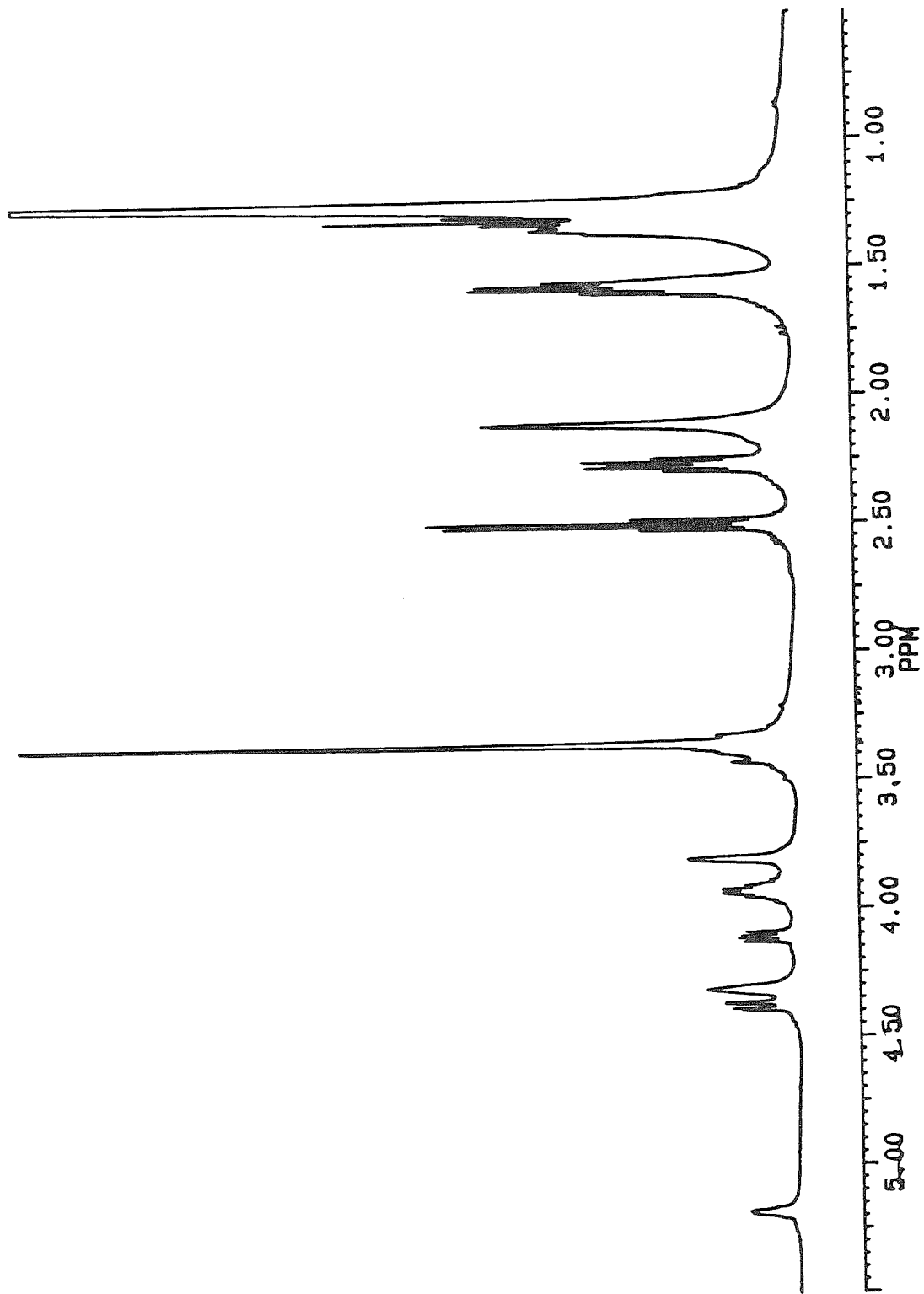
**Figure 3**

Representative  $^1\text{H}$  NMR spectra (500 MHz) of monomeric  $\omega$ -THIOLS in  $\text{CDCl}_3$ :  
A. 1,2-di(16-mercaptohexadecanoyl)-L- $\alpha$ -phosphatidylcholine; B. 1,2-di(15-mercaptopentadecanoyl)-L- $\alpha$ -phosphatidylcholine; C. 1,2-di(12-mercaptododecanoyl)-L- $\alpha$ -phosphatidyl-choline and D. 1,2-di(11-mercaptoundecanoyl)-L- $\alpha$ -phosphatidylcholine.

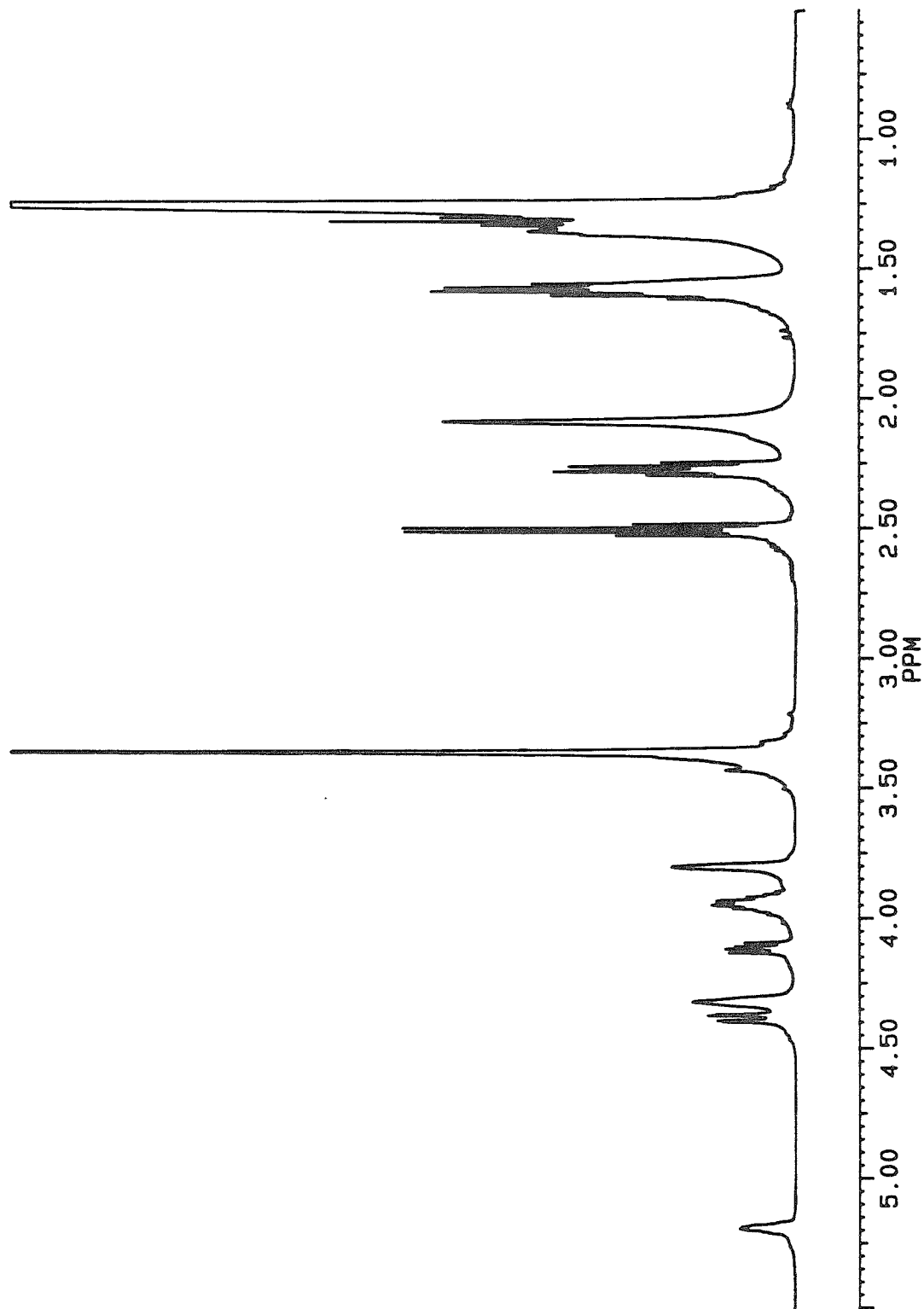
A



B



c



D

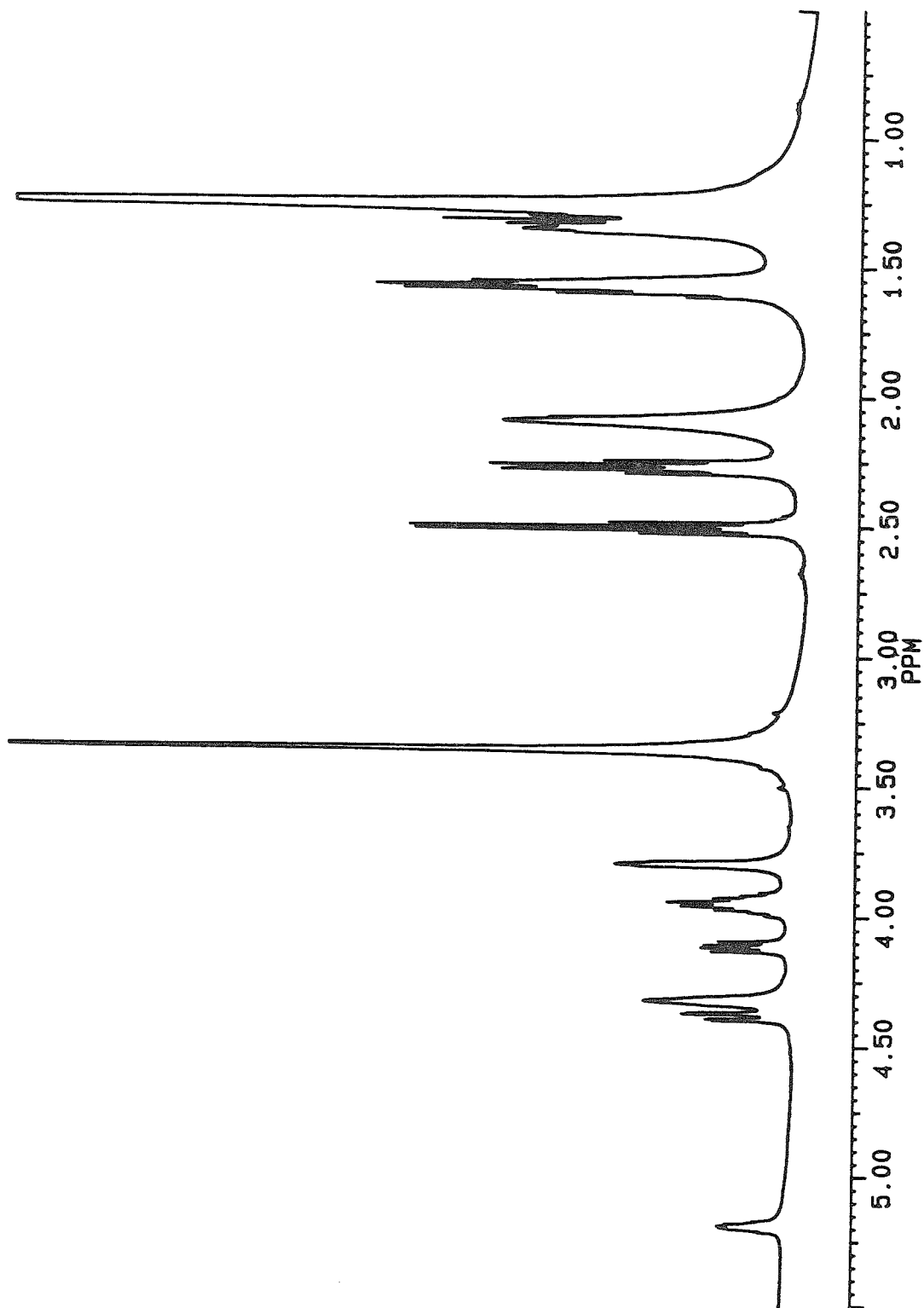
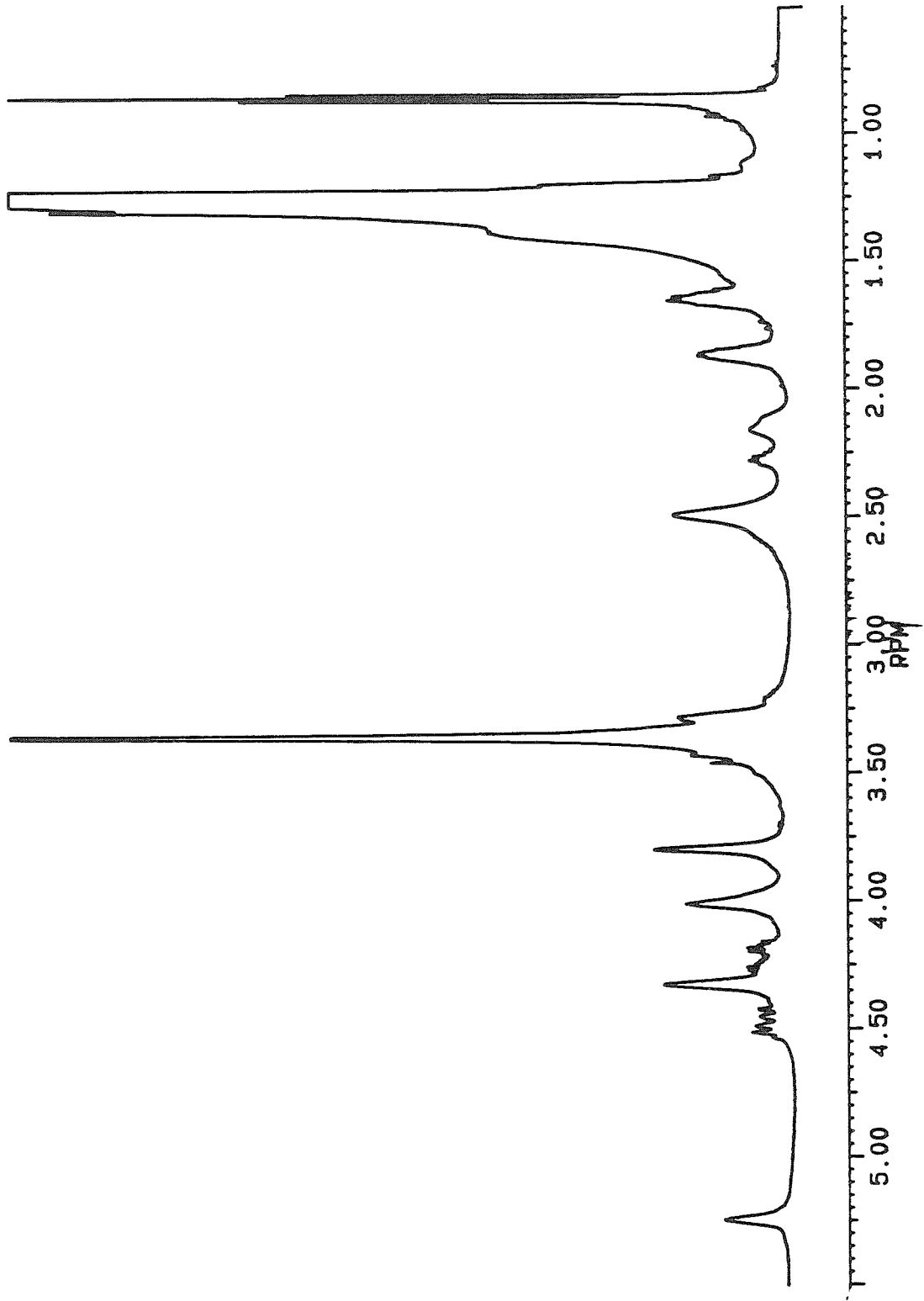


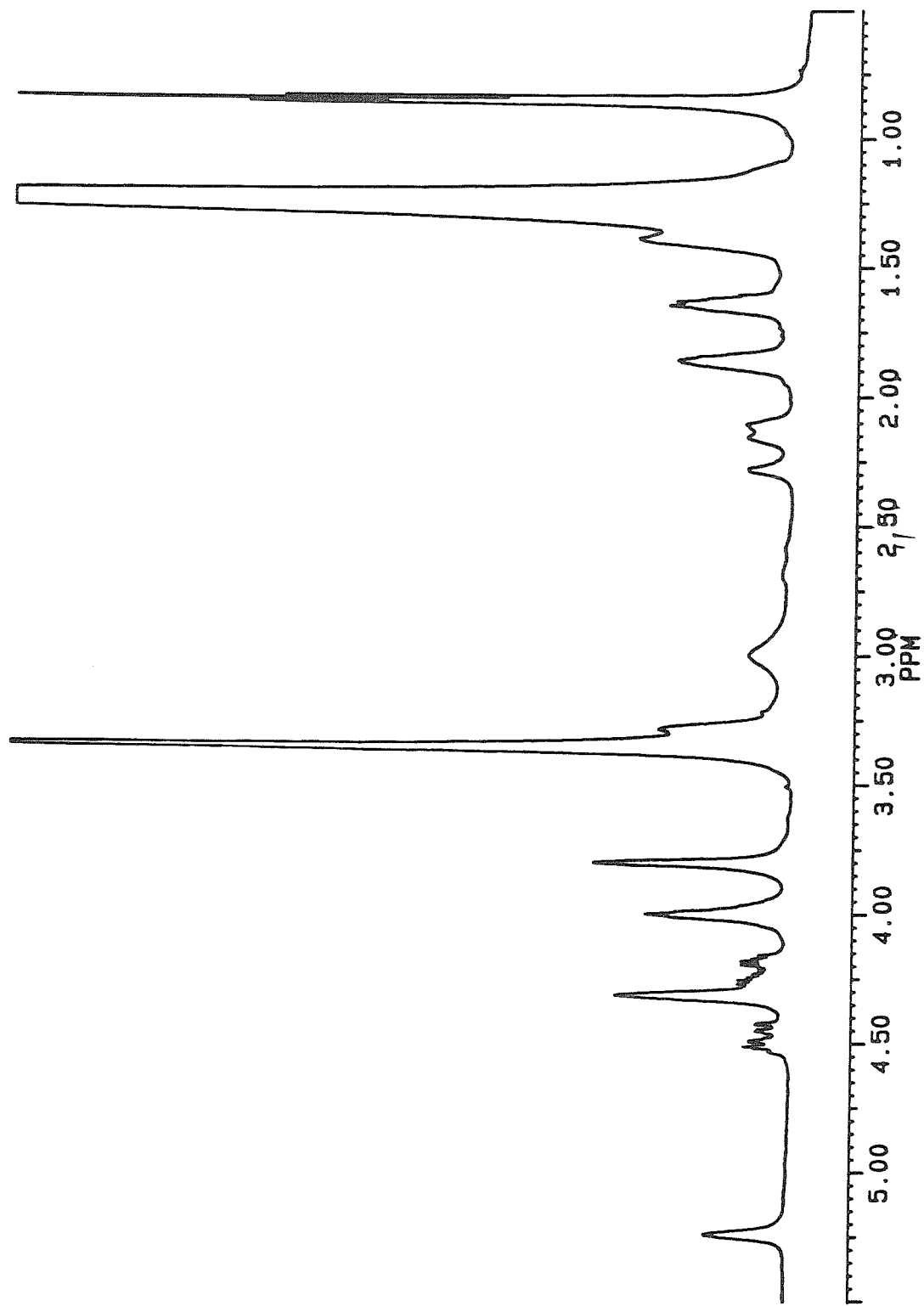
**Figure 4**

Representative  $^1\text{H}$  NMR spectra (500 MHz) of monomeric  $\alpha$ -THIOLS in  $\text{CDCl}_3$ :  
A. 1,2-di(2-mercaptohexadecanoyl)-L- $\alpha$ -phosphatidylcholine; B. 1,2-di(2-mercapto-octadecanoyl)-L- $\alpha$ -phosphatidylcholine; C. 1,2-di(2-mercaptoarachidoyl)-L- $\alpha$ -phosphatidylcholine.

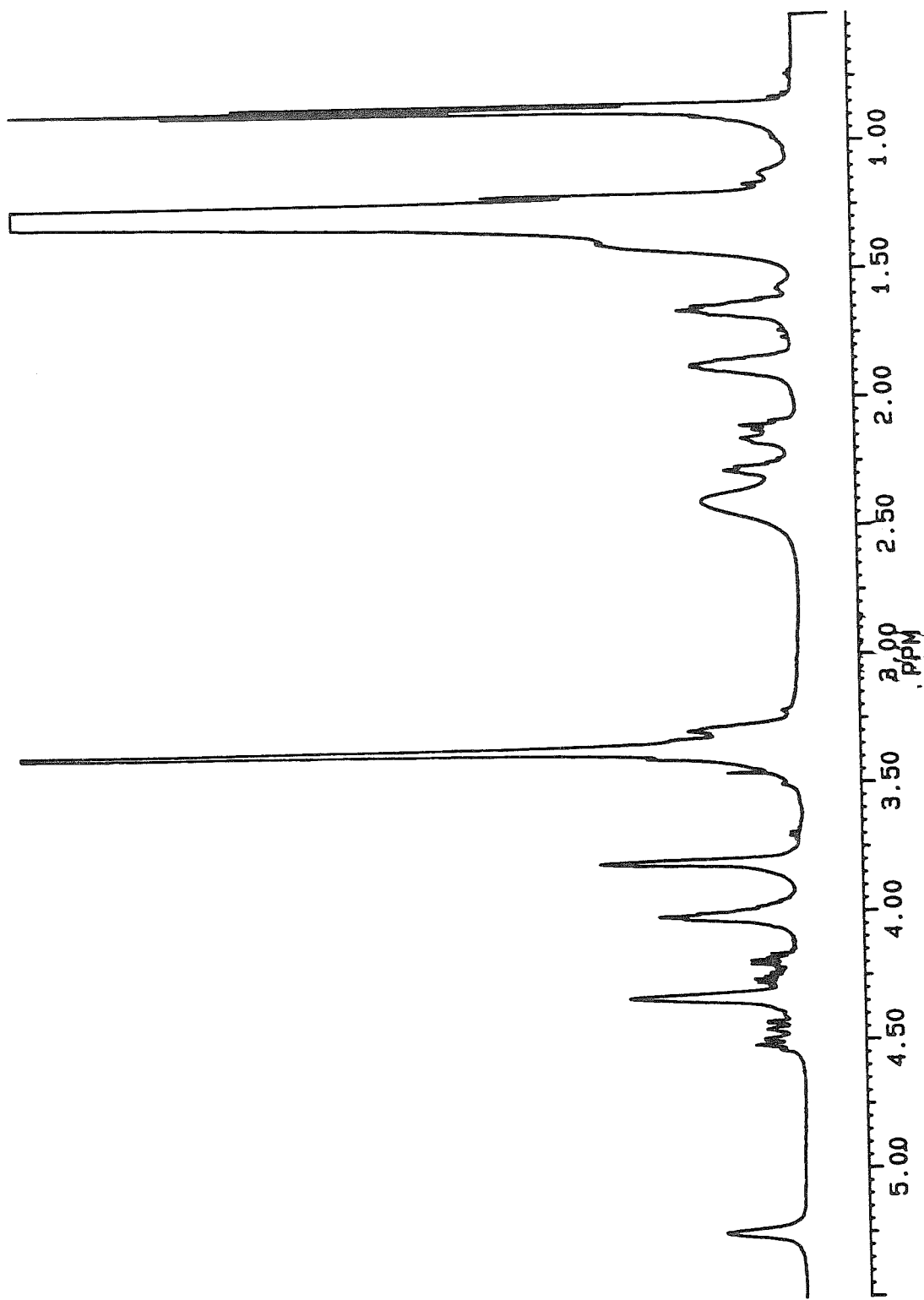
A



B

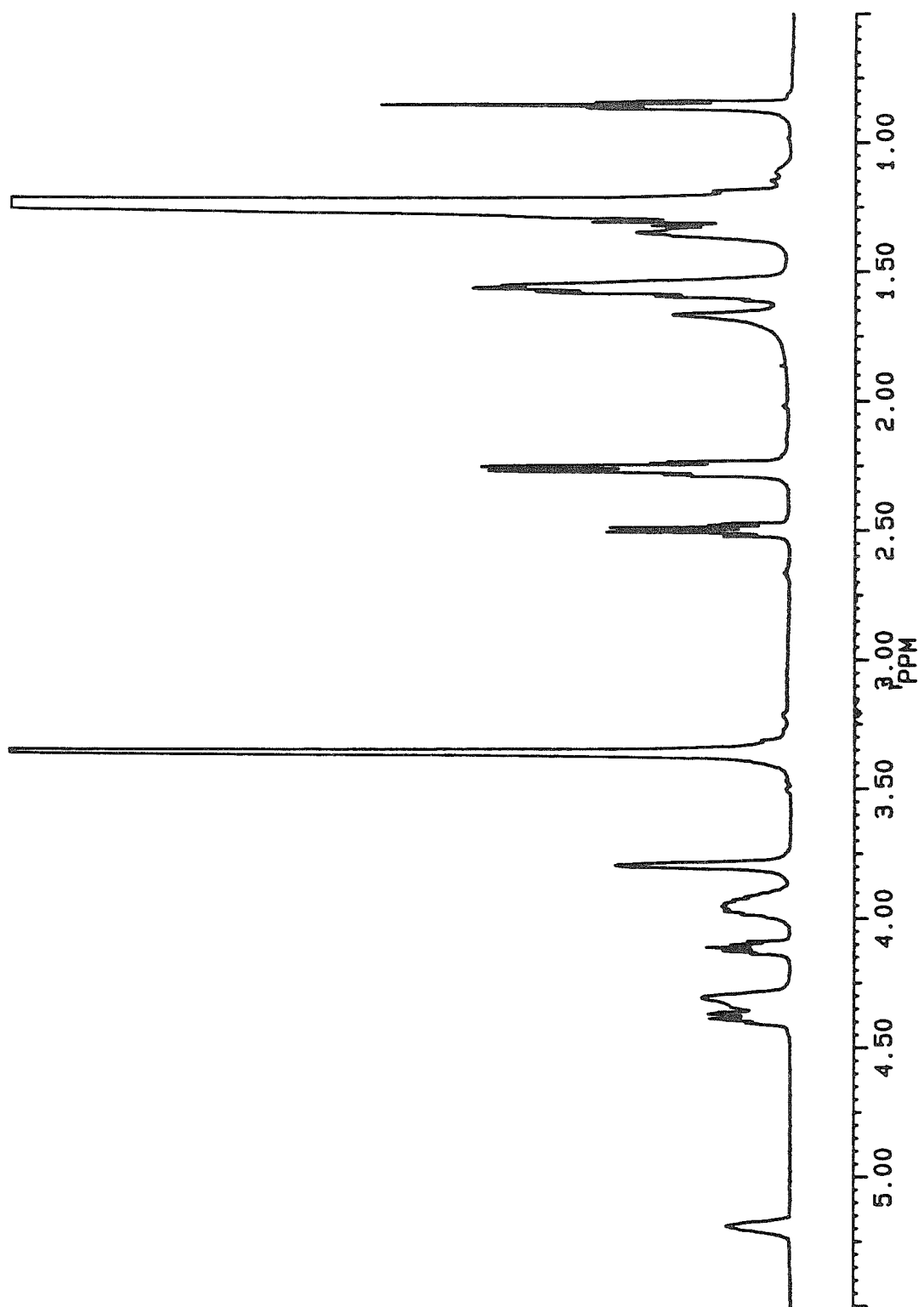


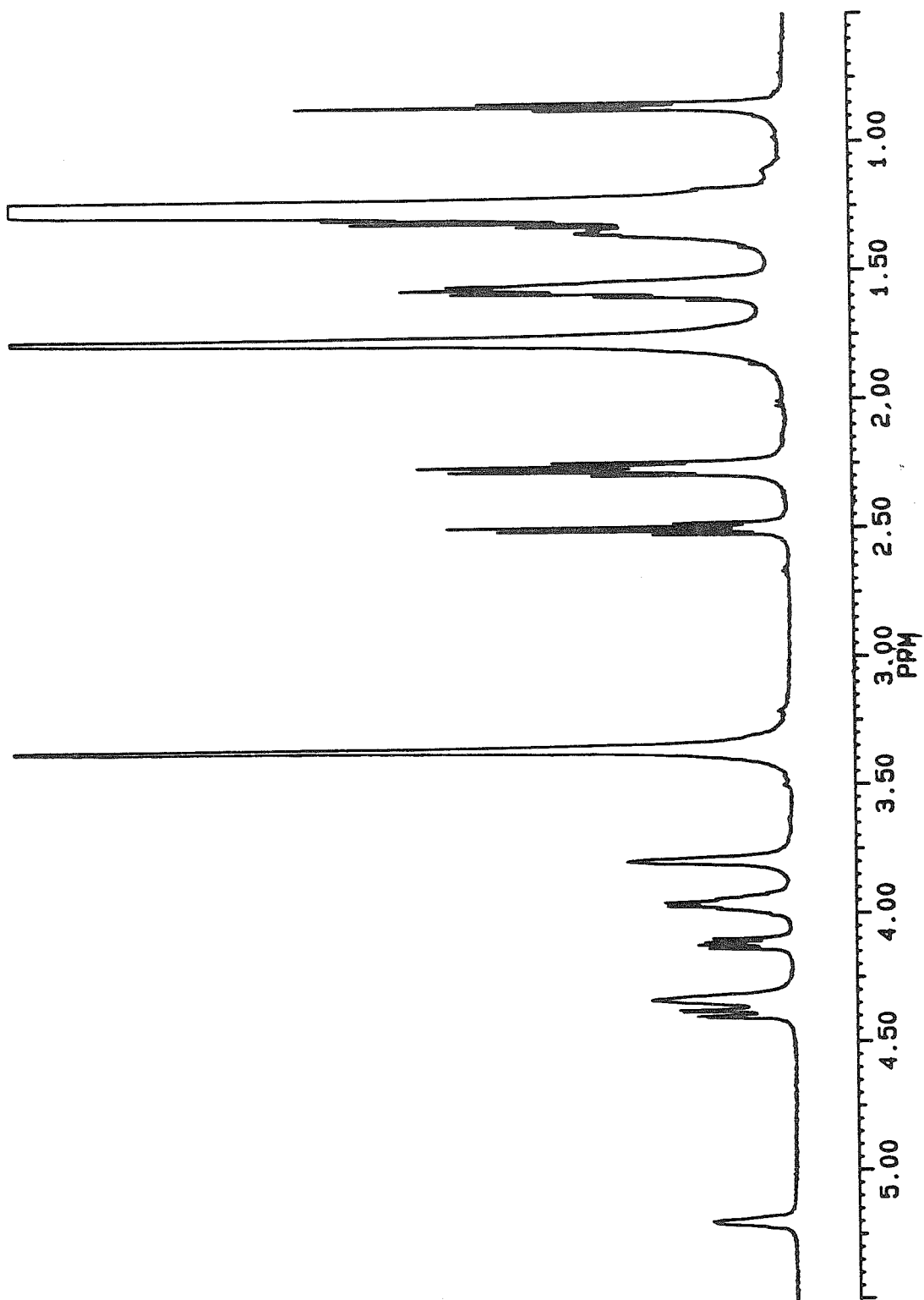
C



**Figure 5**

Representative  $^1\text{H}$  NMR spectra (500 MHz) of mixed-chain  $\omega$ -THIOLS in  $\text{CDCl}_3$ :  
**A.** 1-(hexadecanoyl)-2-(16-mercaptohexadecanoyl)-L- $\alpha$ -phosphatidylcholine; **B.** 1-(octadecanoyl)-2-(16-mercaptohexadecanoyl)-L- $\alpha$ -phosphatidylcholine

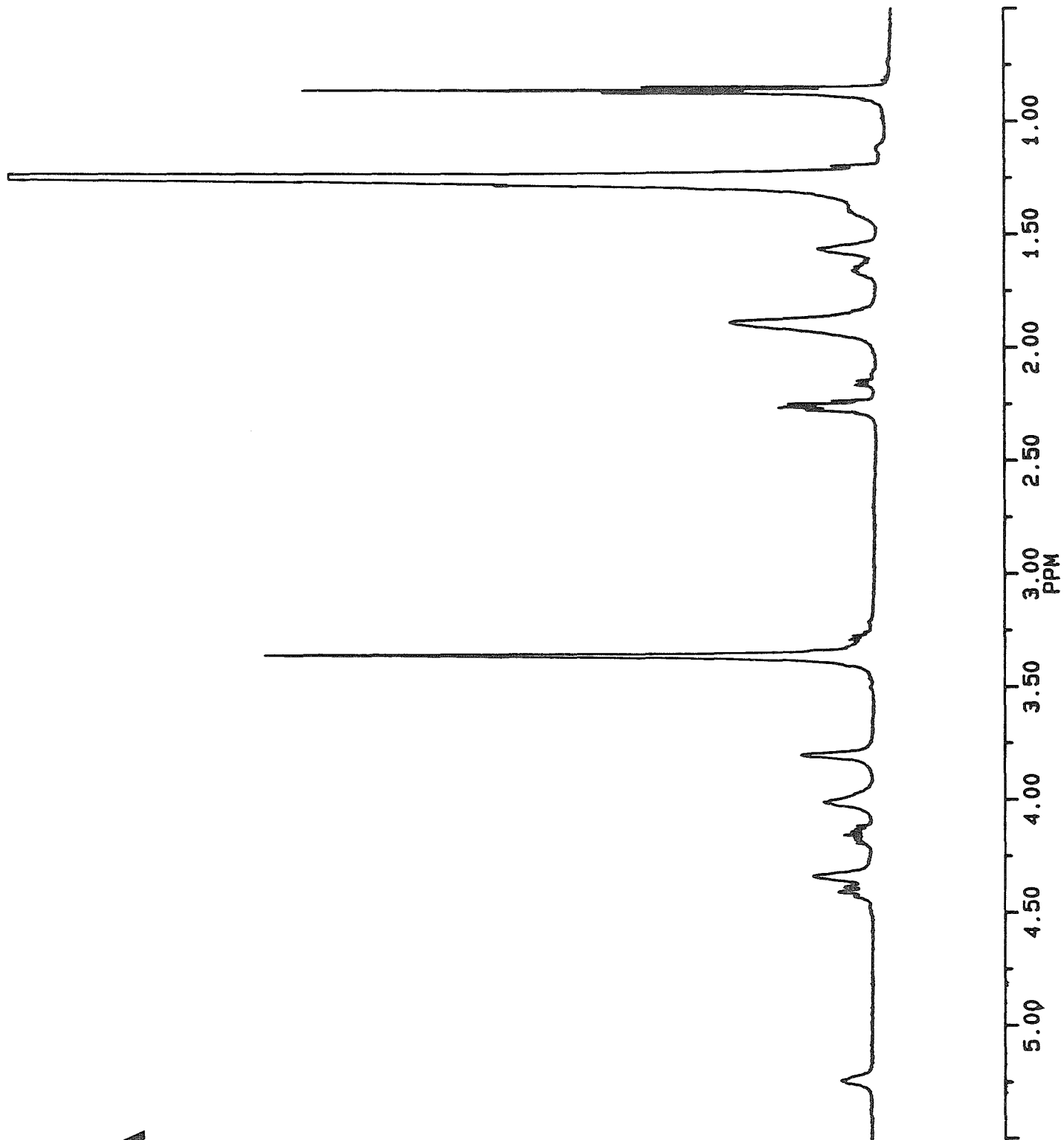
**A**

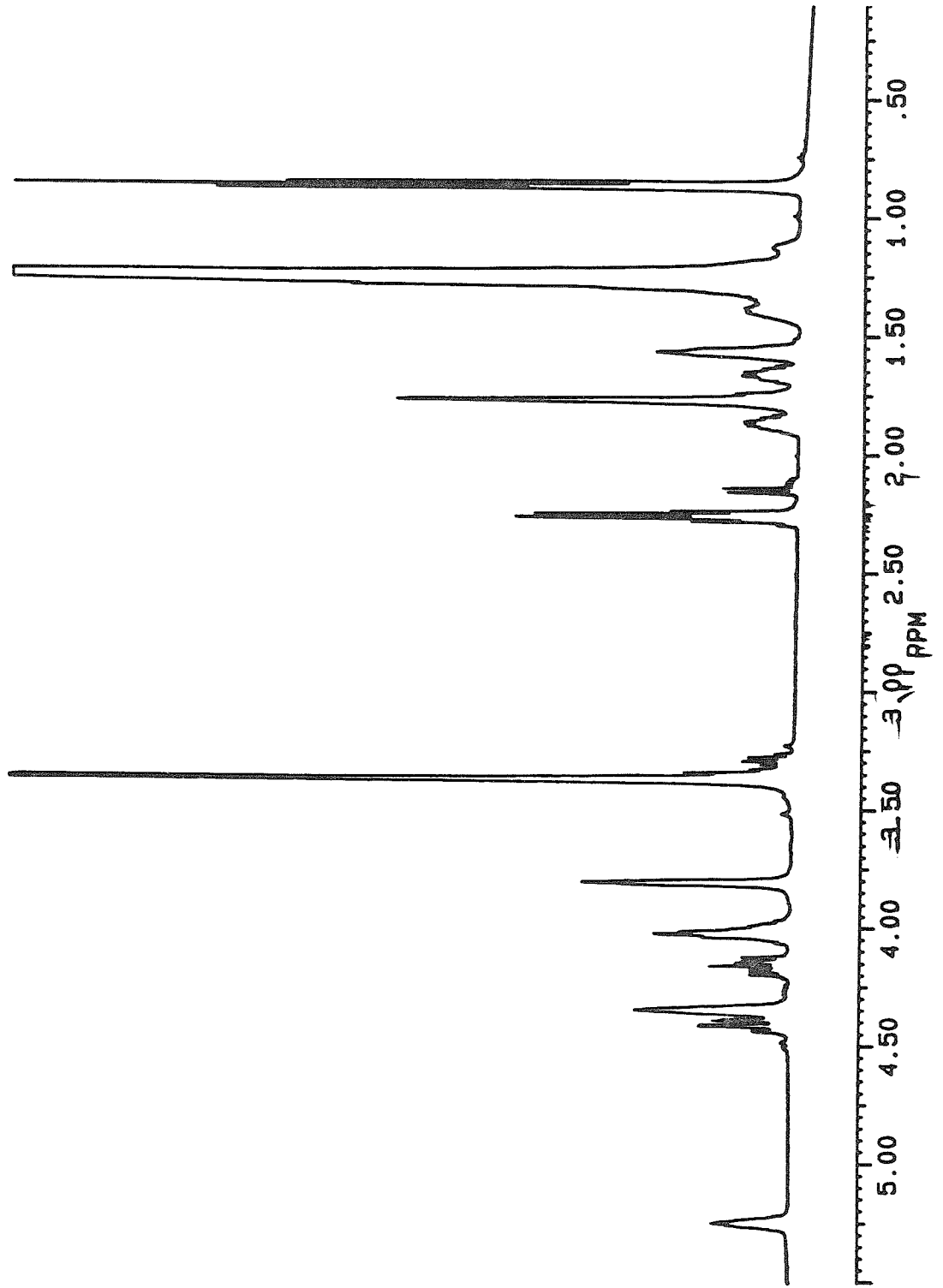
**B**

**Figure 6**

Representative  $^1\text{H}$  NMR spectra (500 MHz) of mixed-chain  $\alpha$ -THIOLS in  $\text{CDCl}_3$ :  
**A.** 1-(octadecanoyl)-2-(2-mercaptooctadecanoyl)-L- $\alpha$ -phosphatidylcholine); **B.** 1-(octadecanoyl)-2-(2-mercaptoarachidoyl)-L- $\alpha$ -phosphatidylcholine)

A



**B**

### Polymerization of Liposomes.

Polymerization of the thiol-containing phospholipid was routinely carried out immediately following preparation of the mercaptophosphatidylcholines. The motivation for doing this was due to the reactivity of the compounds, particularly those with short acyl chains. Storage under argon at  $-20^{\circ}\text{C}$  was insufficient to prevent some oxidation from occurring. Since phospholipid dimers or short oligomers were not readily distinguished from degradation products (i.e., lysolipid), we felt it best to store the compounds as dry powders in the polymerized form to avoid potential artifacts on account of the sample history. As described in the morphology chapter, the polymeric  $\alpha$ -THIOLS form liposomes very readily from the prepolymerized state whereas the  $\omega$ -THIOLS appear to form bilayer fragments whether they have been lyophilized or not.

Method A ; Peroxide Polymerization. Polymerization of the compounds was carried out by the protocol outlined by Regen *et al.* with small modifications of temperature and concentration (1,4). Briefly, samples were prepared at a concentration of 5 mg/ml by dispersion in borate buffer (10 mM borate, 150 mM NaCl, 2 mM  $\text{NaN}_3$ ; pH 8.5) containing 20 equivalents of  $\text{H}_2\text{O}_2$ , pH 8.5.\* The samples were subsequently polymerized for 4-8 h above the phase transition temperature of the monomeric lipid.  $\alpha$ -THIOLS were polymerized 4 h at  $40^{\circ}\text{C}$ ,  $45$ - $50^{\circ}\text{C}$  and  $60^{\circ}\text{C}$  ( $\alpha$ -16,  $\alpha$ -18 and  $\alpha$ -20, respectively). T-THIOLS were polymerized as follows:  $40^{\circ}\text{C}$ , 4 h (N=8-10);  $45^{\circ}\text{C}$ , 4 h (N=11-12);  $50$ - $55^{\circ}\text{C}$ , 4 or 8 h (N=15) and  $60^{\circ}\text{C}$ , 4 or 8 h (N=16).\*\* Mixed-chain lipids were polymerized at a concentration of 10 mg/ml with 20 equivalents of  $\text{H}_2\text{O}_2$ , pH 8.5 for 4 h at the following temperatures:  $50^{\circ}\text{C}$  ( $\omega$ 15-DPL,  $\omega$ 15-DSL);  $60^{\circ}\text{C}$

---

\* In some cases the samples were sonicated prior to polymerization as described in the individual chapters. Unless specifically mentioned, however, the lipids were simply dispersed in buffer.

\*\* N refers to the number of carbons in the fatty acyl chains.

( $\omega$ 16-DPL and  $\alpha$ 18-DSL); 65°C ( $\omega$ 16-DSL). The extent of polymerization was monitored (i) by detection of residual thiol groups using Ellman's reagent in a colorimetric assay or as a TLC spray and (ii) by the retention of the lipid at the origin of TLC plates eluted with 65:25:4 CHCl<sub>3</sub>/MeOH/H<sub>2</sub>O. Following polymerization, samples were dialyzed against deionized water for at least 24 h, lyophilized and stored as dry powders at -20°C. Some variations in temperature and length of polymerization have been utilized but are noted in the chapters. This method of polymerization was used routinely for the experiments described in the preceding chapters unless noted otherwise in the text.

The consequence of the peroxide induced oxidative polymerization has been described by Regen *et al.* for  $\alpha$ -16,  $\omega$ -11, and  $\omega$ -16. In their studies, polymerization was carried out as described above with the exception that for all three lipid types, polymerization was carried out for 4 h at 40°C. Based on analysis of the residual thiol groups, the extent of the reaction and average degree of polymerization ( $X_n$ ) was reported to be 96% ( $X_n = 25$ ), 94% ( $X_n = 17$ ) and 95% ( $X_n = 20$ ) for  $\omega$ -1,  $\omega$ -16 and  $\alpha$ -16, respectively. As described above, for the longer chain lipids, (i.e.,  $\omega$ -16,  $\omega$ -15) the polymerization conditions were slightly more rigorous (higher temperatures were used) in order to polymerize all monomeric lipids above their respective transition temperatures.\* Thus under the conditions which we have employed we anticipated 95-100% conversion to the disulfide.

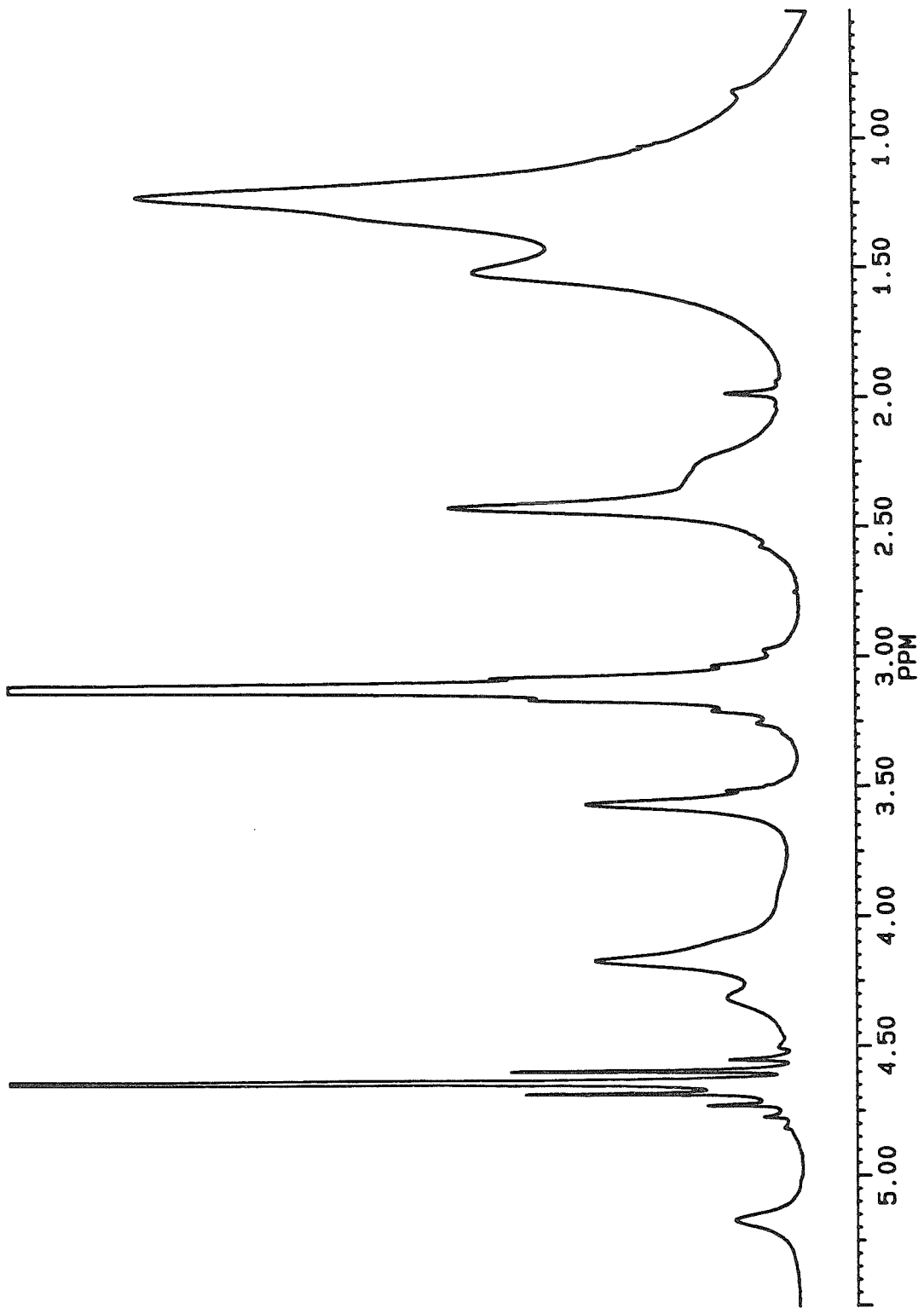
By TLC, the lipids were all found to be thiol negative subsequent to polymerization. NMR was also used to characterize the shorter chain polymerized lipids, which give rise to reasonably resolved features. Figure 7 shows the <sup>1</sup>H NMR spectrum of sonicated monomeric  $\omega$ -11 SUVs in water. The resonance at 4.63 ppm arises from

---

\* See Chapter III for a discussion of the thermal properties of the lipids.

Figure 7

$^1\text{H}$  NMR Spectrum (500 MHz) of sonicated monomeric  $\omega$ -11 SUVs in  $\text{D}_2\text{O}$ . The spectrum was apodized with 1 Hz linebroadening.



HOD present in the sample. All other resonances between 3.5 and 5.5 ppm are assigned to protons from the glycerol backbone and the methylene groups of the headgroup, the resonance at 3.1 ppm is from the choline methyls, and the broad envelope between .75 and 1.75 ppm is from the bulk methylenes of the acyl chains. The asymmetric resonance at  $\approx 2.4$  ppm is due to the overlap between the  $\text{CH}_2\text{SH}$  (low field peak) and  $\text{CH}_2\text{COO}$  (high field shoulder). Upon polymerization, the resonance attributable to the  $\text{CH}_2\text{SH}$  group is shifted downfield to  $\approx 2.65$  ppm ( $\text{CH}_2\text{SS}$ ). As can be seen in the spectra in Figure 8 corresponding to polymerized  $\omega$ -11 and  $\omega$ -10 in  $\text{D}_2\text{O}$ , the reaction appears to be essentially complete. This is visualized even more readily by the spectrum of polymeric  $\omega$ -11 in MeOH (Figure 8).\*

Similar results are shown by analysis of the  $^{13}\text{C}$  spectra. Figure 9A shows the carbon spectra of monomeric  $\omega$ -8 micelles in phosphate buffer.\*\* The detailed resonance assignments are as described in Chapter V. Briefly, the peaks between 60 and 71 ppm arise from the glycerol backbone and headgroup carbons, the peak at 54.3 is from the choline methyls, and the resonances between 20 and 40 ppm are due to the acyl chains.\*\*\* The most important features to note are (i) the lack of any resonance at  $\approx 14$  ppm, which would be due to a terminal methyl group and (ii) the peak at 34 ppm, which is attributed to the superposition of the carbons from the  $\alpha$ -methylene carbon and the  $\text{CH}_2\text{SH}$  carbon ( $\omega$ -methylene). Upon oxidative polymerization the resonance of the  $\omega$ -methylene is shifted to  $\approx 39$  ppm as shown in Figure 9B. The lines are also broadened as a consequence of the polymerization and the increase in the size of the aggregate. Figure 10 shows a spectrum of polymeric  $\omega$ -11 in MeOH (the resonance at

---

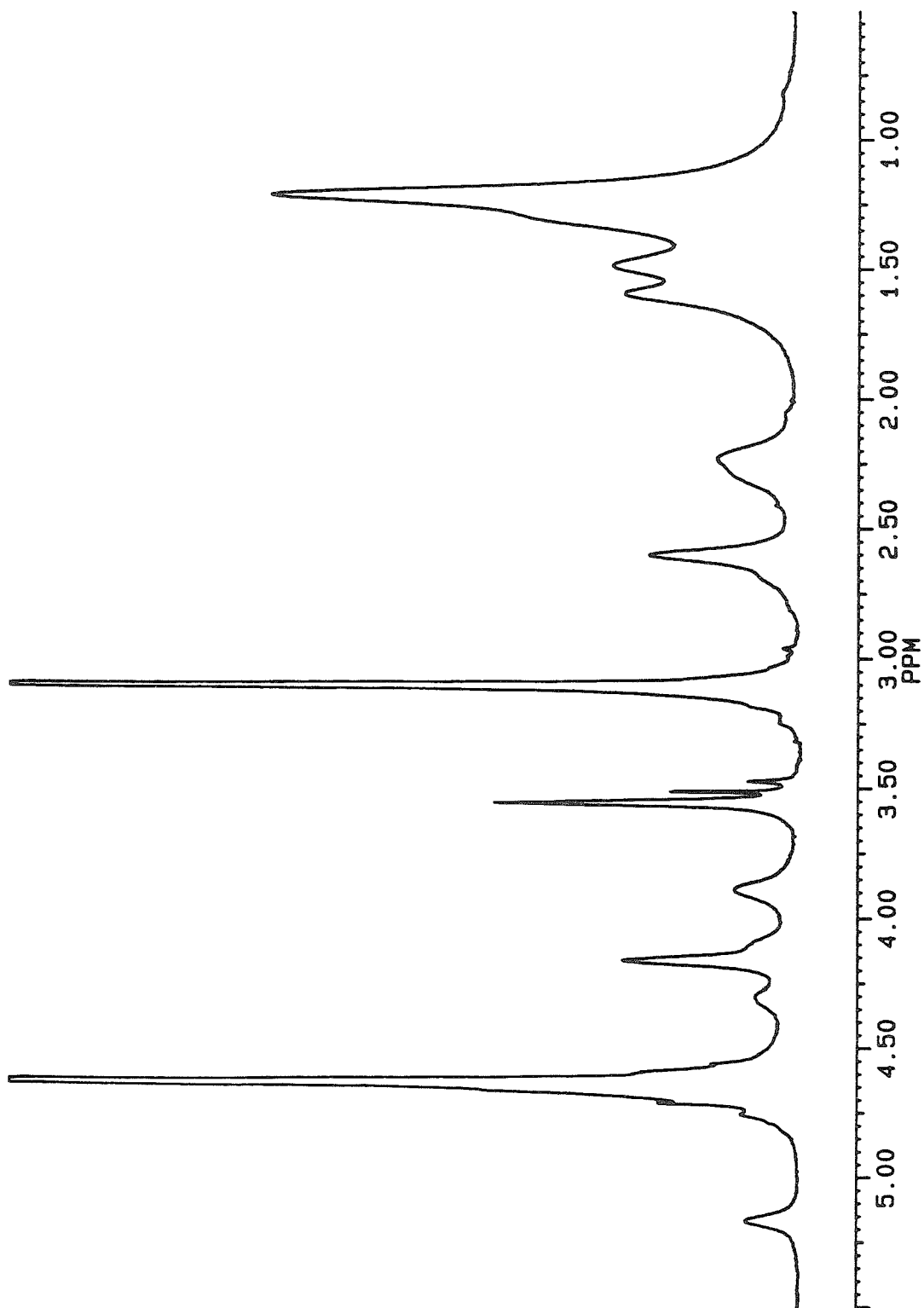
\* The resonances at  $\approx 3.3$  and 4.8 ppm are due to the methanol.

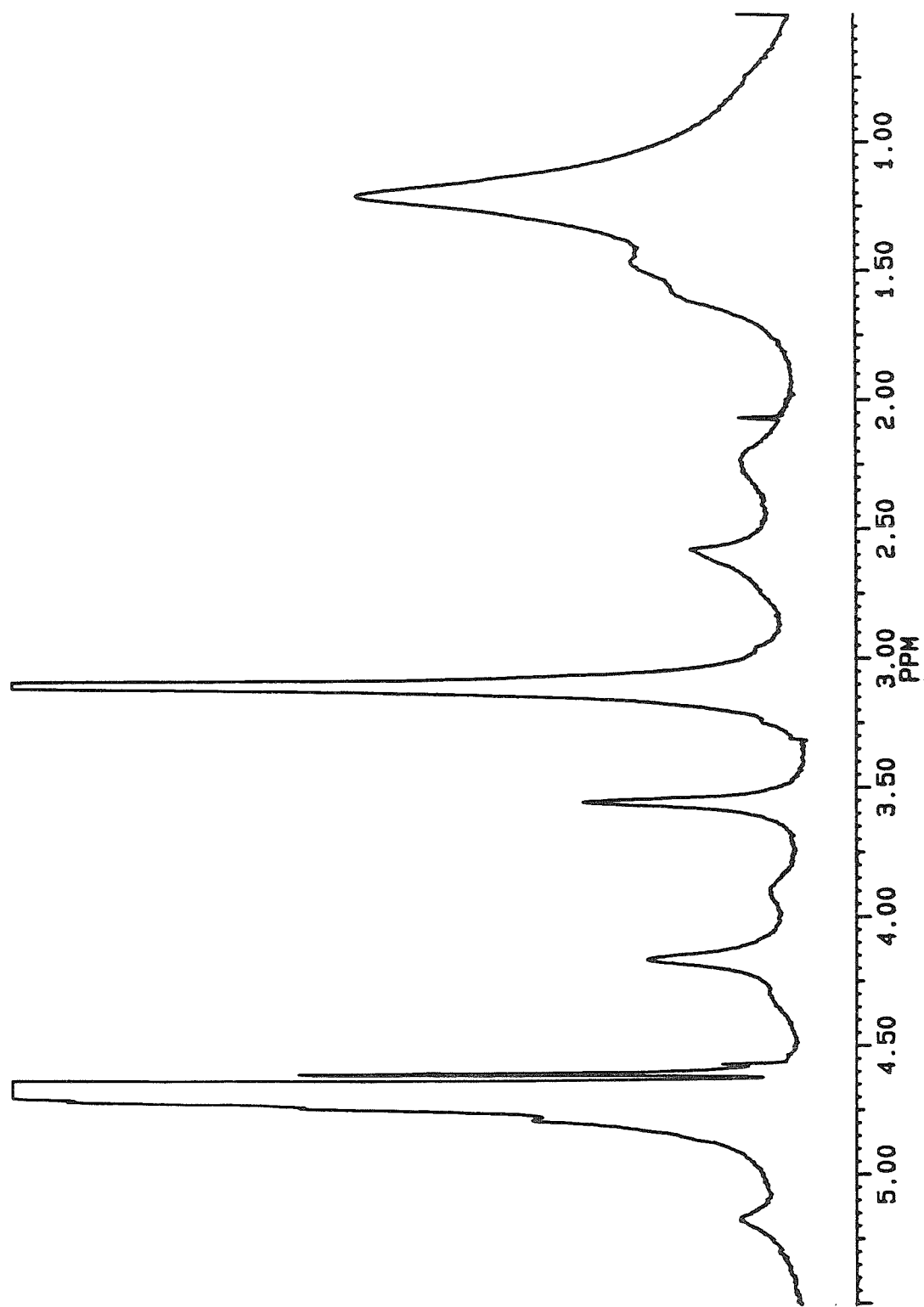
\*\* The resonance seen at  $\approx 57$  ppm is due to EDTA in the sample.

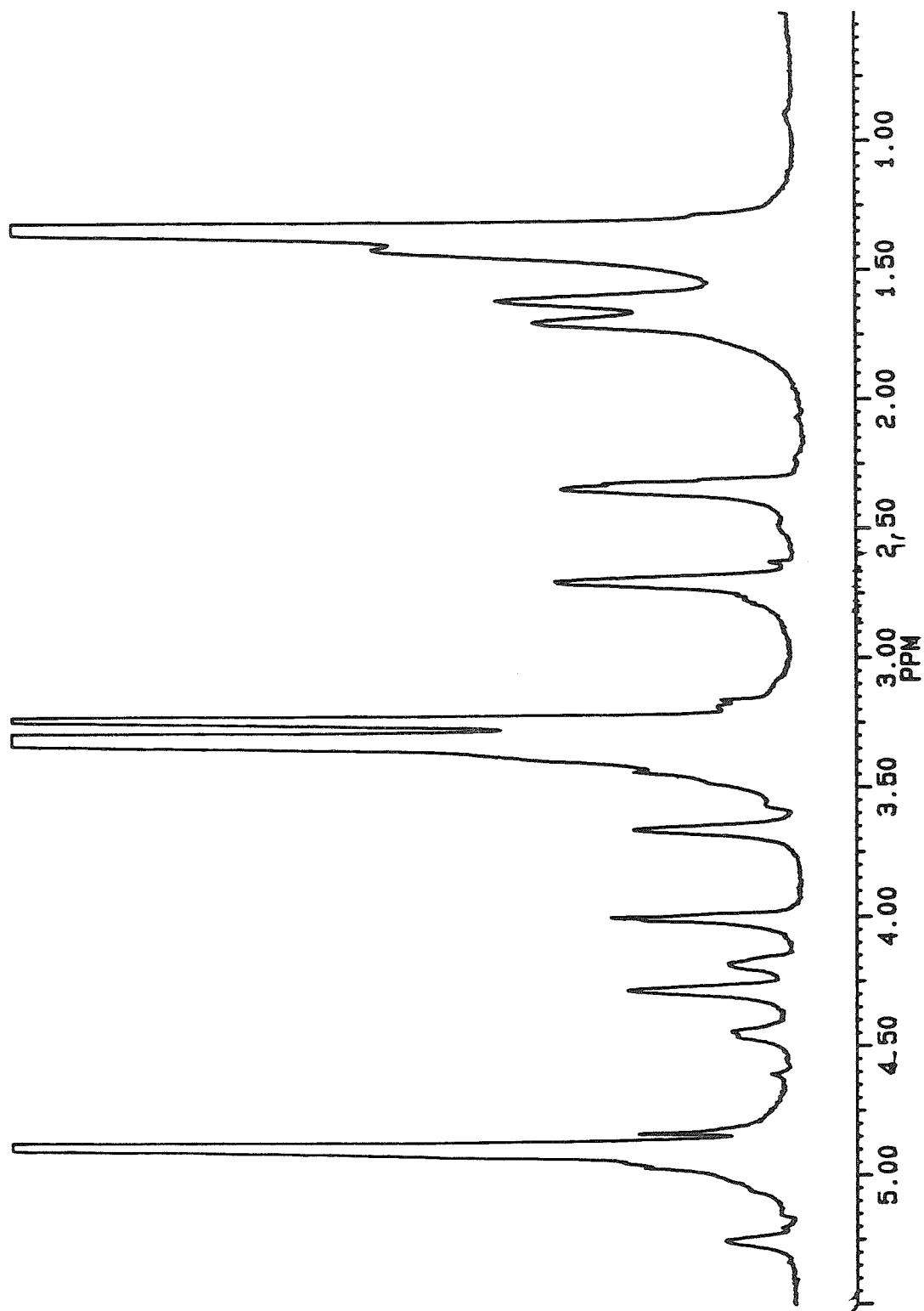
\*\*\* The carbonyl carbon which resonates at approximately 174 ppm was not included in the Figure.

Figure 8

$^1\text{H}$  NMR Spectrum (500 MHz) of polymerized  $\omega$ -THIOLS in  $\text{D}_2\text{O}$  or MeOH. The samples were polymerized by method B (method A yields the same results but the samples are less well resolved). The spectra are apodized with 1 Hz (A and B) and .5 Hz (C) linebroadening: A Polymerized  $\omega$ -10 in  $\text{D}_2\text{O}$ ; B. Polymerized  $\omega$ -11 in  $\text{D}_2\text{O}$ ; C. Polymerized  $\omega$ -11 in MeOH.

**A**

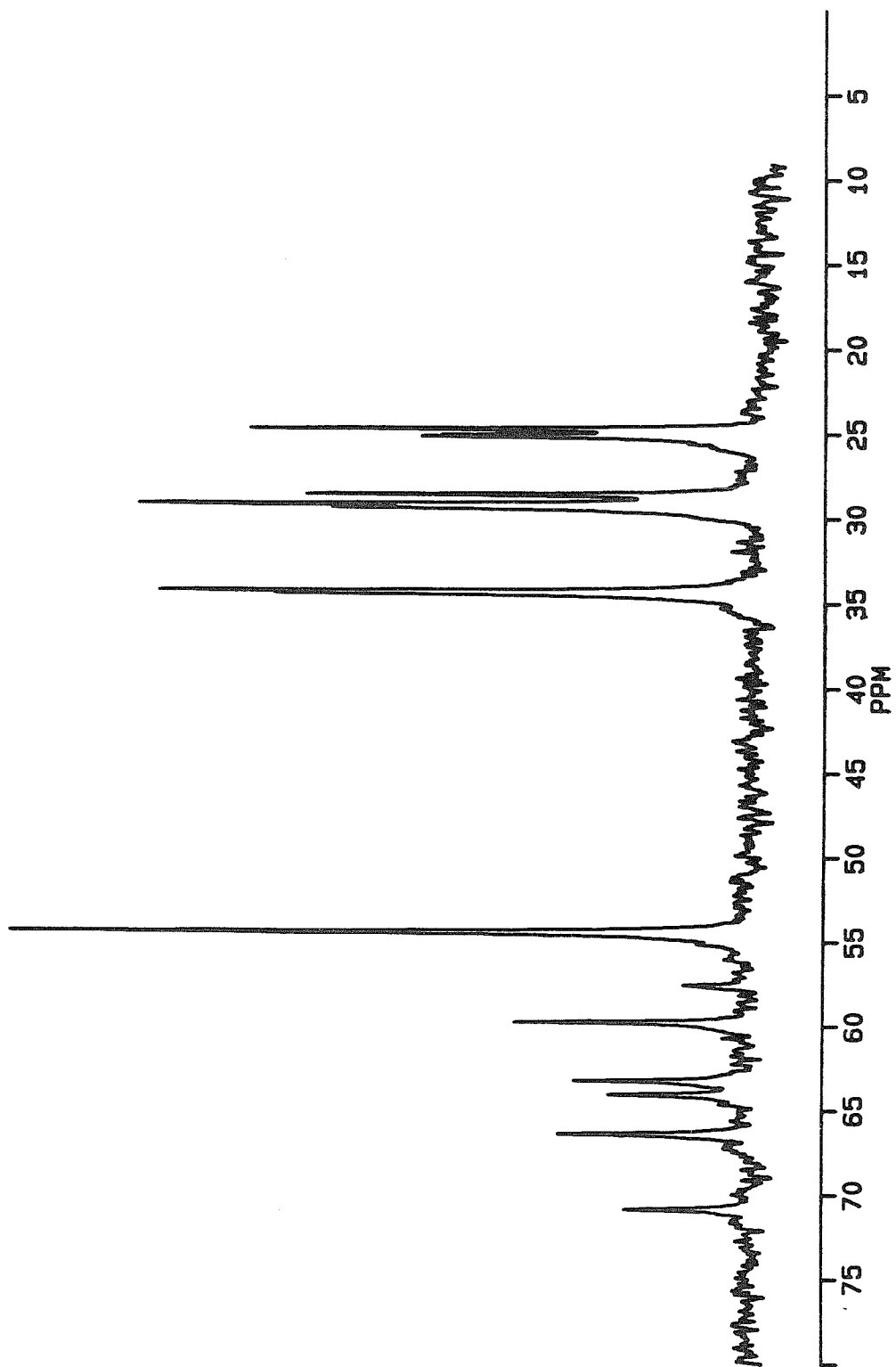


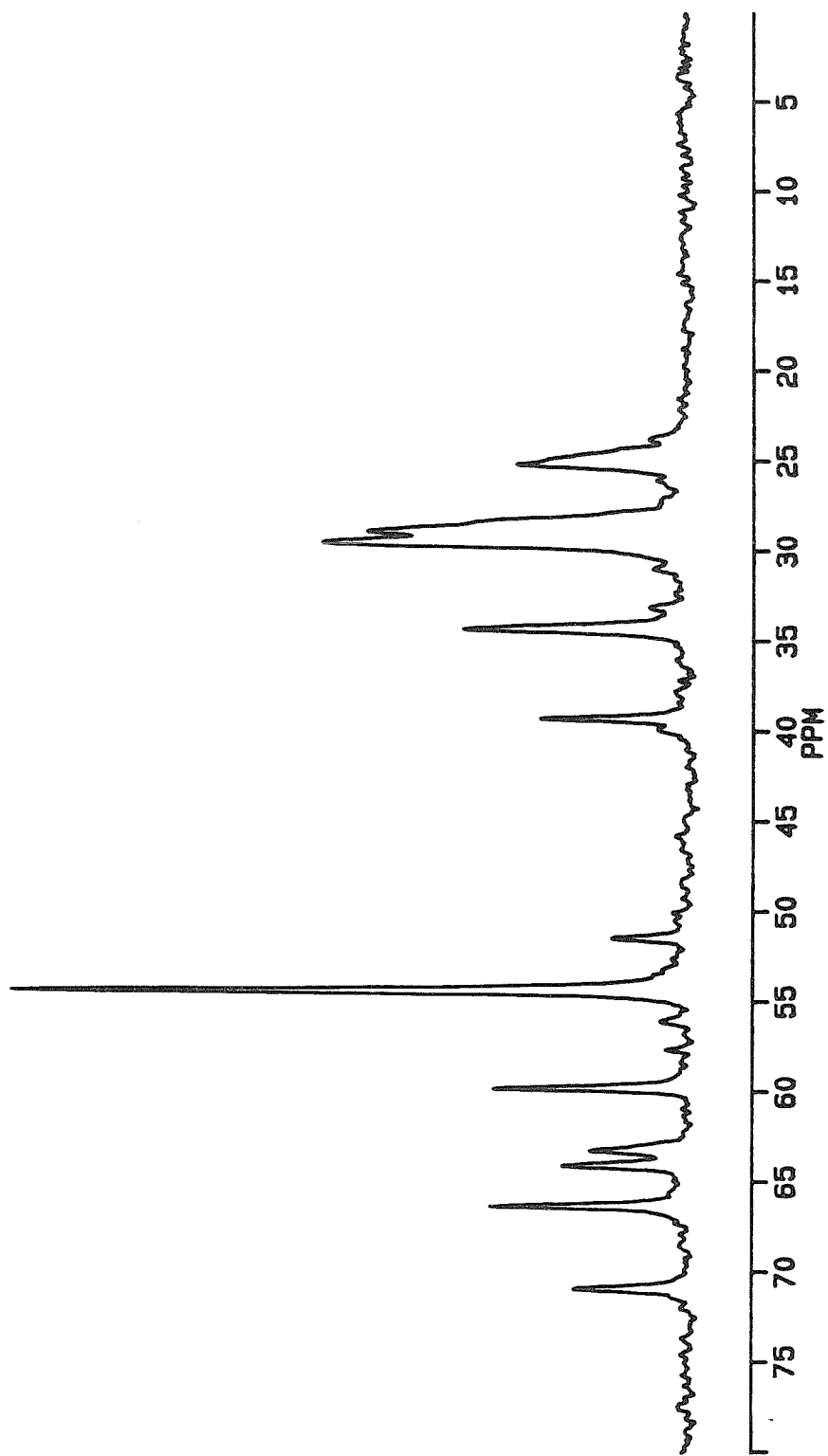


**Figure 9**

$^{13}\text{C}$  spectra (125 MHz) of  $\omega$ -8 "micelles" in phosphate buffer. The spectra are apodized with 10 Hz (A) and 20 Hz (B) linebroadening: **A.** Monomeric  $\omega$ -8 and **B.** Polymeric  $\omega$ -8. The polymerization was carried out by method A.

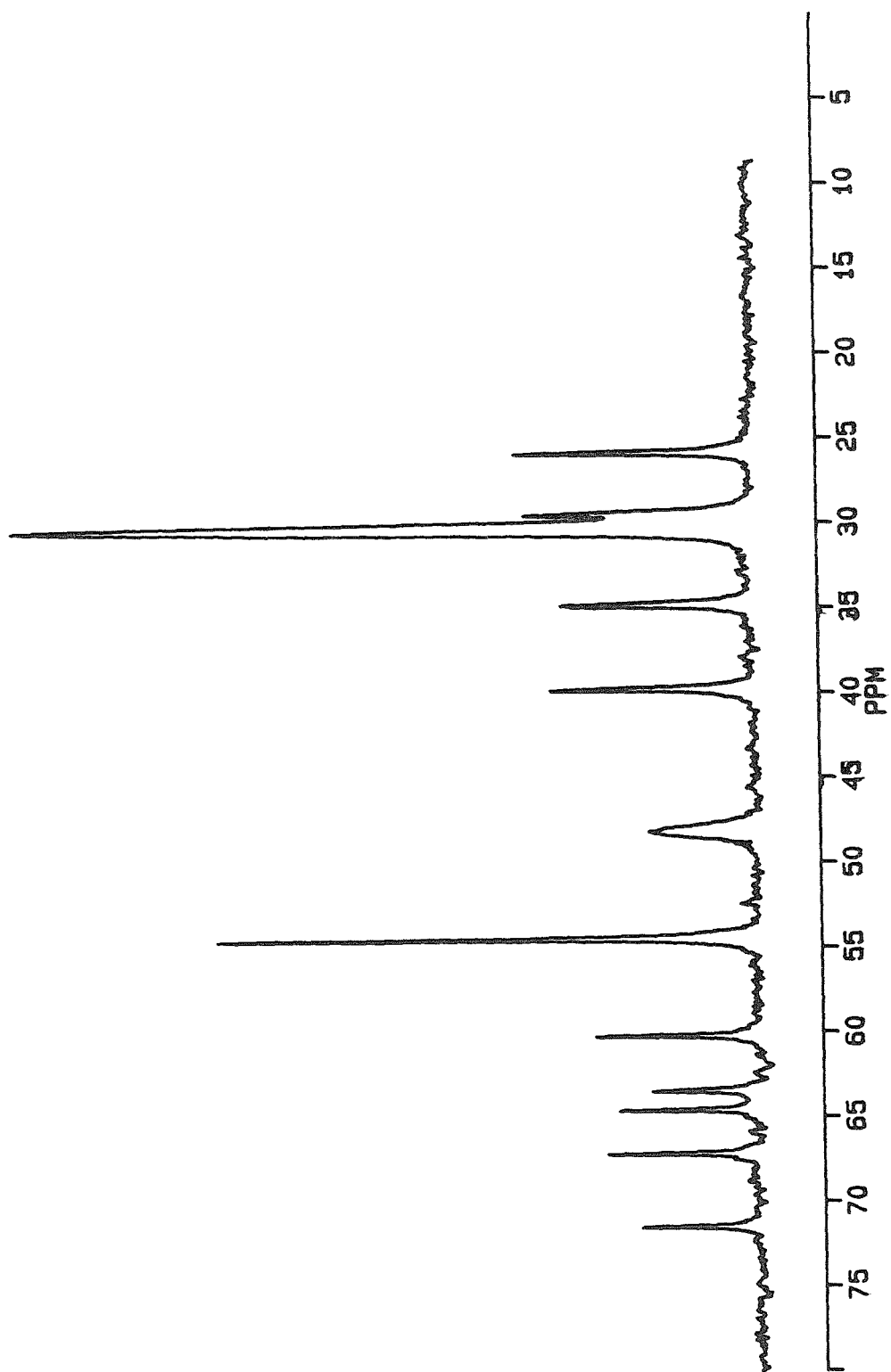
A



**B**

**Figure 10**

$^{13}\text{C}$  spectra (125 MHz) of polymeric  $\omega$ -11 in MeOH. The polymerization was carried out by method A. The spectrum was apodized with 10 Hz linebroadening.



42 ppm is due to the MeOH). As in the case of polymeric  $\omega$ -8, the  $\underline{\text{C}}\text{H}_2\text{S}$  is shifted to 39 ppm, and there is no sign of any terminal methyl groups.

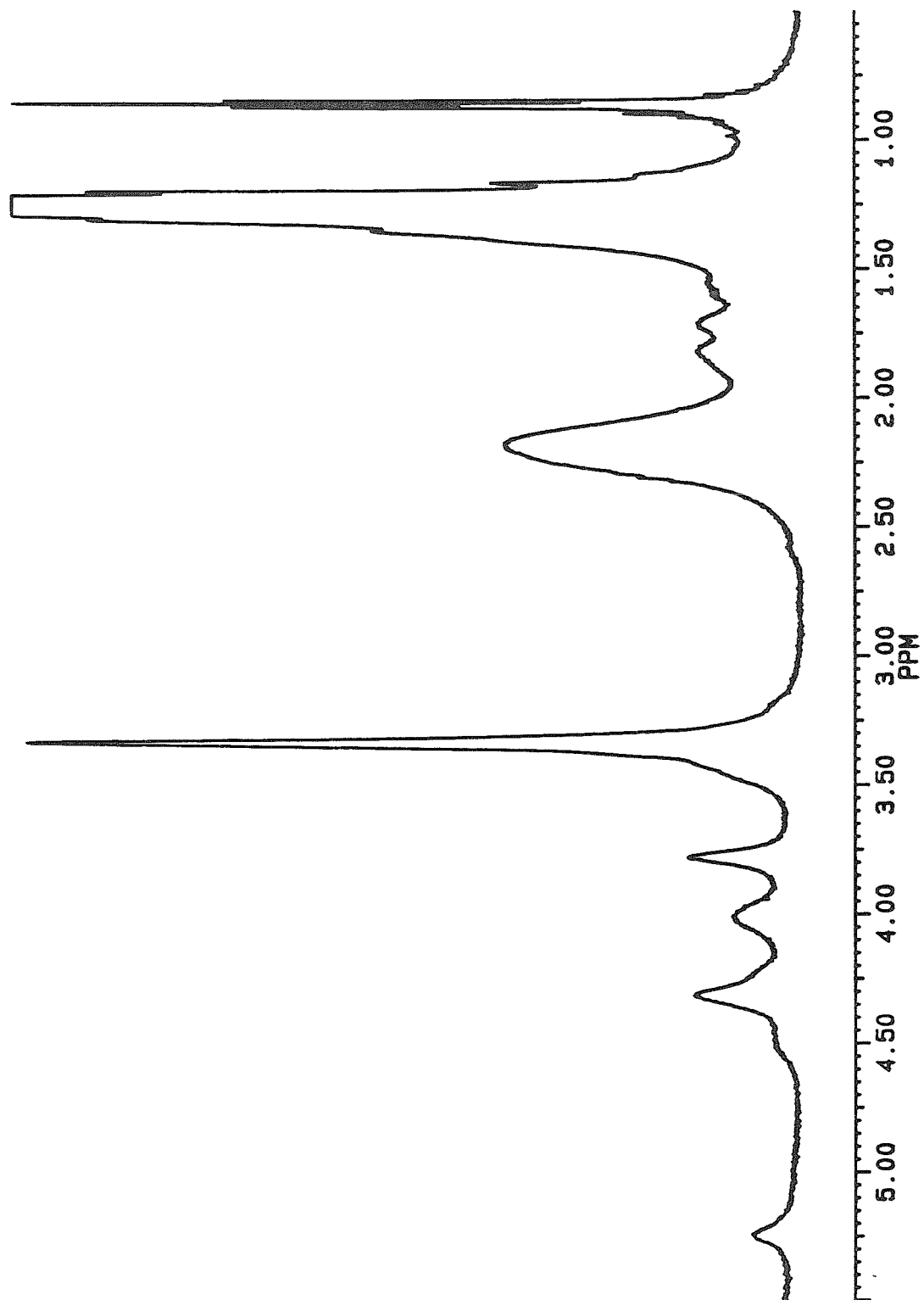
The  $\alpha$ -THIOLS are not as easily characterized by  $^1\text{H}$  NMR due to the broadness of the resonances, the overlap of the  $\underline{\text{C}}\text{H}\text{S}$  methine by the choline resonance and the fact that the  $\underline{\text{S}}\text{H}$  protons are frequently obscured by water. Figure 11 demonstrates the proton spectra of polymerized  $\alpha$ -16 in  $\text{CDCl}_3$ . Clearly all resonances are broadened on account of the polymerization. However the extent of the reaction cannot be monitored in this fashion as the  $\underline{\text{C}}\text{H}\text{SS}$  and any residual  $\underline{\text{S}}\text{H}$  protons are not visible.\*  $^{13}\text{C}$  NMR, however, provides more detailed information. Figure 12A shows the  $^{13}\text{C}$  spectrum of monomeric  $\alpha$ -8 in MeOH. The resonance assignments are as was noted above for monomeric T-8 with the exception that the resonance appearing at  $\approx 14$  ppm is due to the terminal methyl group and the resonance at  $\approx 42$  ppm is due to the  $\underline{\text{C}}\text{H}\text{SH}$  carbon (the broad resonance at  $\approx 48$  ppm is due to MeOH). Upon polymerization, the  $\underline{\text{C}}\text{H}\text{SH}$  carbon disappears completely. At this point it is not certain where the resonance corresponding to the polymerized  $\underline{\text{C}}\text{H}\text{SS}$  arises but based on the spectrum of the protected fatty acid ( $\underline{\text{C}}\text{H}\text{SS}$  resonates at 53 ppm), we suspect that it is buried beneath the resonance of the choline carbon or alternatively, broadened away by rapid spin-spin relaxation due to the rigidity of that region of the phospholipid. The important point, however, is that consistent with the results of Regen *et al.* (1), and thiol analyses that indicate virtually complete disappearance of residual thiol groups following polymerization, the NMR data suggest close to 100% disulfide formation. A reduced extent of reaction might be expected for the long chain  $\omega$ -THIOLS due to the high transition temperature of these lipids. However, under conditions that are slightly

---

\* It should be noted however that these lipids polymerize more readily than the  $\omega$ -THIOLS due to the presence of the thiol group near the membrane interface.

**Figure 11**

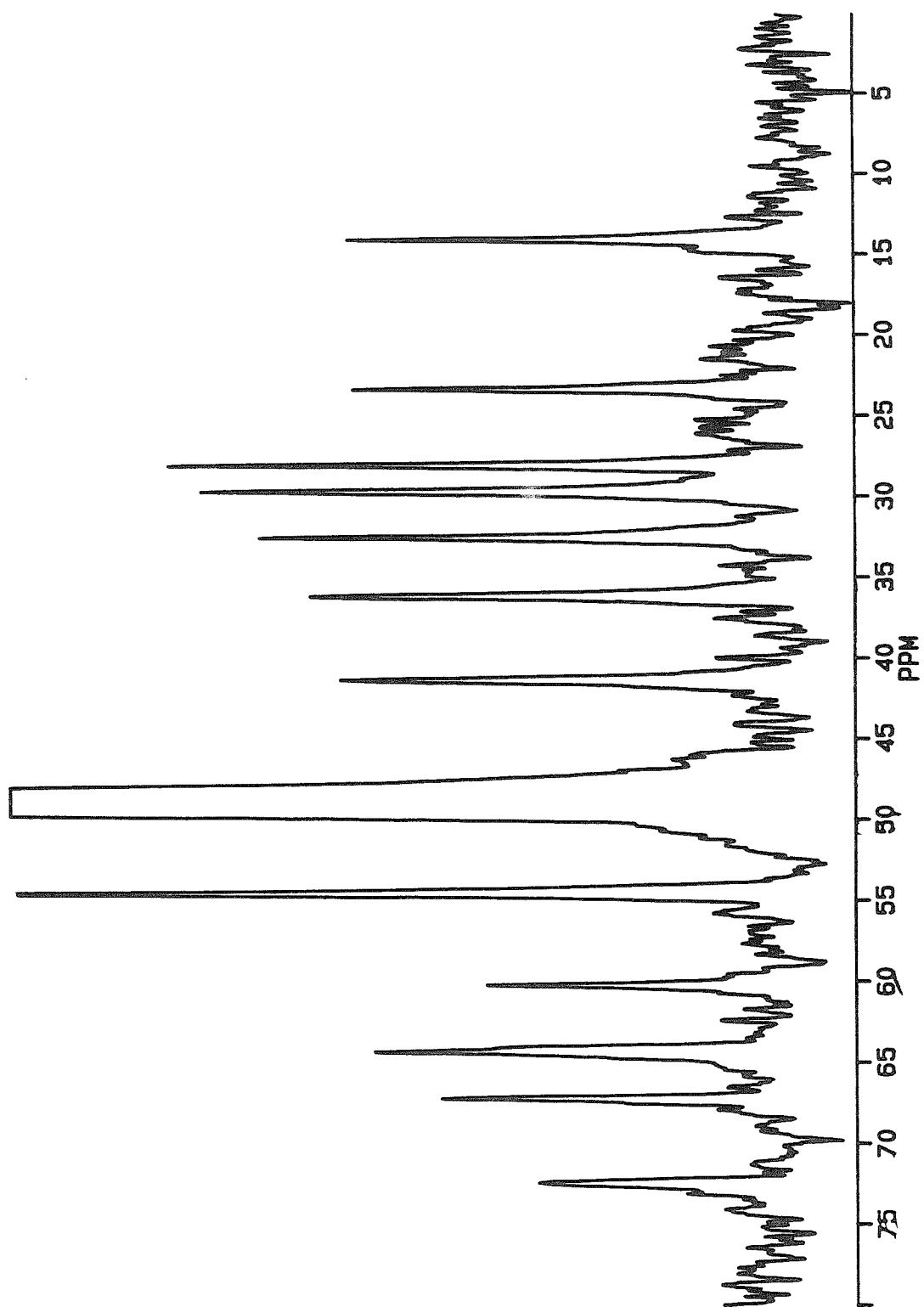
<sup>1</sup>H NMR spectra (500 MHz) of  $\alpha$ -16 in CDCl<sub>3</sub> with 1 Hz linebroadening. The polymerization was carried out by method A.

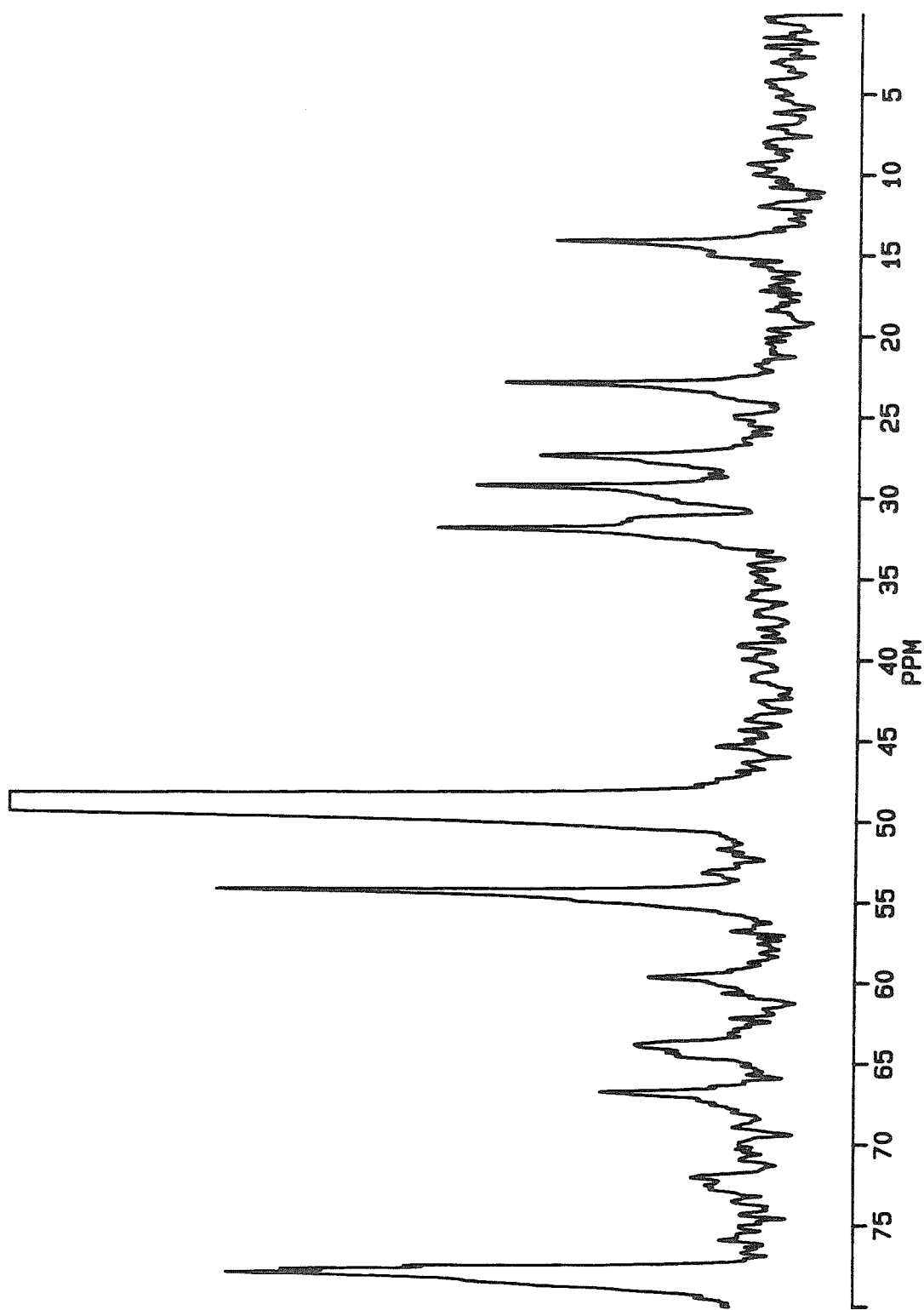


**Figure 12**

$^{13}\text{C}$  spectra (125 MHz) of  $\alpha$ -8 "micelles" in MeOH (A) or 50:50 MeOH/ $\text{CDCl}_3$ . The spectra are apodized with 20 Hz linebroadening: A. Monomeric  $\alpha$ -8 and B. Polymeric  $\alpha$ -8. The polymerization was carried out by method A.

A





milder than what we have used to polymerize  $\omega$ -16, Regen obtained 94% conversion to the disulfide.

Method B ; Cu<sup>+2</sup>/o-Phenanthroline Catalyzed Polymerization For the most part, method A was used to polymerize the lipids. However, a Cu<sup>+2</sup>/o-phenanthroline catalyzed polymerization method was also employed in a few experiments described in Chapter II. The procedure is a modification of that reported in (7) for sulfhydryl oxidation. Briefly, samples were prepared as dispersions in borate buffer (pH 7.4) containing 20 equivalents of H<sub>2</sub>O<sub>2</sub>. To this was added  $\mu$ liter amounts of a 0.025M Cu<sup>+2</sup>/o-Phenanthroline solution until a slight pinkish tint was detected indicating the presence of Cu<sup>+1</sup>(7). The solution was subsequently stirred at room temperature until it attained a slight green tint and the pH began to drop, or the sample was thiol-negative as detected with Ellman's reagent. At this point .1M EDTA (in 10 mM Tris, pH 7.4) was added to quench the reaction. The samples were dialyzed exhaustively with an Amicon dialysis chamber (YM10 filters), first with .1m EDTA to remove copper ions and subsequently with H<sub>2</sub>O/ MEOH to remove o-phenanthroline. The proton spectra of polymeric T-11 in CDCL<sub>3</sub>/MEOH appeared similar to that of an H<sub>2</sub>O<sub>2</sub>-polymerized sample. Samples rehydrated after polymerization by this method seemed to produce smaller aggregate structures than samples prepared by method A. This was shown by preliminary gel permeation chromatography using calibrated columns and by <sup>1</sup>H NMR. Whether this is due to the polymerization or dialysis with organic solvent is not known.

Method C; UV Polymerization. In the first publication of the lipids under study (4), 1,2-di(16-mercaptoundecanoyl)-L- $\alpha$ -phosphatidylcholine ( $\omega$ -11) was reported to be polymerizeable by uv irradiation. The polymerization protocol was carried out as previously described. Specifically, 1 to 5 mg of lipid ( $\omega$ -11) was bath sonicated in 1 ml borate buffer (10 mM borate, 150 mM NaCl, 2 mM NaN<sub>3</sub>; pH 8.5) and

subsequently photolyzed in a cooling bath at 254 nm. The progress of the reaction was monitored by the disappearance of thiol groups using Ellman's reagent and retention of the lipid at the origin of TLC plates eluted with 65:25:4 CHCl<sub>3</sub>/MeOH/H<sub>2</sub>O. Electron micrographs of the polymerized material confirmed the formation and retention of SUVs. However, <sup>1</sup>H NMR indicated that the uv polymerization caused a substantial and complete loss of sulfur as indicated by a diminished resonance at 2.4 ppm (CH<sub>2</sub>SH) and 2.65 ppm (CH<sub>2</sub>SS). Consequently, this polymerization protocol was abandoned.

### REFERENCES

1. Samuel, N.K.P., Singh, M., Yamaguchi, K. and Regen, S.L. (1985) *J. Am. Chem. Soc.* **107**, 42.
2. Habeeb, A.F.S.A in: *Methods in Enzymology* ; Hirs, C.H.W. and Timasheff, S.N., (Eds.); New York: Academic Press; Vol 25, 457.
3. Zahler, W.L. and Cleland, W.W. (1968) *J. Biol. Chem.* **243**, 716-719.
4. Regen, S.L., Yamaguchi, K., Samuel, N.K.P. and Singh, M. (1983) *J. Am. Chem. Soc.* **105**, 6354.
5. Bartlett, G.R. (1959) *J. Biol. Chem.* **234**, 466.
6. Selinger, Z. and Lapidot, Y. (1966) *J. Lipid Res.* **7**, 176.
7. Kobashi, K. (1968) *Biochim. Biophys. Acta.* **158**, 239-245.

---

---

## Chapter IX

### *Concluding Remarks*

---

Technically, we did not achieve the extremely stable liposomes with prolonged vascular half lives that we had initially envisioned at the conception of this project. Needless to say, given our intentions and the implications of liposomal drug delivery, the relatively unspectacular *in vivo* results were perhaps my biggest disappointment and the most frustrating part of the research I have done over the course of the last five and a half years. That is not to say that the lipids studied in this thesis have no utility. There are a variety of other applications of polymerizeable liposomes (even if only for immobilization of recognition molecules and enzymes onto membrane surfaces), which have less strict requirements on the physical properties of the liposomes than drug delivery applications have. But the applications are really only secondary and "icing on the cake." Our original expectations of the potential for these lipid types and our subsequent experimental results only serve to illustrate our current ignorance of the properties of polymerizeable phospholipids. It is hoped that the work described in this thesis will contribute to the deficit by (*i*) offering some insight into the physical

properties of a particular class of polymeric lipids (ii) illustrating both their potential and their caveats when it comes to *in vivo* use and (iii) providing some fundamental information, which may be of help in the rational design of polymerized membranes that possess predetermined properties.